Coventry University

DOCTOR OF PHILOSOPHY

Zinc Rich Paint as Anode System for Cathodic Protection (CP) of Reinforced Concrete Structures and Development of Corrosion/CP Monitoring Probes

Das, Sunil Chandra

Award date:
2012

Awarding institution:
Coventry University

Link to publication

General rights
Copyright and moral rights for the publications made accessible in the public portal are retained by the authors and/or other copyright owners and it is a condition of accessing publications that users recognise and abide by the legal requirements associated with these rights.

- Users may download and print one copy of this thesis for personal non-commercial research or study
- This thesis cannot be reproduced or quoted extensively from without first obtaining permission from the copyright holder(s)
- You may not further distribute the material or use it for any profit-making activity or commercial gain
- You may freely distribute the URL identifying the publication in the public portal

Take down policy
If you believe that this document breaches copyright please contact us providing details, and we will remove access to the work immediately and investigate your claim.

Download date: 23. Dec. 2021

Zinc Rich Paint as Anode System for Cathodic Protection (CP) of Reinforced Concrete Structures and Development of Corrosion/CP Monitoring Probes

By

Sunil Chandra Das

Thesis submitted to the department of Built Environment, Coventry University in partial fulfilment of the requirements for PhD in Civil and Structural Engineering

July, 2012

ACKNOWLEDGMENT

I am most grateful to Dr Eshmaiel Ganjian, my Director of Study, and Dr Homayoon Sadeghi Pouya, my supervisor for their constant enthusiastic support, helpful suggestions and comments throughout the work, without which I could not have possibly been able to complete this work.

I also would like to thank various laboratory staffs and a few MSc students at the Coventry University for their help with my experimental works. I acknowledge and thank the paint Manufacturer for supplying the ZRP material used for this work free of charge. Finally I would like to thank Essex County council for approving and accepting the financial package for the installation of the cathodic protection system designed and engineered using ZRP as an anode system for protecting steel reinforcement of the beams and deck soffit of a bridge structure.

Finally, I would like to thank and dedicate this work to my sons, Sagar and Sumon for their continued encouragements and support. They were always by my side whenever I needed help. I also dedicate this to my wife.

Contents

List of Figures

List of Tables

List of Recent Publications

1) Corrosion mitigation of chloride contaminated reinforced concrete structures: a state-of-the-art review, Das, Pouya and Ganjian, Proceedings of the Institution of Civil Engineers, Construction Materials 164 February 2011, issue CM1, Pages 21-28

2) Zinc Rich Paint as Anode for cathodic protection of Steel in Concrete, Das, Pouya and Ganjian, ACI (American Concrete Institute) Structural and materials Journal, Manuscript Submitted for publication, March 2012.

3) Innovative Cathodic protection of Steel in Concrete using Zinc Rich Paint as Anode system - Field Trial, S.C. Das, H. S. Pouya and E. Ganjian, Structural faults and Repair – 2012 Conference, Edinburgh, 3-5 July 2012. To be Presented.

4) Cathodic Protection to Half Joints of Reinforced Concrete Structures – Case Study, S.C. Das, A. Sharifi and G. Jewell, Structural Faults and Repair – 2012 Conference, Edinburgh, 3 -5 July 2012. To be Presented.

5) Designing a low Carbon Foot-print Anode System for Cathodic protection of R. C. Concrete Structures, S.C. Das, H. S. Pouya and E. Ganjian, Concrete Magazine, Concrete Socity, Paper submitted for publication, April 2012.

6) Recent Advances and Development of Anode Systems for Cathodic Protection of Steel Reinforcement in Concrete Structures, S.C. Das, 16th National Congress on Corrosion Control, 23-25 August 2012, Kolkata, India. To be presented.

ABSTRACT

Since mid-80's cathodic protection (CP) has been recognised as the ''only technique known to stop corrosion regardless of the levels of chloride contamination in concrete'' (FHWA, 1982) and is proved to be the most cost effective means to extend the useful life of the structure.

Cathodic protection is an electrochemical technique to stop/mitigate corrosion by supplying 'current' from an external source in order to suppress the 'internally generated' current flow due to corrosion processes. The 'external' current source could be obtained simply by coupling the steel to another electrochemically more active metal, e.g. zinc; alternatively the 'external' current may be derived from a mains operated low voltage DC power source, viz. transformer/rectifier unit. These two different approaches to supply 'external' current to stop corrosion are generically termed as:
'Sacrificial Anode Cathodic Protection (SACP)' system and
'Impressed Current Cathodic Protection (ICCP)' system, respectively.

Both approaches have proved to be feasible, but the impressed current CP system offers greater flexibility with regard to its ability to provide the necessary current in situations where concrete resistivity is relatively high and variable. The sacrificial anode system is most effective if the concrete resistivity is very low or the anode is placed in a very low resistivity environment such as soil with low resistivity, as the inherent driving voltage is low e.g. the potential difference between zinc and corroding steel in concrete is limited to approximately 0.7 volts.

Other contra-distinction between the two approaches are that the design life of the sacrificial anode systems are usually range between 10 -15 years; on the other hand the design life of the ICCP systems could be well in excess of 60+ years (depending on the type of anode system).

Following the successful application of first CP system, based on impressed current CP (ICCP), on a bridge deck in California, USA 1973, the technology has advanced significantly, particularly the anode systems (which is the main arbiter of a CP system) to deliver the protection current efficiently providing adequate protection (i.e. meeting the criteria recommended in BS EN ISO 12696: 2012 and other International Standards). Most of the CP installations worldwide are operating in ICCP mode. However, due to the escalating cost of anode systems and associated external power supply as well as monitoring/control units for ICCP installation has led researchers to actively pursue different means of developing low cost anode systems. Researchers have mainly focused on sacrificial anode CP (SACP) systems, as SACP does not require an external power supply and control units, but the drawback to this anode system is that it has a shorter life span (usually 10 -15 years compared to 60+ years for ICCP anodes).

This work describes the development of an ICCP anode system design utilising commercially available zinc rich paint (ZRP) as a primary anode material offering an innovative but considerably low cost alternative to currently used materials for ICCP anode systems. It also describes the development of a simple and low cost 'multifunctional' probe for monitoring the performance of the installed CP system, among other functions, such as LPR measurements, macrocell corrosion current measurement, E-log I tests for assessing the current requirements for CP design. For these functions both laboratory investigations and field trial on real life structure were employed.

Laboratory investigations were to determine the essential physical, electrical/electronic, physicochemical and electrochemical parameters necessary for ZRP to act as an efficient anode. The results of the investigations indicated that this specific proprietary ZRP products is highly suitable as ICCP anode material with an anticipated large cost saving in terms of cost of ZRP and easy application procedures together with significant benefits from environmental and health and safety point of view compared to, for example, Thermally Sprayed (TS) Zinc anode system in particular and other ICCP anode system (s) in general as a durable anode system for ICCP installations. This is due to the fact that ZRP anode

system can be applied on concrete substrate like ordinary paint brush, roller (or sprayed)

The analysis of data from the field trial of a fully designed cathodic protection installation for the protection of a bridge deck soffit and beams showed that the ZRP anode system could be considered to be a success and proved that it is capable of protecting reinforcement adequately and effectively.

With regards to the ‘multifunctional’ probe it has been demonstrated the probe can successfully be used as a monitoring device to measure the macrocell corrosion current and as a counter electrode for linear polarisation measurement. Other application as mentioned above however needs further investigation.

Finally, it could be concluded from this work that both the ZRP anode system and the ‘multifunctional’ probe are simple, low cost and possibly offer ‘lowest carbon foot-print’ approach to provide ICCP system design together with means to monitor the CP system performance and the corrosion behaviours using the . ‘multifunctional’ probe.

CHAPTER 1: INTRODUCTION

1.1 Background

The premise of this thesis is to investigate two innovative concepts. The first concept relates to the development of a simple, effective and low cost anode system for the impressed current cathodic protection installation on reinforced /pre-stressed /post tensioned concrete structures. The second strand of this research is to develop a robust but simple and low cost multifunctional probe (coined a term as 'BETA (β)-probe') for monitoring the behaviours of reinforcement corrosion and to assess the performance / effectiveness of the installed cathodic protection systems.

The problems of concrete deterioration due to corrosion of steel reinforcement and/or pre-stressed/post tensional systems in concrete structures are worldwide, and, according to WCO (World Corrosion Organization, with NGO status granted by UN), is costing the nations billions of pounds annually which is equivalent to around 4 to 6% of GDP (Gross Domestic Product). A recent 'White Paper' prepared by G. Schmitt (2009) of WCO, estimated that the direct cost of corrosion is in excess of US$ 2.2 trillion worldwide. On US highway bridges alone this is estimated to be at $8.3 billion overall, with $4.0 billion of that on the capital cost and maintenance of reinforced concrete highway bridge decks and substructures, G. H. Koch et al (2002). In the UK, the Department of Transport's estimate (1989) of salt-induced corrosion damage is a total of £616.5 million on motorway and trunk road bridges in England and Wales. These bridges represent about 10% of the total bridge inventory in the country, E. J. Wallbank (1989). In addition, the indirect costs (e.g. traffic delays, lost productivity etc.) are estimated to be more than ten times the direct cost of corrosion maintenance, repair and rehabilitation. This is over 20 years old statistic and no further estimates for the UK, and other parts of the world, are available but it is considered to be in a similar scale as in US. Only likely difference between various countries in the world, particularly for the either sides of the Atlantic, is the extent of reinforcement corrosion. This is due to a number of factors, mostly the climatic and environmental factors.

There are no simplistic model(s) to predict the rate of deterioration due to corrosion. However, we have sufficient understanding of the corrosion mechanisms and concrete deterioration processes. With the development of various NDT assessment techniques and the recent advances in protection and rehabilitation methods, a large percentage of these costs could be reduced. Various studies estimate that 25 to 30% of annual corrosion costs could be saved if optimum corrosion management practices were employed (WCO, 2002).

For longer-term solution of controlling corrosion, in an official policy statement issued in April 1982, R.A. Barnhart of Federal Highways Administration (FHWA) declared that the application of cathodic protection is proved to be the **'only rehabilitation technique'** to stop/mitigate on-going corrosion of steel reinforcement, particularly for the chloride-contaminated concrete (FHWA Memorandum, 1982). Further, in a report to U.S. Congress, FHWA estimated (in 1991) that up to $50 billion in repair costs could be saved over the period of 30 years by the use of cathodic protection. Alternative options are the replacement of a part of structural repair, massive concrete removal or a continuous programme of patch repairs throughout the life of the structure.

Cathodic protection is an electrochemical technique to stop/mitigate corrosion by supplying 'current' from an external source in order to suppress the 'internally generated' current flow due to corrosion processes. The 'external' current source could be obtained simply by coupling the steel to another electrochemically more active metal, e.g. zinc; alternatively the 'external' current may be derived from a mains operated low voltage DC power source, viz. transformer/rectifier unit. These two different approaches to supply 'external' current to stop corrosion are generically termed as:

'Sacrificial Anode' Cathodic Protection (SACP) system and

'Impressed Current' Cathodic Protection (ICCP) system, respectively.

These two different modes of cathodic protection systems are illustrated in Figures below.

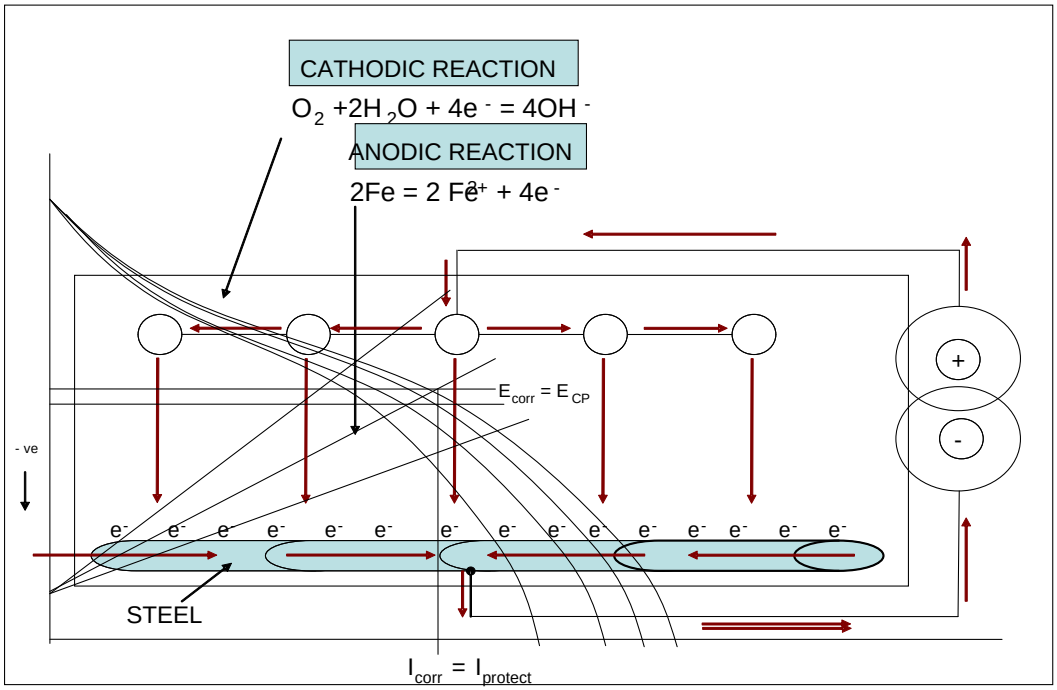

FIGURE 1.1: Circuit Diagram for an Impressed Current CP (ICCP) System
(With super-imposed Polarisation curves).

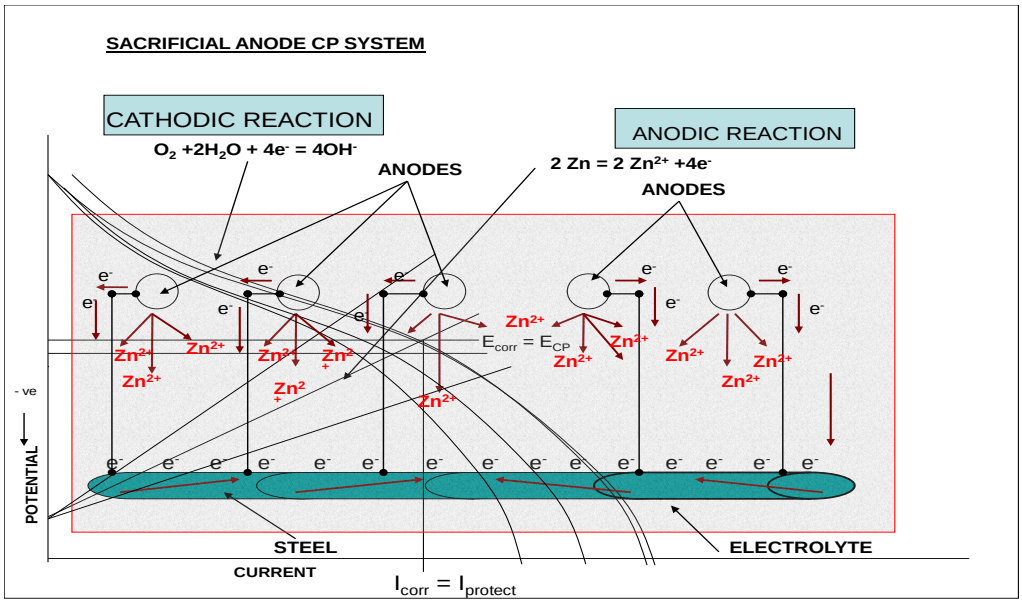

FIGURE 1.2: Circuit Diagram for a Sacrificial CP (SACP) System
(With super-imposed Polarisation curves).

Both approaches have proved to be feasible, but the impressed current CP system offers greater flexibility with regard to its ability to provide the necessary current in situations where concrete resistivity is relatively high and variable. The sacrificial anode system is most effective if the concrete resistivity is very low or the anode is

placed in a very low resistivity environment such as soil with low resistivity, as the inherent driving voltage is low e.g. the potential difference between zinc and corroding steel in concrete is limited to approximately 0.7 volts.

The most important element for any successful cathodic protection system is the design of an effective 'groundbed' (anode) system to distribute the necessary protection current economically and efficiently to the reinforcement. Also, it must be easy to install and possess long term durability. Other components of the CP system are then fairly easily designed to suit the 'groundbed' (anode system), the prevailing corrosion conditions and the environment.

Over the last 30 years, since the first CP system was installed on a concrete bridge deck in 1973 near Sly Park, California by RF Stratfull (RF Stratfull, January 1974), there have been considerable advances and developments in anode materials and anode system ('groundbed') design with real possibility of 'pick N mix' cathodic protection system(s) for above ground R.C. structures.

Not the entire anode systems that are currently in use proved effective or successful or suitable for any types of structural elements. The selection of most suitable anode system (s) ['groundbed' system(s)] would depend on the corrosion morphologies, type of construction (i.e. pre-stressed, post tensioned or conventional reinforced concrete}, the structural geometry, remaining life of the structure, and above all the technically acceptable to provide a long-term corrosion control and cost effective to the owner. Installation methods, operation and maintenance requirements and life cycle cost of the CP system may also play a major role in anode selection.

Vast majority of the installed and operating CP systems globally are ICCP type. More recently, due to escalating costs of impressed current CP anode system (s), there are increasing number of CP installations, particularly in the USA and Canada, are designed utilizing sacrificial anode materials with/without impressed current (M. Funahashi and WT, Young, June 1997 and April 1998 also A.Ip et al. Corrosion 2002). Most popular sacrificial anode systems (with/without impressed current) are based on Thermally Sprayed zinc, aluminium alloys or titanium coatings directly applied on concrete surface (A. Sagues, 1995; BS Covino et al.,

1997; R. Brousseau et. al, 1998). A number of 'purely' sacrificial anode systems are now commercially available (e.g. mortar encapsulated zinc anodes, zinc adhesive anodes, thermally sprayed zinc, thermally sprayed Aluminium-Zinc-Indium alloy anodes etc); but life-cycle analysis shows no significant savings when compared with much durable ICCP anode systems. The present investigation described in this thesis stems from successful experiences with the groundbed design based on utilizing commercially available Zinc Rich Paint (ZRP) as a sacrificial / impressed current anode material. These were 'ad hoc' applications, without much technical performance data, designed to evaluate the performance in real-life situations.

The second strand of the research programme was to develop Corrosion/CP Monitoring Probes. There are number of such monitoring probes available commercially, but they are quite expensive and requires specialist for installation, monitor and data interpretation. The main objective of this part of the programme is to developing a simple and low cost but effective multifunctional probe.

1.2 Research objectives

The specific objectives of this two strands research are to:

Strand 1: Evaluate the performance of zinc rich paints as Anode System for Cathodic Protection (CP) of Reinforced Concrete Structures (including pre-stressed/post tensioned structures) and

Strand 2: Development of Corrosion/CP Monitoring Probes.

The programme of work for the Strand 1 was based on assessing the following three principal properties required from the conductive materials: -

Physical (e.g. Application and adhesion)
Electronic/Electrical and
Electrochemical

Which, when considered together define the ability of the materials to act as an effective anode (ground-bed) for a CP installation.

It is anticipated that this investigation, through a set of experimental methods, will contribute significantly to a more confident evaluation of the performance of Zinc Rich Paint to be used as a CP anode for reinforced concrete structures.

In parallel with the experimental works, the performance of zinc paint anode system will also be evaluated by application to real-life structure.

The second major concept of this research programme (Strand 2) is to investigate the electrochemical parameters, such as in-situ measurement of corrosion rates, macro-cell corrosion current of steel reinforcement in concrete by a simple and low cost embeddable probe.

1.3 Structure of thesis

This thesis is divided into a number of Chapters because of the need to presenting the progression of work for each part independently; at the same time adhering to the methodology for the traditional way of writing a formal dissertation i.e. the main headings to comprise literature review, experimental methods, test programme, results, discussion, and conclusions.

Chapters 2 – 4 of this thesis describes a comprehensive account of experimental programme for the development of a low cost anode system for use in an impressed current CP design, based on Zinc Rich Paint as a primary anode material, together with the full description of a field trial on a real-life structure..

Chapter 5 of this research describes the programme of experimental works undertaken to develop a low cost viable retrofit multifunctional (β-probe) probe for corrosion measurement and CP monitoring. The conception of this 'β-probe' is the response to a number of technical 'why-not' and/or 'if-what' questions regarding the corrosion measurement / CP monitoring techniques. It is hoped, that this part (Part 2) of the investigations, if successful in achieving the set aims and

objectives, will not only compliment the Part 1 of the investigations with regard to assessing the performance of ZRP anode for CP installation but will be useful monitoring tool for CP system with any type of CP installations.

Finally, the concluding chapter (Chapter 6) presents the key findings and main conclusions, highlighting the main practical benefits (such as low cost, low carbon 'foot-print, environmentally friendly and ease of application), limitation of this research together with suggestions for future work.

1.4 Glossary of terms

The Glossary of Terms presented here is mainly in the context of corrosion and cathodic of protection of steel reinforcement in concrete and are not in alphabetical order.

(i) Corrosion

Corrosion is an electrochemical process involving two equal and competing electrochemical reactions i.e. the production and consumption of electrons with no net loss or gain of electrons. One reaction involves loss of electrons, occurring at the anode, and other gains electrons which occurs at the cathode. The first reaction, an anodic reaction (also known as Oxidation or corrosion reaction), causes metal to dissolve into solution as metallic ions liberating electrons. The other accompanying but competing reaction, occurring at cathode (also called the cathodic process or Reduction reaction), consumes electrons by reduction of dissolved chemical species, such as oxygen, chloride etc. Typical examples of anodic and cathodic reactions are:

Anodic reaction:

$$\mathbf{Fe} \longrightarrow Fe^{++} + 2e^{-} \qquad (1.1)$$

Cathodic reactions:

1) $2e^- + ½\ O_2 + H_2O \longrightarrow 2OH^-$ (1.2) or

2) $2H^+ + 2e^- \longrightarrow H_2$ (1.3) or

3) $2Cl^- + 2e^- \longrightarrow Cl_2$. (1.4)

(ii) **Cathodic Protection**

Cathodic Protection is an electrochemical process to mitigate corrosion of metal being exposed in an electrolytic environment (e.g. water, soil, concrete). The process (or technique) involves in supplying electrons (from an external source) to structure to be protected, in order to prevent electrons being generated 'internally. This may be achieved in two ways:

1) By a spontaneous galvanic effect i.e. using metals with more active potentials in the Electrochemical Series than that of the metal to be protected. This is called Sacrificial Anode Cathodic Protection (SACP) system.

2) Electrons (i.e. current) may be delivered from a DC power source through an 'auxiliary' anode (could be consumable or non-consumable). This known as Impressed Current Cathodic Protection (ICCP) system.

(iii) Anode

The part of an electrolytic cell at which the anodic (oxidation or corrosion) reaction takes place. In the context of cathodic protection, anodes contain more active metals (e.g. zinc, aluminium, magnesium etc.) which are used for SACP system or metals (consumable or non-consumable) and other conductive material connected to the positive terminal of a DC power source and is used for ICCP system.

(iv) Anodic Polarisation

Shift in potential from its 'natural potential' to more active (corroding) direction as a result of an applied current.

(v) Cathode

The part of an electrolytic cell at which the cathodic (reduction or electron consuming) reaction occurs. In the context of cathodic protection, this is the being protected.

(vi) Cathodic Polarisation

In the context of cathodic protection, a potential shift from its 'natural potential' to potentials more negative (direction) values, due to the application of current from an external source.

(vii) Potential

A measure of electrochemical reactions at metal (e.g. reinforcement) surfaces with respect to a reference electrode, indicating the condition of metal in terms of a state of corrosion or non-corrosion.

(viii) Natural Potential

In this context, potential of reinforcement (half-cell potential) with respect to a reference electrode (e.g. $Cu/CuSO_4$), measured prior to the application of cathodic protection.

(ix) Polarised Potential

Potential of reinforcement becoming more negative than the ‘natural potential’ or ‘as found potential’ after the application of cathodic protection.

(x) Potential Shift

Potential difference between ‘polarised potential’ and ‘natural potential’. A measure to assess the effectiveness of installed cathodic protection system.

(xi) Potential Decay

In the context of cathodic protection, shift of potential (polarised, IR free, see item xxi) to a less negative potential after the disruption of DC current. It is a measure to determine the effectiveness of the CP system’, usually over a time (e.g. 4 hours).

(xii) Depolarisation

A process of ‘decay’ of reinforcement potential from a ‘polarised state’ (i.e. the measured half-cell potential of the reinforcement with the application of CP current) to a potential of reinforcement in its ‘natural state’ (i.e. the measured half-cell potential of the reinforcement without the influence of an applied CP current).

(xiii) Groundbed

The part of the CP installation where the system anode(s) is (are) placed in the environment close to the structure to be protected.

(xiv) Primary Anode

Usually an anode material made of metallic conductor and used with conductive materials, such as conductive asphalt, conductive paint etc. to deliver current to the conductive anode of the structure to be protected.

(xv) Secondary Anode

‘Secondary Anode’ is the conductive anode material itself (e.g. MMO/Ti, conductive paints, conductive ceramics, metals etc.) and the primary function of this material is to convert ‘electronic current’ to ‘ionic current’ and deliver uniformly the protection current to the reinforcing steel.

(xvi) Anode Extender

Usually a conductive (metallic or non-metallic) material in the form of ‘wire’ used in conjunction with conductive paint material, directly connected to a ‘primary anode’ for distribution of current to the ‘secondary anode’.

(xvii) Embedded (Embeddable) Reference Electrode

Reference electrode is permanently placed within the concrete structure close to but not touching the reinforcement.

(xviii) Constant Current Control

Constant current control means that the current output from the power source, e.g. a transformer-rectifier is set at constant value with the output voltage of the transformer-rectifier automatically adjusting to maintain that current output.

(xix) Constant Voltage Control

Constant voltage control means that the output current of a transformer-rectifier is automatically adjusted so that the output voltage of the transformer-rectifier remains fixed at a set value.

(xx) Potential Control

Potential control means that both the current and voltage output of a transformer-rectifier are automatically adjusted though a feedback system (such

as reference electrodes), whereby the polarised potentials of a cathodically protected structure is maintained to a set value.

(xxi) 'IR Free' Potential

Potential (polarised) of the reinforcement without the contribution from the ohmic (IR) voltage being generated due to flow of current through the concrete between the reinforcement and the reference electrode.

(xxii) Instant (Instantaneous) Off Potential

The potential of the reinforcement measured at the instant (within a time limit of not less than 0.1 and not more than 1.0 seconds) of complete disruption of DC power to the system.

(xxiii) 'IR Drop'

The 'voltage drop' due to flow of current through a resistive medium, such as concrete, between the reinforcement and the location of the reference electrode.

(xxiv) Standard Hydrogen Electrode (SHE)

Electrode comprising of platinum black in a unit activity solution of hydrogen ions (1.05M HCl acid with hydrogen at 101,000 N/m^2 pressure). SHE is defined as zero and used as a primary reference for all electrochemical reactions. Also called as Normal Hydrogen Electrode (NHE).

(xxv) $Cu/CuSO_4$ Half Cell

Copper/Copper sulphate reference electrode (also referred to as CSE). Normal potential of a CSE half-cell vs. SHE (Standard Hydrogen Electrode) is 320 mV.

(xxvi) Ag/AgCl Half Cell

Silver/Silver Chloride reference electrode. Normal potential of an Ag/AgCl half-cell vs. SHE is 240 mV.

(xxvii) Reference Electrode

A reference Electrode is defined as an electrode on which the state of equilibrium of a given reversible electrochemical reaction is permanently secured under constant physico chemical conditions.

(xxviii) Protection Current Density

The current density value (usually in mA/m^2) required to be applied by the cathodic protection to the steel reinforcement, so that the corrosion of the reinforcement is adequately mitigated or controlled.

(xxix) Protection Criteria

The criteria recommended by the national and/or international professional bodies against which the performance of the installed cathodic protection system is assessed to determine the adequacy and efficacy.

CHAPTER 2

ZINC RICH PAINT (ZRP) AS ANODE SYSTEM FOR CATHODIC PROTECTION (CP) OF REINFORCED CONCRETE STRUCTURES

The main goal of this section is to assess all the essential physical, electrical/electronic and electrochemical characteristics of Zinc Rich Paint as an anode system of a cathodic protection installation for reinforced (with or without pre-stressed/post tensioned) concrete structures.

CHAPTER 2: LITERATURE REVIEW

2.1 Introduction

This chapter presents a brief review of the background theories and some technical/practical considerations on corrosion of both steel and zinc in concrete together with some commentaries on the development of Cathodic Protection technologies for reinforced concrete structures to mitigate reinforcement corrosion; leading to the present research work described in this thesis.

Corrosion is a worldwide problem and costs the nations billions of pounds. Corrosion is insidious in nature. Particularly, the corrosion of steel in concrete is only apparent when it is quite advanced and manifests itself progressively in the form of 'rust' stains, cracking, delaminating and finally spalling with exposed and corroding steel reinforcement. Corrosion problem is more acute and accentuated for half-joints of the reinforced/pre-stressed concrete highway bridges. This is due to the fact that half-joints are not easily accessible for NDT inspection and concrete testing.

In 1982, Federal Highway Administration Memorandum proclaimed that Cathodic Protection is the **only rehabilitation technique that has proven to stop corrosion of steel in chloride contaminated concrete** regardless of the chloride content of the concrete. Over the last three decades ever increasing number of successful CP installations worldwide are operational to validate this. For the last ten years, CP technology is extended to provide corrosion protection/prevention to half joints of the cantilever/suspended span bridges and propped cantilever bridges.

There are extensive literature on the subject related to the theoretical understanding of corrosion mechanism (s) and the basis for the applications of cathodic protection to reinforced, pre-stressed/ post tensioned concrete structures. These are briefly discussed in the following sections.

Zinc anodes for CP of reinforced concrete structures can be found in numerous references. However, literature search indicated no prior works on Zinc Rich Paint

(ZRP) as anode (sacrificial or impressed current) for CP of reinforced concrete. The main purpose of this study is to investigate the use of ZRP to provide cathodic protection to chloride contaminated reinforced concrete structures.

2.2 Corrosion Mechanism of Steel in Concrete

The corrosion of steel reinforcement in concrete is an electrochemical process involving two equal, but opposite, reactions; these are the anodic, or oxidation reactions (e.g. $Fe \rightarrow Fe^{++} + 2e^{-}$), and cathodic or reduction reactions (e.g. $O_2 + 2H_2O + 4e^{-} \rightarrow 4OH^{-}$).

Concrete has the inherent ability to protect steel against corrosion. This is due to the high alkalinity of concrete, ranging between 12.5 and 13.7, imparted by the chemical constituents of the cement, in particular calcium hydroxide $Ca(OH)_2$.

In this alkaline environment, a thin film of oxide or hydroxide such as ferric oxide, Fe_2O_3, is formed on the steel surface rendering the steel PASSIVE, i.e. the corrosion rate becomes insignificant.

However, this protection mechanism may break down as a result of one or more changes in the concrete's chemistry, the most common and important factors being:

i) Loss of alkalinity in the concrete
ii) Penetration of aggressive ions to reinforcement depth
iii) A combination of both factors

The main offending ion for the breakdown of passive film on steel reinforcement is chloride in concrete. Chloride salts may be present in concrete from a number of sources:

(a) Calcium chloride deliberately added to the concrete mix at the time of construction as an accelerating admixture. This practice, however, has been prohibited since early 1960's.

(b) Ingress of de-icing salt from an external source, for example in bridge deck or substructure of a bridge.
(c) Ingress from seawater in case of marine structures.
(d) Impurities in the aggregates and/or mixing water.

Chloride acts as a catalyst for oxidation of iron by taking an active part in the reaction. According to Uhlig (1963) it oxidizes the iron to form the complex ion $FeCl_3^-$ and draws this unstable ion into solution, where it reacts with the available hydroxyl ions to form $Fe(OH)_2$. This releases the Cl^- ions back into solution and consume hydroxyl ions, as seen in the following reactions:

$$2Fe + 6Cl^- \rightarrow 2FeCl_3^- + 4e^- \qquad (2.1)$$

This is followed by:

$$FeCl_3^- + 2OH^- \rightarrow Fe(OH)_2 + 3Cl^- \qquad (2.2)$$

The electrons released in oxidation reaction flow through the steel to the cathode surface.

This process would result in a concentration of chloride ion and a reduction of the pH at the points of corrosion initiation, probably accounting for the process of pitting corrosion. The lowered pH at these sites contributes to the continual breakdown of the passive oxide film, ACI SP-102 (2001).

Alternative reactions for complex formation are:

$$Fe^{2+} + 6Cl^- \rightarrow FeCl_6 + 4e^- \qquad (2.3a)$$

or

$$Fe^{3+} + 6Cl^- \rightarrow FeCl_6 + 3e^- \qquad (2.3b)$$

The above reaction removes ferrous (Fe^{3+}) ions from the cathode area, allowing them to be deposited away from the bar, through the reaction:

$$FeCl_6 + 3e^- + 2OH^- \rightarrow Fe(OH)_2 + 6Cl^- \qquad (2.4)$$

This reaction produces rust and releases chloride ion for further reaction with ferrous ions.

In engineering situations, the electrochemical reactions of the corrosion process are more complex than described above.

Electrochemical principles of corrosion can be summarised diagrammatically with the aid of Pourbaix diagrams (pH-potential, based on thermodynamics) (Pourbaix , 1973) and Evan's diagrams (L. L. Shreir et al., 1963); also known as Polarisation diagrams, based on kinetics of the corrosion processes. An example of a well-known form of a potential-pH diagram for the iron-water system and less well-known potential-pH diagram showing experimental condition of iron corrosion in solution containing chloride ions are given in Figure 2.1 and Figure 2.2 respectively, which are based on various electrochemical equilibriums (Pourbaix, 1973).

This image has been removed due to third party copyright. The unabridged version of the thesis can be viewed at the Lanchester Library, Coventry University

Figure 2.1: Potential-pH diagram showing iron corrosion in water (Corrosion-Doctors.org.).

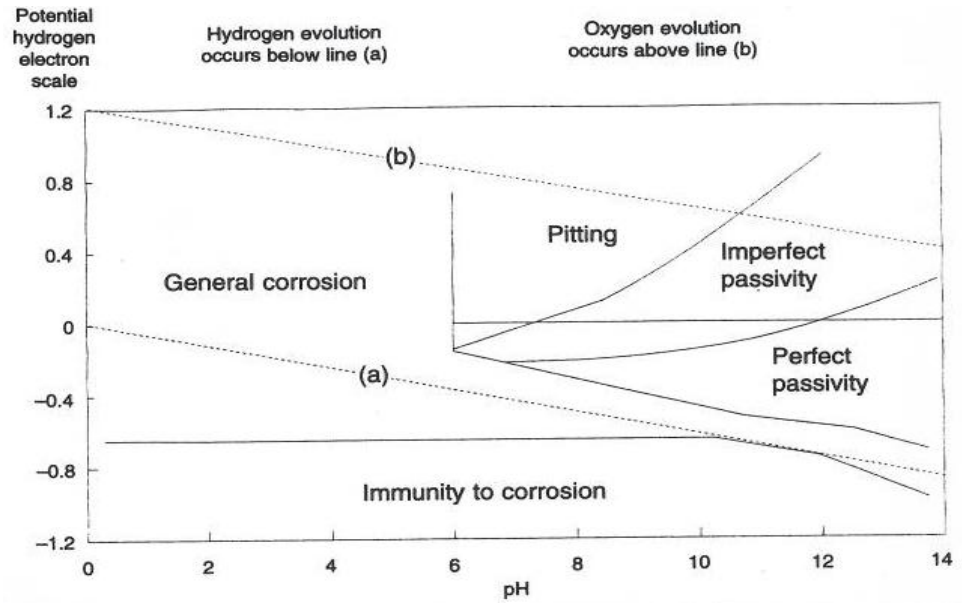

Figure 2.2: Potential-pH diagram showing experimental conditions of iron corrosion in solution containing chloride

However, pH-potential diagrams do not indicate the magnitude or speed at which a corrosion reaction may proceed. The rate of corrosion is controlled by the kinetic factors and this can be graphically represented on a potential vs. current plot, commonly known as 'Evans' or 'Polarisation diagram'. An example of which is given in Figure 2.3.

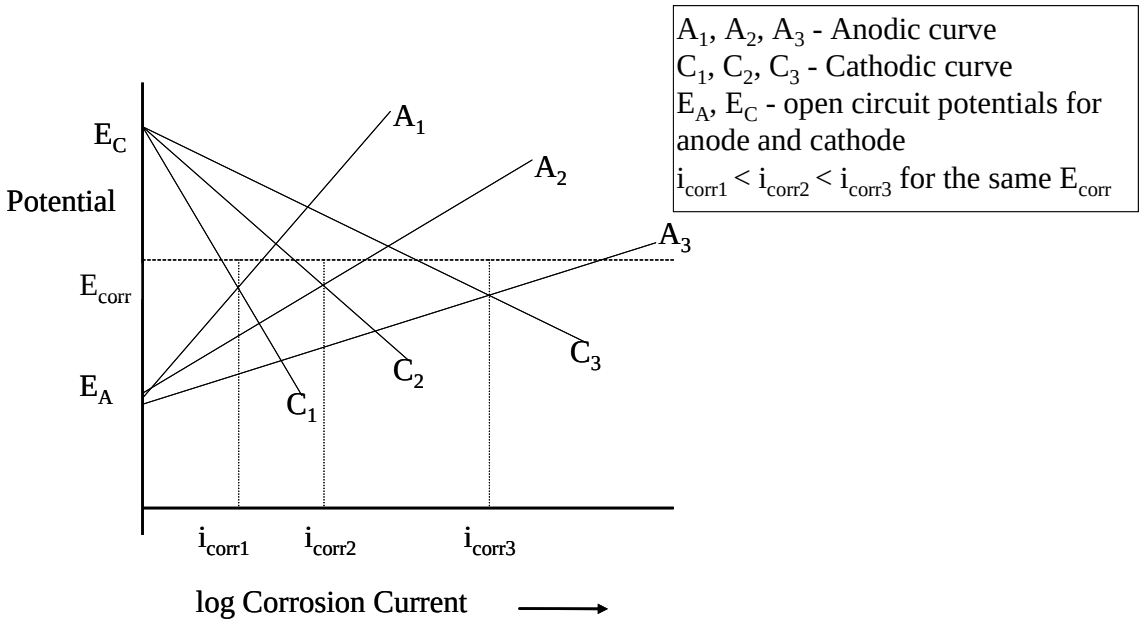

Figure 2.3: Electro-potential verses corrosion current. (Das SC, 1984)

From Figure 2.3, it can be seen that for any particular value of E_{corr} (the measured electro-potential reading) the rate of corrosion could vary by several orders of magnitude due to the logarithmic relationship between corrosion potential and corrosion current.

Among the factors listed above, the availability of oxygen (which depends on the diffusion coefficient of oxygen through concrete cover) and the moisture content in concrete (or relative humidity inside concrete) have the most significant and measurable effects on measured potential. Both entities influence the cathodic reactions of the corrosion process.

This image has been removed due to third party copyright. The unabridged version of the thesis can be viewed at the Lanchester Library

Figure 2.4: Natural and impressed potentials of steel in concrete (Arup, H., 1979)

Due to the inhomogeneous nature of concrete, steel reinforcement may develop electro-potential values over the full ranges for both active and passive states

within the same structure. The range of potential values, both 'natural' and 'impressed' potentials of steel in concrete, is depicted in Figure 2.4 (Arup, H., 1979). The corrosion potential (E_{corr}) of steel in concrete depends on many interacting factors such as:

(a) Relative humidity of the pore system (i.e. moisture content)
(b) Cement / aggregate ratio of the mix
(c) Availability of oxygen, which in turn depends upon other factors including the permeability of concrete and relative humidity.
(d) Distribution of active / passive areas
(e) Presence and type of depassivating ions, e.g. chloride ions or CO_3^- ions
(f) Environmental influences, such as seasonal variations of wetness/dryness, temperature, etc.
(g) Concrete cover to steel reinforcement

These all become cathodically controlled, i.e. the electro-potential tends to be numerically more negative with increasing moisture content (i.e. relative humidity). In addition, electro-potential values tend to be numerically more negative with the depletion of oxygen. This oxygen depletion is caused by decreasing diffusion coefficient as a result of increasing water saturation of the concrete while the corrosion rate remains significantly low. Tuutti, K. (1982), reported that if the RH changes from 65% to 78% the oxygen diffusion coefficient decreases about four fold and at values of 90-95 % RH the cathodic process, which consumes O_2, reaches a limiting situation. On the other hand, Gjorv (1977) and others reported that the concrete resistivity changes by several orders of magnitude as the RH changes from 100% to 50 % with a significant effect on corrosion rates. The overall effect of oxygen depletion and increasing water saturation on electro-potential values is shown in the Figure 2.5 (Das, SC, 1984).

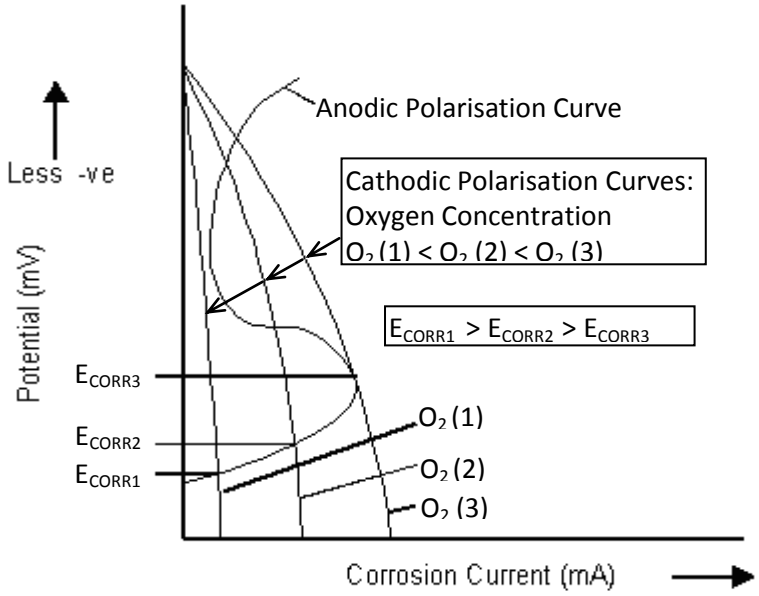

2.5: Effect of Oxygen Concentration On Electro-potentials (Das, SC, 1984)

Further, the electrochemical corrosion of steel reinforcement in concrete, particularly in presence of chloride can occur in different forms due to the different spatial location of anode and cathode (S.Jaggi et al., Eurocorr 2001). These are as follows:

- The first form is as **microcells,** where anodic and cathodic reaction sites are either the same or immediately adjacent, leading to uniform iron dissolution over the whole surface, i.e. corrosion is uniform. Uniform corrosion is generally caused by carbonation of the concrete or by very high chloride content at the reinforcement.

- The second form is as **macrocells,** where a net distinction between corroding areas of the reinforcement, i.e. anodic sites and non-corroding, passive surfaces, i.e. cathodic sites is found.

These two forms of corrosion cells are illustrated in Figure 2.6.

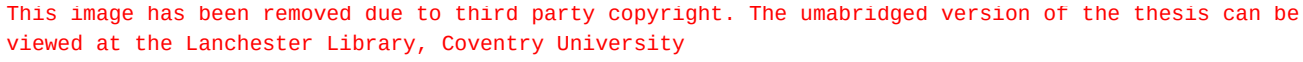

Figure 2.6: Schematic illustration of (a) micro cell corrosion and (b) macro cell corrosion (cement.org 2008).

Microcells occur mainly in the case of chloride induced corrosion, leading to highly localised corrosion in form of pitting. In this situation the anode (more precisely anodic sites) is generally small with respect to the total surface of the reinforcement, which is mostly passive. Macrocell corrosion may lead to locally very high dissolution rate (by a factor of 5 – 10), i.e. reduction of cross-section of the reinforcement may be greatly accelerated due to large cathode/anode area ratio. Local corrosion rates up to 1mm/year have been reported for bridge decks or other chloride contaminated RC structures (B. Elsener, 1995 and 1998; C. Andrade et. al, 2004). This rapid corrosion attack may lead, if not detected early, to structural safety problems.

Macrocells corrosion and the monitor/measurement of macrocell corrosion current are discussed further in details later in Chapter 5 of this document.

2.3 Corrosion and Electrochemistry of Zinc – Brief Review

Detailed discussions on the Corrosion and electrochemistry of zinc can be found in a number of excellent books, such as 'Corrosion and electrochemistry of zinc by Xiaoge Gregory Zhang (Zhang, X. G., 2001). Only the relevant theoretical and technical information are briefly described below.

Zinc and zinc alloys occupy an important place with regards to protection of other metals, in particular steel. Zinc and zinc alloys are the most common and widely used anode materials for the provision of galvanic protection of steel structures exposed in various corrosive environments. It is therefore considered appropriate to appreciate the important theoretical and practical aspects of corrosion behaviours of zinc and its alloys.

The common forms of corrosion on zinc are general corrosion, galvanic corrosion, pitting corrosion and intergranular corrosion. The most important form of corrosion for zinc applications, such as a coating, an anode or zinc dust paint is galvanic corrosion and this galvanic corrosion behaviour of zinc is exploited with advantage to protect steel structures.

Detailed discussion of galvanic corrosion of zinc and its alloys coupled to other metals, except steel is outside the scope of this research project. Therefore, the principles and practical applications of galvanic protection, commonly known as sacrificial cathodic protection, of steel, particularly the steel reinforcement in concrete, by zinc coatings, zinc anodes, zinc-rich paints and other means are reviewed. Various factors that may play roles in galvanic action between zinc coupled steel are discussed.

2.3.1 Theoretical Considerations

Simply, when two dissimilar metals in an electrolyte are electrically connected with each other a current, which is called a galvanic (corrosion) current, from one to the other and the direction of the 'positive' current flows, within the electrolyte, from the metal that has a more negative thermodynamic reversible potential in the

electromotive force (emf) series. This part of the galvanic couple (of the corrosion cell) is the 'anodic' member and the metal with less negative thermodynamic reversible potential becomes 'cathodic' member of the couple. The cathodic member is thus cathodically protected. The electrode potential of metals is expressed by the well known Nernst Equation (L. L. Shreir et al., 1963) as below:

$$E_M = E^0_M + RT/nF \ln a(M^{n+}) \qquad (2.5)$$

Where:

E_M = the standard electrode potential of the metal in the solution of ions at unit activity, i.e. $a(M^{n+}) = 1$.

R = Gas constant,

T = temperature

N = number of electrons involved in the electrode reaction, and

F = Faraday's constant

The electrode potential (i.e. corrosion potential in an aqueous environment) for zinc dissolution,

$$Zn \rightarrow Zn^{++} + 2\,e^-, \qquad (2.6)$$ is given by:

$$E_{Zn} = E^0_{Zn} + RT/2F \ln a(Zn^{++}) = -0.76\ V_{SHE} \qquad (2.7)$$

Where:

E_{Zn} = the electrode potential of the zinc

E^0_{Zn} = the standard electrode potential of the zinc in the solution of ions at unit activity, i.e. $a(M^{n+}) = 1$

R = Gas Constant

T = Temperature

F = Faraday's constant

$a(Zn^{++})$ = ionic concentration of zinc

(cf. for Iron, $Fe \rightarrow Fe^{++} + 2e^-$, $E_{Fe} = -0.44\ V_{SHE}$)

Other possible anodic reactions of Zn/H_2O system are:

$$Zn + 2H_2O \rightarrow Zn(OH)_2 + 2H^+ + 2e^- \qquad (2.8)$$

$$Zn + 2H_2O \rightarrow ZnO_2^{2-}{}_{(aq)} + 4H^+ + 2e^- \qquad (2.9)$$

And their corresponding equilibrium potentials can be obtained from the following simplified Nernst equations:

For the reaction in equation (2.8):

$$E_{Zn} = E^0_{Zn} - 0.059\ pH \qquad (2.10)$$

For the reaction in equation (2.9):

$$E_{Zn} = E^0_{Zn} - 0.12\ pH - 0.059/2 \log a(ZnO_2^{2-}) \qquad (2.11)$$

Historically, the high electro-negativity of zinc is the theoretical basis and used with advantage to provide galvanic protection or 'sacrificial cathodic protection' to steel, when directly coupled together in an electrolyte.

The free corrosion potential of zinc in sea water is about 1.1 volts with respect to a $Cu/CuSO_4$ reference electrode. However, in concrete, the corrosion (or open circuit) potential varies.

2.3.2 Corrosion of Zinc – pH-potential diagram etc.

Zinc is an amphoteric metal i.e. Zinc is capable of reacting chemically either as base or an acid and the corrosion rates of zinc are high in both low and high pH values as shown in the pH- potential diagram below (Figure 2.7).

This image has been removed due to third party copyright. The unabridged version of the thesis can be viewed at the Lanchester Library, Coventry University

Figure 2.7: Potential-pH equilibrium diagram for zinc-water system (Pourbaix, 1973).

Zinc corrodes only very slowly due to the high overvoltage for the reduction of water (i.e., $2H^+ = H_2 + 2e^-$); passivation is possible for values of pH between 9 and 12. At pH 7, zinc does not passivate but corrodes. The effect of pH value on corrosion of zinc is shown in Figure 2.8.

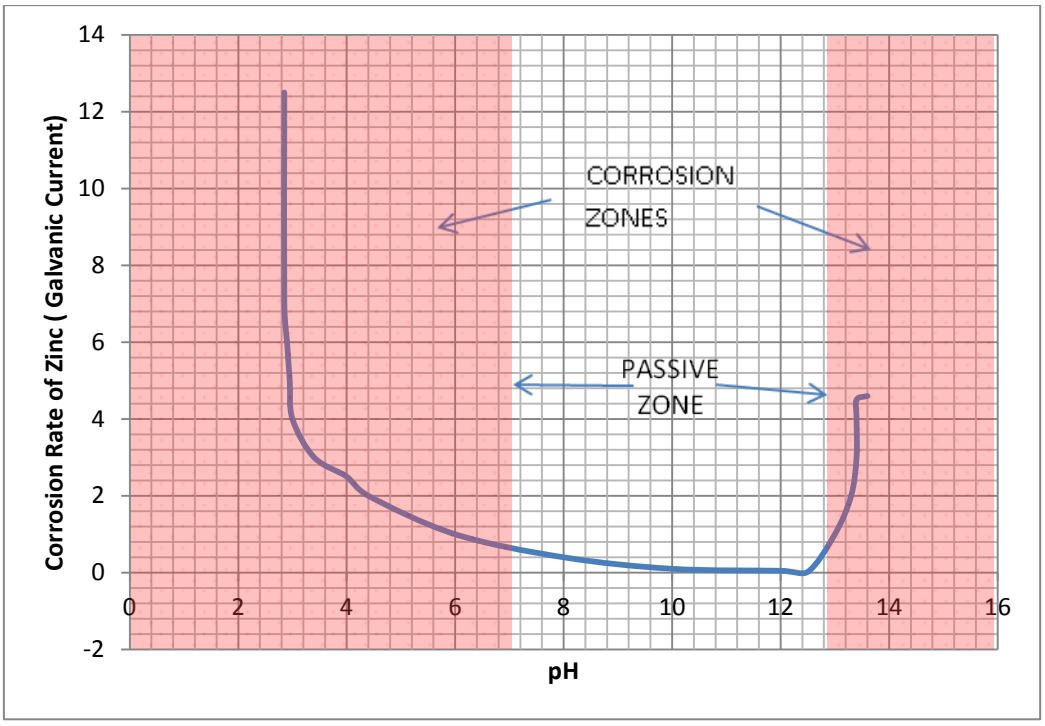

Figure 2.8: Effect of pH value on corrosion of Zinc (after CJ Slunder and WK Boyd, 1971).

2.3.3 Corrosion of Zinc in Concrete

In concrete, the behaviour of zinc is somewhat different. Zinc reacts with hydroxyl ions in plastic concrete and concrete pore solution to form zinc oxide and hydrogen gas. Zinc oxide reacts with calcium ions to form calcium hydroxyzincate. At a pH below 13.3, calcium hydroxyzincate forms a stable coating that passivates the zinc. Above a pH of 13.3, the corrosion products form large crystals that do not provide corrosion protection (Andrade and Macias 1988; Bentur et. al. 1997). A key aspect of providing corrosion protection is the retention of the external layer of pure zinc. Once this layer is lost, the zinc required to form calcium hydroxyzincate is removed and the underlying zinc-iron alloy layers are destroyed (Andrade and Macias 1988). pH values above 13.3 are typical for concrete (Struble 1988).

Zinc provides protection in two ways. It acts as a barrier that prevents access of oxygen and moisture to the protected material, and it acts as a sacrificial anode that corrodes in preference to the protected metal. In air, zinc achieves significant protection itself due to the formation of a hydrated oxide, $Zn(OH)_2$, which in turn

combines with carbon dioxide in the atmosphere to form a protective zinc carbonate layer, ($ZnCO_3$), that prevents further corrosion (Jones 1996).

Most studies to investigate the corrosion behaviour of zinc in concrete, particularly in chloride contaminated concrete, were carried out on galvanised steel reinforcements. The process of galvanising results in the formation of an outer layer of pure zinc that is underlain by several zinc-iron alloy layers; and the corrosion processes are similar to that of ordinary steel reinforcement in chloride contaminated concrete i.e. there is a corrosion initiation stage followed by corrosion propagation. Recent study by D. Darwin et. al (2009) showed that the average critical chloride corrosion threshold of galvanized reinforcement is greater than the threshold for conventional steel and lower than the threshold for ASTM A1035 and 316LN steel. Hydrogen gas evolution did not increase the porosity of the concrete in the non-chromate treated bars relative to that observed for conventional reinforcement. The average time to corrosion initiation at crack locations in bridge decks for galvanized steel is 4.8 years, compared with 2.3 years for conventional steel, and 15 years for ASTM A1035 steel. 316LN stainless steel will not corrode.

Over the years, the ability of galvanized bars to provide corrosion resistance has not been uniformly positive. Probably because zinc is an amphoteric metal, that is, it corrodes in alkaline as well as acid environments. There have been cases in which galvanized bars have performed in a superior manner (McCrum and Arnold, 1993) and other cases in which they have performed ‘high w/c’ly (Manning et al. 1982; Pianca and Schell 2005). The use of chromate treatment also has negative implications because the hexavalent chromate salts that are used to passivate the zinc can cause health problems and are considered to be "potential occupational carcinogens" (NIOSH 2005).

2.4 Cathodic Protection of Steel Reinforcement in Concrete

It is indisputably acknowledged fact that the main cause for corrosion of steel reinforcement in concrete is the presence of chloride (ingress from some external source (s), such as de-icing salts, exposed to marine /coastal exposures etc.) in

concrete and the corrosion process is electrochemical. In an official policy statement issued in April 1982, R. A. Barnhart of Federal Highway Administration (FHWA) stated officially that 'the ONLY rehabilitation technique that has proven to STOP corrosion of steel reinforcement in chloride contaminated bridge decks regardless of chloride content' is Cathodic Protection (CP). Further, in a report to Congress in 1991, FHWA estimates show that up to US$ 50 billion in repair costs could be saved over the next 30 years by the use of cathodic protection (FWHA, 1992).

Nowadays, CP is not only applied to ever increasing number of aging structures already contaminated with chloride but also used 'pro-actively' for preventing structures (initially free of chloride) which are expected to be exposed to corrosion during their design life.

Recent estimate suggests that for the years 2010/2011 alone, globally more than 500,000 m^2 of reinforced concrete structures are protected by the application of cathodic protection as the main means to mitigate/stop on-going or future reinforcement corrosion (private communications with the CP industries). The breakdown of CP usage in different countries around the world is given in Table 2.1 below. The Table also shows that more and more new constructions (more than 45% of the total concrete surface) exposed to aggressive environments, particularly in the Middle-east countries, cathodic protection system is installed as a future corrosion prevention technique.

Table 2.1: Global Usage of Cathodic Protection of Reinforced Concrete Structures for 2010/2011 (private communications)

Country	Installed ICCP Systems for Concrete areas , m^2		ICCP Anode System (s)
	Existing structures	New constructions	
Saudi Arabia		150,000	MMO ribbon
UAE	20,000	50,000	MMO ribbon(for new construction), MMO ribbon, mesh and discrete anodes (for Rehabilitation)
Germany	40,000		MMO –ribbon, mesh, Discrete anodes
Austria	5,000		MMO –ribbon, mesh, Discrete anodes
Switzerland	5,000		MMO –ribbon, mesh, Discrete anodes
Benelux	30,000		MMO –ribbon, mesh, Discrete anodes
France	20,000		MMO –ribbon, mesh, Discrete anodes
USA	20,000		MMO –ribbon, mesh, Discrete anodes, paint, TS zinc anode
Canada	5,000		MMO –ribbon, mesh, Discrete anodes
UK	30,000		MMO –ribbon, mesh, Discrete anodes
Denmark	15,000	15,000	MMO –ribbon, mesh, Discrete anodes
Sweden	10,000		MMO –ribbon, mesh, Discrete anodes
Norway	10,000		MMO –ribbon, mesh, Discrete anodes
China (principally Hong Kong)	5,000		MMO –ribbon, mesh, Discrete anodes
Japan	30,000		MMO –ribbon, mesh, Discrete anodes
South Korea	1,000		MMO –ribbon, mesh, Discrete

			anodes
Australia	15,000		MMO –ribbon, mesh, Discrete anodes

The most critical component of any cathodic protection is the design of an effective 'anodes' system (s) to distribute 'protection current' efficiently and economically to the structural elements to be protected. Also, it must be easy to install and possess long term durability. Other components of the CP system are then fairly easily designed to suit the anode system ('groundbed'), the prevailing corrosion conditions and the environment.

Over the last 30+ years extensive research and field trials led to the developments of a number of anode systems, for both impressed current CP (ICCP) and sacrificial anode CP (SACP) systems. A review document prepared by Eltech Research Corporation for the National Research Council, Washington D. C. (1993) described in detail the advantages and limitations of various anode systems currently available and these anode systems are listed as below.

ICCP Anode Systems, which includes:

- Carbon based anode – which includes surface applied conductive coatings carbon fibres dispersed in cementitious overlay, conductive polymers, carbon based paste that is used as backfill around discrete anodes etc.
- Conductive ceramic anodes
- Activated titanium anodes: mesh, ribbon mesh, solid ribbon, discrete titanium – activated with mixed metal oxides (MMO)
- Thermally sprayed titanium
- Consumable ICCP Anodes: Thermally sprayed zinc (also aluminium alloys)

Galvanic Anode Systems which includes:

- Thermally sprayed zinc
- Thermally sprayed Aluminium-Zinc-Indium
- Mortar Encapsulated Zinc Anodes
- Pressure-sensitive 'Hydrogel' adhesive Zinc

The characteristic attributes of some of these anode systems are given in the Table 2.2 (Corrosion Prevention Association, Technical Note No. 12).

Table 2.2: Impressed current anode types and characteristics (CPA, 2008)

This table has been removed due to third party copyright. The unabridged version of the thesis can be viewed at the Lanchester Library, Coventry University

The inception of this investigation stems from the knowledge that historically Zinc Rich Paints (ZRP) is used as an effective anti-corrosion coating for steel exposed to corrosive environments but literature review identified no prior application of ZRP as anodes for CP system for reinforced concrete structures; however large number of published literature on CP systems (both as sacrificial and impressed current) with thermally Sprayed Metal coatings are available.

Cathodic protection systems using Thermally Sprayed (TS) metal coating, usually zinc as anode material (other anode materials include aluminium-zinc-indium (Al-Zn-In alloys), zinc-aluminium alloys of various compositions, and catalysed titanium) are gaining more and more popularity. TS zinc anodes is also used for impressed current systems. More than 0.2 million m^2 (2 million ft^2) of metallised anodes for Cathodic protection systems are in operation in North America (Costa,J. et.al, 2005). On the other hand, between 1995 (first trial) and 2009 thermally sprayed Al-Zn-In alloys anode system has been installed on more than 15 structures in the USA and Canada, with a total surface area of about 30,00 m^2 (300,000ft^2), (W. Young, et.al., 2009).

2.4.1 Cathodic protection- criteria

The basic theoretical concepts of cathodic protection criteria and the evolving practical criteria for steel in concrete are briefly discussed below.

2.4.1.1 Theoretical considerations

The effectiveness of cathodic protection can be assessed theoretically by criteria based on two different approaches, i.e.

a) Thermodynamics, e.g. potential criteria,

b) Kinetics, e.g. current density criteria

2.4.1.2 Thermodynamics - Potential Criteria

Consider the pH-potential diagram for iron in water as shown in Figures 2.1 – 2.2. after M. Pourbaix (1966). It is evident from these diagrams that metallic iron is thermodynamically stable below a certain potential, depending upon the pH of the electrolyte. These diagrams also show that if the potential of iron in the "corrosion zone" can be depressed far enough to bring the potential into the "immunity zone" then iron would not corrode.

2.4.2 Protection by Immunity

Thermodynamically, to achieve 100% cathodic protection of steel in concrete, the steel's passivity must be changed to immunity by an appropriate drop of the steel to concrete potential. The theoretical protection potential is a function of pH, as can be seen from the potential-pH diagram (Fig. 2.1) and can be calculated from the following equations:

For:	pH < 9.0	E = -0.62 V w.r.t. S.H.E. (2.12)	
	9.0 < pH < 13.7	E = -0.085 -0.059 pH V w.r.t. S.H.E.	(2.13)
	13.7 < pH	E = +0.320 -0.0886 pH V w.r.t. S.H.E.	(2.14)

These are the fundamental criteria for the complete cathodic protection which is often known as "protection by immunity".

2.4.2.1 Protection by Perfect Passivity

Marcel Pourbaix (1973) has demonstrated that steel in a high pH solution containing chloride ions may suffer highly localised corrosion; but this localised corrosion - pitting corrosion strongly depends upon electrode potential, pH and chloride concentration. Furthermore, for a given pH and chloride concentration, there is a unique potential, called pitting potential (Epitt) above which steel corrodes by pitting - this potential could be well above (more positive than) the potential of thermodynamic immunity. By depressing potential to a value below pitting potential, Epitt, adequate cathodic protection may be achieved and is called protection by perfect passivity.

2.4.2.2 Condition for Full Cathodic Protection

The electrochemical theory of corrosion defines that complete cathodic protection would be achieved if the cathodic reactions (electron consuming) are balanced by a supply of sufficient electrons from some source other than the metal to be protected. Corrosion theory also indicates that the corrosion can be stopped if the potential of cathodic areas are polarised to the open circuit potential of the most anodic area, by an external supply of current. The condition to achieve complete cathodic protection may be expressed as below (SC Das, 1984):

$$E_c + \Delta E_c + I_p r_c = E_a \qquad (2.15)$$

Where:

E_c = open circuit potential of cathodic area

ΔE_c = emf of polarisation at cathodic area

I_p = applied current

r_c = resistance of the cathodic path of current

E_a = open circuit potential of anodic area

At this steady state situation anodic current $I_a = 0$ and the total polarisation (due to C.P.) is given by:

$$E_{cp} = \Delta E_c + I_p r_c \qquad (2.16)$$

2.4.3 Kinetics - Current Density Criteria

2.4.3.1 Cathodic protection current requirement

Theoretically, the amount of cathodic protection current required to stop corrosion may be calculated if the rate of natural corrosion is known, which in turn depends on various factors, such as:

a) The extent of cathodic and anodic polarisation due to flow of corrosion current

b) Electrolyte resistance

Wagner, Carl (1952) defined that the minimum current required for complete cathodic protection must satisfy the condition that "the local electrode potential $E_{1(x)}$ of the metal to be protected must be more negative (less noble) at any point (x) than its equilibrium single electrode potential, $E_{1(eq)}$ in the given electrolyte", i.e.

$$E_{1(x)} < E_{1(eq)} \qquad (2.17)$$

Where:

$E_{1(x)}$ is synonymous with the polarised potential with the applied cathodic protection, i.e. E_{cp}

And: $E_{1(eq)}$ is synonymous with the open circuit potential of the anodic area, E_a.

This can be schematically represented by Evan's (polarisation) diagram as shown in Fig. 2.9.

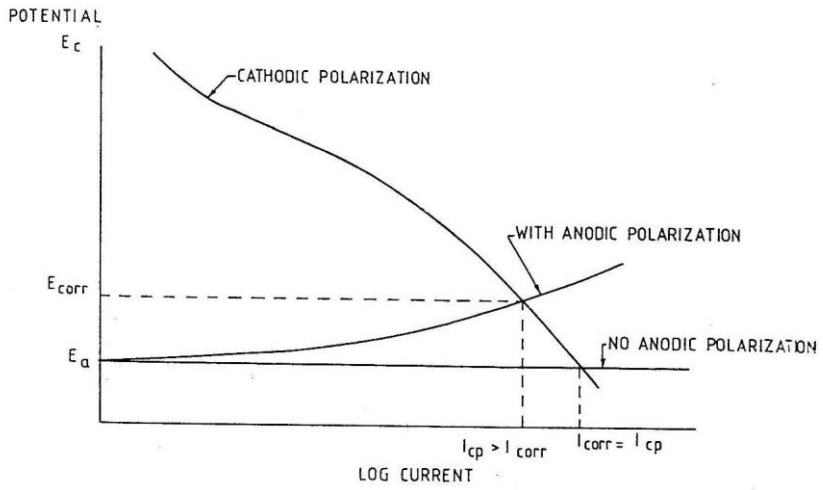

Figure 2.9: Polarisation Diagram showing The Effect of Anodic Polarisation on CP Current (I_{CP}) Requirements (S. C. Das, 1984).

The Figure 2.9 shows that when the metal is polarised slightly beyond the open circuit potential, E_a of the anode (more precisely the anodic area), the corrosion rate becomes zero, and the metal is said to be cathodically protected.

Wagner (1957) also states that "the minimum current for complete cathodic protection can be calculated readily if the geometry is such that the current density and the single electrode potential are the same at all points of the cathode".

If oxygen, dissolved in an electrolyte such as concrete, is the only oxidiser (i.e. cathodic reaction), the minimum current is equivalent to the diffusion rate of oxygen to the metal. Wagner (1952) then developed a set of mathematical expressions to define relationships between the current density J_{ox} necessary to reduce all the available and diffusing oxygen and the maximum variation of the local single electrode potential, ΔE_{max}, which must be greater than the difference E_{corr} (anodic area) E^*, where E^* is defined as the potential for the onset of significant hydrogen evolution by the applied cathodic protection current density.

The detailed discussion of the mathematical models proposed by Wagner is beyond the scope of this thesis. As an example, it is sufficient to cite the following expression for a situation where metal is to be protected by equidistant auxiliary anode:

$$\Delta E_{max} = \frac{J_{ox} c}{\pi \sigma} \ln \coth\left(\frac{\pi d}{c}\right) \qquad (2.18)$$

Where: ΔE_{max} = max difference of the local single electrode potential between different points

J_{ox} = the current density for oxygen reduction

σ = electrolyte conductivity

d = distance between auxiliary anode and metal to be protected

c = distance between adjacent anodes

Rearranging, the above, equation (2.15) can be expressed as:

$$J_{ox} = \frac{\Delta E_{max} \pi \sigma \ln \coth^{-1}\left(\frac{\pi d}{c}\right)}{c} = i_{cp} \qquad (2.19)$$

or

$$i_{cp} = \frac{\Delta E_{\max} \pi \ln \coth^{-1}(\pi d/c)}{cR} \qquad (2.20)$$

Where: R = electrolyte resistivity

Less rigorous mathematical models suggest that at steady state corrosion potential, E_{corr}, the free corrosion rate and the conditions for the complete cathodic protection may be expressed as below:

$$\mathbf{i_{corr} = i_a = i_c} \qquad (2.21)$$

Where: i_{corr} = corrosion current density

i_a and i_c= anodic and cathodic current density

And:

$$\mathbf{i_{corr} = \frac{E_a - E_c}{R_a + R_c}} \qquad (2.22)$$

Where: E_a, E_c = open circuit potential of anode, cathode

R_a, R_c = circuit resistance of all anodic and cathodic areas respectively

Corrosion will stop when $i_a = 0$ and the applied current density $i_{cp} = i_{corr}$, i.e.

$$i_a = 0 = \frac{E_a - E_c}{R_c + R_a} - \frac{i_{cp} R_c}{R_a + R_c} \qquad (2.23)$$

or

$$i_{cp} = \frac{E_a - E_c}{R_c} \qquad (2.24)$$

Theoretical analysis has shown that the free corrosion of steel in concrete is directly proportional to bulk concentration of oxygen, other factors remaining constant. The effect of variations in oxygen concentrations on free corrosion rate and hence the cathodic protection current requirements is diagrammatically presented in Figure 2.10.

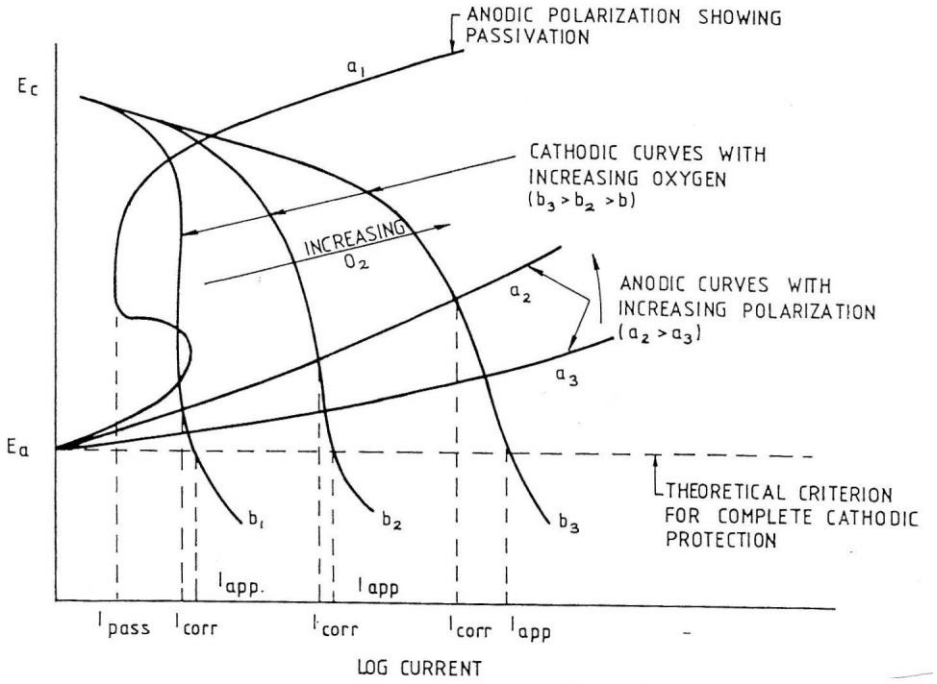

Fig. 2.10: Effect of Oxygen Concentration on I_{corr} = I_{cp} (Das, S. C., 1984)

Note: For the anodic polarisation curves 'a', as oxygen concentration increases so does the I_{corr} and I_{cp}.

This Figure 2.10 shows that the constant current approach to provide cathodic protection is not a technically sound criterion and the reinforcement may be either under or over protected depending on weather and season. During the potential criteria testing, Stratfull and other researchers (NACE, 1984) observed that within each criteria for cathodic protection, there was a considerable change in current density requirement.

However, the assessment or actual determination of the maximum current density requirements is a necessary design parameter.

It has also been pointed out that when the corrosion reaction is completely controlled by oxygen diffusion, the amount of current required to prevent corrosion would be equal to that producing free corrosion. This is only true, however, if no anodic polarisation occurs. In most cases some anodic polarisation will exist and in general the protective current will be greater than the freely corroding current.

2.5 Practical considerations

The theoretical criteria for complete cathodic protection are rather difficult to determine in practice. Therefore, various empirical criteria have evolved over the years in the field of cathodic protection engineering. Most of these criteria have been developed through laboratory experiments or have been empirically determined by evaluating data obtained from successfully operated cathodic protection systems. These are compiled and recommended in NACE, RPO 169-92 (1992) and BS EN ISO 12696 (2012) Standards. The standards, however, cautioned that no one criterion for evaluating the effectiveness of CP has proved to be satisfactory for all conditions and often a combination of criteria is needed for a single structure. The most common criteria are as below:

a) Structure to electrolyte potential more negative than -850 mV, when measured with CP current "ON".

b) Minimum negative voltage shift of 300 mV with current "ON".

c) Minimum negative polarisation voltage shift of 100 mV with current "OFF", to be determined by interrupting the CP current and measuring the polarisation decay.

d) E - log I curve. A structure to electrolyte voltage at least as negative as that originally established at the beginning of the Tafel segment of the E - log I curve.

e) A net protective current from the electrolyte into the structure as measured by an earth current technique applied to predetermined current discharge (anodic) point of the structure.

These practical protection criteria are now being globally accepted and form the basis of national and international Codes of Practice for assessing the effectiveness of the installed cathodic protection systems for buried and/or immersed steel structures.

The criterion for determining the efficiency of cathodic protection to steel in concrete, however, is not well defined. In 1981, a FHWA instigated research

programme looked into the effectiveness and applicability of CP criteria contained in NACE recommended practice for buried/immersed structures to steel in concrete. Although most researchers and practitioners agree that the polarised potential of steel in concrete should not exceed the hydrogen evolution potential (which is approximately -1083 mV CSE (CSE = copper/copper sulphate reference cell) in concrete with 12.5 pH in order to avoid any damaging effects due to cathodic interference, there are considerable arguments over the minimum potential (polarised) level for adequate protection.

More recently, a number of analytical works have been undertaken to establish the minimum criteria and a number of review papers published. The finding of the major works are summarised below:

a) Protection will be effective if the steel-to-concrete potential is polarised to a value somewhat more negative than that of iron in equilibrium with ferrous chloride. This covers a range of -710 to -810 mV CSE.

b) The shifting of structure potential to just sufficiently prevent current discharge would provide adequate cathodic protection. This condition should be satisfied if the polarised potential is more negative than about -400 mV CSE is achieved, since the normal or base potential of steel in concrete is usually in the range from -100 to -300 mV CSE. Recommended minimum values are -510 mV and -710 mV for passive and active steel respectively. However, in wet and high concentration of chloride in concrete, the potential of steel as much as -800 mV CSE was observed and in line with this the "-850 mV CSE" criteria has been extensively used.

c) A laboratory investigations by Vrable et.al (1979) found that the minimum potential (polarised) required to stop corrosion of steel in saturated $Ca(OH)_2$ solution containing chloride (simulating concrete environment), without generating significant amounts of hydrogen, was -770 mV CSE. The protection potential was also found to be related to pitting potential, which in turn depends upon the chloride concentration. The suggested potential criterion for adequate protection

should be such that the polarised potential of steel in concrete is more negative than the pitting potential. The relationship is given in Figure 2.11.

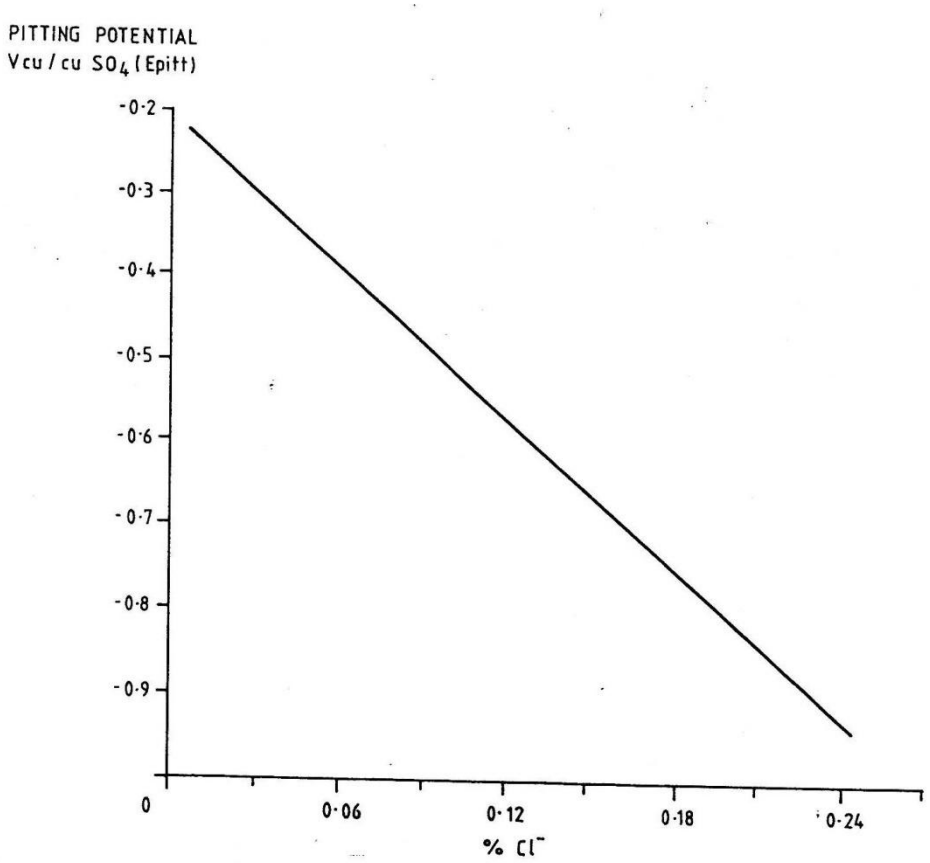

Fig. 2.11: Pitting Potential of Steel in Saturated Ca(OH) (pH=12.3 to 12.7) (Das, S.C. 1984)

d) Other criteria assessed as part of FHWA research programme were:

(i) E - log constant

(ii) Potential shift of 400 mV but without exceeding -1.10V at any location

(iii) "300 mV negative shift"

(iv) "100 mV negative shift"

The divergence in opinion is due to the fact that steel in concrete (unlike steel in soil or immersed in water) does not have an active or corroding potential all through the reinforcement but will have areas of passive or non-corroding potential resulting from the variable moisture content as the structure is exposed to atmosphere.

2.5.1 Standards and codes of practice – present situation

Presently, apart from NACE document RPO290-90 (1990) and BS EN 12696:2000 there is no other official national or international standard on this subject, As a consequence the NACE and BS EN documents are widely used by the industry. More recently, the International Organization for Standardization is in the process of producing an International Standard on Cathodic Protection of Steel in Concrete (ISO 12696- 2012), incorporating the existing standard EN BS 12696:2000 The criteria recommended in the NACE's RP and BS EN 12696:2000 documents are summarised below.

a) Potential shift: a minimum polarisation value obtained during depolarisation tests for a given period.

b) '100 mV potential Decay'

c) Statistical method: a statistical comparison of base potential and polarised potential.

d) The E-log I method: The level of protection determined from an E-log I test.

'100 mV potential decay' with some acceptable variations is the most widely used criterion adopted by the CP specialists worldwide as recommended in BS EN and NACE standards. . This '100 mV decay' is considered to be not always achievable and/or appropriate for some CP anode systems, particularly for the CP design based on sacrificial anode systems and also for thermally sprayed (TS) zinc systems, operating in sacrificial or impressed current mode (Covino et.al, March 2002).

Further difficulty to apply '100 mV decay' criterion for a sacrificial system is that the anodes are normally connected directly to the reinforcement. In view of this CP engineers and researchers are actively perusing and proposing alternative criteria for the assessment of performance and effectiveness of both the sacrificial and impressed current CP system utilizing sacrificial anodes. The statistical method has certain merits and can be theoretically justified in terms of closeness to

Wagner's mathematical models, i.e. the theory predicts that if $i_{corr} = I_{cp,}$ then corrosion will stop and this happens when $E_a = E_c$. Based on theoretical and practical considerations embracing both the 'statistical' and 'depolarisation' criteria, a criterion, called 'CP Index', proposed by Das (S. Das, 1988) which is defined as

$$K_{cp} = (Voff - Vbase)/S \qquad (2.25)$$

Where:

K_{cp} = CP index (a measure to determine the effectiveness of the level of protection).

$Voff$ = the instant off potentials, measured at monitoring points immediately after temporarily switching off the applied power.

$Vbase$ = the potentials measured during commissioning prior to energizing the CP system.

S = the standard deviation of all potentials measured during the initial potential survey and/or the potentials measured prior to energizing the CP system.

The concept of CP Index as a criterion has been further refined by incorporating Wagner's mathematical expressions relating to the maximum polarization, ΔE_{max} , and the minimum density for complete Cathodic protection.

Covino et. al (Covino et.al, March 2002) proposed Performance criteria for TS zinc anode in ICCP mode to be determined and quantified by the CP circuit resistance (CR) and the anode electrochemical age (EA). Anode electrochemical age at time t is defined as the cumulative charge passed across the anode per unit area over the life of the anode and is given by

$$EA(t) = \int J(t)dt \ (coulombs/m^2) \qquad (2.26)$$

Where:

J(t) = CP current density (A/m^2)

t = the time in seconds

The product J(t)*dt is integrated from the beginning to time t.

CP circuit resistance at time t is simply the quotient of voltage, V(t) (volts), between the steel cathode and the Zn anode and the CP current density, J, as expressed as:

$$CR(t) = V(t)/ J(t) \quad (ohms\text{-}m^2) \qquad (2.27)$$

Covino, et al. (Covino et.al, March 2002) also proposed that service life of the thermal sprayed (TS) Zinc anode can be determined by at least three criteria:

1. time for the anode to be consumed
2. Time for bond strength to reach zero; or
3. Time for circuit resistance to reach a level where operating voltages are too high.

2.6 Cathodic protection anodes for RC structures

The most important element of any successful cathodic protection system is the design of an effective anode system to distribute the necessary protection current economically and efficiently to the reinforcement. Also, it must be easy to install and possess long term durability. Other components (e.g. power supply/monitoring equipment etc.) of the CP system can then be selected to suit the anode system, the prevailing corrosion conditions and the environment.

Over the last 30 years there have been considerable advances and development in anode materials and anode system design with real possibility of 'pick N mix' cathodic protection system(s) for above ground RC structures

Conductive coating anodes include a variety of formulations of carbon pigmented solvent or water dispersed coatings, and thermal sprayed zinc. Recently, thermal sprayed titanium has been used experimentally, with a catalysing agent spray applied onto the titanium coating.

Mixed metal oxide coated titanium mesh or grid anode systems are fixed to the surface of the concrete and overlaid with a cementitious overlay which can be poured or pumped into shutters or sprayed.

Discrete anodes are usually installed in purpose cut holes or slots in the concrete. They are either:

- Rods of coated titanium in a carbonaceous backfill;
- Mixed metal oxide coated tubes;
- Strips and ribbon;
- Conductive ceramic tubes in cementitious grout.

Another recent development is the 'Discrete' Zinc Sacrificial Anode System. This is a proprietary zinc sacrificial anode unit embedded within a specifically formulated cementitious mortar and is currently available commercially. The main application of this anode system is for localised protection of steel reinforcement within chloride contaminated concrete by maintaining galvanic protection in areas adjacent to the 'conventional patch repaired' areas and thereby prevents the formation of incipient anodes in neighbouring areas following anti-corrosion treatment and concrete repair to damaged areas.

This anode system is discretely placed within the patch repairs at maximum 750mm centres. The electrical connections are achieved by attaching the wire ties, integral to the anode system tightly to steel reinforcement; and then the areas are instated using appropriate repair mortar.

Not all of the anode systems, mentioned above proved effective or successful or suitable for any types of structural elements. The selection of most suitable anode system(s) would depend on the corrosion morphologies and the structural geometry.

2.7 Zinc Rich Paint as anode for CP (sacrificial or impressed current) of RC Structures.

Literature search revealed no successful prior application of zinc rich paint (ZRP) to provide cathodic protection of RC structures, although a reference of some attempt by one specific ZRP manufacturer, on trial basis, were made but proved unsuccessful due apparently high concrete resistivity (Gjorv O.E., 1977). However, more recently, there have been successful experiences with the anode design

based on utilizing a commercially available zinc rich paint product as a sacrificial / impressed current anode material (S. C. Das, unpublished data).

2.7.1 Zinc Rich Paints

Zinc rich paints (ZRP) are widely used as an alternative to 'hot deep galvanising (HDG)', as an 'under coat' or as a 'top coat' and also as a 'touch-up coat' on galvanised steel to provide corrosion protection of steel in moderately severe environments and corrosive marine atmospheric environments. It is often quoted as 'Cold Galvanising'. Detailed chemistry any formulation of ZRP is outside the scope of present investigation.

Zinc-rich paints must contain either between 65% to 69% metallic zinc by weight or greater than 92% metallic zinc by weight in dry film. Paints containing zinc dust are classified as organic or inorganic, depending on the binder they contain. Inorganic binders are particularly suitable for paints applied in touch-up applications around and over undamaged hot-dip.

2.7.2 Selection of Zinc Rich Paint

Review of commercially available ZRP has identified one proprietary product (namely 'Zinga') as the most promising candidate material for this research. Detailed technical description of this product is given in Appendix E and briefly highlighted as below.

- ZINGA is a single-pack compound containing 99.995% purity electrolytic zinc dust mixed in synthetic resins, pigments and aromatic solvents.
- It is easy to apply by brush, roller, spraying or dipping under any atmospheric condition.
- A dry ZINGA layer consists of 96% zinc, pure to 99.995% and homogeneously dispersed throughout the layer.

- The product is non toxic, hence is safe to use. This is due the fact that it contains high purity zinc with no lead or cadmium present. The product does not contain toluene, xylene or methyl ethyl ketones (MEKs).
- On application it cures to a minimum of 96% zinc content in the dry film. There is no barrier or interface between coatings i.e. every coat merges perfectly with previous coats and therefore can be topped up time and again.

- On the steel surface the coverage is approximately 4 - 5 square metres at 30 - 40 microns.
- Coating has indefinite shelf life.
- Coating can be applied in moist or wet conditions.

Throughout this investigations, the performance of this ZRP coating is compared and contrasted with that of other types of conductive coatings / paints or overlay systems used for CP system designs for reinforced concrete structures, particularly, the adhesion strength and other physicochemical/electrochemical characteristic properties that are essential for any anode material to provide effective and efficient at the same time long life cathodic protection.

CHAPTER 3: EXPERIMENTAL DESIGN: THE PERFORMANCE OF ZINC RICH PAINTS AS ICCP ANODE SYSTEM

In this chapter a comprehensive programme of experiments developed to assess and compare the performance and suitability of the selected Zinc Rich Paint (ZRP) as an anode (groundbed) for the Impressed Current Cathodic Protection (ICCP) system for Reinforced Concrete structures are described in detail.

3.1 Research Plan for Investigations

The specific objective of this part of research is to:
Evaluate the performance of zinc rich paints as Anode System for Cathodic Protection (CP) of Reinforced Concrete Structures.

The programme of work for the above objective was based on assessing the three principal properties required from the conductive materials i. e. Physical – such as application and adhesion, Electronic and Electrochemical. These properties when considered together define the ability of the materials to act as anode.

In parallel with the experimental work, the performance of zinc paint anode system was evaluated by application to real-life structure and is described in Chapter 4.

The project was progressed in the following manner:

Subsequent to an initial selection of material, as per manufacturers' specifications, samples were put through a set of 'screening' tests and then subjected to a full programme of experiments to assess and compare the three principal properties.

Although these experiments were highly interrelated they can be generally divided into: -

1) Experiments oriented towards physical (such as ‘bond strength to concrete substrate) and electrical property (such as cross-film resistance) testing;

2) Experiments oriented towards electrochemical property testing (such as polarisation characteristics, current throwability, current carrying capacity etc.); and

3) Experiments oriented towards environmental durability testing with or without CP curren.

Each part of the experimental works together with the results and discussion are described independently. It is expected that this methodology will help the reader

to appreciate the progression of the work, which involved an integration of many concepts of corrosion science/principles of steel in concrete and the corrosion mitigation technology.

The programme of work together with results and discussion is given below.

3.2 Initial Property Testing

The initial property tests were designed on a 'spot check' basis to establish the possible suitability of the coating material to work as a cathodic protection anode ('groundbed') material. This was required prior to the further in-depth investigations as the material was not originally designed for this application. These preliminary tests were therefore confined to three easily assessable but essential properties, i.e.

1) Physical properties (i.e. application and adhesion, including environmental)
2) Electrical (electronic) properties
3) Electrochemical properties

3.2.1 Assessment of Physical Properties

The purpose of this experimental investigation was to assess the durability aspect (i.e. bond strength) of ZRP coated to concrete substrates. This was achieved through the completion of a number of objectives such as the pull-off test behaviour between two concrete mix designs, under the influence of different factors, like:

1. Short to medium term pull-off bond behaviour between ZRP and concrete substrates (prepared to variable roughness) under the influence of different environmental conditions and natural ageing (without impressed current/galvanic protection)

2. Whether the amount of compaction and the type of mould has any influence upon the obtained pull-off stress values, the type and degree of pull-off fracture observed to concrete coated substrates prepared using a wire brush for:

- Immediately coating and pull-off tested cubes

- Cubes coated and left for 56 days in different environmental conditions

3.2.2 Ease of Application

The concrete specimens were coated using brush applications with generally a 1" brush. It was noted that zinc paint could be applied with relative ease and coating became 'touch-dry' in 1-2 hours.

3.2.3 Adhesion to the Concrete Substrate

Subsequent to the application test, adhesion testing of the coating was undertaken as described below:-

3.2.4 Test Procedure

Detailed experimental test procedures, including concrete mix design, compaction and curing processes, surface preparations, application of ZRP, pull-off (adhesion) test equipment and testing are described in Appendix 'A'; and these are briefly summarised below.

Two types of concrete specimens with two different qualities, representing low water/cement ratio of 0.50 (G) and 'high' water/cement ratio of 0.80 (P) quality concrete were cast; the specimens were 150 x 150 x 150mm ('cube samples').

For adhesion strength (Pull-off tests) determination the concrete surfaces of the 'cube samples' were prepared to remove the cement laitance layer, prior to applying ZRP coatings, and creating three different surface profile defined as (i) very high roughness (VHR, where most of the aggregates were exposed), (ii) high roughness (HR, where some aggregates were exposed) and (iii) medium roughness (MR, where little or no aggregates were exposed). The VHR and HR were obtained with automatic Needle Gun operated with compressed air and the MR profile was achieved by manual wire brushing. The prepared concrete substrates were coated with the ZRP. A total of 4 coats were applied by brush to

achieve a dry film thickness (DFT) of approximately 200-350um. Each coat of paint was applied after allowing the previous coat to dry. The ‘wet’ and ‘dry’ mass of paint was measured after each application of the paint and finally the total mass of dry paint (of a number of coats) was measured to determine the total DFT. The adhesion strength of the ZRP was then determined; first immediately (within 24 hours after the final coat was allowed to dry) and also after allowing the dry paint film to ‘age’ for 54 days. The adhesion strength was determined using an ‘Adhesion Tester, Elcometer 106/6, all in accordance with the procedure recommended in CIRIA (1993) and ELCOMETER (2004).

The tests were conducted as below:

i) High strength aluminium alloy "dollies" (20mm diameter) were bonded onto the test surface by means of an epoxy resin adhesive; and then the adhesive was allowed to cure.

ii) After curing of the resin the Adhesion Tester was placed in position, the "dragging" indicator set to zero and the hand wheel tightened until the pulling force to the dolly caused the break away from the surface.

iii) The pull-off force was then read off the instrument dial, and results converted to bond strength in MPa.

3.3 Results and Discussion

A number of parameters that are considered to affect the adhesion of ZRP on concrete have been investigated, which includes testing carried out for the different concrete qualities, surface preparations (different surface profiles) and concrete ’aging’, with and without the application of impressed CP current. The results of the adhesion (bond) strength are presented in Tables and Figures; and are discussed in detail as below.

Concrete Surface Preparation

Figure 3.1 shows an observational comparison of the varying degrees of surface preparation to ‘low w/c’ and ‘high w/c’ concrete substrates as shown diagrammatically on the left and right respectively.

Observational Comparison: Degree of Aggregate Exposure & Undulations

Based on visual observation and assessment, all concrete substrates prepared to a Very High Roughness (VHR) degree, such as those shown in Figures 3.1(a) and 3.1(b), showed a greater amount of exposed aggregates as well as high undulations compared to other surface preparations like High (HR) and Medium (MR) Roughness. Since a High Roughness (HR) profile was obtained using the same tool for VHR substrates, care and judgment was required not to overly expose or expose a small amount of aggregates. It can be seen from Figures 3.1(c) and 3.1(d) that this substrate roughness achieves an immediate level between VHR and MR profiles in terms of aggregate exposure where Figures 3.1(e) and 3.1(f) for MR profiles exposes a smaller amount of aggregates. With regards to undulations in the surface profile for HR substrates it was hard to quantify by eye exactly which profile i.e. VHR or HR gave a higher undulating (peak to trough) surface. But from the observational experience gathered by the author the undulations were somewhat similar for both VHR and HR profiles with either profile being capable of having a greater amount of undulations. The peak to trough profile, i.e. the amplitude height, for MR profiles were observed to be lesser than for VHR or HR profiles mainly because of the use of a manual operated wire brush tool which essential scrapes the surface and removes the laitance layer. A manual operated wire brush or even a mechanical one does not produce a similar vertical impact like that of a needle gun operated by compressed air. The use of a wire brush in preparing a concrete surface is believed to be similar to a medium sand paper type texture using a sand blasting technique. However, sand blasting like needle gunning relies upon impact to yield concrete roughness. As can be seen in Figures 3.1(e) and 3.1(f) the concrete substrates show a minimum amount of exposed aggregates as opposed to VHR and HR profiles.

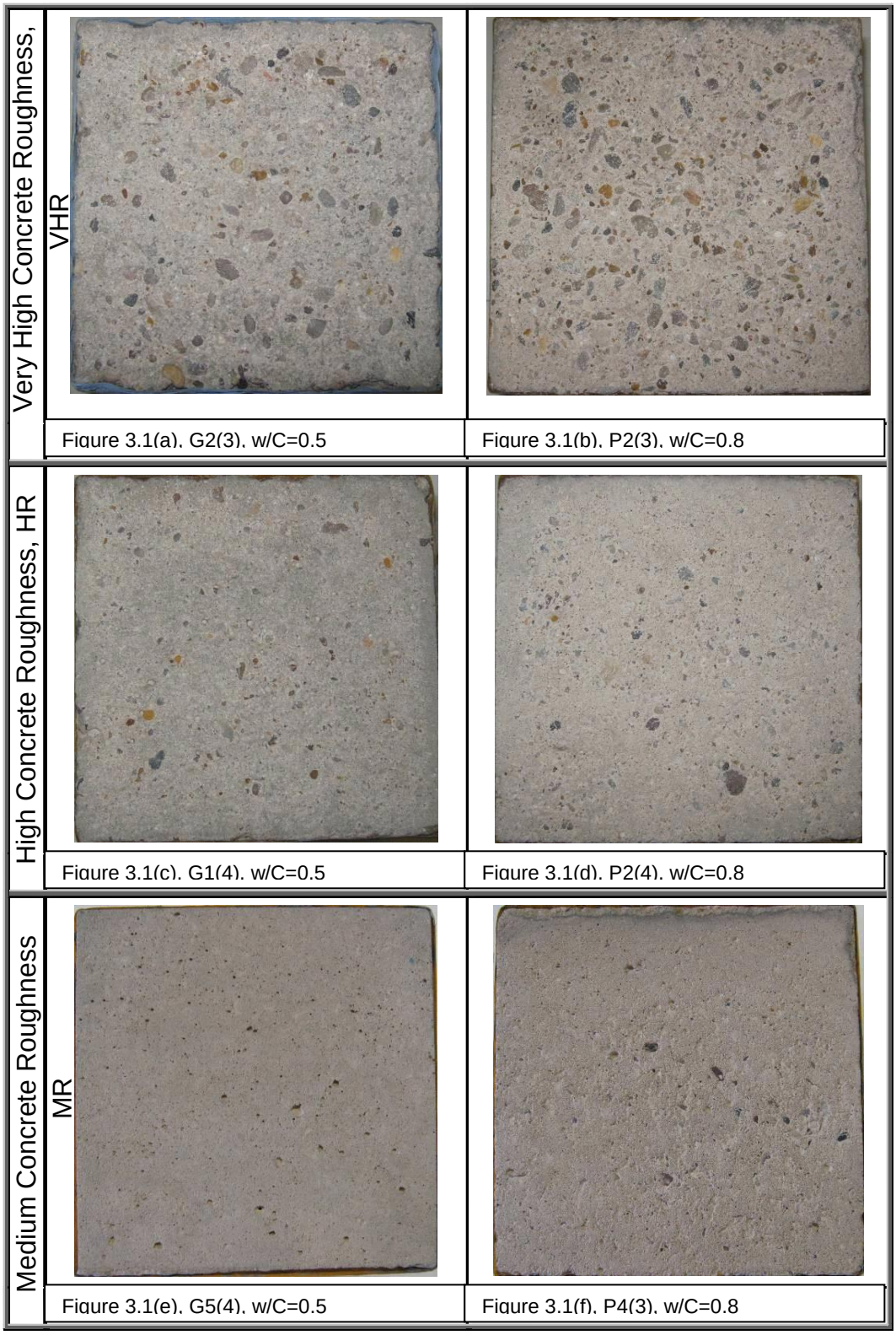

Figure 3.1: Observational comparison of different surface preparation to 'low w/c' concrete (left) and 'high w/c' concrete (right)

Observational Comparison: Presence of Blow Holes

Depending upon the compaction technique of concrete, blow holes can become uncovered on the concrete near to the surface, as a result of roughening the surface with a wire brush. Blow holes were not seen when utilizing a needle gun. Blow hole widths were observed to be up to a few millimetres wide but not greater than approximately 5 millimetres.

Physical Labour Comparison: Time & Effort to Prepare Substrates

Greater time and effort was required in preparing the surface for 'low w/c' concrete substrates than for 'high w/c' concrete substrates, for all grades of roughness. This is primarily due to the high compressive strength as a result of low w/c ratio and high cement content of a concrete mix design. Hence, aggregates were easier to expose for 'high w/c' concrete substrates than it was for 'low w/c' concrete mix designs.

Coating & Pull-Off Testing Time Schedule to Concrete Cubes & Slabs

Table 3.1 shows the dates when cubes and slabs were cast, the number of days within the curing tank and the amount of accumulated days (since cube/slab was cast) to the point of being zinc coated and pull-off tested respectively.

Table 3.1 coating & pull-off testing time schedule to concrete cubes & slabs since cast

Specimen	***Date cast***	***No. of days in curing tank***	***Immediately coated & pull-off tested cubes (days since cast)***	***56 day coated & pull-off tested cubes (days since cast)***
G1 to G3	06/03/10	28	106 - 113	162 - 169
G4 to G7	25/02/10	28	118 - 125	184 - 191
P1 to P3	13/03/10	28	106 - 113	162 - 169
P4 to P5	26/02/10	28	118 - 125	184 - 191
Slab G1 & G2	06/03/10	28	137 - 144 (coated but not tested)	
Slab P3	13/03/10	28		

Immediately Coated & Pull-Off Tested Substrates

Figures 3.2 and 3.3 show the observed pull-off failure mode to different surface preparations (as discussed above) to 'low w/c' and 'high w/c' concretes looking at the substrate end as well as looking at the dolly end respectively.

Terminology Adopted to Observed Pull-Off Failure Types

The terminology adopted to observed pull-off failure types during experimentation is described below and is very much similar to criteria given in BS EN ISO 4624 (BSI, 2003).

- A = failure occurring within concrete substrate
- A/B = failure between concrete substrate and coating
- B/C = inter-coat failure
- -/Y = failure between adhesive and coating

Observational & Numerical Comparison: Pull-Off Test Results

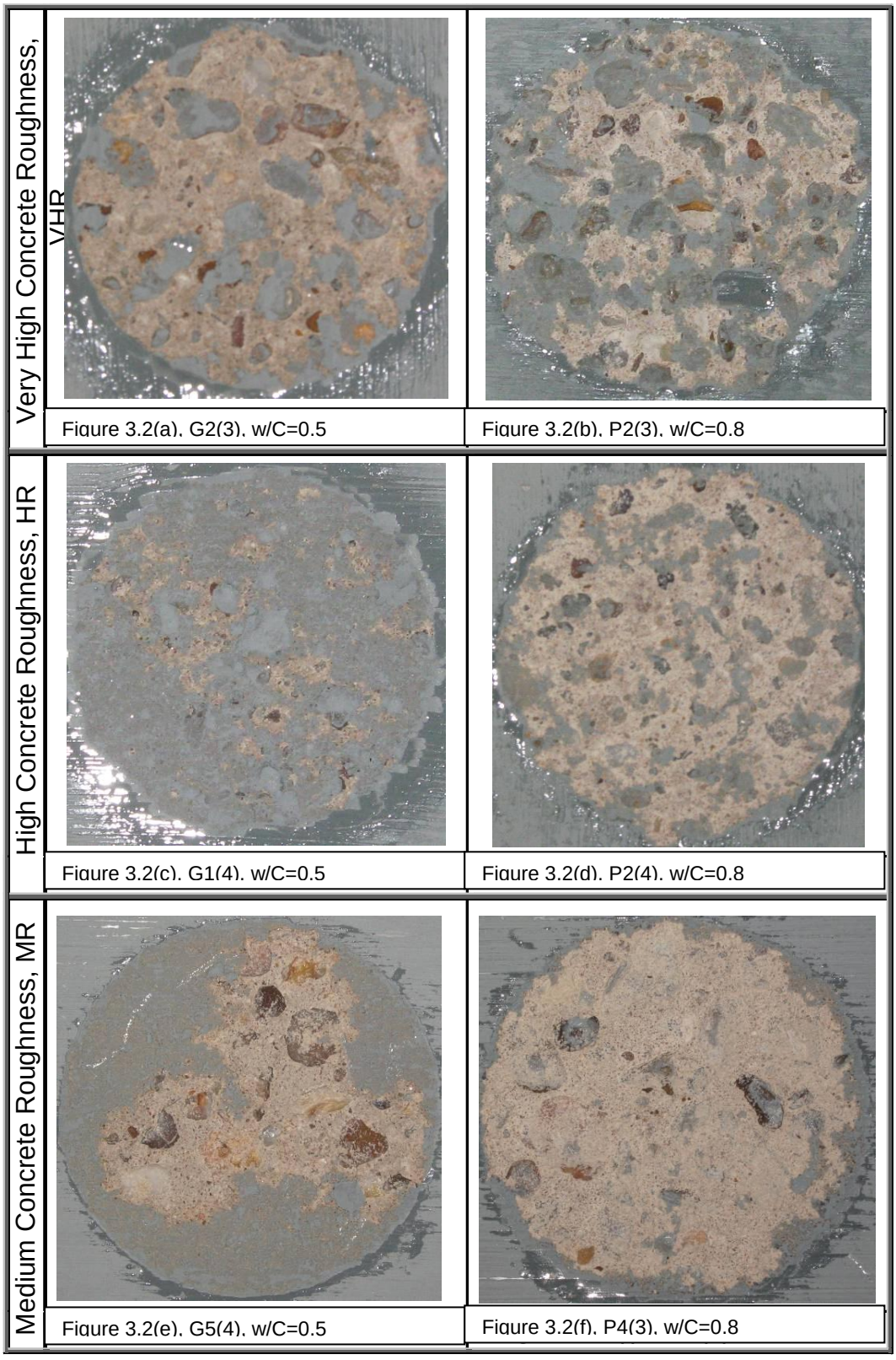

Figure 3.2: Observational pull-off failure comparisons of different surface preparation to 'low w/c' concrete (left) and 'high w/c' concrete (right) looking at substrate end

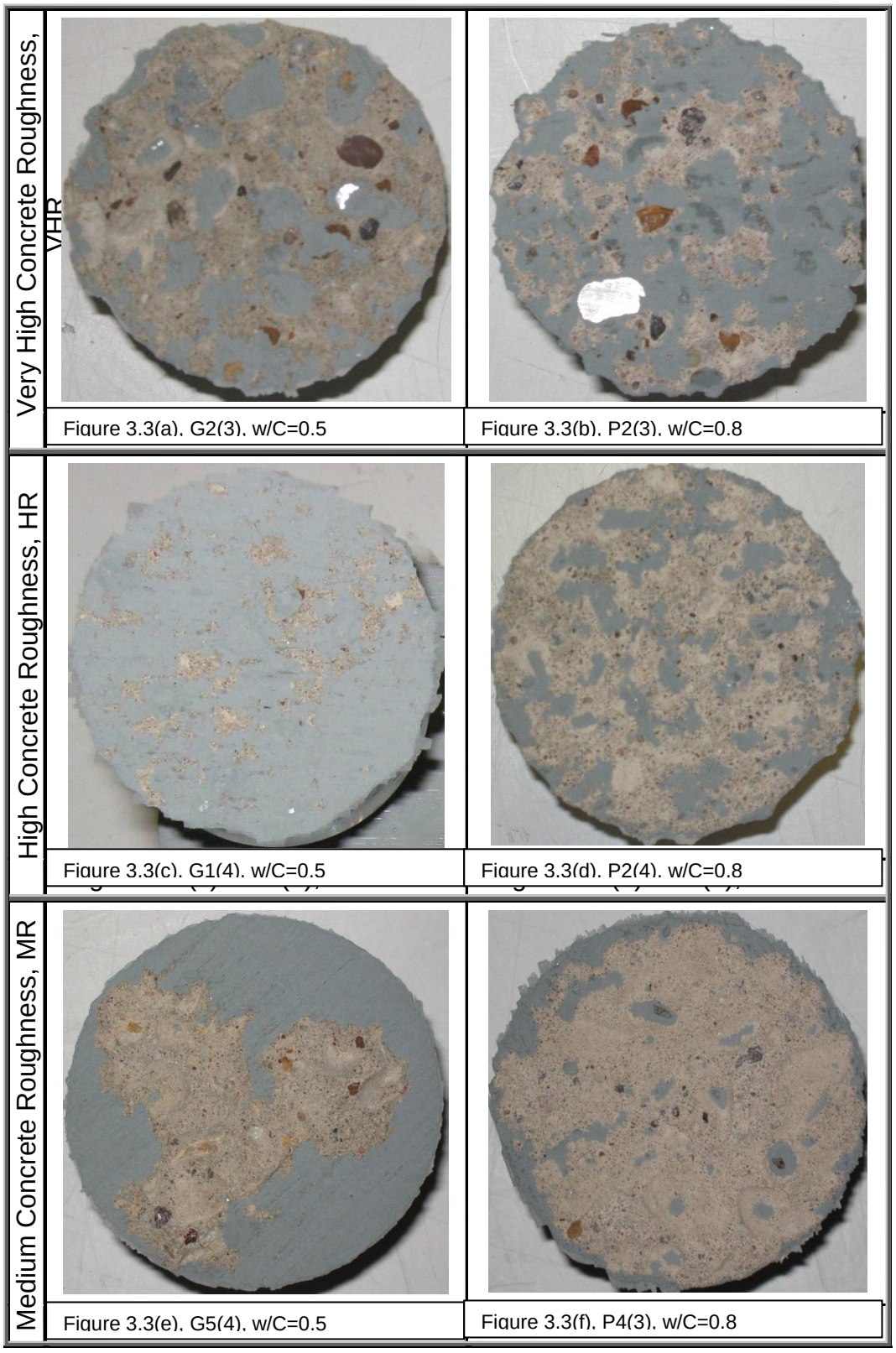

Figure 3.3: Observational pull-off failure comparisons of different surface preparation to 'low w/c' concrete (left) and 'high w/c' concrete (right) looking at dolly end

Pull-off results given in Table 3.2 as well as graphically illustrated in Figure 3.4 show, on average, a medium surface roughness (MR) yields a greater bond between the coating and the substrate compared to VHR and HR results for both ‘low w/c’ and ‘high w/c’ concrete mix designs. This is because of the minimal or, in some cases, the null amount of aggregates exposed in the immediate dolly testing position. As discussed in Section 2.4.11.1 (case study) the amount of aggregates exposed has a direct influence upon the pull-off strength since the bond interface between the coating and the exposed aggregate(s) is weakened due to the inherent smooth surface of the aggregate(s) used in this experiment.

As observed in Figures 3.3(e) and 3.3(f) the amount of concrete depth seen on the dolly end of the failure was greater for MR substrate types than it was for VHR or HR substrate types again as a result of the amount of aggregates being exposed which has an influence on the coatings ability to adhere/anchor itself to suitable locations. Where Zinga was able to find suitable anchor positions pull-off strengths were enhanced and failures showed, as a result, a greater depth of concrete on the dolly end.

Table 3.2: Pull-off tested results (shortly after coating, 1-2 hrs) to 'low w/c (G)' and 'high w/c (P)' dry concrete substrates prepared to different roughness

Variables	$T_{env.}$ (°C)	RH_{env} (%)	$T_{substrate}$ (°C)	DFT (µm)	σ (MPa)	σ_{av} (MPa)	Failure Type*	Area of Fracture (%)
G1.VHR(3)	22.5±1.0	45.5±2.5	23.0±0.25	328	1.75±0.05	1.90	A, B/C, -/Y	A = 70, B/C = 25, -/Y = 5
G2.VHR(3)			23.0±0.25	328	1.95±0.05		A, B/C	A = 75, B/C = 25
G3.VHR(3)			23.5±0.25	343	2.00±0.05		A, B/C, -/Y	A = 70, B/C = 25, -/Y = 5
P1.VHR(3)	24.0±0.5	47.0±3.0	21.0±0.25	299	1.00±0.05	1.13	A, B/C	A = 75, B/C = 25
P2.VHR(3)			22.5±0.25	290	1.00±0.05		A, B/C, A/B, -/Y	A = 60, B/C = 35, A/B & -/Y = 5
P3.VHR(3)			24.5±0.25	304	1.40±0.05		A, B/C, A/B	A = 65, B/C = 30, A/B = 5
G1.HR(4)	23.5±0.5	39.5±1.5	30.0±0.25	391	1.70±0.05	1.65	A, B/C	A = 20, B/C = 80
G2.HR(4)			27.0±0.25	309	1.40±0.05		A, B/C	A = 65, B/C = 35
G3.HR(4)			24.0±0.25	323	1.85±0.05		A, B/C, A/B	A = 60, B/C = 35, A/B = 5
P1.HR(4)	23.5±1.0	46.0±1.0	19.5±0.25	266	0.75±0.05	1.18	A, B/C	A = 75, B/C = 25
P2.HR(4)			19.5±0.25	261	1.30±0.05		A, B/C	A = 80, B/C = 20
P3.HR(4)			19.0±0.25	251	1.50±0.05		A, B/C, A/B	A = 80, B/C = 15, A/B = 5
G4.MR(3)	23.5±0.5	50.5±2.5	24.0±0.25	319	3.40±0.05	2.92	A, B/C	A = 45, B/C = 55
G5.MR(4)	22.5±1.5	35.5±4.5	24.0±0.25	314	3.15±0.05		A, B/C	A = 40, B/C = 60
G6.MR(4)	22.5±1.5	35.5±4.5	24.5±0.25	319	3.50±0.05		A, B/C	A = 40, B/C = 60
G7.MR(1)	23.5±0.5	46.5±7.0	24.0±0.25	304	2.40±0.05		A, B/C	A = 5, B/C = 95
P4.MR(3)	23.5±0.5	50.5±2.5	24.0±0.25	328	2.55±0.05	1.78	A, B/C	A = 95, B/C = 5
P5.MR(1)	22.0±2.0	42.0±2.0	23.0±0.25	305	1.40±0.05		B/C, A/B, -/Y	B/C = 85, A/B = 10, -/Y = 5
P5.MR(2)	22.0±1.0	42.0±3.0	24.5±0.25	319	1.35±0.05		A, B/C, A/B	A = 10, B/C = 80, A/B = 10

KEY: $T_{env.}$ (°C) = environmental temperature, RH_{env} (%) = environmental relative humidity, $T_{substrate}$ (°C) = substrate temperature, DFT (µm) = dry film thickness, σ_{av} (MPa) = average pull-off stress, VHR & HR & MR = very high and high and medium roughnesses respectively . * For the definition of terminology see page 59.

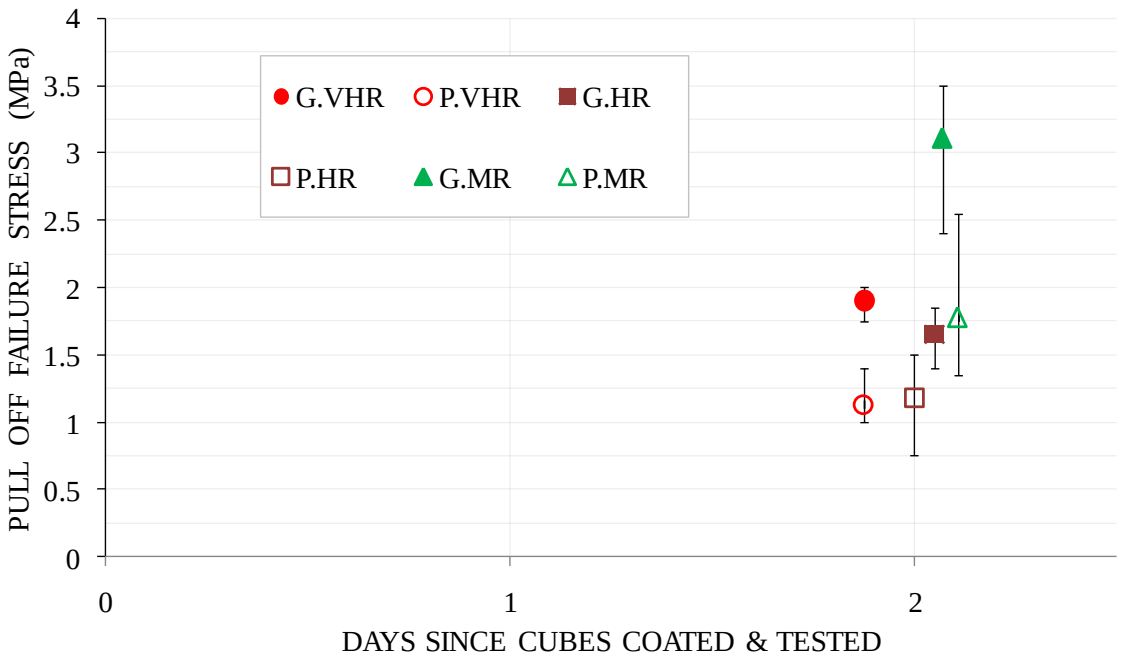

Figure 3.4: Comparison between variable types of substrate roughness when immediately coated and pull-off tested

Note: for each roughness profile shown in Figure 3.4 the data point illustrates the average pull-off stress and the corresponding highs and lows (precisely known as error bars) are the upper and lower range in pull-off values observed respectively. Where G & P = 'low w/c' and 'high w/c' concretes respectively. VHR & HR & MR = very high and high and medium roughness respectively.

Observational & Numerical Comparison: Variations in Pull-Off Failures

However, there were instances, as shown in Figure 3.5 when a variation in pull-off failures was observed to MR substrates for both 'low w/c' and 'high w/c' concrete mix designs. This variation was found to have an impact upon not only the failure type or area of fracture but also the failure stress. For example the range in failure results for VHR profiles was 0.25MPa for 'low w/c' mixes and 0.40MPa for 'high w/c' mixes. Also, the range in failure results for HR profiles was 0.45MPa for 'low w/c' mixes and 0.75MPa for 'high w/c' mixes as seen in Table 3.2 and graphically in Figure 3.4. Whereas for MR substrates the range in failure results was 1.10MPa for 'low w/c' mixes and 1.20MPa for 'high w/c' mixes which is higher than that of VHR and HR profiles.

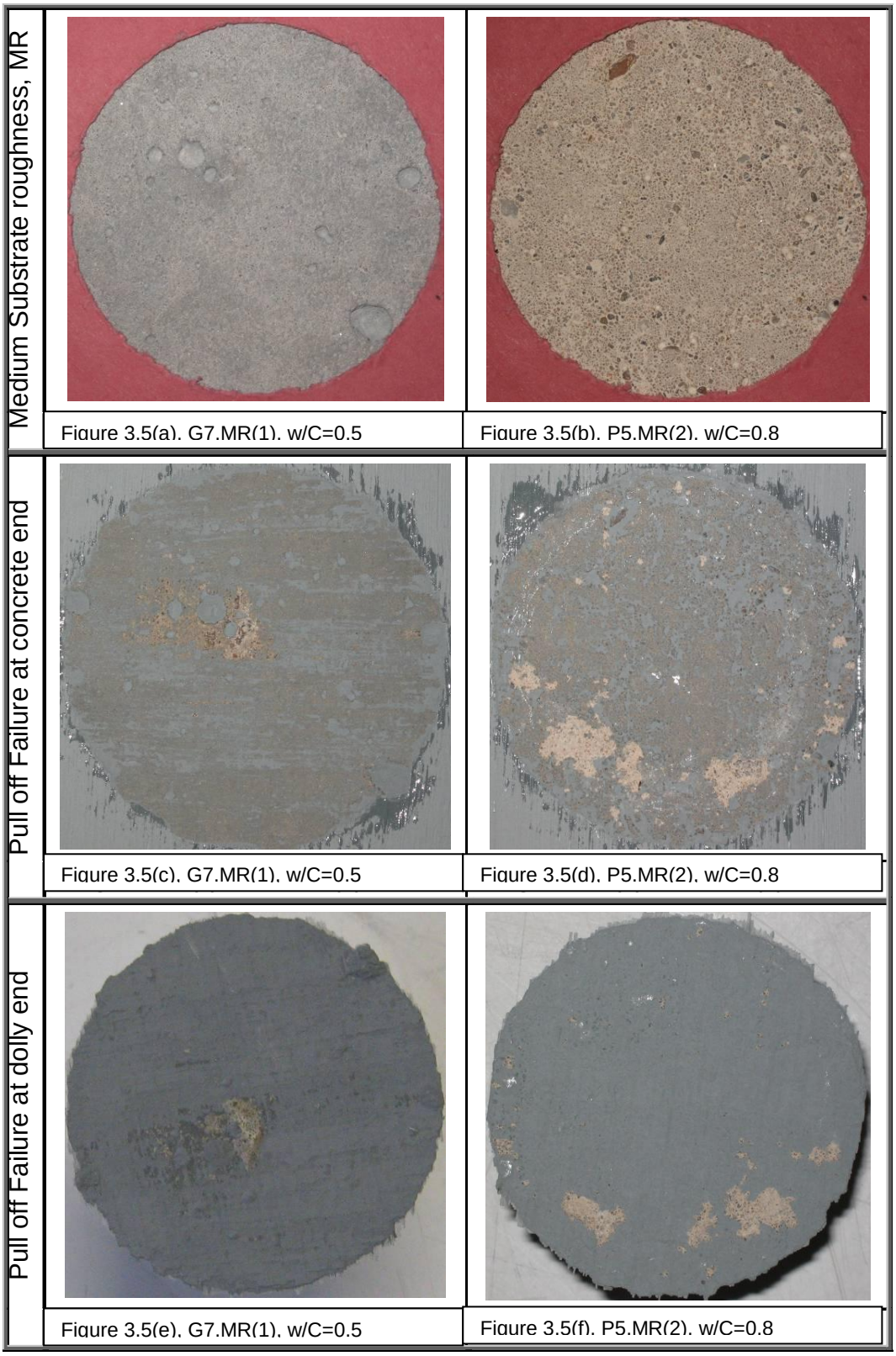

Figure 3.5 variation in observed pull-off failures when producing a medium surface roughness, using a wire brush, to 'low w/c' concrete (left) and 'high w/c' concrete (right)

Factors Influencing Variation in Pull-Off Failures to MR Profiles

Generally speaking, with regards to MR profiles, when a certain amount of concrete was pulled off with the dolly the failure stress was always found to be a higher value. Typical examples are G4(3), G5(4), G6(4) and P4(3) for MR profiles as shown in Table 3.2. However, when pull-off failures illustrate an almost 100 %, or close to 100%, inter-coat type failure (B/C) then a number of factors may play a part in deciding whether the failure stress will be either at the high end or the low end of the range. The possible factors, in the opinion of the author, for a given w/c ratio and cement content are the (i) degree of concrete roughness, (ii) blow hole(s) size and extent, (iii) aggregate type and size, (iv) amount of aggregates exposed, (v) amount and type of compaction during concreting, (vi) undulations in coating/substrate surface, (vii) amount of epoxy resin used (viii) surface carbonation.

For example Figure 3.5(a, c & e) sample G7(1) gave a stress value of 2.40MPa and Figure 3.5(b, d & f) sample P5(2) gave a stress value of 1.35MPa. This is believed to be caused, primarily, by the inability of the coating to adequately bind or adhere to the substrate as a result of inappropriate level of roughness.

Influence of Compaction to the Variation in Pull-Off Failures to MR Profiles

During the compaction process, conducted to initial trial experiments, it was observed that if the mode of the vibrating table was altered to shock table (≈ 8g) an excessive amount of, watery looking, cement paste would run up the vertical sides of the mould and eventually spill out. This would suggest at this level of vibration the effect of compaction would be felt more to the vertical sides of the concrete sample than other horizontal faces. Possibly resulting in a thicker laitance layer to the vertical concrete cube faces.

This resulting effect of compaction was not thought of until the author started to use the wire brush, manually, to yield a MR type substrate, firstly to trial experiments, and then subsequently to the various faces of the cubes and to the bottom face of the slabs. The author discovered that it was much harder to remove the laitance layer or to produce a suitable MR type profile to cubes which were given compaction at a lower vibration (4-7g) than to the cubes that were given

compaction at shock table mode of vibration (≈ 8g). This could be, as discussed above, due to the greater amount of weak laitance produced at the vertical sides of the concrete cubes when compacting at shock table mode. As a result, some substrates were observed to have a favourable roughness such as G4(3), G5(4) and P4(3) because of the ease at which firstly laitance could be removed followed by the appropriate level of roughness produced observed by eye and by human touch. The author noticed the type of mould also seems to play a part, for example the surface laitance layer yielded by a plastic mould was observed not to be influenced much by the level of vibration (shock table: ≈ 8g /normal vibration: 4-7g) as a opposed to the metal mould. This may be because of the plastic mould design and its reduced weight as opposed to the metal mould which is bulkier and much heavier.

Also, in addition to the discussion above, the base face (face resting on the vibrating table) of the cubes and the slabs, compacted at shock table mode, were, similar to the cubes mentioned above in the sense that it was difficult to prepare the surface by wire brush. Again, probably due to the thin laitance layer produced to the base face. This reinforces the point made earlier that the sides of concrete sample are likely to receive more of the effect of compaction than other faces, in this case the base face, when compacting at shock table mode. Hence, the probable reason why variations in pull-off failures (Figure 3.5) were encountered. For further details with regards to comparing short and medium term pull-off data to MR type profiles on issues such as: observed variation in results, concrete strengthening and influence of compaction and type of mould used.

Influence of Needle Gunning to the Variation in Pull-Off Failures to HR Profiles

Figures 3.2(c), 3.3(c), 3.2(d) and 3.3(d) shows the pull-off failures to HR type profiles at the concrete substrate end and dolly end respectively. The results were not that promising for this particular test since for ‘low w/c’ concrete mix designs with an intermediate aggregate exposure (between MR and VHR profiles), the author was expecting stress failure values between MR and VHR profiles but, as can be seen in Table 3.2, and graphically in Figure 3.4, on average the stress failures were the lowest of all grades of roughness. The results for ‘high w/c’

concrete mix designs on the other had were a bit more promising since stress failures, on average, were between MR and VHR profiles but still just above VHR. This might be because of the needle guns in ability to yield an appropriate type of immediate roughness. For example, the needle gun produces vibrating impact through its small diameter sized metal cylinders which are closely packed together with hardly any space between the cylinders refer to Figure 3.6. Because of this design feature possessed by the tool, it was discovered through observation that the impact produced as a result of vibration is very much localized. Also, since the HR profile is an intermediate roughness stage, care was required not to overly expose aggregates. Figures 3.2(c) and 3.3(c) for 'low w/c' concrete substrates show a greater amount of inter-coat failure compared to Figures 3.2(a) and 3.3(a) for a VHR profile. This was mainly because of the point mentioned above that the needle gun is not appropriate to yield an intermediate roughness stage especially to 'low w/c' concrete substrates possessing a high compressive strength since further localized impacts can result in high aggregate exposure and on the other hand minimal localized impacts leads to hardly any change in roughness to the surface. Hence the reason why, on average, the area of fracture results for 'low w/c' concretes had a higher degree of inter-coat type failure as shown in Figures 3.2(c) and 3.3(c). In contrast to 'high w/c' concrete substrates, as mentioned above, the results were slightly favourable because of the lower compressive strength which makes it easier for the needle gun to yield an intermediate roughness stage without overly exposing the aggregates. This is illustrated in Figures 3.2(d), 3.3(d) and Table 3.2 for 'high w/c' concretes where the area of fracture results showed, on average a higher degree of concrete failure at the substrate and dolly end respectively.

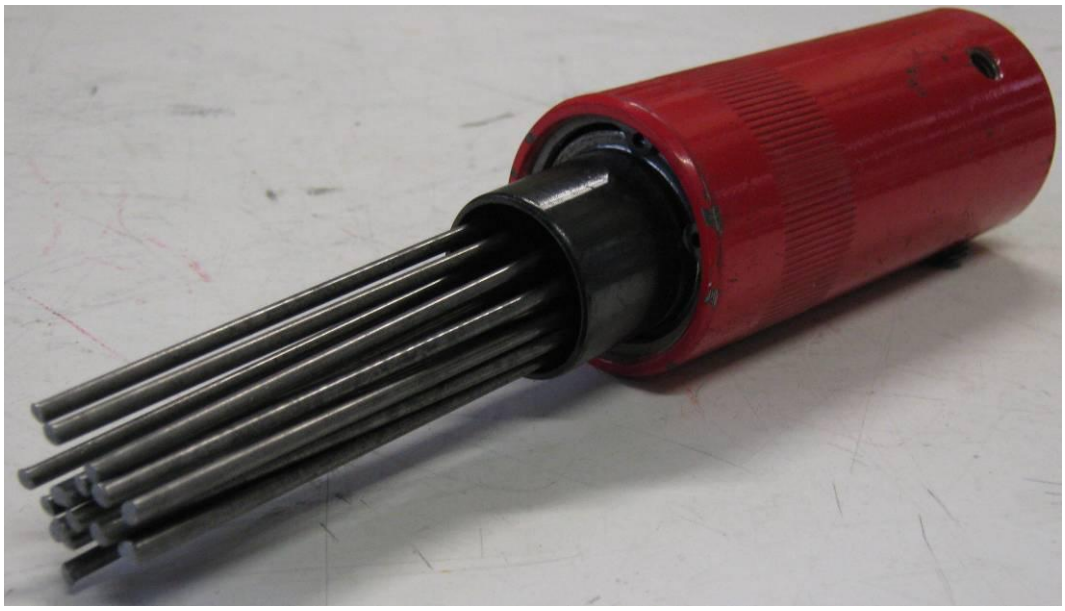

Figure 3.6: Needle gun containing closely packed small diameter sized metal cylinders

Immediately Coated & Pull-Off Tested Substrates (Moist Surface)

To help obtain a moist concrete substrate, general principles laid out in BSI 1542 (1999) were followed. Note: this particular test was carried out only to very high substrate roughness profiles (VHR) because of resource constraints.

Conditioning & Preparation of Substrate

Surfaces 1, 2 and 5 for cubes G3 and P3 were selected for this test. The surfaces of these cubes were wire brushed to begin with, followed by removal of excessive dust and then placed, fully submerged, in a tap water container for approximately 24 hours. At the end of this time period, cubes were taken out of container, wiped clean of any excessive/dripping water, given a very high substrate roughness (VHR), again resulting dust was removed and then finally given a few coats of Zinga.

Observation & Numerical Comparison: Variations in Pull-Off Failures

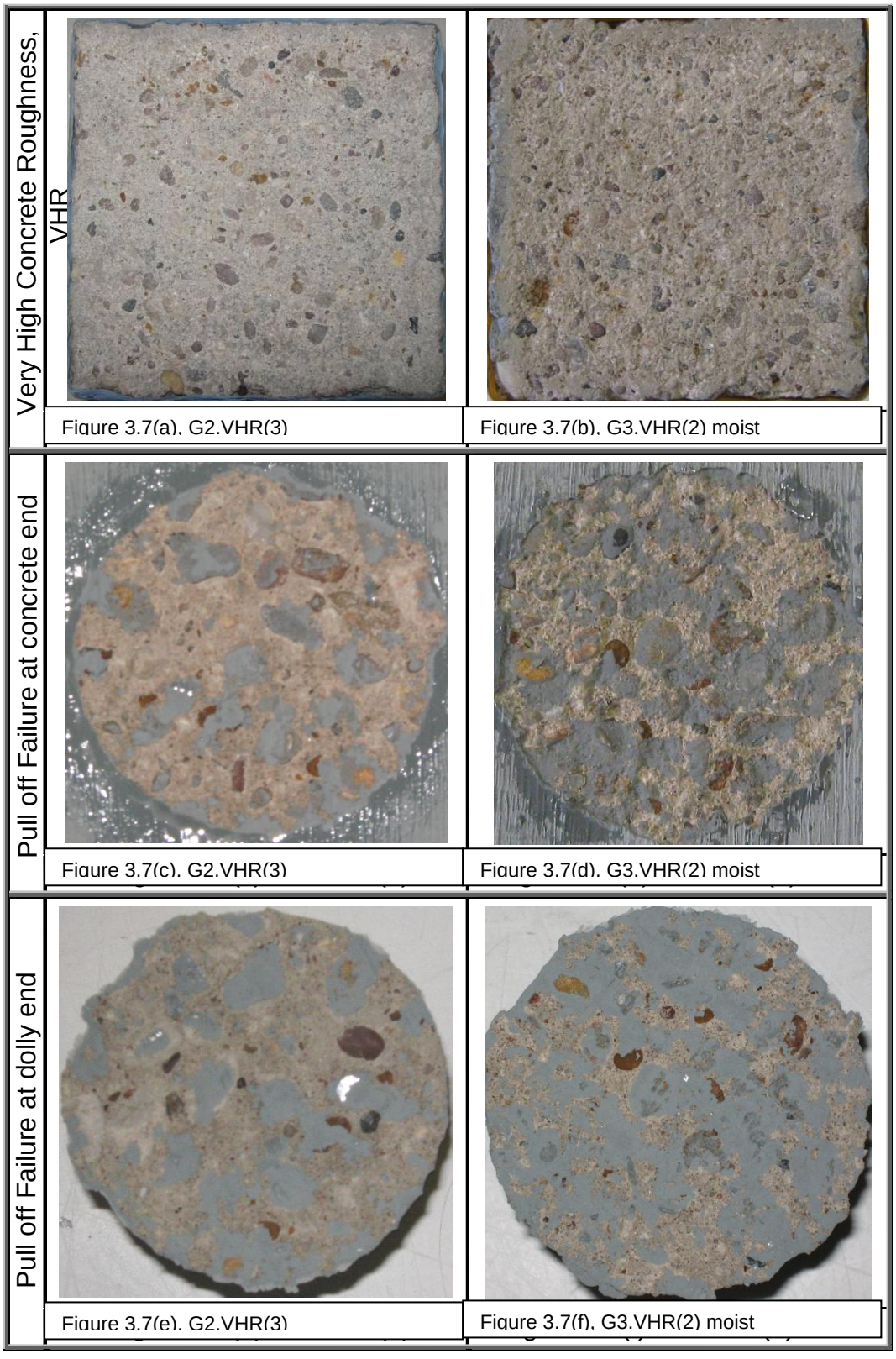

Figure 3.7: Variation in observed pull-off failures for very high substrate roughness (VHR), using a needle gun to 'low w/c' concretes (w/c = 0.50), dry surface (left) & moist surface (right)

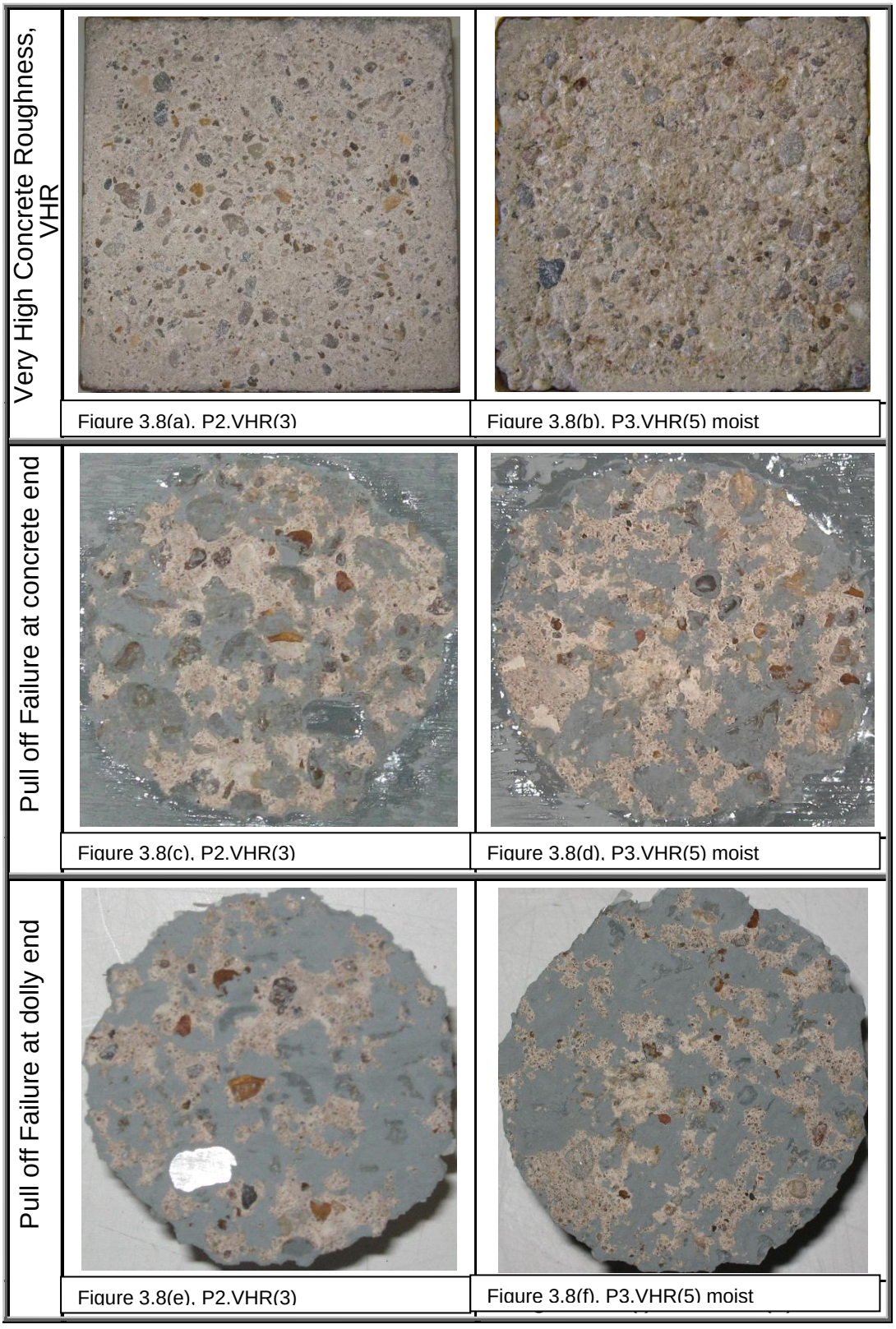

Figure 3.8 variation in observed pull off failures for very high substrate roughness (VHR), using a needle gun to 'high w/c' concretes (w/c = 0.80), dry surface (left) & moist surface (right)

Figures 3.7 and 3.8 shows the variation in observed pull-off failures to ‘low w/c’ and ‘high w/c’ concrete substrates, prepared to a very high roughness profile (VHR), when Zinga is coated to dry surfaces (shown on the left) and to moist surfaces (shown on the right) respectively. It can seen from these Figures 3.7(a), 3.8(a) and 3.7(b), 3.8(b) for both ‘low w/c’ and ‘high w/c’ substrates respectively the appearance of damp concrete in contrast to similar prepared, but dry, concrete substrates. The damp looking concrete can also be seen in the resulting pull-off failures at the substrate and dolly end respectively. Like for example in Figures 3.7(d) and 3.7(f) when comparing with dry concrete samples Figures 3.7(c) and 3.7(e).

Table of results 3.3 and Figure 3.9 graphically shows, on average, a reduction in pull-off strength by as much as 15% for ‘low w/c’ concretes and 27% for ‘high w/c’ concretes respectively as a result of moist substrates when compared to dry substrates with a similar roughness grade (VHR). Interestingly, in one particular case, for surface number 5 cube G3 the failure stress was slightly greater than any individual dry substrate test with the same roughness grade.

Table 3.3: Comparison between immediately coated and pull-off tested dry and moist concrete substrates prepared to very high roughness (VHR)

Variables	$T_{env.}$ (°C)	RH_{env} (%)	$T_{substrate}$ (°C)	DFT (µm)	σ (MPa)	σ_{av} (MPa)	Failure Type*	Area of Fracture (%)
Moist Substrates								
G3.VHR(1)	24.3±1.0	47.5±2.5	26.0±0.25	314	1.40±0.05	1.62	A, B/C, A/B	A = 30, B/C = 65, A/B = 5
G3.VHR(2)	23.5±0.5	46.5±3.5	23.5±0.25	299	1.35±0.05		A, B/C, A/B	A = 45, B/C = 50, A/B = 5
G3.VHR(5)	22.5±1.5	33.5±4.5	24.0±0.25	294	2.10±0.05		A, B/C, A/B	A = 55, B/C = 35, A/B = 10
P3.VHR(1)	24.3±1.0	47.5±2.5	26.0±0.25	333	0.60±0.05	0.82	A, B/C, A/B	A = 30, B/C = 65, A/B = 5
P3.VHR(5)	22.5±1.5	33.5±4.5	23.5±0.25	333	0.95±0.05		A, B/C, A/B	A = 65, B/C = 30, A/B = 5
P3.VHR(2)	22.5±1.5	33.5±4.5	23.5±0.25	309	0.90±0.05		A, B/C, A/B	A = 50, B/C = 45, A/B = 5
Dry Substrates								
G1.VHR(3)	22.5±1.0	45.5±2.5	23.0±0.25	328	1.75±0.05	1.90	A, B/C, -/Y	A = 70, B/C = 25, -/Y = 5
G2.VHR(3)			23.0±0.25	328	1.95±0.05		A, B/C	A = 75, B/C = 25
G3.VHR(3)			23.5±0.25	343	2.00±0.05		A, B/C, -/Y	A = 70, B/C = 25, -/Y = 5
P1.VHR(3)	24.0±0.5	47.0±3.0	21.0±0.25	299	1.00±0.05	1.13	A, B/C	A = 75, B/C = 25
P2.VHR(3)			22.5±0.25	290	1.00±0.05		A, B/C, A/B, -/Y	A = 60, B/C = 35, A/B & -/Y = 5
P3.VHR(3)			24.5±0.25	304	1.40±0.05		A, B/C, A/B	A = 65, B/C = 30, A/B = 5

KEY: $T_{env.}$ (°C) = environmental temperature, RH_{env} (%) = environmental relative humidity, $T_{substrate}$ (°C) = substrate temperature, DFT (µm) = dry film thickness, σ_{av} (MPa) = average pull-off stress, G & P = 'low w/c' and 'high w/c' concretes respectively and VHR = very high substrate roughness

* For definations of the terminology see page 59.

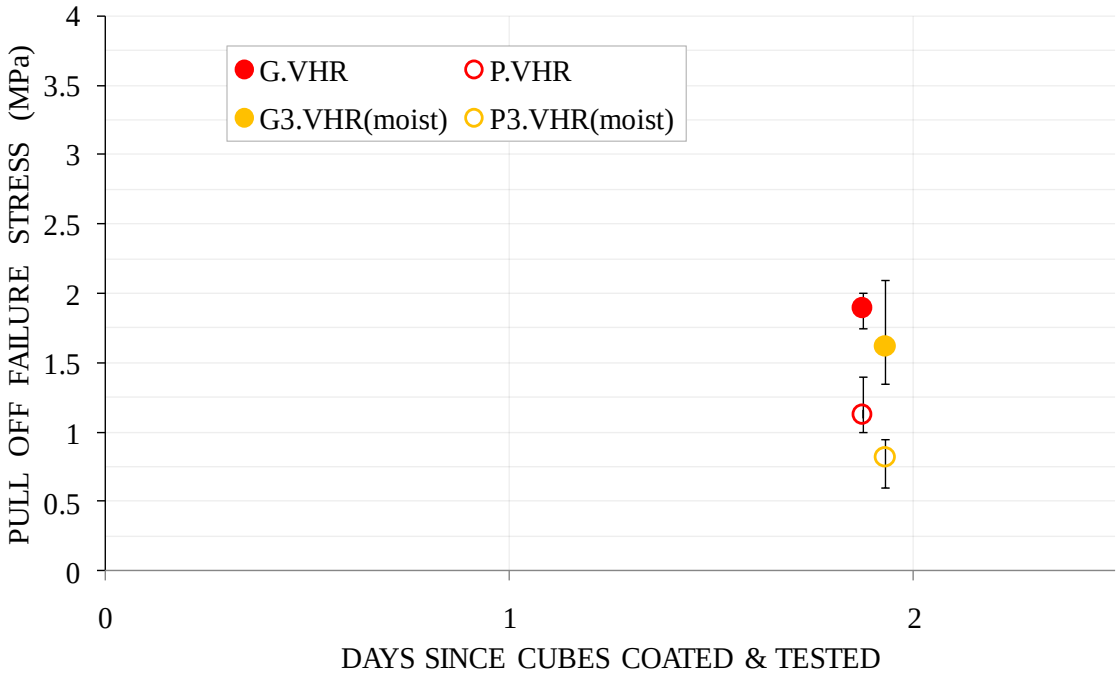

Figure 3.9: Comparison between moist and dry substrates prepared to a very high roughness (VHR) when immediately coated and pull-off tested

Note: each data point in Figure 3.9 is the average pull-off stress and the corresponding highs and lows (precisely known as error bars) are the upper and lower range in pull-off values observed respectively. Where G & P = 'low w/c' and 'high w/c' concretes respectively.

Another observation made was the variation in failure stresses obtained for both 'high w/c' and 'lw w/c' concretes. For example, by referring to Table 3.3 and Figure 3.9 the range for 'high w/c' dry VHR substrates was 0.25MPa whereas for 'low w/c' moist VHR substrates the range gave 0.75MPa. With regards to 'high w/c' substrates, dry surfaces gave a range of 0.40MPa and moist surfaces delivered a range of 0.35MPa for a similar roughness grade (VHR). This may indicate that moist surfaces are capable of introducing more variability in test results however, further research may be required.

To understand the reasons in stress failure variability, the area of fracture results (Table 3.3) needs to be looked at. On average both 'low w/c' and 'high w/c' moist substrates showed an increase in the amount of inter-coat failure (B/C), with a subsequent decrease in concrete failure (A), when compared to 'low w/c' and 'high

w/c' dry substrates. For example, the moist surfaces of 'low w/c' concrete gave on average a 'B/C' failure of 50% and an 'A' failure of 43% whereas for the dry surfaces of same concrete mix this was 25% and 72% for 'B/C' and 'A' failures respectively. With respect to 'high w/c' concrete, the moist surfaces on average a 'B/C' failure of 47% and an 'A' failure of 48% was seen whereas for the dry surfaces of the 'high w/c' concrete this was 30% and 67% for 'B/C' and 'A' failures respectively. The reduced concrete failure, in both 'low w/c' and 'high w/c' concrete mix designs, seems to suggest the coatings in ability to fully adhere/anchor to the moist substrates resulting in a greater inter-coat failure scenario. There was also, on average, a minimal increase in the amount of 'A/B' failure for the moist surfaces of both 'low w/c' and 'high w/c' concretes; again, this is believed to be for similar reasons as expressed above.

56 Day Coated & Pull-Off Tested Substrates

Table 4.1 shows the dates when cubes were cast, the number of days within the curing tank and the amount of accumulated days (from since cubes were cast) to the point of being coated with Zinga up to 56 days and pull-off tested respectively. Note for this particular test only medium (MR) and very high surface roughness (VHR) profiles were considered.

Appearance & Condition of Coated Cubes after 56 Days of Exposure

Figure 3.10 shows the appearance of Zinga coated cubes, prepared to a MR type profile, after being placed, up to 56 days, in variable environmental conditions.

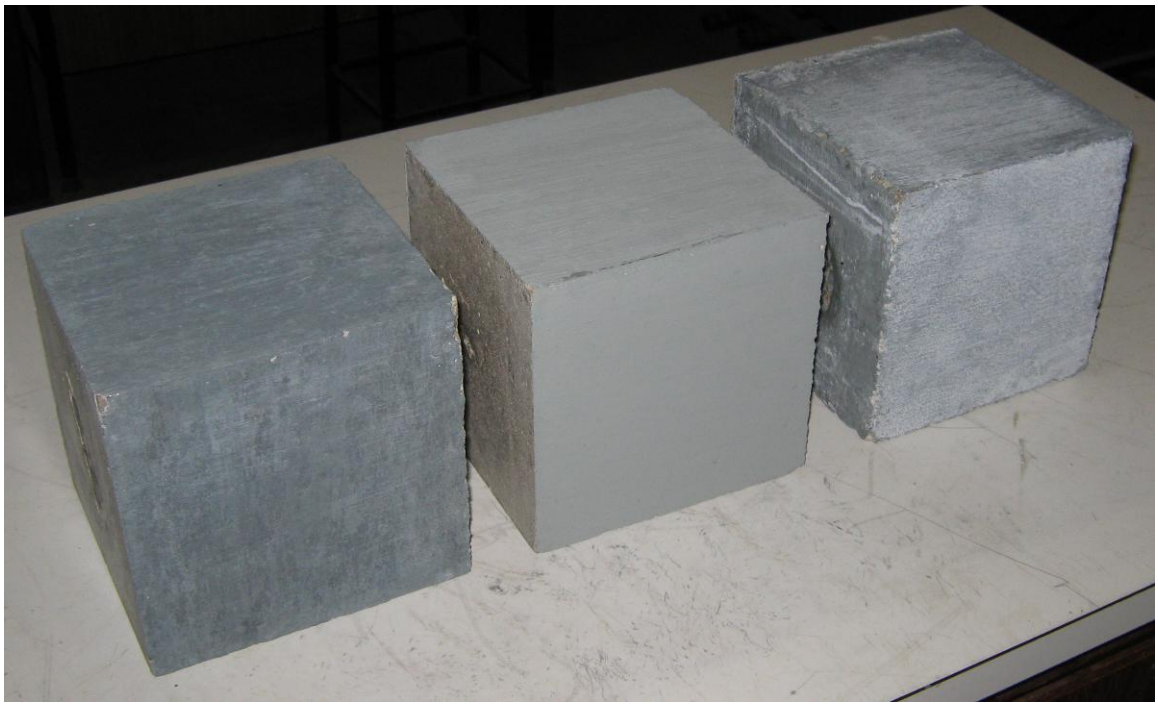

Figure 3.10: Appearance of Zinga coated cubes, prepared to a MR type profile, after being placed up to 56 days in variable environmental conditions.

From left to right as shown in Figure 3.10, coated cubes were placed in an outdoor environment (left), in a temperature control room environment (middle) and again in a temperature control room environment but subjected to daily water spraying (right).

After a few sprays of distilled water to Zinga coated cubes in a temperature controlled environment, upon drying the appearance, initially, showed some slight non uniform white colour stains but with daily spraying, over time, the white stains became more uniform across the selected faces. The observed white colour, as stated by Zinga, does not affect the coatings quality and is a sign of complementary protection known as patina or passive protection of zinc salts which can be removed by fresh water and nylon brush cleaning. The white colour, as suggested by Zinga, may occur due to the following environmental reasons: humidity, temperature, atmospheric pollution, proximity to the coast etc. The possible reasons for the white colour may have been the amount of airborne salts in the temperature control room as a result of other salt related experimental tests and the presence of no continuous fresh air supply (wind). The relative humidity and temperature of the temperature control room was 56 ± 4% and 22.5 ± 1.5°C respectively.

However, unlike coated cubes placed in a temperature control room and with/without frequent water spraying, coated cubes placed in an outdoor environment (Birmingham, UK during the summer months) up to 56 days gave a matt metallic dark grey colour. The author witnessed, after a fairly heavy downpour, the coating to appear uniformly dark grey in colour which occurred several days into the 56 day period. Zinga states natural rain or forced water saturation can help accelerate the barrier (passive) protection in the form of zinc salts and zinc carbonates to the coating surface as well as make the coating harder and by the end of the process the coating will appear uniformly dark grey suggesting the coating has fully polymerised. With regards to the coated cube placed in the temperature control room with no wetting. The initial coating colour was light grey and after 56 days the colour of the coating had changed very little in the direction of dark grey.

The author also observed to cubes prepared to VHR profiles and placed in an outdoor environment, up to 56 days, what seems to be an increase in Zinga surface roughness and/or possibly, as the manufacturer (Zinga) states, an increase in coating hardness. However, observational comparisons made by the author to similar VHR profile prepared cubes placed in a temperature control room (with no wetting) showed very little or no increase in Zinga roughness after a 56 day period. This is may have been as a result of natural outdoor weathering coupled with the fact that the substrate roughness (VHR) yields a highly undulating surface which inevitability leads to a high peak and trough type coated surface profile.

Observation & Numerical Comparison: Pull-Off Test Results

The following sub sections will comprise of comparisons between immediately coated and pull-off tested ‘low w/c’ and ‘high w/c’ concrete cubes and 56 day coated and pull-off tested ‘low w/c’ and ‘high w/c’ concrete cubes for both very high surface roughness (VHR) and medium surface roughnesses (MR) respectively.

Influence of Natural Ageing to VHR Coated Substrates in Different Environments

Figures 3.11 and 3.12 illustrate the observed pull-off failure comparisons to 'low w/c' and 'high w/c' concretes, prepared to a VHR type profile, looking at the substrate end and dolly end respectively. For ease of comparison between cubes placed in different environmental conditions and tested at variable times these Figures have been arranged in manner to enable this. Figures 3.11(a), 3.11(b), 3.12(a) and 3.12(b) (previous shown photographs) were tests carried out within a few days after coating also known as 'immediately coated and pull-off tested' as shown in Section 3.3. Just below are Figures 3.11(c), 3.11(d), .12(c) and 3.12(d) coated cubes G1 and P1 respectively which were placed in a temperature control room (TCR) environment up to 56 days and then tested for pull-off adhesion. Similar to cubes G1 and P1, Figures 3.11(e), 3.11(f), 3.12(e) and 3.12(f) show coated cubes G2 and P2 which were placed in an outdoor environment (Birmingham, United Kingdom) again up to 56 days and then tested for pull-off adhesion.

Table 3.4 and Figure 3.13 shows, regardless of the environmental condition, for the 56 day coated cubes of both 'low w/c' and 'high w/c' concretes, on average an increase in pull-off failures was retrieved when compared to immediately coated and pull-off tested samples (Table 3.2) of the same roughness profile (VHR). This average increase, expressed as a percentage, is 42% for G1, 59% for P1, 27% for G2 and 77% for P2. The author was expecting this increase, since the area of fracture results for immediately coated and pull-off tested samples (VHR type profiles) indicated, on average, at least 65% of the failure occurs within the concrete substrate. Bearing this point in mind and the fact that concrete is likely to gain in strength with time explains the reason for this increase in pull-off stress after a 56 day time period.

	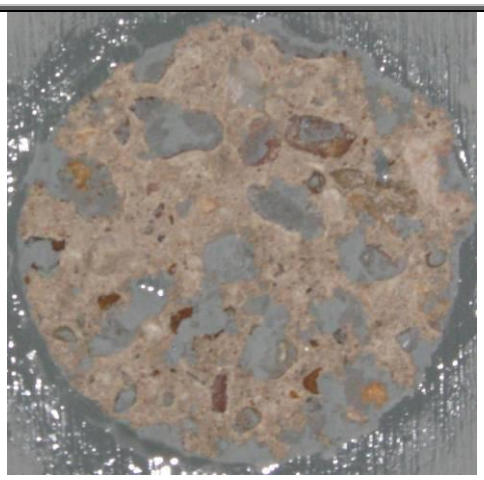	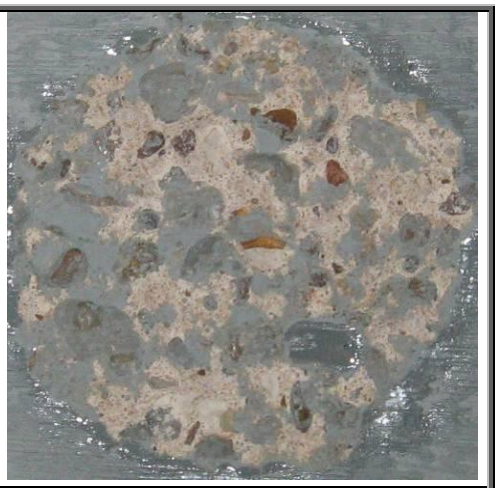
	Figure 3.11(a) – G2(3), w/c = 0.50,	Figure 3.11(b) – P2(3), w/c = 0.80
Very High Concrete Roughness, VHR T = 56 days within TCR	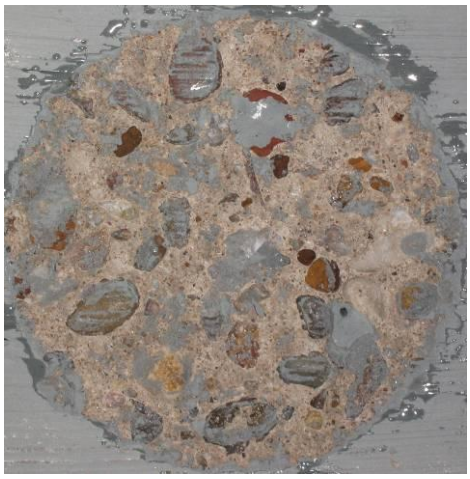	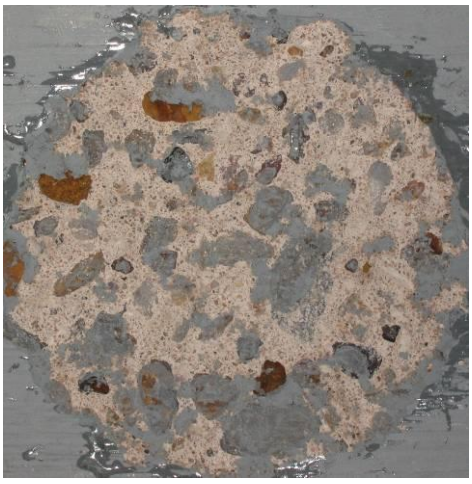
	Figure 3.11(c) – G1(1), w/c = 0.50	Figure 3.11(d) – P1(1), w/c = 0.80
Very High Concrete Roughness, VHR T = 56 days (Outdoor Environment)		
	Figure 3.11(e) – G2(2), w/c = 0.50	Figure 3.11(f) – P2(2), w/c = 0.80

Figure 3.11: Observational pull-off failure comparisons to very high surface roughness 'lo w/c' (left) & 'high w/c' (right) concretes, substrate end, immediately after coating and after 56 days

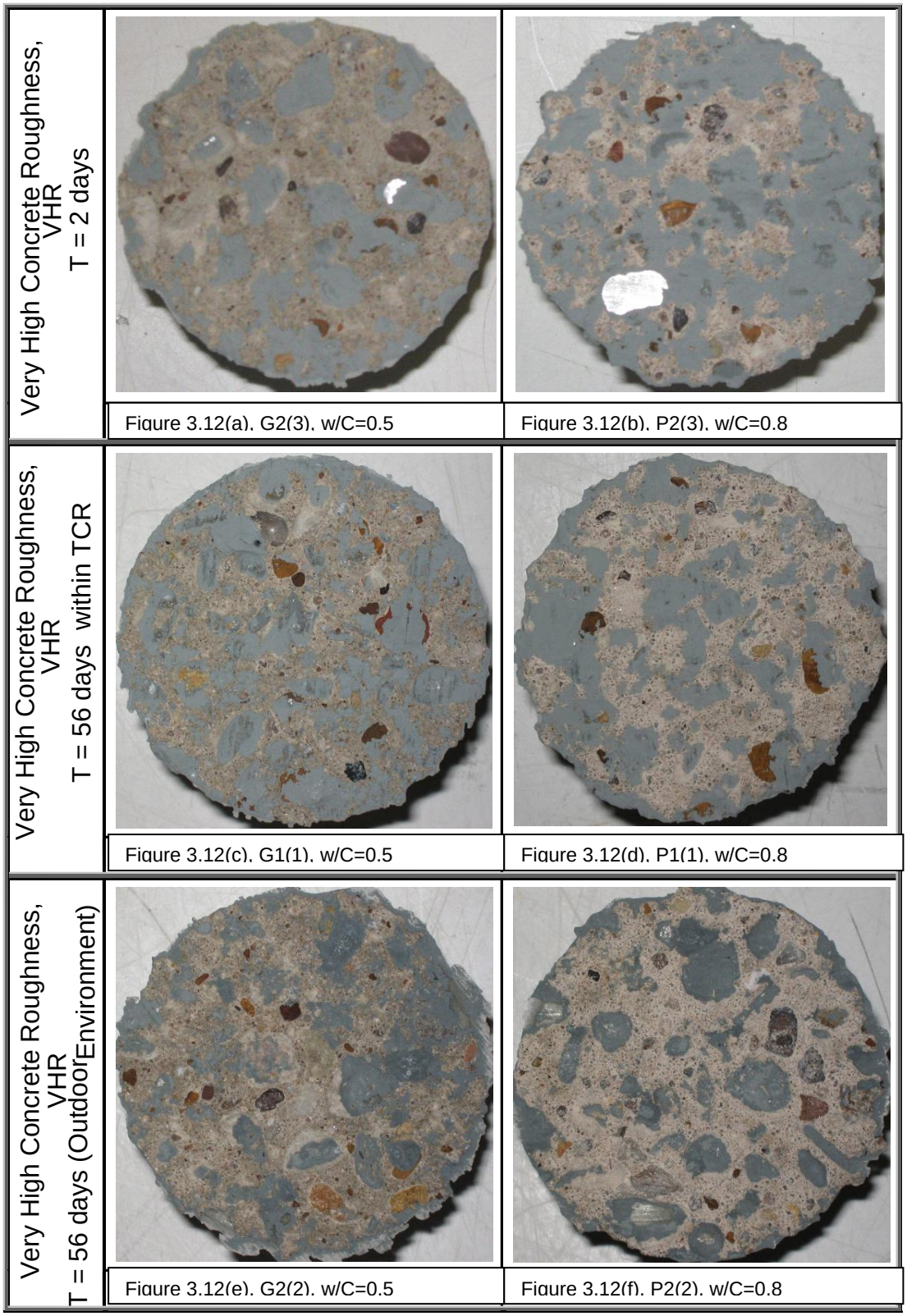

Figure 3.12: Observational pull-off failure comparisons to very high surface roughness for 'low w/c' (left) & 'high w/c' (right) concretes, dolly end, immediately after coating and after 56 days

Table 3.4: Pull-off Test Results: Coated cubes prepared to a very high roughness (VHR) and placed in variable environments up to 56 days.

Variables	$T_{env.}$ (°C)	RH_{env} (%)	$T_{substrate}$ (°C)	DFT (µm)	σ (MPa)	σ_{av} (MPa)	Failure Type*	Area of Fracture (%)
Temperature controlled room (TCR) at RH =56 ± 4 % & T = 22.5 ± 1.5 °C and subject to frequent water spraying								
G1.VHR(1)	24.3±1.0	47.5±2.5	26.0±0.25	328	2.75±0.0	2.70	A, B/C, A/B	A = 85, B/C = 10, A/B = 5
G1.VHR(5)	24.3±1.0	47.0±3.0	25.0±0.25	294	3.20±0.0		A, B/C	A = 55, B/C = 45
G1.VHR(2)	24.0±0.5	47.5±6.5	25.0±0.25	314	2.15±0.0		A, B/C, A/B	A = 65, B/C = 35
P1.VHR(1)	24.3±1.0	47.5±2.5	26.0±0.25	323	1.75±0.0	1.80	A, B/C	A = 80, B/C = 20
P1.VHR(5)	24.3±1.0	47.0±3.0	25.0±0.25	323	2.00±0.0		A, B/C, A/B	A = 70, B/C = 30
P1.VHR(2)	24.0±0.5	47.5±6.5	25.0±0.25	319	1.65±0.0		A, B/C, A/B	A = 65, B/C = 25, A/B = 5
Outdoor environment (OE) subject to natural weathering								
G2.VHR(1)	24.3±1.0	47.5±2.5	26.0±0.25	328	2.50±0.05	2.42	A, B/C, A/B, -/Y	A = 70, B/C = 5, A/B = 5 & -/Y = 20
G2.VHR(5)	24.3±1.0	47.0±3.0	25.0±0.25	328	2.30±0.05		A, B/C, A/B, -/Y	A = 50, B/C = 25, -/Y = 25
G2.VHR(2)	24.0±0.5	47.5±6.5	25.0±0.25	319	2.45±0.05		A, B/C, A/B, -/Y	A = 75, B/C = 5, A/B = 20
P2.VHR(1)	24.3±1.0	47.5±2.5	26.0±0.25	319	1.80±0.05	2.00	A, B/C, A/B	A = 90, B/C = 5, A/B = 5
P2.VHR(5)	24.3±1.0	47.0±3.0	25.0±0.25	299	2.10±0.05		A, B/C, A/B, -/Y	A = 85, B/C & A/B = 5, -/Y = 10
P2.VHR(2)	24.0±0.5	47.5±6.5	25.0±0.25	333	2.10±0.05		A, B/C, A/B, -/Y	A = 75, B/C = 5, A/B = 20

KEY: $T_{env.}$ (°C) = environmental temperature, RH_{env} (%) = environmental relative humidity, $T_{substrate}$ (°C) = substrate temperature, DFT (µm) = dry film thickness, σ_{av} (MPa) = average pull-off stress, G & P = 'low w/c' and 'high w/c' concretes respectively and VHR = very high substrate roughness. * For the definition of terminology, see page 59.

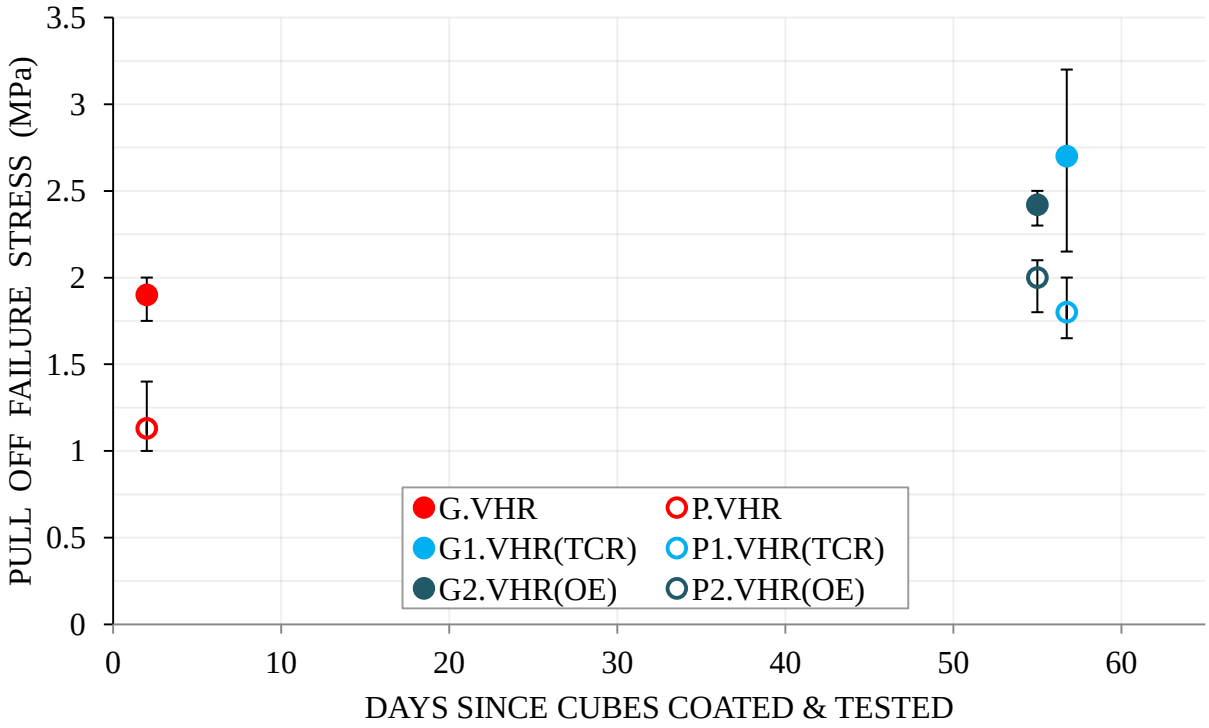

Figure 3.13: Comparison between immediately coated and pull-off tested cubes and 56 day coated and pull-off tested cubes with a very high roughness profile (VHR).

Note: each data point in Figure 3.13 is the average pull-off stress and the corresponding highs and lows (precisely known as error bars) are the upper and lower range in pull-off values observed respectively. Where G & P = 'low w/c' and 'high w/c' concretes, TCR = temperature control room (RH =56 ± 4% & T = 22.5 ± 1.5°C) and OE = outdoor environment.

In terms of comparison to area of fracture results between immediately coated and tested samples and 56 day coated and tested samples. For 'low w/c' concrete mix designs, G1 and G2 both showed, on average, a decline in the amount of failure occurring within the concrete. The concrete failure (A) was found to be on average approximately 66% which is a percentage decrease of 6% from the amount observed to immediately coated and pull-off tested specimens. However, for 'high w/c' concrete mix designs, P1 and P2, the opposite was true both showed, on average, an increase in the amount of failure occurring within the concrete. The concrete failure (A) was found to be on average 73% for P1 and 83% for P2 which is a percentage increase of 9% for P1 and 24% for P2 from the amount previously observed to immediately coated and pull-off tested specimens.

Observation & Numerical Comparison: Variations in Pull-Off Failures

With respect to variability of pull-off stress results, all 56 day coated and pull-off tested samples showed a similar range in results when compared to immediately coated and pull-off tested samples. An exception to this was cube G1 which showed a greater range in pull-off results, as can be seen in Figure 3.13. For example the range in pull-off values for 'low w/c' and 'high w/c' concretes when immediately coated and pull-off tested was 0.25MPa and 0.40MPa respectively. The corresponding range in pull-off values for 56 day coated and then pull-off tested was 1.05MPa for G1, 0.35MPa for P1, 0.20MPa for G2 and 0.30MPa for P2.

With regards to variability of area of fracture results for 56 day coated and pull-off tested cubes when compared to immediately coated and pull-off tested cubes. All 'low w/c' concrete mix design cubes in this matter showed more variability in the amount of failure occurring within the concrete whereas the variability for 'high w/c' concrete mix designs stayed the same. For example G1 showed a range of (A) = 85 – 55 = 30% and for G2 the range was (A) = 75 – 50 = 25% which is higher than immediately coated and tested samples (A) = 75 -70 = 5%. On the other hand 'high w/c' concretes showed no change, for example the range for P1 was (A) = 80 – 65 = 15% and for P2 the range was (A) = 90 – 75 = 15% which is similar to the range observed for immediately coated and tested samples (A) = 75 -60 = 15%.

Influence of Outdoor Weathering & VHR Type Profiles on Abnormal Failures

In the opinion of the author, regardless of the environmental condition 56 day coated cubes were placed, the average pull-off failures were found to be similar for 'low w/c' or 'high w/c' concrete substrates when compared against each other. However, there was some slight variation and in other extreme cases abnormal failures which will be discussed later. For example the average pull-off failure for G1 was 2.70MPa however, for G2 the average was 2.42MPa yielding a difference of approximately 0.30MPa between G1 and G2 results. For 'high w/c' concrete mix designs, the average pull-off failure for P1 was 1.80MPa however, for P2 the average was 2.00MPa yielding a difference of approximately 0.20MPa between P1 and P2 results. It can be seen from Table 3.4, and graphically illustrated in Figure 3.13, the grouped individual pull-off results for P1 and P2 are closely matched with

individual results from each group (i.e. P1 or P2) overlapping to a certain degree. However, there was no intermixing/overlapping of grouped individual pull-off results in the cases of G1 and G2 as shown in Figure 3.13 or Table 3.4 and this was primarily because of G2 where two thirds of the observations were found to be abnormal pull-off failures as a result of significant -/Y failure (between coating and adhesive). Figure 3.14 illustrates a typical abnormal pull-off failure seen to a very high substrate roughness (VHR) for a 'low w/c' concrete substrate when placed, up to 56 days, in an outdoor environment (shown on the left hand side). Figure 3.14 also gives an illustration of a 'high w/c' concrete shown on the right hand side for comparisons purposes to a 'low w/c' concrete mix design. The reading obtained for this particular 'high w/c' substrate (P2 surface 5) was considered acceptable since the observed area of fracture gave around a -/Y of 10% and most importantly the pull-off result for this particular face gave an upper bound value. On the other hand, 'low w/c' concrete cube G2 substrates 5 and 1 showed a great amount of -/Y failure (between the coating and the adhesive) and this is most likely because of an air bubble formation in more than one likely place between adhesive and coating leading to no critical contact.

The explanation for this type of failure has been previously discussed in Section titled 'influence of VHR profiles to observe -/Y type failures'. But just to summarize, this is mainly due to a highly undulated surface possessed by a VHR type profile, hence coating surface is prone to air bubble formation possibly leading to a localized region of no adhesion to the coated substrate. In addition, with respect to 56 day coated and pull-off tested samples, -/Y failure was only observed to cubes exposed to an outdoor environment and the extent of these failures (at least 20% -/Y to both surfaces 5 and 1 of cube G2) has not been seen previously for example, the most -/Y failure recorded to immediately coated and pull-off tested cubes was around 5%. The reason why only those 56 day coated cubes exposed to an outdoor environment suffered in this way is possibly as a result of one or more combination of factors, such as: a weathered Zinga surface, hardened coating by polymerisation, highly undulated concrete substrate and/or coated surface in addition to air bubble formation to epoxy resin or incompatibility of adhesive with respect to outdoor weathered coatings. A possible remedy to help limit this type of failure might be to slightly scratch/roughen the Zinga coating, prior to attaching

dolly, but care is required not to penetrate into the substrate material. Based on the experimental experience gathered by the author in terms of interpretation of a pass or failure criteria to area of fracture results involving a -/Y type failure to concrete substrates prepared to a VHR type profile. In the opinion of the author, where an area of fracture is observed to be greater than around 15% with respect to a -/Y type failure (between coating and adhesive) this may be classified as a failure for that particular pull-off test.

Very High Concrete Roughness, VHR		
	Figure 3.14(a), G2(5), w/C=0.5	Figure 3.14(b), P2(5), w/C=0.8
Pull off failure at substrate end T = 56 days (Outdoor Environment)	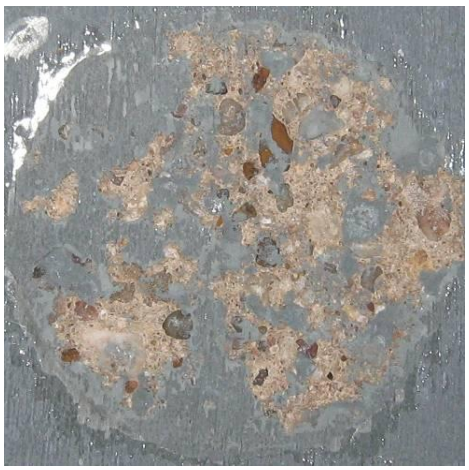	Not Available
	Figure 3.14(c), G2(5), w/C=0.5	Figure 3.14(d), P2(5), w/C=0.8
Pull off failure at dolly end T = 56 days (Outdoor Environment)	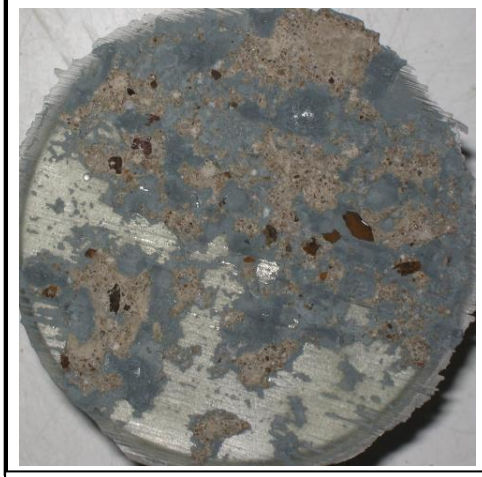	
	Figure 3.14(e), G2(5), w/C=0.5	Figure 3.14(f), P2(5), w/C=0.8

Figure 3.14: Observed abnormal pull-off failures to very high substrate roughness (VHR) 'low w/c' (left) & 'high w/c' (right) concretes when placed, up to 56 days, in an outdoor environment

3.3.1 Influence of Natural Ageing to MR Coated Substrates in Different Environments

Figures 3.15 and 3.16 illustrate the observed pull-off failure comparisons to 'low w/c' and 'high w/c' concretes, prepared to a MR type profile (medium roughness), looking at the substrate end and dolly end respectively. For ease of comparison between cubes placed in different environmental conditions and tested at variable times these Figures have been arranged in manner to enable this. Figures 3.15(a), 3.15(b), 3.16(a) and 3.16(b) (previous shown photographs) were tests carried out within a few days after coating also known as immediately coated and pull-off tested as shown in Section 3.3. Just below are Figures 3.15(c), 3.15(d), 3.16(c) and 3.16(d) coated cubes G4 (surface 1) and P4 (surface 1) respectively which were placed in a temperature control room (TCR) environment up to 56 days whilst being frequently sprayed with distilled water and then tested for pull-off adhesion. Similar to cubes G4 and P4, Figures 3.15(e) and 3.16(e) shows coated cube G5 which was placed in an outdoor environment (Birmingham, United Kingdom) again up to 56 days and then tested for pull-off adhesion.

Table 3.5 and Figure 3.17 shows, regardless of the environmental condition, for both 'low w/c' and 'high w/c' 56 day coated cubes, on average, an increase in pull-off failures was retrieved when compared to immediately coated and pull-off tested samples (Table 3.2) of the same roughness profile (MR). The exception to this was cube G6 which will be discussed later however, the average increase expressed as a percentage is 12.5% for G4, 42% for P4, 12% for G5 and a slight decrease of 1.5% for G6. Other than G6, the author was expecting this increase, since the area of fracture results for immediately coated and pull-off tested samples (MR type profiles) indicated on average at least 33% of the failure occurs within the concrete substrate. Bearing this point in mind and the fact that concrete is likely to gain in strength with time explains the reason for this increase in pull-off stress after a 56 day time period.

Medium Concrete Roughness, MR T = 2 days	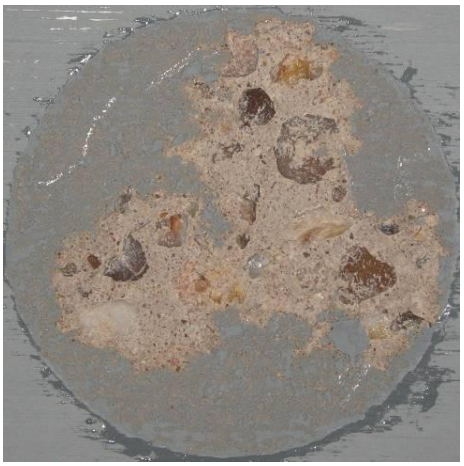	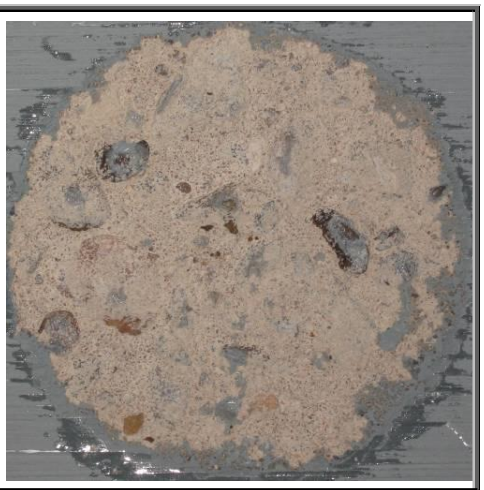
	Figure 3.15(a), G5(4), w/C=0.5	Figure 3.15(b), P4(3), w/C=0.8
Medium Concrete Roughness, MR T = 56 days within TCR (wetted)		
	Figure 3.15(c), G4(1), w/C=0.5	Figure 3.15(d), P4(1), w/C=0.8
Medium Concrete Roughness, MR T = 56 days within TCR	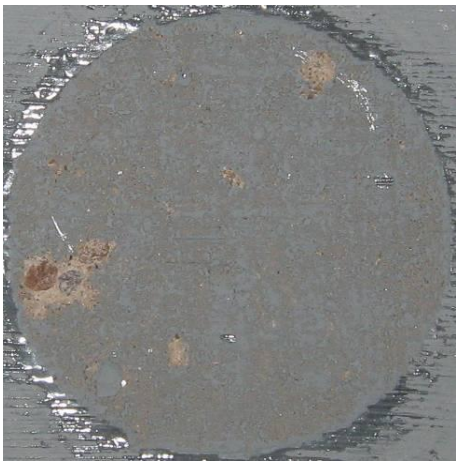	High w/c ratio concrete comparison Not Available
	Figure 3.15(e), G5(1), w/C=0.5	

Figure 3.15: Observational pull-off failure comparisons to medium surface roughness 'low w/c' (left) & 'high w/c' (right) concretes, substrate end, immediately after coating and after 56 days.

Medium Concrete Roughness, MR T = 2 days	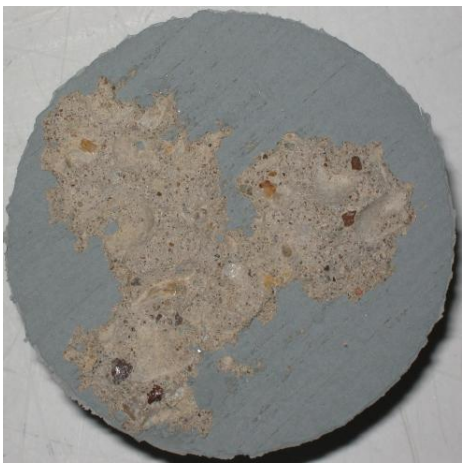	
	Figure 3.16(a), G5(4), w/C=0.5	Figure 3.16(b), P4(3), w/C=0.8
Medium Concrete Roughness, MR T = 56 days within TCR (wetted)		
	Figure 3.16(c), G4(1), w/C=0.5	Figure 3.16(d), P4(1), w/C=0.8
Medium Concrete Roughness, MR T = 56 days within TCR		High w/c ratio concrete comparison Not Available
	Figure 3.16(e), G5(1), w/C=0.5	

Figure 3.16 observational pull-off failure comparisons to medium surface roughness for 'low w/c' (left) & 'high w/c' (right) concretes, dolly end, immediately after coating and after 56 days.

In terms of comparison to area of fracture results between immediately coated and tested samples and 56 day coated and tested samples. For ‘low w/c’ concrete mix designs G5 and G6 both showed, on average, a decline in the amount of failure occurring within the concrete. The concrete failure (A) was found to be on average approximately 5% which is a huge percentage decrease of 85% from the amount observed to immediately coated and pull-off tested specimens.

Table 3.5: Pull-off Test Results - Coated cubes prepared to a medium roughness (MR) and placed in variable environments up to 56 days.

Variables	$T_{env.}$ (°C)	RH_{env} (%)	$T_{substrate}$ (°C)	DFT (µm)	σ (MPa)	σ_{av} (MPa)	Failure Type*	Area of Fracture (%)
Temperature controlled room (TCR) at RH =56 ± 4 % & T = 22.5 ± 1.5 °C and subject to frequent water spraying								
G4.MR(1)	21.0±2.0	50.5±2.5	22.00±0.25	323	>3.50	>3.50	A, B/C	A = 80, B/C = 20
G4.MR(5)	19.0±1.0	70.0±13.0	20.00±0.25	333	>3.50		A, B/C	A = 10, B/C = 90
G4.MR(2)	21.0±2.0	57.0±7.0	22.50±0.25	285	>3.50		A, B/C	A = 90, B/C = 10
P4.MR(1)	21.0±2.0	50.5±2.5	22.00±0.25	343	2.50±0.05	2.53	A, B/C	A = 100
P4.MR(5)	19.0±1.0	70.0±13.	20.00±0.25	294	2.40±0.05		B/C	B/C = 100
P4.MR(2)	21.0±2.0	57.0±7.0	22.00±0.25	314	2.70±0.05		A, B/C	A = 95, B/C = 5
Temperature controlled room (TCR) at RH =56 ± 4 % & T = 22.5 ± 1.5 °C								
G5.MR(1)	21.0±2.0	50.5±2.5	22.00±0.25	319	>3.50	>3.50	A, B/C, -/Y	B/C = 95, A & -/Y = 5
G5.MR(2)	19.0±1.0	70.0±13.0	20.50±0.25	304	>3.50		A, B/C	B/C = 100
G5.MR(3)	21.0±2.0	57.0±7.0	22.50±0.25	299	3.45±0.05		A, B/C	B/C = 100
Outdoor environment (OE) subject to natural weathering								
G6.MR(1)	24.3±0.8	47.5±2.5	22.00±0.25	328	3.50±0.05	3.06	A, B/C	A = 5, B/C = 95
G6.MR(2)	24.3±0.8	47.0±3.0	20.50±0.25	309	>3.50		A, B/C, A/B	A = 20, B/C = 70, A/B = 10
G6.MR(3)	24.3±0.5	47.5±6.5	22.50±0.25	309	2.20±0.05		B/C	B/C = 100

KEY: $T_{env.}$ (°C) = environmental temperature, RH_{env} (%) = environmental relative humidity, $T_{substrate}$ (°C) = substrate temperature, DFT (µm) = dry film thickness, σ_{av} (MPa) = average pull-off stress, G & P = 'low w/c' and 'high w/c' concretes respectively and MR = medium substrate roughness. * For the definition of the terminology, see page 59.

However, for G4 the concrete failure (A) was found to be on average approximately 60% which is a percentage increase of 82% from the amount observed to immediately coated and pull-off tested specimens. With regards to 'high w/c' concrete mix design P4, on average an increase in the amount of failure occurring within the concrete was observed. The concrete failure (A) was found to be on average 65% which is a percentage increase of 86% from the amount previously seen to immediately coated and pull-off tested specimens.

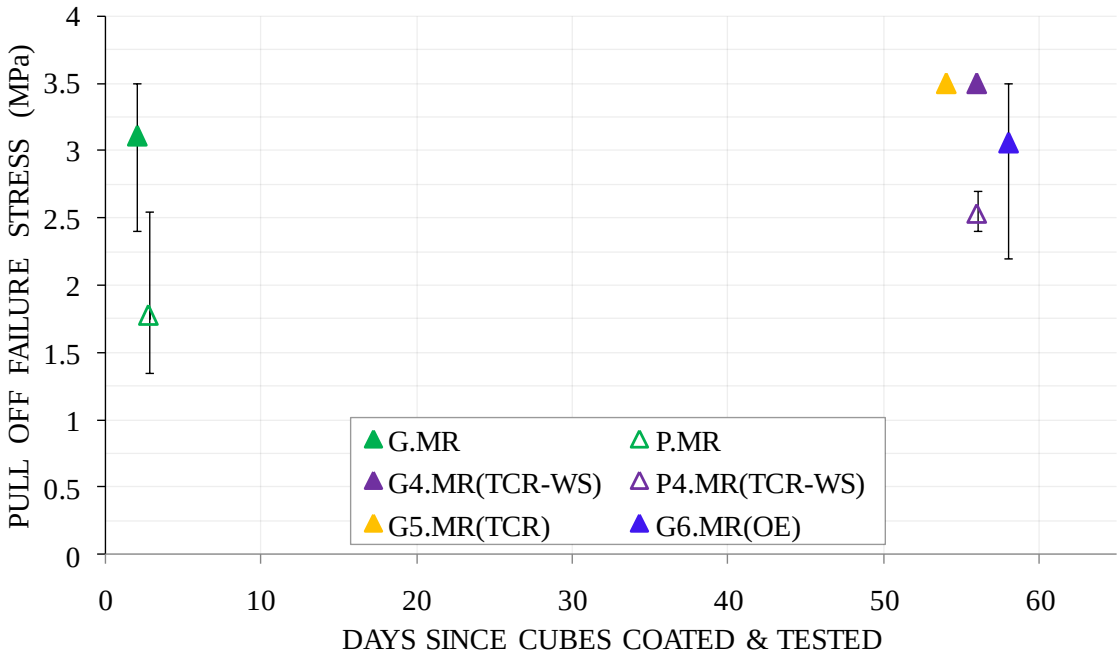

Figure 3.17: Comparison between immediately coated and pull-off tested cubes and 56 day coated and pull-off tested cubes with a medium roughness profile (MR)

Note: each data point in Figure 3.17 is the average pull-off stress and the corresponding highs and lows (precisely known as error bars) are the upper and lower range in pull-off values observed respectively. Where G & P = 'low w/c' and 'high w/c' concretes, TCR = temperature control room (RH =56 ± 4% & T = 22.5 ± 1.5°C), WS = with daily water spraying and OE = outdoor environment.

Observation & Numerical Comparison: Variations in Pull-Off Failures

With regards to variability of results, Table 3.6 shows all the short and medium term pull-off test results carried out to 'low w/c' and 'high w/c' concrete substrates prepared to a medium roughness (MR). For ease of reading and comparison

purposes Table 3.6 provides detailed result analysis such as the average and range in pull-off values per cube as well as the corresponding area of fracture results for each individual surface tested as well as averages per cube in relation to observed failures (A) 'failures occurring within concrete' and (B/C) 'inter-coat failures' only. In addition, information regarding the amount of compaction given using the vibrating table (≈ 8g: shock table or 4-7g: normal vibration) and the type of mould used (metal or plastic) has also shown again for comparison reasons.

Table 3.6: A summarised comparison between immediately coated and pull-off tested cubes and 56 day coated and pull-off tested cubes with a medium roughness profile (MR)

Cube (face)	***σ (MPa)***			***Area of Fracture (%)***		***Average Area of Fracture (%)***		***Adjusted Average Area of Fracture (%)***		***Mode of Compaction (m/s^2)***	***Mould Type***
	Each	Average	Range	A	B/C	A	B/C	A	B/C		
IMMEDIATELY COATED & PULL-OFF TESTED: 'LOW W/C' CONCRETE (W/C = 0.50)											
G4(3)	3.40	3.11	1.10	45	55	33	67	42	58	≈ 8g, Shock	Metal
G5(4)	3.15			40	60					≈ 8g, Shock	Plastic
G6(4)	3.50			40	60					4-7g	Plastic
G7(1)	2.40			5	95					4-7g	Metal
56 DAY COATED & PULL-OFF TESTED: 'LOW W/C' CONCRETE (W/C = 0.50)											
G4(1)	3.50	3.50	0	80	20	60	40	85	15	≈ 8g, Shock	Metal
G4(2)	3.50			90	10						
G4(5)	3.50			10	90						
G5(1)	3.50	3.48	0.05	5	95	2	98			≈ 8g, Shock	Plastic
G5(2)	3.50			-	100						
G5(3)	3.45			-	100						
G6(1)	3.50	3.07	1.30	5	95	8	88			4-7g	Plastic
G6(2)	3.50			20	70						
G6(3)	2.20			-	100						
IMMEDIATELY COATED & PULL-OFF TESTED: 'HIGH W/C' CONCRETE (W/C = 0.80)											
P4(3)	2.55	1.78	1.20	95	5	35	57	95	5	≈ 8g, Shock	Metal
P5(1)	1.40			-	85					≈ 8g, Shock	Plastic
P5(2)	1.35			10	80						
56 DAY COATED & PULL-OFF TESTED: 'HIGH W/C' CONCRETE (W/C = 0.80)											
P4(1)	2.50	2.53	0.30	100	-	65	35	98	2	≈ 8g, Shock	Metal
P4(2)	2.70			95	5						
P4(5)	2.40			-	100						

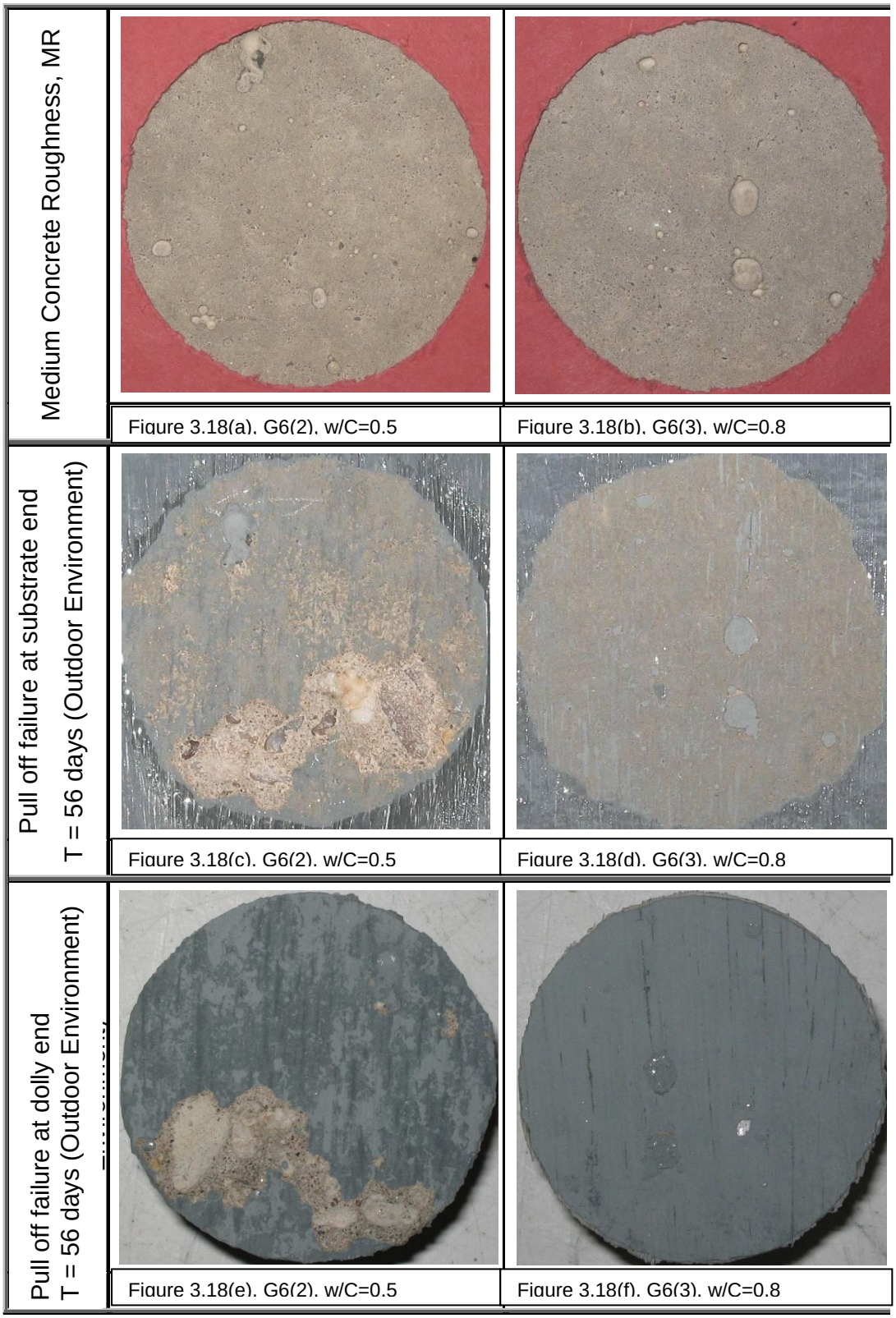

Figure 3.18: Variation in observed pull-off failures to medium substrate roughness 'low w/c' (left) and 'high w/c' concretes (right) when placed, up to 56 days, in a TCR (temperature control room environment) and subject to daily wetting

With reference to Table 3.6, 56 day coated and pull-off tested ‘low w/c’ concrete cubes G4 and G5 gave, on almost every occasion, pull-off values greater than the adhesion tester limit of 3.50MPa and as a result the range in results was essentially near zero for both G4 and G5 cubes. However, variation in area of fracture results was observed to G4 [Figure 3.18 (a), 3.18(c) & 3.18(e)] where the amount of failure occurring within the concrete (A) was 80% for surface 1, 90% for surface 2 and for surface 5 was only 10% which is in contrast to surfaces 1 and 2. Even though surface 5 exhibited a small amount of failure within the concrete this did not negatively impact the pull-off failure stress, however, when the area of fracture for inter-coat (B/C) type failure approaches, or is close to, 100% then there exists the potential to attain a lower pull-off value. The reason for this difference is because substrate number 5 was the base face (face resting on the vibrating table) and the weak laitance layer is likely to be thin since the base face may experience the effects of compaction at a lesser extent compared to the sides. Consequently it is more difficult to produce a suitable roughness by hand using a wire brush.

Unfortunately, cube G6, surface 3 [Figure 3.19 (b), 3.18(d) & 3.18(f)] illustrated a pure 100% inter-coat (B/C) failure which did have a negative impact upon the pull-off failure stress by yielding a lower pull-off value of 2.20MPa. On the left of Figure 3.19 shows surface 2 for the same cube (G6) which, in comparison to surface 3 of G6, pulled out a small percentage of concrete (20%) and as a result gave a pull-off value greater than 3.50MPa. Unlike, G4 and G5, cube G6 gave a range of 1.30MPa in pull-off values which is quite similar to the range in results for immediately coated and pull-off tested samples (1.10MPa).

With regards to ‘high w/c’ concrete cube P4, variation was observed to the area of fracture results [Figure 3.18 (b), 3.18(d) & 3.18(f)], which were very much similar to G4, where the amount of failure occurring within the concrete (A) was 100% for surface 1, 95% for surface 2 and for surface 5 was 0% (B/C = 100%) which is in contrast to surfaces 1 and 2. Just like G4 surface 5, P4 surface 5 was also a base face, compacted to the same level and cast in a metal mould as shown in Table 3.6. Even though surface 5 exhibited a pure 100% inter-coat (B/C) failure this did not have a huge impact upon the pull-off failure stress since surface 5 gave a value of 2.40MPa with the highest pull-off value being 2.70MPa for surface 2

giving a modest range of 0.30MPa. This is quite similar to ‘low w/c’ cube G4 which gave a range of 0MPa however, a higher range in pull-off values is to be expected from ‘high w/c’ concrete mix designs such as P4.

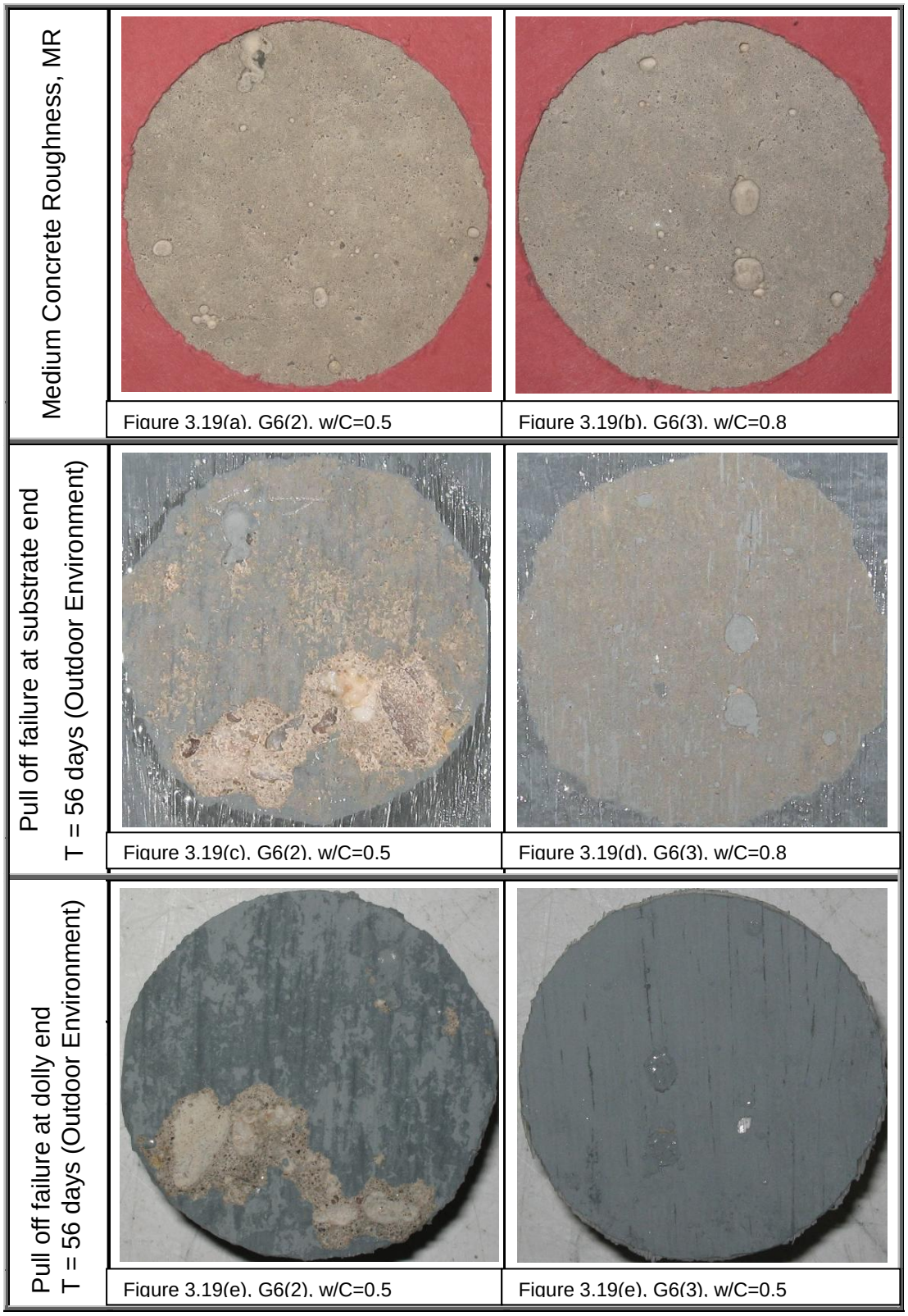

Figure 3.19: Variation in observed pull-off failures to medium substrate roughness to 'low w/c' cube G6 surface 2 (left) & surface 3 (right) when placed, up to 56 days, in an outdoor environment

Observational & Numerical Comparison: Concrete Strengthening

An additional result column, called ‘adjusted average area of fracture (%), is included in Table 3.6 , created an additional results column called ‘adjusted average area of fracture (%)’ is included, which basically discards an inter-coat (B/C) type failure observed to be greater than 80% or only considers a significant amount of failure occurring within the concrete (A) say at least 40%. The intention here is to help develop a simplified model which ignores variation in results. It can be seen from this column that, for ‘low w/c’ and ‘high w/c’ concretes the increase in the amount of failure occurring within the concrete (A) since initially coated and pull-off tested and then after 56 days being coated and pull-off tested is 103% and 3% respectively. Likewise the pull-off stress values, by ignoring variations, for immediately coated and pull-off tested to ‘low w/c’ and ‘high w/c’ concretes the average values are (3.4+3.15+3.5)/3 = 3.35MPa and 2.55MPa respectively. For 56 day coated and pull-off tested cubes the averages, again for ‘low w/c’ and ‘high w/c’ concretes are 3.50MPa and (2.5+2.7)/2 = 2.60MPa respectively. Hence, the increase in pull-off stress values since initially coated and pull-off tested and then after 56 days being coated and pull-off tested is 4.5% and 2% to ‘low w/c’ and ‘high w/c’ concretes respectively. These results are in agreement with the literature review Section regarding concrete strengthening since the observed increase in average pull-off stress and adjusted area of fracture results is more noticeable to ‘low w/c’’ concretes then to ‘high w/c’’ concretes. However, because of the amount of variation seen, further research is required to help improve data correlation.

Influence of Compaction & Type of Mould to Retrieved Pull-Off Results

According to Table 3.6, the retrieved pull-off failure results seem to be influenced by the different levels of compaction and the type of mould used during the concreting process. To help understand and compare these effects the data presented in Table 3.4 has been rearranged and are given in Table 3.7 which has a few additional columns at the end. To help analyse data the author has colour coded pull-off failure stress values and the observed area of fracture results as well as prescribed a pass and failure criteria. Note the word failure described here does not necessary mean that the retrieved pull-off failure results should be discarded but to highlight cases where individual pull-off failure stress values

and/or observed area of fracture results have deviated or introduced variation which can have a potential negative effect upon pull-off results.

Table 3.7: Influence of compaction and mould type to pull-off results (MR prepared cubes)

Cube (face)	*σ (MPa)*		*Area of Fracture (%)*		*Mode of Compaction (m/s²)*	*Mould Type*	*Pass Criteria (σ & Area of Fracture)*	*Pass Criteria (σ alone)*
	Each	Mean	A	B/C				
IMMEDIATELY COATED & PULL-OFF TESTED -'LOW W/C' CONCRETES (W/C = 0.50)								
G4(3)	3.40	3.11	45	55	≈ 8g, Shock	Metal	☑	
G5(4)	3.15		40	60	≈ 8g, Shock	Plastic	☑	
G6(4)	3.50		40	60	4-7g	Plastic	☑	
G7(1)	2.40		5	95	4-7g	Metal	☒	
56 DAY COATED & PULL-OFF TESTED – 'LOW W/C' CONCRETES (W/C = 0.50)								
G4(1)	3.50	3.50	80	20	≈ 8g, Shock	Metal	☑	
G4(2)	3.50		90	10			☑	
G4(5)	3.50		10	90			☒	☑
G5(1)	3.50	3.48	5	95	≈ 8g, Shock	Plastic	☒	☑
G5(2)	3.50		-	100			☒	☑
G5(3)	3.45		-	100			☒	☑
G6(1)	3.50	3.07	5	95	4-7g	Plastic	☒	☑
G6(2)	3.50		20	70			☒	☑
G6(3)	2.20		-	100			☒	
IMMEDIATELY COATED & PULL-OFF TESTED - 'HIGH W/C' CONCRETES (W/C = 0.80)								
P4(3)	2.55	1.78	95	5	≈ 8g, Shock	Metal	☑	
P5(1)	1.40		-	85	≈ 8g, Shock	Plastic	☒	
P5(2)	1.35		10	80			☒	
56 DAY COATED & PULL-OFF TESTED – 'HIGH W/C' CONCRETES (W/C = 0.80)								
P4(1)	2.50	2.53	100	-	≈ 8g, Shock	Metal	☑	
P4(2)	2.70		95	5			☑	
P4(5)	2.40		-	100			☒	☑

[Key: blue coloured text / tick symbol = pass, red coloured text / cross symbol = fail]

To further help distinguish the influence of compaction and type of mould to retrieved pull-off failure results the author has created Table 3.8 which is a simplified version of Table 3.7 by rearranging and mixing short term and medium term data. It can be seen from Table 3.8 that the mode of compaction and type of

mould has four distinct categories, starting at the top of Table 3.8 and then moving towards the base gives (i) ≈ 8g, shock & metal mould, (ii) ≈ 8g, shock & plastic mould, (iii) 4-7g & metal mould and (iv) 4-7g & plastic mould. The data in Table 3.8 has been arranged to indicate the potential likelihood of variation to pull-off failure stress results and the observed area of fracture results where towards the base of Table 3.8 the likelihood of variation is high compared to the top of Table 3.8.

Table 3.8: Slightly altered and rearranged version of Table 3.7

Cube (face)	σ (MPa)	Area of Fracture (%)		Mode of Compaction (m/s^2)	Mould Type	Possible Trend in Retrieved Pull-Off Failure Results
		A	B/C			
G4(1)	3.50	80	20	≈ 8g, Shock	Metal	Increasing likelihood / potential to negatively impact retrieved pull-off stress results ↓ Increasing possibility to observe a greater inter-coat type failure (B/C)
G4(2)	3.50	90	10			
G4(3)	3.40	45	55			
G4(5)	3.50	10	90			
P4(1)	2.50	100	-	≈ 8g, Shock	Metal	
P4(2)	2.70	95	5			
P4(3)	2.55	95	5			
P4(5)	2.40	-	100			
G5(4)	3.15	40	60	≈ 8g, Shock	Plastic	
G5(1)	3.50	5	95	≈ 8g, Shock	Plastic	
G5(2)	3.50	-	100			
G5(3)	3.45	-	100			
P5(1)	1.40	-	85	≈ 8g, Shock	Plastic	
P5(2)	1.35	10	80			
G7(1)	2.40	5	95	4-7g	Metal	
G6(4)	3.50	40	60	4-7g	Plastic	
G6(1)	3.50	5	95			
G6(2)	3.50	20	70			
G6(3)	2.20	-	100			

[Key: blue coloured text = pass, red coloured text = fail]

The pass criteria illustrated in Tables 3.7 and 3.8 is described here as the individual pull-off failure stresses and/or observed area of fracture results per surface which do not vary significantly when tested at the same time and for a particular cube. The general description, with regards to the pass criteria, and the four distinct categories mentioned above is as follows:

(i) ≈ 8g, shock & metal mould: Total surfaces 8. Pass rate = 6/8 = 75%

Even though G4(5) and P4(5) were base surfaces which gave almost 100% inter-coat (B/C) failure the retrieved pull-off failure stress values were similar to its adjacent cube surfaces.
However, if the 2 base surfaces are omitted then this becomes a 100% pass rate.

(ii) ≈ 8g, shock & plastic mould: Total surfaces 1. Pass rate = 0/1 = 0%

This set up gave a lower bound pull-off failure stress indicating an almost 100% B/C failure; hence, a 100% failure rate is assigned, however, further data is needed to reinforce this viewpoint.

(iii) 4-7g & metal mould: Total surfaces 6. Pass rate = 1/6 = 17%

Only one result was shown to satisfy both conditions and this occurred for a 'low w/c' concrete mix design. 4 out of 6 surfaces belonged to 'low w/c' concrete mix designs, where, as mentioned above, only 1 surface satisfied both conditions. However, for the other 3 'low w/c' concrete surfaces, even though an almost 100% B/C failure was observed this did not effect the pull-off failure stress results which was an upper bound value and did not vary significantly. On the other hand, with regards to 'high w/c' concrete surfaces, (2 out of 6 faces) the observed area fracture results showed an almost 100% B/C failure and as a result gave a lower bound pull-off failure stress results when compared to a similar vibrated cube but in a metal mould.

(iv) 4-7g & plastic mould: Total surfaces 4. Pass rate = 1/4 = 25%

A pass a rate of 25% where only one result was shown to satisfy both conditions and this occurred for a 'low w/c' concrete mix design. Even though 2 'low w/c' concrete surfaces gave an almost 100% observed B/C failure this did not effect the pull-off failure stress results which was an upper bound value and did not vary significantly. However, one surface yielded a 100% B/C failure and as a result a lower bound failure stress was obtained introducing variation in results.

Judging by the table of results and the comments made above, the type of mould and level of compaction seems to have an influence in terms of both the pull-off failure results as well as the observed area of fracture results and this effect seems to be greater for 'high w/c' concrete mix designs than for 'low w/c'

concretes. However, further experimental research is required to improve data correlation.

Comparison with Thermal Sprayed Zinc

With reference to the literature review Section, case studies, the following information given is a summarised version of pull-off adhesion strength data between thermal sprayed zinc coatings and concrete substrates for the various stated authors:

- **LEGOUX & DALLAIRE (1995)**

Immediately coated and pull-off tested (no impressed current):

For surfaces roughnessess (RMS) between 0.108mm and 0.030 mm the corresponding pull-off strengths were between 2.25MPa and 1.84MPa respectively (provided the presence of no large aggregate within the immediate test vicinity). However, a lower surface roughness (RMS) of 0.015mm yielded a pull-off strength value of 0.87MPa where a large aggregate was observed.

- **BROUSSEAU, ARNOTT & BALDOCK (1996)**

Coating allowed to age naturally (no impressed current):

Average pull-off failure stresses between the ranges of 2.25MPa to 2.75MPa from 0 to 120 days from application were found. However other, impressed current related tests had shown that the average pull-off stress values were initially approximately 3.5MPa at zero time and at approximately 175 days the average pull-off stress peaked at 3.75MPa under the influence of no current density.

Under the influence of freeze thaw cycling:

Initial average pull-off stress values were approximately 3.0MPa at O cycles and then at 0 to 70 cycles were averaging between approximately 4.0MPa to 2.8MPa.

- **COVINO, et al (2002)**

Coating allowed to age naturally (no impressed current):

Average pull-off failure stresses were initially 1.72MPa and then after being coated for 114 days the average pull-off failure stress was 2.32MPa.

Under the influence of impressed current:

Under the influence of impressed current and frequent water spraying the coated slabs gave a peak pull-off stress value averaging at approximately 3.50MPa at 400kC/m^2.

The literature review test data for the bond strength shown above is fairly similar to the experimental pull-off data for ZRP coated to ‘‘low w/c’’ concrete substrates under the influence of natural ageing. Experimental data for immediately ZRP coated and pull-off tested ‘low w/c’ concretes was on average 3.11MPa. On the other hand, 56 day ZRP coated and pull-off tested ‘low w/c’ concretes gave on average an approximate stress failure of 3.50MPa.

Any comparison between experimental pull-off test data retrieved for ZRP coated concrete substrates and the literature review information shown above for thermal sprayed zinc coatings is difficult and not accurate. This is primarily because, as a stated in the literature review by CIRIA (1993), a consistent approach is needed in sample preparation including any possible natural/electrochemical ageing influence, testing equipment, assessment criteria and accuracy to ensure a proper comparison between the two different material compositions and application techniques. Therefore, experimental ZRP pull-off data and the, as shown, variable pull-off data to thermal sprayed zinc coatings cannot be used to compare against each other, and if the presence of the 4% binder within the dry ZRP film coating actually contributes towards better concrete substrate adhesion could not be confirmed.

Detailed study of the interactions occurring at the ZRP coating / concrete interface regarding the physical, chemical and electrochemical characteristics were outside the scope of the present investigation. However, considerable amount of technical information is available in the literature for the interfacial chemical and electrochemical reactions at the TS zinc coating and concrete. These are considered to be similar to that are identified by the studies carried out in the US and Canada, for the TS zinc / concrete interface, Covino, B. S. et al. (March 2002)., and when zinc is used as anode for CP system (either the galvanic mode or ICCP mode) the reaction steps are:

Step 1: $Zn \rightarrow Zn^{2+} + 2e^{-}$ (3.1)

Step 2: $Zn^{2+} + 2\ H_2O \rightarrow Zn\ (OH)_2 + H_2$ (3.2)

Step 3: $Zn\ (OH)_2 \rightarrow ZnO + H_2O$ (3.3)

At the cathode (i.e. rebar), the usual reaction is:

$O_2 + 2\ H_2O + 4e^- \rightarrow 4OH^-$ (3.4)

The above anodic reactions lead to the formation of zinc minerals such as zinc oxide (ZnO)/$Zn(OH)_2$ followed by 'secondary' mineralisation when combines with other constituents of the environment such as chloride, sulphate or carbonate ions, or minerals in the cement paste to form complex minerals (such as, zinc hydroxycarbonate, zinc hydroxychloride, zinc hydroxysulphate, etc.). With the passage of time the more stable of these minerals will predominate over the less stable minerals in 'Zn oxide layer' which is likely to precipitate at the anode (zinc)-concrete interface. The zinc corrosion products, particularly the zincoxychloride and zincoxysulphate are formed by electro-migration of chloride and sulphate ions from within the concrete to the anode. Covino, B. S. et al. (March 2002). Further, as zinc ions migrate into concrete a reaction 'zone' is developed in the cement paste with zinc replacing Ca and forming a (Ca, Zn)-aluminosilicate. All these may affect the bond strength of the zinc coating leading to premature failure of the anode. However, as discussed in the next section, the results obtained after 40 cycles of accelerated testing in an 'Environmental Chamber' with applied CP current density of 440mA/m^2 (which is 4 times the current density applied to anode recommended in NACE Standard or 200 times the current density used in Oregon DOT Specification) showed some increase in bond strength.

3.3.2 SEM Examination of ZRP/concrete Interface

It has been postulated that the interfacial bond between ZRP and concrete substrate is physico-chemical, rather than the 'pure' mechanical as is the case, according to Covino et. at., (2002) and others. This is reasoned as the ZRP is applied in a liquid form and solidifies on the concrete surface by solvent

evaporation. In order to confirm this hypothesis, pieces of ZRP coated concrete samples, cut out from the test blocks at the end of experimentations. These test specimens were subjected 40 cycles of accelerated 'weathering' in an Environmental Chamber with sustained application of cathodic protection at a constant current of 10 mA. This was an exploratory examination under Scanning Electron Microscope (SEM) to take a few photomicrographs and to compare these with the SEM photomicrographs of the TS zinc obtained by Covino et al., (2002). The SEM examination was undertaken using Low Vacuum mode on a JOEL 6060 LV scanning electron microscope, as shown in Figure 3.20.

Figure 3.20: General view of the SEM, model JOEL 6060

The specimens for the SEM examination were shown in Figure 3.21, labelled as A, B, and C (A: No chloride, B and C: 1% and 3% chloride in the concrete mixes respectively).

Figure 3.21: A view of the ZRP coated samples for SEM examination

Figures 3.22 - 3.27 give SEM photomicrographs of ZRP specimens after environmental testing (40 cycles of electrochemical aging) and Figures 3.28 and 3.29 show examples of TS zinc before and after 'aging'.

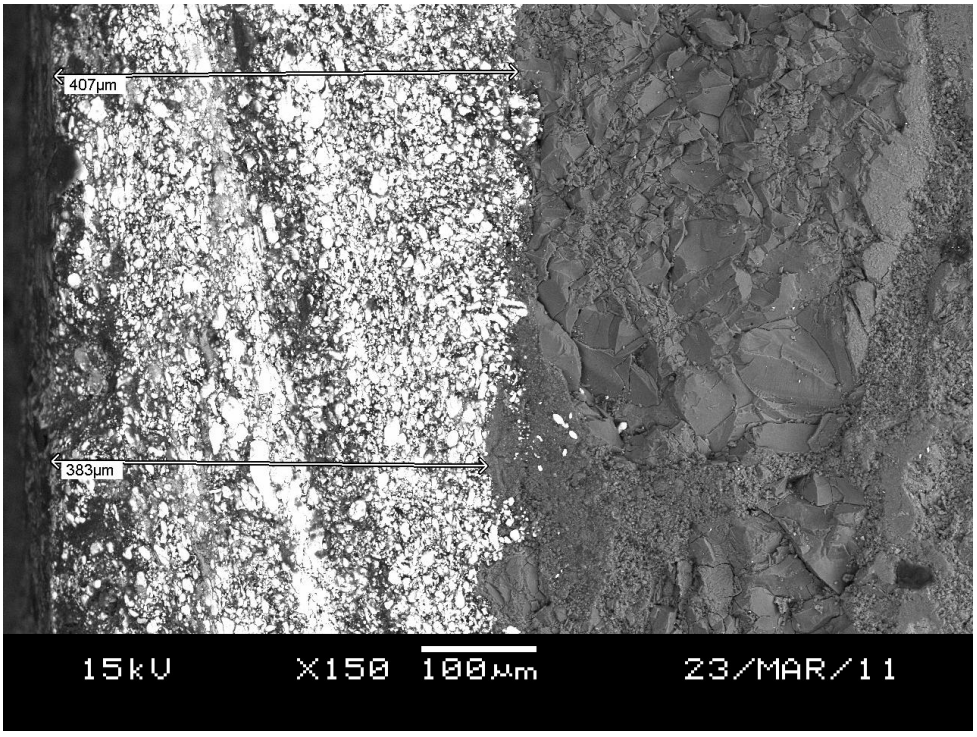

Figure 3.22: SEM Photomicrograph of ZRP Specimen – sample A

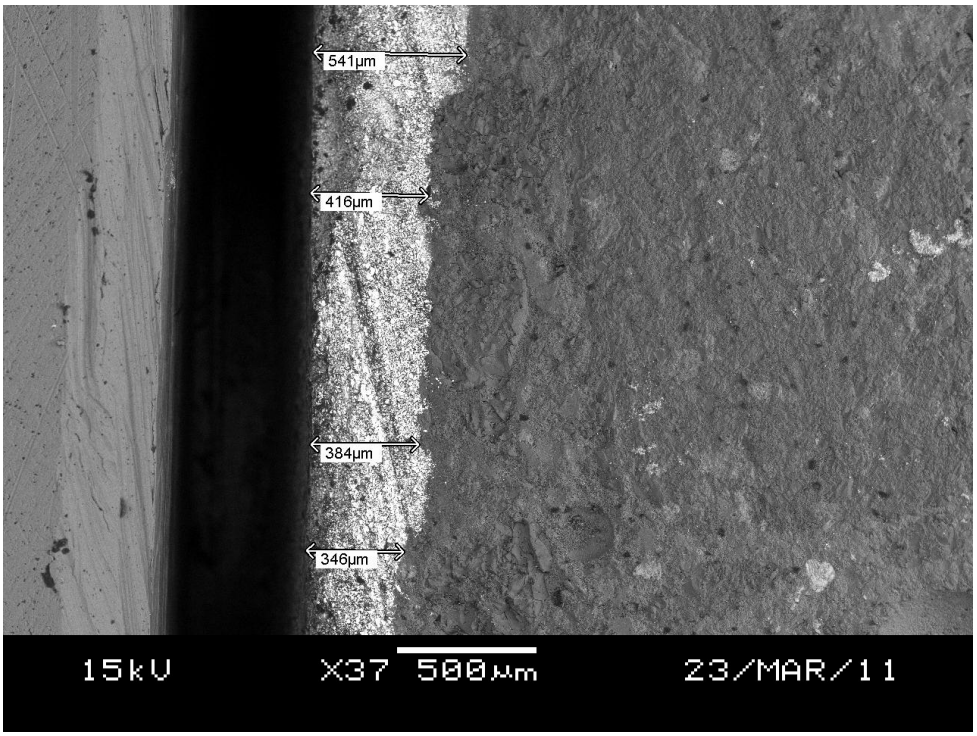

Figure 3.23: SEM Photomicrograph of ZRP Specimen – sample A

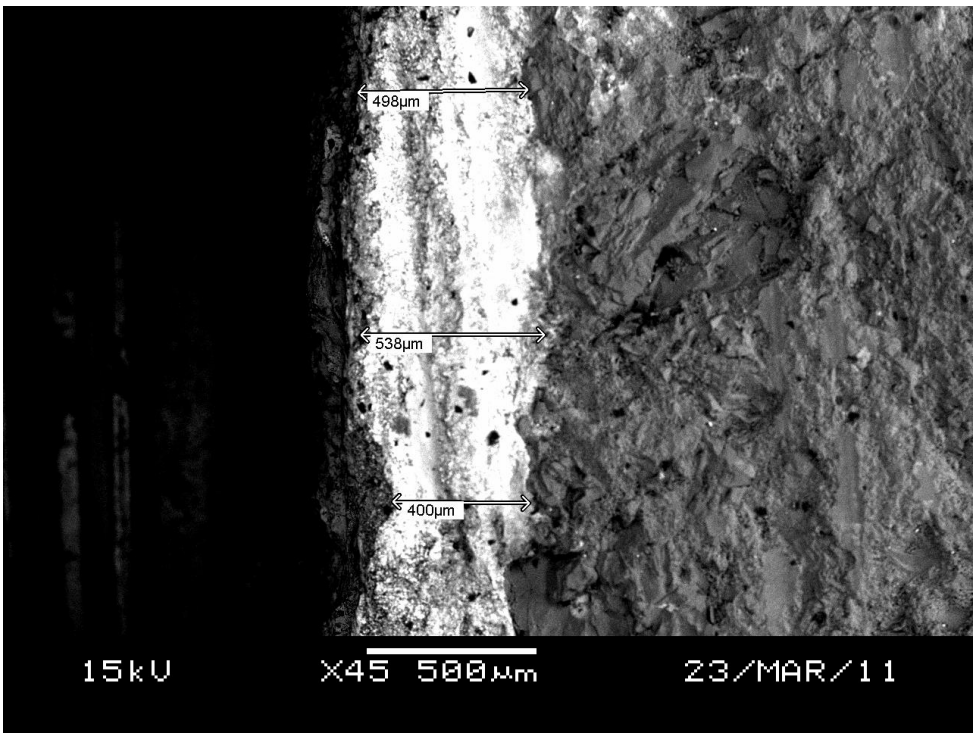

Figure 3.24: SEM Photomicrograph of ZRP Specimen – sample B

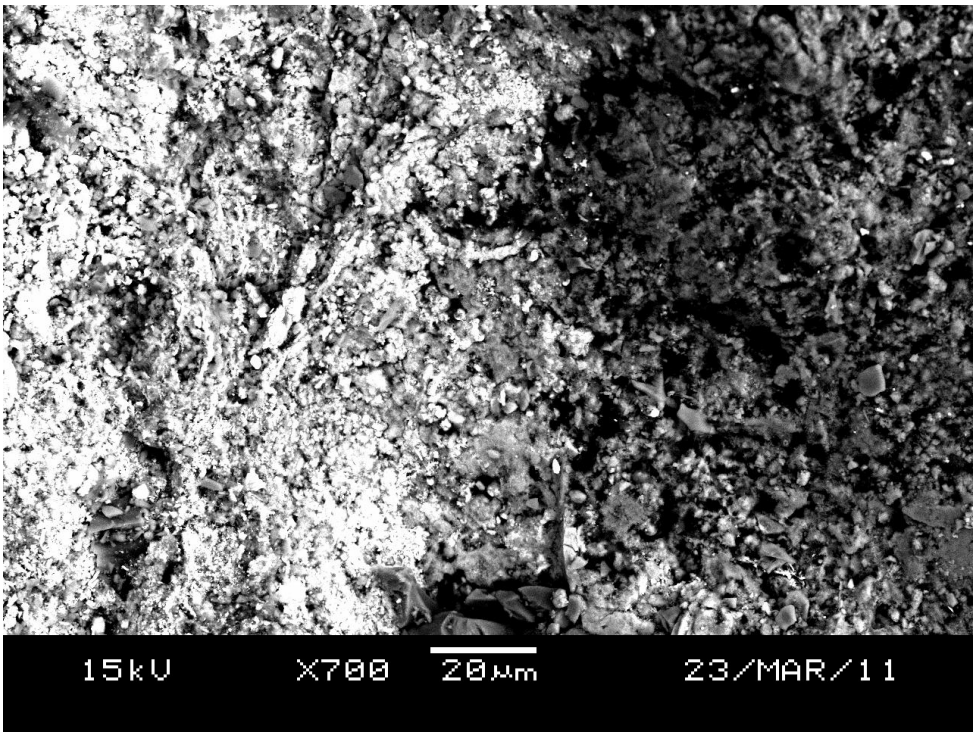

Figure 3.25: SEM Photomicrograph of ZRP Specimen – sample B

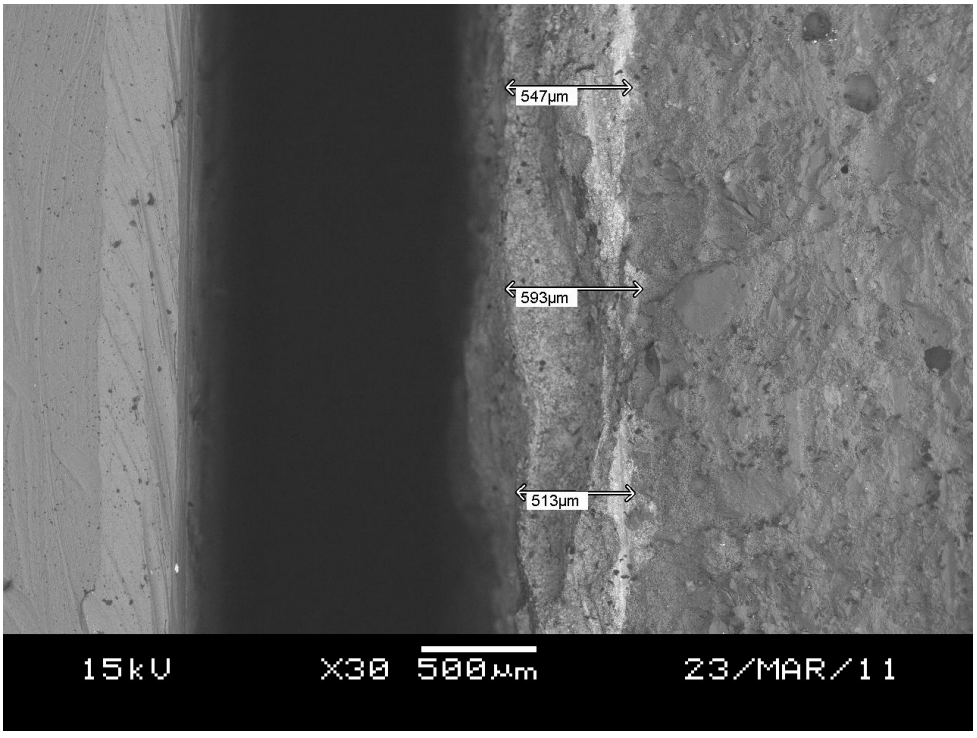

Figure 3.26: SEM Photomicrograph of ZRP Specimen – sample B

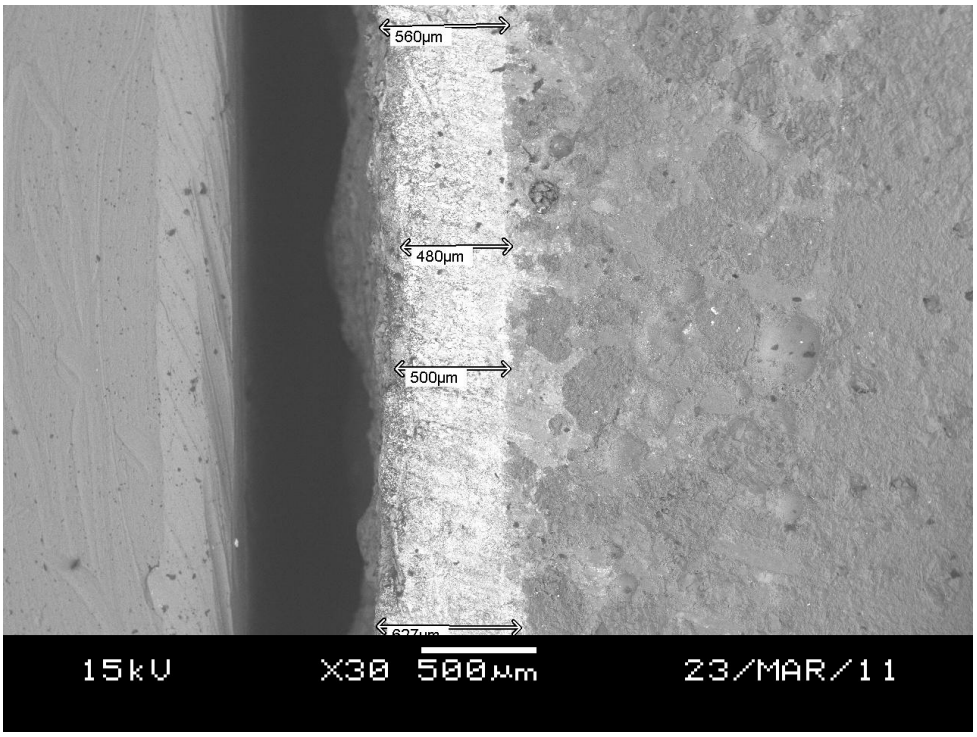

Figure 3.27: SEM Photomicrograph of ZRP Specimen – sample C

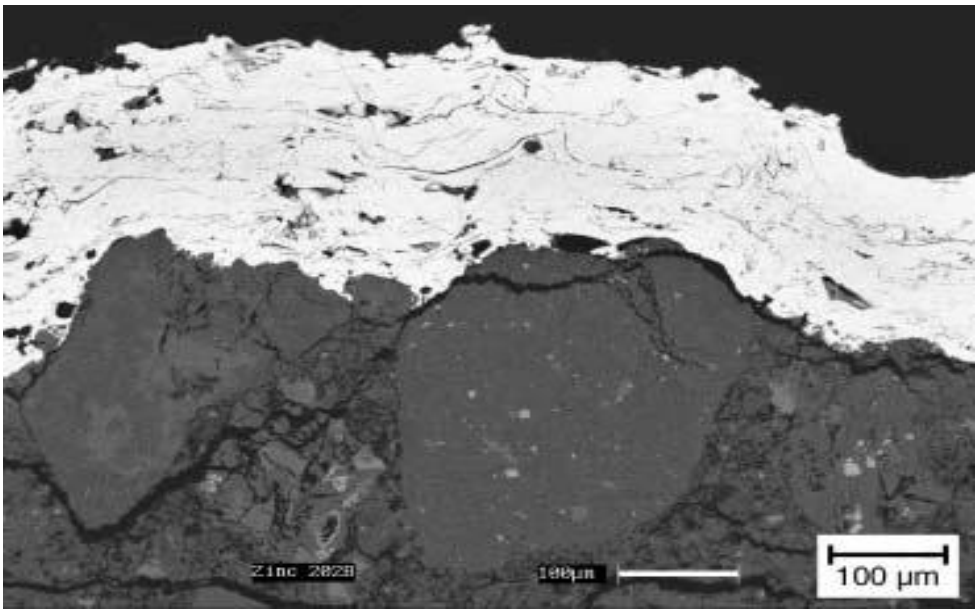

Figure 3.28: SEM photomicrograph of cross-section showing unaged TS Zn anode microstructure and anode-concrete interface for anode on concrete

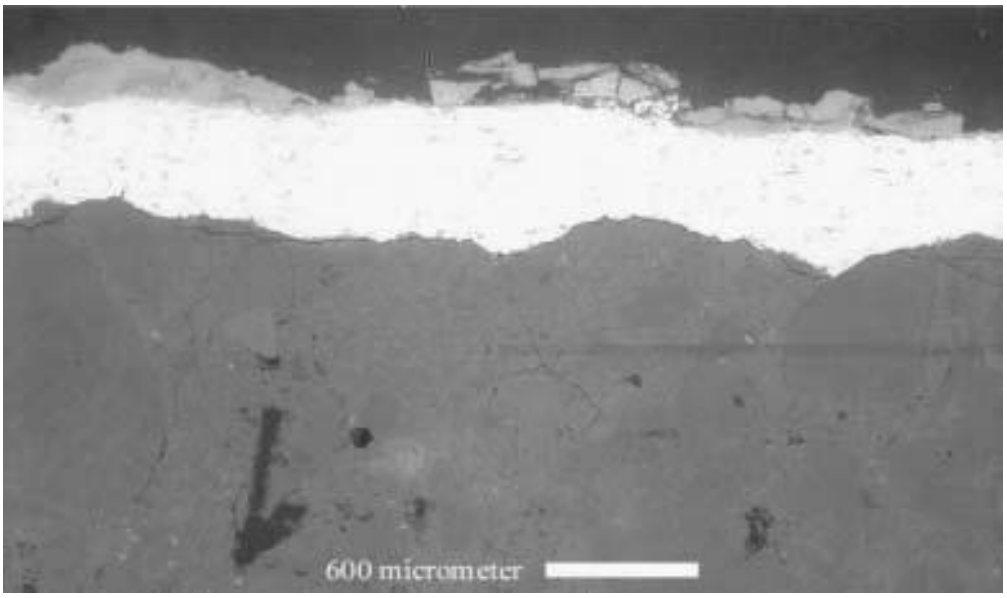

Figure 3.29: SEM photomicrograph of TS Zn anode-concrete interface for the Richmond-San Rafael Bridge SACP zone on the barrel of the south column aged ~ 700 kC/m2 or ~ 10 years' service.

The contra-distinctions between the two sets of SEM photomicrographs were not very apparent, however a closer examination suggests that the ZRP has definitely penetrated deep into concrete matrix. Further SEM analysis including microanalysis (possibly using SEM micro-probe analyser and also other techniques such as petrography, analytical chemical procedures) would be necessary to identify the interfacial chemistry of the ZRP and the concrete constituents. This is to confirm if the postulation that the bond characteristics of ZRP and concrete are a combination of both physical and chemical is correct.

3.3.3 Assessment of Electrical (Electronic) Properties

One of the most essential parameters for a conductive coating (e.g. zinc paint) to act as an anode is to exhibit good electronic conduction across the film in order that impressed current can be distributed. The test procedure developed (by the author) to assess this factor had two aspects:

1) Number of coating applications to obtain an optimum low resistance.
2) Influence of concrete surface condition on electronic resistance.

The property of the coating that was measured to make this assessment was the "cross-film" resistance.

3.3.4 Theory: Cross-Film Resistance Measurement

The cross-film resistance of an electrically conductive coating is expressed by a unit defined as "resistance (ohm) per square".

The resistance of a coating layer is given by

$$R = \rho l/A \qquad (3.5)$$

Where:

R = electrical resistance (ohm)

ρ = bulk resistivity (ohm cm)

l = length of layer (cm)

A = cross sectional area of the layer (cm^2)

For a film of breadth, b, and thickness, t, with current passing between two opposite edges of the film separated by a distance 1, the formula becomes:

$$R = bt \qquad (3.6)$$

and if l = b i. e . a square, then:

$$\rho = Rt \qquad (3.7)$$

This is independent of the size of the square. However, it should be noted that the resistivity of material can be calculated from the 'square' resistance (ohm per square) and the film thickness (i.e. ρ = R.t)

Equation 3.5 also shows that the 'cross film' resistance will, for a given bulk resistivity, be inversely proportional to the coating thickness. Thus it is expected

that the resistance of a coating will tend to be an optimal low when increasing the number of applied coatings.

3.3.5 Cross-film Resistance vs. No. of Coating.

Test Procedure:
Detailed description of the investigation methodology are given in Appendix 'B' and briefly summarised below.

The number of coats required to obtain an optimum "square" resistance was determined by applying the ZRP coating on to 180mm x 250mm hardboard squares with copper strip contacts along two opposite edges. The coatings were built up by repeated application and their "square" D. C. resistances were measured after each application, using a Multi-meter, until the resistance showed little change with further coating applications.

3.3.6 'Cross-film' resistance vs. No. of Coats – Results and Discussion

The results of the 'cross-film' resistance experiments to determine the number of coatings required to achieve an resistance are given in Table 3.9 and are graphically presented in Figures 3.30 – 3.35. The results are mathematically assessed to determine the trend, using the statistical method of 'R^2' factor as shown in Figures 3.31, 3.32, 3.34 and 3.35. In summary the results indicated that the optimum low 'cross-film' resistance is achieve with coats.

Table 3.9: Determination of coating thickness to hardboard samples using a digital calliper.

	Average Thickness				
	Measuring Position: [top end (t) / bottom end (b)]	HB 1(a) (mm)	HB 1(b) (mm)	HB 2 (mm)	HB 3 (mm)
Coat No.	t (hardboard only) =	5.903	5.927	5.913	5.963
	b (hardboard only) =	5.969	5.881	5.835	5.945
	t (hardboard with tape) =	6.130	6.046	N/A	6.064
	b (hardboard with tape) =	6.062	5.994	N/A	6.087
1	t1 =	6.235	6.113	6.164	6.189
	b1 =	6.164	6.103	6.100	6.176
2	t2 =	6.307	6.206	6.163	6.244
	b2 =	6.188	6.144	6.028	6.204
3	t3 =	6.311	6.241	6.251	6.311
	b3 =	6.228	6.172	6.113	6.223
4	t4 =	N/A	N/A	6.307	6.335
	b4 =	N/A	N/A	6.175	6.300
5	t5 =	6.442	6.343	6.382	6.403
	b5 =	6.316	6.262	6.226	6.349
6	t6 =	N/A	N/A	N/A	6.454
	b6 =	N/A	N/A	N/A	6.401
7	t7 =	N/A	N/A	N/A	6.531
	b7 =	N/A	N/A	N/A	6.501
8	t8 =	N/A	N/A	N/A	6.598
	b8 =	N/A	N/A	N/A	6.504
9	t9 =	N/A	N/A	N/A	6.654
	b9 =	N/A	N/A	N/A	6.609
10	t10 =	N/A	N/A	N/A	6.702
	b10 =	N/A	N/A	N/A	6.603
t: coat no. 5/10 (without tape) =		6.208	6.244	6.283	6.612
b: coat no. 5/10 (without tape) =		6.237	6.156	6.109	6.517
t: overall paint thickness =		0.305	0.317	0.370	0.649
b: overall paint thickness =		0.268	0.275	0.274	0.571
Measured Coating Thickness (µm) =		286	296	322	610
Coating Thickness by mass (µm) =					
Theoretical Coating Thickness (µm) **=**		300			600
% Diff. of mass vs theoretical thickness					
% Diff. of measured vs theoretical thickness		4.7%	1.33%	7.33%	1.64%

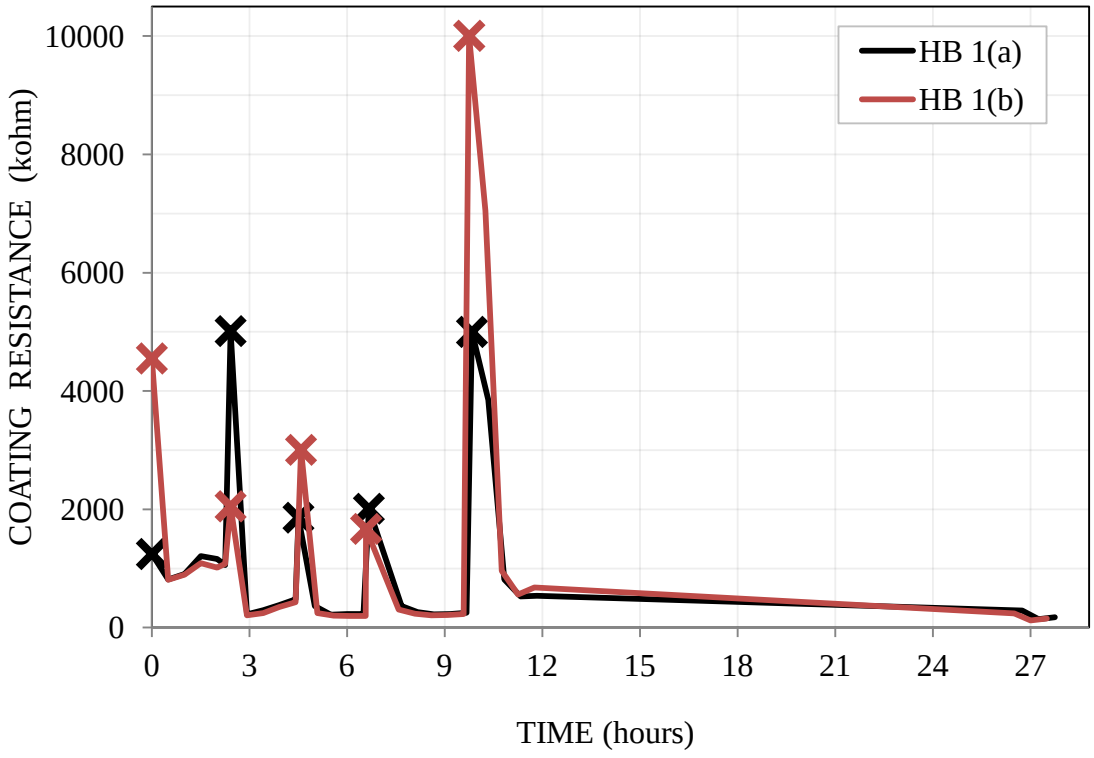

Figure 3.30: Short term graph of coating resistance (kΩ) against time (hrs) for HB 1

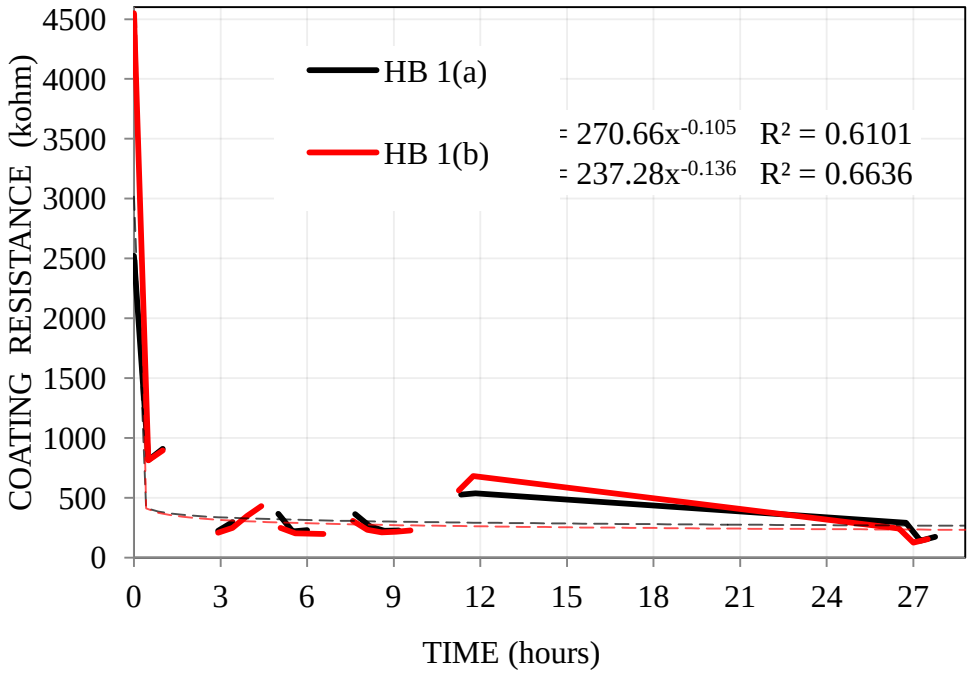

Figure 3.31: Modified and adjusted version of Figure 3.30 above

KEY:	**HB 1(a) & HB 1(b): ≈ 2 – 3hrs drying in an outdoor environment**

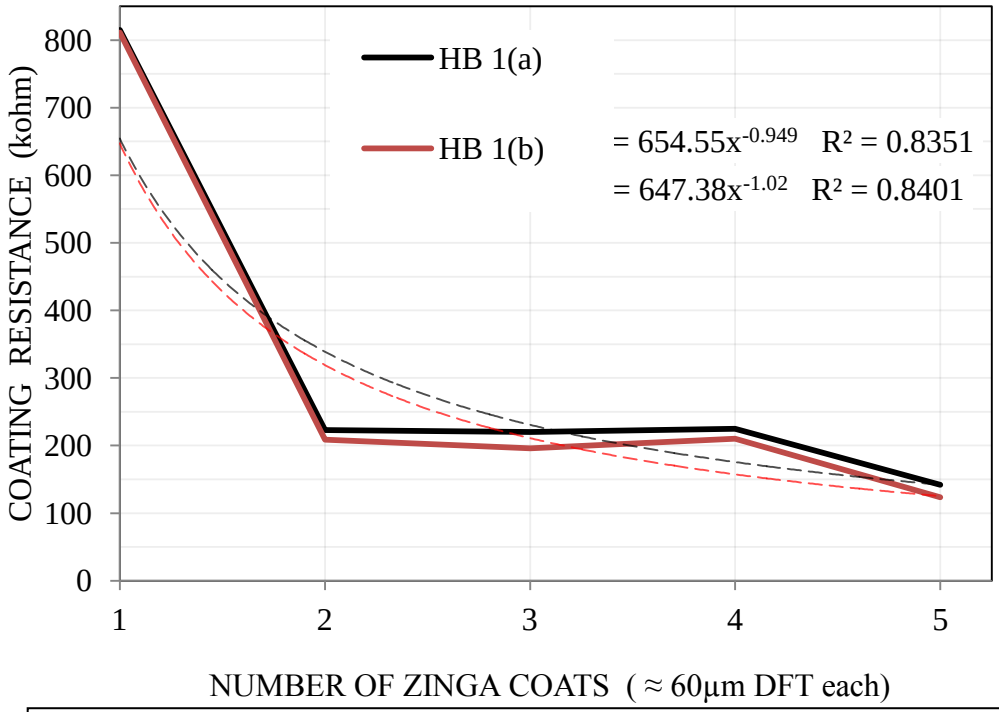

KEY: HB 1(a) & HB 1(b): ≈ 2 – 3hrs drying in an outdoor environment

Figure 3.32: Short term graph of resistance (kΩ) against no. of Zinga coats for HB 1

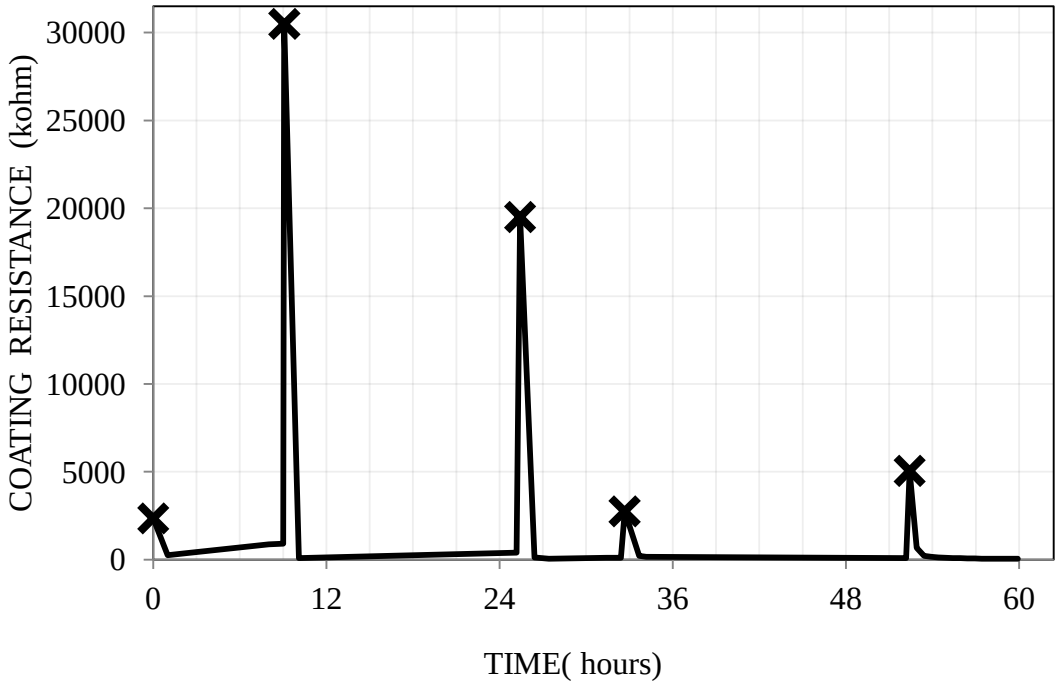

KEY: HB 2: Variable drying time within an outdoor/indoor environment

Figure 3.33 (on previous page): Short term graph of coating resistance (kΩ) against time (hrs) for HB 2

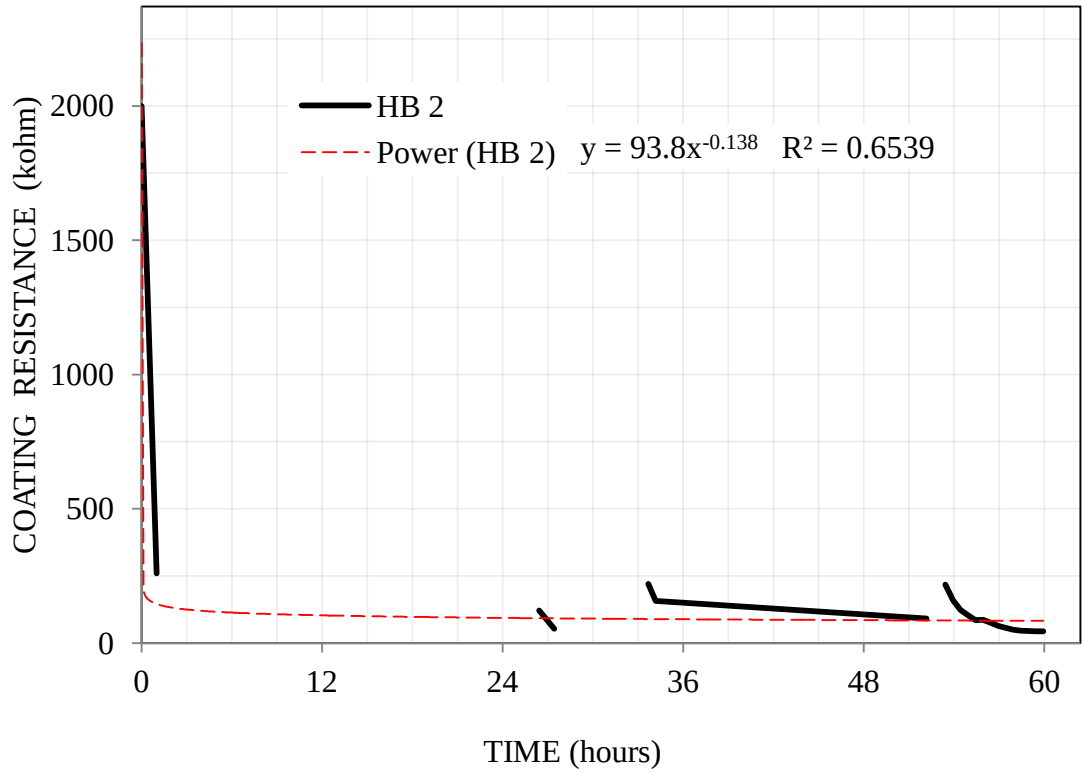

Figure 3.34: Modified and adjusted version of Figure 3.33 above

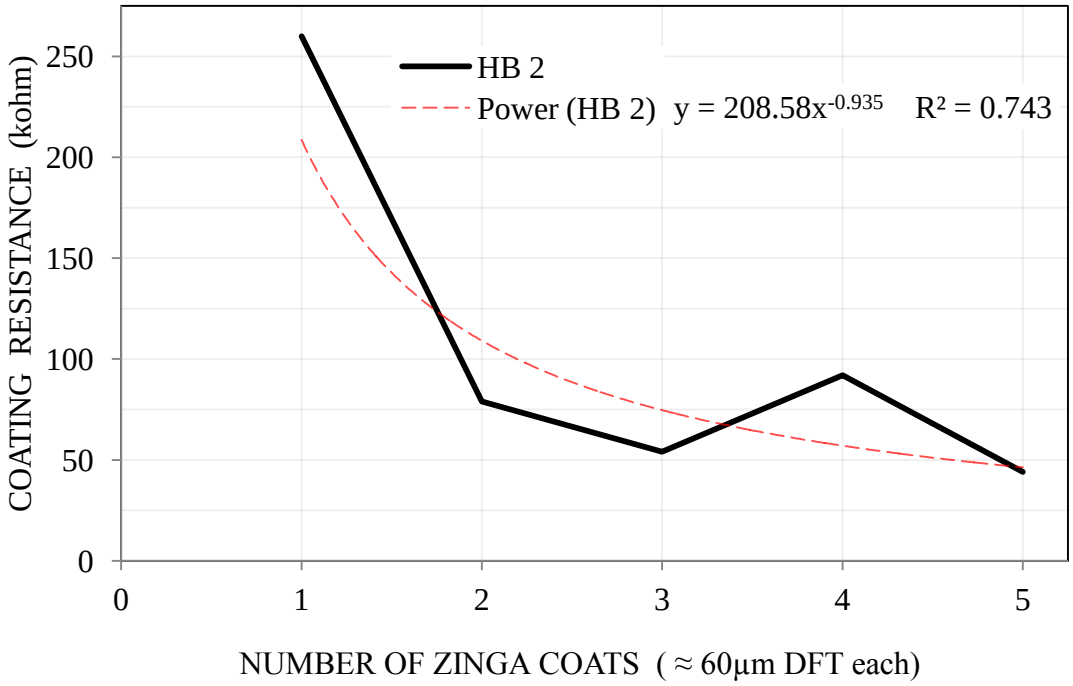

Figure 3.35: Short term graph of resistance (kΩ) against no. of Zinga coats for HB 2

3.4 Electrochemical Property Testing

To test the electrochemical properties of the ZRP coating two sets of Experiments were devised. The first, termed the 'paving slab' tests used coated small slabs of concrete to assess both the applied voltage required to pass various levels of CP current ; and the ability of the coating to maintain a sustained current loading . The second set of tests, termed the 'polarization beam' tests utilized a coated concrete beam sample to assess the ability of the coatings to 'throw' the CP current from a 'primary anode' feeder.

3.4.1 The 'Polarisation Beam Tests'

The principal philosophy behind these experiments is to set up "mini" cathodic protection systems utilizing the zinc coating and to assess the following performance parameters:

i) Current "throwability" i .e. the coating's ability to distribute impressed current uniformly to corroding embedded rebar from "primary" anodes.
ii) Polarisation characteristics of coating.
iii) Cathodic polarisation of the rebar by the coating.

Theoretical considerations – 'current throwability'

The distribution of potential in a uniform conductive electrolyte can be described by the Laplace equation:

$$\nabla^2 E = 0; \text{ or } \delta^2 E/\delta x^2 + \delta^2 E/\delta y^2 + \delta^2 E/\delta z^2 = 0 \quad (3.8)$$

Where:

∇^2 is the Laplace operator.

E is the potential at a point defined by x, y, and z.

There are a number of computer models proposed by researchers, e.g. by Munn, R.S. (August 1982); but the solution of this three-dimensional models of CP (both

SACP and ICCP system) applied to structures are not commonly available or used. The main parameters of these calculations are:

- ☑ Resistance drop through the electrolyte,
- ☑ Potential and overpotential at the cathode,
- ☑ Potential and overpotential at the anode

The detailed discussion of mathematical models to predict the potential distribution and current fluxes in neighbourhood of metallic system in the electrolyte (e.g. steel reinforcements in concrete) is outside the scope of the present work. However, in order to assess the ability of the coating to 'throw' a CP current from a 'primary anode' could be made a mathematical relationship between the voltage drop down the coating and the distance from the primary anode (a function of distance) has been derived. It is considered that the coating to supply an even current density to the embedded steel a plot of the cumulative 'down – coating' voltage drop vs a function of distance from the primary anode should produce a straight line. It was calculated that this function should be:

$$f(\text{distance}) = x - x^2 / 2L \qquad (3.9)$$

Where:

X = distance from the primary anode feed,

L = total length of the coated structural element in question.

The theoretical derivation of 'distance factor' to assess current 'throw-ability' from 'down coating voltage drop' readings measured is described as below:

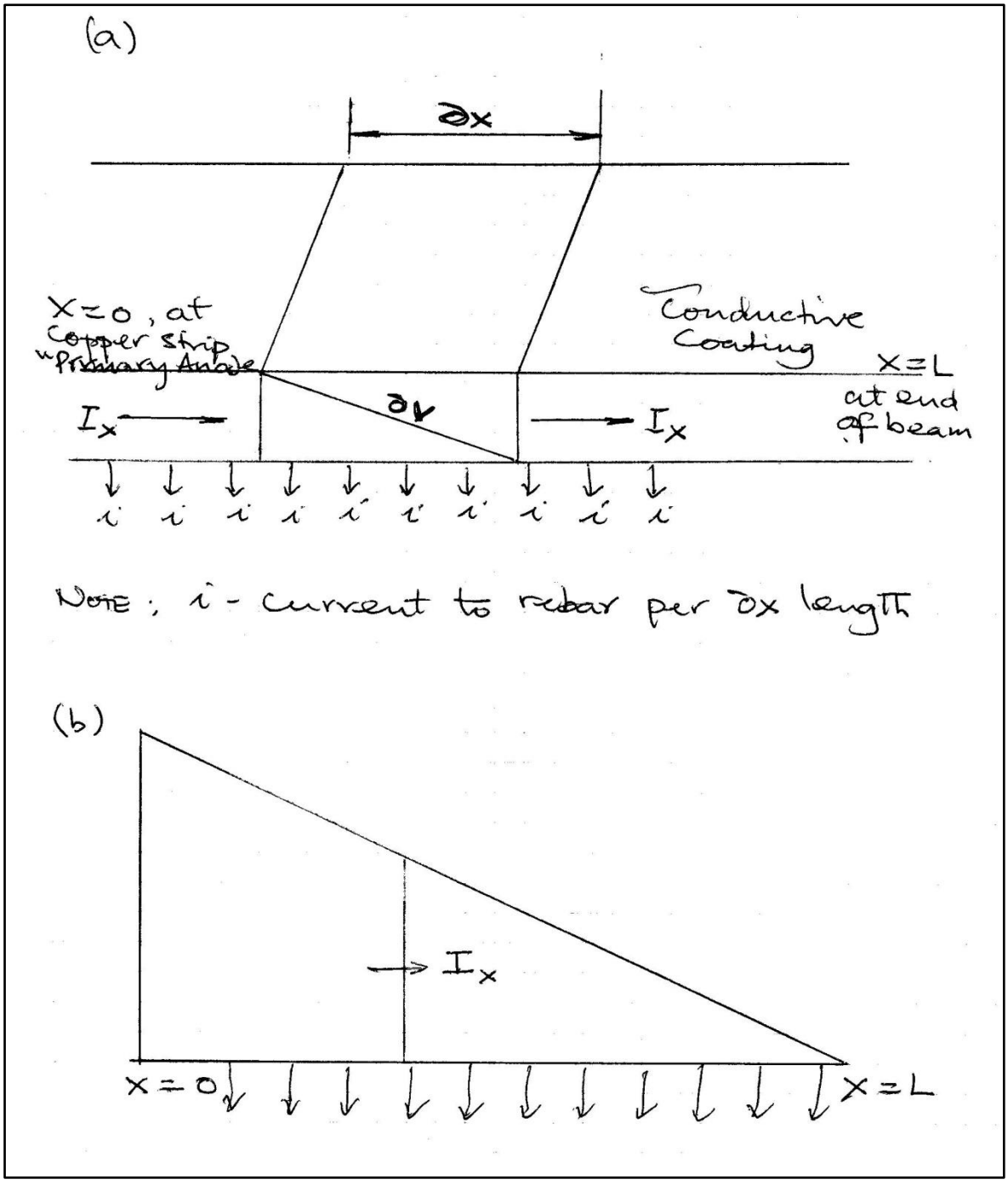

Figure 3.36: Theoretical Model to calculate Current 'throwability'.

Consider the sketches (a) and (b) above, Figure 3.36.

- Assuming an even current spread from the 'primary anode' to end of the coated surface at x =x current passing through the plane is
- Ix = I – xI /L
- I = total current fed to the coating

- If plane at x has a finite but very small thickness,δx (such that over it negligible current passes to the steel reinforcement).
- Then,
- $I_x = V / x.R$
- Putting equations 1) and 2) together
- $I (1 – x / L) = \delta V / \delta x. R$
- In the limiting case where $\delta x \rightarrow 0$, $\delta x \rightarrow dx$, and $IR (1- x / L) = dV/ dx$, or
- $IR (1 – x / L) dx = dV$ (Note - IR is constant).
- Therefore, the voltage drop down the coating is given by;
- $V_{(x)} = IR \int_0^x (1 – x / L) dx$
- $= IR \left[x – x^2 / 2L\right]^x_0$
- Or
- $V_{(x)} = IR (x – x^2 / 2L)$

Thus if R is fairly constant, a plot of voltage drop down the coating i.e. $V_{(x)}$ vs. $[x – x^2 / 2L]$ should give a straight line if the current is being evenly spread to the embedded steel.

This relationship together with the measurement of polarisation of the embedded steel shall be used to assess the evenness of current flow from the coating through the concrete to the steel.

3.4.2 Test Procedure

Full and detailed testing methodology is given in Appendix C1 and is briefly described as below. For these tests, special concrete beam specimens, size 120 x 100 x 800mm long with two 10mm diameter steel bars at 70mm spacing and 50mm cover, were cast. Each end of each reinforcement bar was covered with a 110mm length heat shrink sleeve. This was to prevent bars not to react with the water solution during curing and to avoid rust on the section of the bars outside concrete.

The concrete mix design parameters for these beams are given in Table 3.10 with 2%. 4% chloride by weight of cement deliberately added in order to ensure that the

embedded bars were in a corrosively active state. Three or four miniaturised MMO/Ti reference electrodes were embedded into the beams to monitor the performance parameters of the coating and the steel bars. A Schematic diagram of these beams is shown in Figure 3.37.

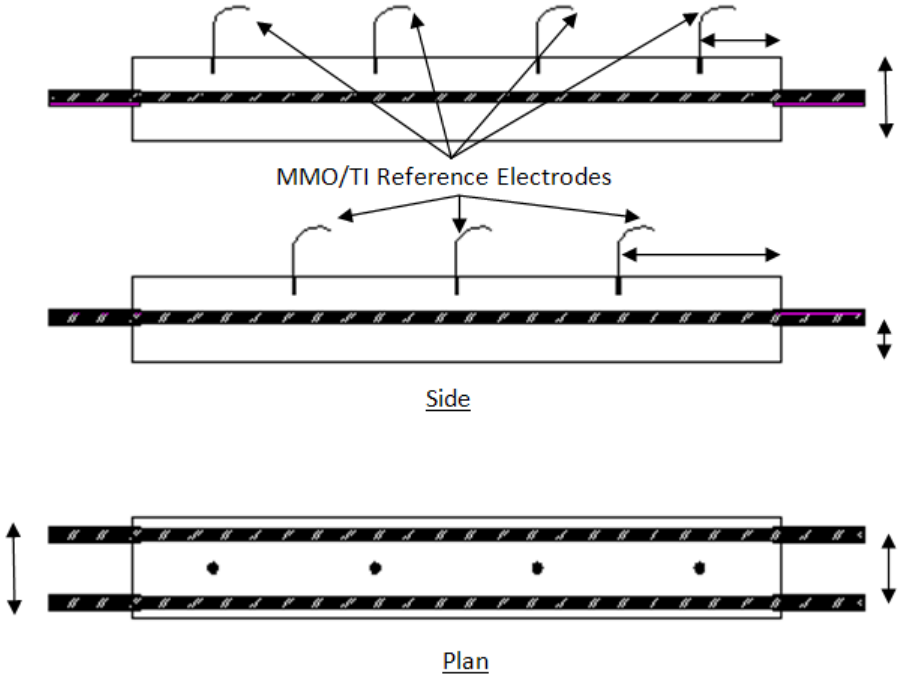

Figure 3.37: Schematic diagram of these beams

3.4.3 Concrete Mix Design – Polarisation Beam Test

Three concrete mixes were made with a target compressive strength of 20 MPa, and the design was carried out with accordance to BS 5328. All mixes have the same water/cement ratio of 0.45, design slump of 160mm as a target for all concrete mixes. In total 3 mixes are made, a control mix which contains no sodium chloride (NaCl) was compared with the other two mixtures which contained chlorides.

The final concrete parameters for the concrete mix are given in Table 3.10 with 0%, 2% and 4 % salt (chloride) deliberately added by weight of cement in order to ensure that the embedded reinforcement is in a corrosively active state. An important note is that the salt is add to the water, mixed until the salt crystals are dissolved and then it is add to the cementitious materials.

Table 3.10: Final mix parameters – Polarisation Beam Test.

Mix	Cement (kg)	Sand (kg)	Gravel (kg)	Water (kg)	Chlorides (kg)
Control. 0% chloride	6.08	12.89	16.54	3.14	0
2% Chloride Contaminated	6.08	12.89	16.54	3.14	0.1216
4% Chloride Contaminated	6.08	12.89	16.54	3.14	0.2432

3.4.4 Calibration of MMO/Ti Electrodes

The calibration process for the MMO/Ti reference electrodes involved a check that the electrodes are working correctly and potentials of the electrode are stable. This is done in a 3.5% chloride solution with reference to a saturated Ag/AgCl reference cell. The MMO/Ti reference electrodes and the Ag/AgCl reference cell were left in the NaCl solution until the measurement of potential with a digital voltmeter. The potential readings were taken between the Ag/AgCl reference cell and the MMO/Ti reference electrodes (one electrode at a time) when stable; this took up to 24 hour. All electrodes behaved in a similar manner. Potential measured in a 3.5% sodium chloride solution was found to be 120 ± 10mV with respect to a Ag/AgCl reference cell.

3.4.5 Concrete Surface Preparation

After 14 days of curing the beam specimens were left to dry in air until the surface was properly dry for the application of the paint. Prior to painting, the concrete surface was roughened by compressed air needle gun and a wire brush. The dust on the surface was cleaned with non-contaminated compressed air.

3.4.6 Coating Applications

The beam specimens were first coated with epoxy pitch paint; this was applied to the base and to the sides of the beam specimens. Two coats of paint were given to each beam. This was to minimise the loss of moisture in the samples during the

investigations. Once the epoxy paint dried up, the top surfaces of the beam samples were cleaned to remove any dust.

Figure 3.38: Shows beam specimens after being coated with epoxy pitch paint

A copper strip (primary electrode) was installed 1cm away from one edge of the top of the beam as shown in schematic Figure 3.39. The top edge of all sides of a specimen is taped around with masking tape to prevent paint from dripping to unwanted areas of the specimen. The top face of the each beam specimen was painted with three coats of the ZINGA paint, using a new clean paint brush, making sure the copper strip was covered with the zinc paint. Each coat of paint layer was left to dry for 24 hours before the next coat was applied. Each beam was weighed before and after each coat of paint. This was to calculate the thickness of each layer of paint and determine the overall thickness of three coats.

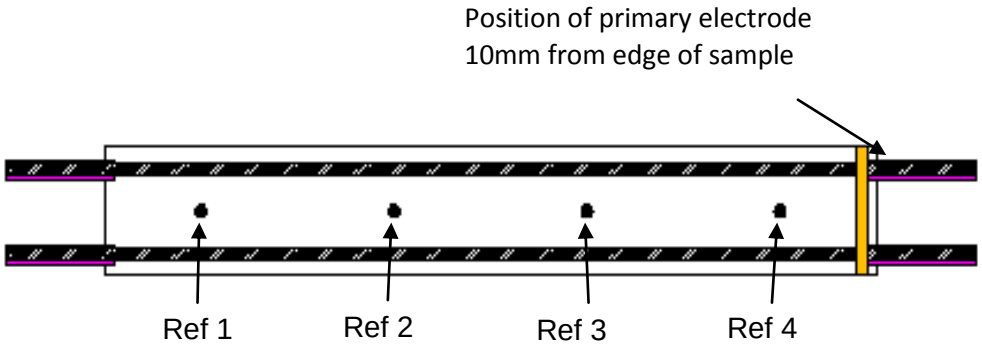

Figure 3.39: Schematic showing the placement of copper strip on a beam specimen

3.4.7 Coating thickness Calculation

The total coating thickness was calculated for each beam specimen as the wet density of zinc paint (ZINGA) is known. Table 3.11 Shows data obtained when coating is applied for each beam and Table 3.12 shows the change in mass for each beam specimen.

Table 3.11: Data of change in mass due to coating application for beam specimens

Mass	Beam 1 Control	Beam 2 2% Chloride Contaminated	Beam 3 4% Chloride Contaminated
Original Mass	23187.50g	24250.50g	23729.50g
Wet Coat 1 Mass	23238.00g	24298.00g	23775.50g
Original Mass + Coat 1 Dry	23231.00g	24291.00g	23770.50g
Wet Coat 2 Mass	23273.00g	24322.50g	23806.50g
Original Mass + Coat 1 Dry + Coat 2 Dry	23266.60g	24316.00g	23795.50g
Wet Coat 3 Mass	23299.05	24348.00g	23825.09g

Table 3.12: Change in mass of coating applied to specimens - Summary.

Change in Mass	Beam 1 Control	Beam 2 2% Chloride Contaminated	Beam 3 4% Chloride Contaminated
Original Mass - Wet Coat 1 Mass = Change in Mass Coat 1	50.50g	48.50g	46.00g
Original Mass + Coat 1 Dry - Wet Coat 2 Mass = Change in Mass Coat 2	42.00g	31.50g	36.00g
Original Mass + Coat 1 Dry + Coat 2 Dry - Wet Coat 3 Mass = Change in Mass Coat 3	32.90g	32.00g	29.59g

The thickness of each wet coat applied was determined using the relationship as below:

$$Density\ \rho = \frac{Mass\ (m)}{Volume\ (v)} = \frac{Mass}{Length \times Hight \times Width} \quad (3.10)$$

$$If\ Height = Thickness\ of\ one\ coat$$

$$\therefore Thickness = \frac{Mass}{Density \times Length \times Width} \quad (3.11)$$

$Where$: $Density = 2670kg/m^3$

$Length = 0.80m$

$Width = 0.12m$

$Mass = Change\ in\ mass\ of\ coating\ kg\ from\ Table\ 3.5\ \therefore\ Change\ in\ Mass\ Coat\ 1$

The above formula 3.11 is used to determine the thickness of each coat and the results are shown in Table 3.13. To get the dry theoretical thickness of the coating the following conversion is used 0.580 × wet film thickness = dry film thickness (shown in Table 3.14), which is given by the manufacturers of ZINGA.

Table 3.13: Wet coat thickness converted to µm

Wet Coat	Beam 1 Control	Beam 2 2% Chloride Contaminated	Beam 3 4% Chloride Contaminated
First Coat Thickness	197 µm	189 µm	179 µm
Second Coat Thickness	164 µm	122 µm	140 µm
Third Coat Thickness	125 µm	125 µm	115 µm

Table 3.14: Total dry coat thickness

Dry Coat	Beam 1 Control	Beam 2 2% Chloride Contaminated	Beam 3 4% Chloride Contaminated
First Coat Thickness	114 µm	110 µm	104 µm
Second Coat Thickness	95 µm	71 µm	81 µm
Third Coat Thickness	73 µm	73 µm	68 µm
Total Thickness	282 µm	254 µm	253 µm

The total dry thickness of paint may vary dependent on the person who is applying the coat. Normally three coats of 'Zinga' represent 180µm dry thickness but the

total dry coating thickness obtained on the beam specimens were more than 250 µm, suggesting very liberal use of paint.

3.4.8 Experiment Setup - Electrochemical Property Investigation

Three specimens prepared for the electrochemical property experiment were setup as shown in Figure 3.40. The potentials are measured between an individual reference electrode and a single reinforcement bar. Initially, the rebar potentials of the beam specimens were monitored for two weeks to determine if they were corroding. The samples are placed in a tank which contains water the samples are partially submerged. The beams are also sprayed regularly with water every two days, to keep them moist. The environmental condition was maintained at constant temperature. This part of the experiment was carried out with accordance of BS EN 12696:2000 Cathodic protection of steel in concrete.

The cathodic polarization characteristics of the coating were monitored at three levels of applied current on the anode surface viz. 10mA, 20mA and 30mA (equivalent to current density values of approximately 100mA/m^2, 200mA/m^2 and 300mA/m^2).. The current was applied for 7 days for each current level and the polarization characteristics monitored every day. After the 7th day the current was switched off for 24 hours and the de-polarisation was monitored over several time intervals throughout the day to obtain a decay potential curve and thus relates to the characteristic cathodic protection of the steel reinforcement.

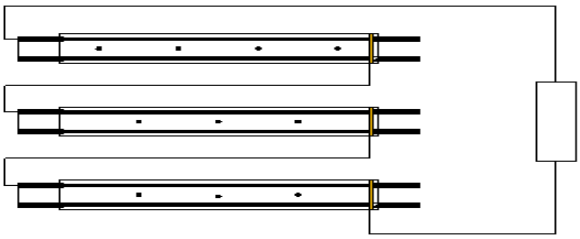

Figure 3.40: Circuit setup of cathodic protection experiment

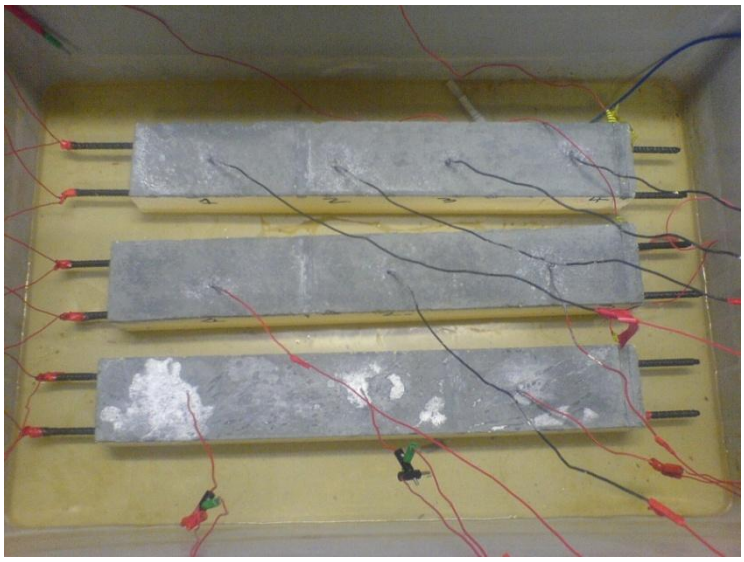

Figure 3.41: Photo of specimens set for cathodic experiment

Two beam specimens are to be prepared by lightly grit blasting/ wire brushing the top surface before applying the zinc coating. The base and the sides of the beams were sealed with an epoxy pitch paint (Epilux 5) to minimise loss of moisture during the experiments.

A detailed method statement of the test regime to be used to assess the various parameters is given in Appendix C1.

3.4.9 Results and Discussion

3.4.9.1 Free Corrosion Potential Results

Free corrosion potentials of the rebars of the three test beam specimens, containing 0%, 2% and 4% were monitored for 14 days. The results are summarised in Table 3.15, Table 3.16 and Table 3.17 for beam specimens' containing 0% chloride, 2% chloride and 4% chloride respectively. The potential readings taken with respect to Ag/AgCl reference electrodes are shown:

Table 3.15: Corrosion potentials (mV) Reference electrodes Vs rebar 1 and 2 for B1 specimen 0% chloride contaminated

Time Period (Days)	Ref 1 Vs Rebar 1 (mV)	Ref 1 Vs Rebar 2 (mV)	Ref 2 Vs Rebar 1 (mV)	Ref 2 Vs Rebar 2 (mV)	Ref3 Vs Rebar 1 (mV)	Ref 3 Vs Rebar 2 (mV)	Average Rebar Potential (mV)
1	-121	-121	-185	-194	-196	-196	-169
2	-112	-112	-202	-202	-204	-204	-173
3	-131	-131	-196	-196	-199	-199	-175
4	-126	-126	-189	-189	-195	-195	-170
5	-114	-134	-194	-193	-194	-194	-171
6	-156	-156	-207	-207	-213	-213	-192
7	-177	-177	-222	-222	-234	-234	-211
8	-124	-123	-232	-232	-226	-226	-194
9	-189	-188	-245	-244	-229	-229	-221
10	-191	-192	-249	-249	-224	-224	-222
11	-192	-191	-252	-252	-225	-225	-223
12	-184	-184	-256	-256	-222	-222	-221
13	-220	-219	-261	-261	-228	-227	-236
14	-219	-218	-218	-267	-225	-283	-238

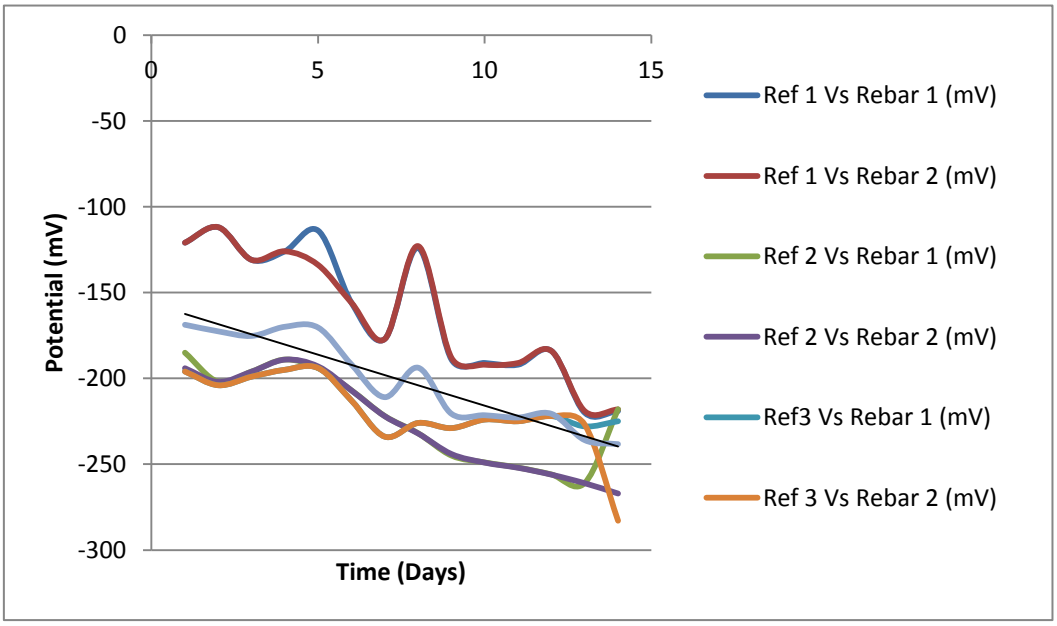

Figure 3.42: Corrosion potentials (mV) Ag/AgCl Reference electrodes Vs rebar 1 and 2 for B1 specimen 0% chloride contaminated

Table 3.16: Corrosion potentials (mV) Reference electrodes Vs rebar 1 and 2 for B2 specimen 2% chloride contaminated

Time Period (Days)	Ref 1 Vs Rebar 1 (mV)	Ref 1 Vs Rebar 2 (mV)	Ref 2 Vs Rebar 1 (mV)	Ref 2 Vs Rebar 2 (mV)	Ref 3 Vs Rebar 1 (mV)	Ref 3 Vs Rebar 2 (mV)	Average Rebar Potential (mV)
1	-331	-331	-323	-323	-309	-309	-321
2	-331	-330	-333	-333	-325	-325	-330
3	-322	-323	-394	-394	-326	-326	-348
4	-320	-320	-378	-378	-324	-324	-341
5	-314	-314	-401	-401	-330	-330	-348
6	-315	-314	-398	-398	-333	-333	-349
7	-326	-336	-425	-425	-345	-345	-367
8	-337	-346	-440	-440	-340	-340	-374
9	-346	-346	-440	-440	-341	-341	-376
10	-412	-410	-447	-447	-356	-356	-405
11	-420	-420	-451	-451	-354	-354	-408
12	-427	-428	-456	-456	-347	-347	-410
13	-435	-435	-460	-460	-346	-346	-414
14	-445	-445	-467	-467	-339	-339	-417

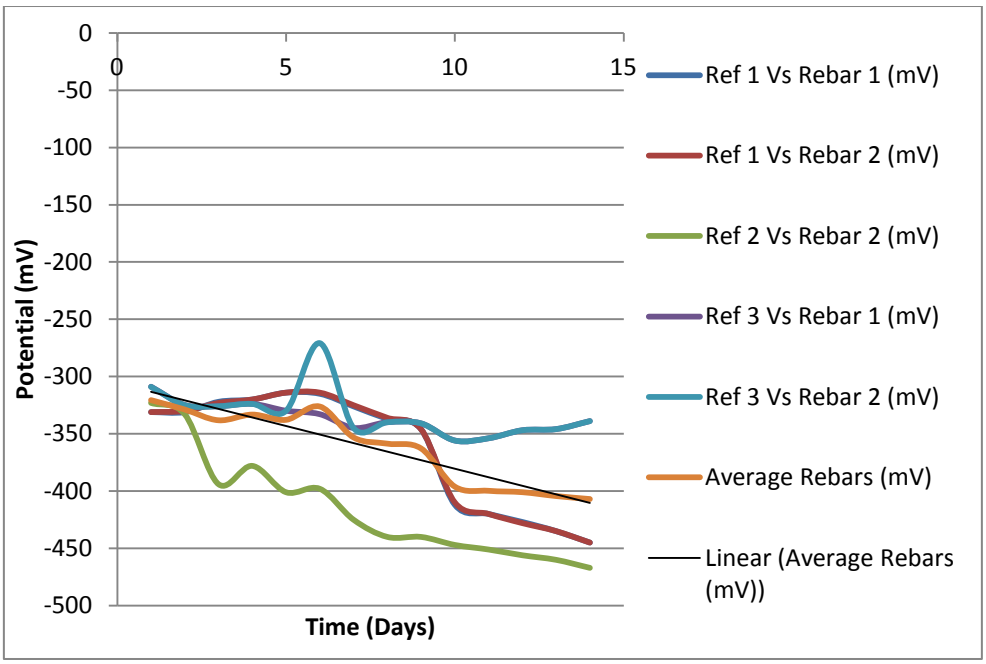

Figure 3.43: Corrosion potentials (mV) Reference electrodes Vs rebar 1 and 2 for B2 specimen 2% chloride contaminated

Table 3.17: Corrosion potentials (mV) Reference electrodes Vs rebar 1 and 2 for B3 specimen 4% chloride contaminated

Time Period (Days)	Ref 1 Vs Rebar 1 (mV)	Ref 1 Vs Rebar 2 (mV)	Ref 2 Vs Rebar 2 (mV)	Ref 3 Vs Rebar 1 (mV)	Ref 3 Vs Rebar 2 (mV)	Ref 4 Vs Rebar 1 (mV)	Ref 4 Vs Rebar 2 (mV)	Average Rebars (mV)
1	-402	-402	-404	-411	-412	-418	-418	-410
2	-404	-406	-412	-413	-414	-421	-421	-413
3	-409	-409	-414	-417	-417	-426	-426	-417
4	-410	-409	-415	-413	-414	-428	-428	-417
5	-410	-410	-424	-416	-416	-429	-429	-419
6	-413	-412	-424	-418	-419	-430	-435	-422
7	-413	-413	-427	-420	-420	-431	-431	-422
8	-418	-418	-430	-425	-425	-435	-440	-427
9	-422	-421	-416	-422	-422	-438	-438	-426
10	-424	-424	-435	-432	-432	-439	-440	-432
11	-424	-425	-428	-431	-431	-447	-447	-433
12	-427	-427	-428	-433	-432	-450	-450	-435
13	-430	-430	-440	-438	-438	-443	-443	-437
14	-440	-439	-448	-450	-450	-449	-450	-447

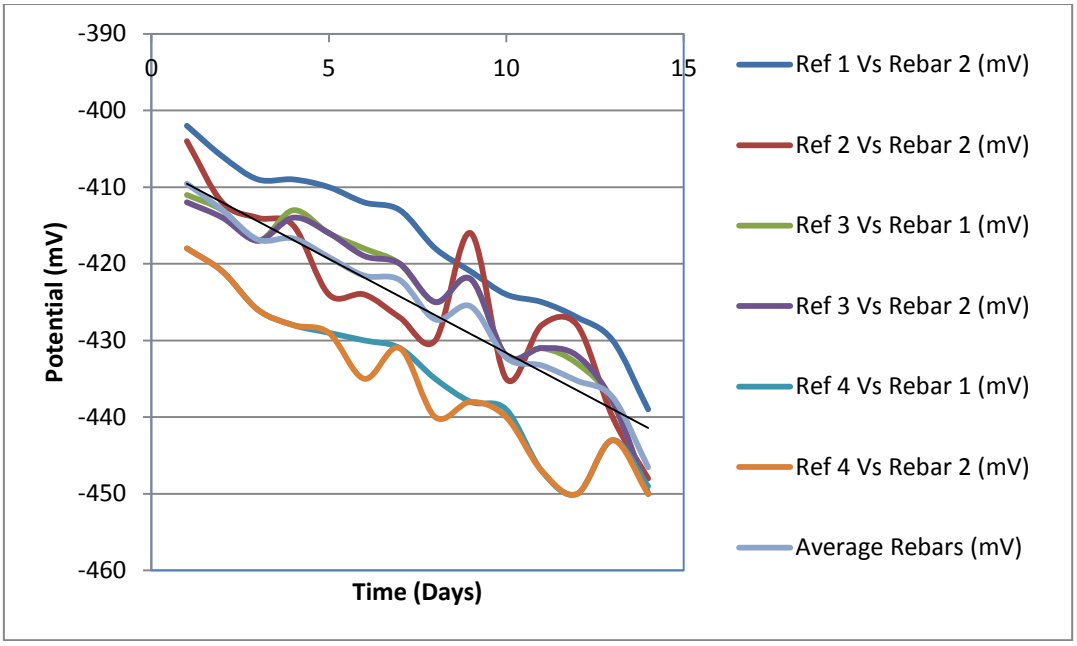

Figure 3.44: Corrosion potentials of Rebar (mV) Reference electrodes 1, 2, 3 and 4 for B3 specimen 4% chloride contaminated

Graphical representation of corrosion potentials is shown in the following figures (Figure 3.45, 3.49, 3.50 and 3.51) for specimens' containing 0% chloride, 2% chloride and 4% chloride. The following figures show the potential distribution of within the reinforced concrete beam specimens, also characterize potential reading taken for 14 days and the results are summarised in Table 3.18. The change in potentials with time were monitored and measured at different positions on the beam.

In accordance with ASTM C 876 – 91 Standard Test Method for Half-Cell Potentials of Uncoated Reinforcing Steel in Concrete, the percentages of potential values more negative than -0.35V and less than –0.20V represent 90% and 10% probability of active corrosion occurring at the time of measurement. For the sample containing 0% of chlorides (Control specimen) the percentages of value less negative than -0.20V was 28% and 24% of values were more negative than -0.35V. The 2% chloride contaminated sample had 0% percentages of potentials less negative than -0.20V 28% and 40 % of potentials were more negative than -0.35V. Finally 100% of potentials values in beam 3 the 4% chloride contaminated sample were more negatively above –0.35V. The higher percentages above represent the level of corrosive activity within a specimen. The higher percentages more negative than -0.35V states high risk of corrosion and less corrosion is when there is more positive potentials than –0.20V. These results also represents, the samples are in active corrosive state and also the level of that activeness.

Table 3.18: Average Corrosion Potentials of Beams 1, 2 and 3

Time Period (Days)	Average Rebar Potential (mV), 0%Cl	Average Rebar Potential (mV), 2% Cl	Average Rebar potential (mV), 4% Cl
1	-169	-321	-410
2	-173	-329	-413
3	-175	-338	-417
4	-170	-333	-417
5	-171	-338	-419
6	-192	-326	-422
7	-211	-353	-422
8	-194	-359	-427
9	-221	-363	-426
10	-222	-396	-432
11	-223	-400	-433
12	-221	-401	-435
13	-236	-404	-437
14	-238	-407	-447

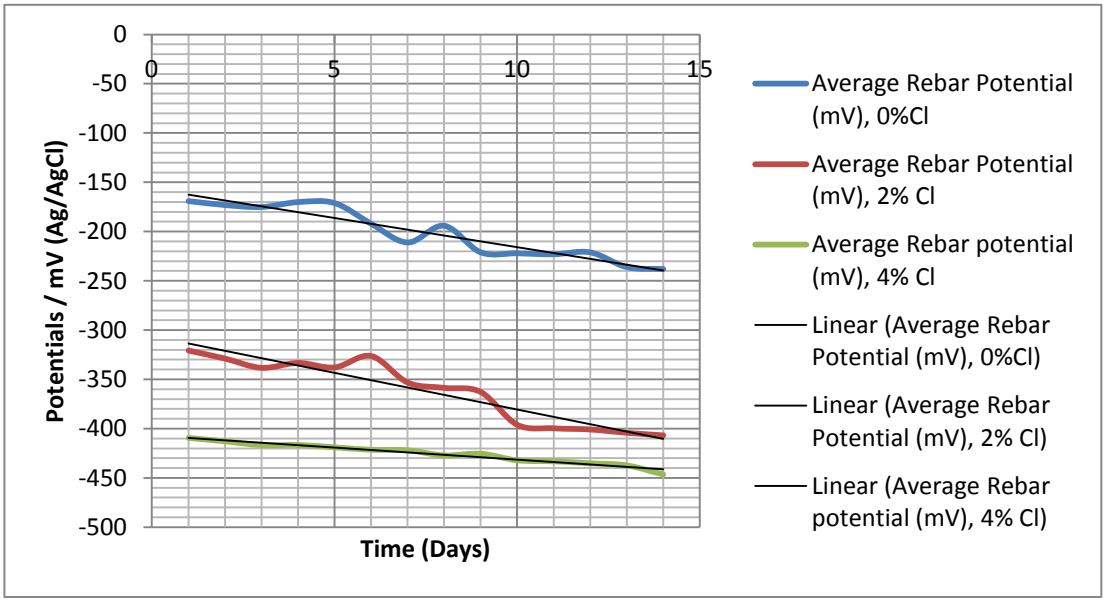

Figure 3.45: Average Corrosion Potentials of Beams 1, 2 and 3

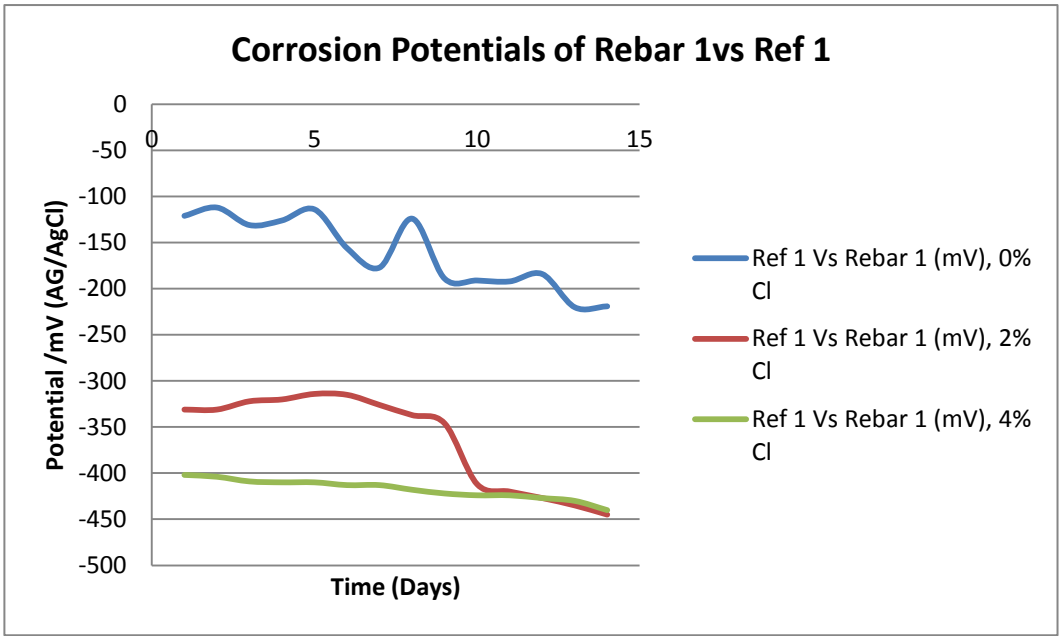

Figure 3.46: Corrosion potentials reference 1 Vs rebar 1

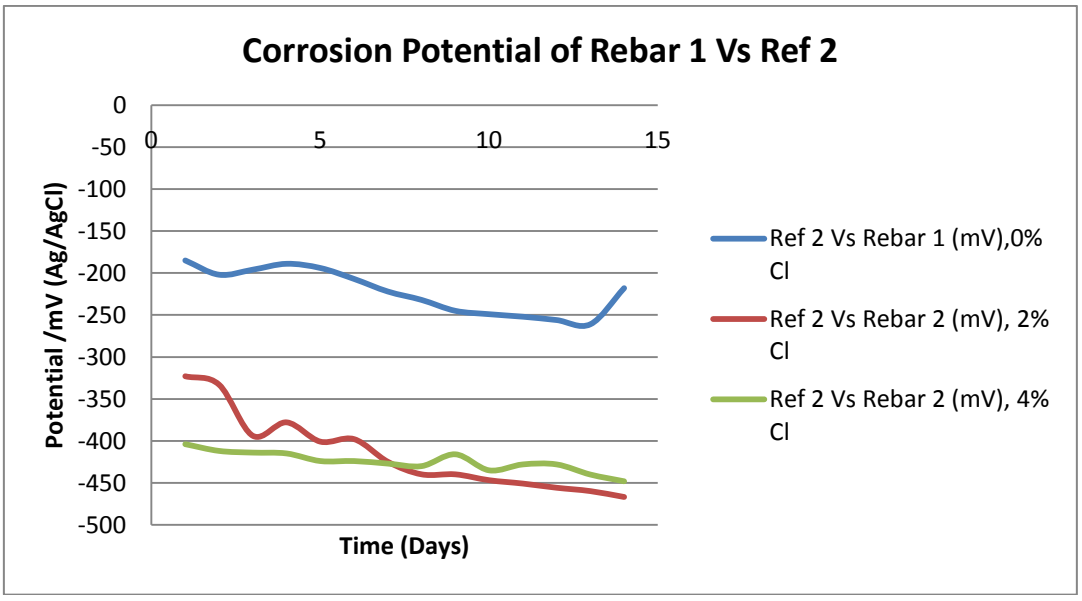

Figure 3.47: Corrosion potentials reference 2 Vs rebar 2

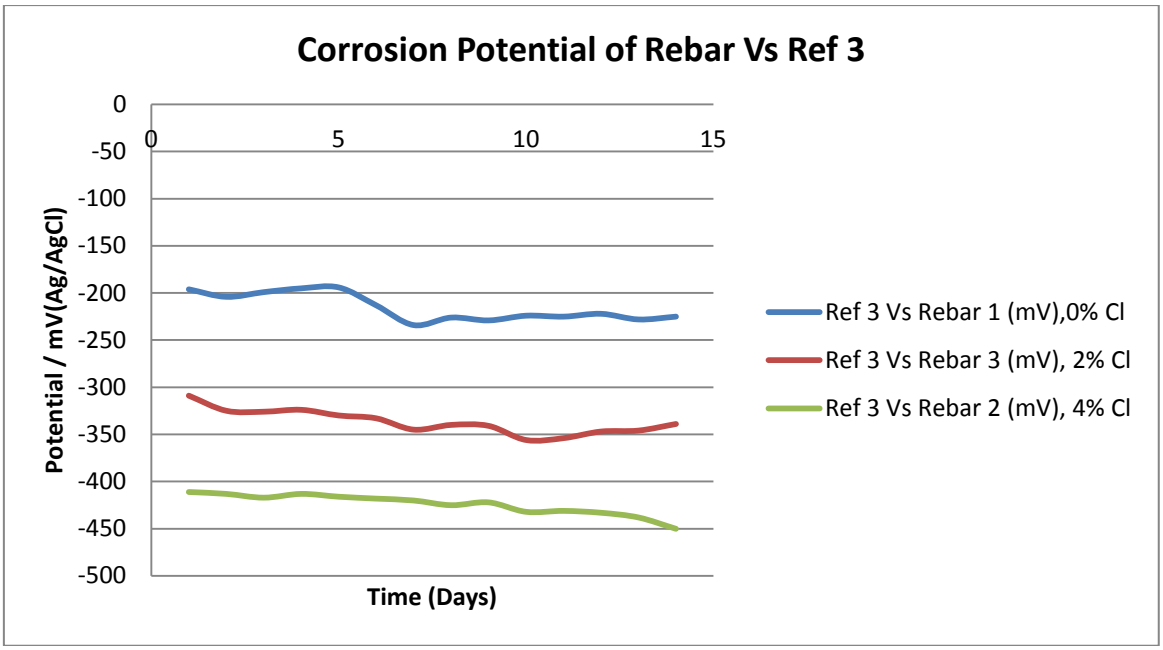

Figure 3.48: Corrosion potentials reference 3 Vs rebar

The results from the above figures (Figure 3.42 - 3.48) show that potential readings from the 4% chloride contaminated sample to be more negative, in the region -414mV to –450mV which is considered to have more corrosive activity present on the steel reinforcement. This is due to the fact they are in the range of severe corrosion (<-400) [Song and Saraswathy, 2006]. Potential readings for the 2% chloride contaminated specimen are in the range of high levels of corrosion activity as potential reading observed are of -314 to -440 after the initial stability of the monitoring reference electrodes. The control sample showed a sign of intermediate risk. This possibly due to fact that a small amount of chlorides was accidentally added to the water solution which partially submerged the samples. Therefore to be critical the known percentage of the chlorides in each sample is not known, due to the pores within the concrete specimens can transport chloride in and out from their self and from contaminated water surrounding them. But the control specimen still showed corrosive potentials less than that obtained for the 2% chloride contaminated and 4% chloride contaminated samples which allowed the experiment to go forwards.

The comparison between the potential readings obtained for rebar 1 and rebar 2 for each sample show pretty much identical potential values observed for every reference electrode. The spacing between the rebar 1 and rebar 2 was relatively close to one another. This shows that the properties of the concrete in a relatively

small distance are consistently similar and do not make any difference on potential readings. Therefore from this point forward the main body of this report will only show and discuss result for rebar 1 verses reference electrodes. All results for Rebar 2 are displayed in Appendices C. Figures 3.49 to 3.51 shows the comparison of the behaviour of individual reference electrodes on each concrete sample.

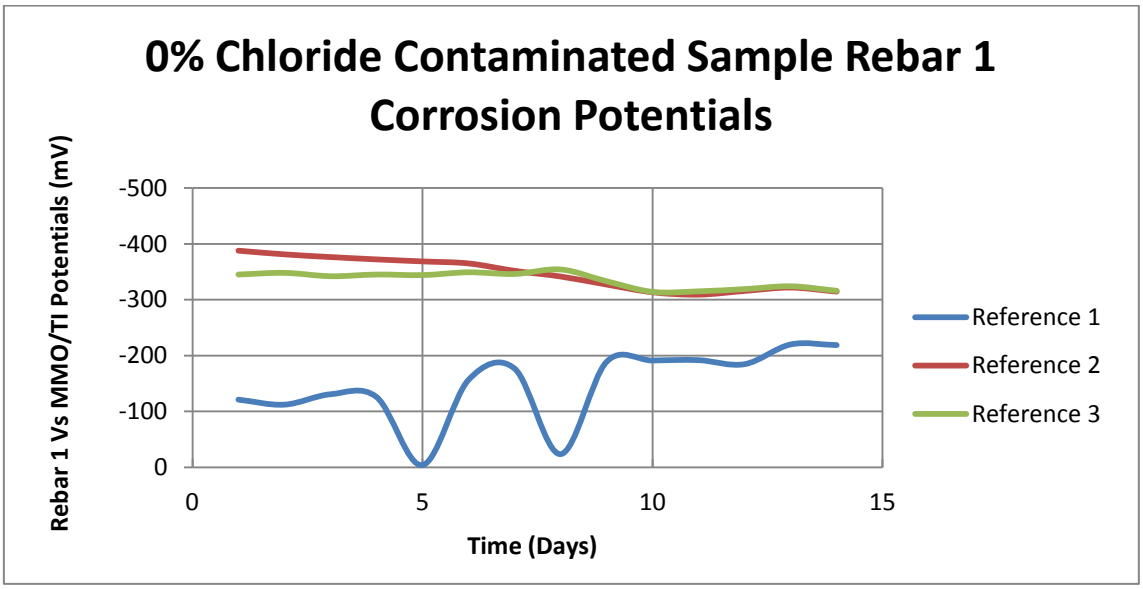

Figure 3.49: Corrosion 0% chloride contaminated specimen

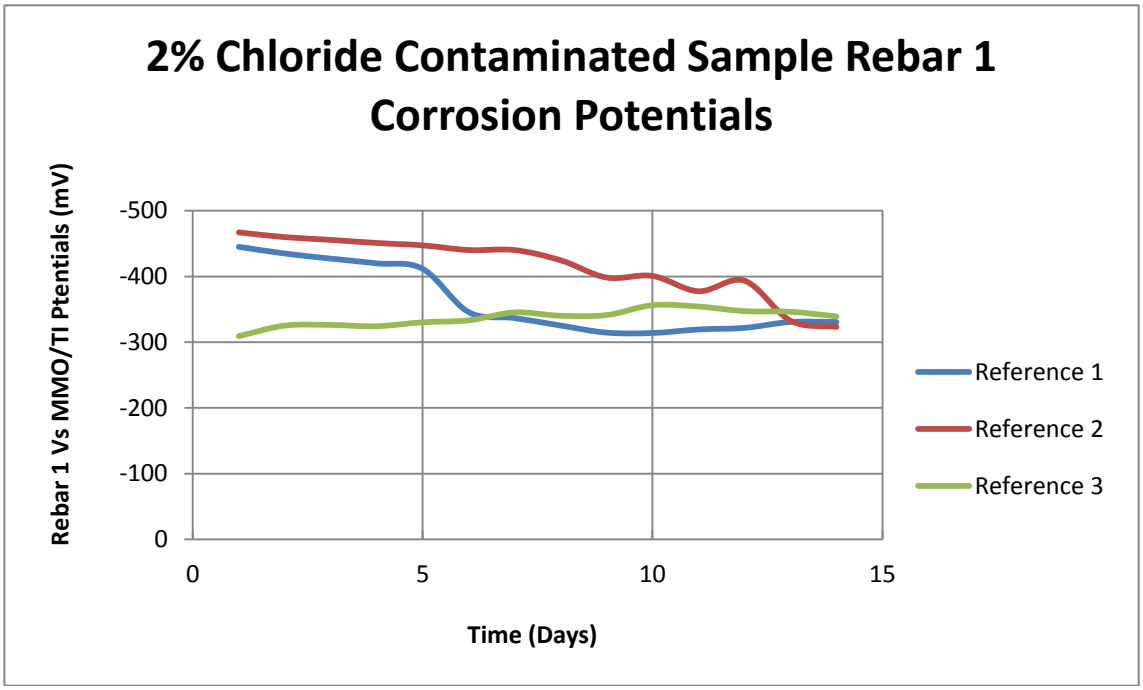

Figure 3.50: Corrosion 2% chloride contaminated specimen

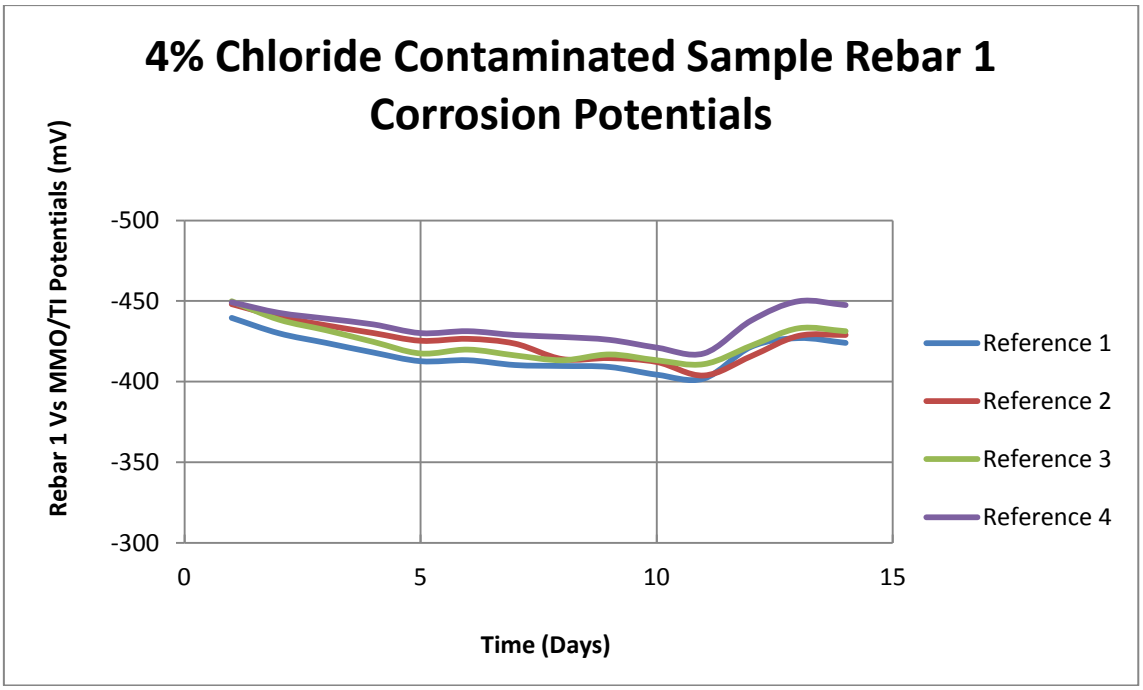

Figure 3.51: Corrosion 4% chloride contaminated specimen

For 4% and the 2% chloride contaminated show comparable potentials across all reference readings, but for the control sample readings observed from reference 1 are in a range -120mV to -216mV compared to more negative readings from reference 2 and 3.

3.4.9.2 Polarisation Results

Potential distributions within the concrete specimens are shown, when assessed at different current densities, in Figures 3.52 - 3.64 and Tables 3.18 – 3.24. These figures and tables represent readings taken on the all beam specimens for 7 days, where the change in polarisation potential with time was monitored and measured at different positions across the specimens.

Table 3.19 Polarisation potentials at 104mA/ m^2 for 0% chloride

Time Period (Days)	Ref 1 Vs Rebar 1 (mV)	Ref 1 Vs Rebar 2 (mV)	Ref 1 Vs Average Rebar (mV)	Ref 2 Vs Rebar 1 (mV)	Ref 2 Vs Rebar 2 (mV)	Ref 2 Vs Average Rebar (mV)	Ref 3 Vs Rebar 1 (mV)	Ref 3 Vs Rebar 2 (mV)	Ref 3 Vs Average Rebar (mV)
1	-247	-247	-247	-325	-326	-325.5	-346	-346	-346
2	-244	-244	-244	-333	-334	-333.5	-353	-353	-353
3	-248	-248	-248	-352	-352	-352	-357	-357	-357
4	-254	-254	-254	-358	-358	-258	-363	-363	-363
5	-233	-233	-233	-364	-364	-364	-369	-369	-369
6	-249	-249	-249	-375	-375	-375	-376	-376	-376
7	-252	-252	-252	-387	-387	-387	-389	-389	-389

Table 3.20 Polarisation potentials at 104mA/ m^2 reference 1 Vs rebar 1

Time Period (Days)	0% Chloride Contaminated Ref 1 Vs Rebar 1 (mV)	2% Chloride Contaminated Ref 1 Vs Rebar 1 (mV)	4% Chloride Contaminated Ref 1 Vs Rebar 1 (mV)
1	-325	-436	-418
2	-333	-442	-436
3	-352	-449	-447
4	-358	-444	-450
5	-364	-443	-460
6	-375	-443	-471
7	-385	-442	-501

Table 3.21 Polarisation potentials at 104mA/ m^2 reference 2 Vs rebar 1

Time Period (Days)	0% Chloride Contaminated Ref 2 Vs Rebar 1 (mV)	2% Chloride Contaminated Ref 2 Vs Rebar 1 (mV)	4% Chloride Contaminated Ref 2 Vs Rebar 1 (mV)
1	-325	-436	-418
2	-333	-442	-436
3	-352	-449	-447
4	-358	-444	-450
5	-364	-444	-460
6	-375	-443	-471
7	-387	-442	-501

Table 3.22 Polarisation potentials at 104mA/ m^2 reference 3 Vs rebar 1

Time Period (Days)	0% Chloride Contaminated Ref 3 Vs Rebar 1 (mV)	2% Chloride Contaminated Ref 3 Vs Rebar 1 (mV)	4% Chloride Contaminated Ref 3 Vs Rebar 1 (mV)
1	-346	-429	-474
2	-353	-445	-481
3	-357	-456	-492
4	-363	-457	-493
5	-369	-456	-504
6	-376	-456	-517
7	-389	-453	-535

Table 3.23: Polarised potentials at 104mA/m^2 reference cells Vs Rebar 1

Time Period (Days)	0% Chloride Contaminated Ref 1 Vs Rebar 1 (mV)	0% Chloride Contaminated Ref 2 Vs Rebar 1 (mV)	0% Chloride Contaminated Ref 3 Vs Rebar 1 (mV)
1	-325	-325	-346
2	-333	-333	-353
3	-352	-352	-357
4	-358	-358	-363
5	-364	-364	-369
6	-375	-375	-376
7	-387	-387	-389

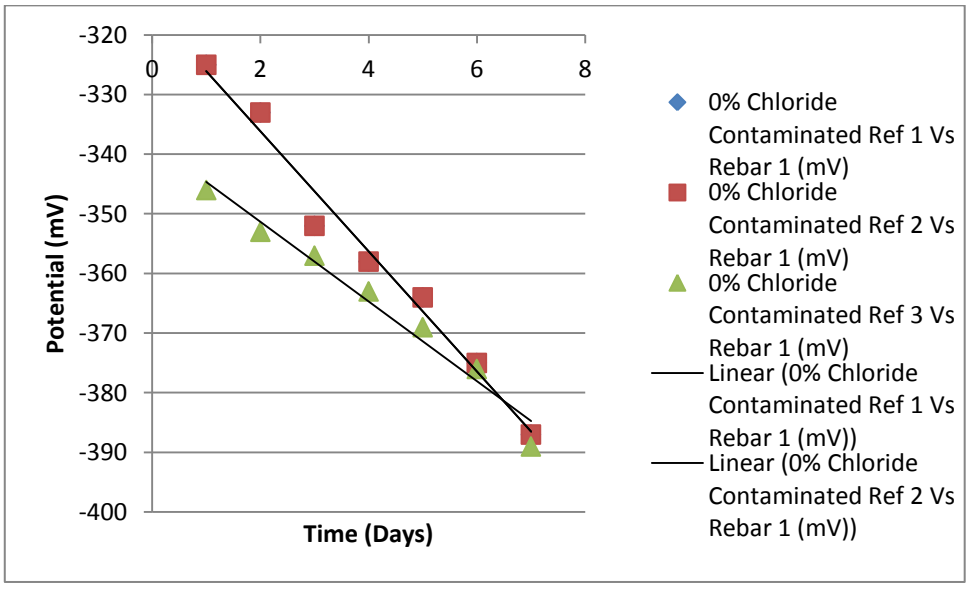

Figure 3.52: Polarised potentials at 104mA/m^2 reference cells Vs Rebar 1

Table 3.24: Polarised potentials at 104mA/m^2 reference cells Vs Rebar 1 (2%)

Time Period (Days)	2% Chloride Contaminated Ref 1 Vs Rebar 1 (mV)	2% Chloride Contaminated Ref 2 Vs Rebar 1 (mV)	2% Chloride Contaminated Ref 3 Vs Rebar 1 (mV)
1	-436	-436	-429
2	-442	-442	-445
3	-449	-449	-456
4	-444	-444	-457
5	-443	-443	-456
6	-443	-443	-456
7	-442	-442	-453

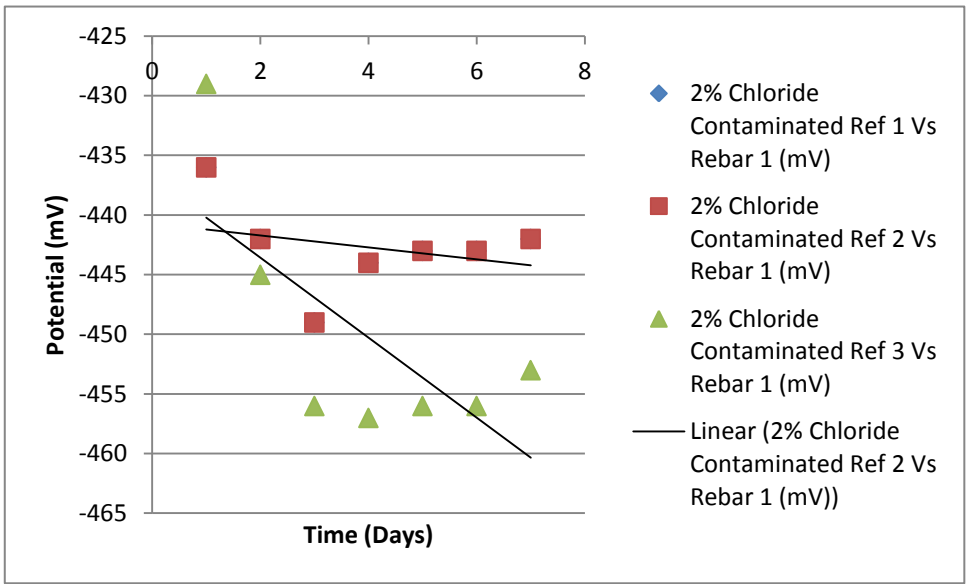

Figure 3.53: Polarised potentials at 104mA/m^2 reference cells Vs Rebar 1 (2%Cl)

Table 3.25: Polarised potentials at 104mA/m^2 reference cells Vs Rebar 1 (4% Cl)

Time Period (Days)	4% Chloride Contaminated Ref 1 Vs Rebar 1 (mV)	4% Chloride Contaminated Ref 2 Vs Rebar 1 (mV)	4% Chloride Contaminated Ref 3 Vs Rebar 1 (mV)
1	-418	-418	-429
2	-436	-436	-445
3	-447	-447	-456
4	-450	-450	-457
5	-460	-460	-456
6	-471	-471	-456
7	-501	-501	-453

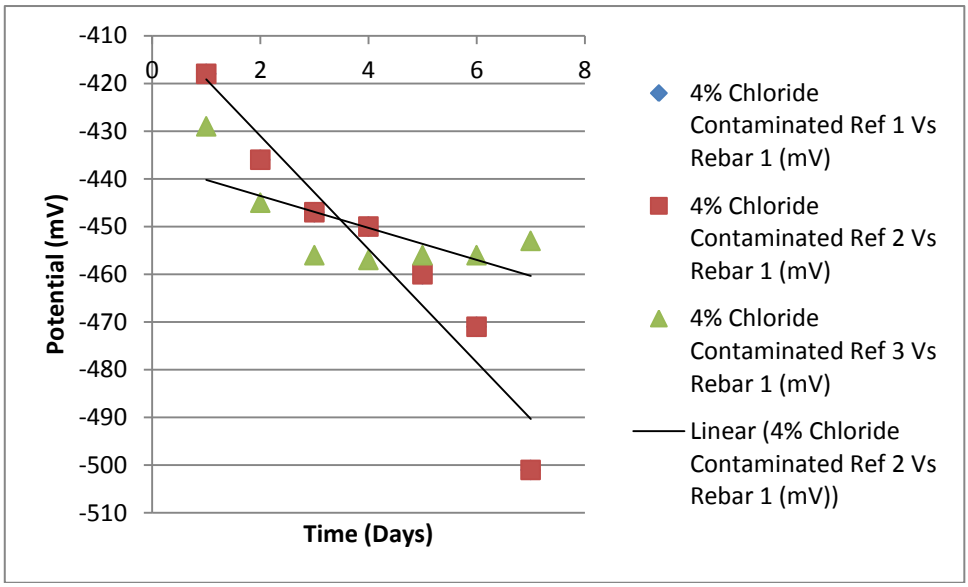

Figure 3.54: Polarised potentials at 104mA/m^2 reference cells Vs Rebar 1 (4%Cl)

With 10mA applied current (which is equivalent to a current density of 104/m^2) the driving volt recorded was 0.12V. Therefore the resistance of the circuit is 12 ohms.

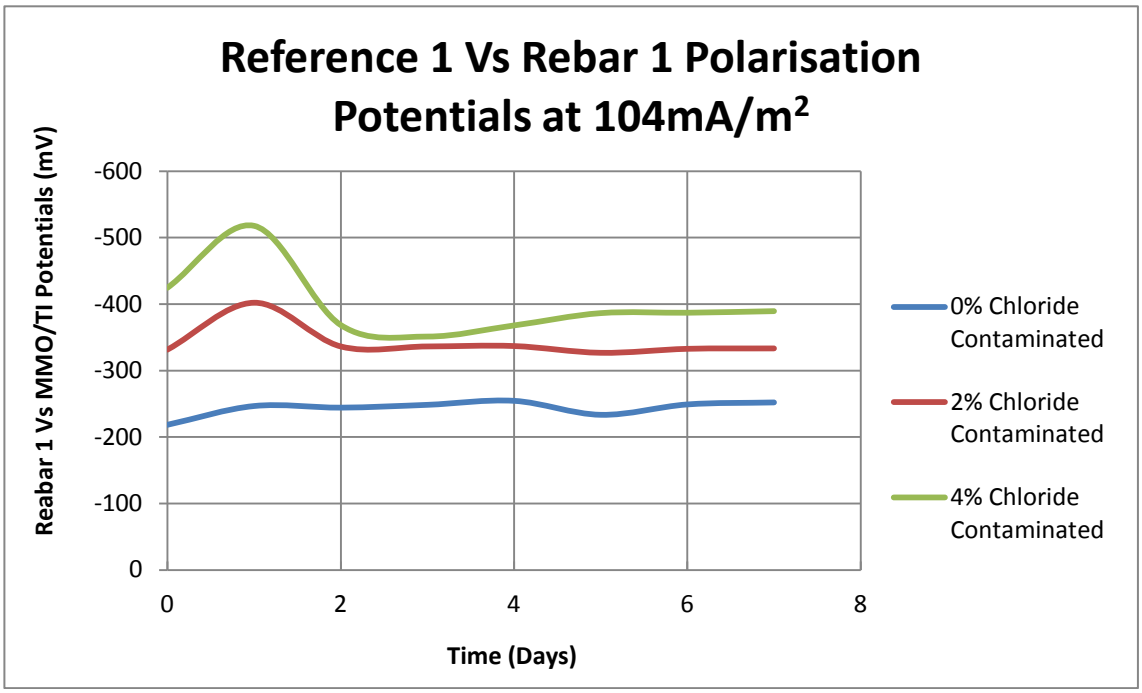

Figure 3.55: Polarisation potentials at 104 mA/m^2 reference 1 Vs rebar 1

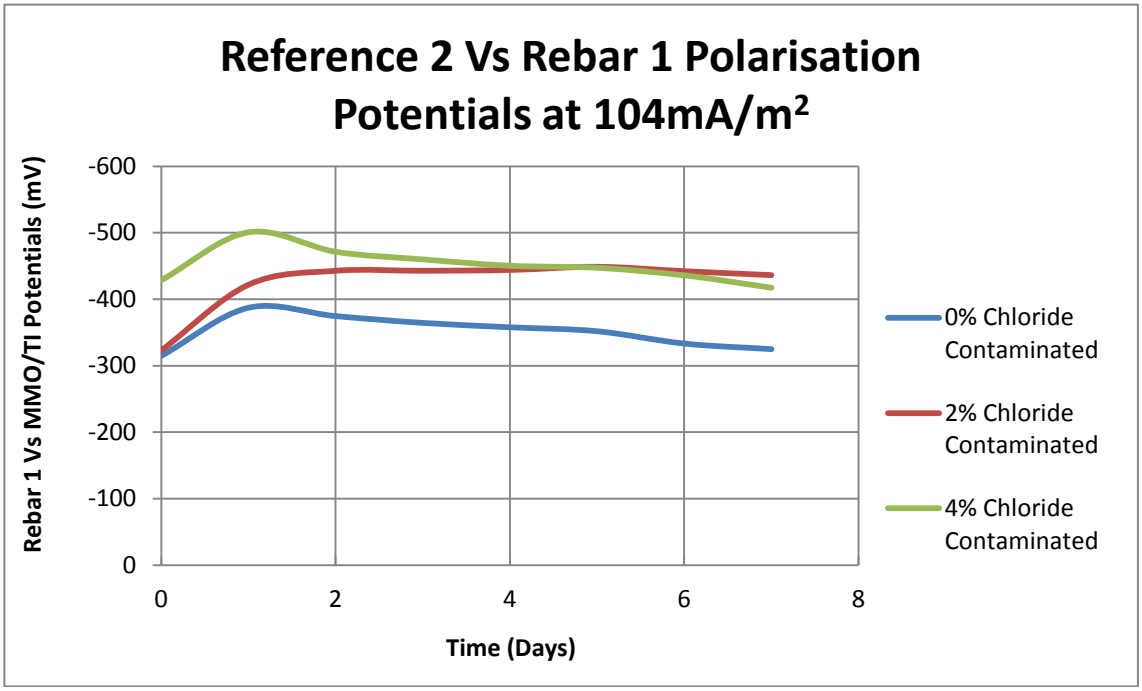

Figure 3.56: Polarisation potentials at 104 mA/m^2 reference 2 Vs rebar 1

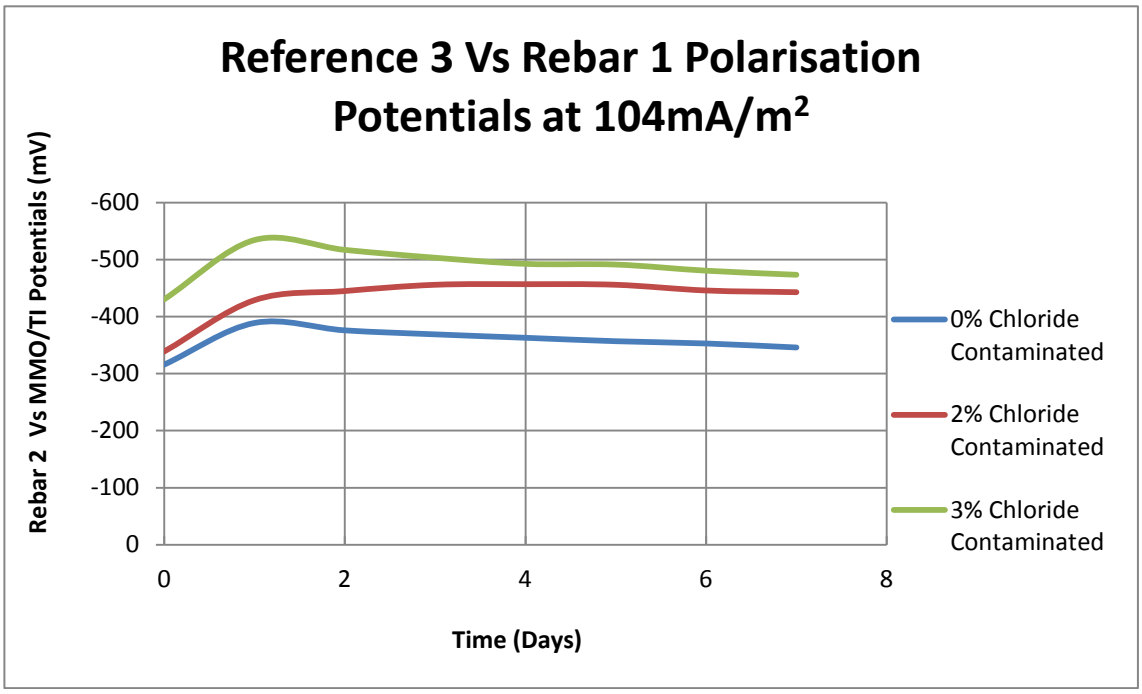

Figure 3.57: Polarisation potentials at 104 mA/m^2 reference 3 Vs rebar 1

Table 3.26 Polarisation potentials at 208mA/ m^2 reference 1 Vs rebar 1

Time Period (Days)	0% Chloride Contaminated Ref 1 Vs Rebar 1 (mV)	2% Chloride Contaminated Ref 1 Vs Rebar 1 (mV)	4% Chloride Contaminated Ref 1 Vs Rebar 1 (mV)
1	-255	-348	-229
2	-260	-348	-306
3	-265	-348	-318
4	-267	-347	-317
5	-267	-247	-320
6	-267	-350	-318
7	-266	-364	-318

Table 3.27 Polarisation potentials at 208mA/ m^2 reference 2 Vs rebar 1

Time Period (Days)	0% Chloride Contaminated Ref 2 Vs Rebar 1 (mV)	2% Chloride Contaminated Ref 2 Vs Rebar 1 (mV)	4% Chloride Contaminated Ref 2 Vs Rebar 1 (mV)
1	-287	-490	-482
2	-289	-489	-481
3	-288	-490	-481
4	-288	-492	-480
5	-289	-490	-481
6	-284	-499	-491
7	-303	-508	-516

Table 3.28: Polarisation potentials at 208mA/ m^2 reference 3 Vs rebar 1

Time Period (Days)	0% Chloride Contaminated Ref 3 Vs Rebar 1 (mV)	2% Chloride Contaminated Ref 3 Vs Rebar 1 (mV)	4% Chloride Contaminated Ref 3 Vs Rebar 1 (mV)
1	-333	-489	-474
2	-334	-591	--481
3	-336	-592	-492
4	-337	-592	-493
5	-338	-594	-504
6	-336	-503	-517
7	-338	-506	-535

When 20mA current is driven to obtain a current density of 208/m^2 the volt recorded was 2.31V. Therefore the resistance is of the circuit is 116 ohms. As where the resistance of the coating in recorded is of a range between 2 to 6MΩ across the samples.

Table 3.29: Polarisation potentials at 208mA/ m^2 reference 3 Vs rebar 1 (0% Cl)

Time Period (Days)	0% Chloride Contaminated Ref 1 Vs Rebar 1 (mV)	0% Chloride Contaminated Ref 2 Vs Rebar 1 (mV)	0% Chloride Contaminated Ref 3 Vs Rebar 1 (mV)
1	-255	-303	-338
2	-260	-284	-336
3	-265	-289	-338
4	-267	-288	-337
5	-267	-288	-336
6	-267	-289	-334
7	-266	-287	-333

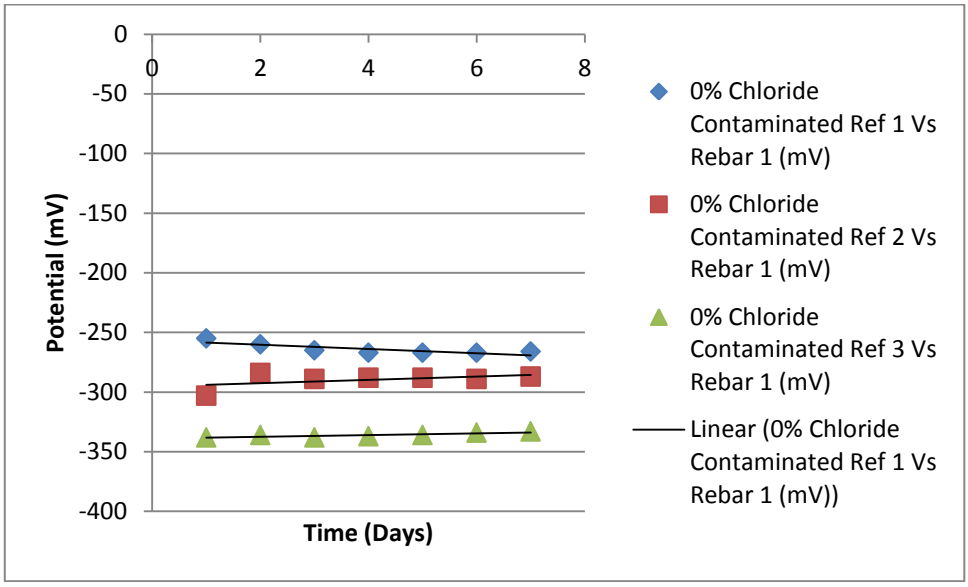

Figure 3.58: Polarisation potentials at 104 mA/m^2 reference 3 Vs rebar 1 (0% Cl)

Table 3.30: Polarisation potentials at 208mA/ m^2 references Vs rebar 1 (2% Cl)

Time Period (Days)	2% Chloride Contaminated Ref 1 Vs Rebar 1 (mV)	2% Chloride Contaminated Ref 2 Vs Rebar 1 (mV)	2% Chloride Contaminated Ref 3 Vs Rebar 1 (mV)
1	-364	-508	-506
2	-350	-499	-503
3	-247	-490	-594
4	-347	-492	-592
5	-248	-490	-592
6	-348	-489	-591
7	-348	-490	-489

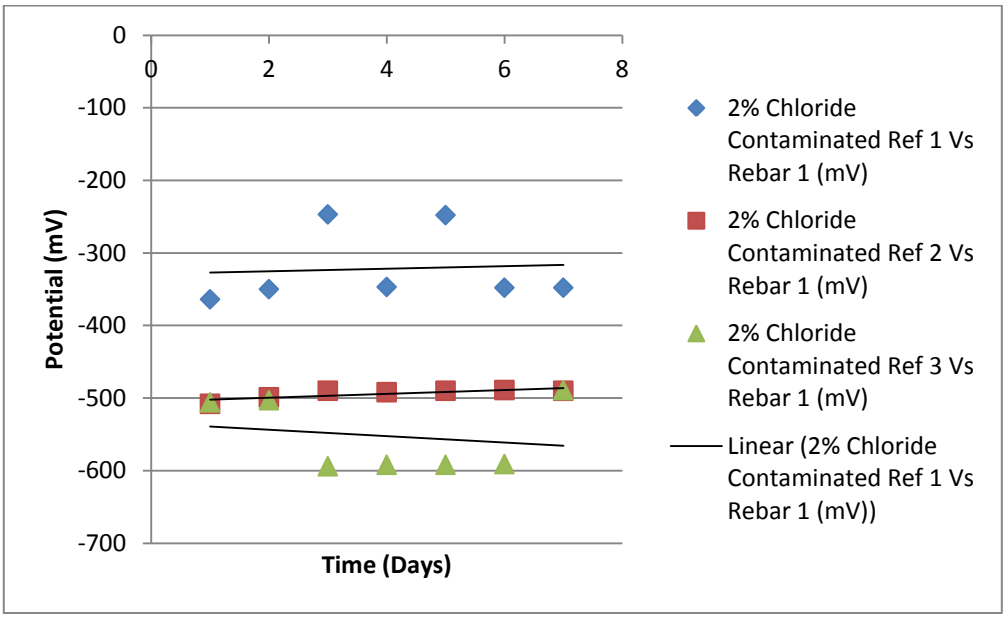

Figure 3.59: Polarisation potentials at 208mA/ m^2 references Vs rebar 1 (2% Cl)

Table 3.31: Polarisation potentials at 208mA/ m^2 references Vs rebar 1 (4% Cl)

Time Period (Days)	4% Chloride Contaminated Ref 1 Vs Rebar 1 (mV)	4% Chloride Contaminated Ref 2 Vs Rebar 1 (mV)	4% Chloride Contaminated Ref 3 Vs Rebar 1 (mV)
1	-229	-516	-535
2	-306	-491	517
3	-318	-481	-504
4	-317	-480	-493
5	-320	-481	-492
6	-318	-481	-481
7	-318	-482	-474

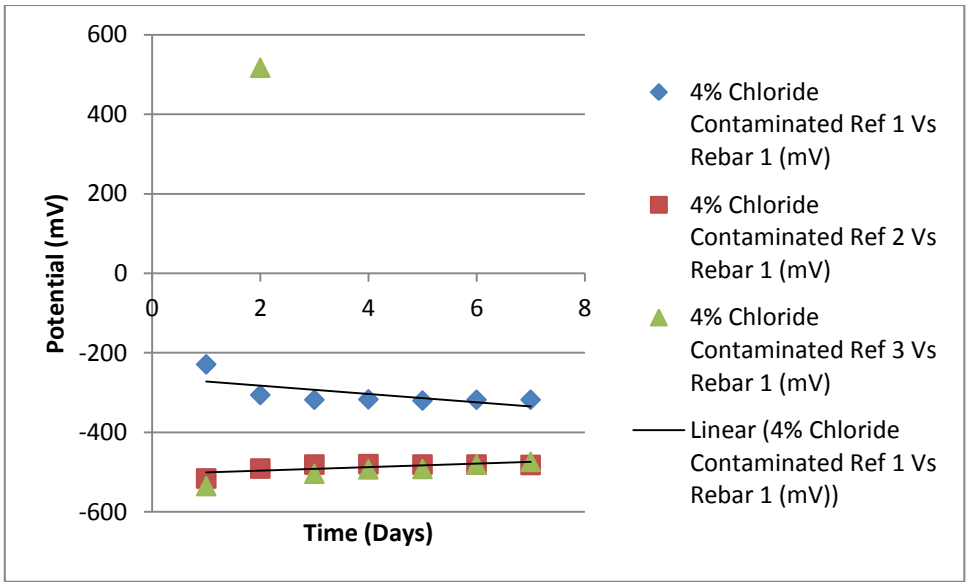

Figure 3.60: Polarisation potentials at 208mA/ m^2 references Vs rebar 1 (4% Cl)

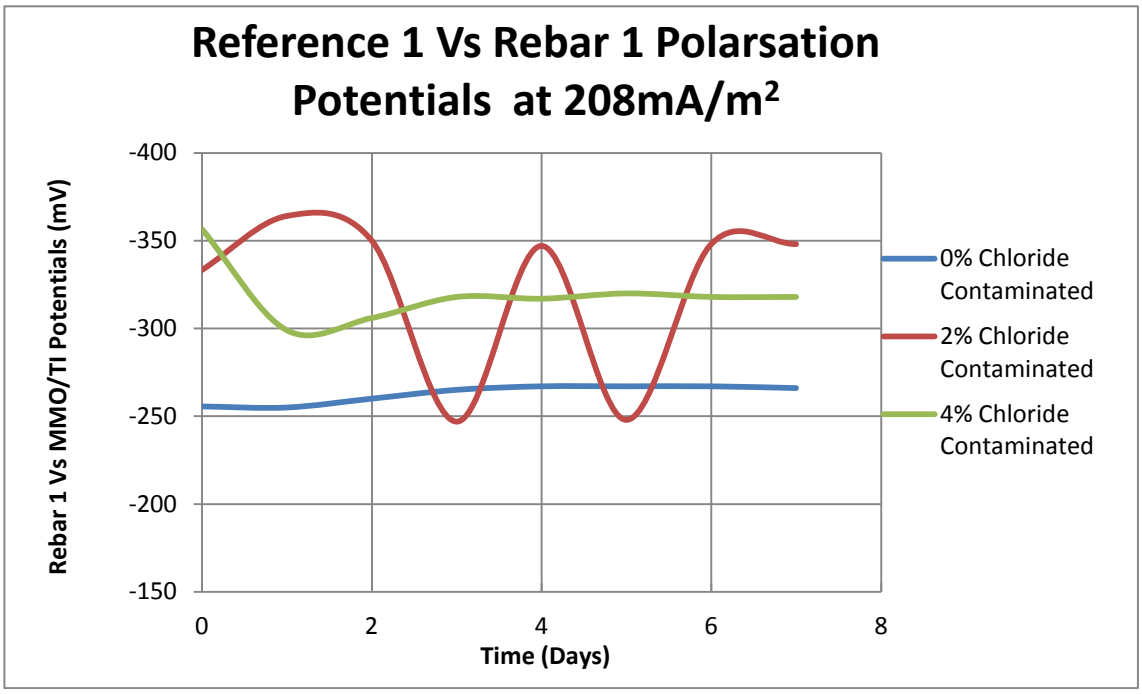

Figure 3.61 Polarisation potentials at 208 mA/m^2 reference 1 Vs rebar 1

The drop in polarisation at days 3 and 5 (Figure 3.48 and Table 3.42) potential for 2% contaminated sample reference 2 to could be to the current flow within the structure of concrete or the structure of the coating. In the case of the cathodic protection the current flows from the zinc coating, passing through the structure of concrete, and then reaching the reinforcement and then this process is repeated until it leaves the third sample to complete the circuit.

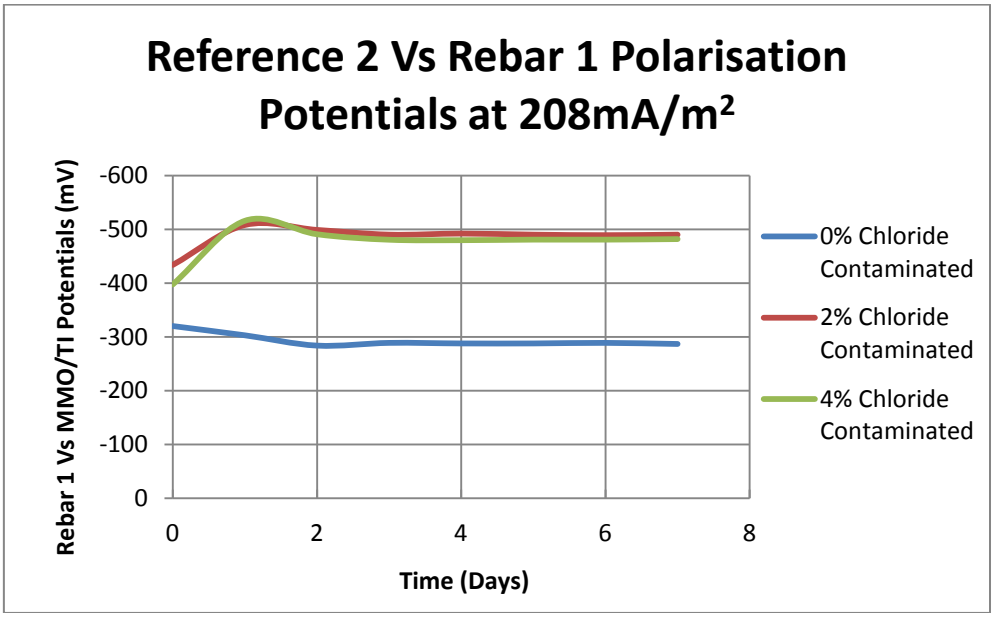

Figure 3.62: Polarisation potentials at 208 mA/m^2 reference 2 Vs rebar 1

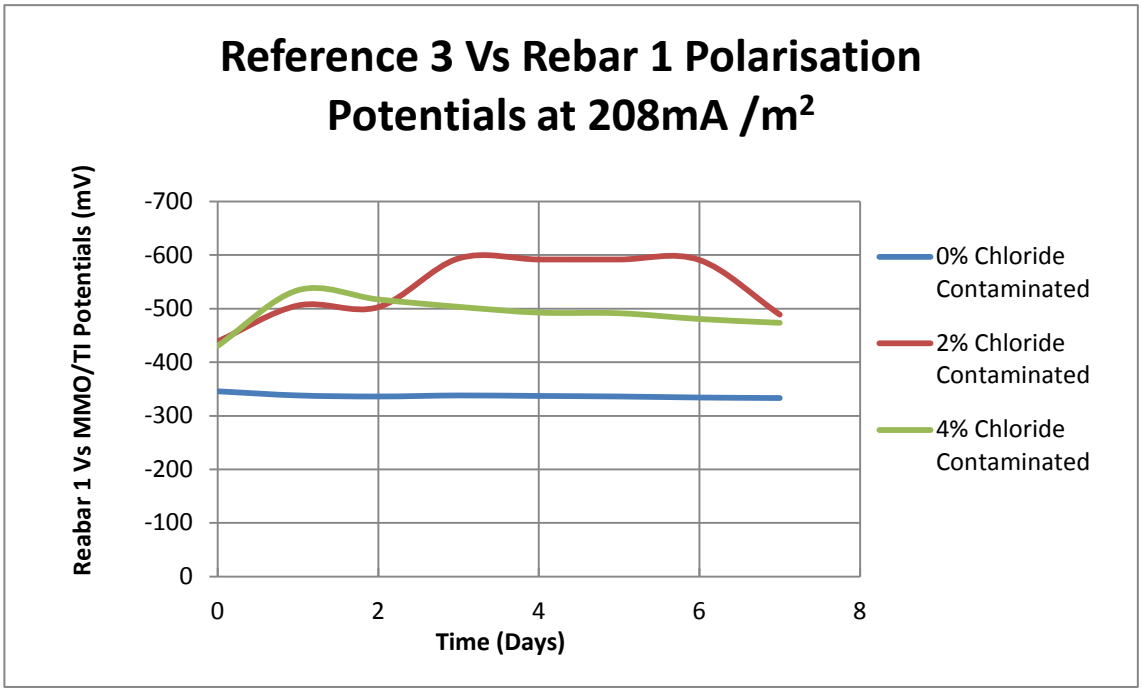

Figure 3.63: Polarisation potentials at 208 mA/m² reference 3 Vs rebar 1

Table 3.32: Polarisation potentials at 313mA/ m² reference 1 Vs rebar 1

Time Period (Days)	0% Chloride Contaminated Ref 1 Vs Rebar 1 (mV)	2% Chloride Contaminated Ref 1 Vs Rebar 1 (mV)	4% Chloride Contaminated Ref 1 Vs Rebar 1 (mV)
1	-263	-567	-314
2	-264	-568	-313
3	-265	-569	-315
4	-267	-570	-316
5	-268	-570	-317
6	-270	-571	-317
7	-269	-572	-318

Table 3.33: Polarisation potentials at 313mA/ m² reference 2 Vs rebar 1

Time Period (Days)	0% Chloride Contaminated Ref 2 Vs Rebar 1 (mV)	2% Chloride Contaminated Ref 2 Vs Rebar 1 (mV)	4% Chloride Contaminated Ref 2 Vs Rebar 1 (mV)
1	-304	-509	-518
2	-305	-510	-519
3	-305	-511	-521
4	-306	-512	-522
5	-308	-513	-522
6	-307	-513	-524
7	-309	-214	-524

Table 3.34: Polarisation potentials at 313mA/ m^2 reference 3 Vs rebar 1

Time Period (Days)	0% Chloride Contaminated Ref 3 Vs Rebar 1 (mV)	2% Chloride Contaminated Ref 3 Vs Rebar 1 (mV)	4% Chloride Contaminated Ref 3 Vs Rebar 1 (mV)
1	-306	-509	-561
2	-306	-514	-562
3	-308	-516	-561
4	-309	-515	-563
5	-309	-515	-563
6	-312	-516	-564
7	-313	-517	-565

When 30mA current is driven to obtain a current density of 313/m^2 the volt recorded was 7.89V. Therefore the resistance is of the circuit is 263 ohms. As where the resistance of the coating in recorded is of a range between 2 to 4MΩ across the samples.

Table 3.35: Polarisation potentials at 313mA/ m^2 reference 1 Vs rebar 1

Time Period (Days)	0% Chloride Contaminated Ref 1 Vs Rebar 1 (mV)	2% Chloride Contaminated Ref 1 Vs Rebar 1 (mV)	4% Chloride Contaminated Ref 1 Vs Rebar 1 (mV)
1	-263	-567	-614
2	-264	-568	-613
3	-265	-569	-615
4	-267	-570	-616
5	-268	-570	-617
6	-270	-571	-617
7	-269	-572	-618

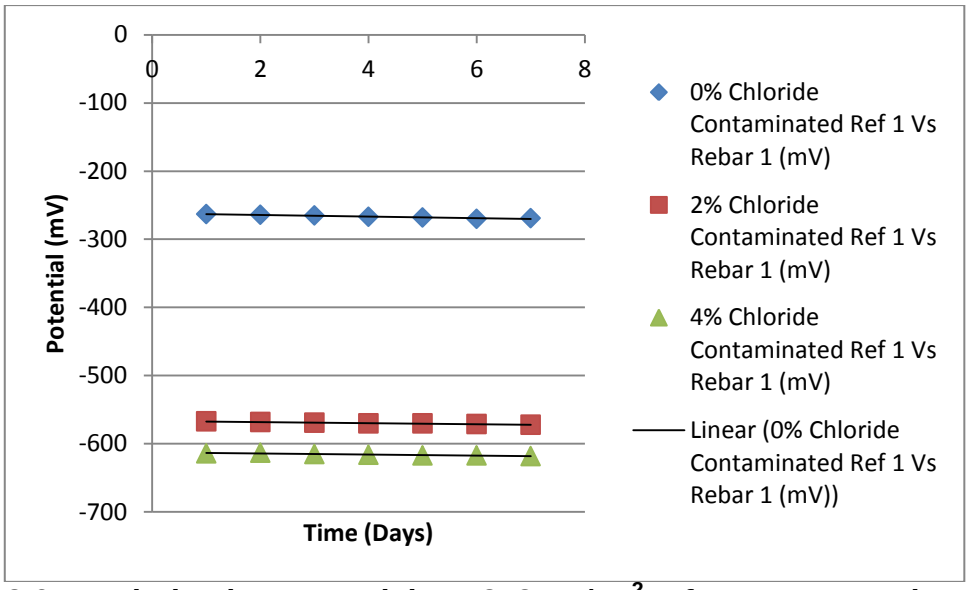

Figure 3.64: Polarisation potentials at 313mA/ m^2 reference 1 Vs rebar 1

Table 3.36: Polarisation potentials at 313mA/ m^2 reference 2 Vs rebar 1

Time Period (Days)	0% Chloride Contaminated Ref 2 Vs Rebar 1 (mV)	2% Chloride Contaminated Ref 2 Vs Rebar 1 (mV)	4% Chloride Contaminated Ref 2 Vs Rebar 1 (mV)
1	-304	-509	-518
2	-305	-510	-519
3	-305	-511	-521
4	-306	-512	-522
5	-308	-513	-522
6	-307	-513	-524
7	-309	-214	-524

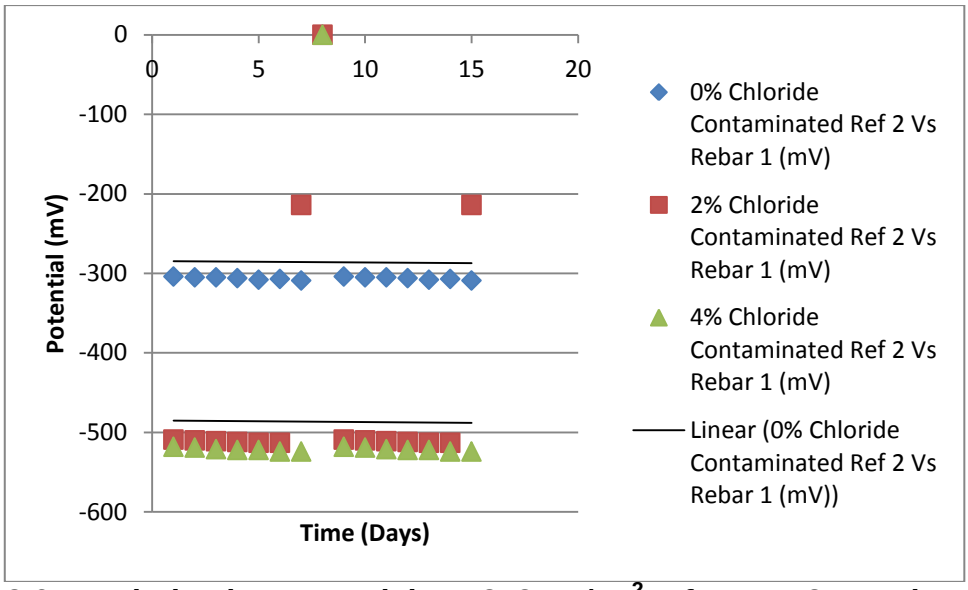

Figure 3.65: Polarisation potentials at 313mA/ m^2 reference 2 Vs rebar 1

Table 3.37: Polarisation potentials at 313mA/ m^2 reference 3 Vs rebar 1

Time Period (Days)	0% Chloride Contaminated Ref 3 Vs Rebar 1 (mV)	2% Chloride Contaminated Ref 3 Vs Rebar 1 (mV)	4% Chloride Contaminated Ref 3 Vs Rebar 1 (mV)
1	-306	-509	-561
2	-306	-514	-562
3	-308	-516	-561
4	-309	-515	-563
5	-309	-515	-563
6	-312	-516	-564
7	-313	-517	-565

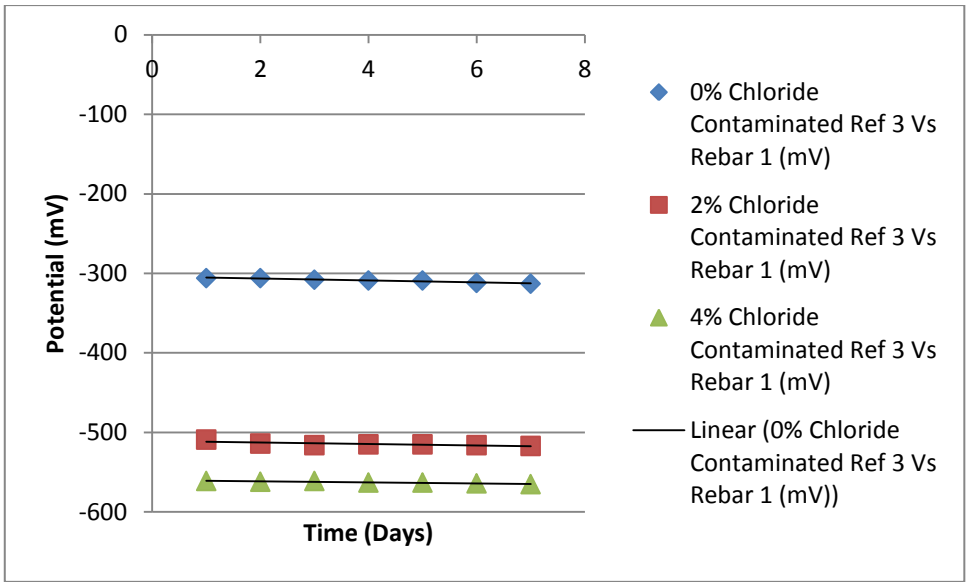

Figure 3.66: Polarisation potentials at 313mA/ m^2 reference 3 Vs rebar 1

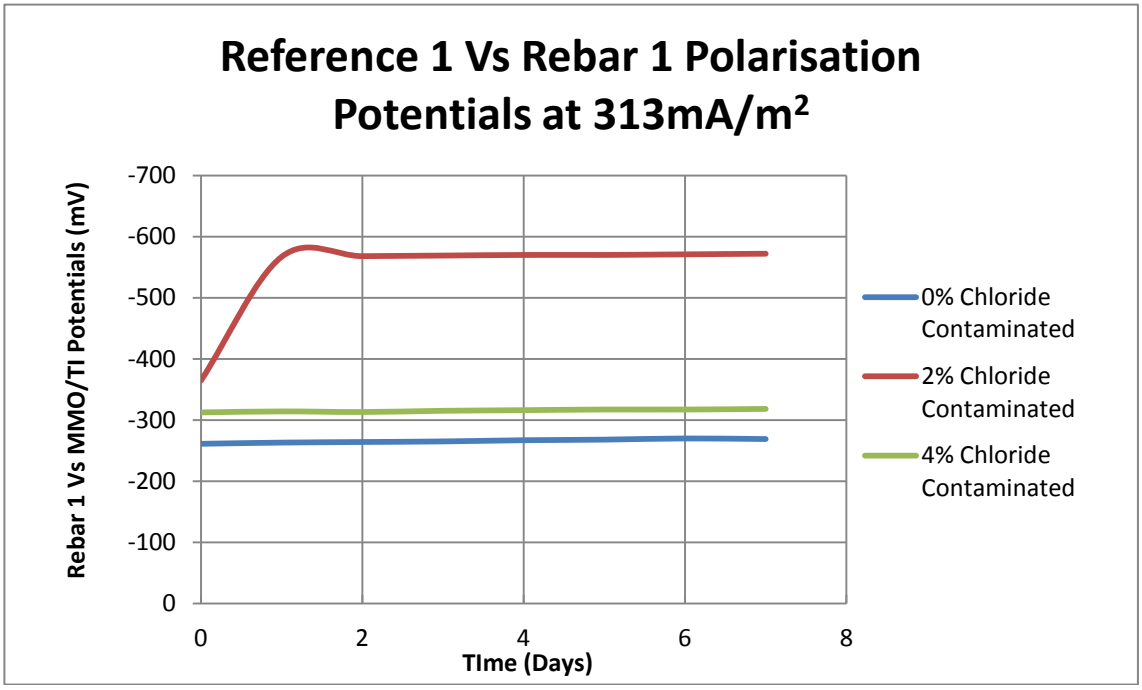

Figure 3.67: Polarisation potentials at 313 mA/m^2 reference 1 Vs rebar 1

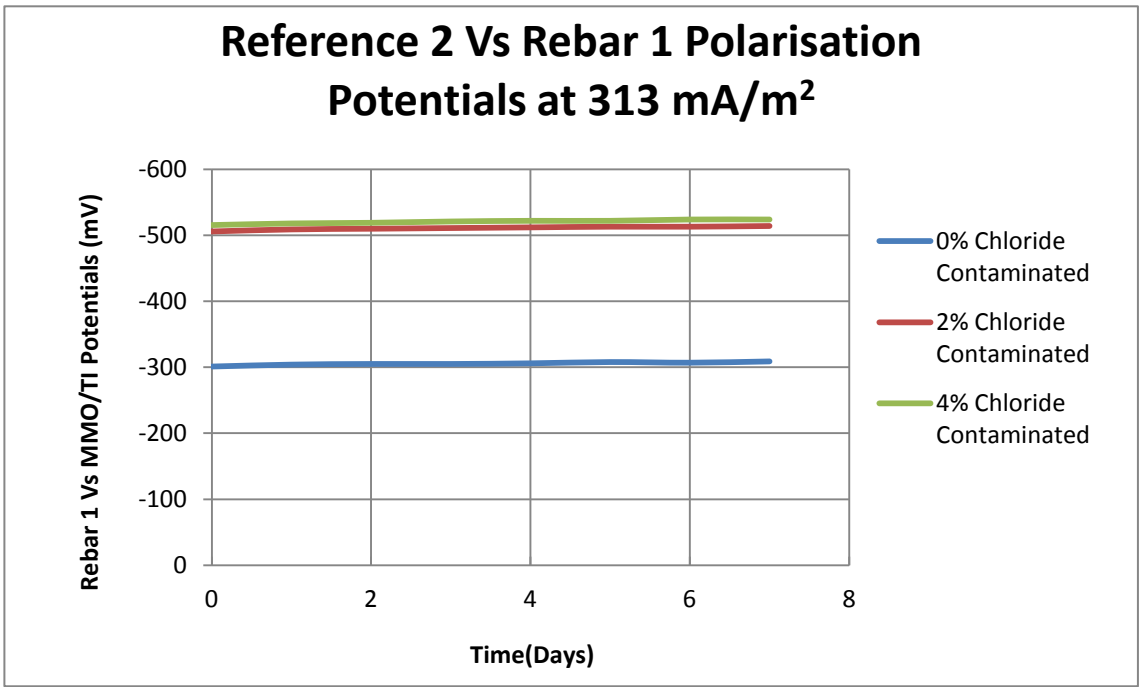

Figure 3.68: Polarisation potentials at 313 mA/m² reference 2 Vs rebar 1

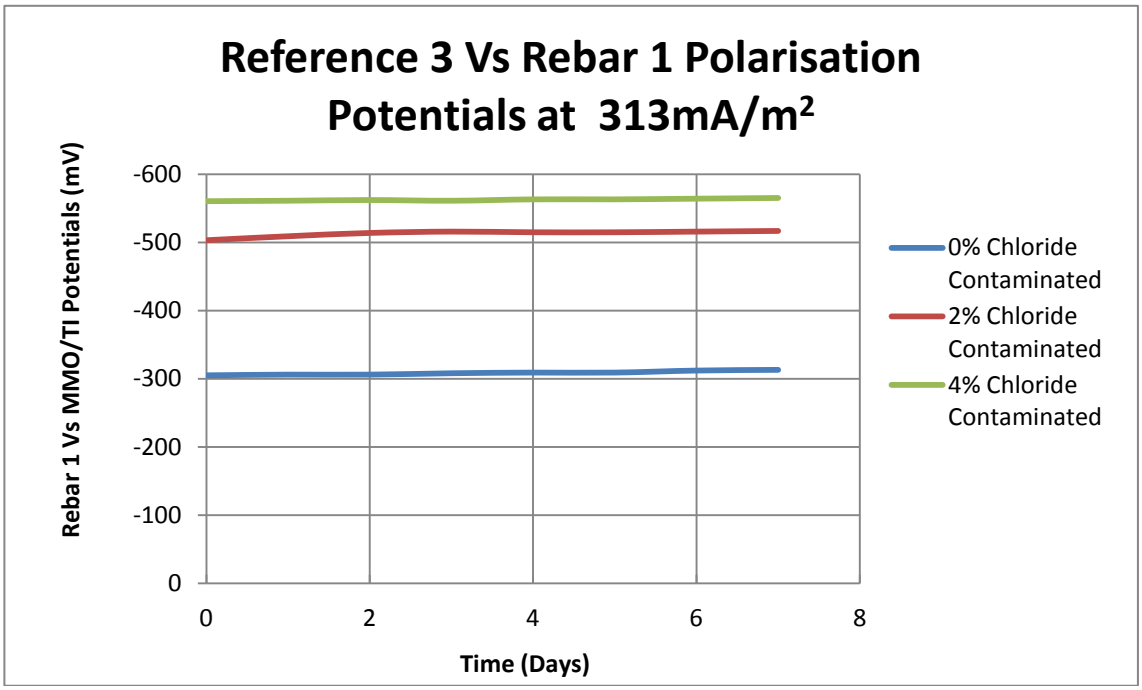

Figure 3.69: Polarisation potentials at 313 mA/m² reference 3 Vs rebar 1

The polarisation results obtained behave in similar lines to those were obtained by Masadeh [2005] for steel anode cathodic system. The potentials obtained are in a range of -250mV to -565mV for all assessed current densities to the surface of the concrete with a general increase of 100mV in the negative direction. The

protection of the steel was not completely, as it is considered by many -770mv is good criteria to be 100% protected. A polarisation shift of 100mv represents protection in the region of 80% against corrosion which was achieved by all samples [Masadeh 2005]. Cathodic protection systems normal starts correctly working after two to four weeks of driving current to get potentials excess of -770mV. All reference electrodes were showing the expected change in potential reading becoming more negative when current was applied.

3.4.9.3 De-Polarisation Results

The de-polarisation results are shown in Figures 3. 70 to 3.78 and the tabulated data is given in Appendix Tables A10 to A18. The de-polarisation readings were taken from 5 minutes after instant off until the readings became stable. In accordance with BS EN 12696:2000 Cathodic protection of steel in concrete de-polarisation readings are taken at intervals of 1 hour, 2hours, 4hours, 8 hours, 1, hours and 24 hours.

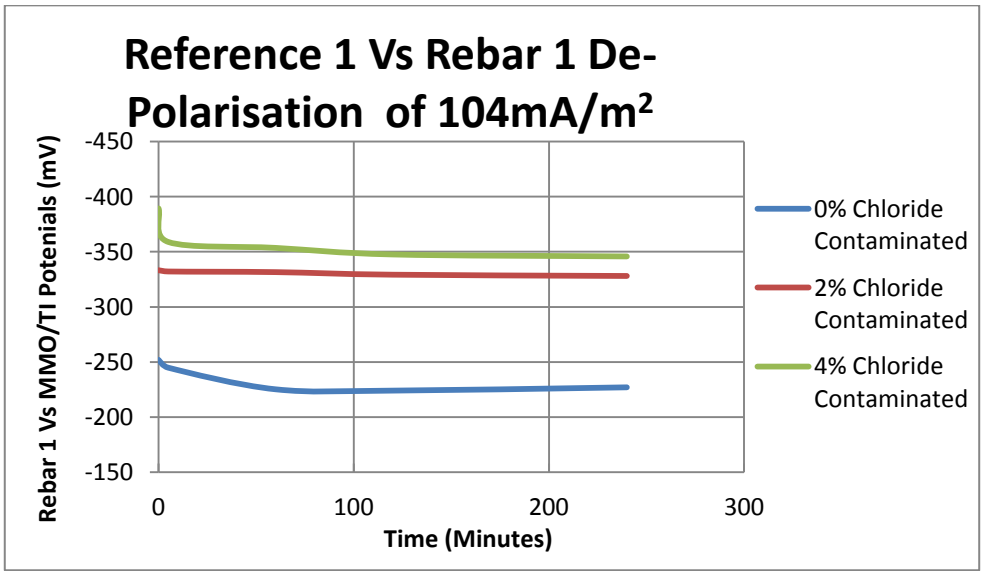

Figure 3.70: De-polarisation potentials at 104 mA/m^2 reference 1 Vs rebar 1

The measurements were relatively stable during the test period. The samples achieved varied decay potential decay within four hours. By the comparison of polarisation and de polarisation data it could be said that beam specimen with 0% chloride contamination is protected and the samples with chlorides are not

protected as there is a increase of potential readings between MMO/TI VS rebar in the negative direction. This is generally represented in Figures 3.63 and 3.64

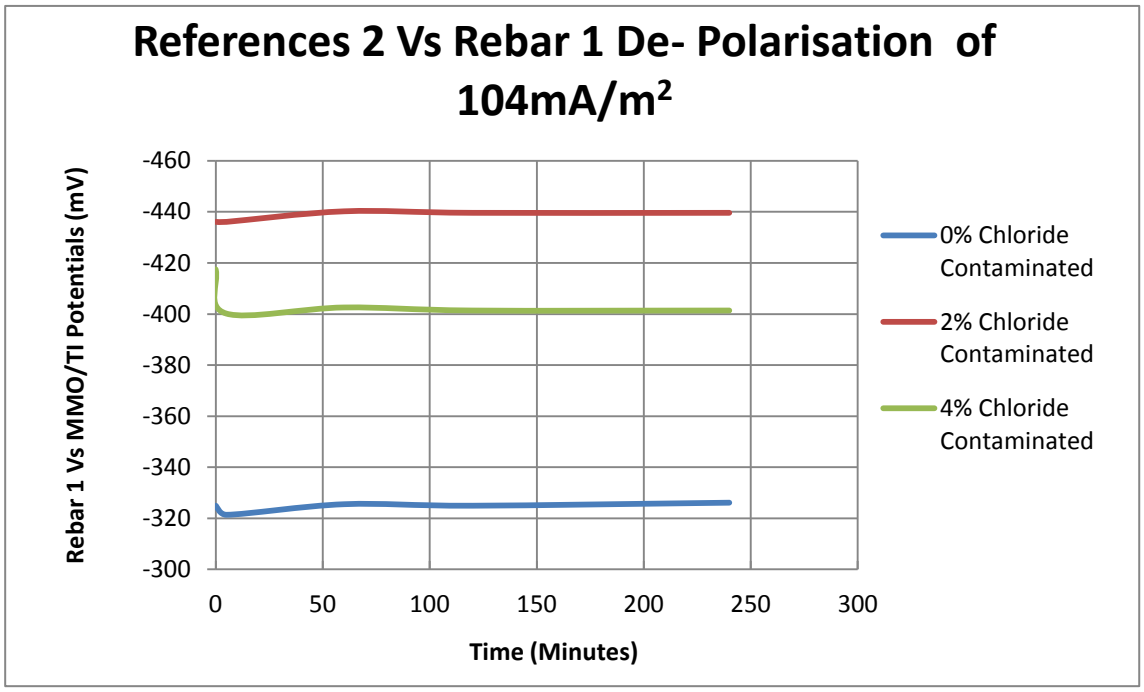

.

Figure 3.71: De-polarisation potentials at 104 mA/m^2 reference 2 Vs rebar 1

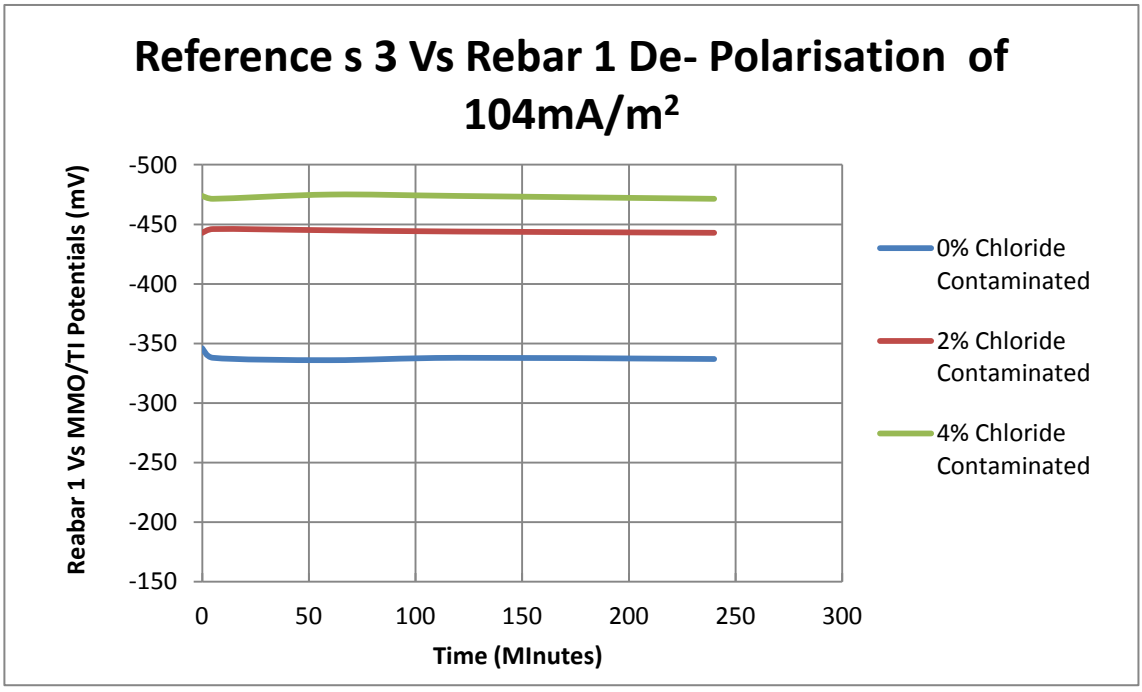

Figure 3.72: De-polarisation potentials at 104 mA/m^2 reference 3 Vs rebar 1

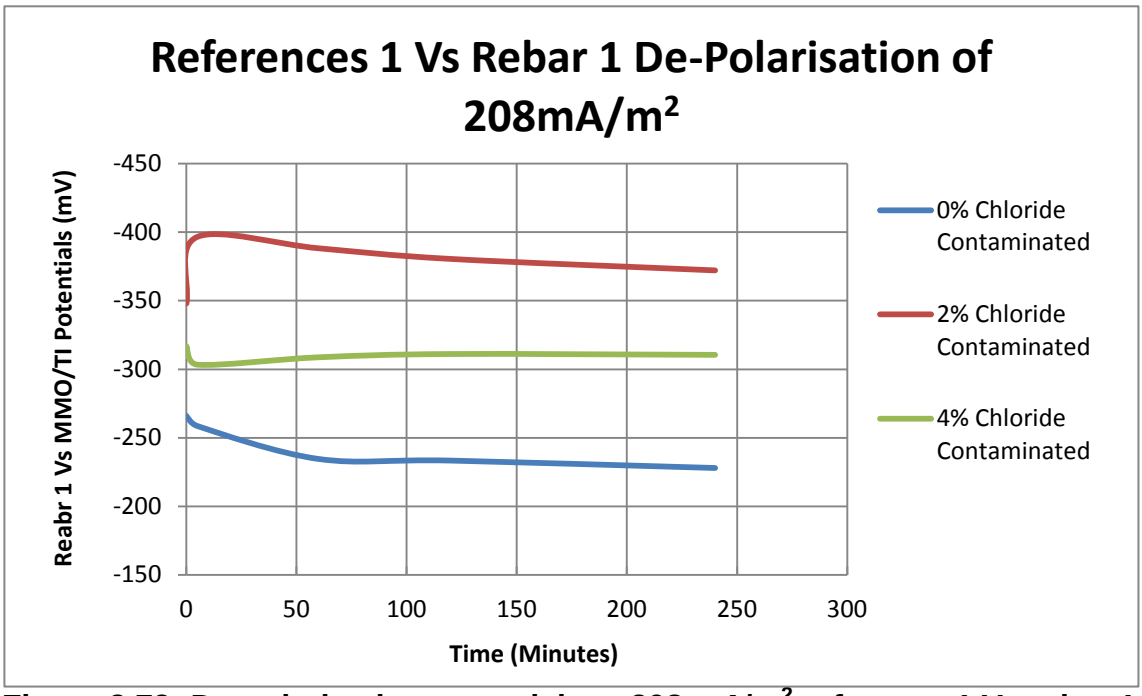

Figure 3.73: De-polarisation potentials at 208 mA/m^2 reference 1 Vs rebar 1

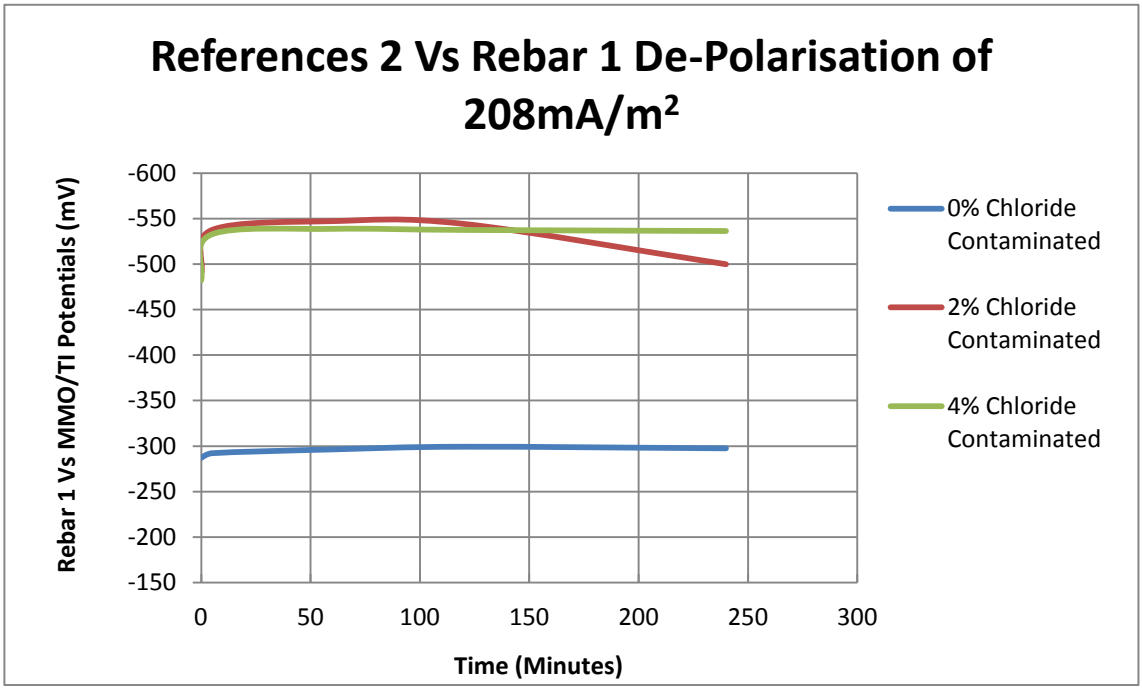

Figure 3.74: De-polarisation potentials at 208 mA/m^2 reference 2 Vs rebar 1

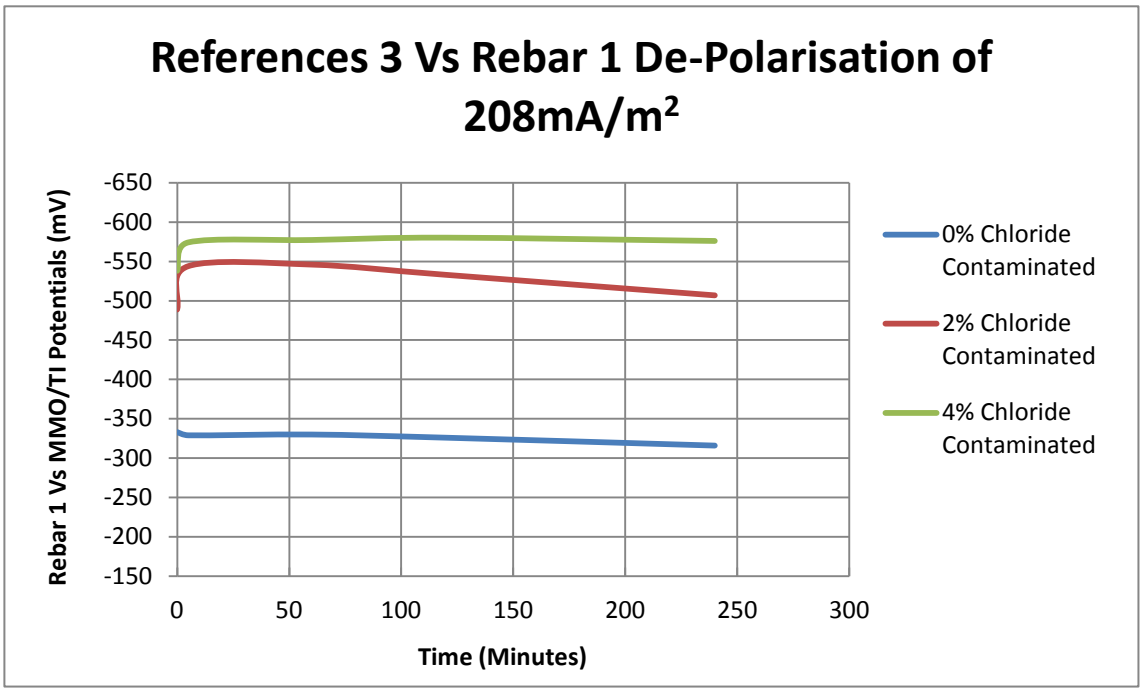

Figure 3.75: De-polarisation potentials at 208 mA/m^2 reference 3 Vs rebar 1

From Figures 3.65 to 3.67 only the control sample is protected, when de-polarisation is observed at 208mA/m2 this is due to an increase of potential in the negative direction from -550 to -575 for specimens contaminated with 4% chloride.

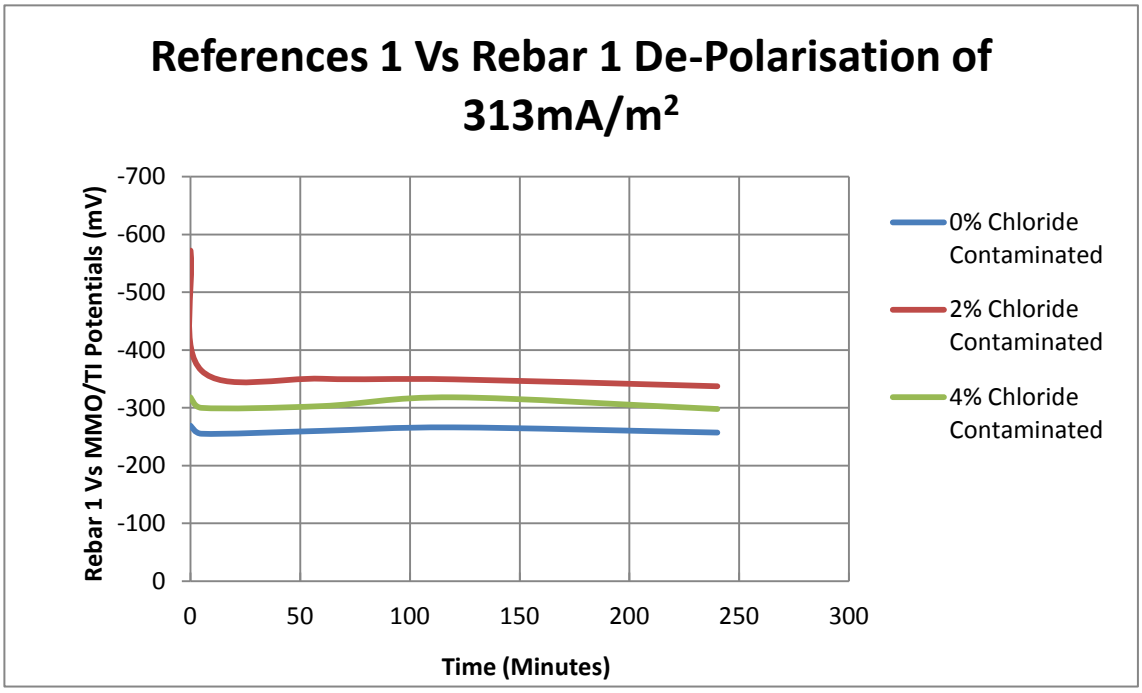

Figure 3.76: De-polarisation potentials at 313mA/m^2 reference 1 Vs rebar 1

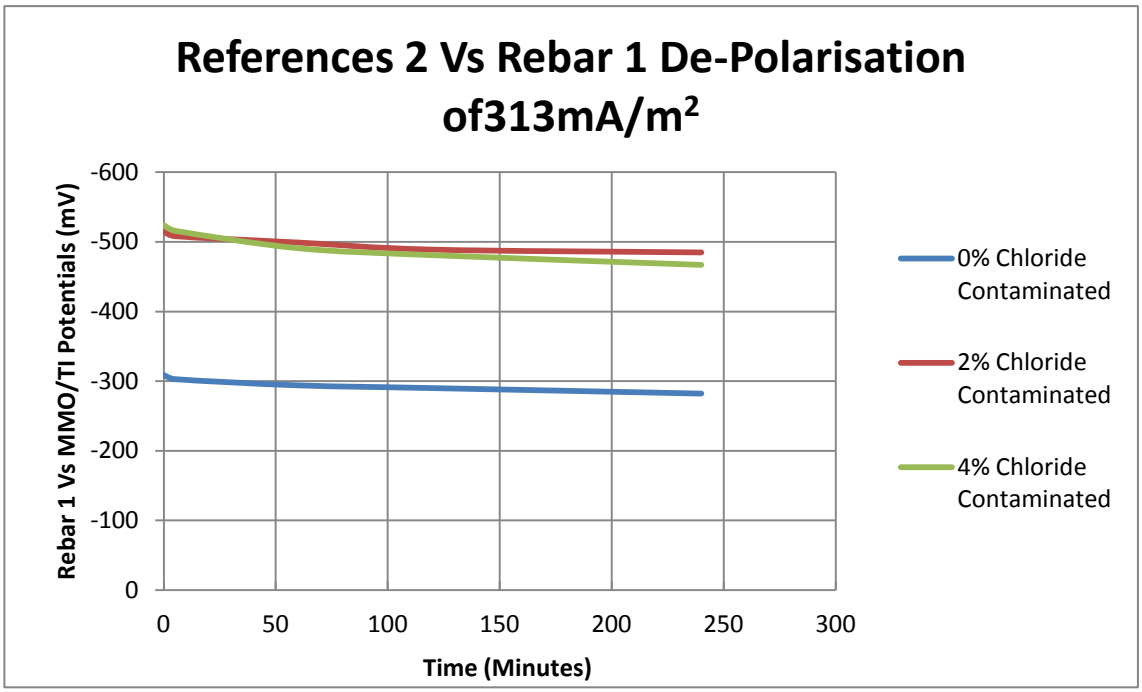

Figure 3.77: De-polarisation potentials at 313mA/m^2 reference 2 Vs rebar 1

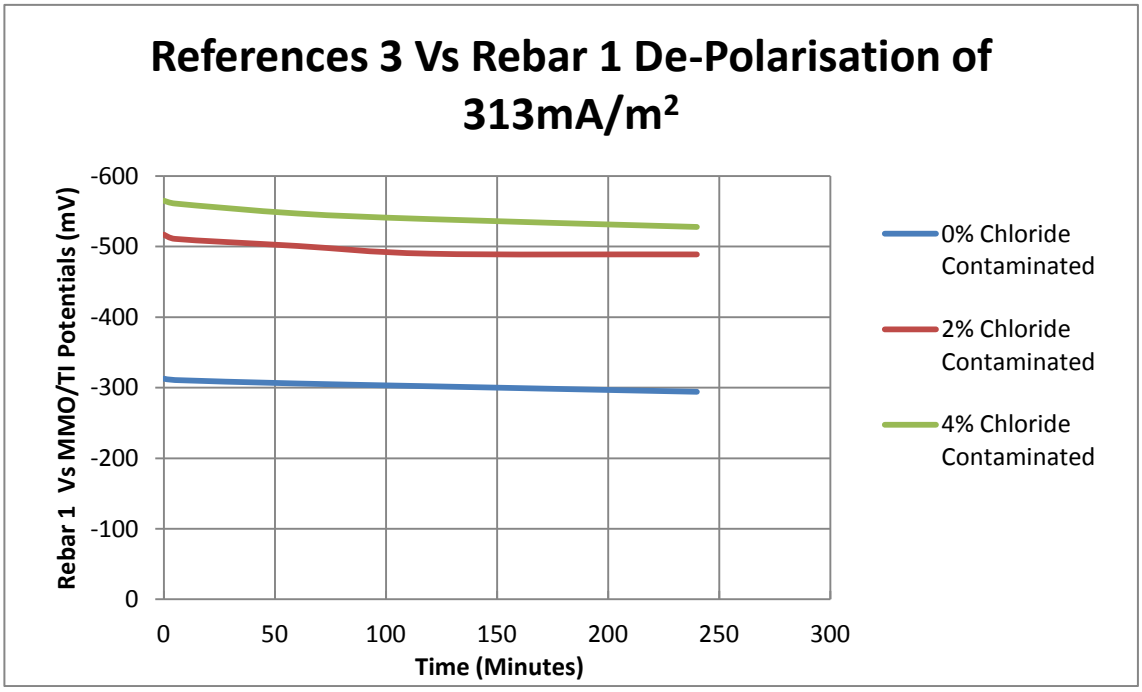

Figure 3.78: De-polarisation potentials at 313mA/m^2 reference 3 Vs rebar 1

When current of 30mA is applied it shows de-polarisation potentials at a current density 313mA/m^2 to the concrete surface, greater than 100mv (Figure 3.78) were obtained indicating that the reinforcement is protected. The de-polarisation also

represents that the samples are not corroding. They are protected. It is recommended that is "*if the potential decays 100 mV or more in 4 hours, the system is assumed to be operating properly. If the potential drop in the 4 hours is less than about 80 mV, the current to the system is increased"* (Kepler *et al*.2000). Therefore the effectiveness of the system will increase.

It was also found out that the current dissipates slightly as the distance is increased from the connection of the primary electrode as shown in Figures 3.66 to 3.68. This is shown by that by lower decay potential reading obtained at reference 1 on samples control and 4% contaminated at current density 208mA/m^2 and 313mA/m^2, but at a current density of 104mA/m^2 potential readings were stable across all samples. This may be due to the high resistance of the coating, a range between 3 to 7MΩ resistance was observed for the coating when a current of 2mA and 3mA was supplied. The resistance measurement was taken between points of the surface of the zinc coating. The overall circuit resistance was of 116Ω and 263Ω respectively, therefore it could be said that the resistance of the coating may disrupt the distribution of the cathodic current. It was also found by Masadeh [2005] that as the distances increase the current flow will dissipate for an open circuit impressed system.

Graphical representation also show an increase in decay which means that current is getting distributing without loss across the surface of the coating as the distance increases. Note, reference 1 is the furthest away at a distance of 580mm for 4% chloride contaminated sample, and 480mm for control sample and 2% chloride contaminated sample and reference 3 is the closest to the connection of the primary electrode at a distance of 80mm for the 4% chloride contaminated sample, and 180mm for 2% chloride contaminated and control specimens.

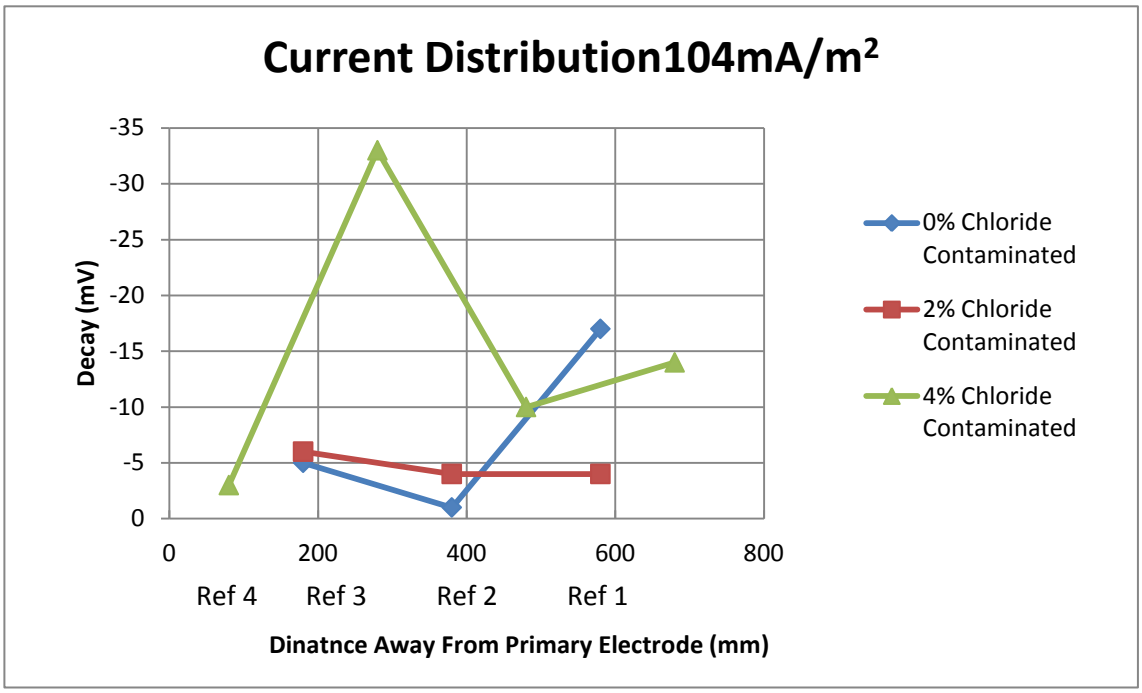

Figure 3.79: Decay Vs Distance at 104mA/m^2

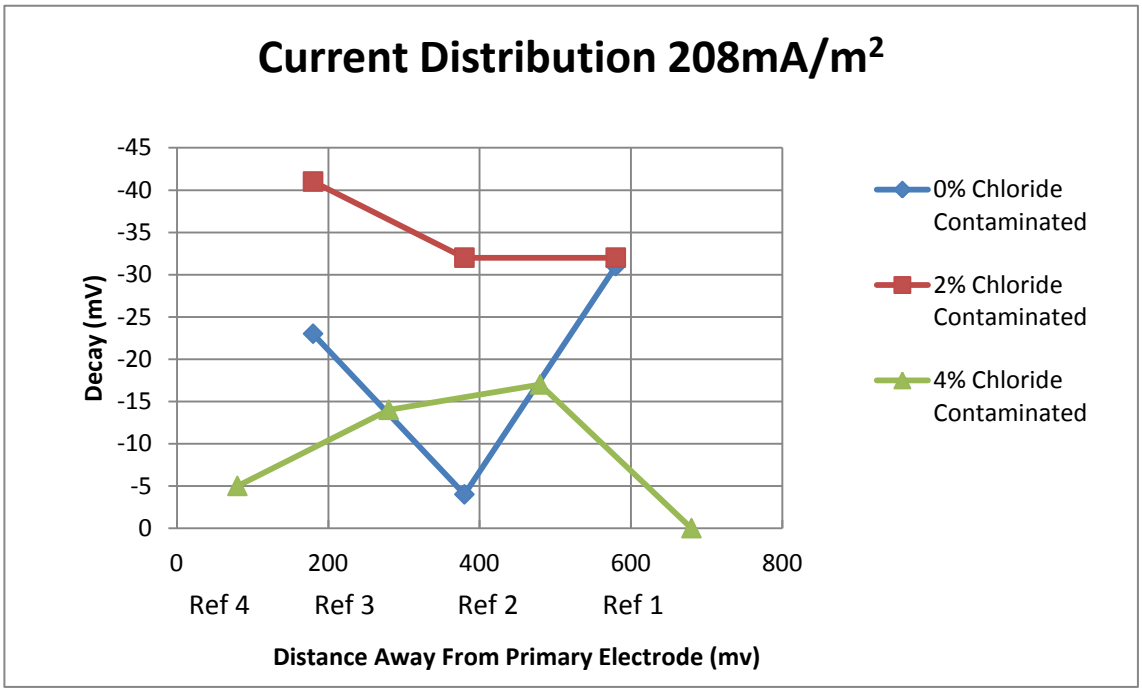

Figure 3.80: Decay Vs Distance at 208mA/m^2

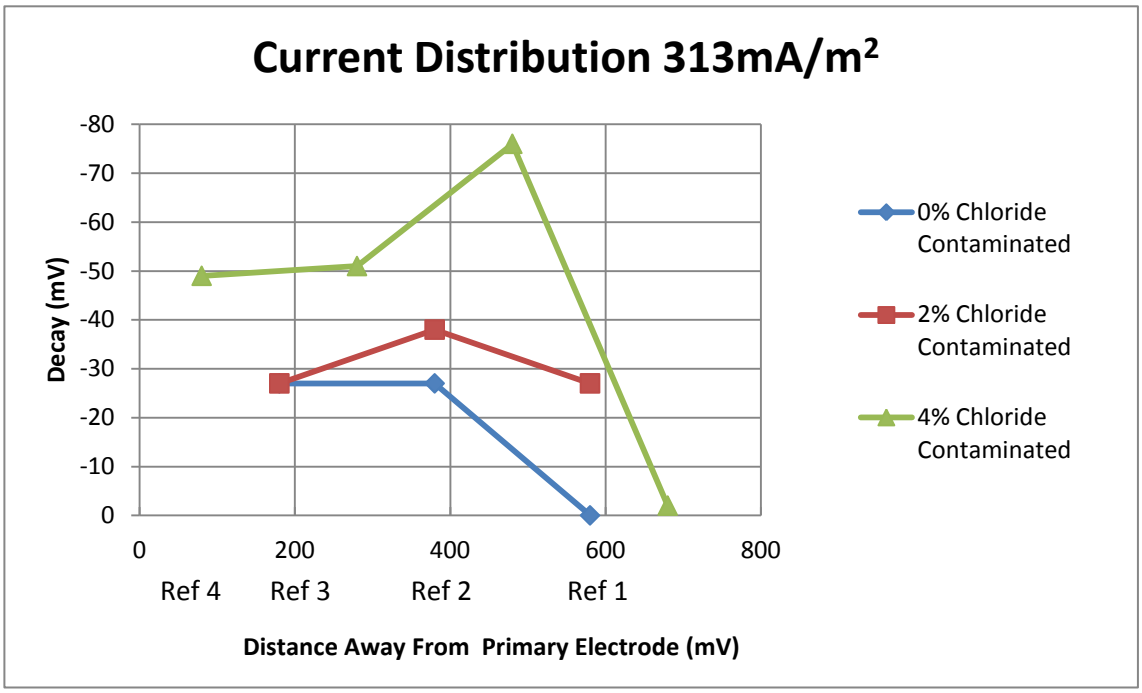

Figure 3.81: Decay Vs Distance at 313mA/m^2

3.4.9.4 Physical Evidence of Results

To confirm the validity of the experimental results at end of each driving current, the samples were visually examined for deterioration and damage. The ZINGA coated surface was closely visually inspected; also a 'forced sello tape test' was carried out to identify if any element of the coating was easily came off from the concrete substrate.

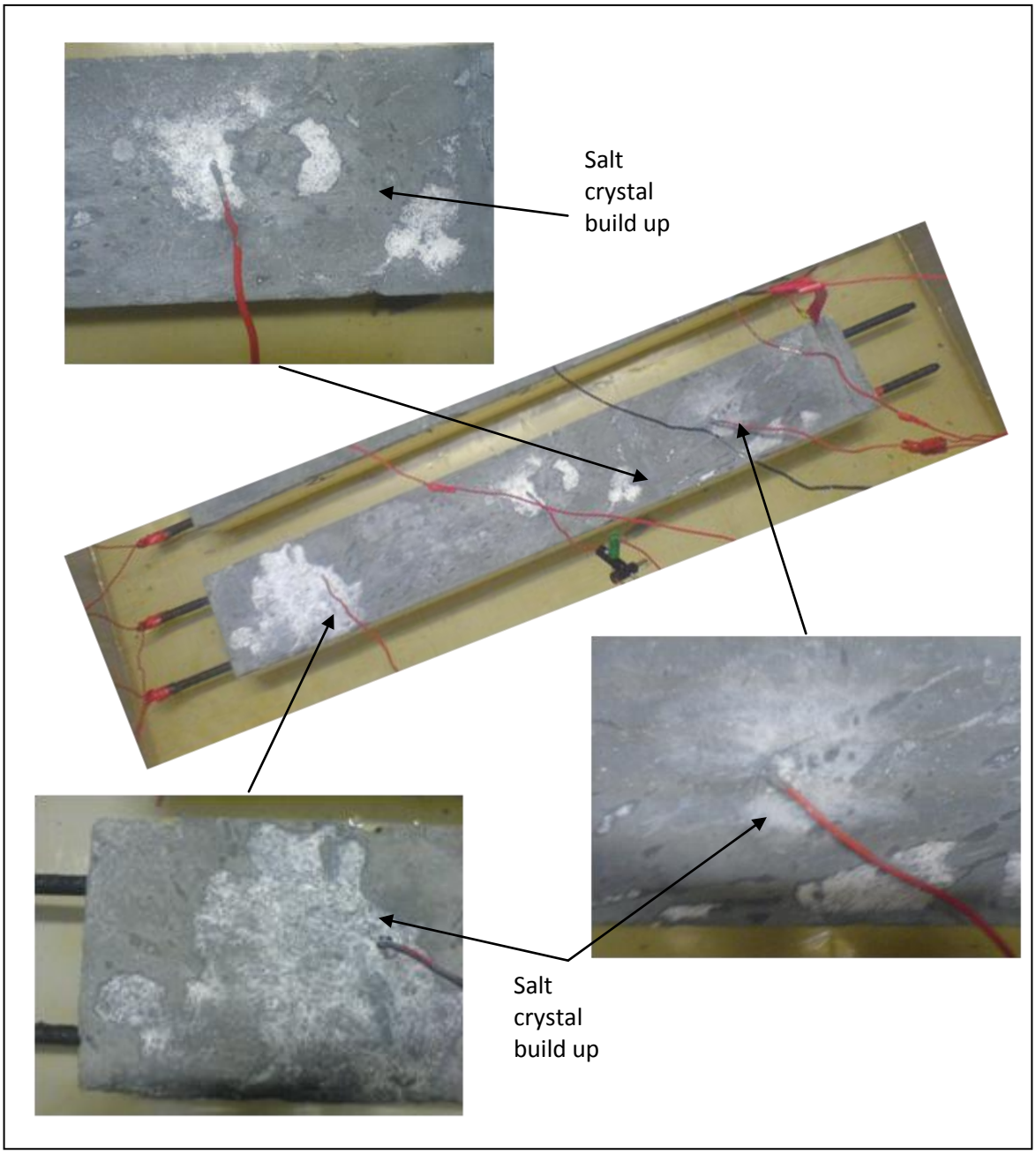

Figure 3.82: Images of chloride build up at the surface of control sample

Figure 3.82 shows the damage to the coating for the control specimen before potential testing began. The damage could be caused by accidental damages by salt contaminated solutions dripping on to the surface of the specimen when other wet sample were lifted out of NaCl solution tank and moved over this specimen, the excess NaCl solution could have dripped on to the surface of the specimen. However, pull-off test (using sello-tape) indicated no loss of adhesion of the paint on concrete surfaces at the affected areas.

Figures 3.83 and *3*.84 show the Beam specimens before and after 'forced sello-tape' tests carried out following the completion of the polarisation experiments at each current density assessed. The figures show no or negligible damage caused to the coating when the sello tape is forced off. This may be due to that the levels of applied current tested were only driven for about 7 days, which may be considered as very short period of time.

Sample	Image Before Sello Tape Test	Image of Sello Tape	Image After Sello Tape Test	Description Damage
Beam 1 Control	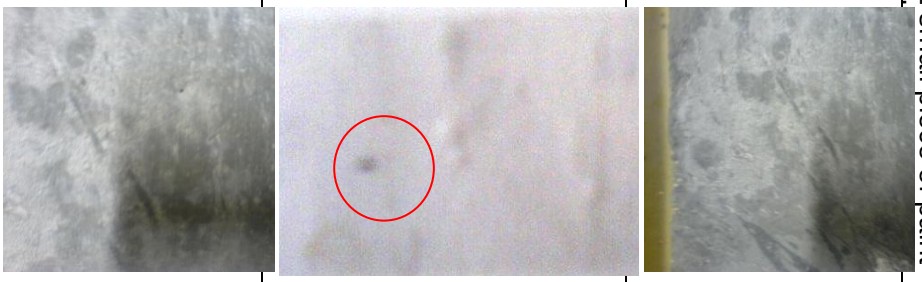			Negligible damage to zinc coating. 1 small piece of paint
Beam 2, 2% Chloride Contaminated	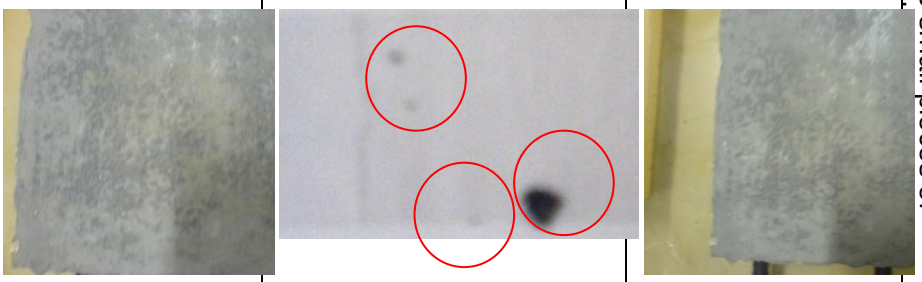			Negligible damage to zinc coating. 3 small pieces of
Beam 3, 4% Chloride Contaminated				Negligible damage to zinc coating. 2 small pieces of paint

Figure 3.83: Visual results of specimens when assessed at current density of 104 mA/m^2

Sample	Image Before Sello Tape Test	Image of Sello Tape	Image After Sello Tape Test	Description Damage
Beam 1 Control				No damage to zinc coating. Salt crystals removed by tape.
Beam 2, 2% Chloride Contaminated	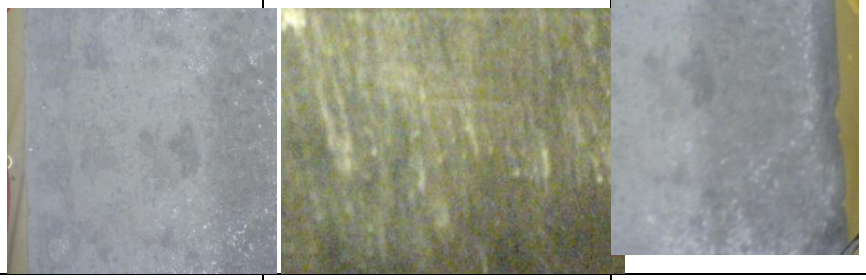			No damage to zinc coating. Salt crystals removed by tape.
Beam 3, 4% Chloride Contaminated	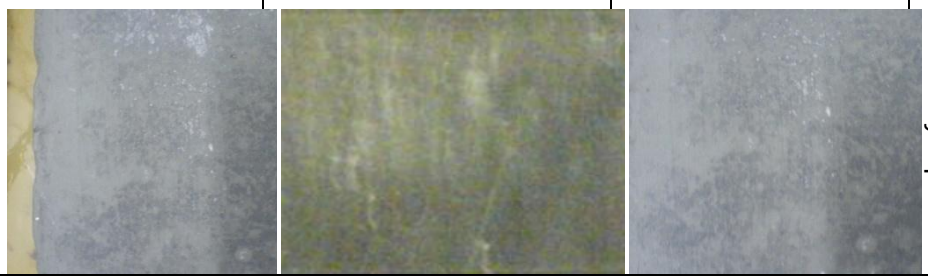			No damage to zinc coating. Salt crystals removed by tape.

Figure 3.84: Visual results of specimens when assessed at current density of 208 mA/m^2

3.5 Electrochemical Tests: Environmental Effects On Performance Of ZRP

3.5.1 Introduction

The main aim of this part to the investigation was to assess the performance and durability of ZRP coating as anode for ICCP system under variable environmental conditions, particularly the effect of changing temperature and relative humidity.
This section briefly outlines methodology of testing and presents the results together with the interpretation and discussion of result. Detailed methodologies of sample preparation and experimental test procedures are give in Appendix C1

3.5.2 Sample Preparation and Experimental Procedures

Sample Preparation:

A total of 3 specimens were used for this experiment. Three concrete blocks of size 150X150x150mm had been prepared. 2 specimens had 1% and 3% of NaCl while concrete mix and 1% and 3.5% NaCl in water and third specimen without any NaCl content. The 3 cubes, labelled, A, B, and C are shown in figure 3.85.

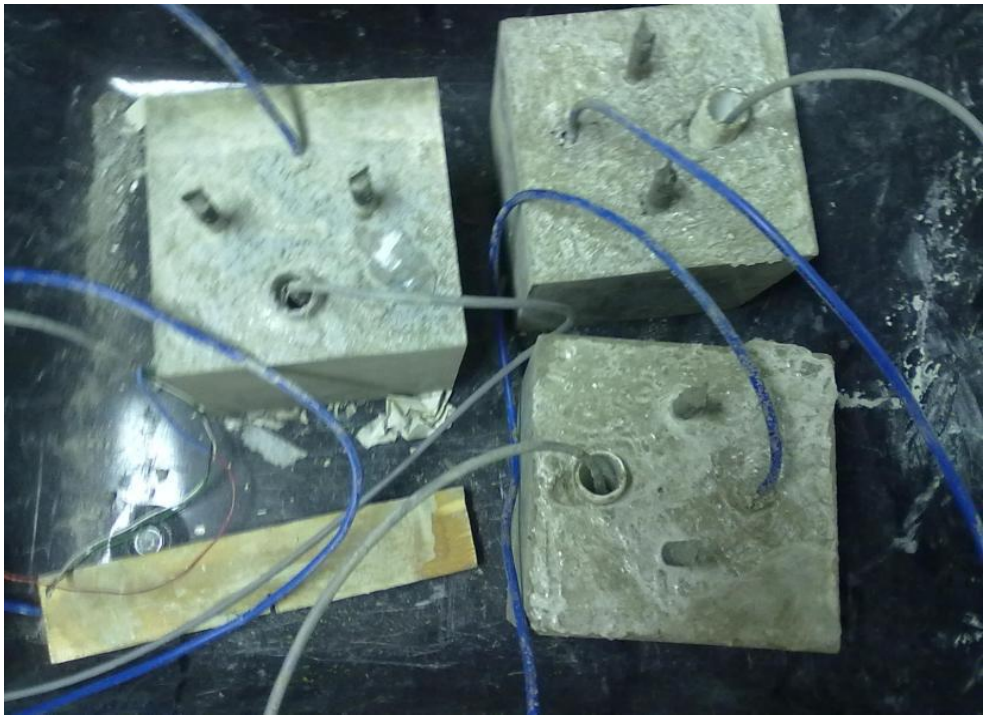

Figure 3.85: Concrete Cube specimens for Environmental Testing

Experimental – Test Procedures.

1. Once the 3 blocks are placed in their respective trays, monitor the potentials of the rebars and also the zinc coating w.r.t Ag/AgCl and MMO/Ti reference electrodes.
2. Measure the corrosion current of the rebars with the 'beta-probes.
3. Monitor as per 1 and 2 above for 1or 2 weeks (or until some decent active corrosion to rebars in blocks with chloride).
4. Place the blocks (with chloride) in the environmental chamber set at 50 ºC , 90% RH and then apply CP at the current set in item 5.
5. Set the DC power supply in constant current mode to supply a constant current of 10.0 mA. (Note: the anode, i.e. Zinc paint, shall be connected to the positive terminal of the power supply).
6. The following parameters shall be measured at 1 h, 24 h, 7 days, 28 days, 40 days (40 cycles in total shall be used)

(a) Cell Voltage and cell current
(b) Anode potential versus the Ag/AgCl reference electrodes.
(c) Cathode (rebars) potential
(d) Corrosion current with the 'beta-probe.
(e) Bond strength between paint and concrete before and after applying the current
(f) Characteristics of interface of zinc paint and concrete after applying current

These three concrete blocks were put in three different trays. Some proportion of water was added in the tray so that the moisture remains in the concrete and the corrosion starts early. Cube A was only with water, cube B with 1% and cube C with 3.5% chloride solution. All the wires were connected with the data logger. The positive channels were connected with the probe and reference electrode and negative channel with steel and copper trip used for zinc paint. Lab Jack software was used to analyse readings on the desktop computer.

After monitoring the corrosion potential and corrosion current for 14 days all three 'cube' specimen were placed in the environmental chamber, as shown in Figure 3. 86.

Figure 3.86: All three cubes placed in the chamber

The environmental chamber was set up at temperature of 20 degree and 50% humidity using software. The results were recorded and displayed on Microsoft excel sheet.

The S!MPATI software used to set up the 24 hour cycle period in which the software set at digital start, the temperature was raised from 20°C to 50°C in 1 hour, then the 50°C temperature was maintained constant for 8 hours, then the temperature was again ramped down from 50°C to 20°C, the remaining time left i.e. 14 hours was kept constant for normal 20°C temperature. In this same way the humidity was also set up from 50% to 90%. This is illustrated in Figure 3. 87.

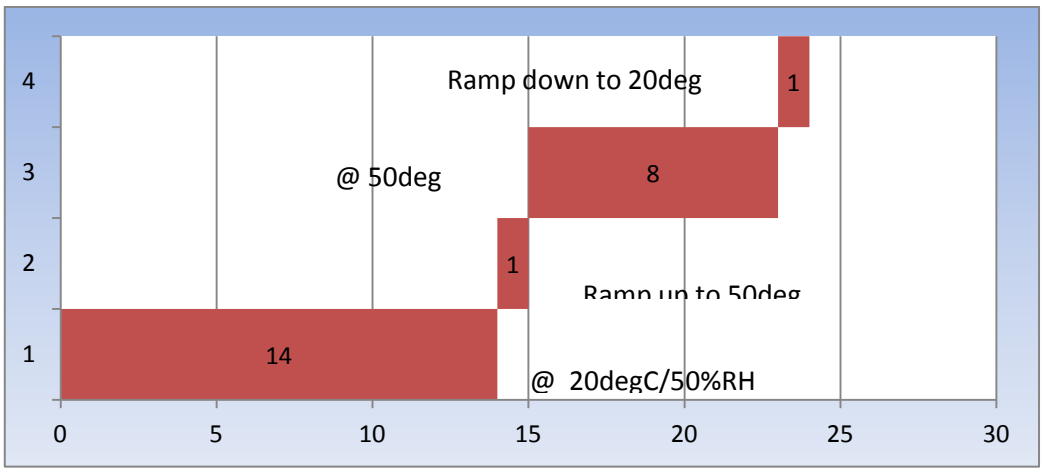

Figure 3.87: '24 hour' cycle – sequence of operation

In this manner 40 cycles had been recorded on the Microsoft excel spread sheet to observe its effect on the Zinc rich paint on all the three concrete blocks and

Once the initial conditioning of the samples was reached they are connected to a DC power supply in constant current mode to supply a constant CP current of 10.0 mA.

The tests were continued for 40 cycles.

Results and discussion

The detailed records all test data obtained in the course of this phase of investigation are tabulated and illustrate graphically and are included in Appendix C1. The findings are summarised and discussed below.

The results given Table 3.38 and Figures 3.88 and 3.89 show the corrosion potentials monitored for 14 days following 28 days curing outside the environmental chamber. All results have been recorded while the environmental chamber was maintaining at 20ºC temperature and 50% humidity, without and with CP.

Table 3.38: Corrosion potential (vs. silver/ silver chloride) and Corrosion current of rebar in cube samples (Test results without CP)

	Cube A (No chloride content)		Cube B (1% chloride content)		Cube C (3.5% chloride content)	
No. of days recorded	**corrosion potential (mV)**	**Corrosion current**	**corrosion potential (mV)**	**Corrosion current**	**corrosion potential (mV)**	**Corrosion current**
1	-306	-38	-358	-39.5	-370	-39
2	-318	-47	-368	-42	-405	-39.5
3	-298	-40	-361	-40	-417	-37
4	-279	-49.5	-342	-44	-428	-42
5	-271	-47	-357	-48.5	-453	-53.5
6	-283	-47.5	-354	-52	-461	-52.5
7	-248	-48	-312	-55	-414	-50
8	-259	-40	-368	-59	-434	-49.5
9	-273	-49	-363	-63	-438	-53.5
10	-289	-53	-357	-72	-440	-62
11	-292	-48	-344	-68	-412	-67
12	-301	-47	-343	-75	-471	-73
13	-312	-42	-396	-73.5	-449	-82
14	-318	-49	-356	-74	-453	-93

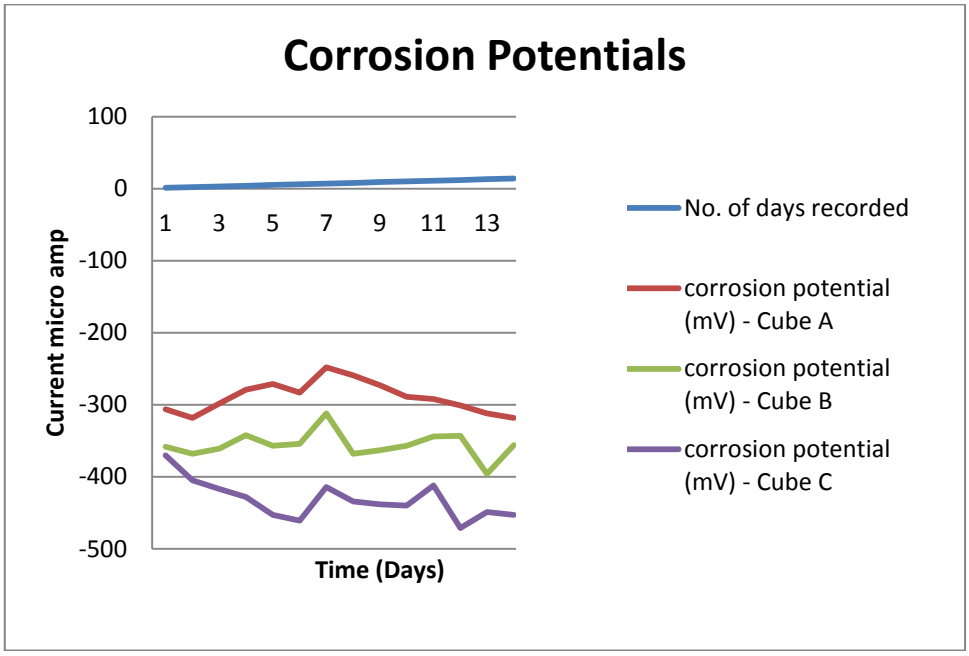

Figure 3.88: Corrosion Potentials (No CP)

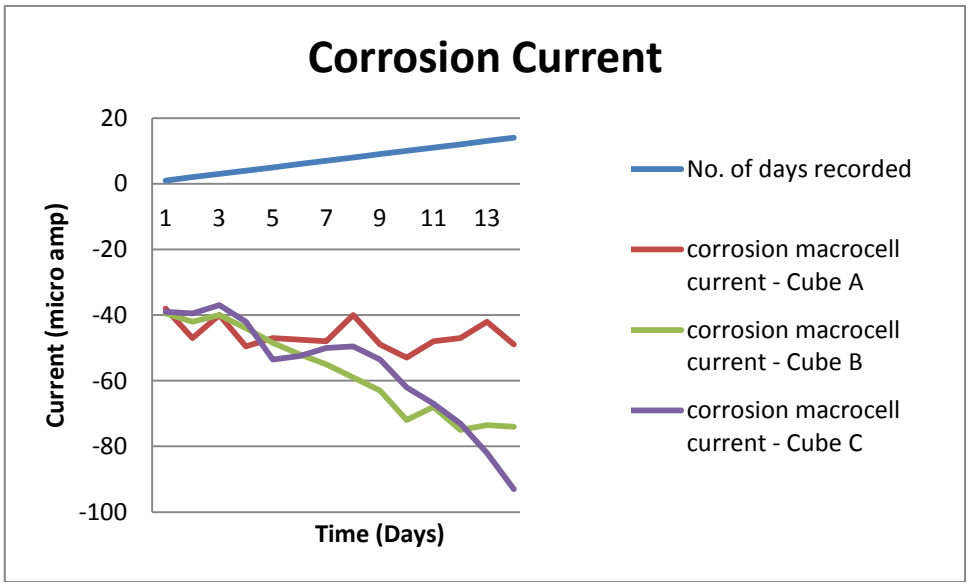

Figure 3.89: Corrosion macrocell current (No CP)

Table 3.39 and Figures 3. 90 and 3.91 show the corrosion potentials and the corrosion macrocell current monitored for 40 cycles with sustained application of CP. All results have been recorded while the environmental chamber was maintaining at 20ºC temperature and 50% humidity, without and with CP.

Table 3.39: Corrosion potential (vs. silver/ silver chloride) and Corrosion current of rebar in cube samples (Test results with CP)

	Cube A (No Chloride)		Cube B (1% Chloride)		Cube C (3.5% Chloride)	
No. of Days	**Corrosion Potential, mV (w.r.t. Ag/AgCl)**	**Corrosion current, mV, measured across 1 ohm**	**Corrosion Potential, mV (w.r.t. Ag/AgCl)**	**Corrosion Current, mV across 1 ohm**	**Corrosion Potential, mV (w.r.t. Ag/AgCl)**	**Corrosion Current, mV across 1 ohm**
1	-353	-49.5	-433	-73.5	-498	-93.5
2	-325	-52	-439	-75	-503	-98
3	-346	-52	-437	-75	-498	-98
4	-388	-52	-428	-75	-429	-98
5	-360	-52	-513	-75	-413	-98
6	-358	-52	-505	-75.5	-430	-98
7	-315	-52	-510	-75	-453	-98
8	-355	-52.5	-529	-74.5	-461	-98
9	-380	-52	-447	-75	-460	-98
10	-365	-52.5	-435	-75	-462	-98
11	-364	-52,5	-498	-75	-464	-98
12	-390	-53	-397	-75	-496	-98
13	-343	-53	-407	-75	-495	-98
14	-325	-53	-441	-75	-487	-98
15	-360	-53	-465	-75	-480	-97,5
16	-358	-53	-436	-75	-482	-97.5
17	-347	-53	-463	-75	-482	-97.5
18	-315	-53.5	-440	-75	-474	-97.5
19	-394	-52	-463	-75	-463	-97.5
20	-360	-52	-450	-75	-461	-97.5
21	-379	-52	-475	-75	-472	-97.5
22	-410	-52.5	-455	-75.5	-467	-87.5
23	-350	-52.5	-445	-75.5	-462	-97.5
24	-380	-52.5	-453	-75.5	-467	-98.5
25	-436	-52,5	-464	-75.5	-465	-98.5
26	-457	-52,5	-430	-75.5	-465	-98.5

27	-339	-52	-416	-75.5	-442	-98.5
28	-340	-52	-418	-75.5	-440	-98.5
29	-319	-52	-443	-75.5	-481	-98.5
30	-355	-52	-416	-75.5	-509	-98.5
31	-274	-52	-400	-75.5	-544	-98.5
32	-301	-52	-430	-76	-549	-98.5
33	-310	-53.5	-450	-76	-545	-98.5
34	-282	-53.5	-443	-76	-540	-98.5
35	-278	-53.5	-448	-76	-512	-98.5
36	-379	-53.5	-470	-76.5	-497	-98.5
37	-283	-53.5	-498	-76.5	-532	-98.5
38	-489	-53.5	-502	-76.5	-551	-98
39	-470	-53.5	-513	-76.5	-570	-98
40	-330	-53.5	-548	-76.5	-591	-98

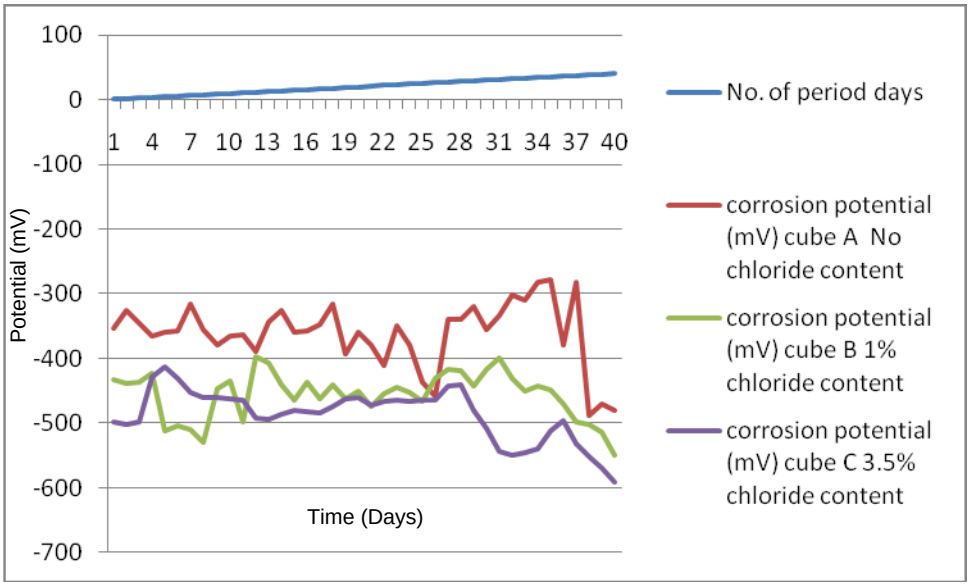

Figure 3.90: corrosion potential results of cube A,B,C

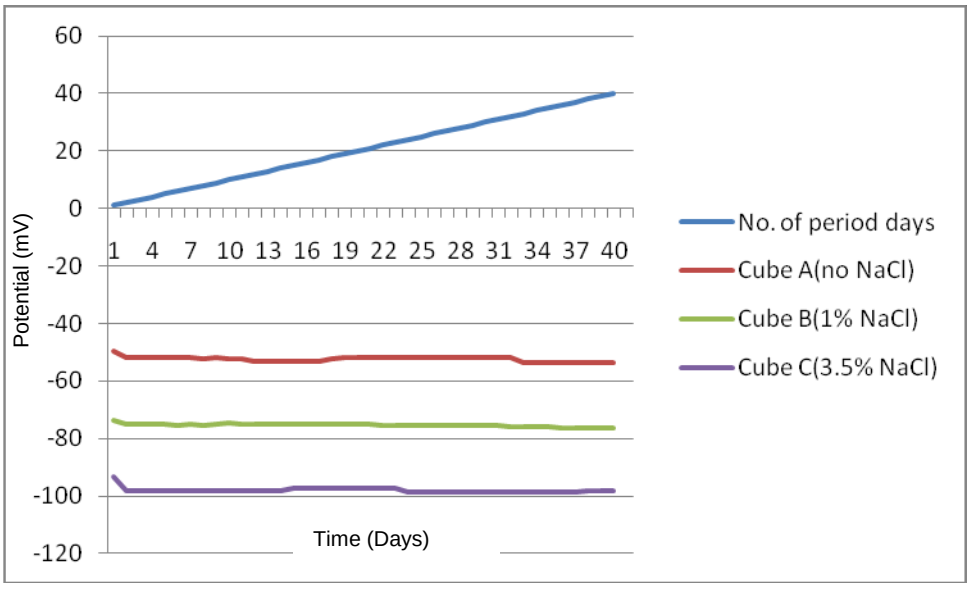

Figure 3.91: shows the macro cell corrosion current results of all cubes.

The corrosion potential results showed that during 14-days period without C.P. both rebar and zinc (with reference to the embedded silver reference electrode) potentials of cubes A and B fluctuating in a state of starting to corrosion. While cube C, it increased significantly, possibly due to high chloride content. The polarised potentials and corrosion current results during the 40 cycles in the chamber with temperature and humidity variations under sustained application of CP current increased. The detailed analyses of the results from the environmental testing allow the following conclusion to be drawn:

- The Zinc coating was found to be durable under large current applied to the samples.
- Deterioration of the coating in the forms of bubbling and seepage was not witnessed due to the current was only being applied for 7 days. However, The cathodic polarisation was observed successfully at the highest current density assessed. The higher the current applied the more polarised the reinforcement became.
- The adhesion (bond) strength values obtained from environmental durability test programme ranged between 1.65 and 2.26 MPa (cf. Adhesion values ranges 1.28 – 2.29 MPa) for TS zinc or for the Cementitious Overlay and carbon based conductive paints, the average value is 1.5 MPa) and the results are summarised in Table 3.40. Environment durability testing, under simulated / accelerated testing regime, showed that the coating exhibited

some increase in bond strength, after 40 cycles at 20 -50^{0}C and 50 -90% RH .

Table 3.40: Bond Strength (with and without CP) under Environmental Conditions

Anode Type	Adhesion Strength, MPa (without CP)	Adhesion Strength, MPa (with CP)	Comments
ZRP Coating	1.65	2.26	Strength increased after 40 cycles of environmental exposure at 50^0 C, 90% HR.
TS Zinc coating	1.28 – 2.29	-	Wetting and drying cycles
Conductive Paint	1.5 (ave.)	-	HA specifications
Cementitious Overlay	Av. 1.5 N/mm^2	-	-

CHAPTER 4: FIELD TRIAL

4.1 Introduction

The use of zinc paint as a ICCP ‘groundbed’ (anode system) is the first of its kind and the main functions of zinc paint are to convert ‘electronic current’ to ‘ionic current’ and to distribute protection current uniformly over the entire surface.

4.2 Brief Description of the Structure

The structure is a single-span monolithic construction with integrated in-situ reinforced concrete (r.c.) deck slabs supported on seven main beams, cantilevered at both ends on r.c. abutments. The structure carries a ‘A-road’ over a tidal Brook and is located in Essex (Figure 4.1).

Figure 4.1: General View of the Bridge

Figure 4.2: General View of the CP installation

4.2.1 Condition Assessment

A number of investigations and tests have been carried out to date and the principal findings have been:

(a) The majority of the longitudinal beams and some areas of deck soffit are showing evidence of severe concrete deterioration and active reinforcement corrosion. The concrete deterioration processes have been going on for some years in the form of cracking and extensive spalling of large areas with exposed and corroding reinforcement.

(b) Chloride ion concentrations determined for the concrete dust samples taken from the beams and soffit were found to be in excess of the threshold value of 0.3% by mass of cement.

(c) Concrete cover to reinforcement in these columns was found to range between >25mm and 35mm.

(d) Analysis of limited half cell potential survey results shows that half cell potential values were less negative than 350 mV. However visual inspection revealed evidence of active corrosion.

In view of the above it was considered essential that further concrete deterioration of the longitudinal beams together with the deck soffit, due to on-going corrosion of the steel reinforcement, be halted or reduced without substantial concrete repair except local repairs of the spalled concrete areas. A low budget solution to mitigate on-going reinforcement corrosion by the application of cathodic protection, utilising ZRP as an anode material, was conceived, following initial success of brief trials with the anode design as a sacrificial / impressed current anode material on a structure exposed to semi-submerged tidal water.

4.3 Cathodic Protection (CP) Design Philosophy

From the above considerations, the proposed cathodic protection system design for the structure was based upon the utilisation of a zinc-rich paint system. However, at the onset provisions of the mains operated external power source was made to provide impressed current Cathodic protection, in case galvanic protection was not possible for this structure.

4.3.1 Design Concept

The design concept of the cathodic protection system for the structure was consisting of the following:

(a) Zinc Rich Paint to provide galvanic protection to the beams and soffit.

(b) Zinc Rich Paint to form anode system for impressed current cathodic protection installation.

4.3.2 C. P. Design

The cathodic protection system for the structure was comprised of the following:

The structure was divided in to 6 no. ‘Anode zones’, for monitoring purpose, comprising of one beam and an adjacent part of the deck soffit (Figure 4.3). The paint was hand applied on the concrete surface by brush, The electrical connection to zinc paint was achieved by means of small (25 mm^2) stainless steel plates fixed on to the concrete surface - one number for each ‘anode zone’ (Figure 4.7). The strings of carbon fibre were laid longitudinally and transversely on to the deck soffit and beams respectively at regular spacing (Figure 4.8). These were to facilitate flow of ‘electronic current’ to zinc paint. A coat of zinc paint itself was used as ‘glue’ to fix the carbon fibre strings on to the concrete surface. In order to achieve an adequate dry film thickness for an estimated design life of 10 years, 3No.coats of paint wwere applied.

Each ‘anode zone’ was provided with 5 No. reference electrodes embedded in the beams and soffit of the bridge deck at select locations (Figure 4.4). The outputs from the power supply unit and other operating functions are controlled through a set of 8No. embeddable Ag/AgCl/KCl reference electrodes only, but the remaining 22 No reference electrodes are to be used for periodic manual monitoring to obtain additional data for closer/finer analysis. This is to evaluate and assess the efficacy and effectiveness of the installed C. P. system. The schematic layout and the wiring diagram of the CP system as installed are given in figures 4.5 – 4.6.

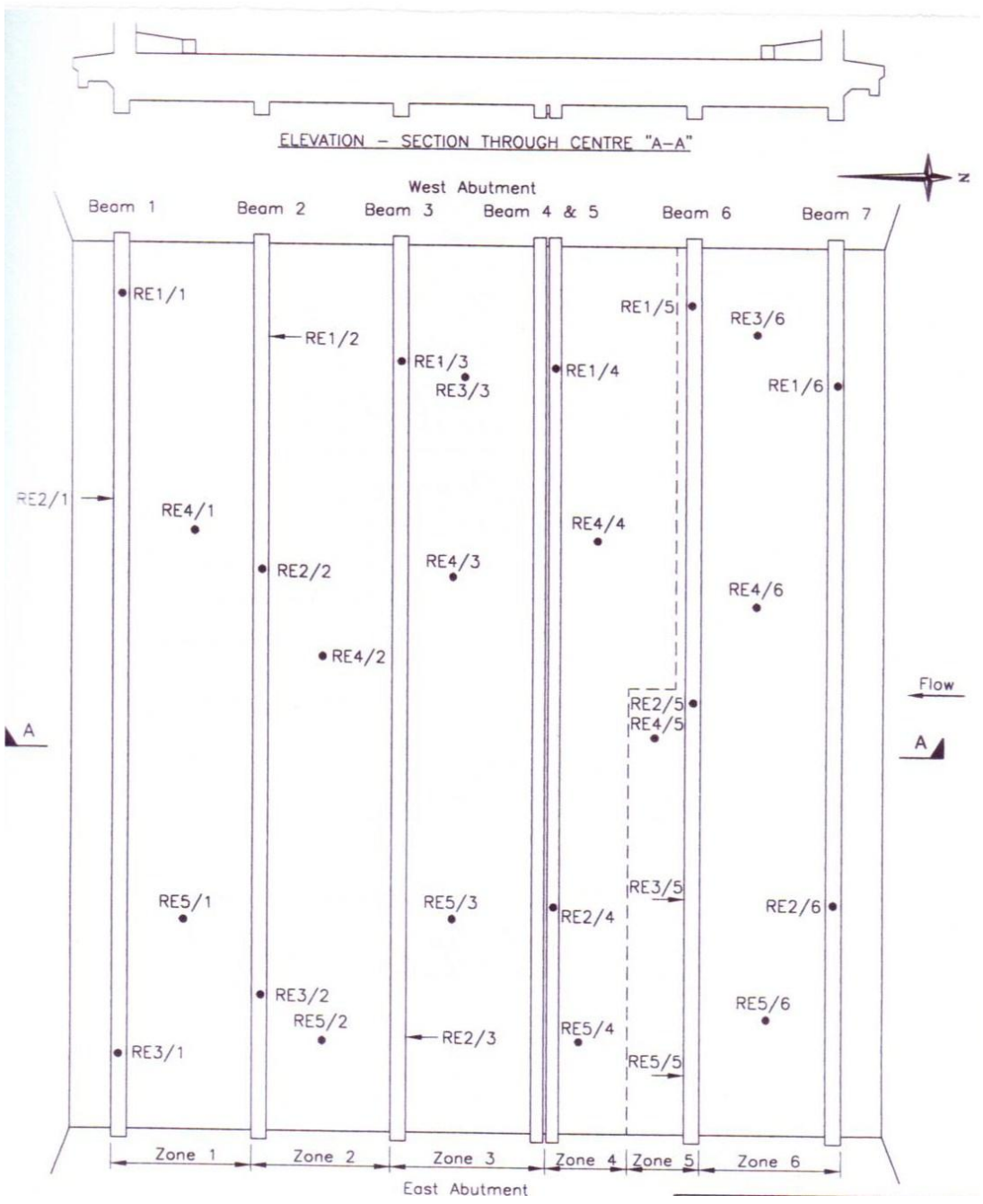

Figure 4.3: Monitoring Zones and Reference (embedded) Electrode Locations

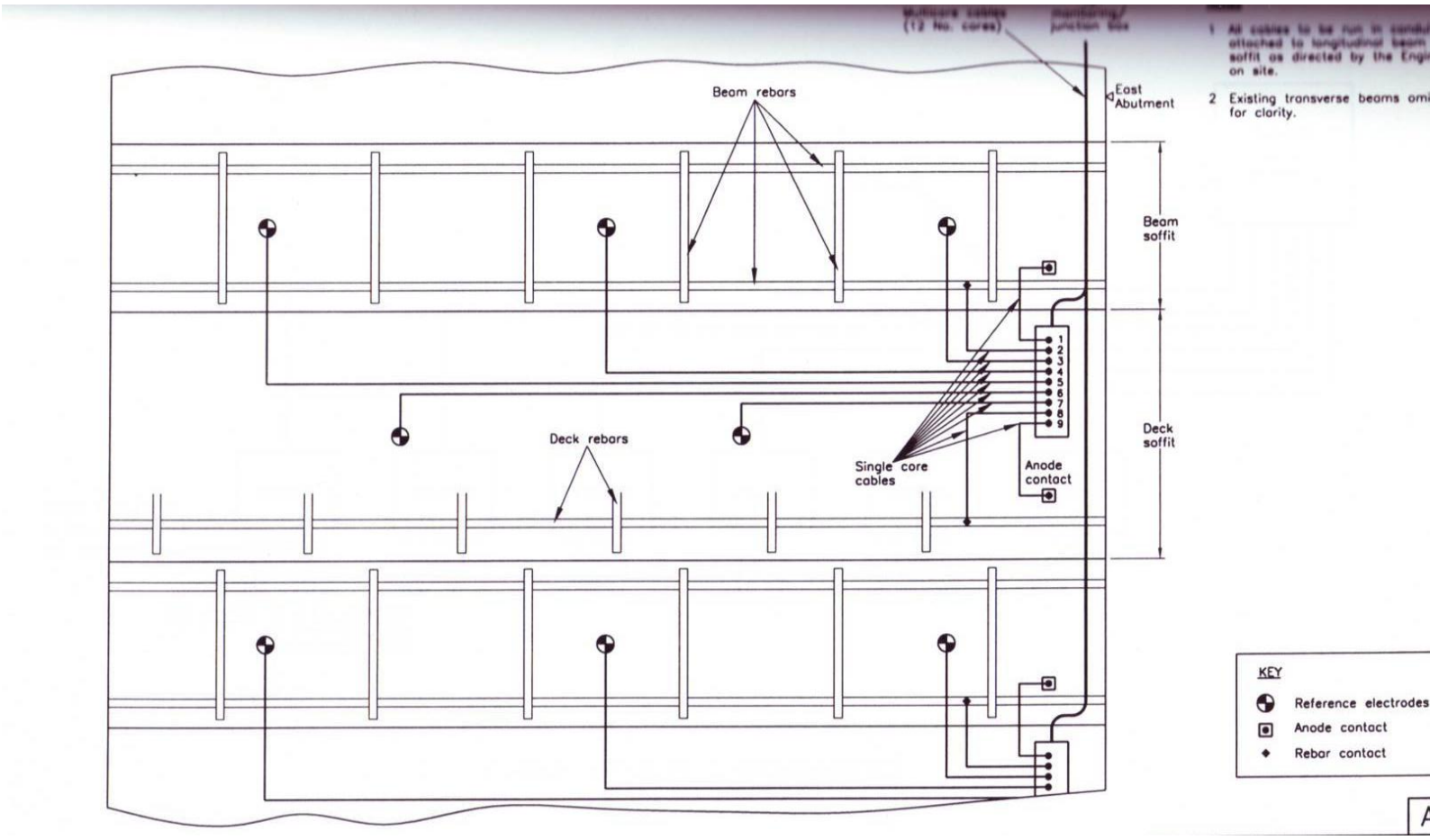

Figure 4.4: Reference Electrodes and anode Connections

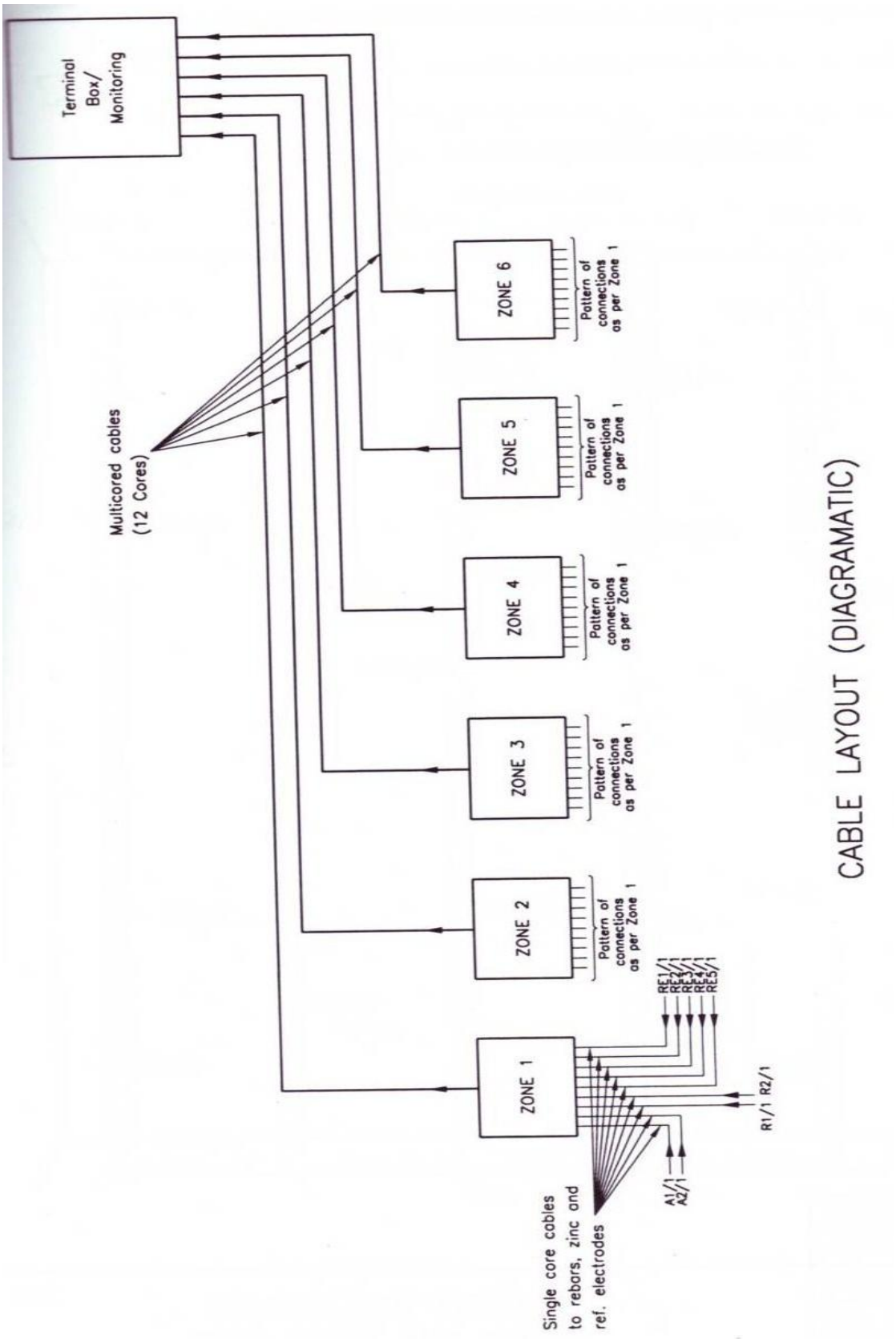

Figure 4.5: CP Electrical wiring Diagram (Schematic)

The ICCP system hardware i.e. Power Supply Unit (PSU), monitoring electrodes etc. are 'software' controlled. That is say that all set-up commands and operation manoeuvres, monitoring, reference inputs, adjusting anode output, making instant-off measurements or complete depolarisation etc. are carried out automatically, once the system is configured through a software via a host PC e.g. a laptop computer.

The ICCP system configuration for Bridge is summarised in Table 4.1 below.

Table 4.1: ICCP SYSTEM CONFIGURATION.

MONITORING ZONE	LOCATION	DESCRIPTION	REFERENCE ELECTRODE I. D.	CONTROL REFERENCE ELECTRODE I. D.	FERRO EYE CHANNEL No.
1	BAY 1	Beam	RE1/1, RE2/1, RE3/1	RE2/1 (REF 8)	10
		Deck	RE4/1, RE5/1	RE4/1 (REF 7)	9
2	BAY 2	Beam	R1/2, R2/2, R3/2		
		Deck	R4/2, R5/2	RE2/2 (REF 6)	8
3	BAY 3	Beam	R1/3, R2/3	RE5/3 (REF 5)	
		Deck	R3/3, R4/3, R5/3		7
4	BAY 4	Beam	R1/4, R2/4	RE3/4 (REF 4)	6
		Deck	R3/4, R4/4, R5/4		
5	BAY 5	Beam	R1/5, R2/5, R3/5	RE2/5 (REF 3)	5
		Deck	R4/5, R5/5		
6	BAY 6	Beam	R1/6, R2/6	RE2/6 (REF 2)	4
		Deck	R3/6, R4/6, R5/6	RE4/6 (REF 1)	3

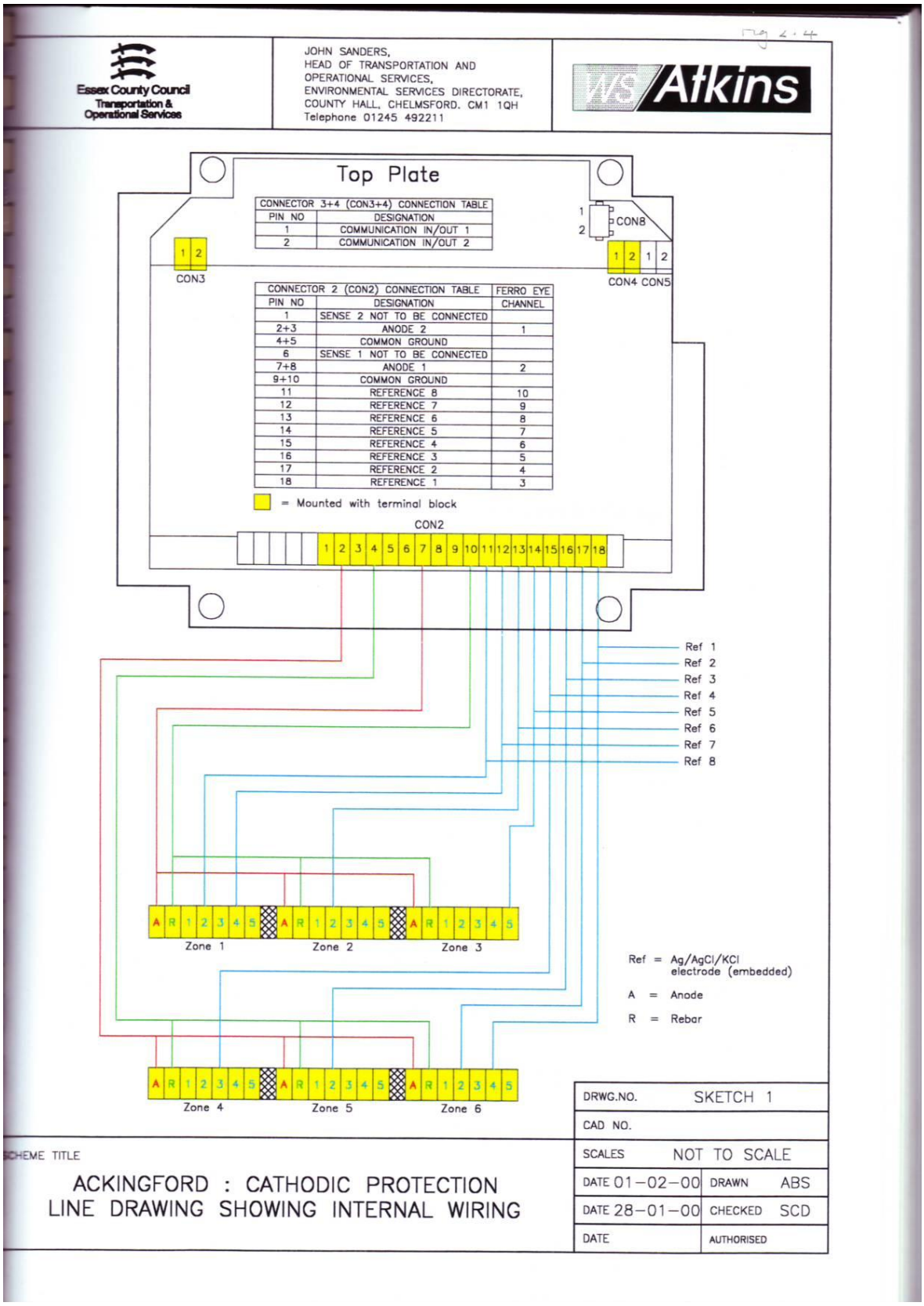

Figure 4.6: Line Drawing showing internal wiring of the Power Supply/ Monitoring Unit.

However, for the trial period, once the PSU was set to operate in constant current mode, all the monitoring was carried out manually.

Some photographs showing various components of the installed system are given in Figures 4.7 – 4.11.

Figure 4.7: Photograph showing Typical Cable Connection to Reinforcement and ZRP anode System.

Figure 4.8: Typical Arrangement of ZRP anode Layout

Figure 4.9: Photograph showing Cable Ducting Layout

Figure 4.10: Photograph showing a Power Supply Unit (PSU) inside the Steel Cabinet

Figure 4.11: Photograph showing a Laptop Connected to the PSU

4.4 Commissioning Test Results

The CP system was initially commissioned to operate as a sacrificial anode cathodic protection (SACP). But the commissioning test results strongly indicated that the ZRP anode system operating sacrificially hardly managed to polarise the reinforcement of this structure; and decided to operate the system in the impressed current cathodic protection (ICCP) mode. In order to test this and waiting for the delivery of the mains operated power supply / monitoring unit, the system was energised using a 6volts Dry cell battery. Straightway the reinforcement was polarised very significantly. The results are summarised in Table 4.2. The system was operated with the dry-cell battery for a period of 15 days and then de-energised and allowed to depolarise for a month (30 days). Finally the system was re-energised and commissioned using mains operated power supply unit with the provision of monitoring the performance of the installed system either manually or automatically. The results are summarised in Table 4.3

All the results given in Tables 4.2 and 4.3 were measured manually at the Termination Box with a portable digital multi-meter (DVM). Some of these results are illustrated graphically in Figures 4.12 – 4.23.

Table 4.2: Initial Energisation Results.

ANODE ZONE	REF. CELL I. D. No.	BASE POT.*	BASE POT+	CP ON Zn alone*	CP ON Zn + BAT.6V (dry cell) after			Depolarised Potential, mV After 30 days 'power off' (Pot. Shift)
					10 min	2hours ++	Potential Shift, mV	
1	RE1/1	-399	-376	-385	-1015	-1099	-723	-608 (232)
	RE2/1	-397	-387	-386	-1061	-1138	-751	-503 {116)
	RE3/1	-404	-371	-370	-1048	-1091	-720	-574 (203)
	RE4/1	-384	-400	-399	-1065	-1080	-680	-614 (214)
	RE5/1	-394	-356	-358	-998	-1007	-651	-598 (242)
2	RE1/2	-224	-320	-318	-747	-783	-463	-635 (315)

	RE2/2	-368	-369	-387	-912	-986	-617	-590 (221)
	RE3/2	-304	-275	-275	-725	-739	-464	-560 (285)
	RE4/2	-360	-272	-280	-851	-846	-574	-556 (284)
	RE5/2	-345	-310	-304	-905	-897	-587	-626 (316)
3	RE1/3	-153	-241	-242	-517	-521	-280	-605 (364)
	RE2/3	-220	-202	-202	-411	-412	-210	-655 (453)
	RE3/3	-253	-251	-260	-555	-546	-295	-656 (405)
	RE4/3	-317	-218	-219	-851	-835	-617	-653 (435)
	RE5/3	-313	-301	-310	-875	-972	-671	-650 (349)
4	RE1/4	-176	-252	-252	-984	-987	-735	-576 (324)
	RE2/4	-234	-209	-210	-883	-834	-625	-588 (379)
	RE3/4	-243	-327	-330	-1088	-1083	-756	-645 (318)
	RE4/4	-223	-228	-227	-887	-809	-581	-538 (310)
	RE5/4	-255	-261	-265	-846	-814	-553	-568 (307)
5	RE1/5	-346	-303	-305	-647	-624	-321	-584 (281)
	RE2/5	-335	-335	-330	-861	-804	-469	-590 (255)
	RE3/5	-331	-317	-320	-727	-693	-376	-594 (277)
	RE4/5	-338	-304	-303	-830	-774	-470	-567 (263)
	RE5/5	-367	-336	-339	-826	-781	-445	-580 (244)
6	RE1/6	-284	-281	-285	-777	-728	-447	-550 (269)
	RE2/6	-315	-286	-280	-864	-800	-514	-581 (295)
	RE3/6	-369	-237	-245	-691	-644	-427	-544 (307)
	RE4/6	-438	-268	-267	-872	-826	-558	-593 (325)
	RE5/6	-319	-307	-306	-943	-897	-590	-599 (292)

Table 4.3: Commissioning & Performance Monitoring Results

Ref. cell No.	Depolarised. Rebar Pot. (1) mV	Open Circuit Potential of Zn Paint mV	Rebar Pot. With CP'On', mV @ 3.8V, 1.5A (2) after 10 mins	Pot. Shift (mV) after 10 mins	Polarised Potential after 12 months, mV	'Instant Off' Polarised Potential after 12 months, mV	Pot.Shift (mV) after 12 months
1	-608	-1002	-689, -800*	81 , 192	-780	-759	151
2	-503	-964	-691, -824*	188 , 321	-798	-748	245
3	-574	-976	-839	265	-819	-802	228
4	-614	-1016	-797	183	-790	-768	154
5	-598	-1109	-831	233	-815	-794	196
6	-635	-1035	-726	91	-715	-702	67
7	-590	-1077	-820	230	-809	-783	193
8	-560	-1055	-838	278	-831	-814	254
9	-556	-1002	-908	352	-891	-857	301
10	-626	-1110	-960	334	-936	-887	261
11	-605	-967	-734	129	-718	-703	98
12	-655	-1038	-829	174	-806	-763	108
13	-656	-1023	-798	133	-791	-748	92
14	-653	-1167	-935	282	-914	-889	236
15	-650	-1000	-827	177	-803	-776	126
16	-576	-920	-649, -1030*	73 , 454	-785	-738	162
17	-588	-915	-723	135	-719	-689	101
18	-645	-953	-1119	474	-989	-898	253
19	-538	-681	-924	386	-906	-872	334
20	-568	-615	-839	271	-811	-786	218
21	-584	-1023	-1021	437	-967	-904	320

22	-590	-788	-739	149	-713	-697	107
23	-594	-943	-813	219	-803	-784	190
24	-567	-920	-957	390	-921	-869	302
25	-580	-766	-890	310	-869	-823	243
26	-550	-1084	-735	185	-709	-673	123
27	-581	-892	-932	342	-913	-847	266
28	-544	-880	-832	288	-817	-758	214
29	-593	-924	-713	120	-703	-657	64
30	-599	-789	-763	164	-751	-719	120

Note:

(1) After 30days following disconnecting the Dry Cell Battery.

(2) 'ON Pot' with the Power Supply unit.

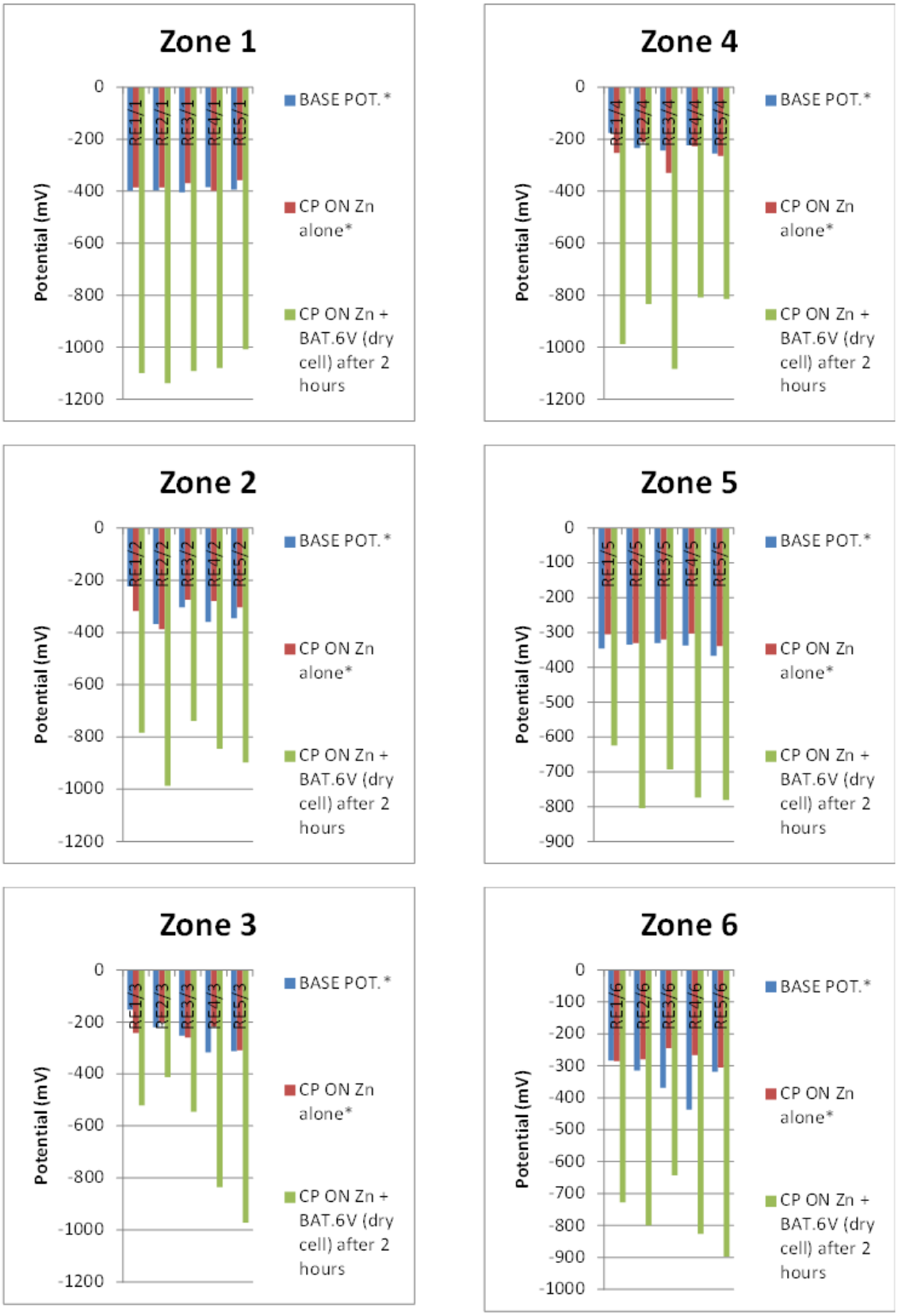

Figure 4.12: Base potentials and Potential shifts by ZRP as SACP /ICCP (Dry cell Battery) Anode System

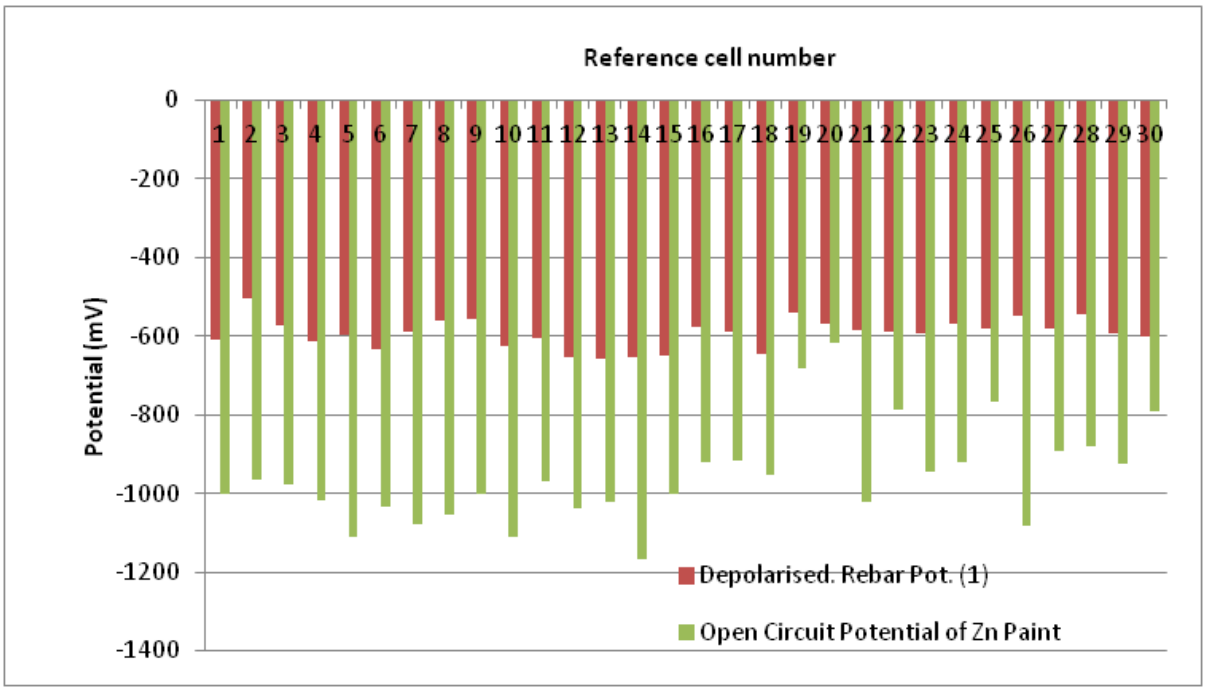

Figure 4.13: Open Circuit Potentials of ZRP and Depolarised Potentials of Rebar after 30 days following disconnection of the Dry Cell Battery

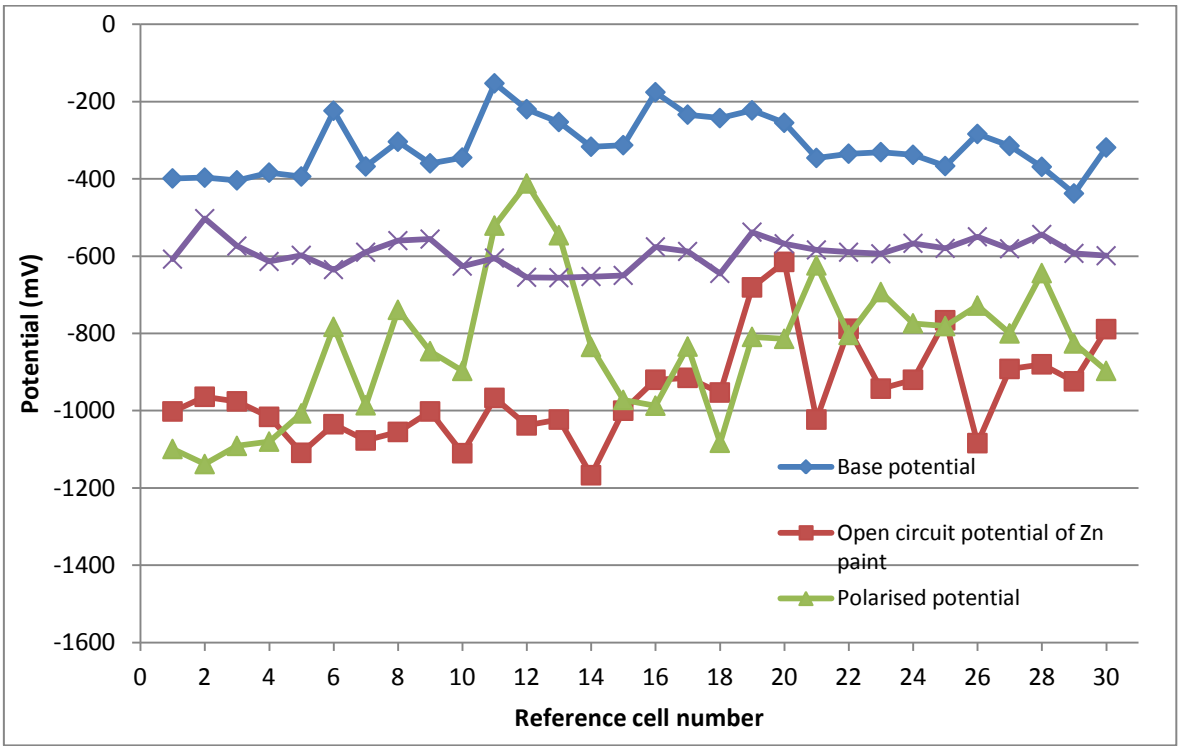

Figure 4.14: Graphs of Commissioning Results with a 6V Dry Cell Battery

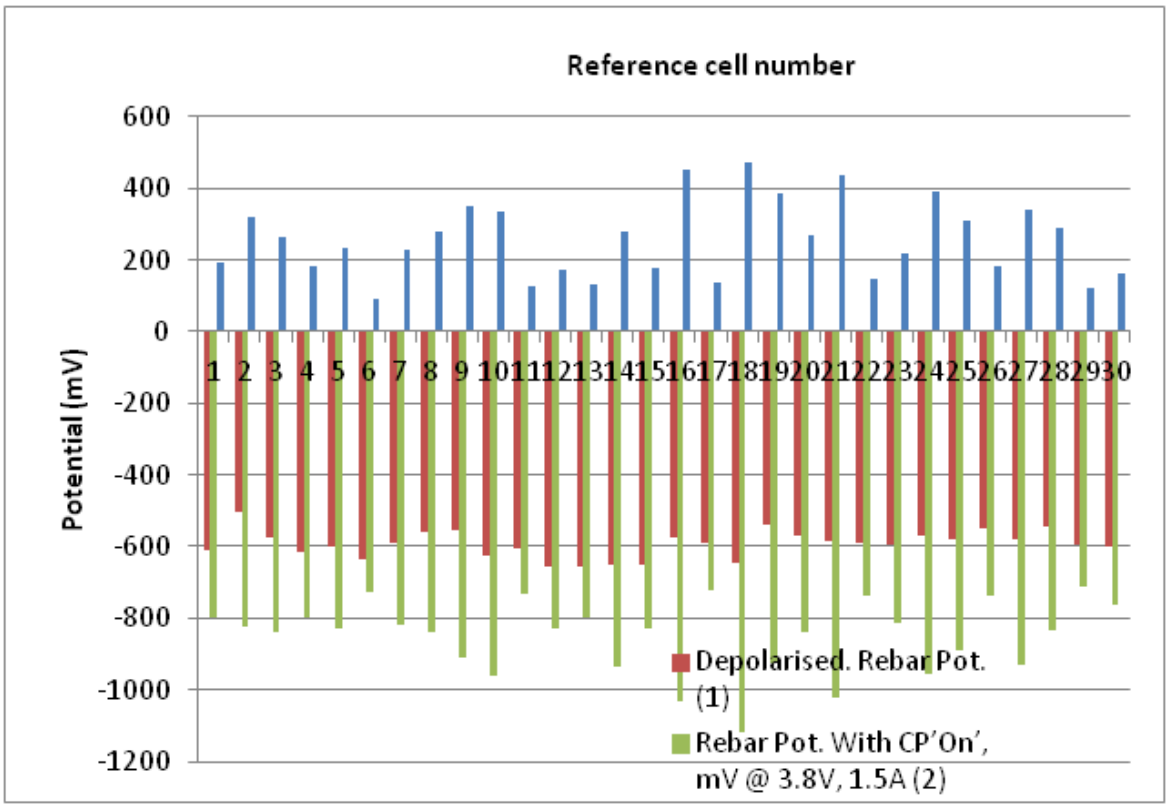

Figure 4.15: Commissioning Results, showing 'ON' potentials and potentials shift after 10 minutes with power on.

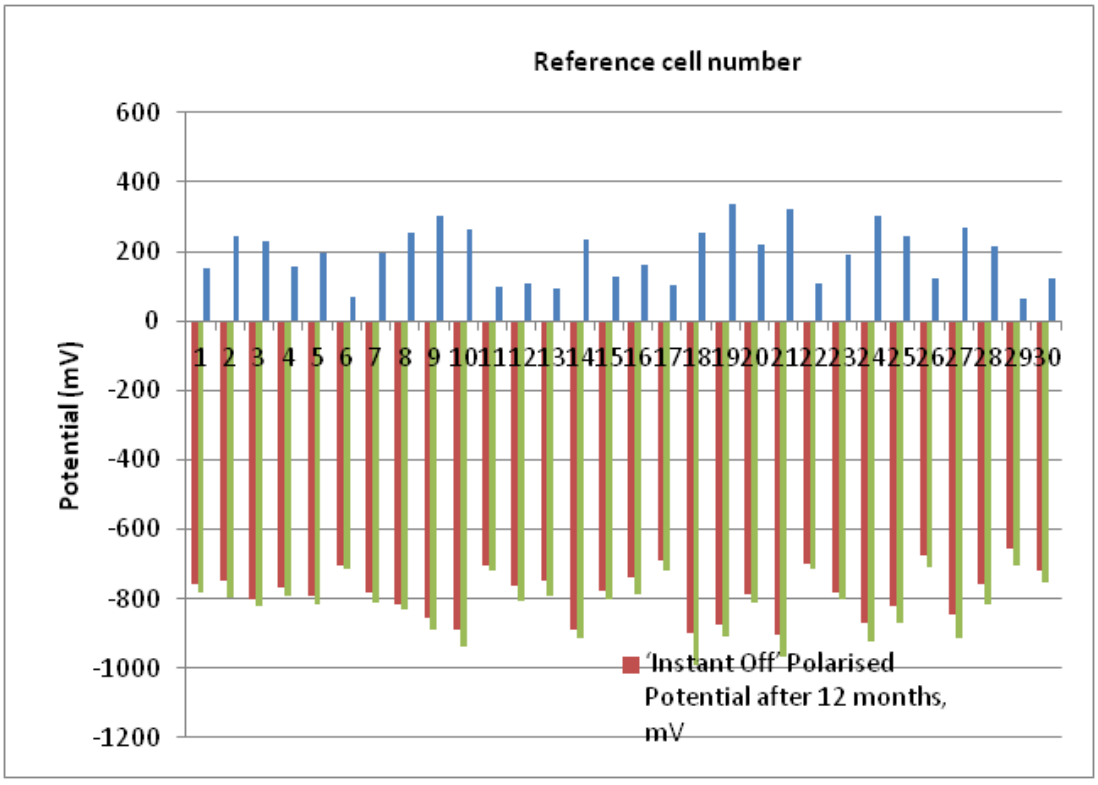

Figure 4.16: Performance Results after 12 months continuous operation.

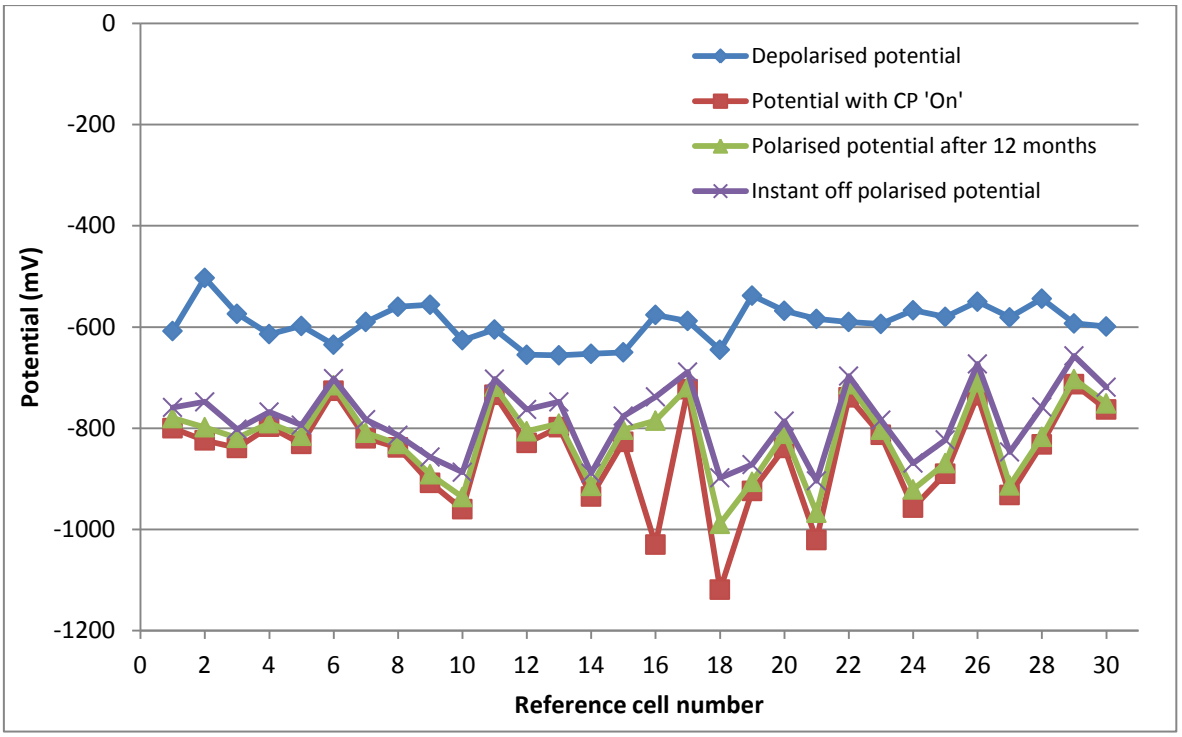

Figure 4.17: Graphs of Commissioning and Performance Results with Mains Operated Power Supply Unit.

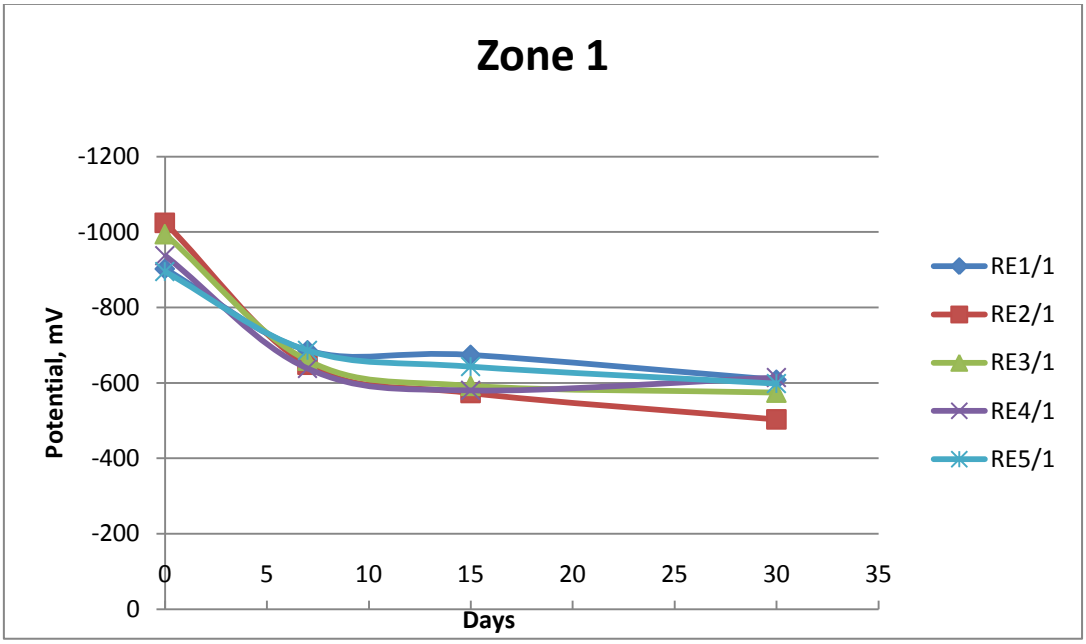

Figure 4.18: Polarisation (Potential) Decay Curve for Anode Zone 1.

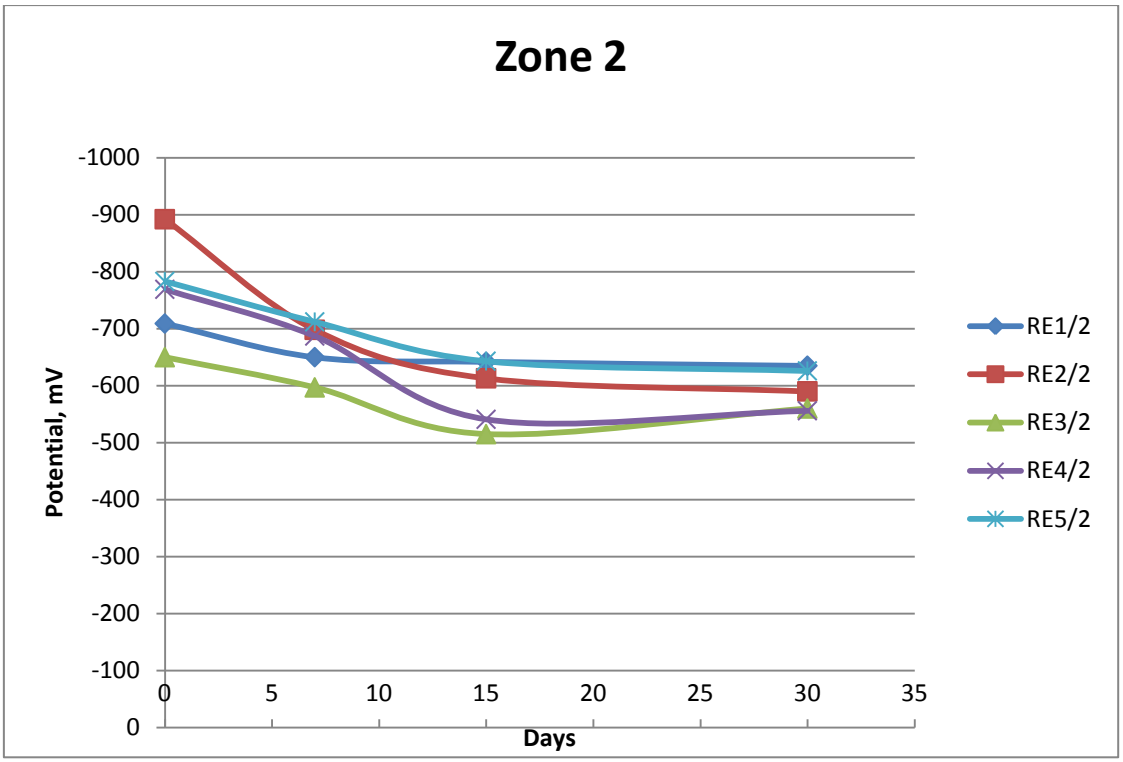

Figure 4.19: Polarisation (Potential) Decay Curve for Anode Zone 2

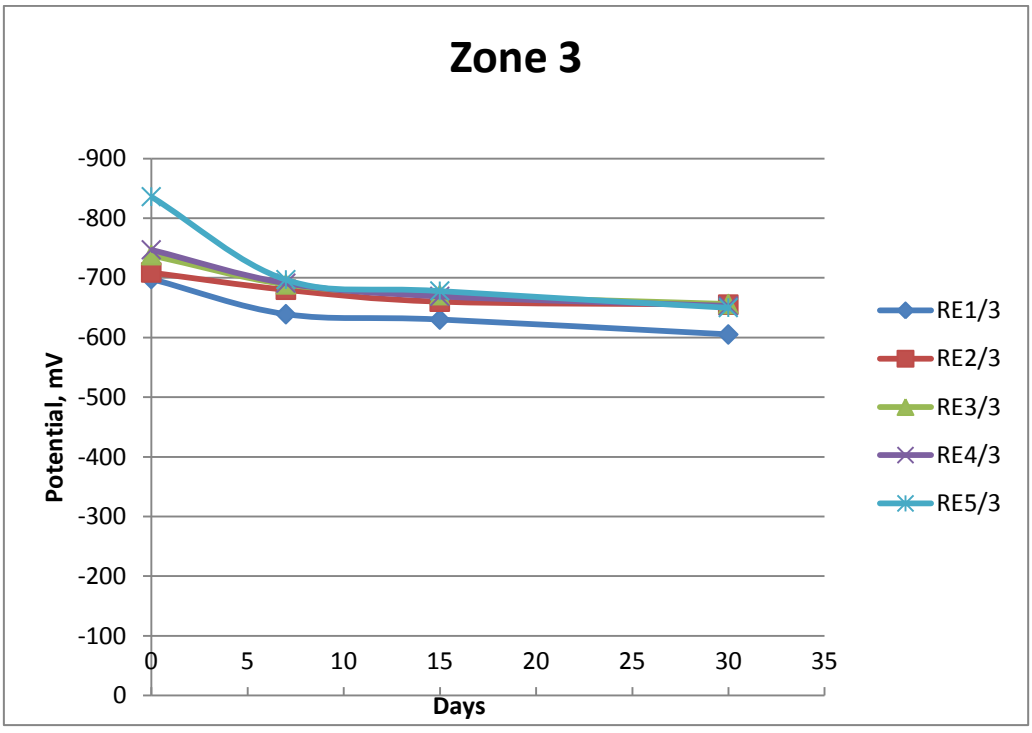

Figure 4.20: Polarisation (Potential) Decay Curve for Anode Zone 3

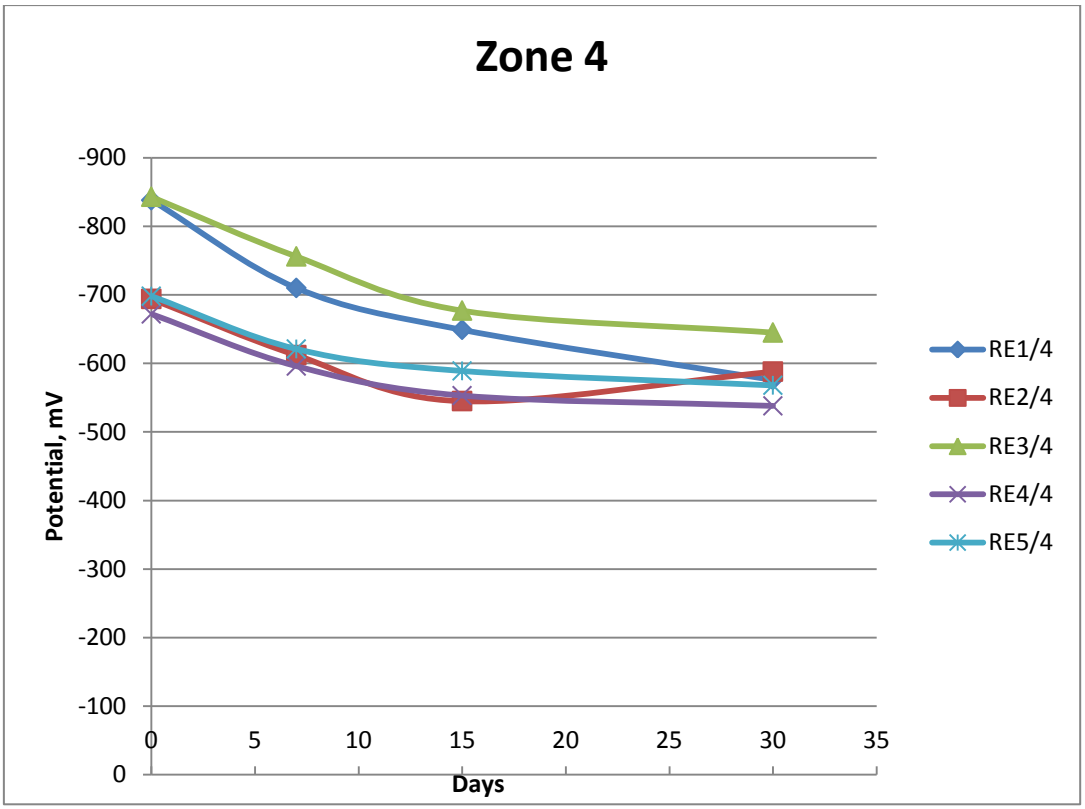

Figure 4.21: Polarisation (Potential) Decay Curve for Anode Zone 4

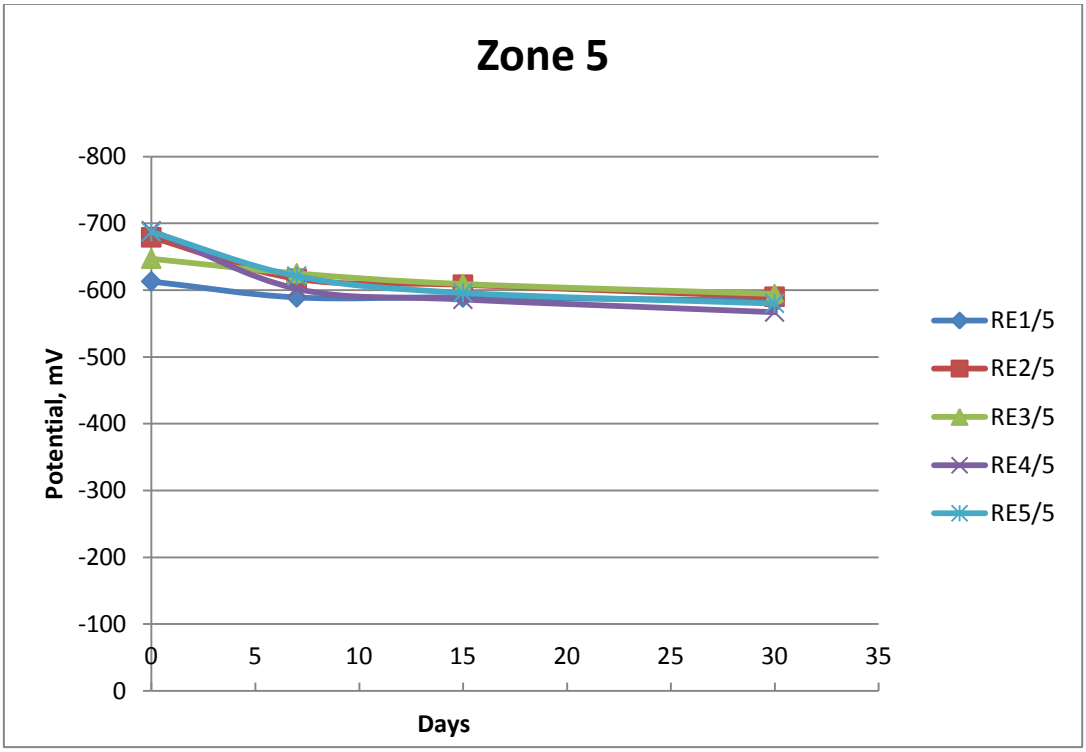

Figure 4.22: Polarisation (Potential) Decay Curve for Anode Zone 5

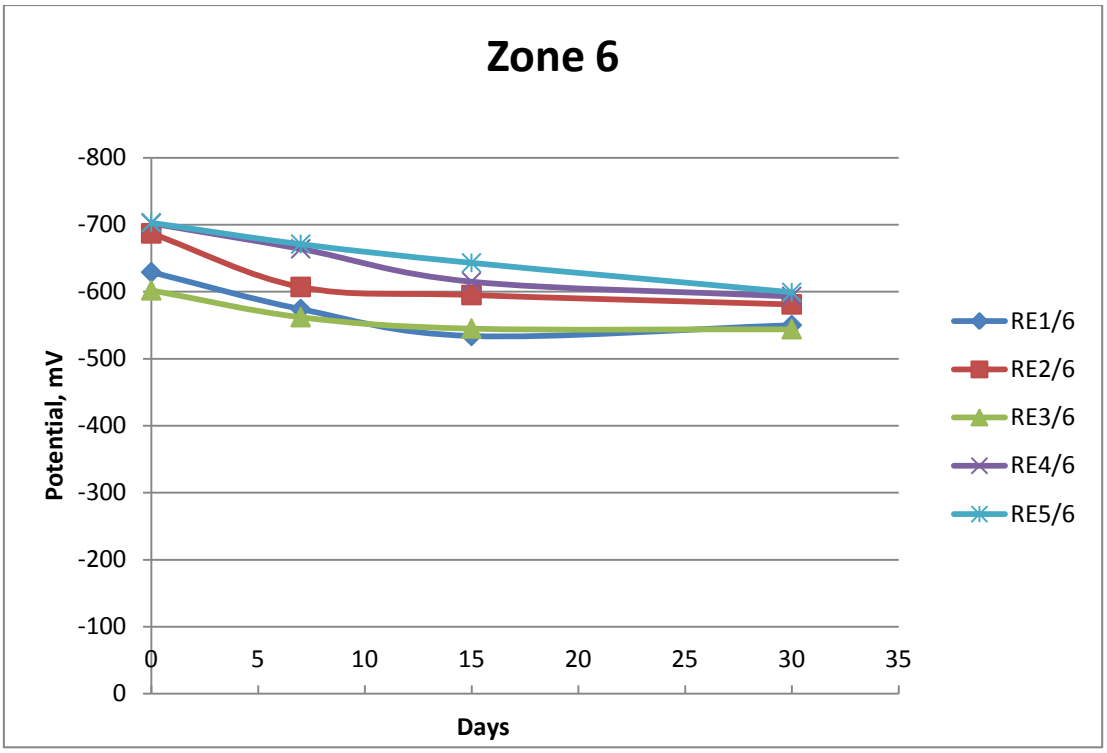

Figure 4.23: Polarisation (Potential) Decay Curve for Anode Zone 6

4.5 Discussion

Zinc rich paints (ZRP) are widely used for over 8 decades as an alternative to 'hot deep galvanising (HDG)', as an 'under coat' or as a 'top coat' and also as a 'touch-up coat' on galvanised steel to provide corrosion protection of steel in moderately severe environments and corrosive marine atmospheric environments. It is often quoted as 'Cold Galvanising'.

Zinc-rich paints must contain either between 65% to 69% metallic zinc by weight or greater than 92% metallic zinc by weight in dry film. Paints containing zinc dust are classified as organic or inorganic, depending on the binder they contain. Inorganic binders are particularly suitable for paints applied in touch-up applications around and over undamaged hot-dip galvanized areas (The American Galvanizers Association (AGA, internet access, July 2011).

The use of zinc rich paint (ZRP) as a ICCP anode material ('groundbed') is the first of its kind and the main functions of zinc paint are to convert 'electronic current' to 'ionic current' and to distribute protection current uniformly over the entire surface.

The main aim of this field trial was to confirm that these fundamental requirements are achievable.

Results presented in Table 4.2 and Figures 4.12 – 4.14 show that the initial attempt to use ZRP anode material to provide Cathodic protection sacrificially hardly managed to polarise the steel reinforcement of the structure but by connecting to a simple 6V dry cell battery as an external power source the steel reinforcement was polarised significantly. The potential shift (potential different between 'on' potentials and the 'base' potentials at embedded reference electrode locations ranged between 210 mV and 756 mV. After continuous operation with the Dry Cell Battery for a period of 15 days the battery was then disconnected and the system was allowed to depolarise for a month (to replace the battery with a mains operated power supply unit). The measured depolarised potential after a month still retained significant levels of polarisation with potential shifts of 116mV - 453mV from the 'base' values (Figures 4.18 – 4.23). This suggests that the potential decay on this structure is very sluggish.

Table 4.3 and Figures 4.15 – 4.17 give the results of the commissioning and performance of the installed ICCP system. The system was operating at 3.8 V, 1.5A and monitored for a period of 12 months. Finally the system was set to operate at 1.5A constant current mode. The results, for the first 12 months, strongly indicated that the ZRP anode system is feasible to provide and maintain adequate Cathodic protection. The values of the open circuit potential of the ZRP measured at reference electrode locations suggest that the protection current would be uniformly distributed over the entire concrete surface under protection Figures 4.13 and 4.14.

Finally, visual inspection of structure at 12 months showed no evidence of deterioration of the ZRP anode system.

CHAPTER 5: DEVELOPMENT OF A MULTIFUNCTIONAL CORROSION / CP MONITORING PROBE

This chapter describes the second strand of the research programme i.e. to develop Corrosion/CP Monitoring Probes. The main objective of this programme is to develop a simple and cost effective multifunctional probe to measure corrosion rate (based on two-probe LP technique), corrosion potential and corrosion (macro-cell) current of steel in on-site concrete.

5.1 Introduction

The corrosion of steel in concrete is a dynamic process that requires proper monitoring and assessment in order to quantify its progression. Difficulties in undertaking satisfactory monitoring and assessment remain a major problem. This study aims to develop a simple, multifunctional and cost-effective embeddable probe to measure corrosion rate of steel in on-site concrete. In this work, a multifunctional 'Beta' (coined the term) probe was developed to investigate corrosion activities, qualitatively and quantitatively, by electrode potential measurements, macro-cell corrosion current measurement tests and linear polarization resistance measurement in different Reinforced Concrete specimens immersed partly in 3% NaCl solution, and partly in fresh water. The electrode potential test results indicated high corrosion risk possibly due to the saturated state of the test specimens. However, the corrosion rate results from both macro-cell and linear polarization tests are low and approximately the same. Conclusions and recommendations were made on the degree of accuracy of the probe and how it may be modified for practical suitability.

5.2 Research Questions / Motivation

Socio-economic impact of concrete deterioration due to reinforcement corrosion of infrastructures is felt across the world. Asset Management Team (AMT) responsible for the rehabilitation of deteriorating structures is increasingly concerned that a simple 'patch repair' of the affected areas of the structure is ineffective, particularly if the concrete deterioration is primarily due to corrosion of

steel reinforcement. For long term rehabilitation strategies of maintain the integrity and extending the serviceable life to match the ‘design life’ of the structures it is essential that the structures are monitored in real-time to determine the extent and the cause (s) of determination. Extensive research and development over the last four decades or more various NDT (non-destructive techniques) are available to identify and quantify the extent of the problems but some of these NDT techniques to monitoring and determination of the rate of on-going corrosion, particularly for quantitative analysis, that are available commercially require not only considerable knowledge and experience to undertake field measurements and data interpretation but quite expensive.

Recognizing the intricate and expensive nature of the vast available modern monitoring techniques this research attempts to develop a relatively simple and cost-effective on-site method of determining corrosion rate of reinforcing steel in concrete. Intuitively, a too expensive and complex device will not be used in practice.

5.2.1 Aim

Recognizing the practical importance of this subject, this research attempts to develop a distinct, simple, multifunctional and cost-effective embeddable probe for measuring corrosion current (of corrosion rate), in on-site RC structures for purposes of early warning of significant corrosion damage, prediction of residual life so that appropriate interventions in real-time for remedial action to mitigate corrosion of steel reinforcement and maintain the integrity of the structures.

The rate of corrosion of steel in concrete remains the key factor for evaluating the extent of corrosion damage and for predicting the life expectancy of deteriorated RC structures. Corrosion probes such as Corrowatch, Schiessel, Force probe etc are common and available in the market. Their applications are without direct contact with the embedded reinforcing bars, hence, they simulate only nearest to actual corrosion damage on structures.

Other common non-destructive electrochemical methods suitable for measuring corrosion rate include alternating current (AC) impedance method, Electrochemical Noise method and Linear Polarization Resistance (LPR) method. However, LPR method remains the simplest and the most suitable for on-site structures; but with varying degrees of accuracy.

The main aim of this part of the investigation is to develop a simple, cost effective 'mulitifunctional' probe not just to measure the macro-cell corrosion current (corrosion rate) but is designed to incorporates LPR measurement in its applications as a "quick check method," for verifying the corrosion rate results. Further it is also conceived to be used as 'temporary anode' system for 'E- log I' test for assessing the cathodic protection current requirement together with the provision to monitor the performance of the CP system qualitatively or quantitatively.

5.2.2 Objectives

- To couple a laboratory based embeddable corrosion rate monitoring probes.
- To monitor the performance of the probes in different reinforced concrete specimens under different corrosive environments.
- To determine macro cell corrosion currents and evaluate corrosion penetration.
- To compare the results of the embeddable probe with that of linear polarization resistance method for purpose of validity.

5.2.3 Scope of research

The scope of this chapter covers the development of 'Beta-Multifunctional probe' for measuring macro cell corrosion current (corrosion rate) of reinforcing steel in on-site concrete only. Macro cell corrosion current measurement technique, using modified ASTM G109-92 test method for determining macro-cell current and to verify such test results with LPR method, was employed to generate data of macro cell corrosion current. This is to assess the performance of the probe. Sets of

experiments were designed to simulate chloride induced corrosion on deteriorated reinforced concrete. The study incorporates extensive discussion on methods of measuring rate of corrosion on-site, it however excludes studies on corrosion control, full structural assessment and repair of damaged structures. Other conceptual ideas of using the probe 'counter electrode' for LPR measurement and to use as a 'temporary anode system' for 'E – log I' tests and to use as a permanent performance monitoring probe for assessment of CP system shall be investigated as future development works.

5.3 Literature Review

5.3.1 Introduction

Reinforcement corrosion is insidious in nature and its initiation and early stages of propagation cannot be detected visually. Yet early detection of corrosion in reinforced concrete structures as generally advocated can provide the opportunity of early interception in its progression, thereby ensuring the safety of the structure. If corrosion process is left unchecked until cracking or spalling occurs, then the costs of repair are significantly higher because much of the concrete cover and the badly corroded section (s) of the reinforcement must be replaced especially where pitting occurs. Because of the enormous direct and indirect cost of deterioration of reinforced concrete structures due to corrosion, particularly the chloride induced corrosion, a number of different corrosion monitoring methods and techniques have been developed. This is not only to identify and quantify the extent and rate of deterioration but also to assess and evaluate the performance and effectiveness of the corrosion mitigation/protection methods.

Some techniques are exclusively suitable for laboratory investigation purposes; others are designed for use either as 'in-situ' or 'embeddable' devices on real life structures. The most commonly used techniques for evaluating the condition of steel reinforcement in concrete are based on the assessment of the electrochemical parameters of the corrosion process (s). Rodriguez et al. (1994) made a detailed study of available monitoring techniques and evaluated them with regards to their performance in terms of the reliability and repeatability, ease and speed of individual measurement, qualitative or quantitative information provided.

Structural health monitoring (SHM) has recently gained popularity in most developed nations of the world where premium is placed on conservation of resources and sustainability. Modern infrastructural managers no longer repose on mere visual and routine inspections, as these are found not adequately enough to formulate strategic maintenance scheme. It is now clear to most practitioners that there are difficult-to-access locations within some structures that can best be appraised with monitoring devices installed at the time of construction or 'retrofit' at locations of interest. Structures protected from corrosion either by Cathodic Protection or other protective measures are also require to be closely monitored to ensure their performances during the service life of a structure. In reality, the import of real-time information on structural performance or degradations afforded by some monitoring devices cannot be overemphasized as it readily fosters proactive maintenance planning and programming. Hence, in order to enhance sustainability, and develop easier and reliable methods of assessing the present and future performance of in-service structures, researchers in the field of corrosion are actively involved in developing new monitoring techniques.

5.3.2 Corrosion Monitoring Techniques

It is universally acknowledged fact that no single technique may provide comprehensively the overall condition evaluation of the structure in question for the purpose of early intervention or repairs. Therefore, engineers involved in the structural conditions assessment require adequate knowledge of the working principle, performance and limitations of each device at their disposal. Such understanding is necessary to avoid potential pitfalls associated with data acquisitions and interpretations.

Concrete Society Technical Report No. 60 (2004) provides the best practice guidance on the main tests that are routinely used and on several advanced tests for determining corrosion activity. It describes the theoretical background to the tests, the type of equipment and its use, and most importantly, gives advice on the interpretation of the results. This section briefly reviews the current practice and

the state of art on corrosion monitoring techniques for both laboratory and on-site conditions.

5.3.2.1 Laboratory and On-site Corrosion Measurements

A number of corrosion measurement techniques have been developed for laboratory and on-site measurements to evaluate and quantify different corrosion parameters. These are discussed in the subsequent sections. Traditionally, most of these techniques are developed and used extensively in the laboratory to institute building codes and spin new corrosion protection system (Bentur *et al*., 1997). However, many of these techniques are improved on and readily available on commercial scale, for field measurements of corrosion activities. For instance, the on-site embeddable linear polarization sensor shown in Figure 5.1, as presented by Ha-Won Song and Velu Saraswathy, exhibits parallel working principle with the one developed for laboratory test.

This image has been removed due to third party copyright. The unabridged version of the thesis can be viewed at the Lanchester Library, Coventry University

Figure 5.1 Embeddable Linear Polarization sensor (Int. Journal of Electrochemical Science 2007)

5.3.2.2 Visual Techniques and Mass Loss

These techniques had been in practice since early 1900s. Visual techniques undertaken in laboratories involve observations to the possibility of steel corrosion

in concrete and the subsequent impacts on concrete specimen. Detailed procedures to carrying out the techniques are specified in ASTM G46-94 (Standard Guide for Examination and Evaluation of Pitting Corrosion). Bentur *et al*. (1997) explained that a detailed analysis of these techniques is almost always destructive because it requires the removal of steel from its environment, by breaking open the concrete and examining the steel. However in field surveys, visual inspections often set precedence for other detailed corrosion surveys. It may start as a casual 'look over' that spots a problem and end up as a rigorous logging of every defect seen on the concrete surface (Concrete Society, 1984).
On the other hand, the mass loss or gravimetric technique requires that the bars be weighed prior to and after exposure, and rust scales be carefully cleansed in order to determine the amount of steel loss. This method has been identified by Vassie (1978) and Bentur *et al*. (1997) as not without error because of the possibility of introducing mass loss which may be unrelated to corrosion activities.

Orthodox investigator like Knudson (1907) carried out extensive experimental work using these techniques to verify the possibility of electrolytic action on metals insulated with concrete. In his work he explained in details his keen observations after subjecting two samples of (RC) to electrolysis for a period of thirty days. The experiment consists of three sample blocks with wrought-iron pipe positioned in each block. Two samples immersed in two different solutions (fresh and sea water) were connected in series with 0.1A of steady current flowing through the loop. The conclusions drawn at the end of the experiment reflected loss in weight of the irons, obvious cracks on concrete samples during electrolysis and rust deposits on the metals when the samples were crushed open. The third sample however did not show any of those electrolytic effects; it was only immersed in sea water with no impressed current flowing through it. This approach helps demonstrate not only the possibility and effects of corrosion on steel in concrete, but also the metal loss can be converted to corrosion rate by Faraday's law;

$$m = MIt/zF \qquad (5.1)$$

Where: m = mass of steel consumed
M = Atomic weight of metal (56g for Fe)
I = current (amperes)
t = time (seconds)

z = ionic charge (2 for Fe – Fe^{2+} + $2e^{-}$)

F = 96,500 A.s

However, it is intrusive and destructive in nature while attempting to determine and quantify the extent of damage on the embedded bars. In RILEM report (1988) it is stated that such techniques do not suggest any differential or instantaneous corrosion rates, but only a mean value may be represented. Detailed appraisal of these techniques is presented in RILEM report (1988).

5.3.2.3 Electrochemical Techniques

A number of electrochemical techniques have been developed to directly measure corrosion activities in concrete, due to electrochemicallity of corrosion process(s) of steel in concrete. These techniques are used to determine corrosion parameters on which various corrosion models have been proposed for the prediction of the residual service life of the structure and to help make informed decisions to any intervention measure. The main parameters measured include the following:

- Corrosion Potential
- Concrete Resistivity
- Corrosion Rate
- Macro cell corrosion current

In addition to the above, many researchers have proposed techniques to measure corrosion current directly (although no such devices to measure corrosion current are commercially available yet), particularly the ‘macro’/’micro’ cell corrosion current, since the corrosion of steel in chloride contaminated concrete is predominately due to the formation of corrosion micro or macro cells.

5.3.2.4 Corrosion Potential Measurements

This is the most widely used technique (because of its simplicity) and is described in American National Standards ASTM C-876 to assess the on-going corrosion

activities of steel reinforcement in concrete. It is measured as a potential difference with respect to a reference electrode This potential difference is called corrosion potential, ($E_{corr,}$), and in accordance with C Wagner (Journal of the Electrochemical Society, 1952) is defined as a single electrode potential which corresponds to the intersection of the potential-current density curve for dissolution of metal (anodic current density. I_a) and that for reduction of the oxidizing agent (Cathodic current density, i_c) the potential at which the anodic and cathodic reaction rates are in equilibrium and which is indicative of thermodynamic tendency for corrosion reaction to occur. For a metal in a homogeneous solution, the corrosion potential developed within a particular environment is unique to describe the thermodynamic tendency of metal to corrode. In contradistinction, for a metal in an inhomogeneous environment, such as steel reinforcement in concrete, E_{corr} varies considerably from location to locations.

Two different methods are currently being used to measure corrosion potentials of steel reinforcement in concrete, including:

i) Half – cell potential and potential mapping measurement:

This method makes use of a single reference electrode connected to the embedded corroding steel, either as illustrated by Ha-Won Song and Velu Saraswathy (2007) in Figure 5.2 or embedded in close proximity with the steel (i.e. as permanent installation in on-site condition) to establish corrosion potential.

This image has been removed due to third party copyright. The unabridged version of the thesis can be viewed at the Lanchester Library, Coventry University

Figure 5.2: Schematic representation of Half-cell Measurement (Int. Journal of Electrochemical Science 2007).

The choice of positioning the reference electrode is governed by the type of data required. Where potential mapping is to be incorporated especially for field surveys, it is important that the reference electrode be movable in order to detect changes in potential at different locations of the structure. The preferred reference electrode for site use is the silver/silver chloride/potassium chloride (SSC) electrode, although Copper/Copper Sulphate electrode is still quite widely used as per ASTM Standard C876, (Concrete Society Report NO. 60). The relative potential values with respect to a Standard hydrogen electrode (SHE) of different reference electrodes commonly used in the laboratory and/or site measurement is given in Table 5.1

Table 5.1: Reference electrodes for measurement and calibration (Concrete Society, Technical Report 60, 2004)

This table has been removed due to third party copyright. The unabridged version of the thesis can be viewed at the Lanchester Library, Coventry University

For normal outdoor concrete the minimum acceptable input impedance of the digital voltmeter (DVM) is 10 M-ohms, for dry concrete the input impedance should not be less than 100 M-ohms; and the DVM should have as high a resolution as possible, preferable +. 0.1 mV, although values can be recorded to the nearest 5 mV (Concrete Society Technical Report No. 60) this technique are clearly described in ASTM C876 (Standard Test Method for Half-Cell Potential of Reinforcing Steel in Concrete).

ASTM criteria for interpretation of corrosion as presented in Table 5.2 are extensively discussed by Ha-Won Song and Velu Saraswathy (2007), Bentur *et al*. (1997), Vassie (1991) and RILEM report (1988). The criteria was originally

developed empirically and is commonly known as 'Van Daveer' criteria (1975), which was later incorporated in to ASTM-C876 document.

Table 5.2: ASTM (C876) Criteria for Corrosion Interpretation. (Modified to include other reference electrodes)

Half cell Potential Reading (V)			**Corrosion activity (% probability)**
CSE	SCE	Ag/AgCl	
>-0.200	>-0.125	>-0.100	<90% Probability, No corrosion
-0.200 to -0.350	-0.125 to -0.275	-0.100 to –0.250	An increasing probability of corrosion
<-0.350	<-0.275	< -0.250	Greater than 90% probability of corrosion

However, the adoption of the method and interpretation of data as described in ASTM standard calls for caution in order to avoid erroneous result or assessment. In RILEM report (1988), it is clear that good contact between the concrete and the reference electrode should be ensured to minimize ohmic drop. Also apparent is that the criteria for potential range of corrosion probability indicated by ASTM standard, as given in Table 5.2, which were developed in the USA mainly in relation to bridges, is an empirical observation based on chloride contamination and may not fully represent conditions for the presence of carbonation in concrete. Furthermore, half-cell potential readings can be affected by many factors, such as polarization due to limited oxygen diffusion. If oxygen diffusion is restricted, such as fully immersed or water saturated structures, reinforcement potentials values can be very highly negative without any actual corrosion (Arup 1983; Elsner and Bohni 1992). Existence of high resistance 'latence' layer on concrete, corrosion products on the reinforcement, the age of the concrete, reference electrode position, cement type, and presence of cracks were reported as factors affecting the half cell potential values (Alonso et al. 1998; Browne et al. 1983; Elsener et al. 2003).

Finally, half cell potential is a thermodynamic parameter and therefore does not provide any information about the rate of corrosion but only indicates the tendency to corrosion. Therefore, it is usually necessary to use other monitoring methods.

ii) Half-cell Potential Mapping

A fuller understanding of the corrosion condition is given by drawing a potential 'map' of the area surveyed (Concrete Society, 2004). The measured values of the half-cell potentials are plotted (manually or automatically) on the map and lines are drawn between points of equal potential. These 'contour' lines identify anodic areas (where corrosion is possible) and Cathodic areas (where risk of corrosion is less). The greater the potential difference between the anodic and cathodic areas, the steeper the gradient of potential lines and greater the possibility of significant corrosion in the anodic areas (Concrete Society, 2004). A typical half-cell potential contour map is shown in Figure 5.3 (a).

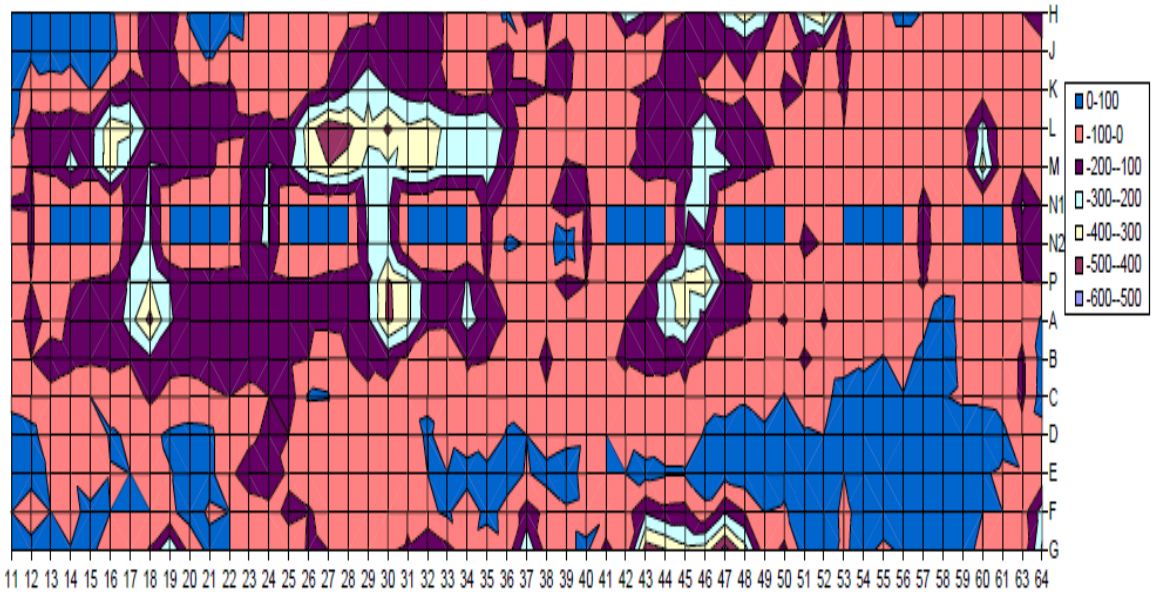

Figure 5.3(a): Typical example – Half-cell potential Contour Map.

iii) Surface Potential Measurement:

Unlike the previously discussed method, this method uses two matching half – cells, one held in a fixed position and the other moved across the concrete surface as shown by Ha-Won Song and Velu Saraswathy (2007) in Figure 5.3 (b).

This image has been removed due to third party copyright. The unabridged version of the thesis can be viewed at the Lanchester Library, Coventry University

Figure 5.3 (b): Schematic representations of surface potential Measurements (Int. Journal of Electrochemical Science 2007).

This method is particularly useful where direct contact with reinforcing steel is not feasible. It is possible to obtain comparative potential data between the two cells in contact with the concrete, one fixed and the other moved across the surface (Concrete Society Technical Report No. 60, 2004). In a way, the possibility of corrosion correlates to the degree of potential different indicated between the cells. With proper interpretation of result, a reliable potential contour map can be made. These methods are in no doubt only suitable for concrete with uncoated rebars where direct contact to the rebars or contact between the concrete and rebars is not feasible. Again, like all half-cell potential methods, they do not provide information on corrosion rate.

5.3.2.5 Concrete Resistivity Measurements

Electrical resistivity of concrete is a function of many factors of which the quality of concrete has a great bearing, and it is apparent that concrete resistivity has a huge control on the rate of corrosion, as the concrete pores serve as crucible where corrosion reactions are thermodynamically maintained. This has been demonstrated by Stratfull (1968) and Vassie and Cavalier (1981) with a common conclusion that the corrosion rate, once the reinforcing steel is active, is significantly controlled by the concrete resistivity. In this respect, advances in corrosion monitoring have developed easy methods of detecting the degree of resistance that can be exhibited by concrete to electric flows; including AC and DC

techniques discussed by Ha-Won Song and Velu Saraswathy (2007). In the DC measurement, an electric field is applied between the two embedded electrodes and the resulting current is measured as a voltage drop over a small resistance. But review by Bentur *et al*. (1997) stated clearly that due to the high resistivity of concrete, a large DC source or lower AC voltage is always required for testing concrete resistivity or conductivity. The AC method on the other hand may either take the form of a two-probe or four-probe method. The latter is generally believed to be more accurate; however, it is more expensive. The most common type is the modified 4-pins 'Wenner' technique, which requires the flow of an alternating current between the two outer electrodes and the potential different measured across the two inner probes as shown schematically in figure 5.4

This image has been removed due to third party copyright. The unabridged version of the thesis can be viewed at the lanchester Library, Coventry University

Figure 5.4: Schematic representation of four-probe Wenner-type resistivity measurement (Int. Journal of Electrochemical Science 2007).

With a known current 'I' flowing through the outer probes and a measured voltage 'V' between the inner probes, resistance '**R**' is calculated as:

$$\mathbf{R} = \mathbf{V/I}. \qquad (5.2)$$

And concrete resistivity '**ρ**' is given by:

$$\boldsymbol{\rho = 2\,\pi\,a\,R\ (Ohm.cm)} \qquad (5.3)$$

Where:

a= inner electrode distance (cm),

R= Resistance (Ω).

Other procedures for determining concrete resistivity are presented in ASTM C1202-94 (Test Method for Electrical Indication of Concretes' Ability to Resist Chloride Ion Penetration) and reviewed by and Bentur *et al*. (1997).

While no known mathematical relation exists between concrete resistivity and corrosion current, researchers, through laboratory and field observations, have proposed empirical correlations as illustrated in Table 5.3 between these two parameters.

Table 5.3: Corrosion risk from Resistivity (Int. Journal of Electrochemical Science 2007)

Resistivity (Ohm.cm)	Corrosion Risk
Greater than 20,000	Negligible
10,000 – 20,000	Low
5,000 – 10,000	High
Less than 5,000	Very high

5.3.2.6 Corrosion Rate Measurements

This section relates to one of the main focus of this study. Corrosion rate measurement is paramount in assessing the degree of deterioration of reinforced concrete structures. Such measurement is required to obtain direct information for developing effective maintenance scheme and for predicting the remaining service life of a structure. Different non-destructive methods such as alternating current (AC) impedance, electrochemical noise method, linear polarization resistance and various embeddable corrosion sensors have been developed to carry out corrosion rate measurement. However, it is a generic notion in literature that AC impedance and electrochemical noise are unsuitable for use in the field for corrosion rate measurement of steel in concrete.

Hence, for the purpose of this study, this section only examines the applications of linear polarization resistance method and embeddable probes method for evaluating corrosion rate in reinforced concrete structures.

i) Linear Polarization Resistance Method:

This method has been described as the simplest method of evaluating instantaneous corrosion rate of reinforcing steel in concrete. Traditionally, it was developed from the Stern-Geary theory and its application for field purpose is classified as non-destructive as it only requires localized damage to the concrete cover in order to allow electrical connection to the rebar (Ha-Won Song and Velu Saraswathy, 2007). The method of polarization resistance is based on the algebraic solution of the Tafel equations for the respective oxidation (anodic) and reduction (Cathodic) reactions. The Tafel equation relates the rate of an electrochemical reaction (expressed as current density, i) to the overpotential (termed as polarisation, V) and the relationship between polarization and current density can be expressed, as:

Anodic polarization $\eta_a = \beta_a \log (i_a / i_0)$ (5.4)

Cathodic polarization $\eta_c = \beta_c \log (i_c / i_0)$ (5.5)

Where η_a and η_c are the anodic and cathodic polarization over-potentials, β_a and β_c are known as the Tafel constants, i_a and i_c are the anodic and cathodic current densities, and i_0 corresponds to the exchange current density. at the exchange current is the current at equilibrium, i.e. the rate at which oxidised and reduced species transfer electrons with the electrode. The Tafel equation was first deduced experimentally and was later shown to be a limiting case of the Butler-Volmer equation, one of the most fundamental relationships in electrochemistry. It describes how electrical current on an electrode depends on the electrode potential, considering that both a cathodic and an anodic reaction occur on the same electrode:

$$I = A.\, i_0.\, \{\exp[(1-\alpha)nF/RT.\,(E - E_{eq})] - \exp[\alpha nF/RT.(E - E_{eq})]\} \quad (5.6)$$

Where:

I = electrode current, A

i_0 = exchange current density, A/m^2

E = electrode potential, V

E_{eq} = equilibrium potential, V

A = electrode active surface area, m^2

T = absolute temperature, K

n = number of electrons involved in the electrode reaction

F = Faraday constant

α = so-called symmetry factor, dimensionless.

The above equation is valid when the electrode reaction is controlled by electrical charge transfer at the electrode (i.e. electrode reaction is under activation controlled). For the case when the electrode reaction is under 'mass-transfer' (i.e. diffusion) controlled, the value of the current becomes limiting current, $i_{limiting}$ and this is expressed by the equation:

$$\mathbf{I_{limiting} = nFD/\delta * C^*} \qquad (5.7)$$

Where:

D is the diffusion coefficient;

δ is the diffusion layer thickness;

C^* is the concentration of the electroactive (limiting) species in the bulk of the electrolyte.

nFD = same definitions as above.

Now, the corrosion rate of a given metal in a corrosive electrolyte (e.g. Steel in concrete) is defined (in absence of external currents) where total oxidation current (e.g. for reaction: $Fe \rightarrow Fe^{++} + 2e^-$) and the total reduction current (e.g. for reaction: $2H^+ + 2e^- \rightarrow H_2$) are equal. The electrode potential corresponding to this condition of zero net current is called the 'Corrosion Potential', E_{corr}, and the common value of the current at this corrosion potential is called the 'Corrosion Current', i_{corr} (M Pourbaix, 1973). This can be expressed as:

At E_{corr},

$$\mathbf{i_a = i_c = 0 \text{ or } i_a = i_c = i_{corr}} \qquad (5.8)$$

The rate of any electrochemical reaction can be represented by a curve, if the potential of a reacting electrode, E, is plotted against the flow of 'reaction current' density, i. These curves are called 'Tafel Curves' or simply 'polarisation curves'. An example is illustrated in Figure 5.5

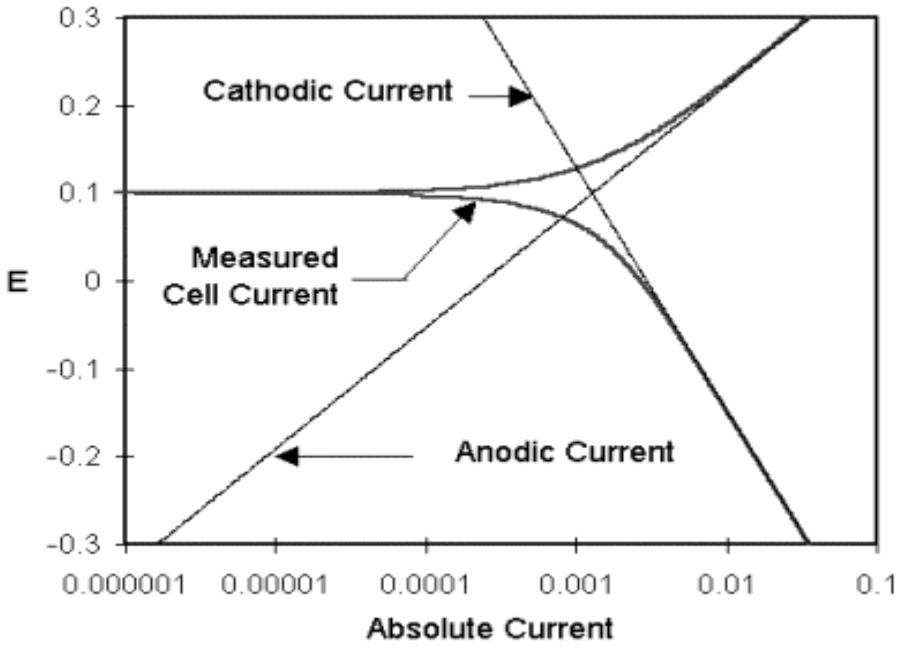

Figure 5.5: Tafel curve, *Corrosion Process Showing Anodic and Cathodic Current Components* and extrapolation of the Tafel region to the equilibrium potential

The polarisation curve is the sum i_{total} of cathodic current density (i_c) and anodic current density (i_a) and both of them depend on the overvoltage exponentially, Tafel Constant $\boldsymbol{\beta_a}$ and $\boldsymbol{\beta_c}$ defining the slope of the curves. This can be expressed as:

$$\mathbf{i_{total} = i_a + i_c = i_{corr} \{[exp(E - E_{corr})/ \beta_a] + [exp(E_{corr} - E)/ \beta_c]\}} \qquad (5.9)$$

The basis for this equation lies in the mixed potential theory proposed by Wagner and Traud in 1938, (F. Mansfeld, Corrosion, 2006).

This image has been removed due to third party copyright. The unabridged version of the thesis can be viewed at the Lanchester Library, Coventry University

Figure 5.6: Ideal Linear Polarization Curve (corrosion-doctors.org 2008)

Note: i_{corr} is used in equations above instead of i_o and the polarization = $(E - E_{corr})$

The determination of these two branches of the Tafel curves is easily performed in the laboratory by 'intentiostatic (also called as galvanostatic), potentiostatic or by potentiokinetic methods.

Under potentiostatic conditions, the equilibrium potential of the reinforcing steel is polarized by varying its value by a fixed amount and monitoring the current decay after a fixed time (Ha-Won Song and Velu Saraswathy (2007). So, a sharp increase in current is indicative of corrosion activities (Bentur *et al*., 1997). In the galvanostatic test, a small fixed current is applied to the rebar and the resulting potential change is recorded after a fixed time. In the same vein, a sharp decrease in potential to negative values under this test is indicative of corrosion activities. Polarization in this context, as the name suggests, is the application of external power source, usually low voltage DC supply, to the rebar such that the corrosion potential ($\mathbf{E_{corr}}$) of the rebar undergoes a shift from its equilibrium state, i.e. for a change of potential, $\Delta\mathbf{E = E - E_{corr}}$, there is a corresponding change in current, $\Delta\mathbf{i = i - i_{corr}}$**.** Depending upon whether galvanostatic or potentiostatic circuits are used either i or $\Delta\mathbf{E}$, may be the independent variables. In both cases, it is recommended that conditions should be selected such that the change in potential falls within

Stern-Geary range, i.e. Δ**E < 10- 30 mV** (Stern and Geary, 1957), where the potential change (Δ**E**) is assumed almost always proportional to the applied current density (Δ**i**), then the corrosion current may be calculated by rearranging equation 5.9 and substituting the exponential function $\exp^x$ ($x \rightarrow 0$) with x, the Stern-Geary formula results:

$$\mathbf{i_{total} = i_{corr}\,[E - E_{corr}] * [1/\beta_a + 1/\beta_c]} \qquad (5.10)$$

According to Stern-Geary (1957) the quotient $\Delta E / I$, called the polarization resistance ($\mathbf{R_p}$), and is defined as the slope of the potential – current density curve at the free corrosion potential, as illustrated in by Figure 5.6, Pierre R. Roberge (2008). This slope, obviously, as discussed by Stern and Geary (1957), is inversely proportional to the instantaneous corrosion rate ($\mathbf{I_{corr}}$) as Δ**E** tends to zero in equation (16).

$$\mathbf{\Delta E/\Delta i}_{\ \Delta E} \Big| \longrightarrow \mathbf{0 = R_p = B/\,I_{corr}} \qquad (5.11)$$

Where:

i = current density applied

I_{corr} = corrosion rate ($\mu A / cm^2$)

R_p= polarization resistance ($\Omega.cm^2$)

B= proportionality constant (Stern-Geary Constant) = $(\beta a * \beta c)/ 2.303(\beta a + \beta c)$

The basis for the Stern and Geary equation that is used in polarisation resistance technique also lies on the mixed potential theory, and the derivation of the equation is completely mathematical and the no assumptions are needed to derive this equation beyond those for validity of Tafel equation. Furthermore, the assumption of linearity between voltage and current is not needed (F. Mansfeld and K. B. Oldham, 1971).

In order to estimate the corrosion rate using equation (16), the values of two Tafel slopes and the polarisation resistance, all measured at the corrosion potential, would be needed. Obtaining a good estimates for Tafel slopes, particularly for in-situ measurements on real-life structure, can be very difficult.

However, for steel in concrete, the value of B has been documented to vary from 13 to 52 mV for wide range of systems (Stern 1958). However, for steel reinforcement in concrete Andrade et.al (Andrade and Gonzales 1978) recommended the value of 26 mV for bare steel in active state and for galvanized steel and 52 mV for bare steel in the passive state. In the literature the B value of 26 mV is widely used (including most of the commercially available LPR measuring devices). Since polarization resistance, $\Delta \mathbf{E} / I$ is intimately dependent upon the Tafel constants, $\mathbf{i_{corr}}$ values calculated from LPR data can produce an error by a factor of 2.2 unless Tafel constants are known for a given situation (M. Pourbaix, 1973). N.D. Greene and R.H. Gandhi (1982) have suggested that no assumed value for Stern-Geary Constant, B, is required to calculate corrosion rate from LPR measurement; instead they developed a computer program, called 'Betacrunch' in Basic language for PC (Personal Computer) where simply three sets of measured values of $\Delta \mathbf{E}$ and $\mathbf{I_{applied}}$ are needed as data input, then the program algorithm automatically determines the actual Tafel constants $\boldsymbol{\beta_a}$ and $\boldsymbol{\beta_c}$ to calculate corrosion rate. It is the intension of the present investigation to use this computer program in conjunction with the proposed multi-functional '**β**-probe' to be used as a counter electrode for linear polarization resistance measurement.

The R_p measurements provide an instantaneous corrosion rate, greatly influenced by climatic changes (temperature, humidity). Exposure conditions especially temperature and concrete humidity can alter icorr in chloride contaminated concrete by a factor of up to 10 (Andrade, C., et. al, 1996 and Zimmermann, L et.al, 1997) and therefore an average corrosion rate can only be estimated after integrating R_p data over time (Elsener, B., 2005). Once an average corrosion rates are determined by R_p measurements, it is possible with varying degree of accuracy to estimate the corrosion rate ($\mathbf{I_{corr}}$) in terms of section loss of the rebar by introducing Faraday's law of electrolysis. In RILEM report (1988), it is suggested that the accurate assessment of this method could be ascertained when I_{corr} vs time curves are integrated to obtained the 'total corrosion current' and converting it to section loss as shown in equation (17) and (18); the value may also be checked against the gravimetric loss obtained from the same steel sample.

$$\int_0 \mathbf{I_{corr}}\ \mathbf{dt} = \mathbf{I_{corr\ T}} \qquad (5.12)$$

Applying Faraday's law, mass loss is given by:

$$m = M \cdot t \cdot I_{corr\,T} / n F \quad (5.13)$$

Where:

M= Molecular weight (56 for steel or iron)

t= Time

n= Ionic charge (2 for $Fe \rightarrow Fe^{2+} + 2e^{-}$)

F= Faraday's constant (96500C/mol)

Typical corrosion rate conversion table based on Faraday's principle is illustrated below in Table 5.4.

Table 5.4: Tabular representation between the most common corrosion units in usage: corrosion current (mA cm^{-2}), mass loss (g m^{-2} day^{-1}) and penetration rates (mm y^{-1} or mpy) (corrosion-doctors.org 2008).

	mA cm^{-2}	mm $year^{-1}$	mpy	g m^{-2} day^{-1}
mA cm^{-2}	1	3.28 M/nd	129 M/nd	8.95 M/n
mm $year^{-1}$	0.306 nd/M	1	39.4	2.74 d
mpy	0.00777 nd/M	0.0254	1	0.0694 d
g m^{-2} day^{-1}	0.112 n/M	0.365 /d	14.4 /d	1

1 mA cm^{-2} = (3.28 M/nd) mm y^{-1} = (129 M/nd) mpy = (8.95 M/n) g m^{-2} day^{-1}

Where:

mpy = milli-inch per year

n = number of electrons freed by the corrosion reaction

M = atomic mass

d = density

For steel or iron, this gives an approximate value of: 1 mA cm^{-2} = 11.6 mm y^{-1} = 456 mpy = 249 g m^{-2} day^{-1}.

In the frequent case of chloride induced localised corrosion, the average corrosion rate determined from R_p measurements underestimate the real, local penetration rates by a factor of 5 – 10 (Elsener, B., Materials Science Forum, 192 – 194, 1995, 857- 866., Flis, J et. al, 1993 and Elsener, B, 1998; Andrade, C., et. al (2004). Assuming localised corrosion at the point with active corrosion, the local penetration rate could vary between 0.15 and 0.3 mm/year at temperature of 6 ^{0}C and increased up to 1 mm/year at 30 ^{0}C. This makes the residual lifetime calculations difficult or uncertain and from an engineering point of view such high local reduction in cross-section of the reinforcement is very dangerous for safety of the structures.

ii) **Embeddable probes method:**

Different electronic configurations of probes are available on commercial scale across the globe with varying degrees of accuracy in determining corrosion deterioration in reinforced concrete structures. Prominent probe is the Embeddable Corrosion Instrument (ECI) which provides comprehensive, real-time corrosion information on reinforced concrete structures within a digital network (Ha-Won Song and Velu Saraswathy (2007). The ECI is versatile and capable of detecting five corrosion quantities simultaneously, viz: linear polarization resistance, open circuit potential, resistivity, chloride ion concentration and temperature. Unlike other commercially available ones, more often than not, ECI gives clearer picture of the causes and sign of corrosion. Its inclusion in RC structures can best be done as illustrated in Figures 5.7 – 5.11.

These images have been removed due to third party copyright. The unabridged version of the thesis can be viewed at the Lanchester Library

Figure 5.7: ECI Sensor during operation (Int. Journal of Electrochemical Science 2007).

Figure 5.8: Isolated ECI Sensor (vatechnologies.com 2008).

Some other commercially available ones illustrated in Figures 5.8 to 5.12 are Schiessel probe, Corrowatch probe, Force probe, C-probe type CP 100 and CORROATER; their compositions and performances are reviewed extensively by Dubravka *et al* (2008).

These images have been removed due to third party copyright. The unabridged version of the thesis can be viewed at the Lanchester Library, Coventry University

Figure 5.9: Schiessel probe (ndt.net 2008)

Figure 5.10: Corrowatch probe (ndt.net 2008)

These images have been removed due to third party copyright. The unabridged version of the thesis can be viewed at the Lanchester Library

Figure 5.11: FORCE probe (ndt.net 2008)

Figure 5.12: C-probe type CP 100 (ndt.net 2008)

This image has been removed due to third party copyright. The unabridged version of the thesis can be viewed at the Lanchester Library, Coventry University

Figure 5.13: CORROATER (ndt.net 2008).

iii) Macro cell Corrosion Current Measurement

Another important aspect to the development of the proposed 'multi-functional **β**-probe' is to measure corrosion current, hence the corrosion rate, of the steel reinforcement in chloride contaminated concrete due to the formation of macro-cell corrosion. In addition, it is the intension of this investigation to assess if the probe could be used as a 'counter electrode' for the linear polarisation measurement together with a separate role to assess the current requirement for an effective cathodic protection by 'E – log I' tests and also to monitor the performance of the operating cathodic protection installation by monitoring the direction of current flow with the formation of a corrosion macro cell.

This section briefly reviews the literature with regard to the fundamental principles for the formation and morphology of macro-cell corrosion of steel reinforcement in concrete together with the methodology of 'in situ' measurement of macro cell corrosion current.

In section 2.2 the spatiality of the anodic and cathodic reactions occurring on steel reinforcement in chloride contaminated concrete leading to the formation of

macrocell corrosion cells with a corresponding flow of ‘macrocell’ corrosion current has been defined.

As stated in section 2.2 the corrosion morphology of steel in chloride contaminated concrete is dominantly due to the formation of ‘macro cells’ leading to highly localised corrosion. A typical example of macro cell corrosion is shown in figure below.

Figure 5.14: An example of macro cell Corrosion.

The spatial locations of ‘anodic’ and ‘cathodic’ sites a ‘short-circuited’ corrosion cell is formed and the total corrosion current, $I_{corr,\ total}$ is given by the driving voltage (i.e. potential difference between uncoupled anode and cathode), ΔV, divided by the resistance of the electrolyte, $R_{El} + R_A + R_{c,}$ where R_A and R_C are the resistance of the anodic and cathodic reactions:

$$I_{corr,\ total} = \Delta V / (R_{El} + R_A + R_{c,}) \qquad (5.14)$$

The values of ΔV are reported to be ranging between 0.25 and 0.50 V (Raupach, M., and Gulikers, J., 2000; and Elsener, B., 1998). According to Jaggi, S., et al., (2001) the electrolyte resistance R_{EL} contains the geometry factor anode / cathode ratio (e.g. increases for small anodes) and the resistivity of the concrete, which in turn are affected by, among other factors, the relative humidity and temperature. On the other hand, the resistance components, R_A and R_C, are influenced by the kinetics of the anodic dissolution of the steel in pitting conditions and cathodic oxygen reduction reaction.

In its simplest form, macrocell corrosion current measurement involves embedding a small piece of steel (same as reinforcement steel, if possible) cast in high chloride concrete, forming a small concrete cylinder, to create a 'galvanic' corrosion cell between the probe and the steel reinforcement. Many researchers frequently used this approach in laboratory and also in the field to study corrosion behaviours and are being developed as an ASTM procedure (ASTM G109-92). The procedure to measure the macrocell corrosion current (or 'galvanic corrosion current') is obtained by connecting the probe to the positive terminal and the reinforcement to the negative terminal of a voltmeter through a shunt resister (1 or 10 ohm). The reading is voltage polarity (+ or -), which indicates the direction of current flow. A negative (-) reading indicates that the steel reinforcement is corroding. Thus, this can provide qualitative information regarding the corrosion activities on the reinforcement. Macrocell corrosion probe may be used to estimate the local current density collected on the steel, if the surface area of the probe is known. Therefore, the probe may be used to confirm that local corrosively active sites ('hot spots') receive sufficient current from the CP system. This is indicated by a reversal of net current flow between the macrocell probe and the reinforcement after the CP system has been energised. Further, the probe could be used as a 'temporary anode' to undertake 'E – log I' test (at an initial stages of CP system design) for assessing the current density required to provide adequate cathodic protection.

Finally, the macrocell (or galvanic cell) probe can be used as a 'counter electrode' for LPR measurement. In this case, the value of the polarisation can be calculated from the potential shift, ΔE, of the corroding steel and the measured value of the macro cell corrosion current, I_{mac}:

$$R_p = \Delta E / I_{mac} \qquad (5.15)$$

A number of researchers employed macrocell (or galvanic cell) corrosion measurement technique to predict the instantaneous corrosion rate of steel reinforcement. Gulikers et. al., (1984) have demonstrated that the corrosion rate calculated from the test results obtained macro cell current measurements and using equation // above are in good agreement with the corrosion rates with the polarisation resistance, Rp, obtained from normal polarisation procedure.

According to Gulikers et. al., for practical purposes the galvanic polarisation method (as they call it) may give a reasonable alternative to LPR measurements.

5.4 Experimental design

5.4.1 Background

This section outlines the development of the probe design, equipment, materials and procedure used to prepare the test specimens employed for the research work i.e. to investigate the usefulness of the new probe to monitor number of parameters relating to the corrosion behaviour of the reinforcement steel in concrete, together with the assessment of the effectiveness of the cathodic protection system. These parameters includes (i) macro cell corrosion current measurement, (ii) act as a counter electrode for linear polarisation measurement, (iii) use as a 'temporary anode' to conduct E-logI test to assess the current requirements for adequate cathodic protection and also (iv) to monitor the performance of the operating cathodic protection installation. The research work incorporates both experimental and mathematical methods to assess and evaluate the performance of the probe.

Relevant experimental techniques that historically have been employed to investigate corrosion rate due to macro-cell phenomena associated with reinforcing steel in concrete are those described in ASTM G109-92 (Test Method for Determining the Effects of Chemical Admixtures on the Corrosion of Embedded Steel Reinforcement in Concrete Exposed to Chloride Environments) and Southern Exposure Method. For the purpose of this study, ASTM 109-92 test method has been adopted with necessary modifications.
The results obtained from the macro-cell test were validated / compared with data from the LPR measurements, 'two-probes' embedded electrode method.

5.4.2 Materials and Equipment

The following equipment and materials were used for the experimental tests:

- Voltmeter: FLUKE 110 TRUE RMS MULTIMETER: used for measuring corrosion potentials.

- Data logger / Amplifier: Lab Jack U3-LV. Used for recording real-time corrosion potentials.
- Mixer: For mixing concrete used in the concrete specimen tests.
- Silver / Silver Chloride Electrode (Ag/AgCl): The reference electrode is used to measure the corrosion potential of the bars and the macro cell probe.
- Wire: Insulated lead wire is used to make the electrical connections to the bars.
- Compacted sand sample: Used as a trial specimen.
- Concrete: The concrete consists of Portland Type I cement, crushed limestone as coarse aggregate, River sand as fine aggregate, tap water.
- Salt: Sodium Chloride.
- Anode: Conductive ceramic anode provides cathodic protection from corrosion by salt water.
- Reinforcing steel: Carbon steel (Mild and High-yield).
- Potentiostat: TYPE DT 2110 (HI-TEK INSTRUMENTS), for conducting Linear Polarization Test.
- Desktop computer: For collecting real-time information from data logger.

Probe Construction and electrical Circuit:

The probe is made up of 20mm diameter carbon steel disc encased in 50mm long water-tight pvc tube (epoxy filled). To enable an interaction between the probe and the corrosive environment, only the front end of the disc (i.e. the cross section of the bar) was exposed to form an interface with the concrete / sand environment while the other end was connected to 4 lead cables which deliver the potential difference developed at the disc – concrete / sand interface. One of the cables was however connected with 1 Ohm resistor to enable the measurement of cell current. The probe circuit diagram is illustrated in Figure 5.20.

1 ohm resistors: Coupled with probe to measure corrosion current.

Various stages of the probe construction and the materials and equipment used to set up the experiments are illustrated in Figures 5.17 – 5.19, 5.21 – 5.23.

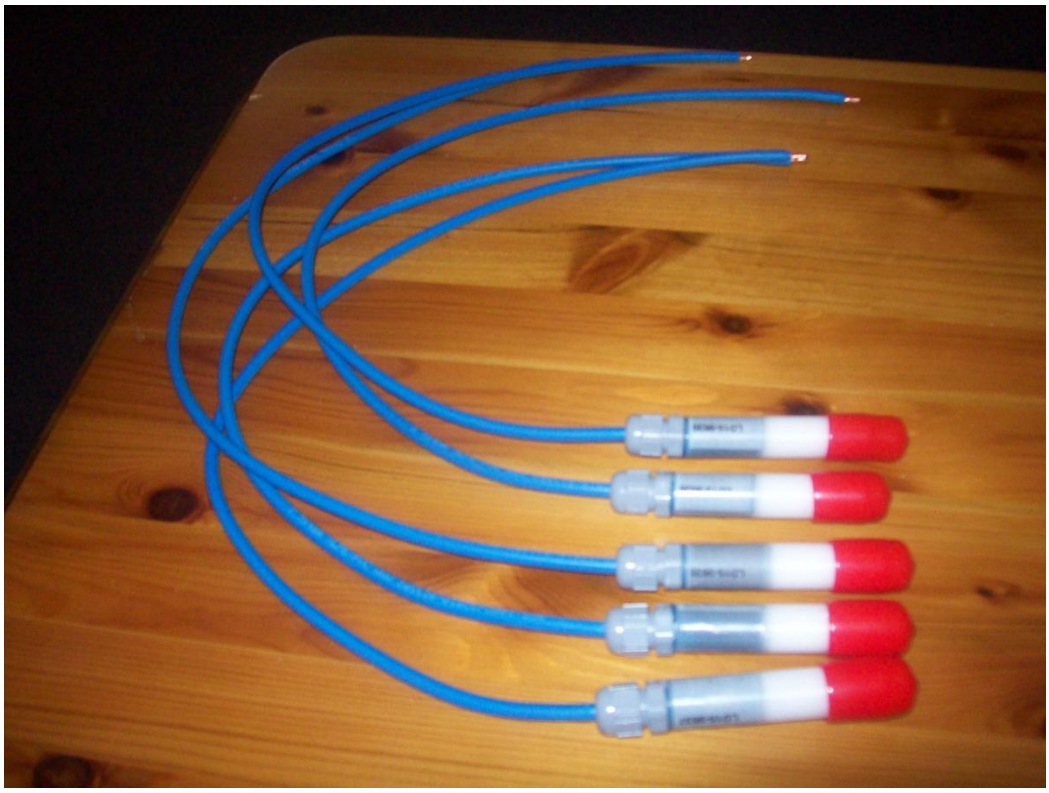

Figure 5.15: Reference Electrodes, Ag/AgCl.

Figure 5.16: Conductive ceramic anodes

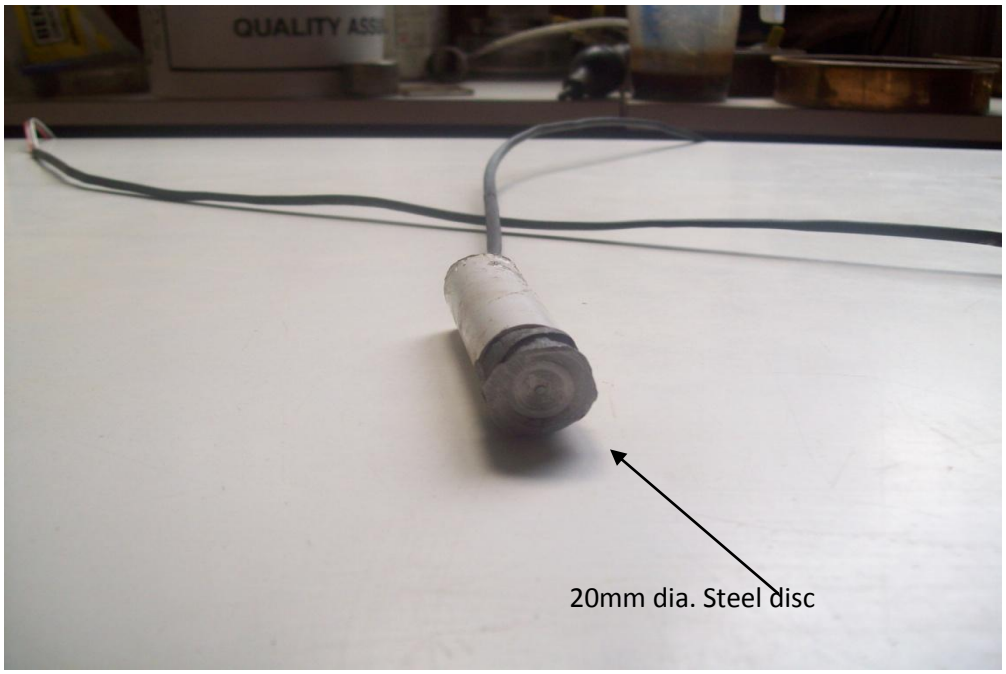

Figure 5.17: Probe before embedment

Figure 5.18: Probes before embedment

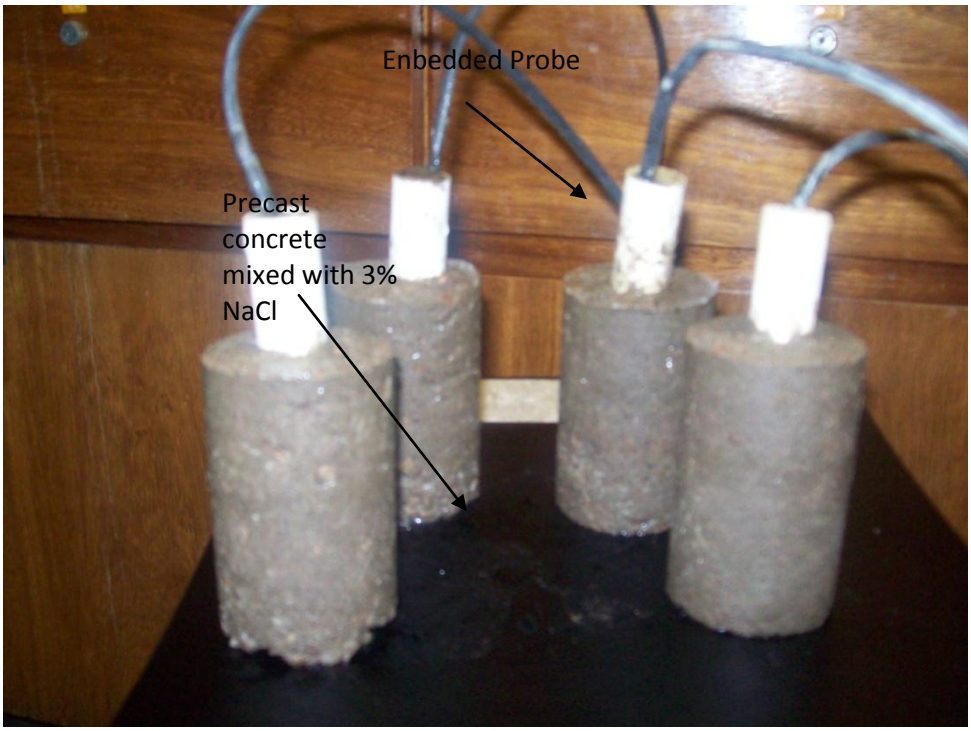

Figure 5.19: Probes after embedment

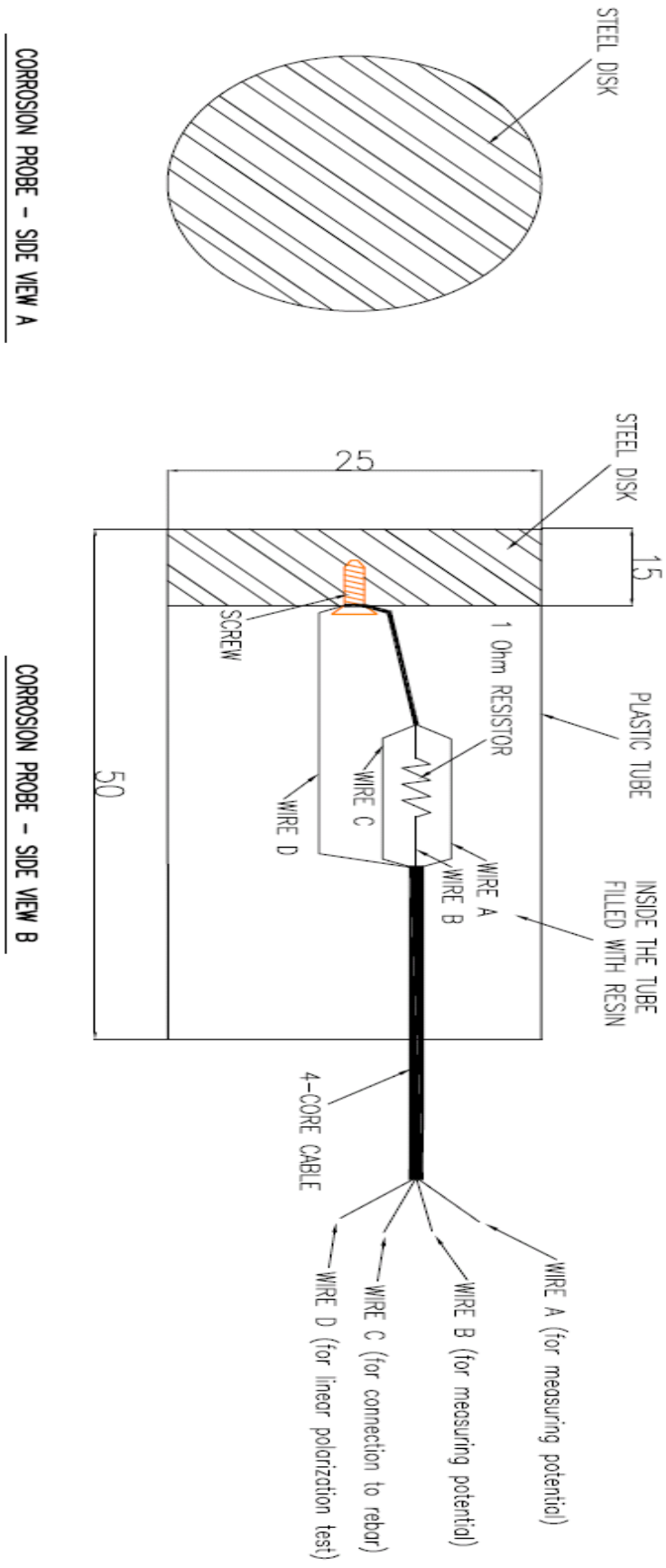

Figure 5.20: Probe circuit

Figure 5.21: Data logging device

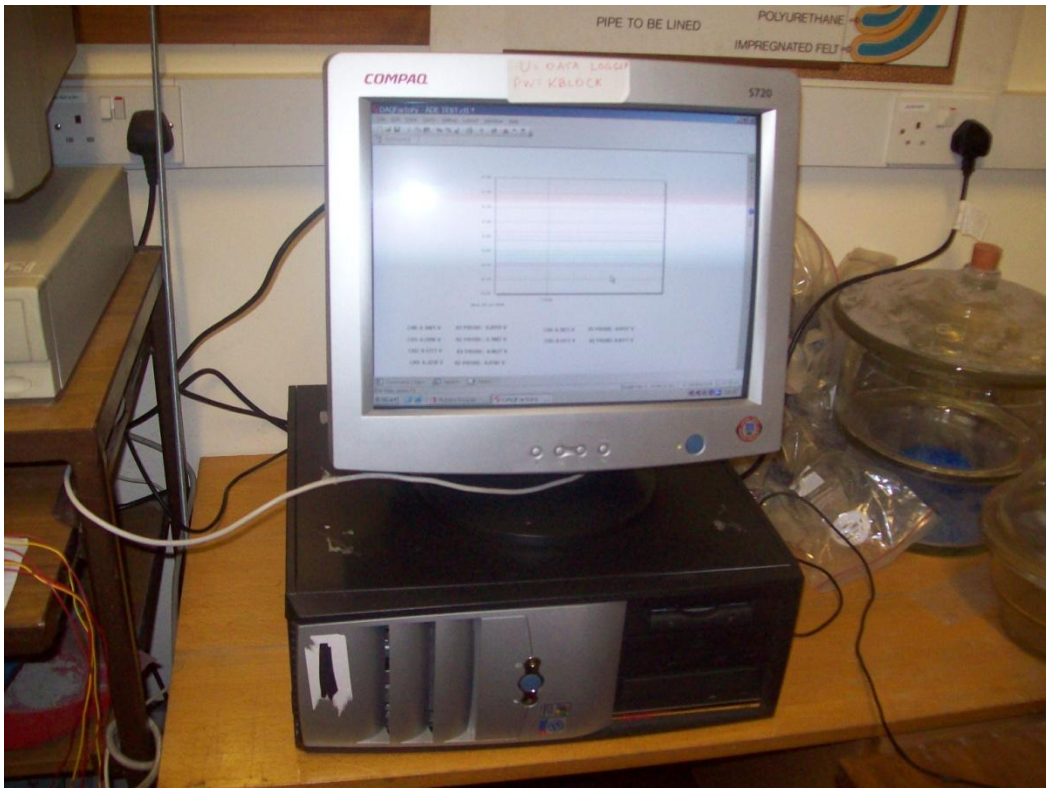

Figure 5.22: Desktop computer

Figure 5.23: Potentiostat

5.4.3 Research Methodology

Experimental, mathematical, graphical and tabular approaches were employed to undertake this study. Details of the methods employed for the experimental focus are considered under the following:

Test specimen preparation and Testing

Test procedure

The mathematical approaches range from simplified equations to complex statistical methods in managing data and estimating quantities on which findings, conclusions and recommendations were based.

5.4.4 Test specimen preparation and Testing

A total of 6 specimens were used for the experiment. These consist of 2 compacted soil specimens mixed with 3.5% of Sodium Chloride solution, and 4

concrete slab specimens. Each soil specimen wooden form illustrated in Figures 5.24 and 5.25 has the following internal dimensions: 350mm x 350mm x 80mm, and contains one Ag/AgCl electrode, one probe, one anode and two embedded 10mm diameter high yield steel of 450mm long. The concrete specimens illustrated in Figures 5.26 and 5.27; each sample is sized 300mm x 300mm x 100mm, with 4 no. embedded 10mm diameter mild steel. The mild steel are of two sets: 2 test bars (350mm long) and 2 dormant bars (300mm long). All bars were electrically isolated.

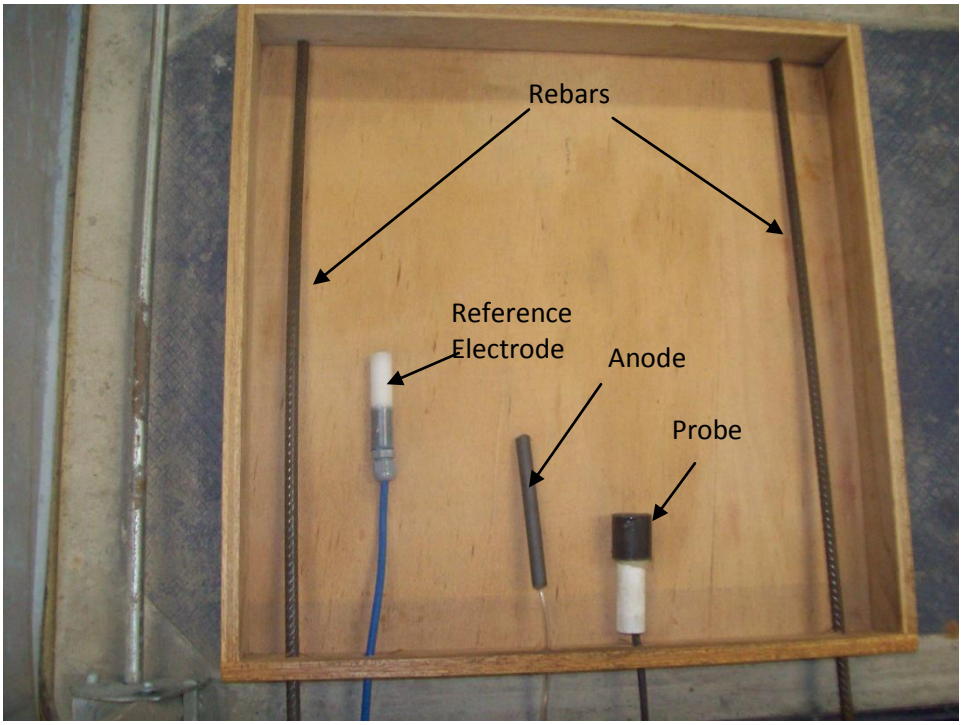

Figure 5.24: Wooden form with test components

Figure 5.25: Soil specimen under test

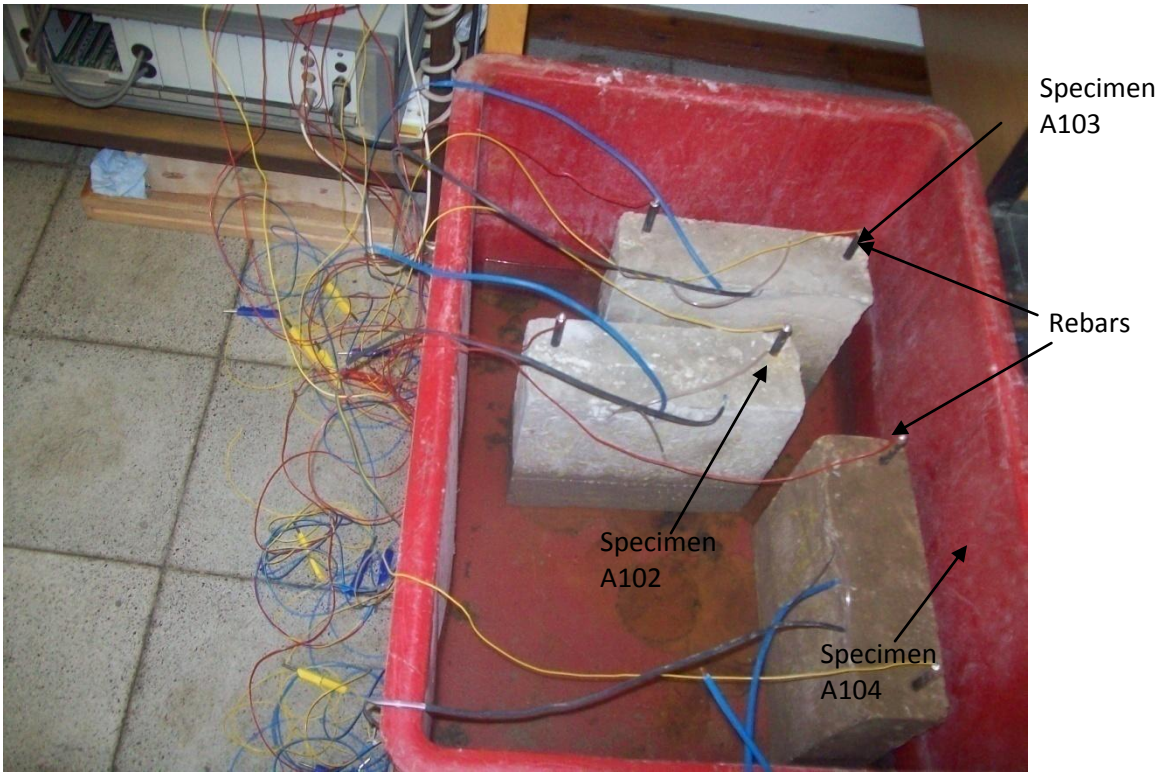

Figure 5.26: Concrete specimens in salt solution during the testing period

Figure 5.27: Concrete specimens in fresh water during the testing period

The compacted sand experiment was undertaken as a trial test in the event of likely problems and uncertainties that may crop up when carrying out the concrete specimen tests. This however was found useful as it made a good precedence.

The compacted soil specimens were prepared with the mixture of fine aggregate (sand) and 3.5% salt solution (NaCl). The samples were kept moist throughout the test period to ensure ionic conductivity.

The concrete specimens were prepared to simulate corrosion of steel in 'high w/c' quality concrete of two different grades (w/c ratio 0.53% and 0.83%). One sample (sample A101) was partly immersed in fresh water and three samples (samples A102, A103 and A104) was partly immersed in NaCl solution. Table 5.5 summarizes the material make-up and exposure conditions of each specimen. Table 5.6 provides a summary of the material composition for the 'sand specimen'.

Table 5.5: Specimen Concrete Mix Proportions and Exposure conditions

Mix Type	Specimen	Water (Kg/m^3)	Cement OPC (Kg/m^3)	Fine Agg. (Kg/m^3)	Coarse Agg. (Kg/m^3)	3% NaCl (Kg)	w/c Ratio	Exposure Condition
1	A101	159	300	885	1140	-	0.53	Fresh water
	A102	159	300	885	1140	-	0.53	3% NaCl solution
2	A103	166	200	200	1300	-	0.83	3% NaCl solution
	A104	166	200	200	1300	0.46	0.83	3% NaCl solution

Table 5.6: Material composition for sand specimens

Specimen Designation	Specimen Type	Material Composition	Specimen Size
101A	Compacted Sand	Soil dry wt.= 12.25kg NaCl wt.=0.429kg Wt. of water=3.52kg	350mm x 350mm x 80mm
102B	Compacted Sand	Soil dry wt.= 12.25kg NaCl wt.=0.429kg Wt. of water=3.52kg	350mm x 350mm x 80mm

5.4.5 Test Procedure

The experimental work was undertaken in two phases. The initial (trial) tests were carried out on the soil specimens to ascertain the practicality of the electrical circuit designed for the probe and the general configuration of the specimens. The second tests were carried out on the concrete specimens, having understudied the behaviour of the probe in the trial tests. While no amendment was carried out on the probe circuit itself, it was necessary to modify the experimental tests in terms of the material design and possible corrosion measurements that could be undertaken. The configuration of the specimen is illustrated in Figure 5.22, 5.26 and 5.27 depicting the positions of the rebars, probe, reference electrode and the anode.

The procedure for undertaking the compacted-sand specimen tests is as follows:
The bars were cut to the desired length (i.e. 450mm).

The bars were then inserted through the holes drilled on the face of the wooden forms, with about 100mm lengths projecting outward to enable connection with lead cables.

The probe, anode and reference electrode were positioned as shown in Figure 5.24.

The mixture of sand, salt and water was then placed in the prepared wooden forms and compacted in three layers with trowel.

The outward ends of the bars, probe, anode and reference electrode were connected to lead cables to enable links with necessary measuring devices.

The specimens were then stored and left undisturbed for 3 days in the temperature controlled room (25^0C), in the laboratory, before the testing period commenced.

Daily wetting of the specimens with fresh water was also carried out to prevent the soil from dry out and to ensure internal conductivity.

Modifications to this experiment were made as follows:

After about 20 days testing period, it was observed that the probe and the bars were corroding concurrently and about the same rate from their equilibrium potentials, since the concentration of chloride was uniform within the soil specimens. Hence, the potential difference values indicated by the multimeter with respect to reference electrode may not be useful for the purpose of this study since the anodic current is meant to be generated either by the probe or the rebars. In the event where the anodic site interchanges between the probe and the rebars, false readings are inevitable, it thus becomes necessary to redesign the corrosive environments such that corrosion activities favour one site over the other. This however necessitated the eventual modification to the soil specimen. The slight modification was to vary the concentration of chloride within the specimen matrix and monitor the effects. To achieve this, the soil/salt environment around one of the embedded bars in each sample was scooped out and replaced with compacted salt-free soil. The samples were however left for about 3 days before commencing further reading to allow enough time for the rebars to adjust their potentials thermodynamically to the new environment.

In order to incorporate the modification employed in the soil specimen tests into the concrete tests, it became imperative to create a separate but more corrosive

environment for the probe or the rebars within the concrete matrix of the concrete specimens. The approach, of course, relates to the ASTM G109-92 principle where 3% salt solution ponding is often used to set up macro-cell current in embedded rebars as shown in Figure 5.30 by Javier *et al*. (2002). To simulate this, the bare face of the probe was embedded in a fresh 50mm diameter cylindrical concrete (100mm long) mixed with 3% NaCl as shown in Figure 5.27 to form a monolithic precast unit. The precast unit was positioned as before along side the rebars, reference electrode and anode. This enabled the probe to corrode faster than the adjacent rebars thereby setting up the required macro-cell current. However, for the purpose of practical application, in existing corroding structures, the inclusion of 3% salt in the probe environment will be unnecessary. This is because for a corroding rebar in concrete, it is easy for the macro-cell current to be detected when connected to a non-corroding probe. The expression governing the change in the potential difference between these two electrodes is given by:

$$\Delta E = E_{probe} - E_{rebar} \qquad (5.16)$$

It should be noted that the equation only becomes valid where only one electrode corrodes. So, all efforts must be to keep the potential of one electrode constant and enforce potential variations on the other electrode.

The procedure for carrying out the concrete specimens tests was as follows:
The bars were cut to the desired length, 350mm.
The bars were then inserted through the holes drilled on the face of the wooden form, with about 50mm lengths projecting outward to enable connection with lead cables.
The probe (precast unit), anode and reference electrode were positioned as shown in Figure 5.27.
The prepared concrete mix was then placed in the prepared mould and compacted with tapping rod.
The outward ends of the bars, probe, anode and reference electrode were connected to lead cables accordingly to enable links with necessary measuring devices.
The specimens were cured in fresh water tank for 21 days, fully immersed.

The specimens were then removed from the water and allowed to stay in air for 3 days.
Specimen A101 was then 1/3 immersed in fresh water and stored in temperature controlled room (25^0C), in the laboratory.

Specimens (A102, A103 and A104) were equally 1/3 immersed, but in 3% NaCl solution and stored in the temperature controlled room (25^0C), in the laboratory.
The specimens were left undisturbed for 3 days before the testing period commenced.

This image has been removed due to third party copyright. The unabridged version of the thesis can be viewed at the Lanchester Library, Coventry University

Figure 5.28: Schematic representation of macro-cell measurement of rebars in accordance to ASTM G109-92 (iri.ku.edu 2002)

5.4.6 Corrosion Potential and Macro-cell Tests

All the 6 specimens prepared for the experimental study, both corrosion potential test and macro-cell test were conducted concurrently. The corrosion potential test determines the relative tendency of a material to corrode in a given environment. The corrosion potentials of the reinforcing bars and the probes were measured with respect to the embedded silver / silver chloride electrodes as schematically represented in Figure 5.29. Readings were taken daily with multimeter, and automatic data logging device.

Macro-cell test is used to measure the corrosion rate of steel. However, it should be acknowledged that macro-cell current only provides a fraction of the whole, but useful and widely employed by engineers as an easy means of detecting corrosion activities in RC structures. In this experiment, the macro-cell test was carried out by direct measurement of voltage drop across the 1 ohm resistor between the probe and the embedded rebars using automatic data logging device as illustrated in Figure 5.30. The voltage drop obtained from the macro-cell readings can easily be converted to corrosion current density and rate of corrosion by using the simplified faraday's equation 5.17 given below or the Conversion table, Table 5.4 in section 5.3.2.5.

$$\textbf{Rate} = 11.6\, i_c \ \textbf{(µm/yr.)} \qquad (5.17)$$

Where:

i_c = corrosion current density, ($\mu A/cm^2$)

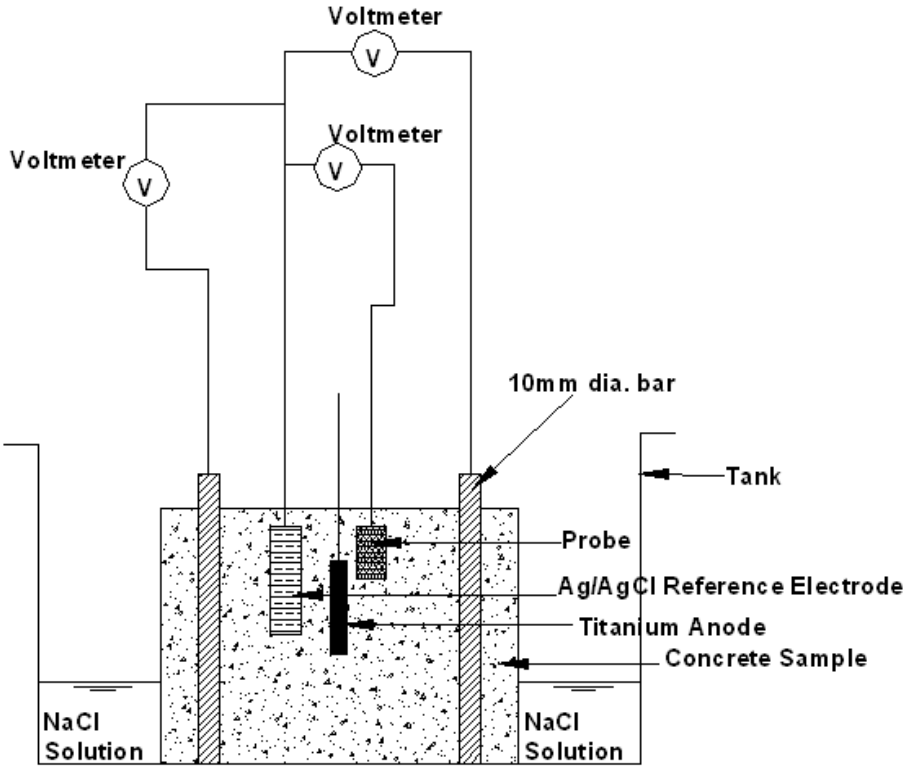

Figure 5.29: Schematic representation of corrosion potential measurements of rebars and probe.

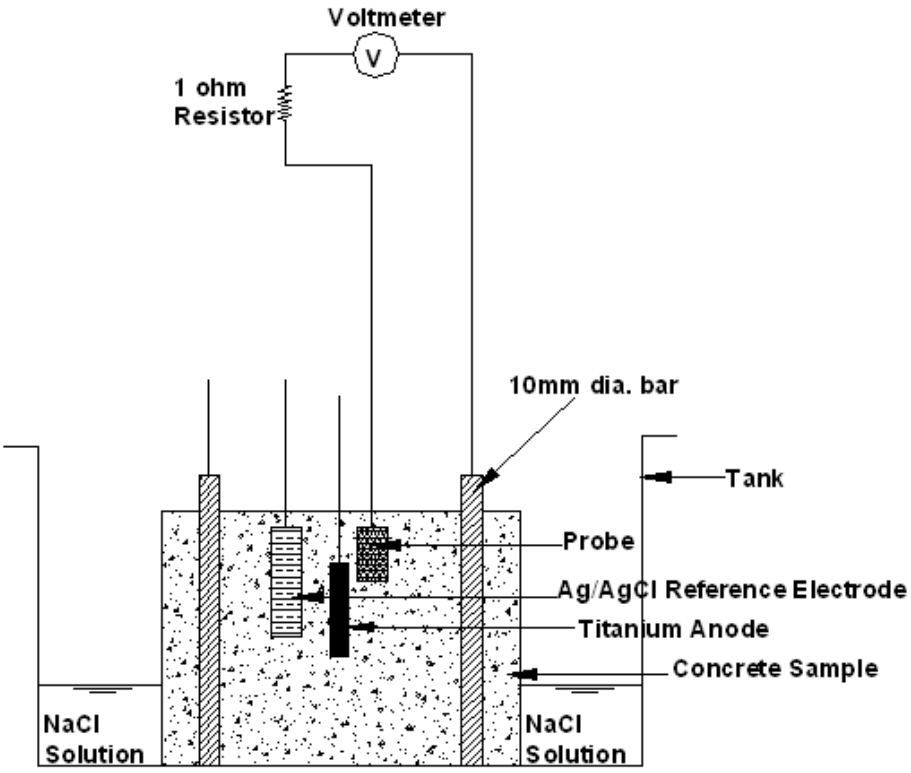

Figure 5.30: Schematic representation of macro-cell measurements between probe and rebars.

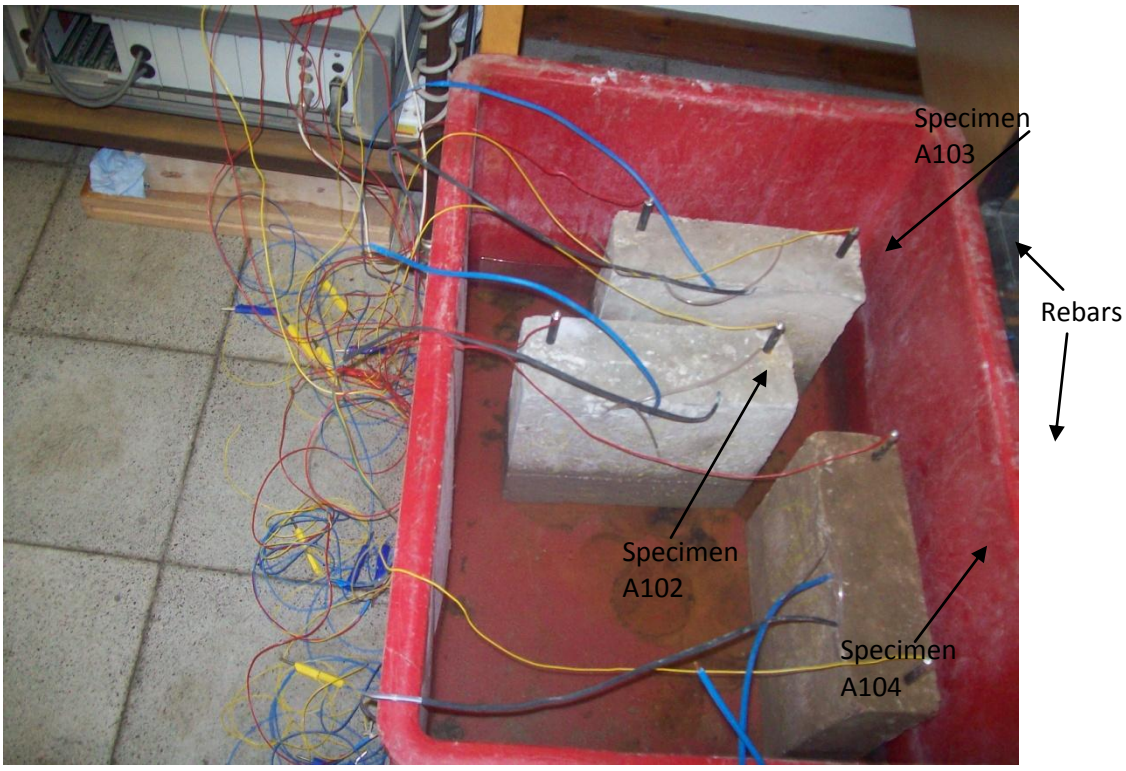

Figure 5.31: Corrosion potential test setup with concrete specimens in Salt solution (A102, A103 & A104).

Figure 5.32: Corrosion potential test setup with concrete specimens in fresh water (A101)

5.4.7 Concrete Cube Test

Standard compressive strength tests were carried out on four concrete cubes made to accompany each mix design at 28 days. The specimen cube test result is given in Table 5.7.

Table 5.7: Cube Test Result

Cube No	Cube Size (mm)	Specimen Designation	Max. Load (KN)	Av. Max. Load (kN)	Stress At Max. Load (MPa)	Av. Stress At Max. Load (MPa)	W/C Ratio
1	100	A101, A102	232.19	224.085	23.22	22.41	0.53
2	100		221.39		22.14		
3	100		219.44		21.94		
4	100		223.32		22.33		
5	100	A103, A104	120.54	136.685	12.05	13.67	0.83
6	100		179.19		17.92		
7	100		125.69		12.57		
8	100		121.32		12.13		

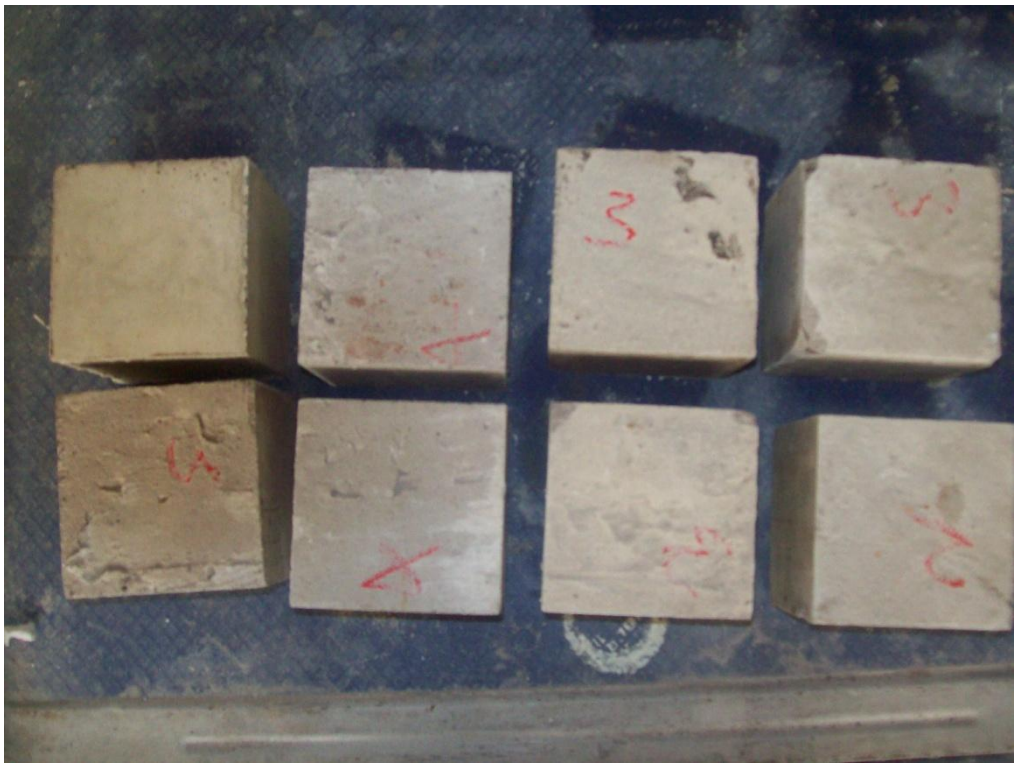

Figure 5.33: Cube Samples

Figure 5.34: Concrete cube sample representing Specimen A101

Figure 5.35: Concrete cube sample representing Specimen A102

Figure 5.36: Concrete cube sample representing Specimen A103

Figure 5.37: Concrete cube sample representing Specimen A104

Figure 5.38: Concrete cube Crush Test

5.4.8 Linear Polarization Resistance Test

This test was undertaken to validate the results obtained from the macro-cell test. Potentiostatic approach was adopted to achieve this as schematically shown in Figure 5.39, and the procedure is as follows:

For each of the concrete specimen, the probe, one test rebar and reference electrode were connected to the working, secondary and reference electrode terminals of the potentiostat respectively.

The rest potential of the working electrode (probe) with respect to the reference electrode was measured and recorded using multimeter.

For each polarization reading, the rest potential was varied with successive low DC supply of 20mV, above the rest potential; the corresponding decay current was monitored and recorded after 30 seconds.

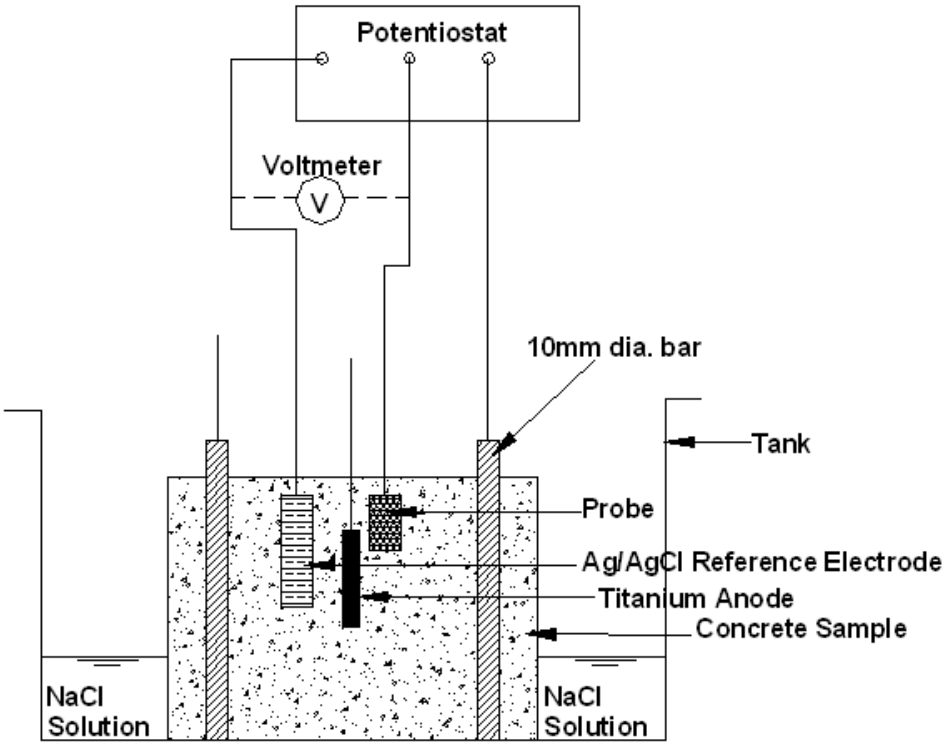

Figure 5.39: Schematic representation of Linear polarization measurement.

5.5 Results and Discussion

This section presents and discusses the results obtained in the corrosion potential tests, macro-cell tests and linear polarization resistance tests. The results and discussion cover only the second phase of the experiment which relates to the concrete slab tests.

5.5.1 Corrosion Potential Test

Average daily corrosion potential results are shown in Tables 5.8 to 5.12 and Figure 5.40 to 5.43. By convention, the more negative the corrosion potential, the greater the likelihood of corrosion. As presented in Table 5.2, when the corrosion potential versus the silver / silver chloride electrode is more negative than –250mV, the corrosion state is classified as severe; at values in the upward of –250 mV, there is greater than 90% probability that corrosion is occurring; when the potential falls between –100 mV to - 250 mV, the risk of corrosion assumes an intermediate state, and at values less negative than -100mV, the risk is low to about 10% probability (ASTM C 876).

Table 5.8: Corrosion potential in mV of Silver / Silver Chloride Electrode versus Probe and Rebars in Specimen A101 during the 30 days testing period.

Test Period (days)	Probe (mV)	Rebar 1 (mV)	Rebar 2 (mV)
1	-489	-542	-509
2	-490	-549	-511
3	-491	-551	-516
4	-491	-555	-518
5	-518	-559	-504
6	-520	-559	-502
7	-523	-558	-502
8	-523	-558	-503
9	-524	-558	-501
10	-526	-558	-499
11	-531	-556	-496
12	-533	-554	-491
13	-536	-553	-486
14	-541	-559	-489
15	-541	-559	-488
16	-541	-559	-488
17	-540	-559	-488
18	-541	-559	-486
19	-539	-559	-484
20	-537	-561	-485
21	-536	-561	-485
22	-536	-561	-484
23	-535	-562	-484
24	-535	-562	-484
25	-552	-564	-498
26	-562	-565	-505
27	-569	-565	-511
28	-573	-566	-514
29	-610	-572	-514
30	-650	-579	-515

Table 5.9: Corrosion potential in mV of Silver / Silver Chloride Electrode versus Probe and Rebars in Specimen A102 during the 30 days testing period.

Test Period (days)	Probe (mV)	Rebar 1 (mV)	Rebar 2 (mV)
1	-542	-619	-649
2	-512	-630	-625
3	-510	-625	-625
4	-508	-622	-622
5	-502	-620	-622
6	-504	-615	-618
7	-507	-607	-610
8	-507	-602	-609
9	-508	-602	-609
10	-508	-596	-608
11	-535	-650	-610
12	-536	-647	-608
13	-536	-640	-607
14	-537	-630	-605
15	-539	-590	-602
16	-550	-586	-599
17	-550	-584	-597
18	-550	-584	-592
19	-551	-584	-592
20	-550	-583	-592
21	-551	-581	-591
22	-551	-579	-589
23	-552	-578	-588
24	-552	-574	-572
25	-554	-573	-580
26	-555	-571	-581
27	-551	-571	-581
28	-549	-569	-579
29	-549	-568	-578
30	-548	-567	-576

Table 5.10: Corrosion potential in mV of Silver / Silver Chloride Electrode versus Probe and Rebars in Specimen A103 during the 30 days testing period

Test Period (days)	Probe (mV)	Rebar 1 (mV)	Rebar 2 (mV)
1	-507	-640	-651
2	-525	-646	-657
3	-520	-646	-654
4	-514	-645	-650
5	-513	-642	-647
6	-512	-640	-641
7	-512	-640	-641
8	-512	-638	-639
9	-541	-633	-636
10	-541	-633	-635
11	-541	-633	-635
12	-542	-631	-633
13	-542	-631	-633
14	-542	-630	-632
15	-555	-627	-628
16	-555	-627	-628
17	-555	-627	-628
18	-556	-625	-625
19	-556	-625	-625
20	-557	-620	-617
21	-557	-620	-617
22	-557	-620	-617
23	-559	-615	-611
24	-559	-615	-609
25	-560	-613	-606
26	-560	-613	-606
27	-559	-611	-606
28	-557	-608	-606
29	-555	-608	-607
30	-554	-606	-608

Table 5.11: Corrosion potential in mV of Silver / Silver Chloride Electrode versus Probe and Rebars in Specimen A104 during 30 days testing period

Test Period (days)	Probe (mV)	Rebar 1 (mV)	Rebar 2 (mV)
1	-581	-585	-554
2	-568	-604	-563
3	-565	-603	-564
4	-563	-603	-564
5	-560	-602	-567
6	-560	-600	-569
7	-561	-600	-569
8	-561	-592	-571
9	-562	-585	-572
10	-498	-611	-575
11	-498	-605	-575
12	-498	-605	-575
13	-499	-600	-575
14	-499	-598	-576
15	-518	-586	-580
16	-522	-588	-589
17	-523	-588	-589
18	-525	-588	-589
19	-526	-590	-582
20	-527	-592	-578
21	-529	-590	-578
22	-531	-590	-578
23	-531	-590	-578
24	-533	-589	-578
25	-534	-588	-578
26	-533	-586	-579
27	-533	-586	-580
28	-533	-586	-580
29	-533	-584	-582
30	-533	-584	-582

The erratic nature of the values presented in Table 5.8 to 5.12 may be difficult to interpret directly, hence, a clearer view of the data can be appreciated when the natural measure of the corrosion potential dispersal is understood as shown in Table 5.13; assuming the centre of the data is measured about the mean value. The data is normalized and distributed by using the statistical principles of standard deviation and standard error of the mean. These are expressed mathematically in equation 5.18 to 5.21:

Mean:

$$\bar{x} = \frac{1}{N}\sum_{i=1}^{N} x_i \qquad (5.18)$$

Standard deviation:

$$\sigma = \sqrt{\frac{1}{N}\sum_{i=1}^{N}(x_i - \bar{x})^2} \qquad (5.19)$$

Standard error:

$$\sigma_{\bar{X}} = \frac{\sigma}{\sqrt{n}}, \qquad (5.20)$$

Confidence interval for the mean:

$$\bar{X} = \pm Z\sigma_{\bar{X}}, \qquad (5.21)$$

Where:

$\bar{X}$ = mean

$\sigma_{\bar{X}}$ = standard error

σ = standard deviation

Z = value corresponding to cumulative density function of the normal distribution

n or N = size of the sample

Table 5.12: Summary table of Corrosion potential of Silver / Silver Chloride Electrode versus Probe and Rebars in Specimen A101, A102, A013 and A104 in 30 days testing period

Specimen	Test Electrode	Mean Potential (mV)	Standard Deviation (mV)	Standard Error	True Potential (mV)
A101	Probe	-537.77	32.94	Lies between 6.01 and 18.03 of the mean value.	Lies between -551.55 and -523.99
	Rebar 1	-559.4	6.65	Lies between 1.21 and 3.64 of the mean value.	Lies between -560.18 and - 554.62
	Rebar 2	-498	11.72	Lies between 2.14 and 6.42 of the mean value.	Lies between -502.91 and -493.09
A102	Probe	-535.13	19.35	Lies between 3.53 and 10.59 of the mean value.	Lies between -543.22 and -527.04
	Rebar 1	-598.23	25.59	Lies between 4.67 and 14.01 of the mean value.	Lies between -608.4 and -587.52
	Rebar 2	-600.53	18.06	Lies between 3.30 and 9.90 of the mean value.	Lies between -608.1 and -592.96
A103	Probe	-542.5	18.52	Lies between 3.38 and 10.14 of the mean value.	Lies between -550.25 and -534.75
	Rebar 1	-626.93	12.18	Lies between 2.22 and 6.67 of the mean value.	Lies between -632.03 and -621.83
	Rebar 2	-627.6	15.95	Lies between 2.91 and 8.73 of the mean value.	Lies between -634.27 and -620.93
A104	Probe	-534.57	23.38	Lies between 4.27 and 12.8 of the mean value.	Lies between -544.35 and -524.79
	Rebar 1	-593.27	7.93	Lies between 1.45 and 4.34 of the mean value.	Lies between -596.59 and -593.27
	Rebar 2	-575.63	8.00	Lies between 1.46 and 4.38 of the mean value.	Lies between -578.98 and -575.28

From Table 5.5 and Table 5.11, a direct tabular contrast can be developed as presented in Table 5.13.

Table 5.13: Tabular Comparison of Test Specimens

Specimen Designation	Probe	Rebar 1	Rebar 2	Compressive Stress (MPa)	Exposure Condition
True Potentials in A101 (mV).	Between -551.55 and -523.99	Between -560.18 and -554.62	Between -502.91 and -493.09	22.41	Fresh water
True Potentials A102 (mV).	Between -543.22 and -527.04	Between -608.4 and -587.52	Between -608.1 and -592.96	22.41	NaCl solution
True Potentials A103 (mV).	Between -550.25 and -534.75	Between -632.03 and -621.83	Between -634.27 and -620.93	13.67	NaCl solution
True Potentials A104 (mV).	Between -544.35 and -524.79	Between -596.59 and -593.27	Between -578.98 and -575.28	13.67	NaCl solution

From Table 5.13, it seems both the quality of concrete and exposed conditions have slight influence on the corrosion tendencies of the test electrodes as it reflects on the embedded rebars potentials. Logically, steel embedded in a 'high w/c' quality concrete and in a more corrosive environment is expected to corrode faster than steel in a better quality concrete and in a lesser corrosive environment. A direct analogy of this is illustrated clearly in Table 5.13 where corrosion tendency is least both on Rebar 1 and Rebar 2, in specimen A101. While it may be suspected that specimen A103 exhibits the highest corrosion probability for these same reasons, such effects were of little influence on specimen A104. For clarity purpose, graphical illustrations of corrosion patterns are appended in Figure 5.40 to 5.43 with further discussions.

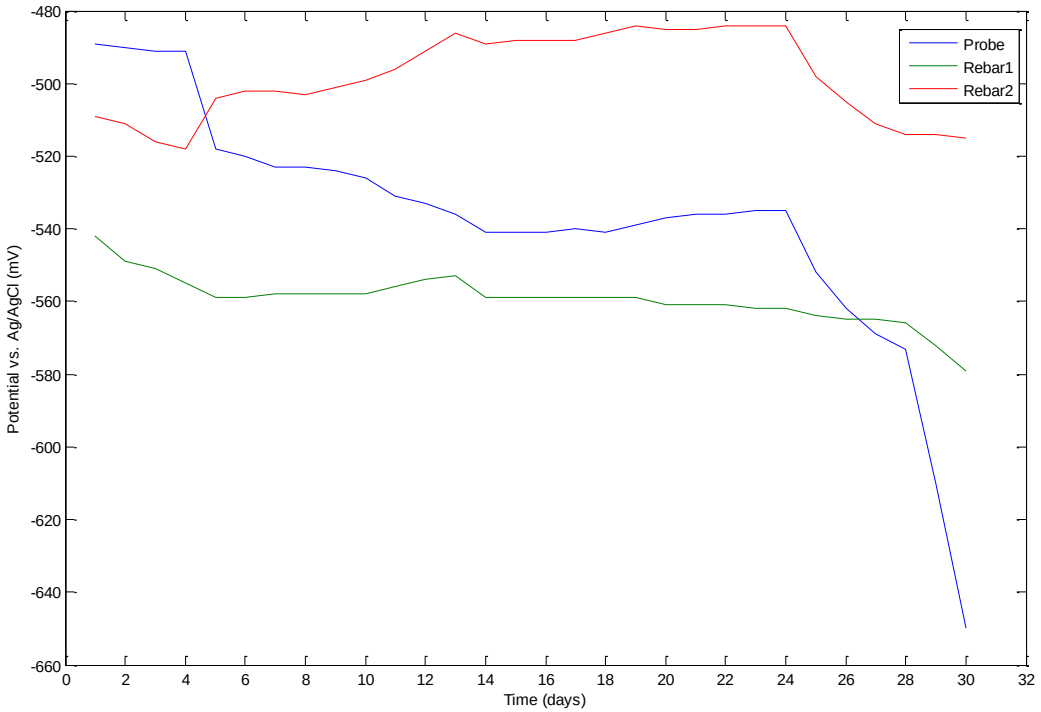

Figure 5.40: Average Corrosion Potential – Time Curve for Probe and Rebars in Specimen A101

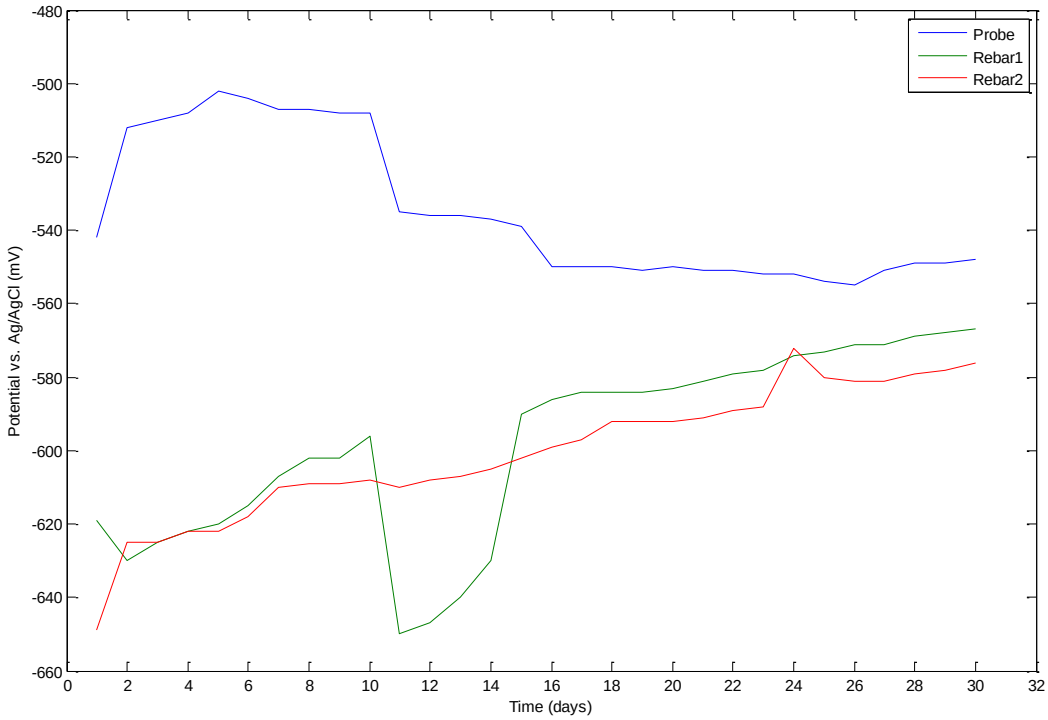

Figure 5.41: Average Corrosion Potential – Time Curve for Probe and Rebars in Specimen A102

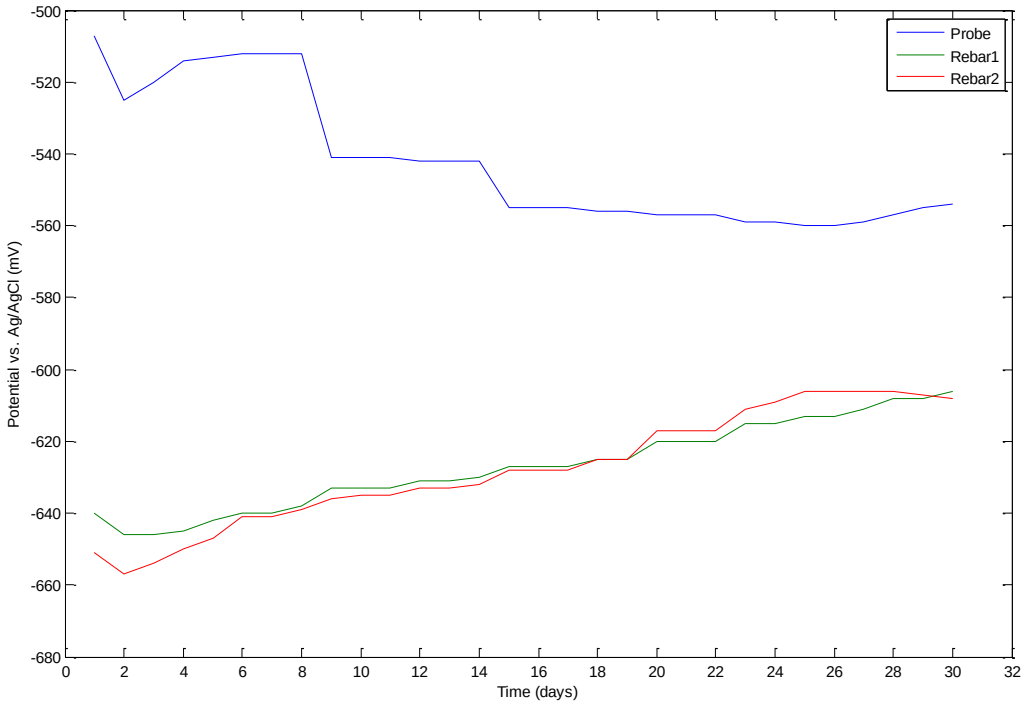

Figure 5.42: Average Corrosion Potential – Time Curve for Probe and Rebars in Specimen A103

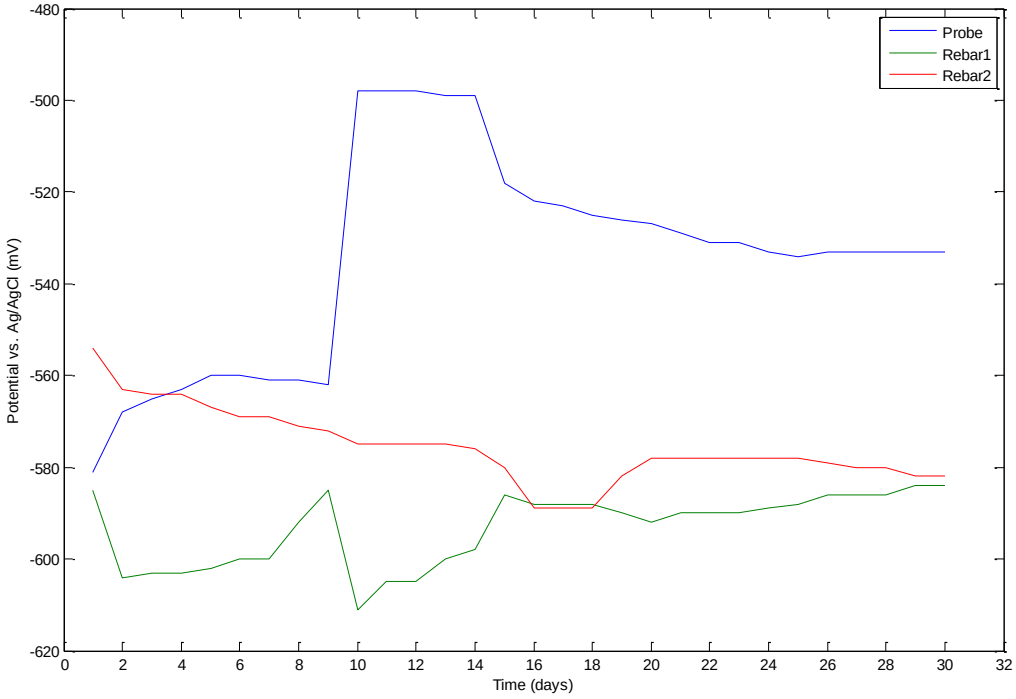

Figure 5.43: Average Corrosion Potential – Time Curve for Probe and Rebars in Specimen A104

Generally, a glance at Table 5.13 and Figure 5.40 to 5.43 shows that all the test electrodes in the four concrete specimen tests exhibit high possibility of corrosion, since the true corrosion potentials and the pattern of corrosion indicated by each are in higher negative values than -250mV (with respect to Ag/AgCl). From Table 5.2 such high corrosion potentials are indicative of severe state of corrosion. However, in order to expound the behaviour of each test electrode in each specimen, it is important to investigate the corrosion patterns as illustrated in Figure 5.40 to 5.43.

In specimen A101, shown in Figure 5.40, the probe corrosion potential increased steadily from -489mV to -650 mV and in higher magnitude than those of Rebar 1 and Rebar 2, unlike in other specimens where the probe potential was relatively lower. This possibly reflects the low effects of fresh water in which specimen A101 was immersed during the testing period on the adjacent rebars. Comparatively, the situation where the corrosion potentials of the rebars in specimen A102, A103 and A104 were higher than that of probe can be explained as due to the effect of salt solution in which the specimens were partly immersed during the testing period. The ingress of chloride at the immersed zone of the specimen is capable of interfering with the passive layer around the rebars either by preventing its formation or breaking it down in order to initiate corrosion process. Such interference is aggravated by the hygroscopic nature of chloride, as it absorbs and retains water to launch early corrosion attack on the rebars. In regard to this experiment, the interference of chloride could possibly be due to infiltration of NaCl solution, salt leaching from the probe precast unit embedded in the concrete specimens or inclusion of sodium chloride in concrete – specimen A104. In literature, it is claimed that the most vulnerable zone to corrosion attack on the rebars under this situation are regions just above the salt water level. Such regions are easily prone to localized corrosion attack and that may have contributed to the early high corrosion values indicated by the reference electrode.

However, experience has shown that the high corrosion potential exhibited by the rebars in all the concrete specimens over a period of 51 days (21 days curing period and 30 days testing period) may not be the actual state of the rebars for obvious reasons already discussed in section 5.3. This is because the values

indicated by reference electrode may sometimes correspond to the thermodynamic feasibility of corrosion reaction the test electrodes may be undergoing, and not necessarily the actual corrosion state. So caution should be taken when interpreting and adopting results obtained by reference electrode. Under this circumstance, the saturated state of the concrete specimens during curing with little or no oxygen availability within the concrete matrix, and possible variations in temperature and internal moisture content of concrete during the testing period may have contributed to the early high corrosion potential values indicated by the reference electrode, especially as more pronounced at the beginning of the testing period when the concrete pores were fully saturated. It is apparent that decline in the concrete internal moisture content will invariably reduce the corrosion possibilities of the rebars. The effect of this was conspicuous on specimen A102 and A103, as the corrosion potentials of the rebars tend towards less negative values in Figure 5.41 and 5.42 respectively. Concisely, in specimen A102, the decline pattern changed from -619 mV to -567 mV and -649 mV to -576 mV in Rebar 1 and Rebar 2 respectively. In specimen A103, the corrosion potential of Rebar 1 declined from -640 mV to -606mV while that of Rebar 2 changed from -651 mV to -608 mV. This phenomenon is generally perceived as a major weakness of using reference electrode to measure corrosion potential of embedded steel in saturated concrete. Hence, to ascertain the credibility of such results, other complementary corrosion tests like corrosion rate test must be undertaken. In the tentative, the corrosion potentials should be assumed high but subjective, until the actual corrosion rate of the test electrodes are analysed in the subsequent sections.

5.5.2 Corrosion Macro-cell Test

This test is a matching test to the corrosion potential test as it helps to estimate the rate of penetration of macro-cell corrosion current. Average daily voltage drop across the 1 ohm resistor between the probe and the rebars, and their respective corrosion rate results are shown in Table 5.14 to 5.18 and Figure 5.44 to 5.54. The corrosion rate can be determined by using Table 5.4 or equation 5.17 as earlier stated. The corrosion current is determined by adopting Ohm's law. With a known

resistance and a measure voltage drop within the mesh, the current can be obtained easily by using equation (5.22).

$$I = V/R \qquad (5.22)$$

This is further converted to corrosion current density which is the amount of current passing through the unit area of the probe steel disc (anode), and is given by:

$$Ic = V/RA \qquad (5.23)$$

Where,

V= voltage drop across the resistor, mV

R= resistance of the resistor, ohm

A= area of exposed steel disc, cm^2

This corrosion current density in $\mu A/cm^2$ can then be converted to corrosion rate in µA/year by using equation (27).

$$Rate = Ic\ (11.6 \times 10^{-3}) \qquad (5.24)$$

Hence, the time to cracking / spalling in year, can be estimated thus:

$$Time = e / Rate\ of\ corrosion \qquad (5.25)$$

Where:

e = loss in reinforcement diameter (µm)

As discussed in section 5.3, ASTM G109 is the only standard for measuring macro cell corrosion rates of steel in concrete. In reinforced concrete this technique involves the measurement of current passing through the concrete surface.

Table 5.14: Corrosion current of Probe versus Rebars in Specimen A101 during the 30 days testing period

Test Period (Days)	Probe vs. Rebar1 (mV)	Probe vs. Rebar 2 (mV)	Average Corrosion Potential (mV)	Corrosion Current (μA)	Current Density (μA/cm^2)
1	-55	-21	-38	-38	-12.09
2	-66	-28	-47	-47	-14.96
3	-43	-14	-28.5	-28.5	-9.07
4	-41	-21	-31	-31	-9.8
5	-37	-25	-31	-31	-9.8
6	-31	-28	-29.5	-29.5	-9.39
7	-25	-35	-30	-30	-9.55
8	-21	-42	-31.5	-31.5	-10.03
9	-15	-52	-18.5	-18.5	-5.89
10	-17	-53	-35	-35	-11.14
11	-19	-55	-37	-37	-11.78
12	-20	-56	-38	-38	-12.09
13	-20	-58	-39	-39	-12.41
14	-23	-54	-38.5	-38.5	-12.25
15	-25	-52	-38.5	-38.5	-12.25
16	-26	-52	-39	-39	-12.41
17	-26	-51	-38.5	-38.5	-12.25
18	-28	-37	-32.5	-32.5	-10.34
19	-27	-31	-29	-29	-9.23
20	-29	-28	-28.5	-28.5	-9.07
21	-32	-28	-30	-30	-9.55
22	-39	-25	-32	-32	-10.18
23	-43	-136	-89.5	-89.5	-28.48
24	-48	-136	-92	-92	-29.28
25	-49	-136	-92.5	-92.5	-29.44
26	-49	-136	-92.5	-92.5	-29.44
27	-94	-136	-115	-115	-36.6
28	-84	-136	-110	-110	-35.01
29	-74	-136	-105	-105	-33.42
30	-72	-128	-100	-100	-31.83

Table 5.15: Corrosion current table of Probe versus Rebars in Specimen A102 during the 30 days testing period

Test Period (Days)	Probe vs. Rebar 1(mV)	Probe vs. Rebar 2 (mV)	Average Corrosion Potential (mV)	Corrosion Current (µA)	Current Density (µA/cm^2)
1	-97	-117	-107	-107	-34.05
2	-120	-113	-116.5	-116.5	-37.08
3	-119	-120	-119.5	-119.5	-38.03
4	-105	-120	-112.5	-112.5	-35.81
5	-97	-100	-98.5	-98.5	-31.35
6	-89	-100	-94.5	-94.5	-30.08
7	-91	-74	-82.5	-82.5	-26.26
8	-75	-69	-72	-72	-22.92
9	-53	-64	-58.5	-58.5	-18.62
10	-39	-47	-43	-43	-13.69
11	-42	-42	-42	-42	-13.37
12	-49	-38	-43.5	-43.5	-13.84
13	-56	-34	-45	-45	-14.32
14	-34	-31	-32.5	-32.5	-10.34
15	-25	-27	-26	-26	-8.27
16	-17	-25	-21	-21	-6.68
17	-17	-26	-21.5	-21.5	-6.84
18	-18	-26	-22	-22	-7.00
19	-18	-28	-23	-23	-7.32
20	-280	-28	-154	-154	-49.01
21	-250	-28	-139	-139	-44.24
22	-284	-28	-156	-156	-49.65
23	-110	-28	-69	-69	-21.96
24	-274	-28	-151	-151	-48.06
25	-95	-28	-61.5	-61.5	-19.57
26	-57	-28	-42.5	-42.5	-13.53
27	-34	-29	-31.5	-31.5	-10.03
28	-25	-29	-27	-27	-8.59
29	-19	-29	-24	-24	-7.64
30	-17	-27	-22	-22	-7.00

Table 5.16: Corrosion current table of Probe versus Rebars in Specimen A103 during the 30 days testing period

Test Period (Days)	Probe vs. Rebar 1(mV)	Probe vs. Rebar 2 (mV)	Average Corrosion Potential (mV)	Corrosion Current (µA)	Current Density (µA/cm^2)
1	-136	-145	-140.5	-140.5	-44.72
2	-115	-129	-122	-122	-38.83
3	-134	-138	-136	-136	-43.28
4	-125	-129	-127	-127	-40.42
5	-115	-116	-115.5	-115.5	-36.76
6	-109	-109	-109	-109	-34.69
7	-93	-96	-94.5	-94.5	-30.08
8	-91	-93	-92	-92	-29.28
9	-87	-89	-88	-88	-28.01
10	-72	-73	-72.5	-72.5	-23.07
11	-69	-71	-70	-70	-22.28
12	-65	-69	-67	-67	-21.32
13	-62	-68	-65	-65	-20.69
14	-59	-62	-60.5	-60.5	-19.26
15	-55	-60	-57.5	-57.5	-18.30
16	-53	-45	-49	-49	-15.60
17	-53	-53	-53	-53	-16.87
18	-54	-54	-54	-54	-17.19
19	-53	-54	-53.5	-53.5	-17.03
20	-42	-53	-47.5	-47.5	-15.12
21	-43	-43	-43	-43	-13.69
22	-58	-45	-51.5	-51.5	-16.39
23	-57	-46	-51.5	-51.5	-16.39
24	-57	-47	-52	-52	-16.55
25	-59	-49	-54	-54	-17.19
26	-59	-49	-54	-54	-17.19
27	-51	-53	-52	-52	-16.55
28	-51	-54	-52.5	-52.5	-16.71
29	-52	-55	-53.5	-53.5	-17.03
30	-52	-55	-53.5	-53.5	-17.03

Table 5.17: Corrosion current table of Probe versus Rebars in Specimen A104 during the 30 days testing period

Test Period (Days)	Probe vs. Rebar1 (mV)	Probe vs. Rebar 2 (mV)	Average Corrosion Potential (mV)	Corrosion Current (µA)	Current Density (µA/cm^2)
1	-4	-28	-16	-16	-5.09
2	-37	-7	-22	-22	-7.00
3	-41	-7	-24	-24	-7.64
4	-35	-9	-22	-22	-7.00
5	-28	-10	-19	-19	-6.05
6	-24	-11	-17.5	-17.5	-5.57
7	-115	-78	-96.5	-96.5	-30.71
8	-111	-79	-95	-95	-30.24
9	-103	-79	-91	-91	-28.96
10	-75	-61	-68	-68	-21.64
11	-71	-58	-64.5	-64.5	-20.53
12	-69	-55	-62	-62	-19.73
13	-65	-51	-58	-58	-18.46
14	-61	-49	-55	-55	-17.50
15	-58	-47	-52.5	-52.5	-16.71
16	-54	-44	-49	-49	-15.60
17	-54	-49	-51.5	-51.5	-16.39
18	-53	-53	-53	-53	-16.87
19	-52	-55	-53.5	-53.5	-17.03
20	-58	-58	-58	-58	-18.46
21	-57	-58	-57.5	-57.5	-18.30
22	-55	-57	-56	-56	-17.82
23	-55	-56	-55.5	-55.5	-17.66
24	-54	-55	-54.5	-54.5	-17.35
25	-53	-54	-53.5	-53.5	-17.03
26	-53	-53	-53	-53	-16.87
27	-52	-53	-52.5	-52.5	-16.71
28	-52	-54	-53	-53	-16.87
29	-51	-53	-52	-52	-16.55
30	-51	-53	-52	-52	-16.55

Table 5.18: Summary of Corrosion rate for Specimen A101, A102, A013 and A104

Specimen	Mean Current density ($\mu A/cm^2$)	Standard Deviation ($\mu A/cm^2$)	Standard Error	True Current density limit ($\mu A/cm^2$)	Corrosion Rate limit (µm/yr.)
A101	-16.31	9.68	Lies between 1.77 and 5.30 of the mean value.	Lies between -20.36 and -12.26	Upper=0.24 Lower=0.14
A102	-21.84	14.38	Lies between 2.63 and 7.87 of the mean value.	Lies between -27.85 and -15.83	Upper=0.323 Lower=0.183
A103	-23.25	9.43	Lies between 1.72 and 5.16 of the mean value.	Lies between -28.37 and -22.15	Upper=0.329 Lower=0.256
A104	-16.63	6.52	Lies between 1.19 and 3.57 of the mean value.	Lies between -19.4 and -13.9	Upper=0.225 Lower=0.161

On average, the corrosion activities on all the test specimens as presented in Table 5.18 indicated low penetration rate, ranging between 0.14 and 0.329 µm/year. For purpose of clarity, the general sign convention adopted under this test is to interpret a more positive value as less corrosive state. Values below 1.0 µm/year are assumed as low corrosion rates and within permissible passive state as indicated by research findings of Portland Cement Association. Hence, the corrosion rates shown in Table 5.18 are indicative that all the test electrodes are still within their passive state.

However, it is worthwhile to investigate the trend of corrosion rate as illustrated by each test specimen in order to establish facts relating to the aim and objectives of this study. The figures plotted in Figure 5.42 to 5.54 are meant for this purpose and they represent real-time variations of corrosion current and corrosion rate generated from the data logging device for a period of 20,000 minutes.

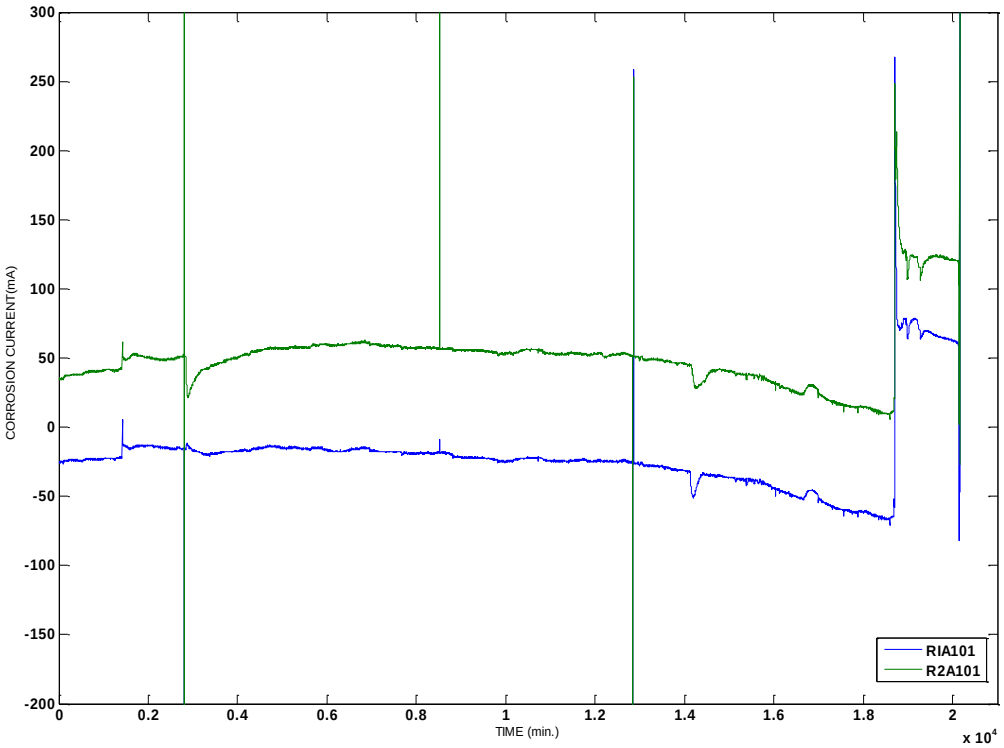

Figure 5.44: Variation of Corrosion Current with Time for Specimen A101

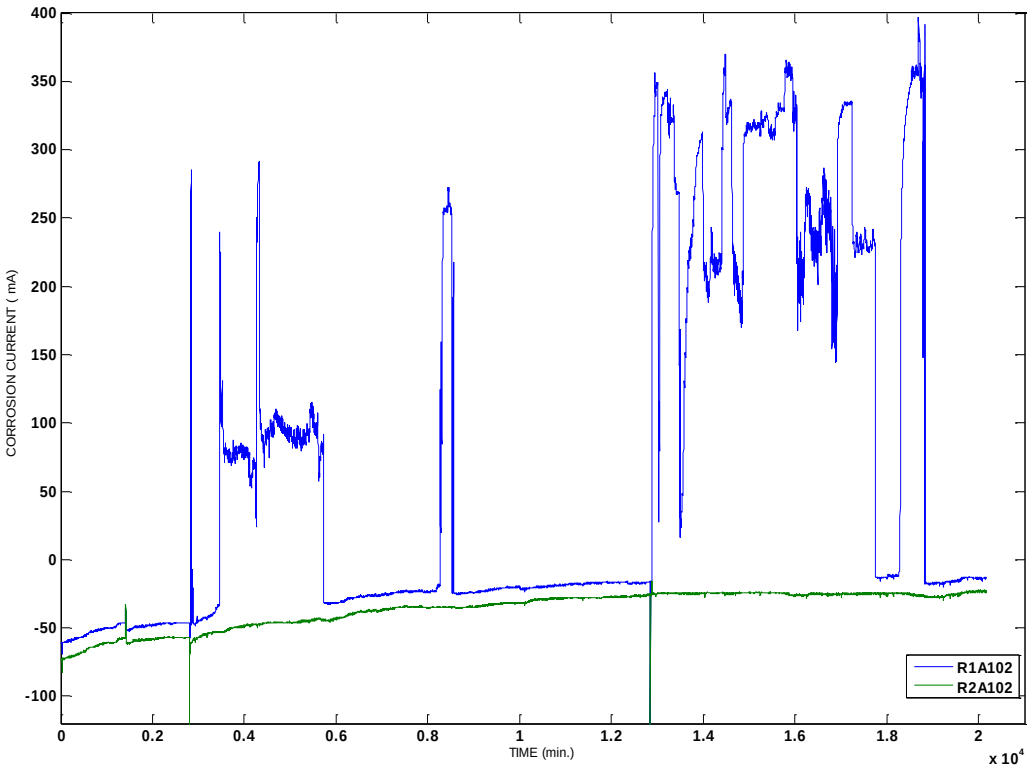

Figure 5.45: Variation of Corrosion Current with Time for Specimen A102

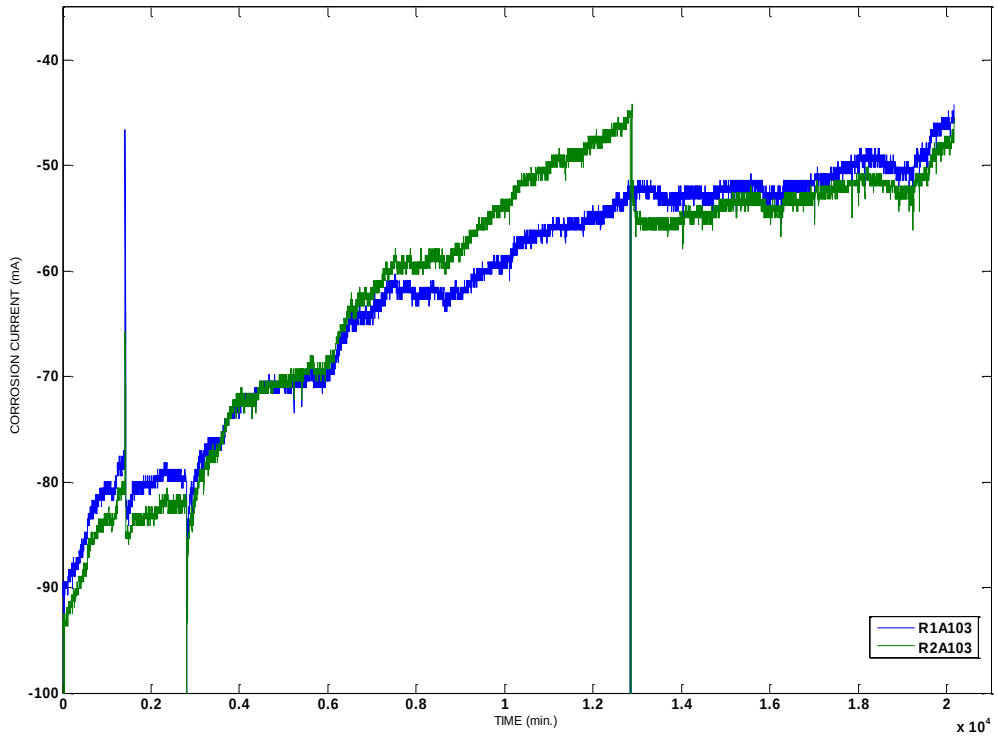

Figure 5.46: Variation of Corrosion Current with Time for Specimen A103

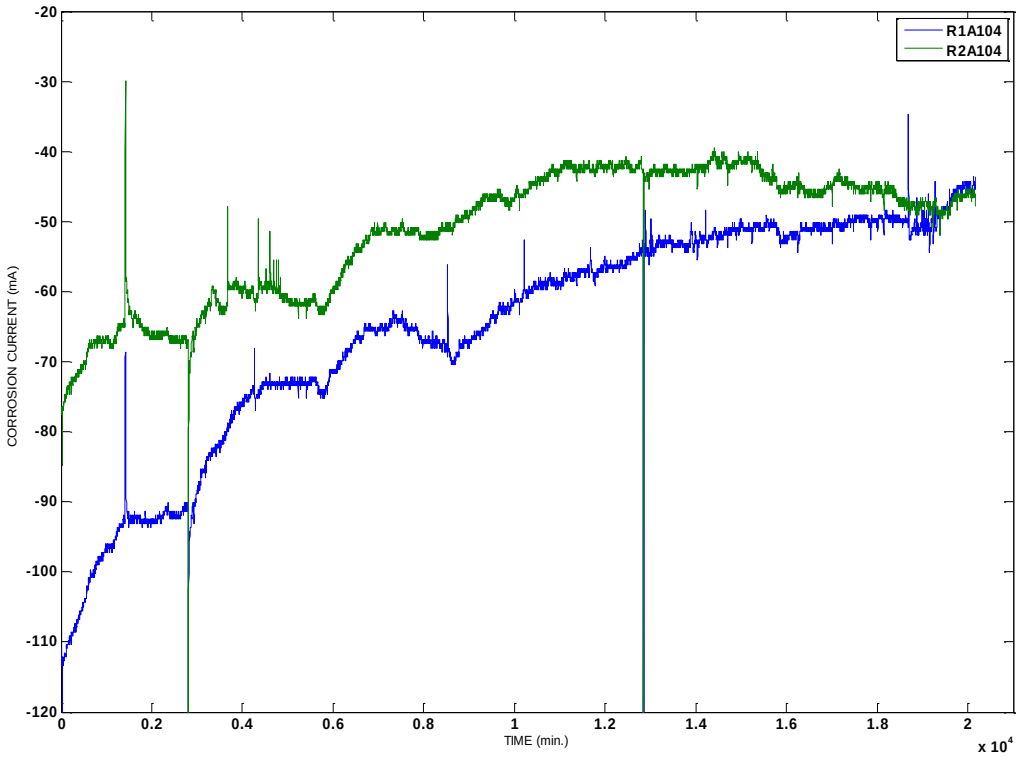

Figure 5.47: Variation of Corrosion Current with Time for Specimen A104

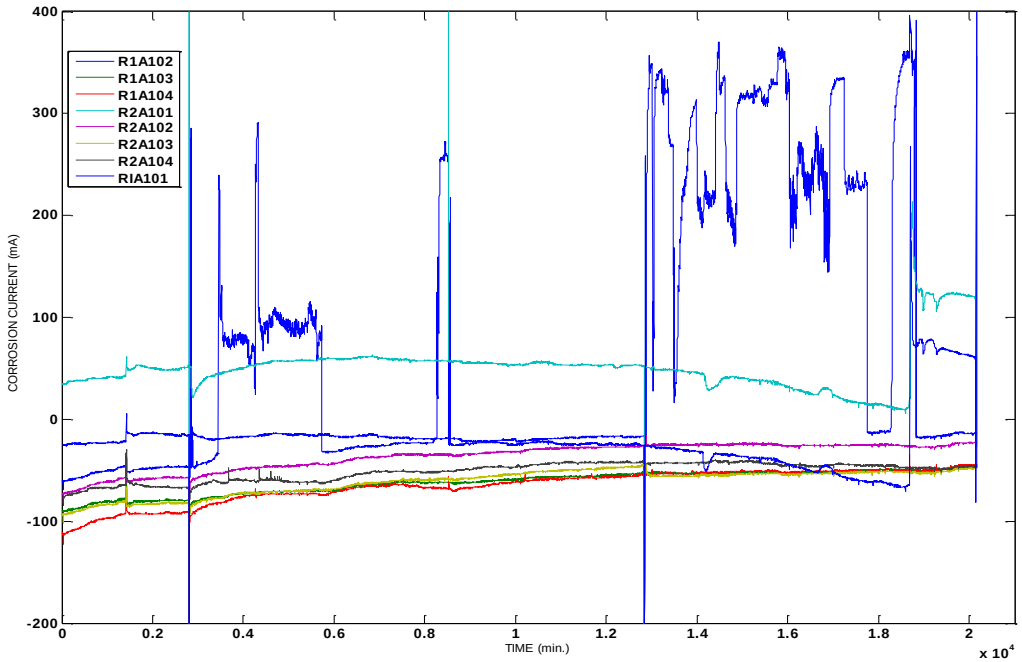

Figure 5.48: Superimposed fluctuation of Corrosion Current for Specimen A101, A102, A103 and A104

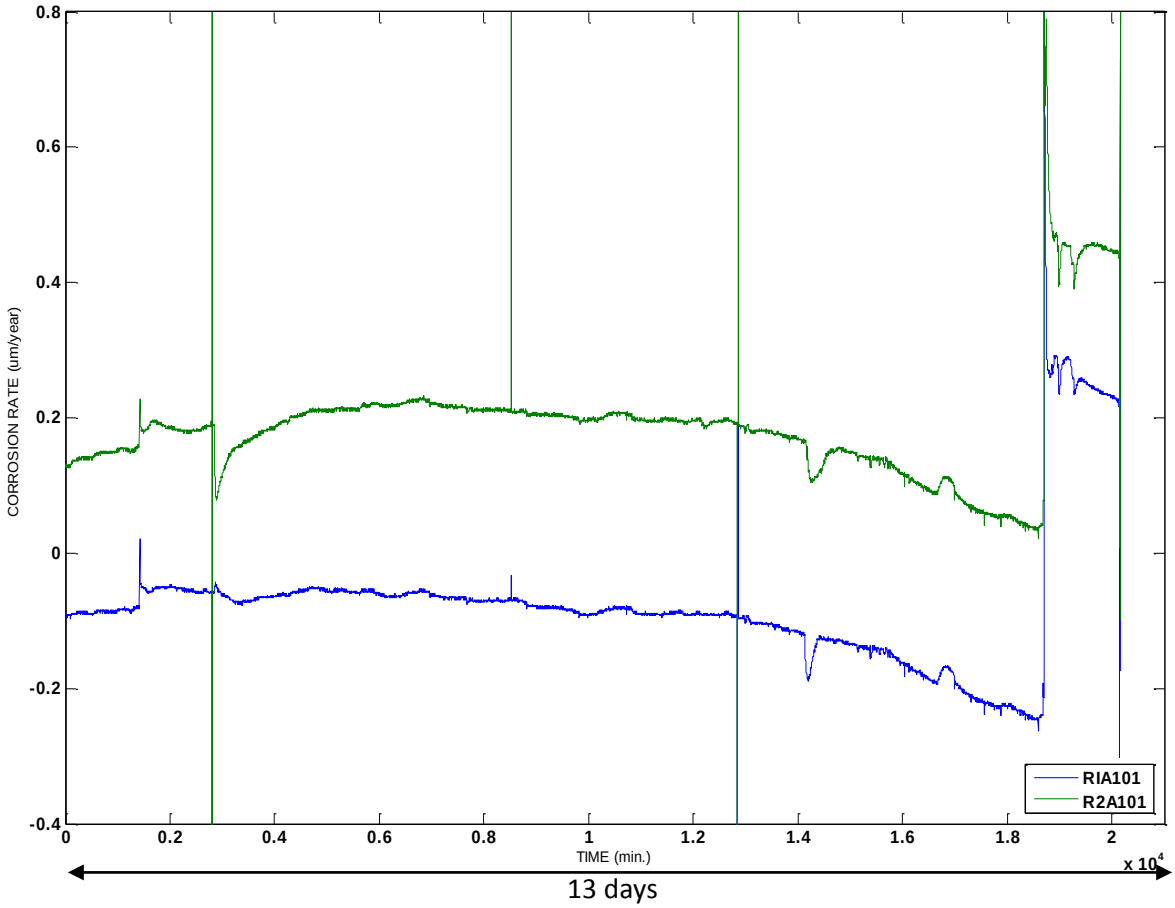

Figure 5.49: Variation of Corrosion rate with Time for Specimen A101

In specimen A101 as shown in Figure 5.47, the corrosion rate pattern between the Probe and Rebar 1 increased from -0.1 to - 0.23 µm/year up to the 12th day of the testing period, while that of Probe and Rebar 2 increased from +0.12 to +0.07 µm/year. On the average, between the probe and the rebars in specimen A101, Figure 5.52 indicates an increase from +0.02 to -0.10 µm/year. The corrosion rate therefore can be said to be low and within passive state.

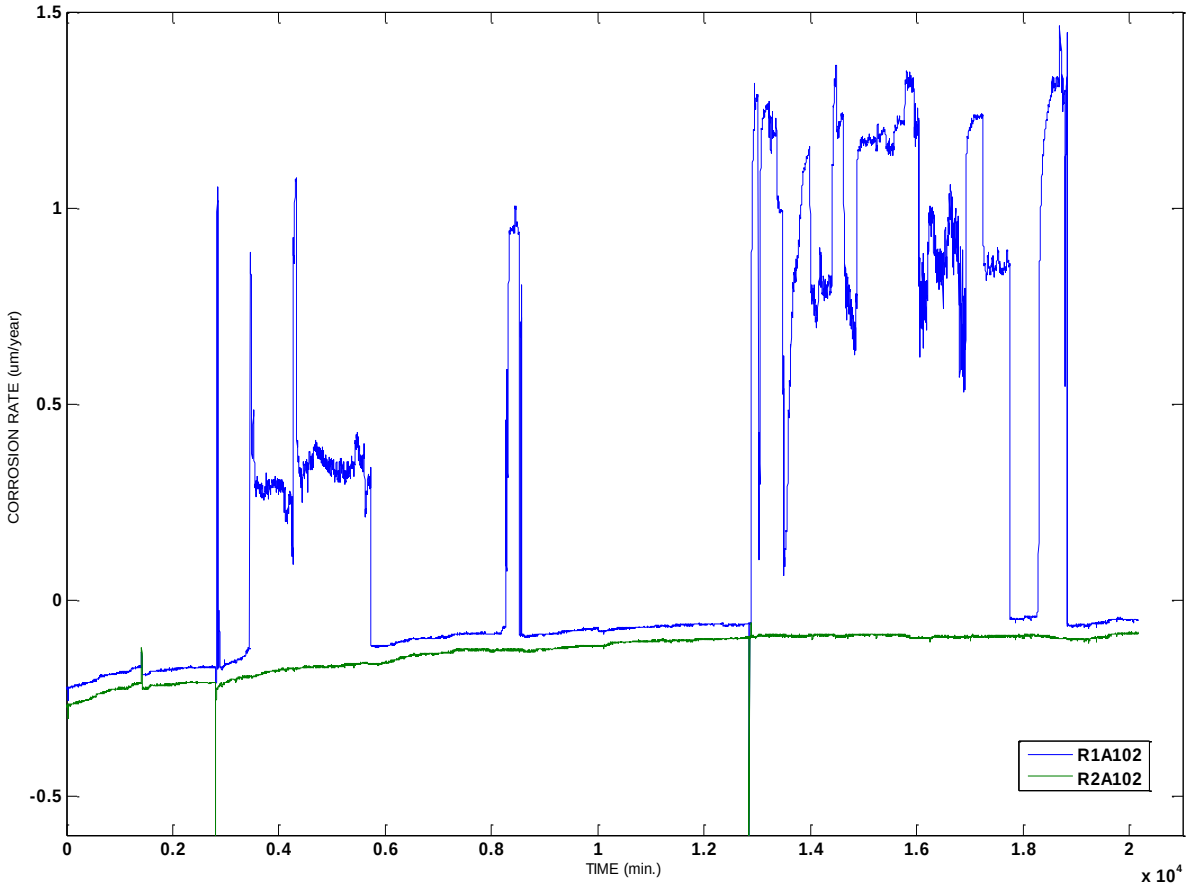

Figure 5.50: Variation of Corrosion rate with Time for Specimen A102

In specimen A102 illustrated in Figure 5.50, the corrosion rate pattern between the Probe and Rebar 1 declined from -0.09 to -0.02 µm/year, while that of Probe and Rebar 2 declined from -0.10 to – 0.04 µm/year. On the average, the corrosion variation as shown in Figure 5.51 declined between -0.24 and -0.07 µm/year which falls within the permissible limit of passivity. However, the corrosion rate here is greater than in specimen A101.

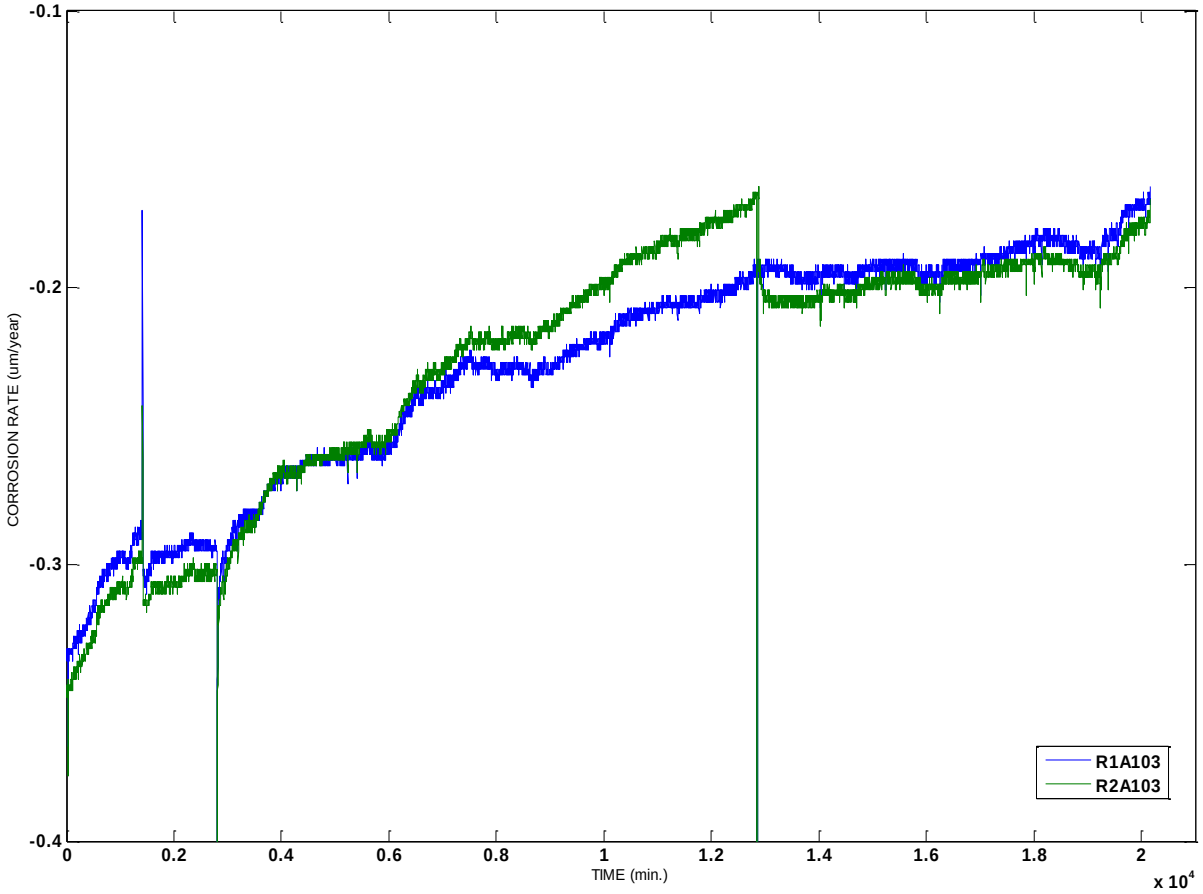

Figure 5.51: Variation of Corrosion rate with Time for Specimen A103

In specimen A103, corrosion rate declined from -0.33 to -0.23 µm/year and from -0.34 to -0.22 µm/year between Probe and Rebar 1, and between Probe and Rebar 2 respectively as shown in Figure 5.50. On the average, as illustrated in Figure 5.52, the corrosion rate variation lies between –0.36 and -0.20 µm/year. Comparatively, corrosion rate in specimen A103 is higher than that of specimen A102.

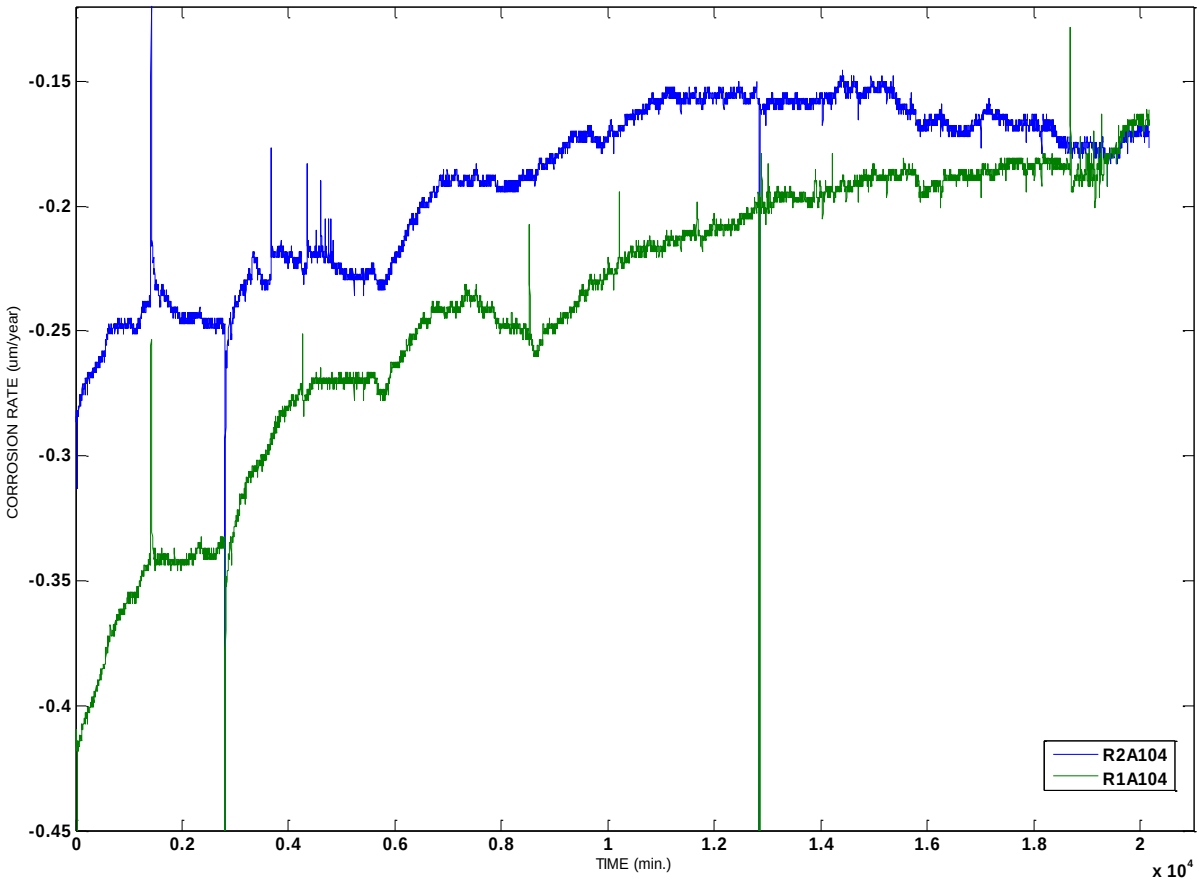

Figure 5.52: Variation of Corrosion rate with Time for Specimen A104

In specimen A104, Figure 5.51 shows a decline of -0.28 to -0.17 µm/year and -0.42 to -0.16 µm/year between the Probe and Rebar 1, and Probe and Rebar 2 respectively. On the average, as illustrated in Figure 5.53, the corrosion rate variation lies between -0.36 and -0.20 µm/year. The corrosion rate in specimen A104 is thus equal to that in specimen A103.

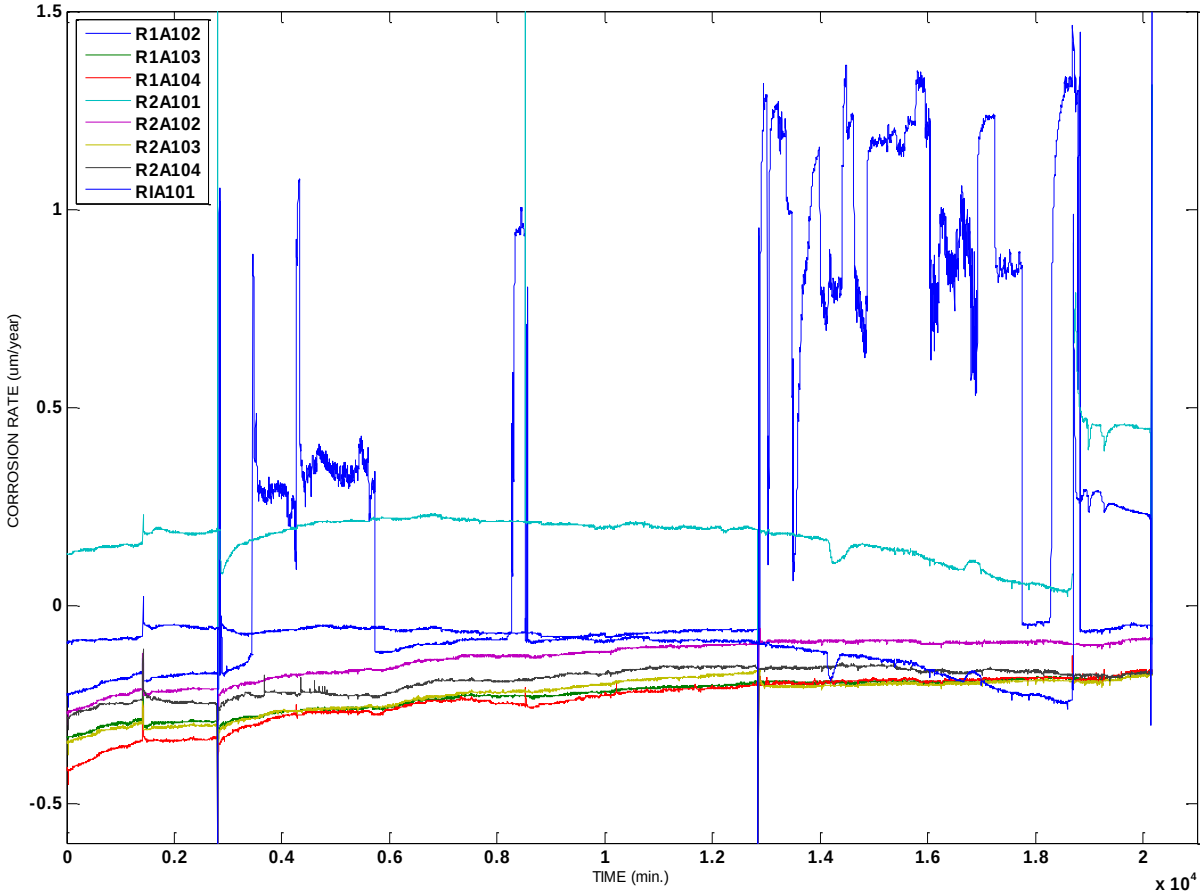

Figure 5.53: Superimposed fluctuation of Corrosion rates for Specimen A101, A102, A103 and A104

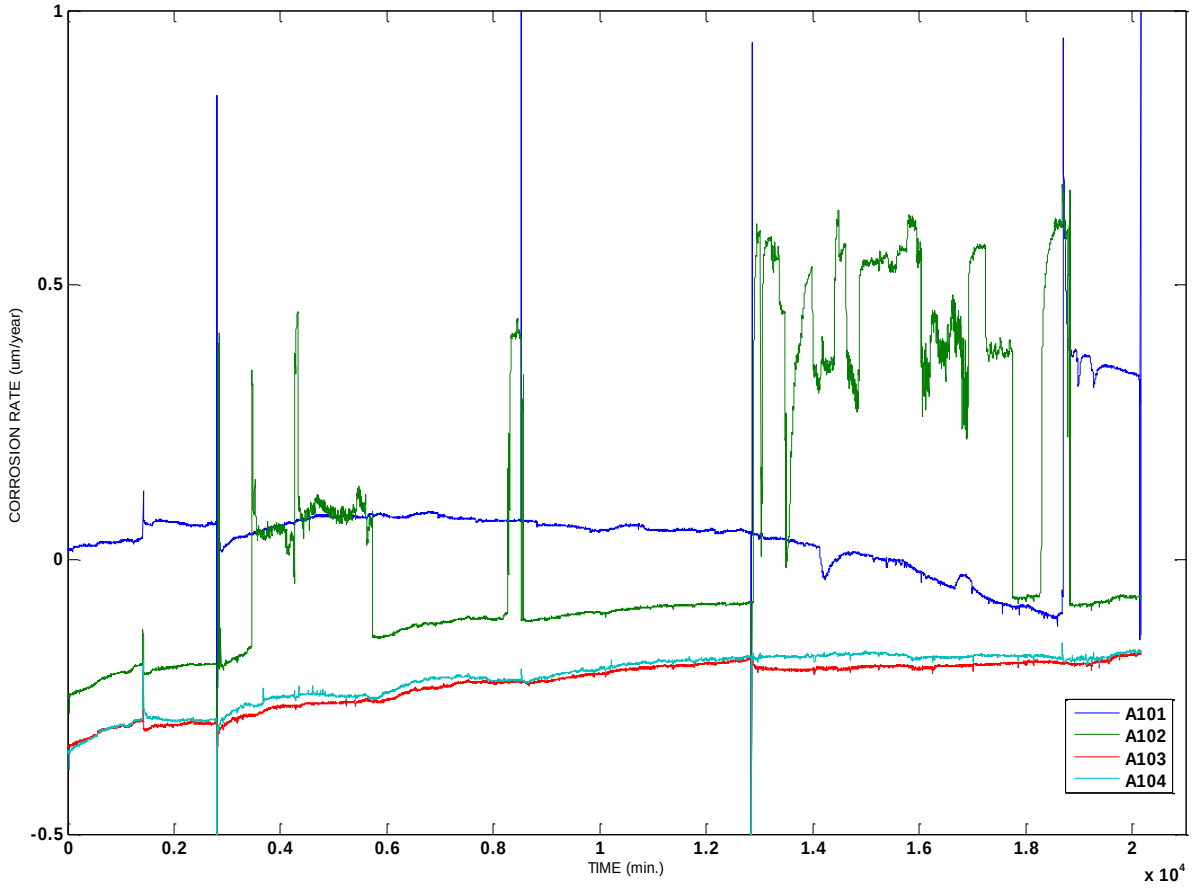

Figure 5.54: Average fluctuation of Corrosion rates for Specimen A101, A102, A103 and A104

Furthermore, it is important to point out potential errors that may accompany result interpretation as discussed for each of the test specimen. With the exception of specimen A101 where the corrosion rate increases, the decline values exhibited by other specimens, especially rapid decline in corrosion rate of specimen A103 and A104 in Figure 5.51 and 5.52 respectively, should not be taken as absolute, except it is ascertained that the anodic site (probe) where corrosion is expected to occur is fixed. Any swap in the anodic reaction between the probe and the rebars will invariably distort the result.

From the material design perspective, there are indications that the rebars in specimen A103 and A104 may be undergoing rapid corrosion process due to the 'high w/c' quality of concrete they were embedded in. With w/c ratio 0.83 and 13.67 MPa average compressive strength, it is logical to suspect some degree of corrosion penetration on the rebars. This is because high w/c ratio increases both

permeability and conductivity properties of concrete. In the event of such phenomenon, the corrosion potentials of the rebars may rise to measure up with that of corroding probe and the voltage drop across the resistor becomes inevitably low in respect of equation (19). Clear view of this can be seen in Figure 5.41, 5.42, 5.51 and 5.52. This possibly reveals the weakness of this method and somewhat makes it unsuitable in conditions where likely chances of corrosion are feasible on the probe and the rebars simultaneously.

Comparing the macro-cell test results to the corrosion potential test results, one can find a considerable degree of variance, but the results are complementary and more informing. The exaggerating outcome in the corrosion potential tests cannot be completely obviated in this type of experiment, as more time is required to monitor and justify the overall results obtained so far.

5.5.3 Linear Polarization Resistance Test

A measure of both micro-cell and macro-cell corrosion can be obtained with the linear polarization test, which uses a working electrode, a secondary electrode and a reference electrode to establish a polarization curve by imposing a range of potentials on the test (working) electrode and measuring the resulting current. In this experiment, the probe in each specimen served as the working electrode while one of the rebars in each sample was used as the secondary electrode. The procedure is as discussed in section 5.3. The test was carried out on the 30th day of the testing period and the results are given in Table 5.19 to 5.22 and Figure 5.55 to 5.58.

Table 5.19: Linear Polarization result for Specimen A101

Potential Shift V (V)	Observed Current I (µA)	Calculated Current Density Ic (µA/cm2)
-0.260	-1.9	-0.60
-0.280	-1.7	-0.54
-0.300	-1.5	-0.48
-0.320	-1.4	-0.45
-0.340	-1.3	-0.41
-0.360	-1.3	-0.41
-0.380	-1.3	-0.41
-0.400	-1.2	-0.38
-0.420	-1.1	-0.35

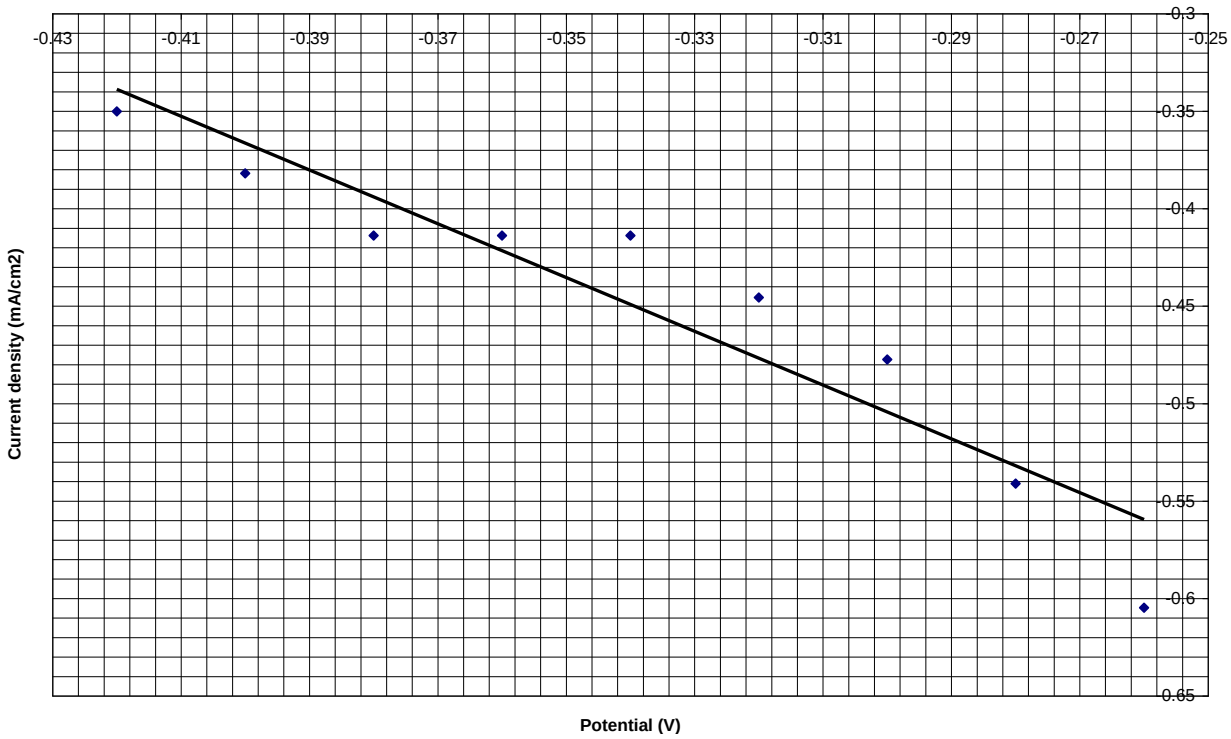

Figure 5.55: Linear Polarization curve for Specimen A101

Table 5.20: Linear Polarization result for Specimen A102

Potential Shift V (V)	Observed Current I (µA)	Calculated Current Density Ic (µA/cm2)
-0.392	-2.83	-0.90
-0.412	-2.85	-0.91
-0.432	-2.85	-0.91
-0.452	-2.88	-0.92
-0.472	-2.9	-0.92
-0.492	-2.9	-0.92
-0.512	-3	-0.95
-0.532	-3.1	-0.99
-0.552	-3.2	-1.02

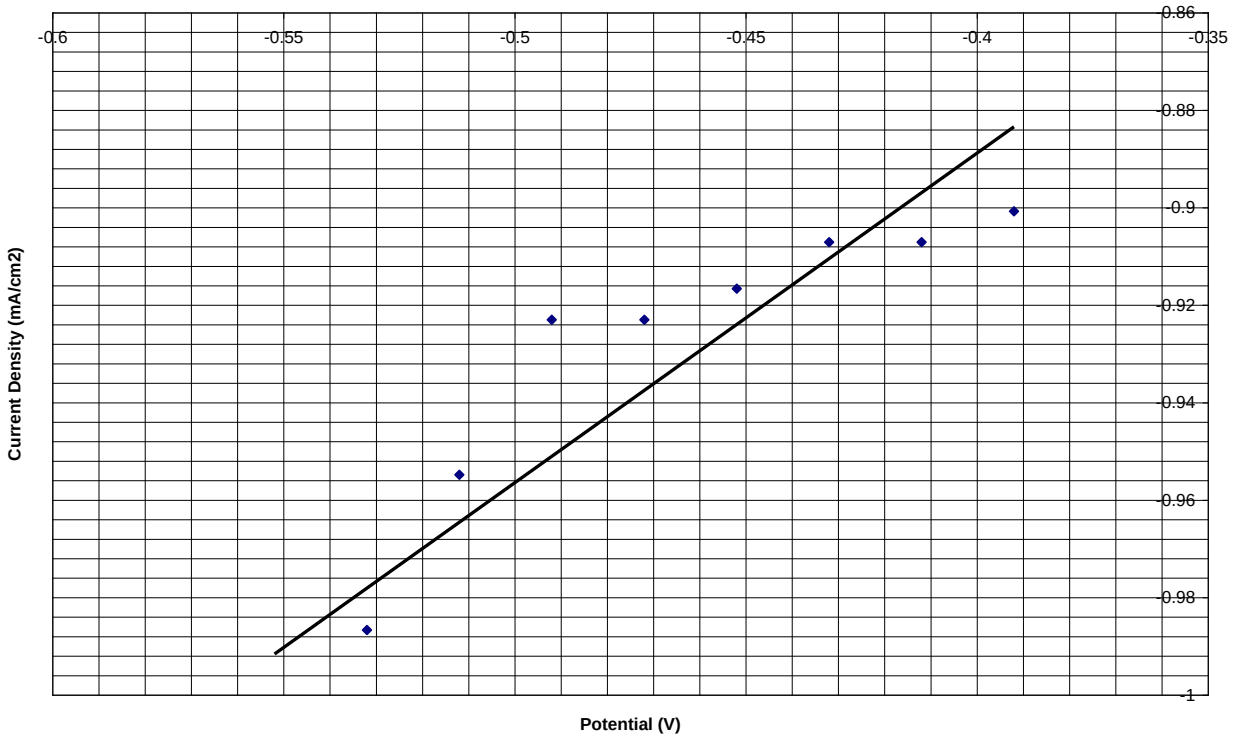

Figure 5.56: Linear Polarization curve for Specimen A102

Table 5.21: Linear Polarization result for Specimen A103

Potential Shift V (V)	Observed Current I (µA)	Calculated Current Density Ic (µA/cm2)
-0.551	-9.31	-2.96
-0.571	-9.32	-2.97
-0.591	-7.15	-2.28
-0.611	-7.1	-2.26
-0.631	-7.01	-2.23
-0.651	-6.96	-2.22
-0.671	-6.95	-2.21
-0.691	-6.9	-2.20
-0.711	-7.03	-2.24

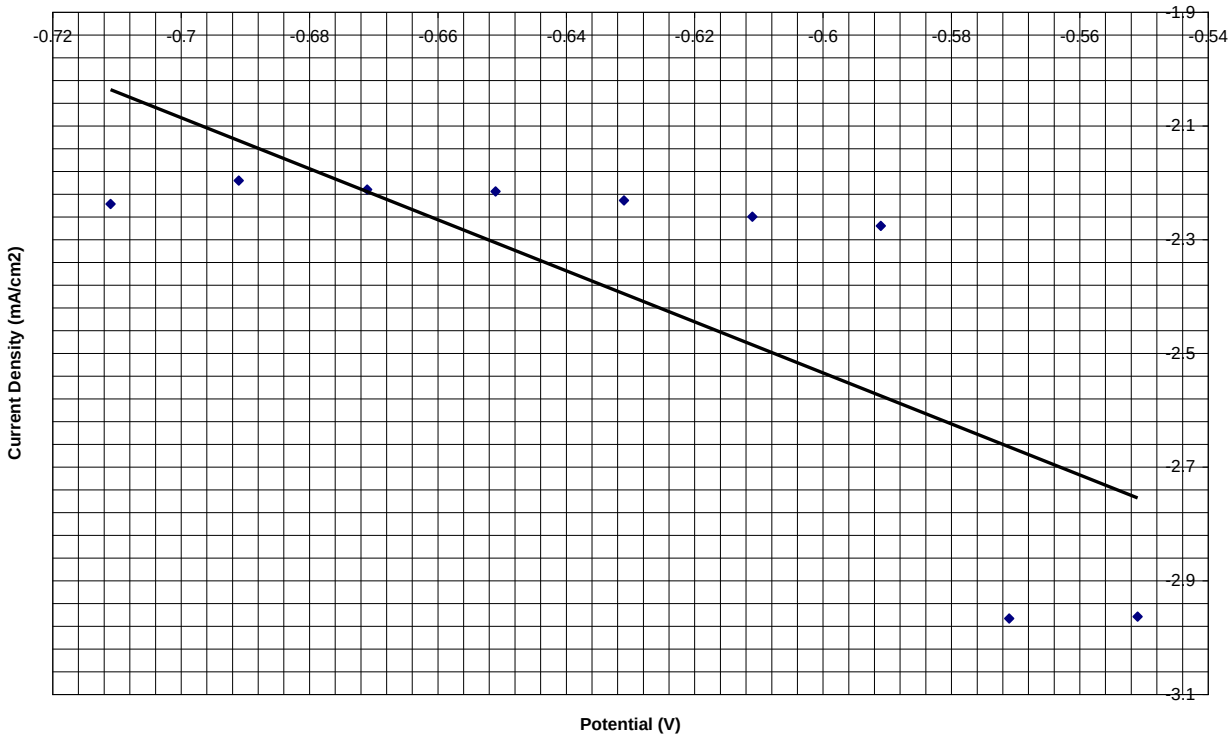

Figure 5.57: Linear Polarization curve for Specimen A103

Table 5.22: Linear Polarization result for Specimen A104

Potential Shift V (V)	Observed Current I (µA)	Calculated Current Density Ic (µA/cm2)
-0.355	-13.36	-4.25
-0.375	-13.29	-4.23
-0.395	-13.29	-4.23
-0.415	-13.3	-4.23
-0.435	-13.34	-4.25
-0.455	-13.55	-4.31
-0.475	-13.65	-4.34
-0.495	-13.68	-4.35
-0.515	-13.69	-4.36

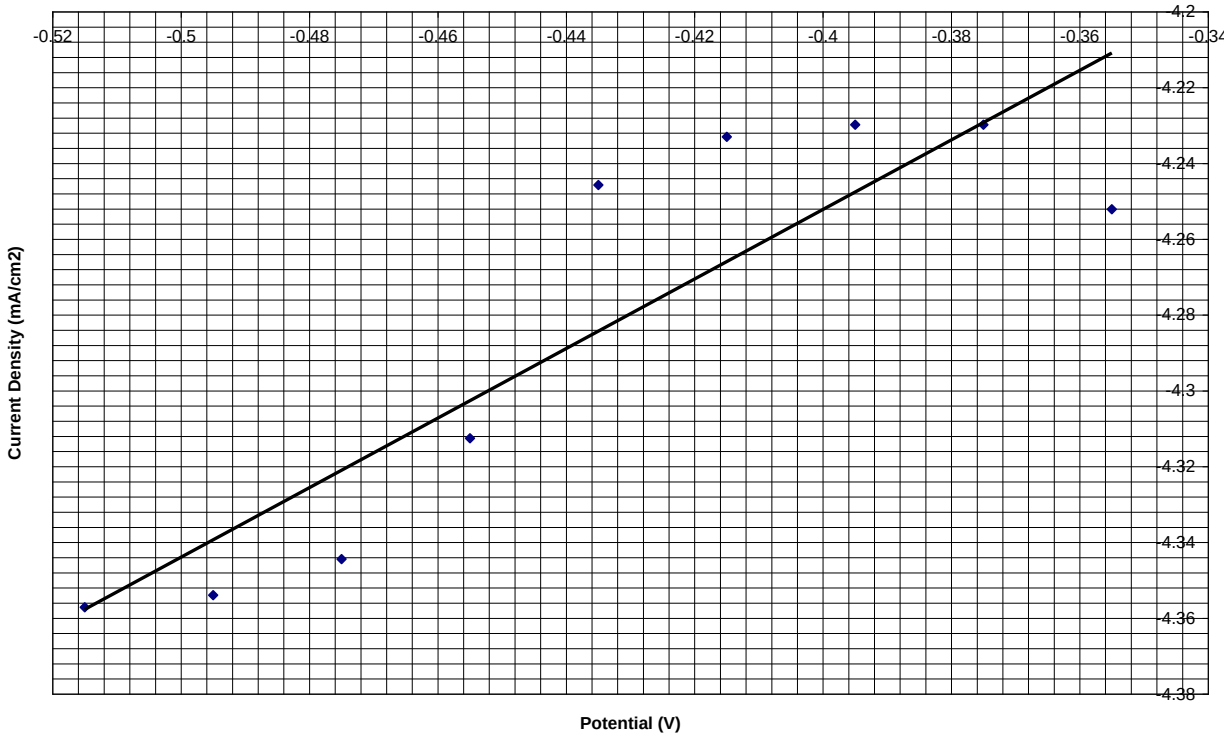

Figure 5.58: Linear Polarization curve for Specimen A104

From tables 5.19 to 5.22 and figures 5.55 to 5.58, representing LPR test results for specimen A101, A102, A103 and A104, the average slopes which correspond to the polarization resistance are as follows:

Specimen A101 = 0.82 Ω.cm^2

Specimen A102 = 4.00 Ω.cm^2

Specimen A103 = 1.25 Ω.cm^2

Specimen A104 = 1.25 $\Omega.cm^2$

These values can then be related to the corrosion rate using equation 5.15, where B ranges between 26 and 52mV. Table 5.23 gives the summary of their corresponding corrosion rates.

Table 5.23: Tabular representation of Corrosion Rate from Linear Polarization Test for Specimen A101, A102, A103 and A104

Specimen	Average Slope. R_p ($\Omega.cm^2$)	Constant. B (mV)	Corrosion rate. Ic ($\mu A/cm^2$)	Corrosion Rate R (µm / year)
A101	0.82	26	31.70	0.37
	0.82	52	63.40	0.74
A102	4.00	26	6.50	0.075
	4.00	52	13.00	0.15
A103	1.25	26	20.80	0.24
	1.25	52	41.60	0.48
A104	1.25	26	20.80	0.24
	1.25	52	41.60	0.48

From Table 5.19 and Figure 5.55, the approximate linear polarization resistance (**Rp**) due to potential shift in specimen A101 from -260mV to -420 mV and the eventual current decay is estimated to be 0.82 $\Omega.cm^2$. This apparently yields a corrosion penetration ranging between 0.37 and 0.74 µm/year which on the average falls within allowable passive corrosion rate. Also, the steady decline in the decay current as shown in Table 5.21, from -1.9 mA to -1.1 mA is somewhat indicative of no corrosion activity.

In specimen A102 where the decay current rises sharply between -2.83 mA to -3.20 mA with an average linear polarization resistance of 4.00 $\Omega.cm^2$ as illustrated in Figure 5.55, Table 5.22 and Table 5.23, the corresponding corrosion rate ranges between 0.075 to 0.15 µm/year. These values suggest that corrosion rate is low and within the permissible range of passivity.

The corrosion rates in specimen A103 and A104 are equal just as in the macro-cell results but range between 0.24 and 0.48 µm/year as seen in Table 5.21, 5.22 and 5.23. The corresponding linear polarization resistance for each is approximately 1.25$\Omega.cm^2$ as illustrated in Figure 5.57 and 5.58. The corrosion penetrations therefore are low and below active corrosion rate.

In order to have a reasonable comparison between LPR test results and macro-cell test result, Table 5.23 and Figure 5.54 are integrated to achieve this. In Table 5.24, values under the macro-cell corrosion rate correspond to the maximum and minimum values for each test specimen represented in Figure 5.54. Comparatively, it is obvious in Table 5.24 that corrosion rate values deduced from both LPR tests and macro-cell test are not exactly the same but do have approximate correlation. Also, it is evident in both results that corrosion activities are still very low and within permissible corrosion rate limits of steel passivity. Corrosion effects on specimen A103 and A104 are approximately equal as shown by both tests.

Table 5.24: Tabular comparison between LPR and Macro-cell Test results

Specimen	LPR Corrosion Rate R (μm / year)	Macro-cell Corrosion Rate R (μm / year)
A101	0.37	0.02
	0.74	0.1
A102	0.075	0.07
	0.15	0.24
A103	0.24	0.20
	0.48	0.36
A104	0.24	0.20
	0.48	0.36

CHAPTER 6: CONCLUSIONS AND RECOMMENDATIONS

6.1 ZRP Anode Material investigations - Conclusions

Based on the results of this investigation, both laboratory and field trial, and the interpretation and discussions of results the following conclusions are made:-

1. ZRP coating used had better adhesion properties to concrete substrate than those reported for the TS zinc coating, conductive overlay or the conductive (carbon based) paints. The adhesion values obtained for the ZRP ranged between 1.65 MPa and 3.5 MPa with and without applied CP current.
2. The bond strength results obtained from the environmental durability testing showed that the strength value increased between Zinc paint and concrete when the current was applied for 40 days 40 cycles). The results of this investigation showed greater bond strength results than thermal spray zinc under cyclic wetting and drying conditions.

3. The electrical 'cross-film' resistance of the ZRP coating was found to decrease exponentially to an optimum minimum resistance value with three coats (brush applied) producing approximately 200 - 250 µm dry film thickness (DFT).

4. The polarised potentials and the CP current of the reinforcements monitored during the 40-cycle environmental testing showed increased levels of polarisation on all cube samples and the results also showed that the 'potential shift' is higher for higher chloride content in concrete.

5. Accelerated environmental test results showed that ZRP coating was capable of withstanding / supporting high levels of current, more than 400mA/m^2 for a total of 40 cycles at 20 – 50 ^{0}C and 50 – 90% RH, without showing any evidence of coating deterioration or loss of bond strength. The current density used for the environmental durability test was nearly 180 times greater than the design current density normally specified and

operated CP systems using TS zinc anodes [Cf. 2.2mA/m^2 current density as per Oregon DOT specification].

6. The total charge pass in 40 cycles was calculated to a 427 A-h/m^2. In accordance with the NACE Standard TM0294 -2001, the total charge density of 38,500 A-h/m^2 of actual anode surface area equates to a serviceable anode life of 40 years if operated at a current density of 110 mA/m^2 of anode surface for 40 years. This represents a predicted anode life of approximately 20 years at normal operating current density of 10 mA/m^2 or some 100 years at a 2.2 mA/m^2, as recommended by the Oregon DOT Specification.

7. The results from the electrochemical tests showed that the higher the applied current density on anode the higher is the extent of polarisation, as expected. The higher the levels of polarisation, the higher the chloride content in the concrete. The cumulative charge (in kilo-coulombs/m^2) passed across the anode per unit area is calculated to be approximately 380kC/m^2. Again, the adhesion tests (pull-off tests using sellotape) at end of electrochemical testing showed no deterioration of the bond strength.

8. Electrochemical tests also showed that the 'current throwability' from the primary anode connection extends at least up to 600mm without significant current attenuation. This suggests that the ZRP coating is capable of distributing protection current uniformly.

9. The service life of the anode system could be determined from the accelerated test in accordance with the NACE Standard TM0294 -2001, total charge density of 38,500 A-h/m^2 of actual anode surface area equates to a serviceable anode life of 40 years if operated at a current density of 110 mA/m^2 of anode surface for 40 years (NACE Standard TM0294, 2000). The service life of the anode system determined from the accelerated test indicated that three coats (Dry Film Thickness of 250 µm) could be well in excess of 15 years at current density of 20 mA/m^2.

10. The service life of the ZRP coating (or TS zinc coating) would depend on the chemical/ electrochemical reactions at the zinc coating-concrete interface and the nature and extent of the reaction products (i.e. the ‘primary’ and ‘secondary’ minerals deposits due to dissolution of zinc as CP anode); which in turn affects the adhesion strength of the coating to concrete substrate.

11. Results of the field trial showed that the initial attempt to use ZRP anode material to provide Cathodic protection sacrificially hardly managed to polarise the steel reinforcement of the structure but by connecting to a simple 6V dry cell battery as an external power source the steel reinforcement was polarised significantly. The potential shift (potential difference between ‘on’ potentials and the ‘base’ potentials at embedded reference electrode locations ranged between 210 mV and 756 mV. After continuous operation with the Dry Cell Battery for a period of 15 days the battery was disconnected and the system was allowed to depolarise for a month (to replace the battery with a mains operated power supply unit). The measured depolarised potential after a month still retained significant levels of polarisation with potential shifts of 116mV - 453mV from the ‘base’ value. This suggests that the potential decay on this structure is very sluggish.

12. The results of the commissioning and performance of the installed ICCP system operating at 3.8 V, 1.5 A, and monitored for a period of 12 months strongly indicated that the ZRP anode system is feasible to provide and maintain adequate Cathodic protection.

13. The values of the open circuit potential of the ZRP measured at reference electrode locations suggest that the protection current would be uniformly distributed over the entire concrete surface under protection.

14. The ICCP installation utilising ZRP anode system for the field trial could be considered to be a success and proved that ZRP anode system is capable of protecting adequately and effectively.

15. Finally, annual visual inspections of the structure at showed no evidence of deterioration of the ZRP anode system.

6.2 Probe Development - Conclusions

A relatively simple, multifunctional and low-cost embeddable probe capable of measuring corrosion rate of steel in on-site concrete structures was successfully developed.

It is evident from the experimental tests conducted on the probe, results analysis and discussion that the probe is simple in material composition, easy to use, relatively cheap and capable of detecting direct corrosion current in reinforcing bars which can be related to corrosion rate as shown in this work.

It has also been proved that the applied method can be used for linear polarisation test which could serve as a control test or quick check method for verifying the performance of the probe. The probe can also measure corrosion potentials of embedded steel in concrete when integrated with standard reference electrode.

1. The corrosion potential tests indicated that the probe could be used to monitor not only the corrosion state of the steel reinforcement but could also be a useful device to track the direction of current (either 'galvanic' corrosion current or the applied CP current). In the case of tracking CP current the effectiveness of the CP installation could be assessed.

2. The corrosion rates, as shown by the macro-cell test results and the linear polarization test results, were generally low and within allowable range of steel passivity. Passive steel in concrete normally exhibits corrosion penetration between 0.1 to 1.0 µm/year. The macro-cell test results and the linear polarization test results are approximately the same. Considering the limitations and accuracy of the results obtainable from much more expensive and sophisticated commercially available LPR measurement devices and the R_p values calculated from the macrocell corrosion (galvanic

corrosion) measurements appeared to be an attractive low cost alternative procedure, using this probe.

3. This work has been demonstrated that the applied method is capable of detecting corrosion current which can be related directly to corrosion rate (and steel section loss) of steel in concrete, structural life expectancy and time of remedial action.

4. The accuracy of the probe was perceived to be affected under conditions where there are likely chances of corrosion possibility on the probe and the rebars simultaneously as shown by the declined trend of corrosion rates in specimen A103 and A104. In view of this, much longer period of testing is required.

6.3 Recommendations for future work

In consideration of the above discussion and conclusions of the present investigations further future works recommended is:

6.3.1 ZRP Anode Material

The scope of the present investigations, both the laboratory testing and the field trial, was restricted by time constraints, particularly the chemical and electrochemical properties characterisation would require longer term experiments. In view of this, it is recommended that the performance of ZRP should be undertaken. The specific areas of future works should include:

1. It is postulated the higher bond strength values (compared to TS zinc coating) is possibly due to physico-chemical bond rather than 'pure' mechanical bond. This should be verified by studying the ZRP/concrete interfacial chemistry, using techniques such as scanning electron microscopy including spectroscopy, petrography etc.

2. Longer term electrochemical testing under varying environmental condition to identify and quantify the functionality of the ZPR for sustaining installed CP and for better estimate of life expectancy of the ZRP.

6.3.2 'β-Probe'

The short time performance results obtained from the applied method may not satisfactorily justify its reliability, hence, it is recommended that further investigation be undertaken to verify long term performance of the method and the multifunctionality of the 'β-probe'. These are:

1. When undertaking longer term assessment of the applied method, other parameters like temperature variations, concrete internal moisture content variations and pH tests should be incorporated, since they have considerable influence on corrosion rate. Hence, a reliable mathematical model can be developed in order to advance the practicality of the method.

2. In addition, during the course of the present investigation two more equally important conceptual ideas were not possible i.e. (i) the use of the probe as a counter electrode for LPR measurement, incorporating the 'Betacrunch' program. This should be translated into some software program down-loadable to some hand held electronic device (s) such as 'smart phone'. It is also suggested the future works should include developing a inexpensive, portable (preferably hand held) low voltage power supply unit. This is to deliver variable but constant current (s) for LPR measurement on real-life structures.

3. Further work should be undertaken to test the functionality of the probe for 'E- log I' testing. This is to generate real-time data for estimating the current requirement of CP design.

REFERENCES

ACI Materials Journal, Mar/Apr 2009 by Darwin, David, Browning, JoAnn, O'Reilly, Matthew, Xing, Lihua, Ji, Jianxin, internet access, 22 Nov, 2010.

Andrade, C., Alonso, C., Gulikers, J., Polder, R., Cigna, R., Vennesland, O., Salta, M., Raharinaivo, A., Elsener, B., Material and Structures, 37, p. 623 – 624, 2004.

Apostolos, J.A., et. al (1984). Cathodic protection of reinforced concrete by using metallized coatings and conductive paints. Record no. 926.p.222-28. Transportation Research Record: Washington DC.

Arup, H., 'Steel in Concrete - Electrochemical corrosion', Newsletter No. 2, Kerrosioncentralen, Glostrup, Copenhagen, 1979.

Arup, H. (1983), The Mechanism of the Protection of Steel by Concrete. In: Alan P. ed. *Corrosion of Reinforcement in Concrete Construction*. Ellis Horwood Limited, 151 – 157.

ASTM C876-91, (1991), 'Standard Test Method for Half-Cell Potential of Reinforcing Steel in Concrete,' *ASTM International*, West Conshohocken, pp. 434 – 439.

ASTM G109-92, (1992), 'Test Method for Determining the Effects of Chemical Admixtures on the Corrosion of Embedded Steel Reinforcement in Concrete Exposed to Chloride Environments,' *ASTM International*, West Conshohocken, pp. 452 – 455.

Barovsky, N., Bozhinov, G., Sandor, P. and Simeonov, Y. (1983) Durability of Reinforced Concrete in Sea Water. In: Alan P. ed. *Corrosion of Reinforcement in Concrete Construction*. Ellis Horwood Limited, 19 – 38.

Bentur, A., Berke, N.S. and Diamond, S. (1997) *Steel corrosion in concrete*, 1st edn. E & FN SPON.

BRE Digest 434, Corrosion of reinforcement in concrete: electrochemical monitoring, BRE

(Building Research Establishment), Garston, Watford, U. K., November 1998.

Brousseau, R. et.al., Sprayed Titanium Coatings for the Cathodic Protection of Reinforced Concrete, Journal of Thermal Spray Technology, Vol. 7(2), June 1998.

Brousseau, R., Arnott,M., and Dallaire, S., The adhesion of metallized zinc coatings on concrete, Corrosion/93, No. 93331, NACE, Houston TX, 1993.

Brousseau, R., Arnott,M., and Baldock, B., Improving the Adhesion of Zinc Coating Used to Metallize concrete, Marer. Perform., Vol33 (No.1), 1994.

BS EN 12696:2000, Cathodic Protection of steel in concrete, BSI, London.

BS EN ISO 12696: 2012, Cathodic Protection of steel in concrete, BSI, London.

BS EN ISO 4624: (2003), Pull-off test for Adhesion, BSI, London.

Bullard, S. J., Covino, B. S. Jr., Holcomb, G.R., and McGill, G. E., Bond strength of thermally-sprayed

CIRIA (1993) ‘Technical Note 139, Standard test for repair materials and coatings for concrete, Part 1: Pull-off tests’. U.K, London: CIRIA.

Clear, K., Measuring Rate of Corrosion of steel in Field Concrete Structures, Paper No. 88-0324, 68th Annual Meeting of Transportation Research Meeting, 1989.

Concrete Society Technical Report No. 60 (2004), Electrochemical tests for reinforcement corrosion.

Corrosion monitoring http://www.corrosion-club.com [9 June 2008]

Corrosion Prevention Association, Monograph No. 12, Budget Cost and Anode Performance Information for Impressed Current Cathodic Protection of Reinforced Concrete Highway Bridges, 2008.

Corrosion Prevention Association, Monograph No. 11, Impressed Current Anodes for the Cathodic Protection of Atmospherically Exposed Reinforced Concrete, 2006.

Costa, J and Etcheverry, L (2005), Corrosion and corrosion Control, ICRJ’s Concrete Repair Bulletin, September/October 2005.

Covino, B. S. Jr,; Cramer, S. D.; Bullard, S. J.; Holcomb, G. R.; Russell, J. H.; and Collins, W. K.; ‘Performance of Zinc Anodes for Cathodic Protection of Reinforced Concrete Bridges, Final Report, SPR 364, Oregon Department of Transportation Research Group, FHWA, Washington D. C., March 2002.

Cramer, S. D., et al, Prevention of Chloride-induced Corrosion Damage to Bridges, ISIJ International, Vol. 42, (2002), No. 12, p. 1376 – 1385.

Das, S.C. (1984) Cathodic Protection Criteria for Steel in Concrete – Some Theoretical and Practical considerations. In: *International Conference on Corrosion and Protection of Steel in Concrete*, **2**, University of Sheffield, 1362 – 1374.

Das, S.C. (1988): An alternative Criterion for the Assessment of Cathodic Protection Systems for Steel in Concrete” by Sunil Das. Industrial Corrosion, September 1988.

Das, S.C. (2000) Inspection, Maintenance and Repair / Rehabilitation of Concrete Structures to ensure Durability. In: *Durability of Concrete Structures*, Technical Session 1, Aurangabad, India, 71 – 80.

Dubravka, B., Dunja, M. and Dalibor, S. *Non-destructive corrosion rate monitoring for reinforced concrete structures* http://www.ndt.net [5 July 2008].

ELCOMETER (2004) ‘Elcometer 106 Scale 6 Operating Instructions; coatings on concrete adhesion tester and concrete tensile tester’. Elcometer Ltd.

Elsener, B., Corrosion Rate of steel in concrete – Measurements beyond the Tafel law, Corrosion Science, Vol.47, p. 3019 -3033, 2005.

Elsener, B., Corrosion Rate of steel in concrete – from laboratory to reinforced concrete structures., in: Mietz, J, Elsener, B., Polder, R. (Ed.), Corrosion of Reinforcement in Concrete, EFC Publication No. 25, 1998, p. 92 – 103.

Elsener, B., Materials Science Forum 192 – 194, 1995.

Embedded corrosion instrument
http://www.vatechnologies.com/eciIndex.htm [15 May 2008].

Gjorv,O.E.,et al,'Electrical Resistivity of Concrete in the oceans',The 9th Annual Offshore Conference in Houston, May 2-5 1977, pp 585-588.

Greene, N. D and Gandhi, R. H, Betacrunch Version 1.0, Materials Performance, 21, 1982.

Greene, N. D and Gandhi, R. H, Betacrunch Version 2.0, Materials Performance, July 1987.

Hansson, C.M., Poursaee, A. and Jaffer, S.J. (2007) *Corrosion of reinforcement bars in concrete*, PCA R&D 3013. Portland Cement Association, Illinois.

Ha-Won, S. and Velu, S. (2007) Corrosion Monitoring of Reinforced Concrete Structures – A Review. *International Journal of Electrochemical Science,* **2**, 1-28.

Holcomb, G. R., Covino, B. S. Jr., Cramer, S. D., Russell, J. H., Bullard, S. J., Collins, W. K.; Humectants to Augment Current from Metallised Zinc Cathodic Protection Systems on Concrete, Final Report, SPR 384, Origon Department of Transportation Research Group, FHWA, December 2002.

House of Culture *Collapse of Berlin Congress Hall*
http://www.hkw.de/en/hkw/gebauede/architektur/index.php [23 June 2008].

Hyoung, S.S. and Stephen, G.M. (2007) On-Site Measurements on Corrosion Rate of Steel in Reinforced Concrete. *Journal of the American Concrete Institute*, **104**(6), 638 – 642.

Invention of Battery http://d-training.aots.or.jp/ioe/ioe2-1.html [24 July 2008]

ISIS Canada Research Network, *Civionics*
http://www.isiscanada.com/innovations/civionics [27 July 2008]

Jaggi et.al (2001), Macrocell Corrosion of steel in concrete – Experiments and Numerical Modelling, Eurcorr 2001, Italy.

Knudson, A.A. (1907) Electrolytic corrosion of iron and steel in concrete. In: *214th Meeting of the American Institute of Electrical Engineers*, New York, 231 – 245.

Legoux J.G. Dallaire, S (1995), 'Adhesion Mechanisms of Arc-Sprayed Zinc on Concrete, Journal of Thermal Spray technology, vol. 4(4) 1995 -395. (JTTEE5 4:395-400).

McGill, G. E., Cramer, S.D., Covino, B. S.. Jr.,Bullard, S. J., Holcomb, G. R., Collins, W. K., Gover, R. D., and Wilson, R.D., Field application of an arc-sprayed titanium anode for cathodic protection of reinforcing steel in concrete –final report. SPR 365, FHWA-OR-RD-99-13, Washington , DC: Oregon Department of Transportation and Federal Highway Administration, 1999.

Mansfeld, M and Oldham, K. B, A modification of the Stern-Geary linear polarisation equation, Corrosion Science, Vol. 11, p. 787, 1971.

Mansfeld, F, The Polarisation Resistance Technique for Measuring Corrosion Currents, Advances in Corrosion Engineering and Technology (F0ntana, M. G. and Staehle, H, ed), 6, ch.3, Plenum Press, 1976.

NACE Standard TM0294: Testing of Embeddable Impressed Current Anodes for Use in Cathodic Protection of Atmospherically Exposed Steel-Reinforced Concrete, NACE international, Houston, Texas, 2001.

Manning, D. G., Escalante, E., and Whiting, D., 'Panel Report – Galvanisd Rebar as a Long-term Protective System, Washington, D. C., 1982.

Peter, P. (2002) *Concrete Reinforcement Corrosion: From Assessment to Repair Decision*. The Institute of Civil Engineers, Design and Practice Guides, 1st edn. Thomas Telford.

Pierre, R. R. *Corrosion Theory* htt:***//***www.corrosion-doctors.org [7 May 2008].

Pourbaix, Marcel (1973), Lectures on Electrochemical Corrosion, Plenum Press, 1973.

Pourbaix, Marcel, et.al (1966), Atlas of Electrochemical Equilibria in Aqueous Solutions, Pargainon Press, 1966.

Protection of Reinforced Concrete Bridges, Final report, SPR 364.

Raupach, M., Chloride induced macrocell corrosion of steel in concrete – theoretical background and practical consequences, Construction and Building Materials, 10, p. 237, 1996.

Raupach, M.,and Gulikers,J., Investigation on Cathodic control of Chloride Induced reinforcement corrosion in Concrete – corrosion Mechanism and Protection, EFC Publication No. 31. Ed Mietz, J., Polder, R., and Elsner, B.,IMO Communications, London,2000.

Rob, L. and Wynne, E. (2006) *Chemistry*,3rd edn. Palgrave Macmillan.

Rosa, E.B., Burton, M. and Peter, O.S. (1912) Electrolysis of Concrete. *Engineering News*, **68**(25), 1162 – 1166.

Schell, H. C., and Manning, D. G., Evaluating the performance of cathodic protection systems on reinforced concrete bridge substructures, Material Performance, July 1985.

Schiessl, P. (1988) *Corrosion of steel in concrete*, Report of the Technical Committee 60-CSC. RILEM, the International Union of Testing and Research Laboratories for Material and Structures.

Schmitt, Gunter, Global Needs for knowledge, Dissemination, Research, and Development in Materials Deterioration and Corrosion Control, World Corrosion Organisation, White Paper, (2009).

Scully, J. R, Polarisation Resistance method for Determination of Instantaneous Corrosion Rates, Corrosion, Vol.56, p.199 (2000).

Slater, J.E. (1983) *Corrosion of metals in association with concrete*, ASTM Special Technical Publication 818. American Society for Testing and Materials.

Stern, M.S. and Geary, A.J. (1957) Electrochemical Polarization I: A Theoretical Analysis of the Slope of Polarization Curve. *Journal of Electrochemical Society*, **104**(1) 56 – 63.

Trethewey, K.R. and Chamberlain, J. (1995) *Corrosion for Science and Engineering*, 2nd Edn. Longman (UK).

Tullmin, M. *The Corrosion Journal for the Online Community* http://www.corrosionsource.com [13 July 2008].

Tuutti, K., Corrosion of Steel in Concrete, Swedish Cement and Concrete Research Institute, Stockholm, 1982.

Uhlig, H., Corrosion and Corrosion control: An Introduction to Corrosion Science and Engineering, Pub. John Wiley & Sons (1963).

Van Daveer, J. R., 'Techniques for evaluating reinforced concrete bridge decks', Journal of the American Concrete Institute, December 1975, pp 697-704.

Vassie, P.R.W. (1978) *The Corrosion of Steel in Environments simulating the liquid phase of concrete*, TRRL Supplementary Report 396. Transport and Road Research Laboratory, Crowthorne, Berkshire.

Vrable, J. B., Cathodic protection ofreinforcedconcrete bridge decks. NCHRP Report 180, Washington, DC: Transportation Research Board. 1977.

Wagner, Carl, Contribution to the Theory of Cathodic Protection, Journal of the Electrochemical Society, January 1952.

Wagner, Carl, Contribution to the Theory of Cathodic Protection, Journal of the Electrochemical Society, October 1957.

Wagner, C and Traud, W, On the Interpretation of Corrosion Processes Through Superposition of Electrochemical Partial Processes and on the Potential of Mixed Electrodes, Z. Electrochem.Ang. Physik. Chemie, Vol.44,p. 391, 1938 –translation by Mansfeld, F, Corrosion, Vol.62, p. 843, 2006.

Wood and Neikirk (2008) Development of Wireless Sensors to Monitor Corrosion in Civil Infrastructure Systems http://www.weewave.mer.utexas.edu [1 May 2008].

World Corrosion Organisation (WCO),

Young, W. T., Clem Firlotte, P. E., Funahashi, P. E., Evaluation of Al-Zn-In Alloy for Galvanic cathodic protection of Bridge Decks, Final Report for Highway IDEA Project 100, Transportation Research Board of the National Academics, Washington DC, August 2009.

Zhang, X. G., Corrosion and Electrochemistry of zinc, Plenum press, New York, NY, 1996.

PUBLICATIONS

1) "Cathodic Protection - A Long Term Solution to Chloride Induced Corrosion?" by: R. McAnoy, J.P. Broomfield & S.C. Das: Conference Proceedings, Structural Faults and Repair 1985, London, 1985.

2) "An alternative Criterion for the Assessment of Cathodic Protection Systems for Steel in Concrete" by Sunil Das. Industrial Corrosion, September 1988.

3) "A Novel Approach to Stop Reinforcement Corrosion of Sub-terranean Structures by Cathodic Protection" by S C Das, Conference Proceedings, Structural Faults and Repair, University of Edinburgh, 1993.

4) "Monitoring is the Key", S C Das, Highways, June 1993.

5) "Cathodic Protection of R.C. Structures" by S C Das, The Structural Engineer, Vol. 71, No 22, November 1993.

6) "Cathodic Protection Criteria for Steel in Concrete - Some Theoretical and Practical Considerations" by S C Das, International Conference on Corrosion and Protection of Steel in Concrete, University of Sheffield, 24-29 July 1994

7) "Downhole Potential Calculator" by S.C. Das, UK Corrosion and Eurocorr`94,31 October - 3 November 1994, Bournemouth, UK. Conference Proceedings, Vol 4, pp 213 - 221.

8) "Inspection and NDT testing of Concrete Structures: Pre-requisites for Rehabilitation Strategies" by S C Das, International Seminar on Failures, Rehabilitation and Retrofitting of Bridges and Aqueducts, 17 - 19 November 1994, Bombay, India.

9) "Computer Aided Quantitative Interpretation of Electropotential Survey Results for RC Structures" by S.C.Das and I. McMahon, Structural Faults and Repairs -'95, 3-5 July 1995, London.

10) "Inspection, Maintenance And Rehabilitation of Concrete Structures by S.C.Das, ING-IABSE Seminar on 'Durablity of Structures', 4-5 February 2000, Aurangabad, India.

11) Cathodic protection in marine environments, by Dr S. El-Belbol and S. C. Das, Concrete Engineering, summer, 2001.

12) Cathodic Protection for Reinforced Concrete Structures – a Proven Technique to Stop Corrosion by Ali Sharifi and Sunil Das, Asia Bridge Summit, Shanghai, China, March 2008.

13) Corrosion mitigation of chloride contaminated reinforced concrete structures: a state-of-the-art review, Das, Pouya and Ganjian, Proceedings of the Institution of Civil Engineers, Construction Materials 164 February 2011, issue CM1, Pages 21-28

14) Zinc Rich Paint as Anode for cathodic protection of Steel in Concrete, Das, Pouya and Ganjian, ACI (American Concrete Institute) Structural and materials Journal, Manuscript Submitted for publication, March 2012.

15) Innovative Cathodic protection of Steel in Concrete using Zinc Rich Paint as Anode system - Field Trial, S.C. Das, H. S. Pouya and E. Ganjian, Structural faults and Repair – 2012 Conference, Edinburgh, 3-5 July 2012. To be Presented.

16) Cathodic Protection to Half Joints of Reinforced Concrete Structures – Case Study, S.C. Das, A. Sharifi and G. Jewell, Structural Faults and Repair – 2012 Conference, Edinburgh, 3 -5 July 2012. To be Presented.

17) Designing a low Carbon Foot-print Anode System for Cathodic protection of R. C. Concrete Structures, S.C. Das, H. S. Pouya and E. Ganjian, Concrete Magazine, Concrete Socity, Paper submitted for publication, April 2012.

18) Recent Advances and Development of Anode Systems for Cathodic Protection of Steel Reinforcement in Concrete Structures, S.C. Das, 16th National Congress on Corrosion Control, 23-25 August 2012, Kolkata, India. To be presented.

APPENDICES

APPENDIX A: ADHISION TEST

A1 Concrete Mix Design, Compaction & Curing Processes

The concrete mix design, curing and compaction processes to the concrete slabs and cubes for two types of intended concretes: 'low w/c' (low water/cement ratio of 0.50) and 'high w/c' (high water/cement ratio of 0.80) is summarised in Table A1. Some cube specimens will be cast in different 150mm^3 moulds (plastic or metal) and vibrated at different accelerations: low vibration (4-7g) or shock table mode vibration (≈ 8g). However, all slabs will be compacted at a lower vibration (not shock table mode) to prevent damage and movements of internal elements including the timber formwork, refer to Section 3.4.3 for more details.

Table A1: mix design, compaction and curing process to concrete cubes and slabs

Component		Concrete Mix Design	
		Good 'G'	'high w/c' 'P'
Water/Cement Ratio		0.50	0.80
Ordinary Portland Cement (kg/m^3)		300	200
Water (kg/m^3)		150	160
Uncrushed Coarse Aggregate (kg/m^3) (4.75-10mm size)		1300	1175
Fine Aggregate (kg/m^3) (Sand) ≈ 65% passing 600µm sieve		670	867
Slump Test (mm)		≈ 10	≈ 20
Amount of compaction (vibrating table) (m/s^2)	shock table mode of vibration (≈ 8g)	Cubes: G1 to G5	Cubes: P1 to P5
	lower vibration (4-7g)	Slabs: G1 & G2 Cubes: G6 & G7	Slab: P3
Curing Process (2 days after demoulding specimens)		Fully immersed in curing tank for 28 days then allowed to dry in air prior to zinc coating	

A comprehensive step by step process adopted throughout the experimental stages is given below.

A2 Conditioning of Substrate

After 28 days underwater curing, all concrete cubes will be allowed to age (dry in air) for at least a month prior to coating and pull-off tested. This is because, as suggested by CIRIA (1993), repairs/coatings are unlikely to be applied before the concrete has reached 28 days and concrete is generally mature at the time of coating application or repair. Therefore, CIRIA (1993) recommends substrates should be at least 28 days old prior to the application of coatings.

A3 Surface Preparation

With regards to point 1 above (Section 3.3.1) Table A2 shows the tools and engineering judgment which will be required to obtain different levels of concrete substrate roughness. The information contained in Table 3.2 was determined through initial trial experimentation and after reviewing literature. The roughness terminology adopted, as shown in Table A2 and throughout this report will be as follows:

VHR = Very High Concrete Roughness (using machined operated needle gun)
HR = High Concrete Roughness (using machined operated needle gun)
MR = Medium Concrete Roughness (using hand operated wire brush)

Table A2: Summary illustrating the methodology and engineering judgment used to obtain different levels of concrete substrate roughness through trial experimentation

Substrate Roughness Degree (Terminology)	Tool Utilised	Manual/ Automatic	Degree of Aggregates Exposed
Very High Roughness (VHR)	Needle Gun (compressed air)	Automatic	Most Aggregates Exposed
High Roughness (HR)	Needle Gun (compressed air)	Automatic	Some Aggregates Exposed
Medium Roughness (MR)	Wire Brush	Manual	Little/None Aggregates Exposed

Prior to coating, and just after the cube is given a prescribed substrate roughness, (i) excess dust present on the surface will be removed by using an air compressor unit, (ii) temporary tape will be used to seal the upper outer sides and corners to each cube to help prevent Zinga paint spilling over, (iii) the mass of the cube will be measured as a reference point and then (iv) the temperature of the substrate,

as well as the temperature and relative humidity of the surrounding environment, will be checked using a thermometer and hydrometer respectively.

A4 Application of ZRP Coating

Each prepared substrate will receive a total of 4 or 3 Zinga coats to achieve a total theoretical dry film thickness (DFT) between approximately 200-350µm. The waiting times between each applied coat will be in accordance with the manufacturers instructions, however, as a means check the coating will be touched to see if dry and prior to recoating the mass of the cube will be measured. Immediately after applying Zinga, the wet film mass will be measured per coat and then accumulated in order to determine the combined wet film thickness to each coated surface which then will be converted into the composite DFT using Equation A1 from CONCRETE SOCIETY (1997). After applying the final coat of Zinga the cubes will be allowed to dry overnight and then the procedure for pull-off testing will commence the very next day for short term tests. However, for medium term tests (56 day coated & pull-off tested) this will be delayed until the coated surface has aged up till 56 days from the time it was first coated.

$$\text{Coverage } (\text{m}^2/\text{kg}) = \frac{10 \text{ x } \% \text{ solids content by volume}}{\text{dry film thickness in } \mu\text{m} \times \text{relative density (wet)}} \qquad (A1)$$

Where for Zinga: the solids content by volume is 58%, the relative wet density is 2.67 kg/dm^3 as shown in Table 2.1 and the cube coverage area per surface is 150mm^2.

A5 Pull-Off Test Procedure

Elcometer Apparatus:

Elcometer 106/6 Adhesion Tester including a base support ring and a ratchet spanner

5 No. of 50.8mm (2”) diameter high-tensile aluminium dollies, length of dolly is 30mm which is not less than half of dolly diameter (25.4mm) hence satisfies BSI 4624 (2003) recommendation. See Figure A1.
Adhesives: Araldite (precision) slow setting, two pack epoxy resin

Figure A1: placement of adhesion tester upon concrete test cube with attached dolly

Ensure dolly and test areas are clean, free of oil, moisture, dust and roughened with abrasive paper and then degreased with a suitable solvent prior to the application of adhesive. Use a minimum amount of adhesive, both hardener and resin mixed together with approximately equal volumes to produce an even coated film over entire dolly surface area and use within one hour after mixing. Push dolly firmly against substrate in order to squeeze out excess adhesive which should then be immediately removed with paper towel.
CIRIA (1993) states do not allow a direct bond between the dolly and substrate to occur as a result of excessive use of adhesive. Allow adhesive to cure for 24 hours at 25°C. Note according to ELCOMETER (2004) lower temperatures can require extended curing times up to 3 days or more.

Immediately after adhesive has cured, inspect and ensure dolly is aligned in a perfectly vertical plane to allow for a uniform pressure distribution i.e. pure tensile

load avoiding any bending moments. The author decided not to score the coating since according to COVINO, et al (2002) pre-scoring of the zinc coating around the dolly did not improve reproducibility of pull-off measurements and was not carried out in future tests.

Position base support ring over dolly and ensure it lies flat on substrate. Slacken the nut of the adhesion tester device, set the dragging indicator to zero and carefully engage claw with dolly. Hold device in position with one hand, to ensure no rotation and/or bending of device exists, whilst tightening the nut using a ratchet spanner with the other hand, at a uniform and even rate i.e. (rate of stress not greater than 1MPa per second but time to failure within 90 seconds). BSI 4624 (2003)

Record the failure stress from engraved scale and then immediately slacken the nut by reversing the ratchet spanner to remove all the force from the unit. Record the failure type and then estimate the area of fracture as a percentage. An example is given in standard BSI 4624 (2003).

Note: according to ELCOMETER (2004) for valid test results the coating will be observed to fully adhere to dolly. However, when coating is partly covered by the dolly this can be considered as a partial adhesion failure but if no coating is seen on the dolly, then this is declared as a failure with respect to the adhesive. This may be as a result of incorrect/insufficient mixing, incompatibility with coating, strength etc. ELCOMETER (2004).

A6 ADHESION TESTS – Analysis of Results

A6.1 Concrete Surface Preparation

Figure A2 shows an observational comparison of the varying degrees of surface preparation to ‘low w/c’ and ‘high w/c’ concrete substrates as shown diagrammatically on the left and right respectively.

A6.2 Observational Comparison: Degree of Aggregate Exposure & Undulations

All concrete substrates prepared to a Very High Roughness (VHR) degree, such as those shown in Figures A2(a) and A2(b), showed a greater amount of exposed aggregates as well as high undulations compared to other surface preparations like High (HR) and Medium (MR) Roughness. Since a High Roughness (HR) profile was obtained.

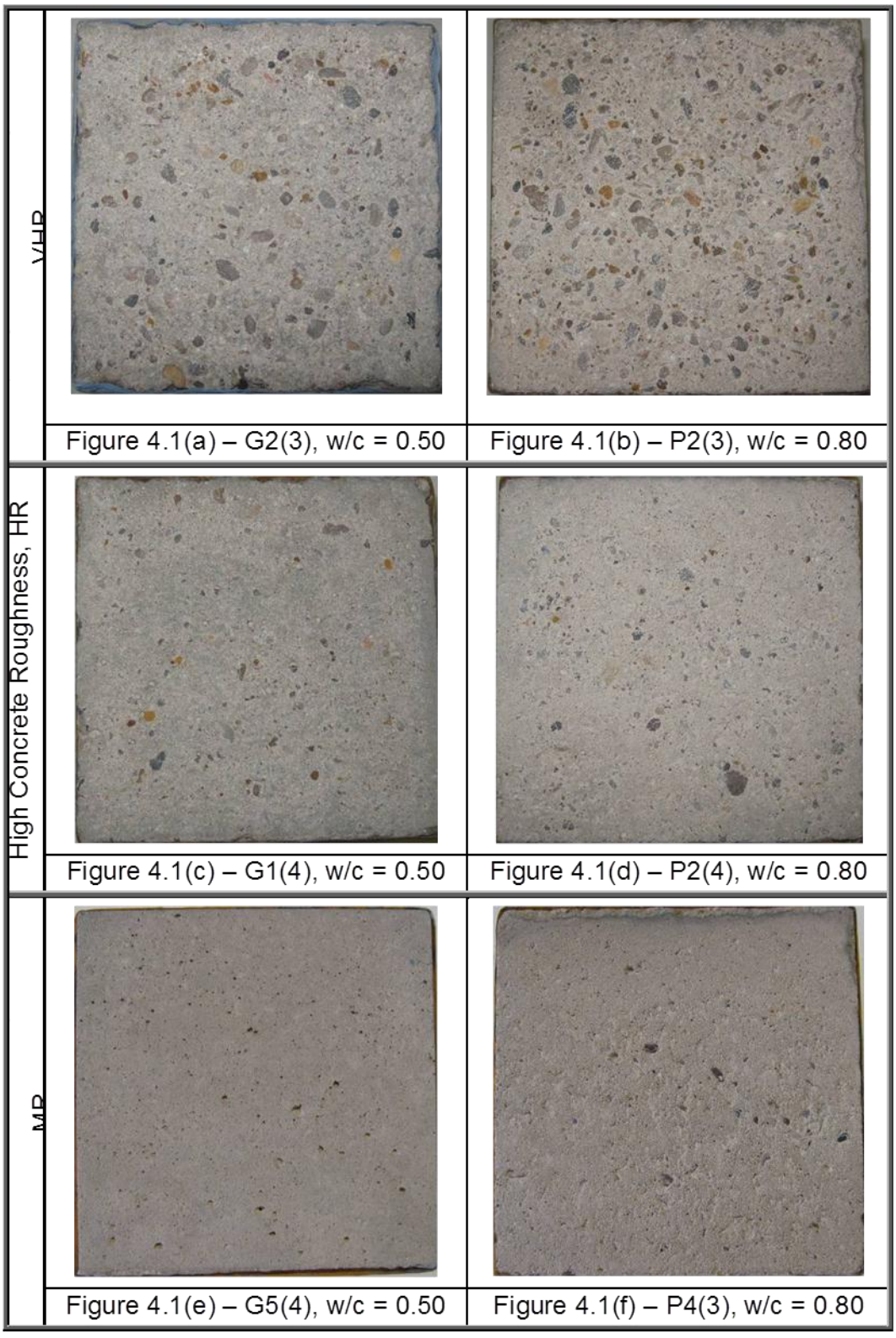

Figure A2: observational comparison of different surface preparation to 'low w/c' concrete (left) and 'high w/c' concrete (right)

It can be seen from Figures A2(c) and A2(d) that this substrate roughness achieves an immediate level between VHR and MR profiles in terms of aggregate exposure where Figures A2(e) and A2(f) for MR profiles exposes a smaller amount of aggregates. With regards to undulations in the surface profile for HR substrates it was hard to quantify by eye exactly which profile i.e. VHR or HR gave a higher undulating (peak to trough) surface. But from the observational experience gathered by the author the undulations were somewhat similar for both VHR and HR profiles with either profile being capable of having a greater amount of undulations. The peak to trough profile, i.e. the amplitude height, for MR profiles were observed to be lesser than for VHR or HR profiles mainly because of the use of a manual operated wire brush tool which essential scrapes the surface and removes the laitance layer. A manual operated wire brush or even a mechanical one does not produce a similar vertical impact like that of a needle gun operated by compressed air. The use of a wire brush in preparing a concrete surface is believed to be similar to a medium sand paper type texture using a sand blasting technique. However, sand blasting like needle gunning relies upon impact to yield concrete roughness. As can be seen in Figures A2(e) and A2(f) the concrete substrates show a minimum amount of exposed aggregates as opposed to VHR and HR profiles.

A7 Coating & Pull-Off Testing Time Schedule to Concrete Cubes

Table A3 shows the dates when cubes were cast, the number of days within the curing tank and the amount of accumulated days (from since cube/slab was cast) to the point of being zinc coated and pull-off tested respectively.

Table A3: Coating & pull-off testing time schedule to concrete cubes since cast

Specimen	Date cast	No. of days in curing tank	Immediately coated & pull-off tested cubes (days since cast)	56 day coated & pull-off tested cubes (days since cast)
G1 to G3	06/03/10	28	106 – 113	162 - 169
G4 to G7	25/02/10	28	118 – 125	184 - 191
P1 to P3	13/03/10	28	106 – 113	162 - 169
P4 to P5	26/02/10	28	118 – 125	184 - 191

A8 Immediately Coated & Pull-Off Tested Substrates

Continuing on from Figure A2, Figures A3 and A4 go on to show the observed pull-off failure comparisons to different surface preparations (as discussed above) to 'low w/c' and 'high w/c' concretes looking at the substrate end as well as looking at the dolly end respectively.

A8.1 Terminology Adopted to Observed Pull-Off Failure Types

The terminology adopted to observed pull-off failure types during experimentation is shown below and is very much similar to criteria given in BSI 4624 (2003).

A = failure occurring within concrete substrate

A/B = failure between concrete substrate and coating

B/C = inter-coat failure

-/Y = failure between adhesive and coating

A8.2 Observational & Numerical Comparison: Pull-Off Test Results

Pull-off results given in Table A4 as well as graphically illustrated in Figure A5 show, on average, a medium surface roughness (MR) yields a greater bond between the coating and the substrate compared to VHR and HR results for both 'low w/c' and 'high w/c' concrete mix designs. This is because of the minimal or, in some cases, the null amount of aggregates exposed in the immediate dolly testing position. As discussed in Section 3.3 the amount of aggregates exposed has a direct influence upon the pull-off strength since the bond interface between the

coating and the exposed aggregate(s) is weakened due to the inherent smooth surface of the aggregate(s) used in this experiment.

As observed in Figures 4.3(e) and 4.3(f) the amount of concrete depth seen on the dolly end of the failure was greater for MR substrate types than it was for VHR or HR substrate types again as a result of the amount of aggregates being exposed which has an influence on the coatings ability to adhere/anchor itself to suitable locations. Where Zinga was able to find suitable anchor positions pull-off strengths were enhanced and failures showed, as a result, a greater depth of concrete on the dolly end.

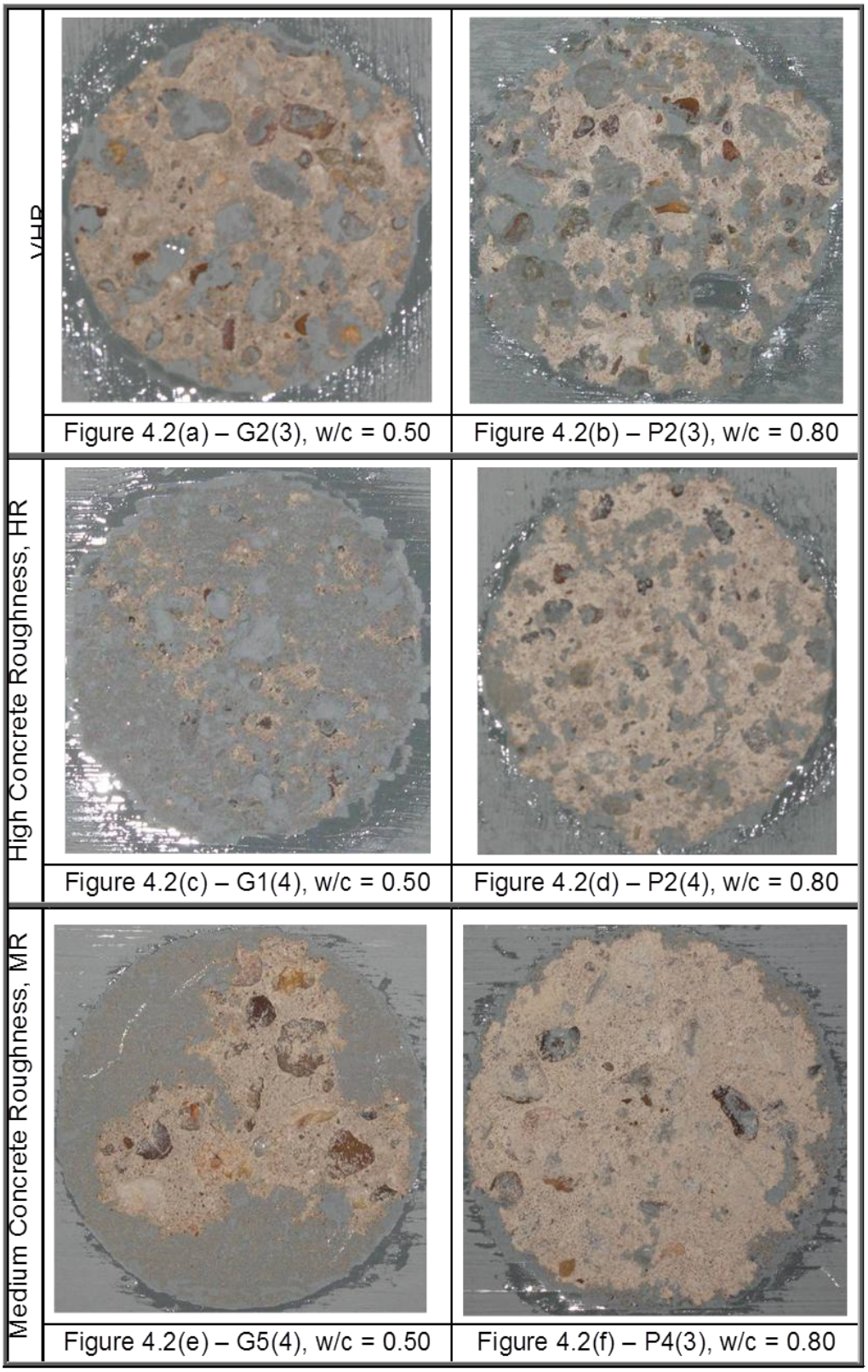

Figure A3: observational pull-off failure comparisons of different surface preparation to 'low w/c' concrete (left) and 'high w/c' concrete (right) looking at substrate end.

VHR		
	Figure 4.3(a) – G2(3), w/c = 0.50	Figure 4.3(b) – P2(3), w/c = 0.80
High Concrete Roughness, HR		
	Figure 4.3(c) – G1(4), w/c = 0.50	Figure 4.3(d) – P2(4), w/c = 0.80
Medium Concrete Roughness, MR		
	Figure 4.3(e) – G5(4), w/c = 0.50	Figure 4.3(f) – P4(3), w/c = 0.80

Figure A4: Observational pull-off failure comparisons of different surface preparation to 'low w/c' concrete (left) and 'high w/c' concrete (right) looking at dolly end.

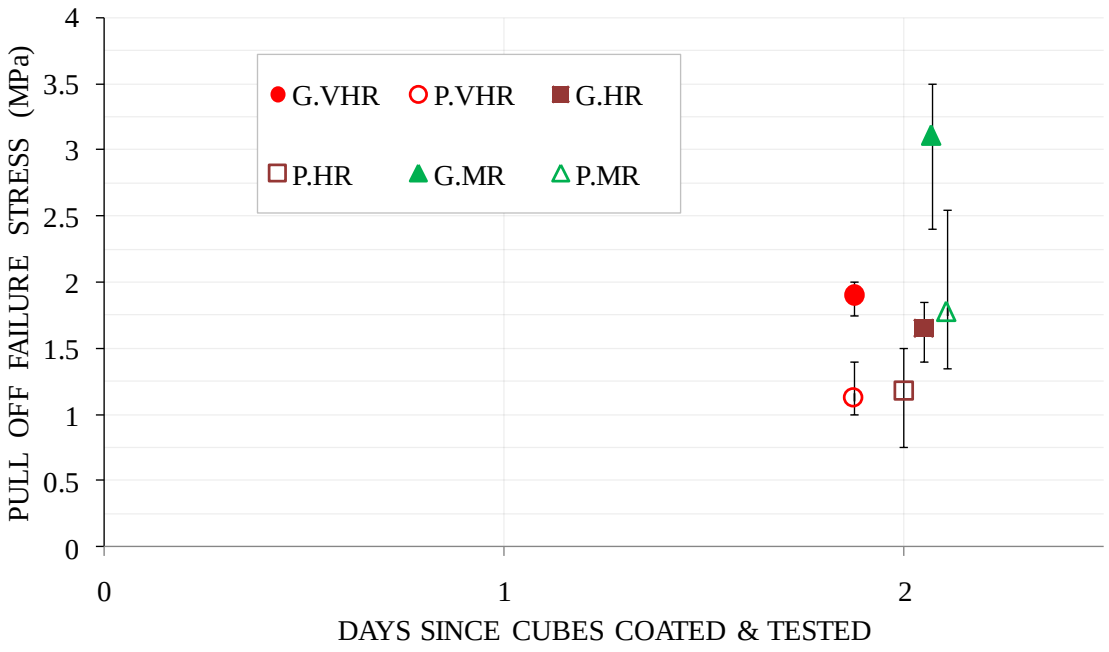

Figure A5: Comparison between variable types of substrate roughness when immediately coated and pull-off tested

Note: for each roughness profile shown in Figure A5 the data point illustrates the average pull-off stress and the corresponding highs and lows (precisely known as error bars) are the upper and lower range in pull-off values observed respectively. Where G & P = 'low w/c' and 'high w/c' concretes respectively. VHR & HR & MR = very high and high and medium roughnesses respectively.

A8.3 Observational & Numerical Comparison: Variations in Pull-Off Failures

However, there were instances, as shown in Figure A6 when a variation in pull-off failures was observed to MR substrates for both ‘low w/c’ and ‘high w/c’ concrete mix designs. This variation was found to have an impact upon not only the failure type or area of fracture but also the failure stress. For example the range in failure results for VHR profiles was 0.25MPa for ‘low w/c’ mixes and 0.40MPa for ‘high w/c’ mixes. Also, the range in failure results for HR profiles was 0.45MPa for ‘low w/c’ mixes and 0.75MPa for ‘high w/c’ mixes as seen in Table A4 and graphically in Figure A6. Whereas for MR substrates the range in failure results was 1.10MPa for ‘low w/c’ mixes and 1.20MPa for ‘high w/c’ mixes which is higher than that of VHR and HR profiles.

Figure A6(a) – G7.MR(1), w/c = 0.50

Figure A6(b) – P5.MR(2), w/c = 0.80

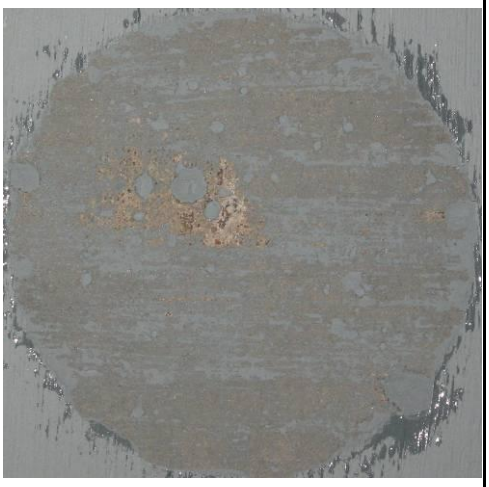

Figure A6(c) – G7.MR(1), w/c = 0.50

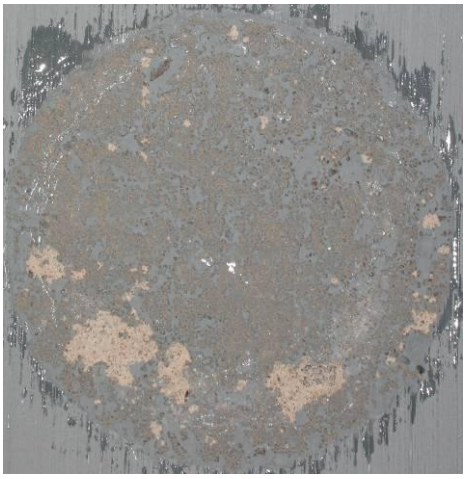

Figure A6(d) – P5.MR(2), w/c = 0.80

Figure A6(e) – G7.MR(1), w/c = 0.50

Figure A6(f) – P5.MR(2), w/c = 0.80

Figure A6 (on previous page): Variation in observed pull-off failures when producing a medium surface roughness, using a wire brush, to 'low w/c' concrete (left) and 'high w/c' concrete (right).

A8.4 Governing Factors Influencing Variation in Pull-Off Failures to MR Profiles

Generally speaking, with regards to MR profiles, when a certain amount of concrete was pulled off with the dolly the failure stress was always found to be a higher value. Typical examples are G4(3), G5(4), G6(4) and P4(3) for MR profiles. However, when pull-off failures illustrate an almost 100 %, or close to 100%, inter-coat type failure (B/C) then a number of factors may play a part in deciding whether the failure stress will be either at the high end or the low end of the range. The possible factors, in the opinion of the author, for a given w/c ratio and cement content are the (i) degree of concrete roughness, (ii) blow hole(s) size and extent, (iii) aggregate type and size, (iv) amount of aggregates exposed, (v) amount and type of compaction during concreting, (vi) undulations in coating/substrate surface, (vii) amount of epoxy resin used (viii) surface carbonation.

For example Figure A6(a, c & e) sample G7(1) gave a stress value of 2.40MPa and Figure 4.5(b, d & f) sample P5(2) gave a stress value of 1.35MPa. This is believed to be caused, primarily, by the inability of the coating to adequately bind or adhere to the substrate as a result of inappropriate level of roughness.

A8.5 Influence of Compaction to the Variation in Pull-Off Failures to MR Profiles

During the compaction process, conducted to initial trial experiments, the author observed that if the mode of the vibrating table was altered to shock table (≈ 8g) an excessive amount of, watery looking, cement paste would run up the vertical sides of the mould and eventually spill out. This would suggest at this level of vibration the effect of compaction would be felt more to the vertical sides of the concrete sample than other horizontal faces. Possibly resulting in a thicker laitance layer to the vertical concrete cube faces.

This resulting effect of compaction was not thought of until the author started to use the wire brush, manually, to yield a MR type substrate, firstly to trial experiments, and then subsequently to the various faces of the cubes and to the bottom face of the slabs. The author discovered that it was much harder to remove the laitance layer or to produce a suitable MR type profile to cubes which were given compaction at a lower vibration (4-7g) than to the cubes that were given compaction at shock table mode of vibration (≈ 8g). This could be, as discussed above, due to the greater amount of weak laitance produced at the vertical sides of the concrete cubes when compacting at shock table mode. As a result, some substrates were observed to have a favourable roughness such as G4(3), G5(4) and P4(3) because of the ease at which firstly laitance could be removed followed by the appropriate level of roughness produced observed by eye and by human touch. The author noticed the type of mould also seems to play a part, for example the surface laitance layer yielded by a plastic mould was observed not to be influenced much by the level of vibration (shock table: ≈ 8g /normal vibration: 4-7g) as a opposed to the metal mould. This may be because of the plastic mould design and its reduced weight as opposed to the metal mould which is bulkier and much heavier.

Also, in addition to the discussion above, the base face (face resting on the vibrating table) of the cubes and the slabs, compacted at shock table mode, were, similar to the cubes mentioned above in the sense that it was difficult to prepare the surface by wire brush. Again, probably due to the thin laitance layer produced to the base face. This reinforces the point made earlier that the sides of concrete sample are likely to receive more of the effect of compaction than other faces, in this case the base face, when compacting at shock table mode. Hence, the probable reason why variations in pull-off failures (Figure A6) were encountered. For further details with regards to comparing short and medium term pull-off data to MR type profiles on issues such as: observed variation in results, concrete strengthening and influence of compaction & type of mould refer to Sections 3.3.

A8.6 Influence of Needle Gunning to the Variation in Pull-Off Failures to HR Profiles

Figures A3(c), A4(c), A3(d) and A4(d) shows the pull-off failures to HR type profiles at the concrete substrate end and dolly end respectively. The results were not that promising for this particular test since for ‘low w/c’ concrete mix designs with an intermediate aggregate exposure (between MR and VHR profiles), the author was expecting stress failure values between MR and VHR profiles but, as can be seen in Table A4, and graphically in Figure A5, on average the stress failures were the lowest of all grades of roughness. The results for ‘high w/c’ concrete mix designs on the other hand were a bit more promising since stress failures, on average, were between MR and VHR profiles but still just above VHR. This might be because of the needle gun’s inability to yield an appropriate type of intermediate surface profile.

APPENDIX B: HARDBOARD EXPERIMENTS

A number of similar size and type of compressed hardboard (wood pulp) specimens with attached connections comprising of thin copper strips and electrical wiring were manufactured. The ends of the electrical wiring and the copper strips were soldered together and to seal the joint from possible corrosion, especially in the case of coated concrete slabs subjected to frequent water spraying, an adequate length of heat shrinkable sleeves (with inner adhesive) were utilised as waterproofing. The completed connection comprising of a thin copper strip with attached wiring were fixed to the opposite sides of the hardboard substrate using a two part epoxy resin, as well as some small weights, to firmly hold into position. But prior to making this connection, to hardboard and concrete substrates, the rear face of each copper strip was given a suitable roughness using an emery cloth to achieve suitable bonding. Immediately before coating Zinga, to both hardboard and concrete surfaces, the exposed copper strip face was given an appropriate roughness to yield a satisfactory bond between the Zinga paint and copper strip as well as to remove other contaminates such as corrosion products. This appropriate roughness to the copper strip was found, through practical experimentation, whilst using a coarse grade emery cloth which is likely to conform to the required substrate roughness stated by Zinga. After roughening the copper strip, the surface was wiped clean/degreased with a small amount of cloth soaked in methylated spirit. In addition, to prevent Zinga paint spilling over the sides of test subjects, tape was used to seal outer sides and corners. The tape was then eventually removed upon completion of test. The substrate temperature of both hardboard and concrete specimens were then checked using a thermometer. Finally, an appropriate amount of Zinga (a wet film mass of known amount) was brush applied and measured, whilst at the same time, being placed upon a weighing machine to enable accurate mass measurement. It was found, in previous trial experimentation, the use of an ordinary paint brush would cause brush marks in the coated substrate as well as brush hair loss within the paint container and then appearance of hairs in the coated surface. To prevent any future occurrence of this matter, a ‘low w/c’ quality brush of Hamilton range was utilised.

The mass measurement of the reinforced concrete slab, through trail experimentation, was found to be a lot more complicated and difficult. This was because of a number of reasons: firstly, from a physical point of view the slabs were heavy and fairly large in

size with plenty of extruding wires and a rebar. Secondly, due to the sheer amount of wires, if these wires were not incorporated into the mass measurement of the slab then this would effect the accuracy of slab mass measurement. For example, this was because of the variable reactions of the wires when coming into contact with the ground which therefore directly impacts the mass recorded on the scale. The implications for this is very important since to accurately determine the wet film mass (which can be several grams or more), displayed values need to be stable and accurate. To counter this particular problem the author used two methods either a small length of timber was attached to the extruding rebar and then the remaining wires were rotated around this length of timber and firmly attached to ensure no loose wire touches the ground. In the other case no timber, or any other attachments for that matter, was used but wires were simply placed into a carrier bag and then using any spare wire to firmly wrap around the bag and the extended rebar.

For each slab, the mass measurements were then checked several times over and found to be stable within a half a gram.

All hardboard specimens will be given a total of 5 coats with the exception of Hardboard number 3 (HB 3) which will be given several or more. Each measured coat will be aimed at achieving a wet film mass of 12.4g which corresponds to a theoretical dry film thickness of 60µm. A total of 5 Zinga coats will be applied to achieve a composite, theoretical dry film thickness of 300µm. The exception to this will be hardboard number 3 (HB 3) which will be given several or more coats in order to obtain a optimum minimum resistance as well as observe how data correlates to a particular mathematical relationship. For all hardboard specimens, when each applied coat has become sufficiently dry to handle an attempt will be made to measure the resulting thickness of paint by using a digital vernier calliper (0-150mm range). Since the apparatus is incapable of measuring the central hardboard region, readings will be taken in the only available position which will be between the copper strips along the top and bottom ends of the hardboard specimens. Along each top/bottom end length, at least 20 evenly spaced measurements will be carried out and then an average of both the top and bottom end lengths will be calculated.

APPENDIX C: PERFORMANCE OF ZINC PAINT

C1 Electrochemical Property Testing: Effect of Environmental Condition on Zinc Paint

C1.1 Objectives

The main aim of this investigation is to assess the effect of humidity and temperature on the performance of zinc paint with and without CP. The parameters chosen were:
Temperature Range: between 29 deg C and 50 deg. C.
Humidity Range: 50% and 90%.

C1.2 Sample Preparation

The methodology of sample preparation for this set of tests is:

- 3 concrete blocks (one control + two with different chloride levels); 150x150 x150mm with two rebars +1 No. B-probe + 1 No. Reference electrode. Connect cables to various elements and insulate the connections with heat-shrink sleeves.
- Cast the concrete blocks with all the probes etc. as above, one block no chloride, one block 1% chloride and the third one with 3% chloride added to the concrete mix. Remove the blocks from moulds and cure.
- Wire brush the top face of the blocks and weigh each block.
- Apply 3No. Coats of Zinc paint on each top face (allow time between coats for each coat to dry).
- Weigh each block with zinc coating. This is important and required for determining the Zinc coating thickness.
- Place blocks (flat –top face up) in plastic trays; Fill (partially without covering the top zinc coated surface) one tray with distilled water, one tray with 1% chloride solution, one tray with 3.5% chloride solution.

[IMPORTANT: All cables (free ends) shall be out of solutions at all times].

C1.3 Experimental – Test Procedures

1. Once the 3 blocks are placed in their respective trays, monitor the potentials of the rebars and also the zinc coating w.r.t Ag/AgCl and MMO/Ti reference electrodes.
2. Measure the corrosion current of the rebars with the ‘beta’-probes.
3. Monitor as per 1 and 2 above for 1or 2 weeks (or until some decent active corrosion to rebars in blocks with chloride).
4. Place the blocks (with chloride) in the environmental chamber
5. The operation cycles of the environmental is shown diagrammatically in Figure C1.1.
6. Set the DC power supply in constant current mode to supply a constant current of 17.8 mA. (Note: the anode, i.e. Zinc paint, shall be connected to the positive terminal of the power supply).
7. The following parameters shall be measured at 1 h, 24 h, 7 days, 28 days, 42 days, 56 days.

    (a) Cell Voltage and cell current
    (b) Anode potential versus the Ag/AgCl and MMO/Ti reference electrodes.
    (c) Cathode (rebars) potential
    (d) Corrosion current with the ‘beta-probe.
    (e) Bond strength between paint and concrete before and after applying the current.
    (f) Characteristics of interface of zinc paint and concrete after applying current.

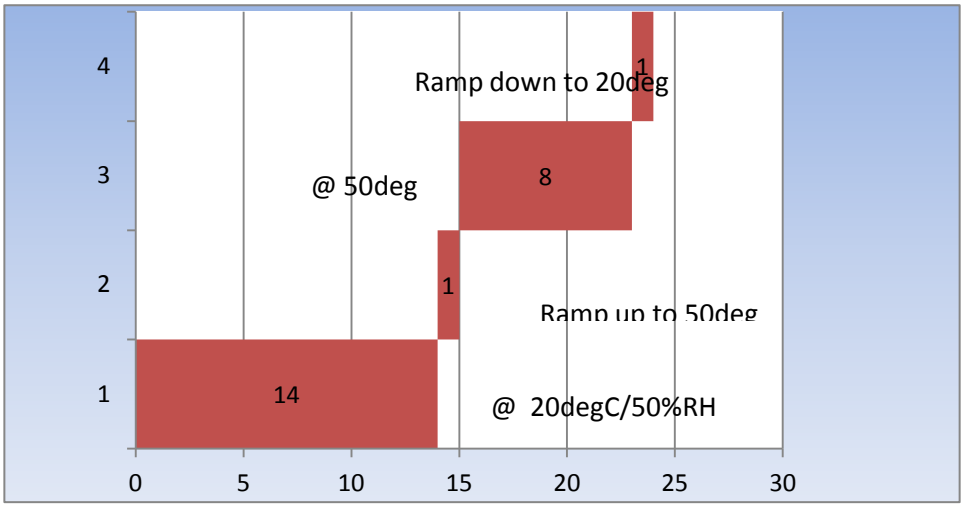

Figure C1: Environmental Cycle

C1.4 RESULTS

All data obtained in the course of this phase of investigations are miticulaously recoded and are tabulated and graphically illustrated where necessary. These are given in tables and Figures below.

Table C1: Mix proportions used and exposure conditions

Mix type	specimen	water	cement	Fine	coarse	NaCl	slump	Exposure condition
1	A	0.73	1.52	3.25	4.17	-	160 m m	Only fresh water
2	B	0.73	1.52	3.25	4.17	1.00 %	160 m m	1%NaCl
3	C	0.73	1.52	3.25	4.17	3.00 %	160 m m	3.5% NaCl

The results corrosion potential obtained while the specimen were in the environmental chamber were measured at maintained temperature of 20 ^{0} C and 50% RH.

Table C2: results of corrosion potential of rebar vs. silver/ silver chloride in cube A with no chloride content in concrete and while in solution. Test results of 14 days without CP.

No. of period days recorded	corrosion potential (mV)cube A(No chloride content)	corrosion potential (mV)cube B(1% chloride content)	corrosion potential (mV)cube C(3.5% chloride content)
1	-306	-358	-370
2	-318	-368	-405
3	-298	-361	-417
4	-279	-342	-428
5	-271	-357	-453
6	-283	-354	-461
7	-248	-312	-414
8	-259	-368	-434
9	-273	-363	-438
10	-289	-357	-440
11	-292	-344	-412
12	-301	-343	-471
13	-312	-396	-449
14	-318	-356	-453

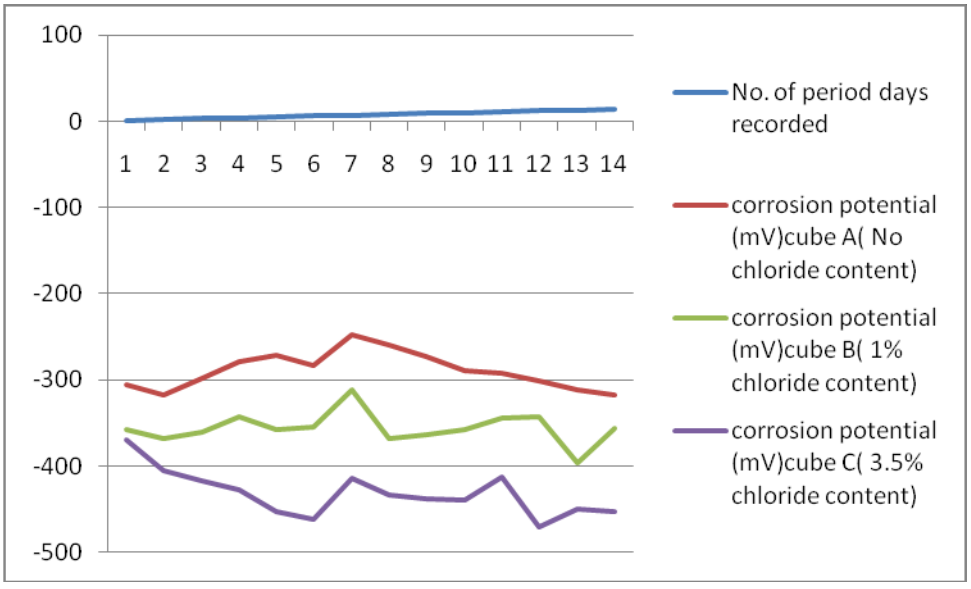

Figure C2: corrosion potential of rebar vs. reference electrode.

Table C3: results of corrosion potential of Zinga vs. silver/ silver chloride in cube A without using chloride content 1. Test results of 14 days without CP.

No. of period days recorded	corrosion potential (mV)cube A(No chloride content)	corrosion potential (mV)cube B(1% chloride content)	corrosion potential (mV)cube C(3.5% chloride content)
1	-306	-358	-370
2	-318	-368	-405
3	-298	-361	-417
4	-279	-342	-428
5	-271	-357	-453
6	-283	-354	-461
7	-248	-312	-414
8	-259	-368	-434
9	-273	-363	-438
10	-289	-357	-440
11	-292	-344	-412
12	-301	-343	-471
13	-312	-396	-449
14	-318	-356	-453

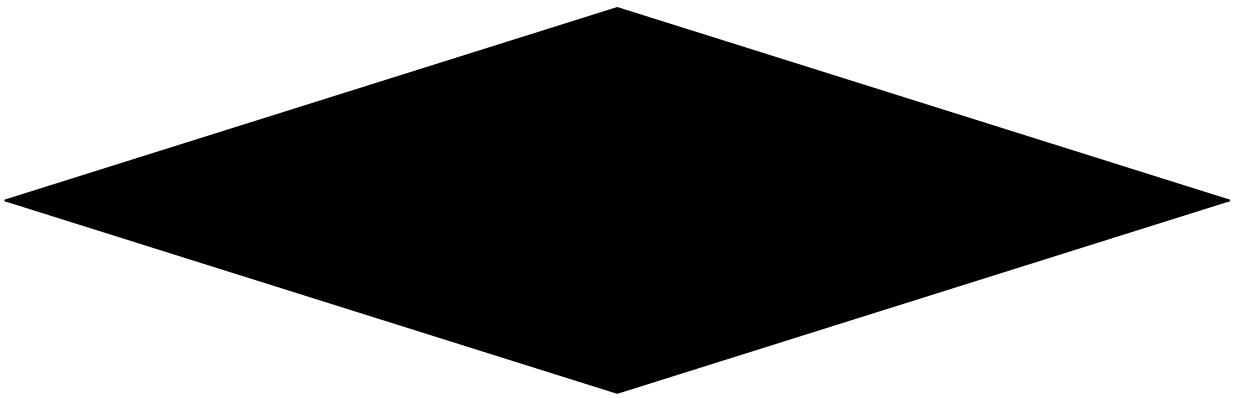

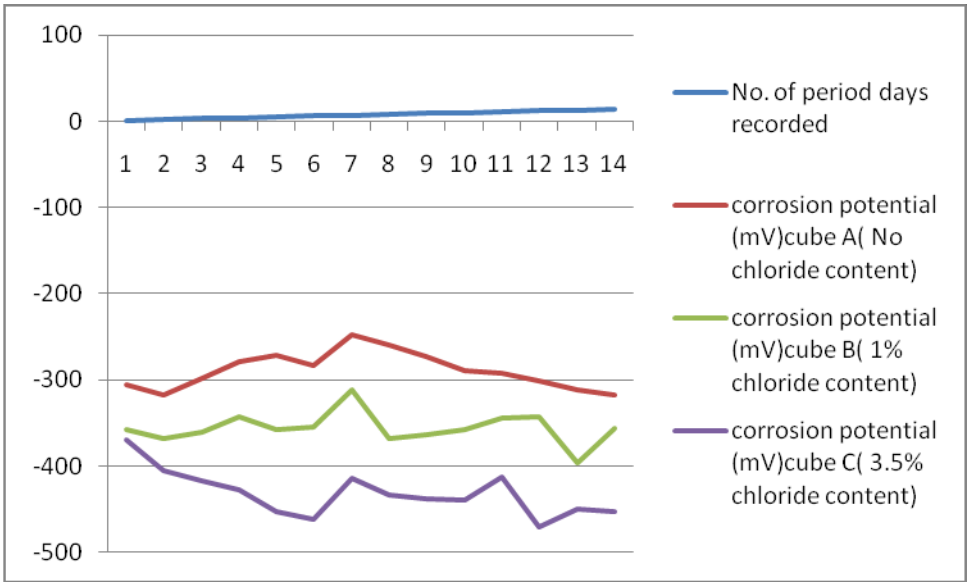

Figure C3: corrosion potential of zinga vs. reference electrode.

Table C 4 : corrosion current of Rebar Vs Probe of Cube A, B, C having different chloride content for the period of 14 days without applying CP.

No. of period Days	Cube A(no NaCl)	Cube B(1% NaCl)	Cube C(3.5% NaCl)
1	-38	-39.5	-39
2	-47	-42	-39.5
3	-49	-40	-37
4	-49.5	-44	-42
5	-47	-48.5	-53.5
6	-47.5	-52	-52.5
7	-48	-55	-50
8	-40	-59	-49.5
9	-49	-63	-53.5
10	-53	-72	-62
11	-48	-68	-67
12	-47	-75	-73
13	-42	-73.5	-82
14	-49	-74	-93

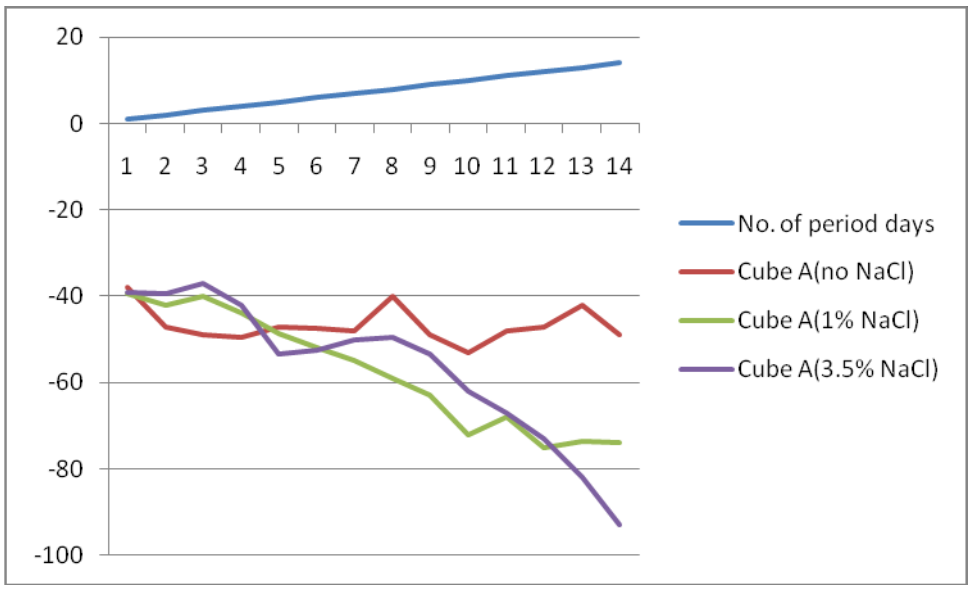

Figure C4: Results on corrosion macro cell current in cubes A,B,C.

Table C5: Results of corrosion potential of cube A, B, C when kept in environmental chamber and raising the temperature and humidity.

Reference electrode vs. rebar

No. of period days	corrosion potential, mV		
	cube A No chloride content	cube B 1% chloride content	cube C 3.5% chloride content
1	-353	-433	-498
2	-325	-439	-503
3	-346	-437	-498
4	-366	-428	-429
5	-360	-513	-413
6	-358	-505	-430
7	-315	-510	-453
8	-355	-529	-461
9	-380	-447	-460
10	-365	-435	-462
11	-364	-498	-464
12	-390	-397	-496
13	-343	-407	-495
14	-325	-441	-487
15	-360	-465	-480
16	-358	-436	-482
17	-347	-463	-482
18	-315	-440	-474
19	-394	-463	-463
20	-360	-450	-461
21	-379	-475	-472
22	-410	-455	-467
23	-350	-445	-462
24	-380	-453	-467
25	-436	-464	-465
26	-457	-430	-465
27	-339	-416	-442
28	-340	-418	-440
29	-319	-443	-481
30	-355	-416	-509
31	-274	-400	-544

32	-301	-430	-549
33	-310	-450	-545
34	-282	-443	-540
35	-278	-448	-512
36	-379	-470	-497
37	-283	-498	-532
38	-489	-502	-551
39	-470	-513	-570
40	-330	-548	-591

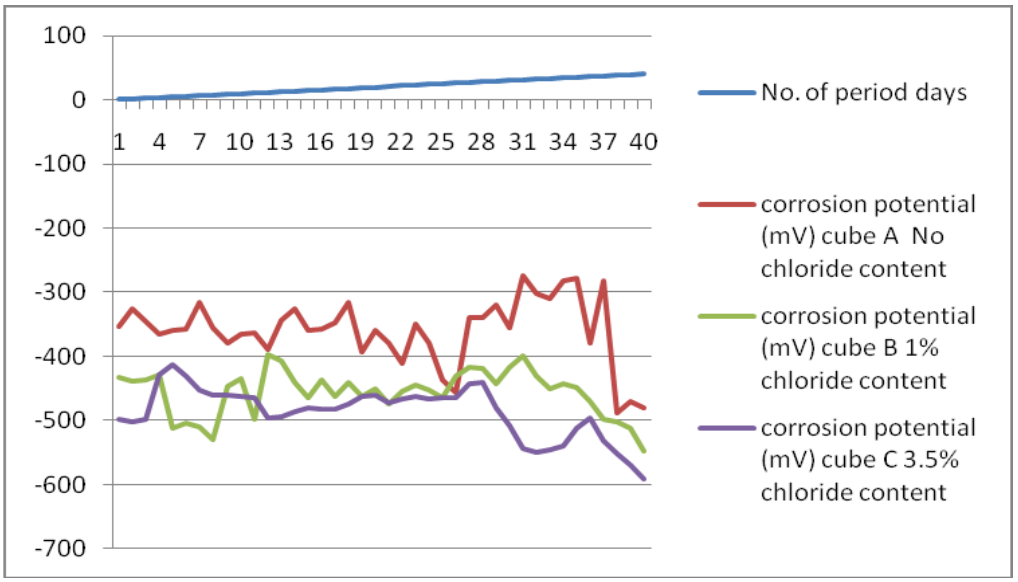

Figure C5: Corrosion potential results of cube A, B, C

Table C6: Results of corrosion potential of cube A, B, C when kept in environmental chamber and raising the temperature and humidity. Reference electrode vs. Zinga (applied on concrete surface)

No. of period days	corrosion potential (mV) cube A No chloride content	corrosion potential (mV) cube B 1% chloride content	corrosion potential (mV) cube C 3.5% chloride content
1	-353	-433	-498
2	-325	-439	-503
3	-346	-437	-498
4	-366	-422	-429
5	-360	-513	-413
6	-358	-505	-430
7	-315	-510	-453
8	-355	-529	-461
9	-380	-447	-460
10	-365	-435	-462
11	-364	-498	-464
12	-390	-397	-492
13	-343	-407	-495
14	-325	-441	-487
15	-360	-465	-480
16	-358	-436	-482
17	-347	-463	-484
18	-315	-440	-474
19	-394	-463	-463
20	-360	-450	-461
21	-379	-475	-472
22	-410	-455	-467
23	-350	-445	-465

24	-380	-453	-467
25	-436	-466	-465
26	-458	-430	-465
27	-339	-416	-442
28	-340	-418	-441
29	-319	-443	-481
30	-356	-416	-509
31	-333	-400	-544
32	-301	-430	-549
33	-310	-450	-545
34	-282	-443	-540
35	-278	-448	-512
36	-379	-470	-497
37	-283	-498	-532
38	-489	-502	-552
39	-470	-514	-570
40	-481	-549	-592

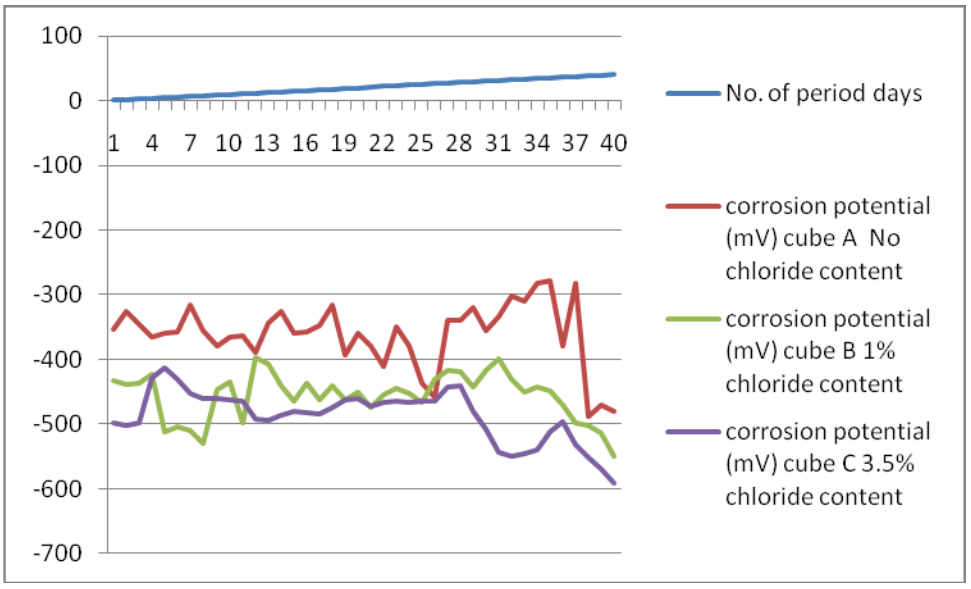

Figure C6: corrosion potential results of cube A, B, C

Table C7: Results of corrosion current of cube A, B, C when kept in environmental chamber and raising the temperature and humidity.

No. of period days	Cube A(no NaCl)	Cube B(1% NaCl)	Cube C(3.5% NaCl)
1	-49.5	-73.5	-93.5
2	-52	-75	-98
3	-52	-75	-98
4	-52	-75	-98
5	-52	-75	-98
6	-52	-75.5	-98
7	-52	-75	-98
8	-52.5	-75.5	-98
9	-52	-75	-98
10	-52.5	-74.5	-98
11	-52.5	-75	-98
12	-53	-75	-98
13	-53	-75	-98
14	-53	-75	-98
15	-53	-75	-97.5
16	-53	-75	-97.5
17	-53	-75	-97.5
18	-52.5	-75	-97.5
19	-52	-75	-97.5
20	-52	-75	-97.5
21	-52	-75	-97.5
22	-52.5	-75.5	-97.5
23	-52.5	-75.5	-97.5
24	-52.5	-75.5	-98.5
25	-52.5	-75.5	-98.5
26	-52.5	-75.5	-98.5

27	-52	-75.5	-98.5
28	-52	-75.5	-98.5
29	-52	-75.5	-98.5
30	-52	-75.5	-98.5
31	-52	-75.5	-98.5
32	-52	-76	-98.5
33	-53.5	-76	-98.5
34	-53.5	-76	-98.5
35	-53.5	-76	-98.5
36	-53.5	-76.5	-98.5
37	-53.5	-76.5	-98.5
38	-53.5	-76.5	-98
39	-53.5	-76.5	-98
40	-53.5	-76.5	-98

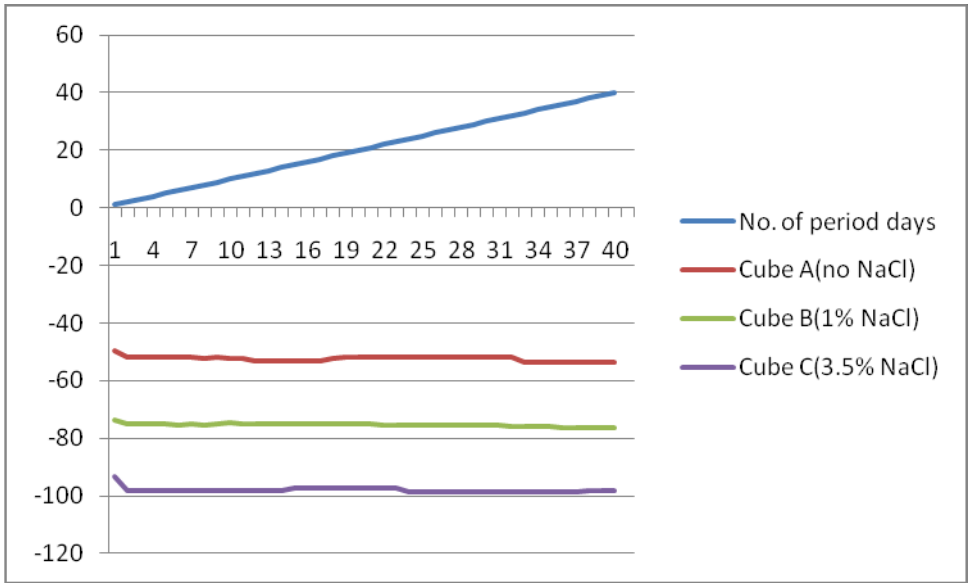

Figure C 7 : Macro cell corrosion current results of all cubes

Figure C8: Effect of temperature and humidity after 40 days cyclic period on cube A

Figure C9: Effect of temperature and humidity after 40 days cyclic period on cube B having chloride content

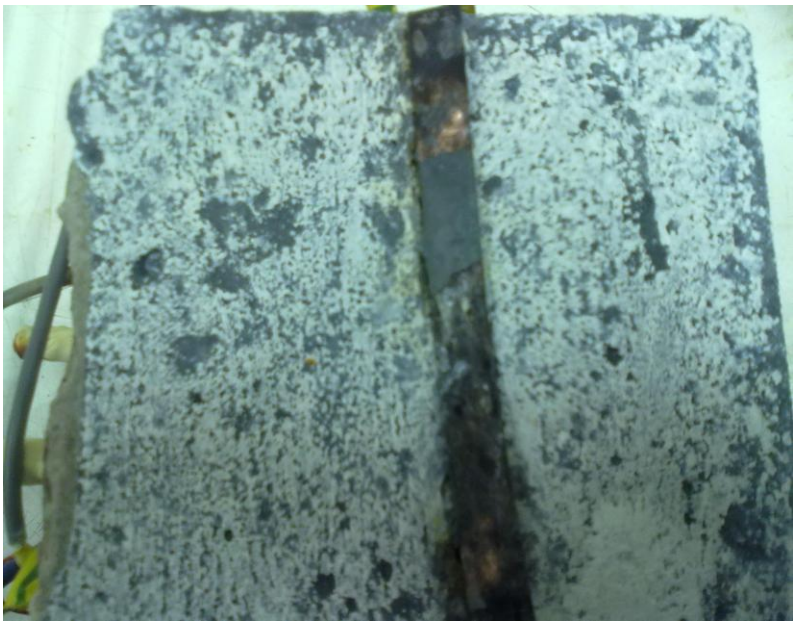

Figure C10: Effect of temperature and humidity after 40 days cyclic period on cube C having chloride content

Figure C11: Dolly showing the results before current applied of cube A

Figure C12: Surface showing the results before current applied of cube A

Figure C13: Dolly showing the results after current applied of cube A

Figure C14: Surface showing the results after current applied of cube A

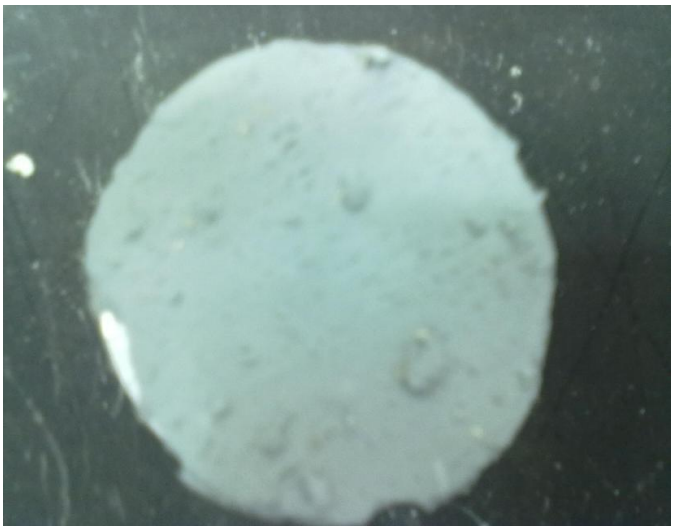

Figure C15: Dolly showing the results before current applied of cube B

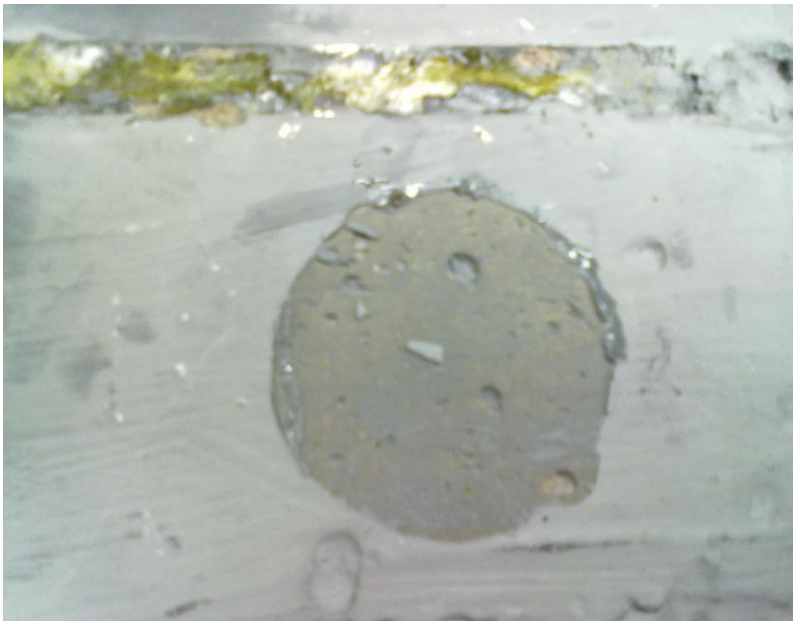

Figure C16: Surface showing the results before current applied of cube B

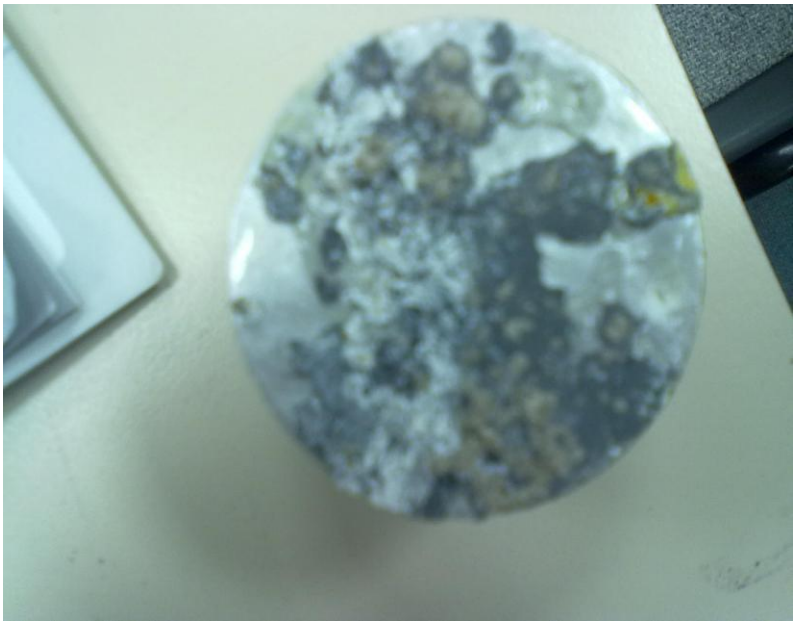

Figure C17: Dolly showing the results after current applied of cube B

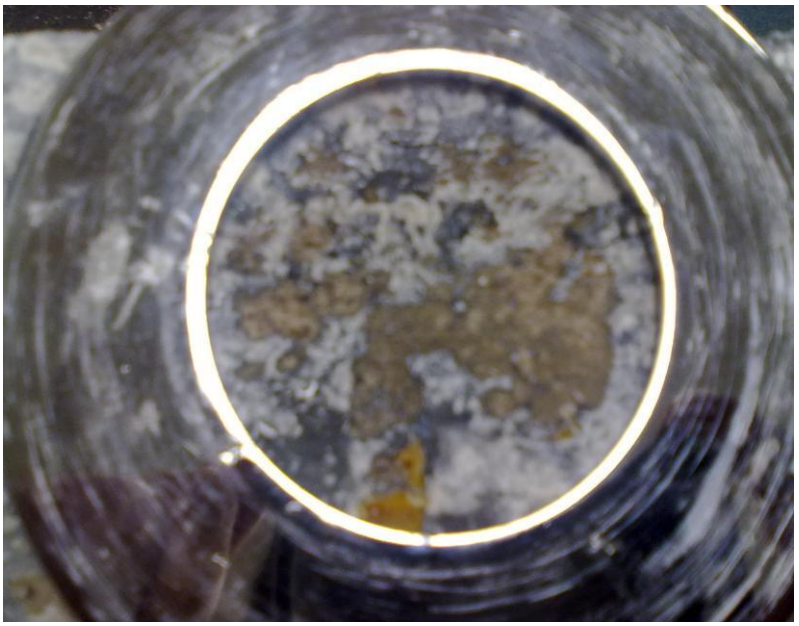

Figure C18: Surface showing the results after current applied of cube B

Figure C19: Dolly showing the results before current applied of cube C

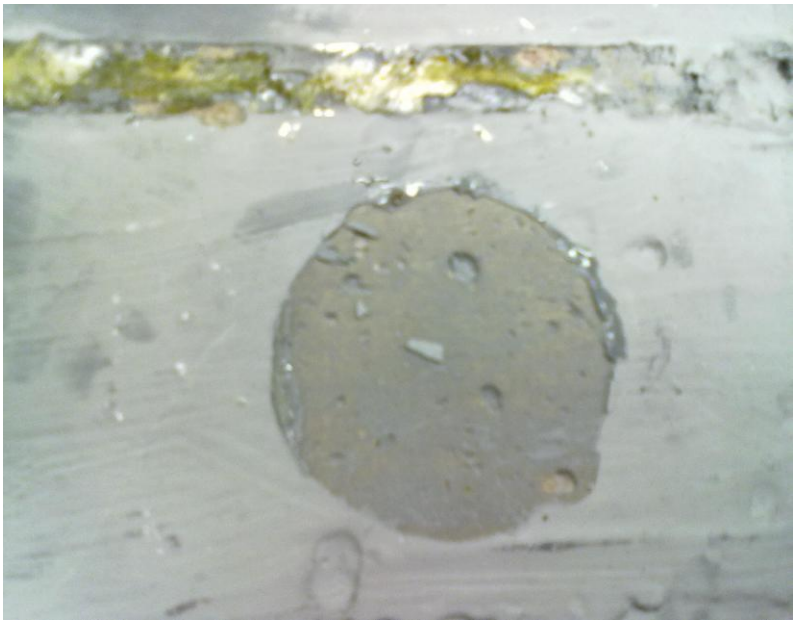

Figure C20: Surface showing the results before current applied of cube C

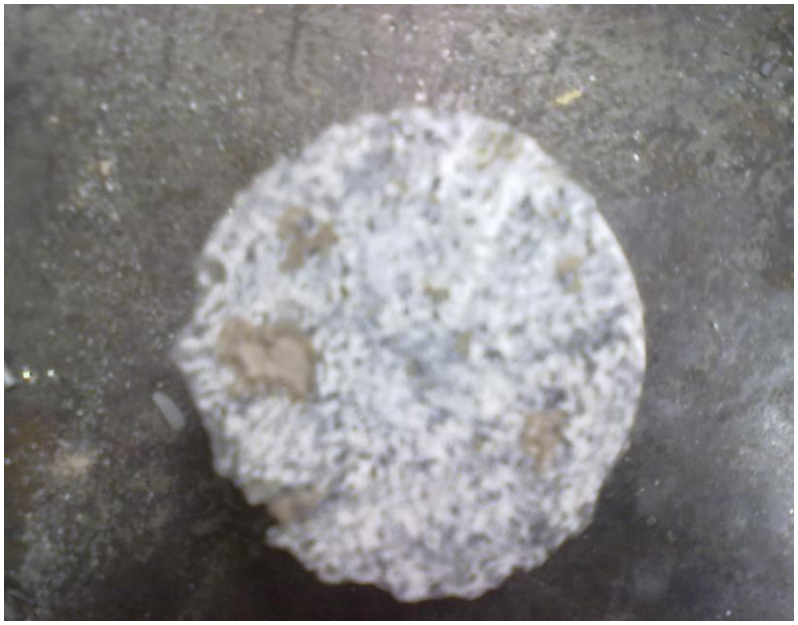

Figure C21: Dolly showing the results after current applied of cube C

Figure C22: Surface showing the results after current applied of cube C

Table C8: Bond strength test results of all three cubes before and after applied current on zinga

Sample	Test results before	Test results after
	(MPa)	(MPa)
A	1.50	2.0
B	1.85	2.5
C	1.60	2.3

C2.0 Electrochemical Property Testing: 'Beam Specimen' - Test results tables and graphs

Table C9: Polarisation potentials at 104mA/ m^2 for 0% chloride contaminated sample

Time Period (Days)	Ref 1 Vs Rebar 1 (mV)	Ref 1 Vs Rebar 2 (mV)	Ref 2 Vs Rebar 1 (mV)	Ref 2 Vs Rebar 2 (mV)	Ref 3 Vs Rebar 1 (mV)	Ref 3 Vs Rebar 2 (mV)
1	-247	-247	-387	-387	-389	-389
2	-244	-244	-375	-375	-376	-376
3	-248	-248	-364	-364	-369	-369
4	-254	-254	-358	-358	-363	-363
5	-233	-233	-352	-352	-357	-357
6	-249	-249	-333	-334	-353	-353
7	-252	-252	-325	-326	-346	-346

Table C10: Polarisation potentials at 104mA/ m^2 for 2% chloride contaminated sample

Time Period (Days)	Ref 1 Vs Rebar 1 (mV)	Ref 1 Vs Rebar 2 (mV)	Ref 2 Vs Rebar 1 (mV)	Ref 2 Vs Rebar 2 (mV)	Ref 3 Vs Rebar 1 (mV)	Ref 3 Vs Rebar 2 (mV)
1	-402	-402	-422	-422	-429	-429
2	-336	-336	-443	-442	-445	-445
3	-336	-336	-443	-441	-456	-456
4	-337	-337	-444	-443	-457	-457
5	-327	-327	-449	-449	-456	-456
6	-333	-332	-442	-443	-446	-446
7	-333	-333	-436	-436	-443	-443

Table C11: Polarisation potentials at 104mA/ m^2 for 4% chloride contaminated sample

Time Period (Days)	Ref 1 Vs Rebar 1 (mV)	Ref 1 Vs Rebar 2 (mV)	Ref 2 Vs Rebar 1 (mV)	Ref 2 Vs Rebar 2 (mV)	Ref 3 Vs Rebar 1 (mV)	Ref 3 Vs Rebar 2 (mV)	Ref 4 Vs Rebar 1 (mV)	Ref 4 Vs Rebar 2 (mV)
1	-518	-517	-501	-501	-535	-533	-517	-517
2	-369	-371	-471	-473	-517	-517	-502	-501
3	-351	-352	-460	-459	-504	-504	-491	-490
4	-368	-367	-450	-450	-493	-495	-484	-484
5	-386	-386	-447	-447	-492	-493	-484	-484
6	-387	-387	-436	-436	-481	-481	-473	-473
7	-389	-389	-418	-418	-474	-474	-467	-467

Table C12: Polarisation potentials at 208mA/ m^2 for 0% chloride contaminated sample

Time Period (Days)	Ref 1 Vs Rebar 1 (mV)	Ref 1 Vs Rebar 2 (mV)	Ref 2 Vs Rebar 1 (mV)	Ref 2 Vs Rebar 2 (mV)	Ref 3 Vs Rebar 1 (mV)	Ref 3 Vs Rebar 2 (mV)
1	-255	-254	-303	-303	-338	-338
2	-260	-260	-284	-294	-336	-337
3	-265	-266	-289	-288	-338	-338
4	-267	-267	-288	-290	-337	-337
5	-267	-266	-288	-287	-336	-336
6	-267	-266	-289	-289	-334	-334
7	-266	-265	-287	-288	-333	-333

Table C13: Polarisation potentials at 208mA/ m^2 for 2% chloride contaminated sample

Time Period (Days)	Ref 1 Vs Rebar 1 (mV)	Ref 1 Vs Rebar 2 (mV)	Ref 2 Vs Rebar 1 (mV)	Ref 2 Vs Rebar 2 (mV)	Ref 3 Vs Rebar 1 (mV)	Ref 3 Vs Rebar 2 (mV)
1	-364	-365	-508	-508	-506	-506
2	-350	-249	-499	-498	-503	-503
3	-247	-348	-490	-490	-594	-594
4	-347	-346	-492	-489	-592	-592
5	-248	-348	-490	-489	-592	-592
6	-348	-347	-489	-490	-591	-591
7	-348	-347	-490	-490	-489	-493

Table C14: Polarisation potentials at 208mA/ m^2 for 4% chloride contaminated sample

Time Period (Days)	Ref 1 Vs Rebar 1 (mV)	Ref 1 Vs Rebar 2 (mV)	Ref 2 Vs Rebar 1 (mV)	Ref 2 Vs Rebar 2 (mV)	Ref 3 Vs Rebar 1 (mV)	Ref 3 Vs Rebar 2 (mV)	Ref 4 Vs Rebar 1 (mV)	Ref 4 Vs Rebar 2 (mV)
1	-300	-299	-516	-516	-561	-563	-547	-556
2	-303	-306	-491	-492	-547	-549	-532	-532
3	-319	-318	-481	-480	-538	-539	-524	-525
4	-320	-317	-480	-481	-538	-537	-523	-523
5	-319	-320	-481	-480	-532	-538	-523	-523
6	-320	-318	-481	-480	-538	-538	-522	-523
7	-317	-318	-482	-480	-538	-536	-523	-524

Table C15: Polarisation potentials at 313mA/ m^2 for 0% chloride contaminated sample

Time Period (Days)	Ref 1 Vs Rebar 1 (mV)	Ref 1 Vs Rebar 2 (mV)	Ref 2 Vs Rebar 1 (mV)	Ref 2 Vs Rebar 2 (mV)	Ref 3 Vs Rebar 1 (mV)	Ref 3 Vs Rebar 2 (mV)
1	-263	-263	-304	-304	-306	-306
2	-264	-264	-305	-305	-306	-306
3	-265	-265	-305	-305	-308	-308
4	-267	-267	-306	-306	-309	-309
5	-268	-268	-308	-308	-309	-309
6	-270	-270	-307	-308	-312	-312
7	-269	-270	-309	-309	-313	-313

Table C16: Polarisation potentials at 313mA/ m^2 for 2% chloride contaminated sample

Time Period (Days)	Ref 1 Vs Rebar 1 (mV)	Ref 1 Vs Rebar 2 (mV)	Ref 2 Vs Rebar 1 (mV)	Ref 2 Vs Rebar 2 (mV)	Ref 3 Vs Rebar 1 (mV)	Ref 3 Vs Rebar 2 (mV)
1	-567	-567	-509	-509	-509	-509
2	-568	-568	-510	-510	-514	-514
3	-569	-569	-511	-511	-516	-516
4	-570	-570	-512	-512	-515	-515
5	-570	-570	-513	-513	-515	-515
6	-571	-571	-513	-513	-516	-516
7	-572	-572	-514	-514	-517	-517

Table C17: Polarisation potentials at 313mA/ m^2 for 4% chloride contaminated sample

Time Period (Days)	Ref 1 Vs Rebar 1 (mV)	Ref 1 Vs Rebar 2 (mV)	Ref 2 Vs Rebar 1 (mV)	Ref 2 Vs Rebar 2 (mV)	Ref 3 Vs Rebar 1 (mV)	Ref 3 Vs Rebar 2 (mV)	Ref 4 Vs Rebar 1 (mV)	Ref 1 Vs Rebar 3 (mV)
1	-314	-314	-518	-519	-561	-561	-547	-547
2	-313	-314	-519	-519	-562	-562	-548	-548
3	-315	-315	-521	-521	-561	-561	-501	-501
4	-316	-316	-522	-522	-563	-563	-501	-501
5	-317	-317	-522	-522	-563	-563	-503	-502
6	-317	-317	-524	-524	-564	-564	-504	-504
7	-318	-318	-524	-525	-565	-565	-554	-554

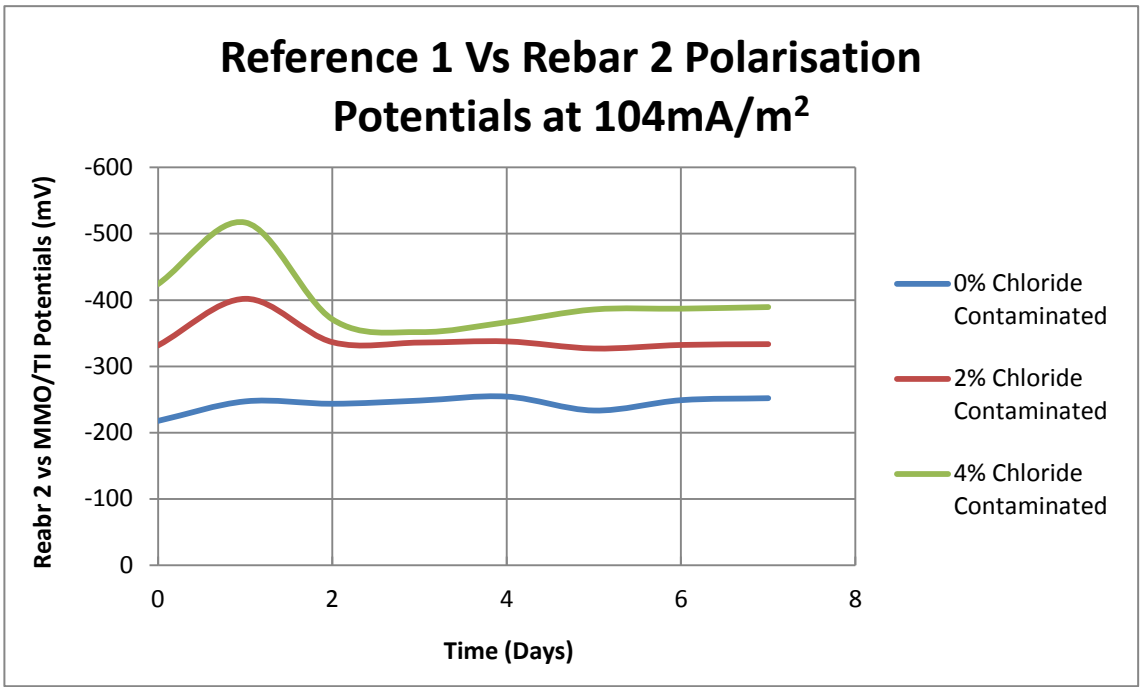

Figure C23: Polarisation potentials at 104 mA/m^2 reference 1 Vs rebar 2

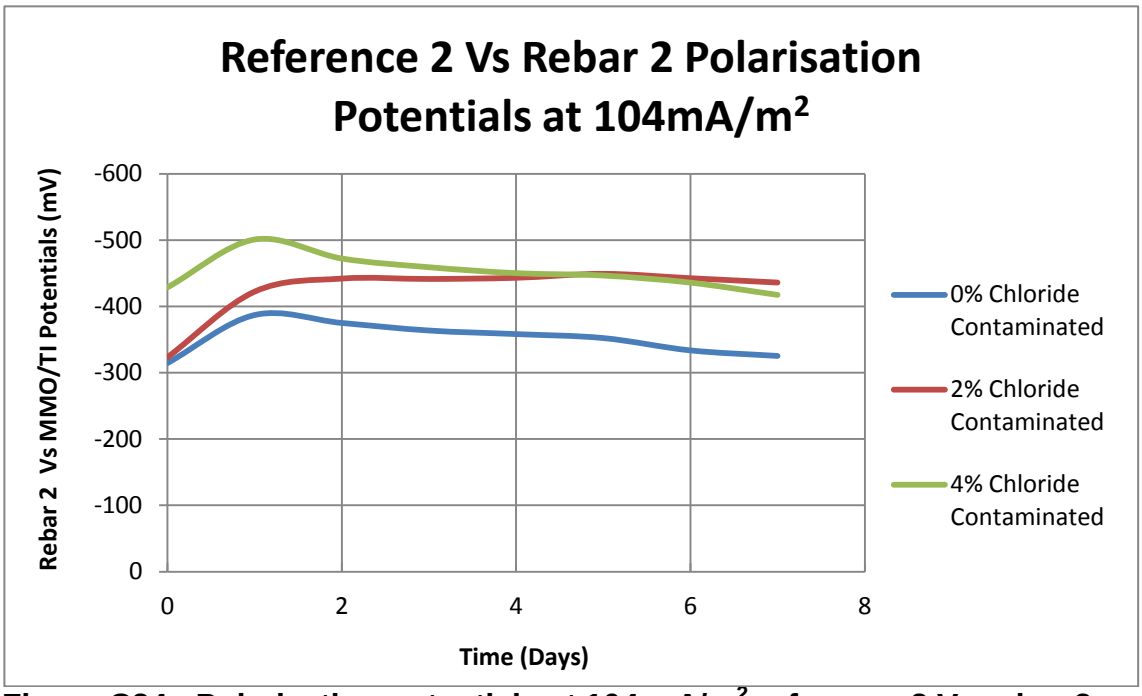

Figure C24: Polarisation potentials at 104 mA/m^2 reference 2 Vs rebar 2

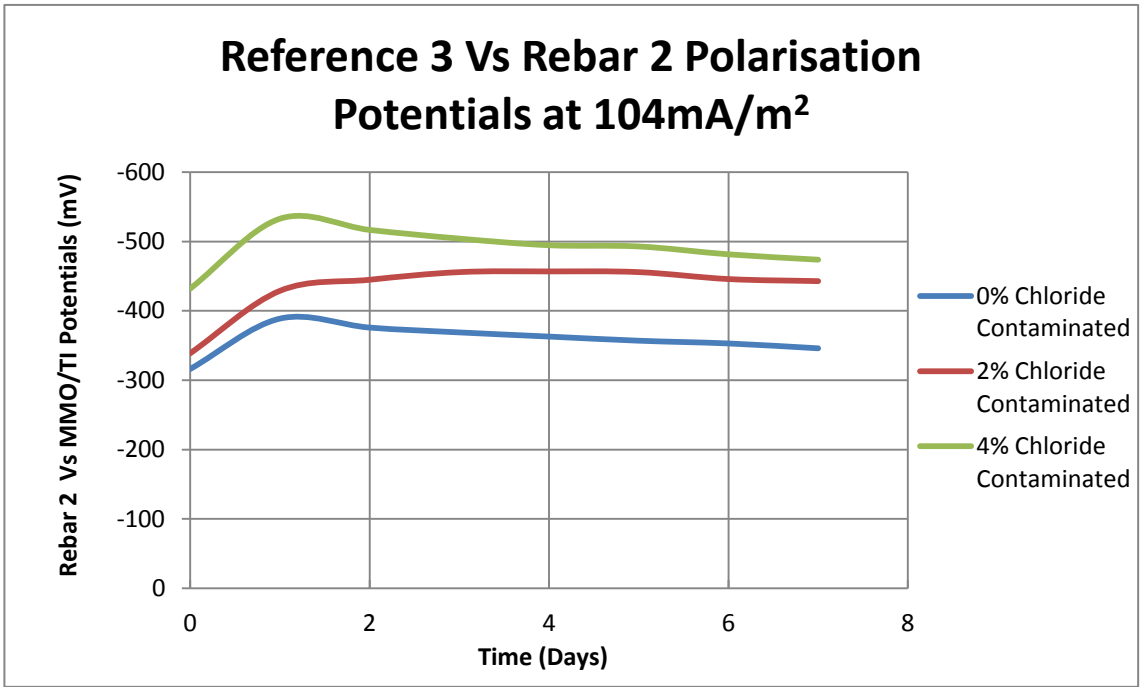

Figure C25: Polarisation potentials at 104 mA/m^2 reference 3 Vs rebar 2

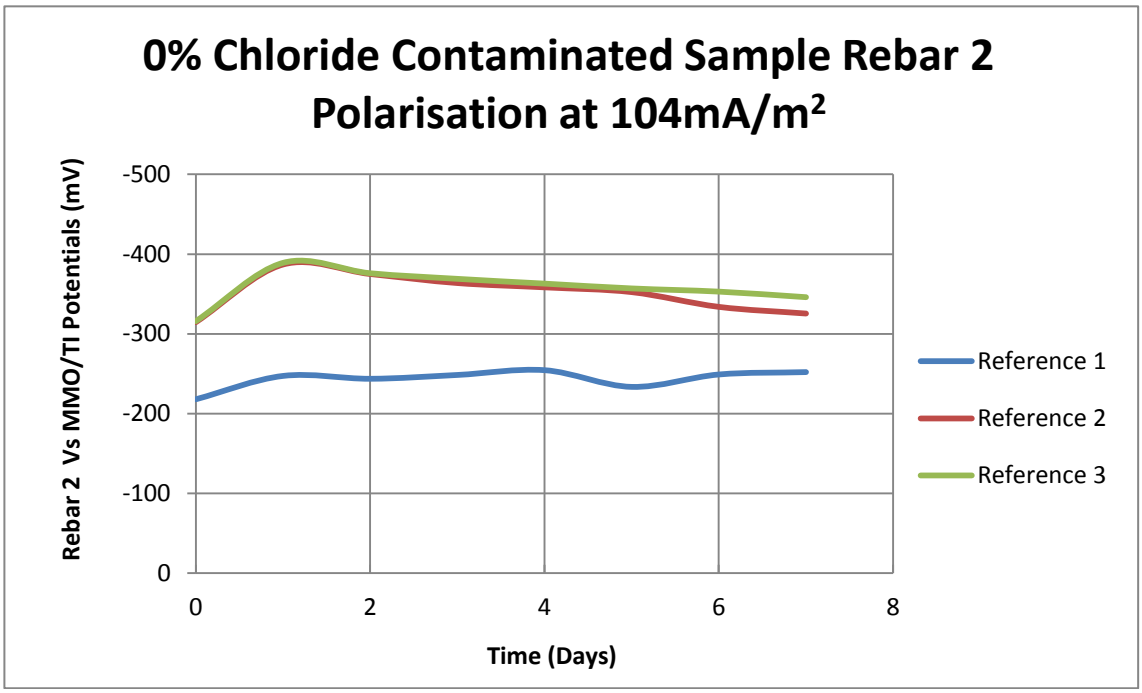

Figure C26: Polarisation potentials at 104 mA/m^2 of 0% chloride contaminated sample rebar 2

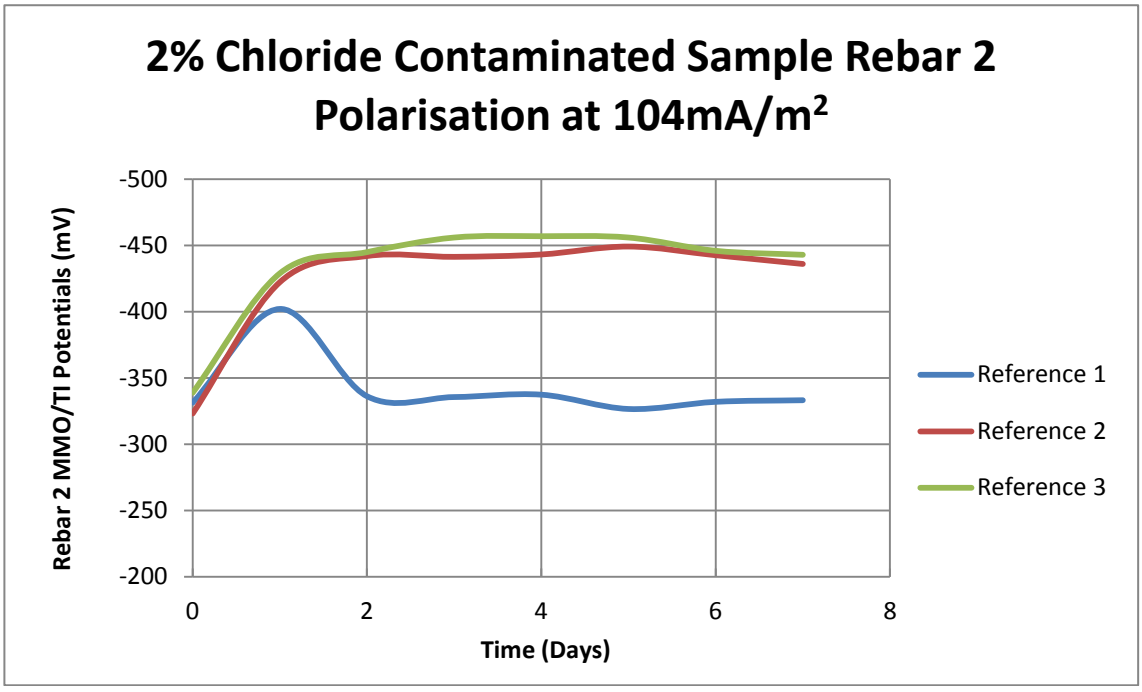

Figure C27: Polarisation potentials at 104 mA/m^2 of 2% chloride contaminated sample rebar 2

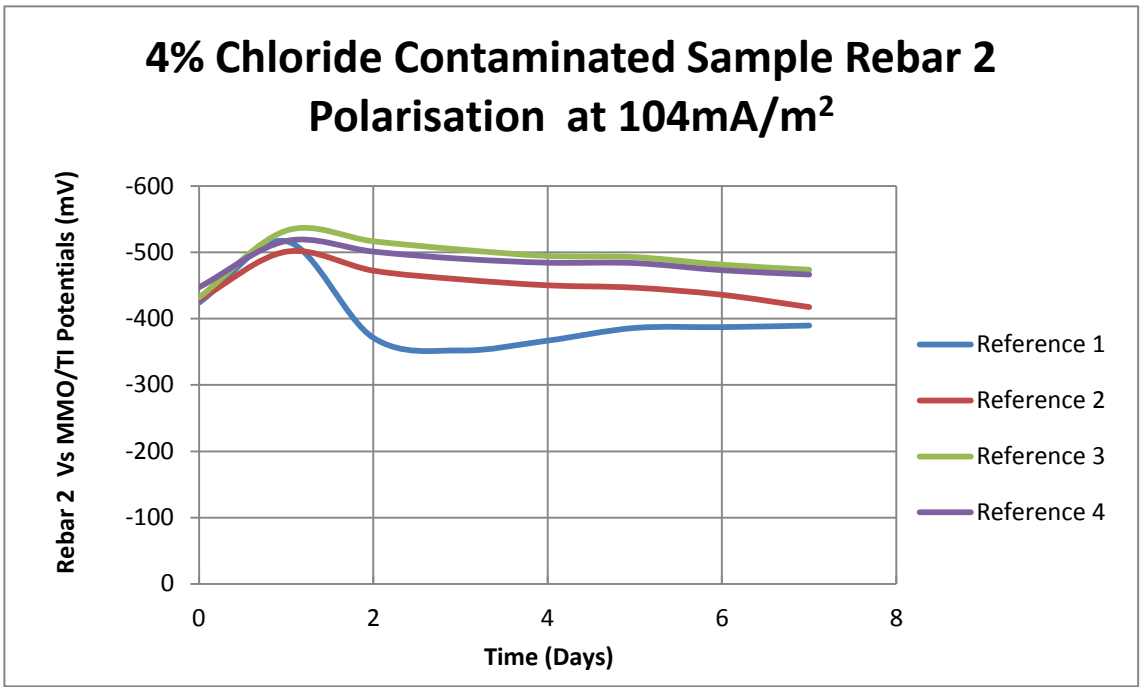

Figure C28: Polarisation potentials at 104 mA/m² of 4% chloride contaminated sample rebar 2

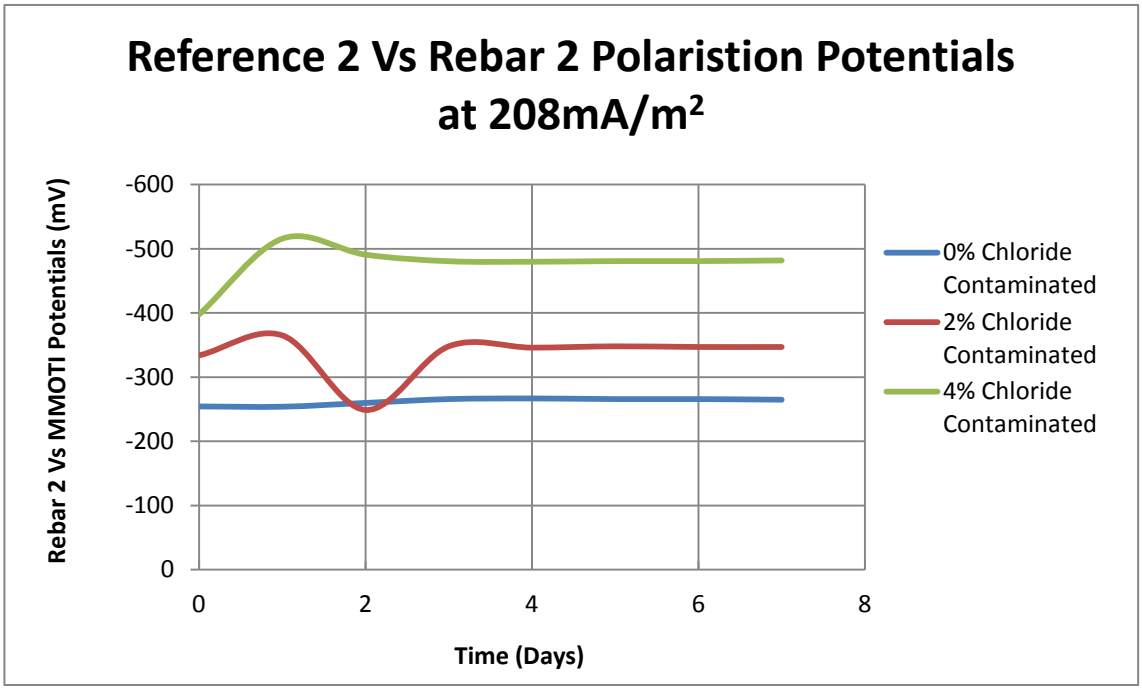

Figure C29: Polarisation potentials at 208 mA/m² reference 1 Vs rebar 2

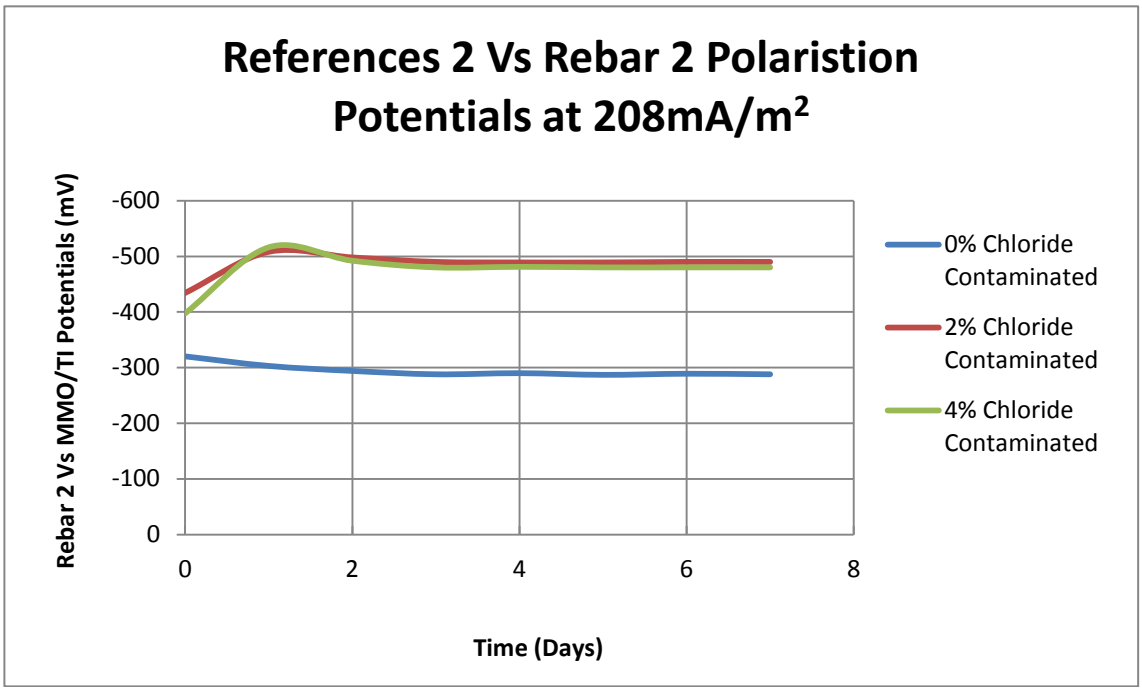

Figure C30: Polarisation potentials at 208 mA/m^2 reference 2 Vs rebar 2

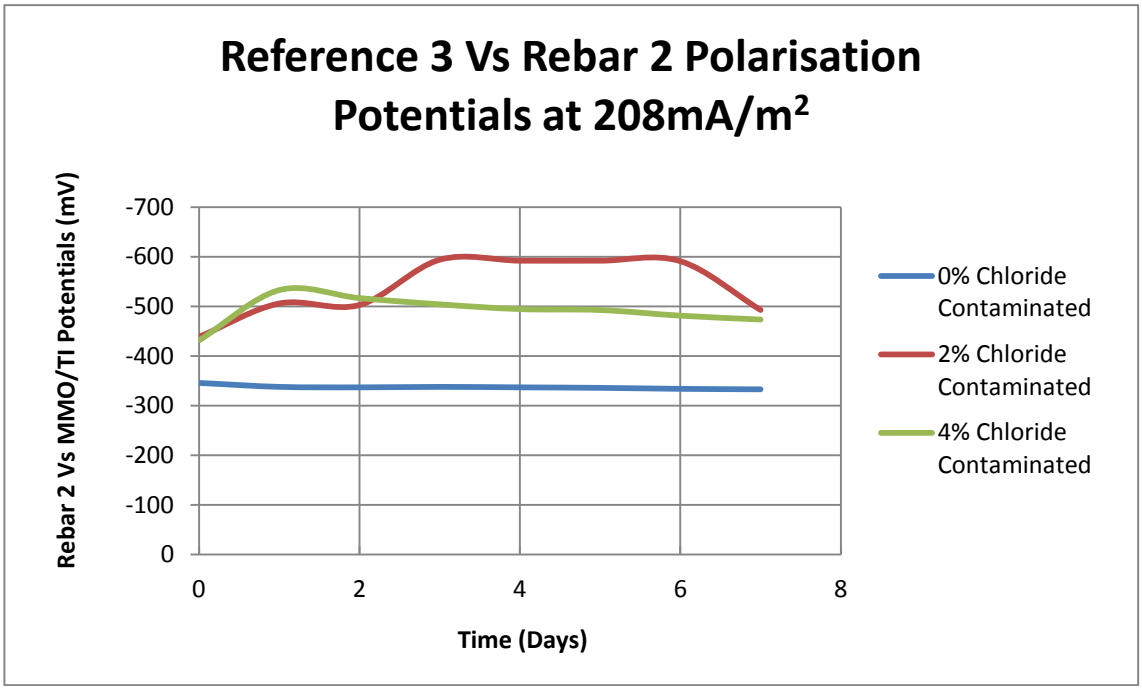

Figure C31: Polarisation potentials at 208 mA/m^2 reference 3 Vs rebar 2

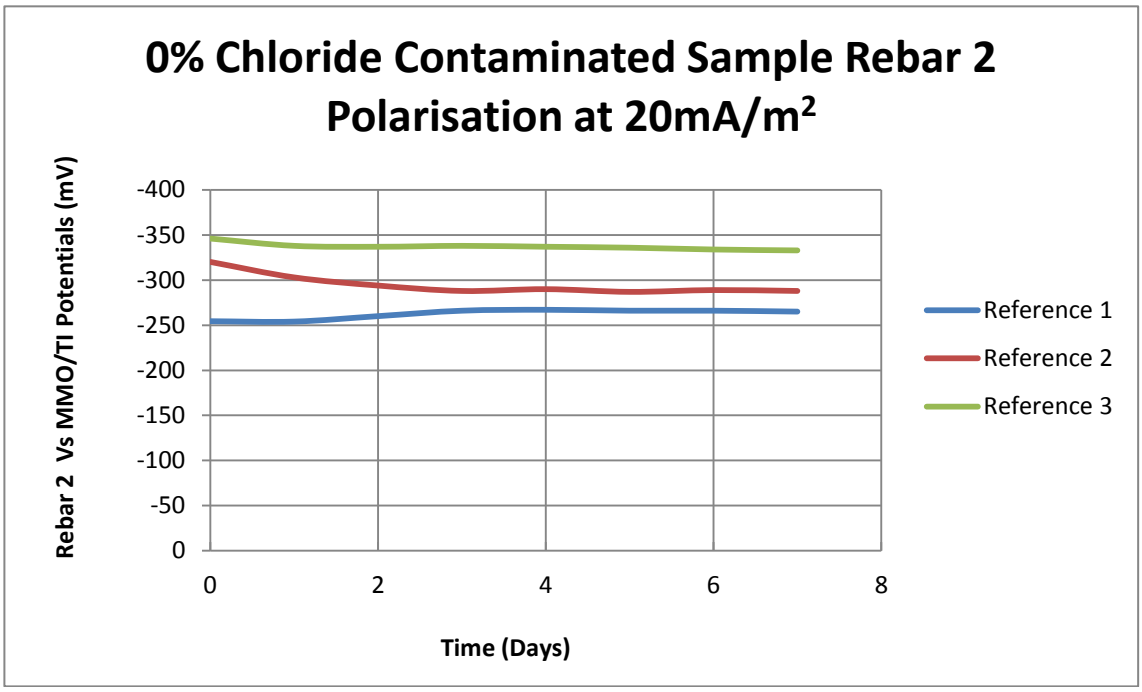

Figure C32: Polarisation potentials at 208 mA/m^2 of 0% chloride contaminated sample rebar 2

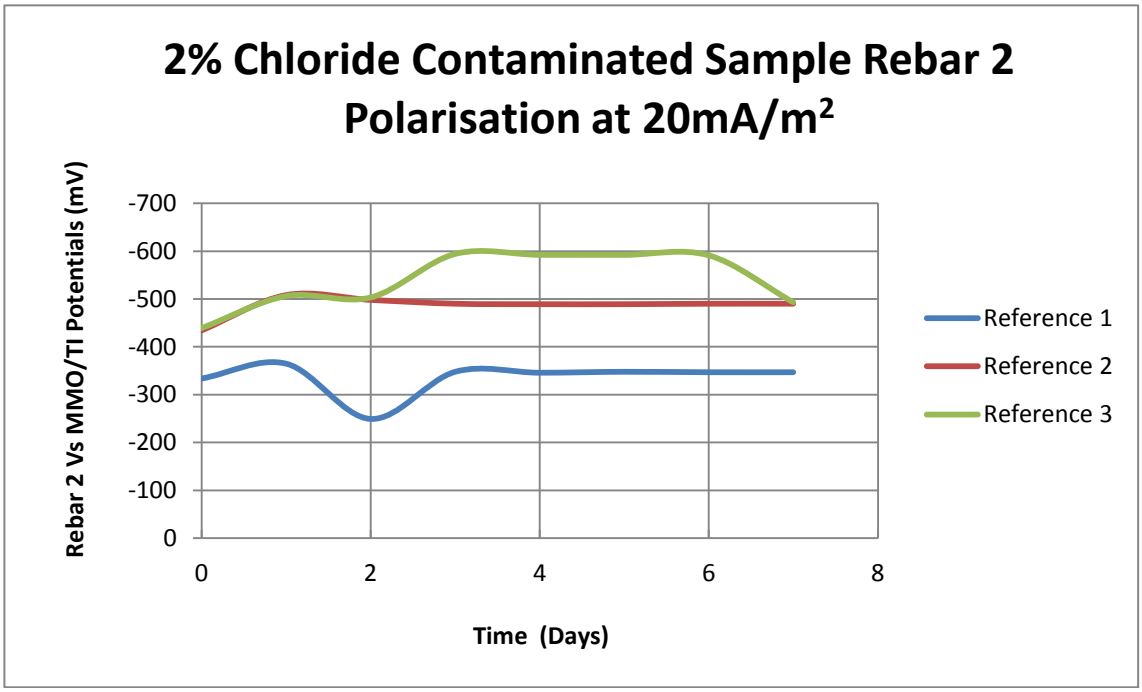

Figure C33: Polarisation potentials at 208 mA/m^2 of 2% chloride contaminated sample rebar 2

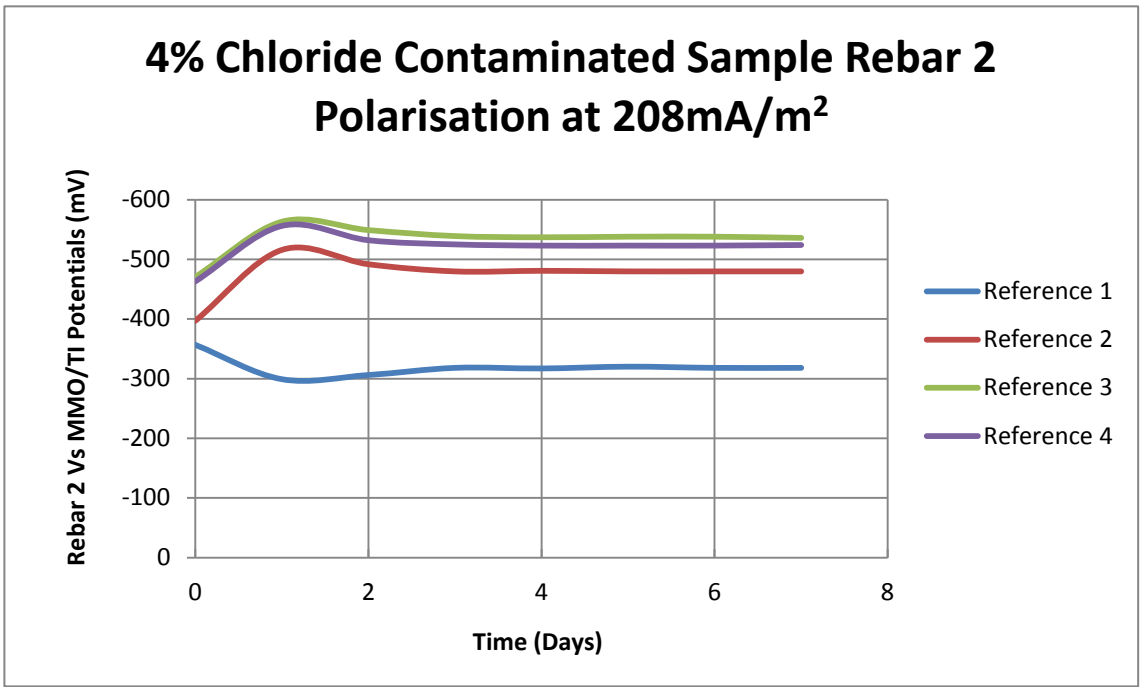

Figure C34: Polarisation potentials at 208 mA/m^2 of 4% chloride contaminated sample rebar 2

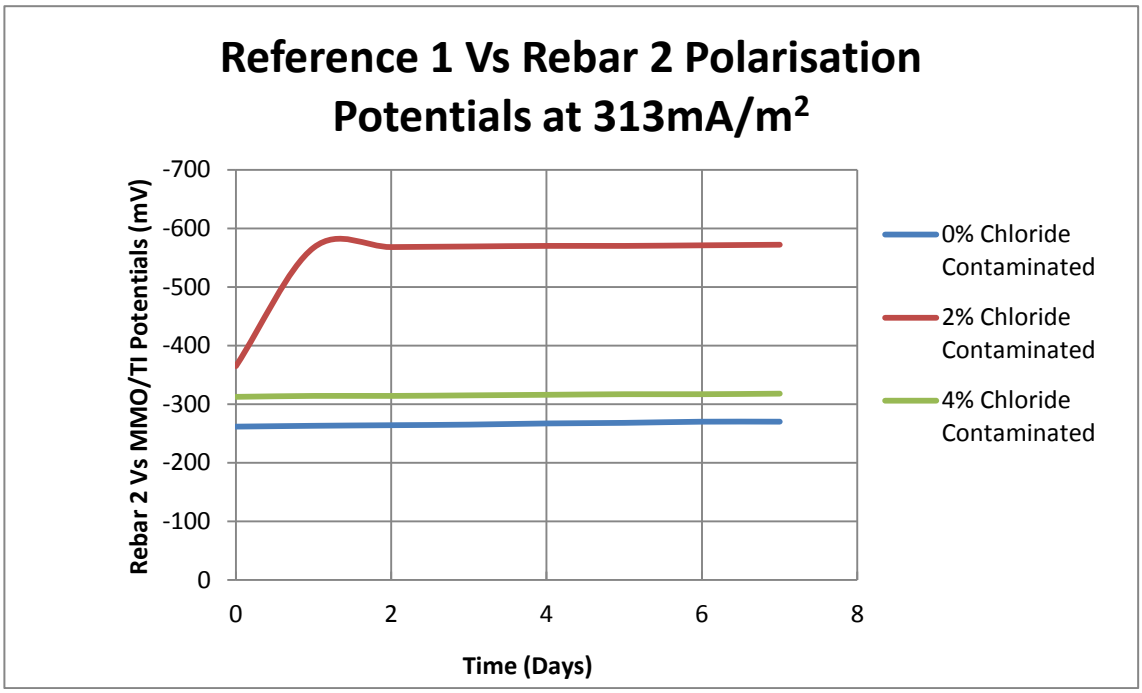

Figure C35: Polarisation potentials at 313 mA/m^2 reference 1 Vs rebar 2

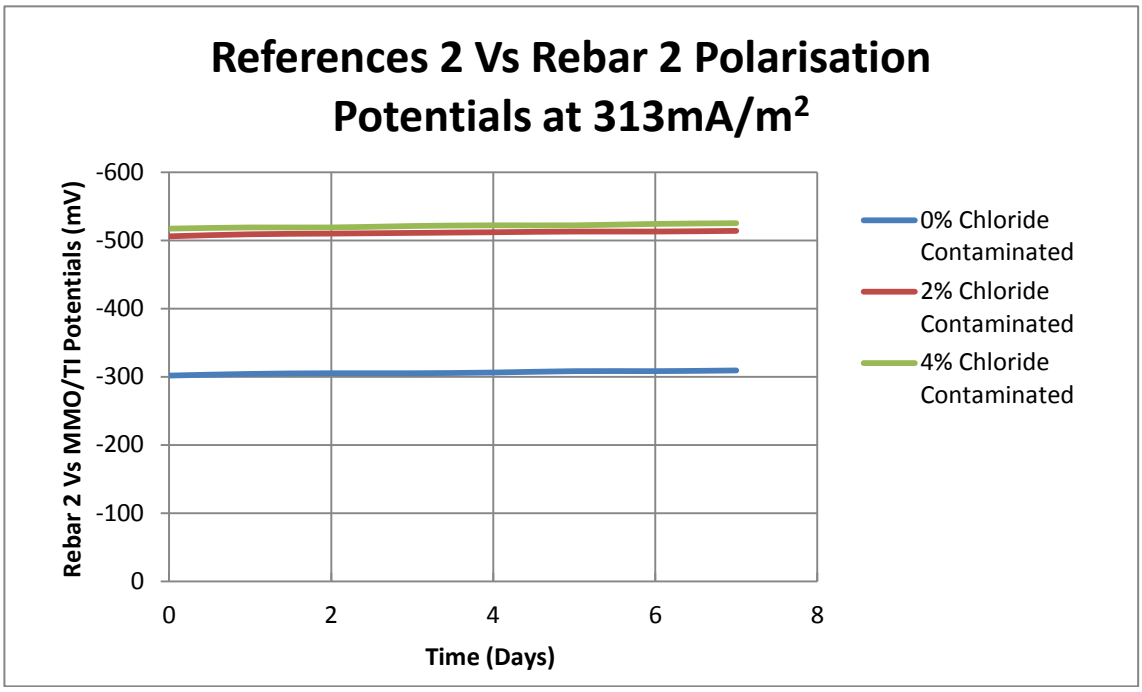

Figure C36: Polarisation potentials at 313 mA/m^2 reference 2 Vs rebar 2

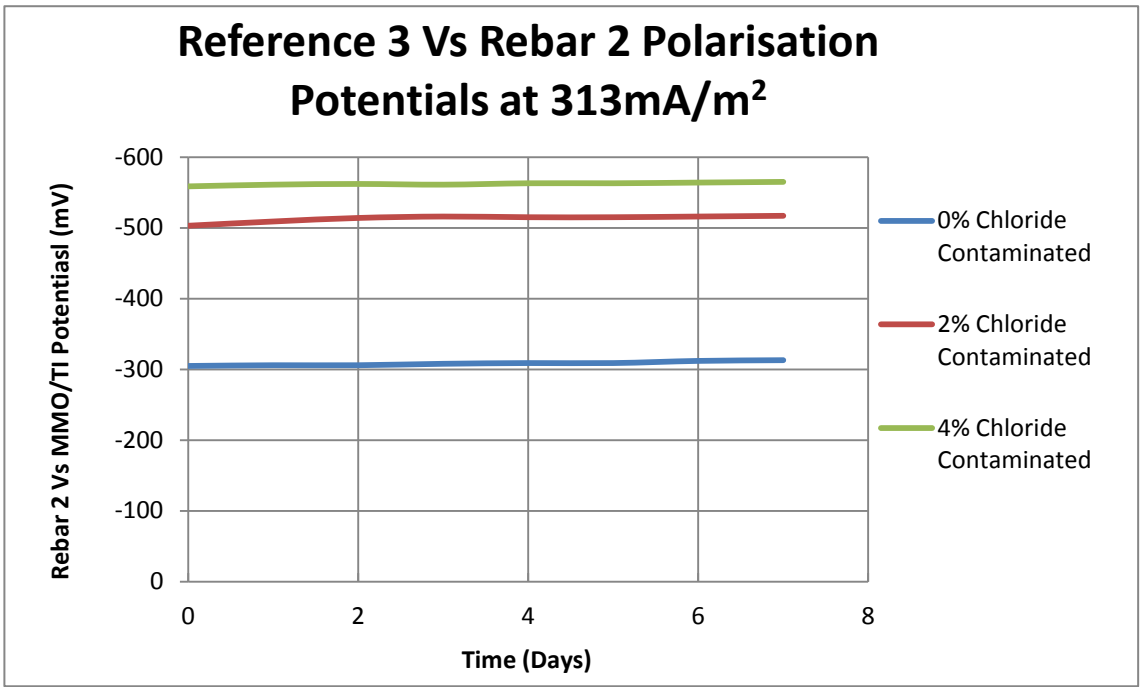

Figure C37: Polarisation potentials at 313 mA/m^2 reference 3 Vs rebar 2

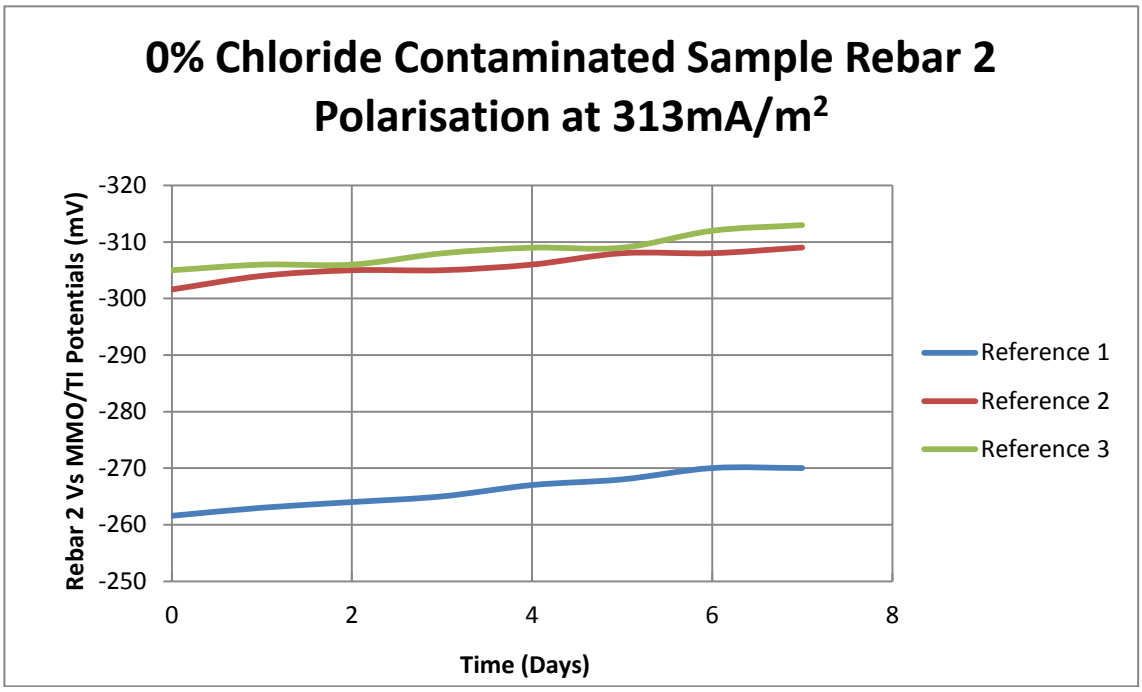

Figure C38: Polarisation potentials at 313mA/m^2 of 0% chloride contaminated sample rebar 2

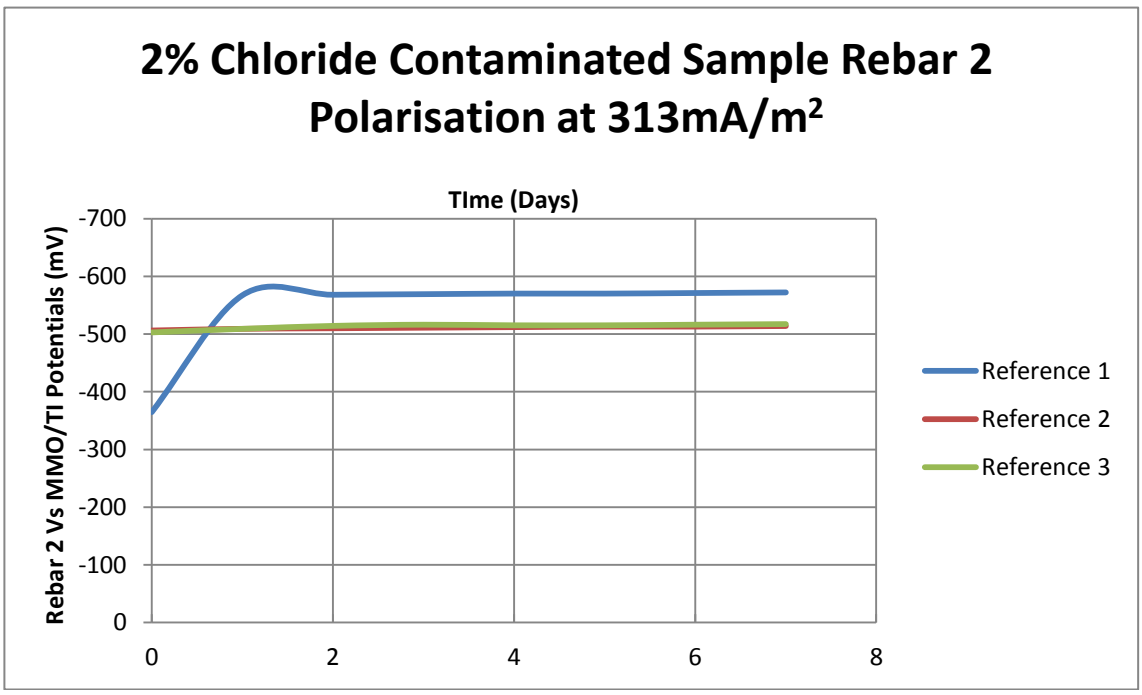

Figure C39: Polarisation potentials at 313mA/m^2 of 2% chloride contaminated sample rebar 2

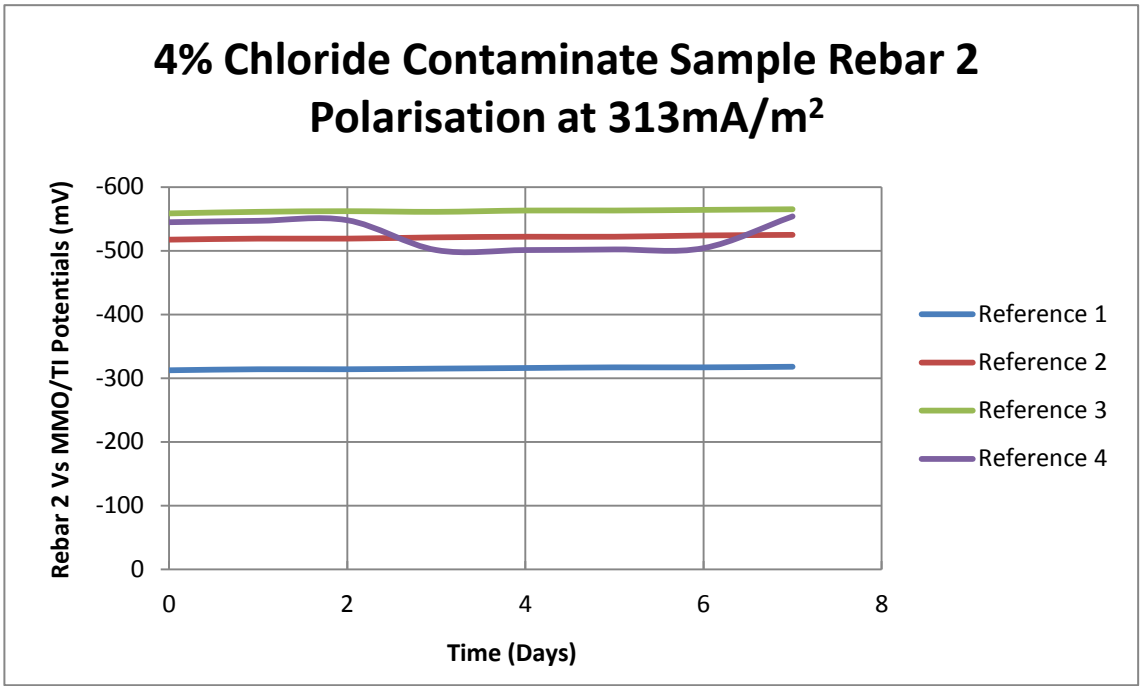

Figure C40: Polarisation potentials at 313mA/m^2 of 4% chloride contaminated sample rebar 2

Table C18: De-polarisation potentials at 104mA/ m^2 for 0% chloride contaminated sample

Time Period (Minutes)	Ref 1 Vs Rebar 1 (mV)	Ref 1 Vs Rebar 2 (mV)	Ref 2 Vs Rebar 1 (mV)	Ref 2 Vs Rebar 2 (mV)	Ref 3 Vs Rebar 1 (mV)	Ref 3 Vs Rebar 2 (mV)
0	-252	-252	-325	-326	-346	-346
5	-245	-245	-321	-321	-338	-338
60	-225	-226	-326	-325	-336	-337
120	-224	-224	-325	-325	-338	-338
240	-227	-227	-326	-326	-337	-337
480	-228	-228	-324	-325	-336	-336
720	-254	-254	-321	-319	-334	-334
1440	-256	-254	-320	-320	-333	-333

Table C19: De-polarisation potentials at 104mA/ m^2 for 2% chloride contaminated sample

Time Period (Minutes)	Ref 1 Vs Rebar 1 (mV)	Ref 1 Vs Rebar 2 (mV)	Ref 2 Vs Rebar 1 (mV)	Ref 2 Vs Rebar 2 (mV)	Ref 3 Vs Rebar 1 (mV)	Ref 3 Vs Rebar 2 (mV)
0	-333	-333	-436	-436	-443	-443
5	-332	-333	-436	-435	-446	-458
60	-331	-331	-440	-441	-445	-445
120	-329	-329	-440	-440	-444	-444
240	-328	-328	-440	-440	-443	-443
480	-329	-328	-439	-440	-440	-440
720	-333	-333	-432	-432	-446	-445
1440	-333	-334	-434	-434	-439	-439

Table C20: De-polarisation potentials at 104mA/ m^2 for 4% chloride contaminated sample

Time Period (Minutes)	Ref 1 Vs Rebar 1 (mV)	Ref 1 Vs Rebar 2 (mV)	Ref 2 Vs Rebar 1 (mV)	Ref 2 Vs Rebar 2 (mV)	Ref 3 Vs Rebar 1 (mV)	Ref 3 Vs Rebar 2 (mV)	Ref 4 Vs Rebar 1 (mV)	Ref 1 Vs Rebar 3 (mV)
0	-389	-389	-418	-418	-474	-474	-467	-467
5	-359	-360	-400	-401	-471	-470	-467	-467
60	-354	-354	-403	-401	-475	-473	-469	-470
120	-348	-350	-401	-403	-474	-473	-468	-468
240	-346	-346	-401	-404	-471	-473	-469	-468
480	-345	-346	-403	-404	-471	-475	-467	-467
720	-391	-389	-408	-409	-470	-472	-463	-463
1440	-357	-357	-398	-397	-468	-471	-464	-463

Table C21: De-polarisation potentials at 208 mA/ m^2 for 0% chloride contaminated sample

Time Period (Minutes)	Ref 1 Vs Rebar 1 (mV)	Ref 1 Vs Rebar 2 (mV)	Ref 2 Vs Rebar 1 (mV)	Ref 2 Vs Rebar 2 (mV)	Ref 3 Vs Rebar 1 (mV)	Ref 3 Vs Rebar 2 (mV)
0	-266	-265	-287	-288	-333	-333
5	-259	-259	-292	-292	-329	-329
60	-235	-235	-296	-298	-330	-330
120	-233	-234	-299	-298	-326	-326
240	-228	-229	-297	-299	-316	-316
480	-248	-250	-301	-302	-316	-316
720	-256	-256	-305	-305	-311	-311
1440	-261	-262	-301	-302	-306	-306

Table C22: De-polarisation potentials at 208 mA/ m^2 for 2% chloride contaminated sample

Time Period (Minutes)	Ref 1 Vs Rebar 1 (mV)	Ref 1 Vs Rebar 2 (mV)	Ref 2 Vs Rebar 1 (mV)	Ref 2 Vs Rebar 2 (mV)	Ref 3 Vs Rebar 1 (mV)	Ref 3 Vs Rebar 2 (mV)
0	-348	-347	-490	-490	-489	-493
5	-397	-397	-538	-538	-544	-544
60	-388	-389	-547	-547	-546	-546
120	-380	-381	-544	-545	-533	-533
240	-372	-373	-500	-501	-507	-507
480	-362	-362	-502	-501	-508	-507
720	-366	-366	-507	-507	-503	-503
1440	-365	-365	-506	-506	-503	-503

Table C23: De-polarisation potentials at 208 mA/ m^2 for 4% chloride contaminated sample

Time Period (Minutes)	Ref 1 Vs Rebar 1 (mV)	Ref 1 Vs Rebar 2 (mV)	Ref 2 Vs Rebar 1 (mV)	Ref 2 Vs Rebar 2 (mV)	Ref 3 Vs Rebar 1 (mV)	Ref 3 Vs Rebar 2 (mV)	Ref 4 Vs Rebar 1 (mV)	Ref 1 Vs Rebar 3 (mV)
0	-317	-318	-482	-480	-538	-536	-523	-524
5	-303	-305	-533	-533	-574	-573	-559	-559
60	-309	-311	-539	-539	-577	-580	-562	-563
120	-311	-311	-538	-538	-580	-579	-562	-562
240	-311	-311	-536	-537	-576	-577	-562	-561
480	-311	-310	-532	-533	-575	-573	-558	-558
720	-309	-309	-527	-528	-569	-569	-554	-554
1440	-312	-312	-516	-517	-560	-559	-545	-545

Table C24: De-polarisation potentials at 313 mA/ m^2 for 0% chloride contaminated sample

Time Period (Minutes)	Ref 1 Vs Rebar 1 (mV)	Ref 1 Vs Rebar 2 (mV)	Ref 2 Vs Rebar 1 (mV)	Ref 2 Vs Rebar 2 (mV)	Ref 3 Vs Rebar 1 (mV)	Ref 3 Vs Rebar 2 (mV)
0	-269	-270	-309	-309	-313	-313
5	-255	-254	-303	-303	-311	-311
60	-260	-260	-294	-294	-306	-306
120	-266	-266	-290	-290	-302	-302
240	-257	-257	-282	-283	-294	-294
480	-263	-263	-285	-286	-288	-288
720	-264	-264	-276	-277	-286	-286
1440	-264	-263	-280	-280	-284	-284

Table C25: De-polarisation potentials at 313 mA/ m^2 for 2% chloride contaminated sample

Time Period (Minutes)	Ref 1 Vs Rebar 1 (mV)	Ref 1 Vs Rebar 2 (mV)	Ref 2 Vs Rebar 1 (mV)	Ref 2 Vs Rebar 2 (mV)	Ref 3 Vs Rebar 1 (mV)	Ref 3 Vs Rebar 2 (mV)
0	-572	-572	-514	-514	-517	-517
5	-364	-365	-508	-508	-511	-511
60	-350	-349	-499	-498	-501	-501
120	-349	-348	-489	-490	-490	-490
240	-337	-337	-485	-485	-489	-489
480	-340	-340	-478	-477	-484	-484
720	-340	-340	-474	-474	-575	-575
1440	-340	-340	-467	-467	-571	-571

Table C26: De-polarisation potentials at 313 mA/ m^2 for 4% chloride contaminated sample

Time Period (Minutes)	Ref 1 Vs Rebar 1 (mV)	Ref 1 Vs Rebar 2 (mV)	Ref 2 Vs Rebar 1 (mV)	Ref 2 Vs Rebar 2 (mV)	Ref 3 Vs Rebar 1 (mV)	Ref 3 Vs Rebar 2 (mV)	Ref 4 Vs Rebar 1 (mV)	Ref 1 Vs Rebar 3 (mV)
0	-318	-318	-524	-525	-565	-565	-554	-554
5	-300	-300	-516	-516	-561	-563	-547	-546
60	-303	-306	-491	-492	-547	-549	-532	-532
120	-318	-318	-481	-481	-539	-539	-524	-524
240	-298	-298	-467	-467	-528	-528	-517	-517
480	-303	-304	-457	-456	-521	-520	-510	-509
720	-316	-315	-450	-450	-514	-518	-504	-503
1440	-316	-315	-440	-442	-510	-510	-498	-498

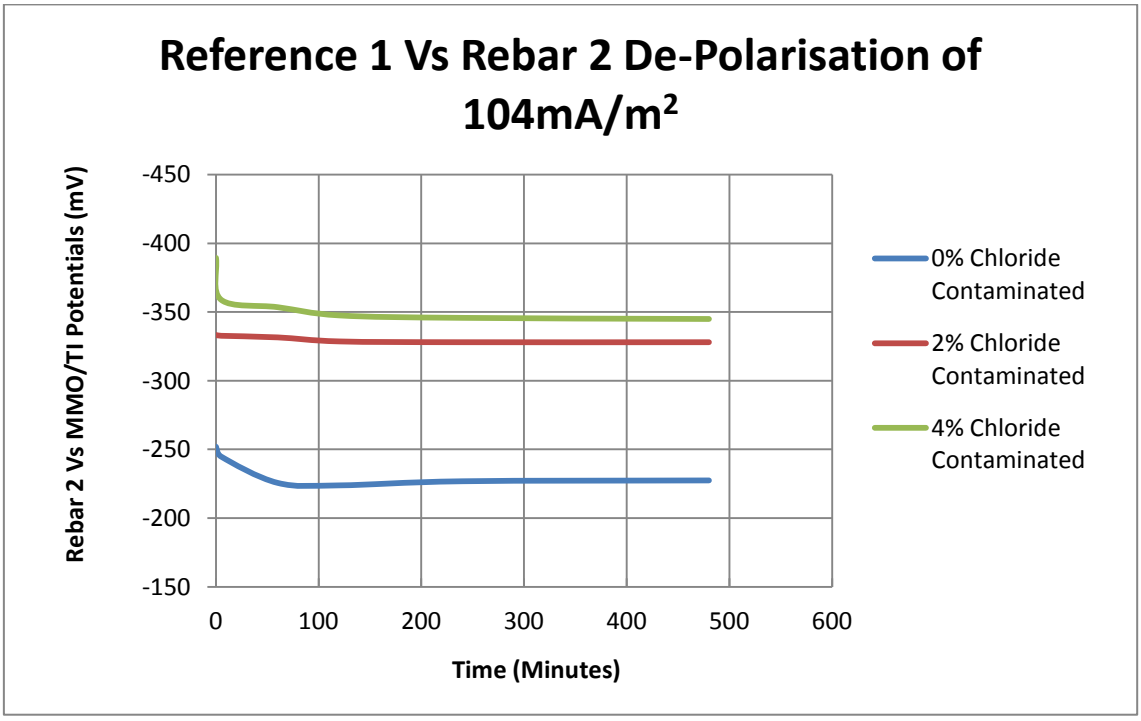

Figure C41: De-polarisation potentials at 104 mA/m^2 reference 1 Vs rebar 2

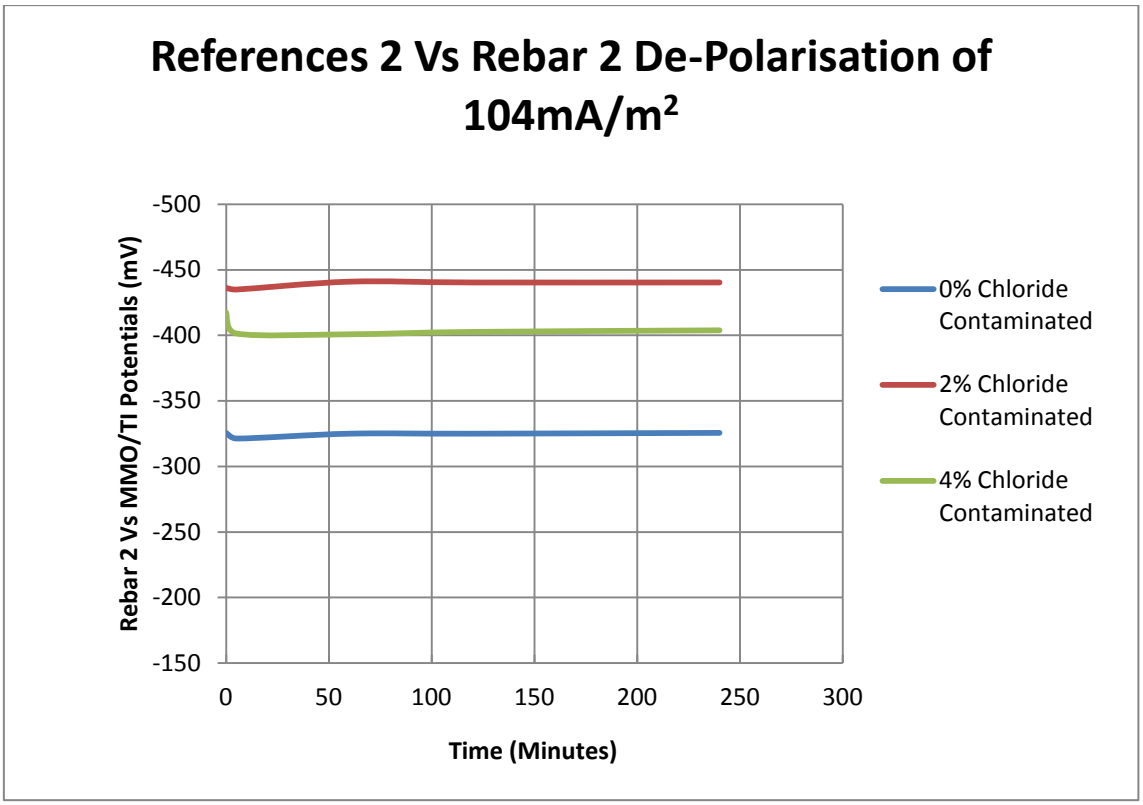

Figure C42: De-polarisation potentials at 104 mA/m^2 reference 2 Vs rebar 2

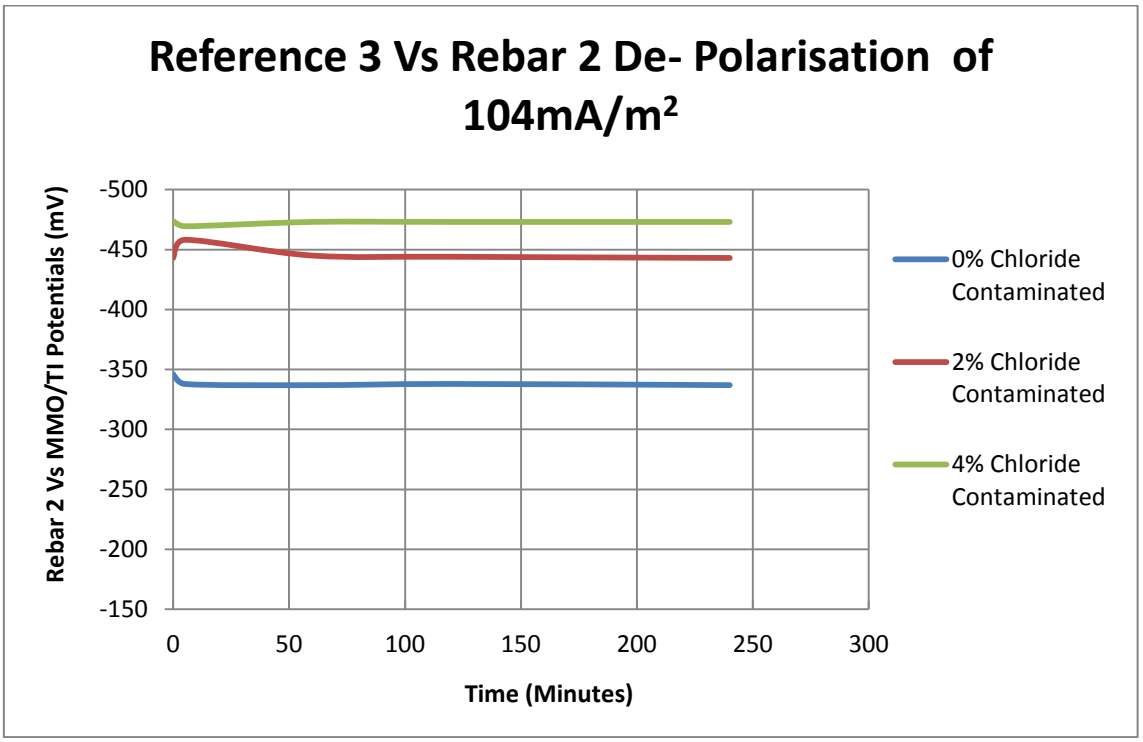

Figure C43: De-polarisation potentials at 104 mA/m^2 reference 2 Vs rebar 2

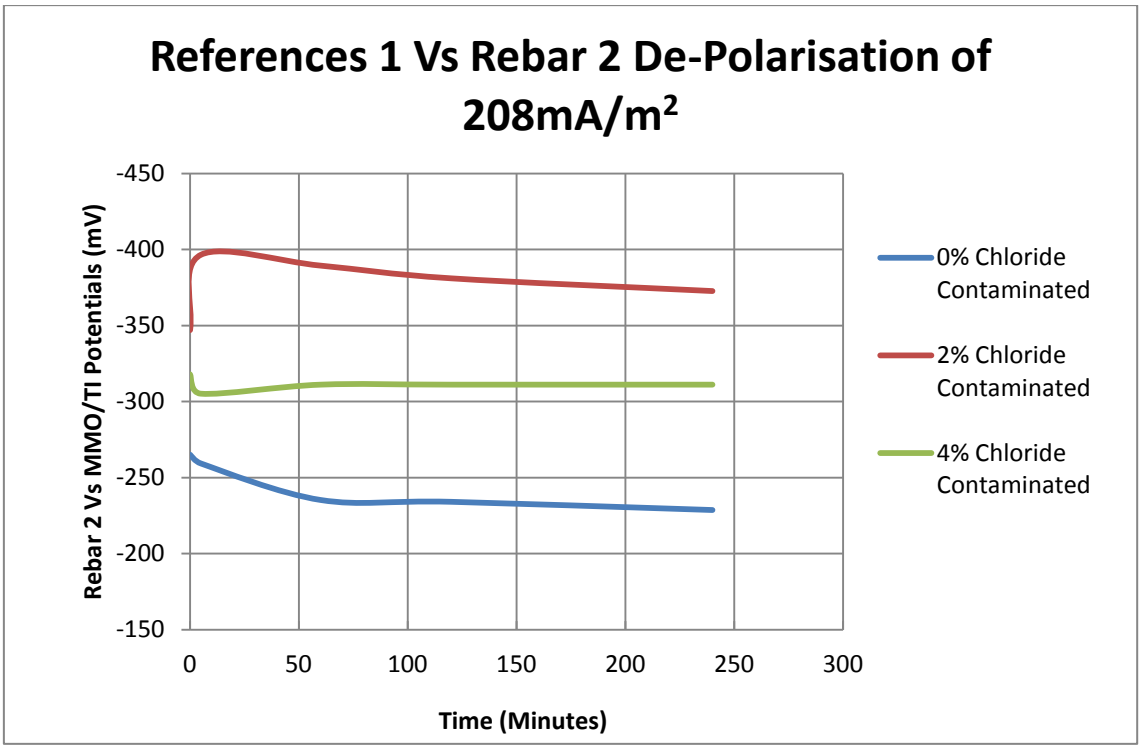

Figure C44: De-polarisation potentials at 208 mA/m^2 reference 1 Vs rebar 2

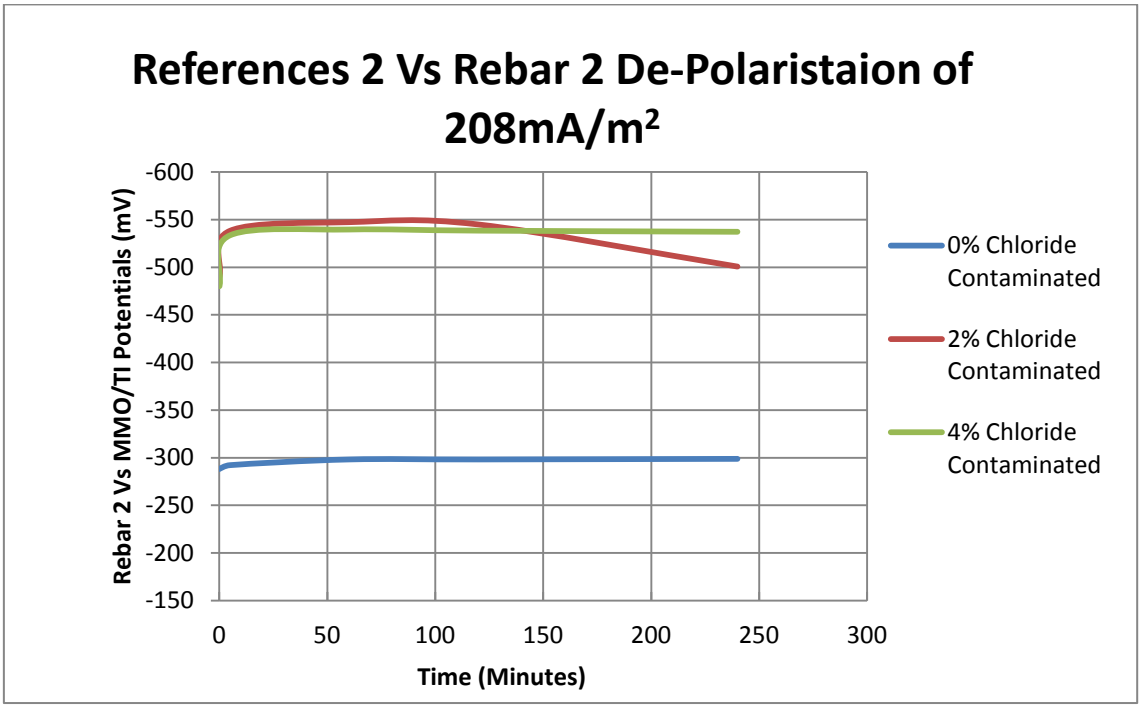

Figure C45: De-polarisation potentials at 208 mA/m^2 reference 2 Vs rebar 2

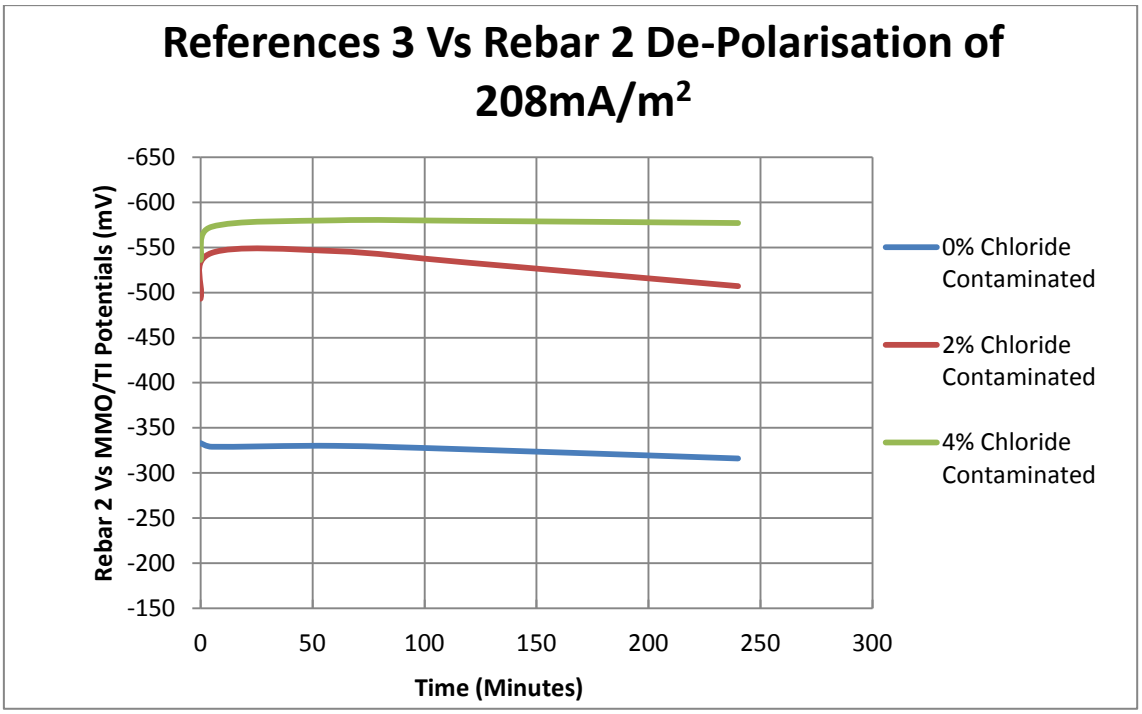

Figure C46: De-polarisation potentials at 208 mA/m² reference 3 Vs rebar 2

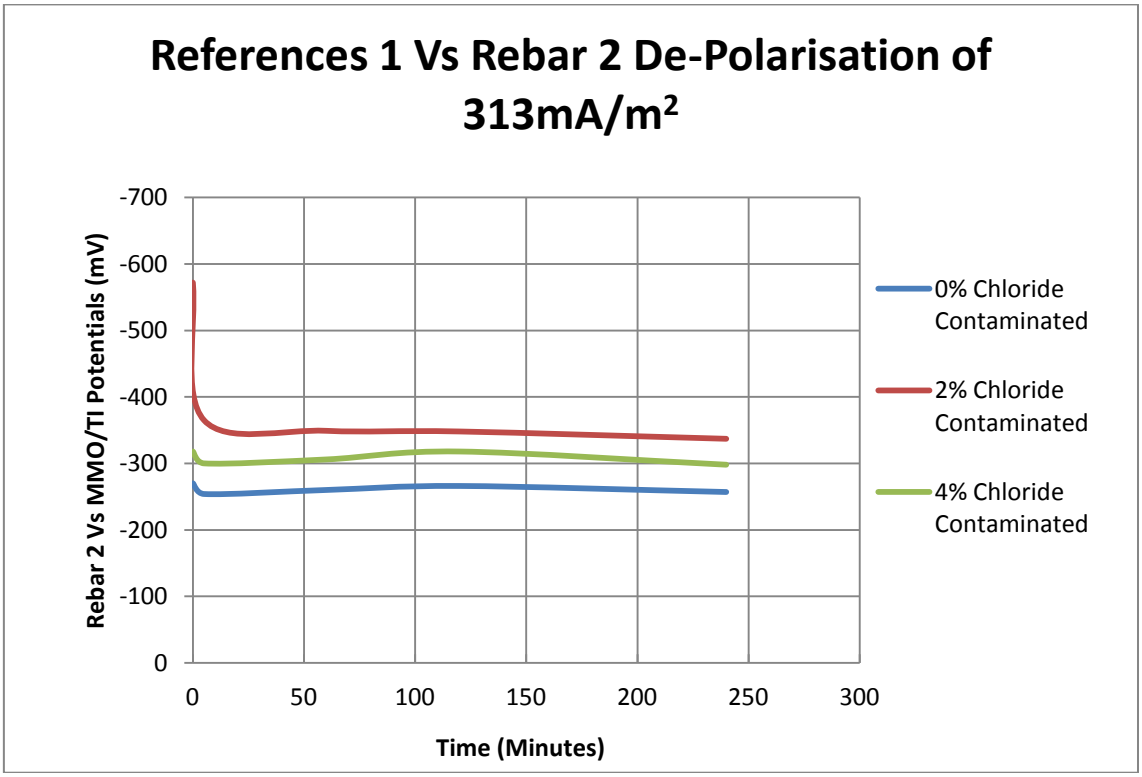

Figure C47: De-polarisation potentials at 308 mA/m² reference 1 Vs rebar 2

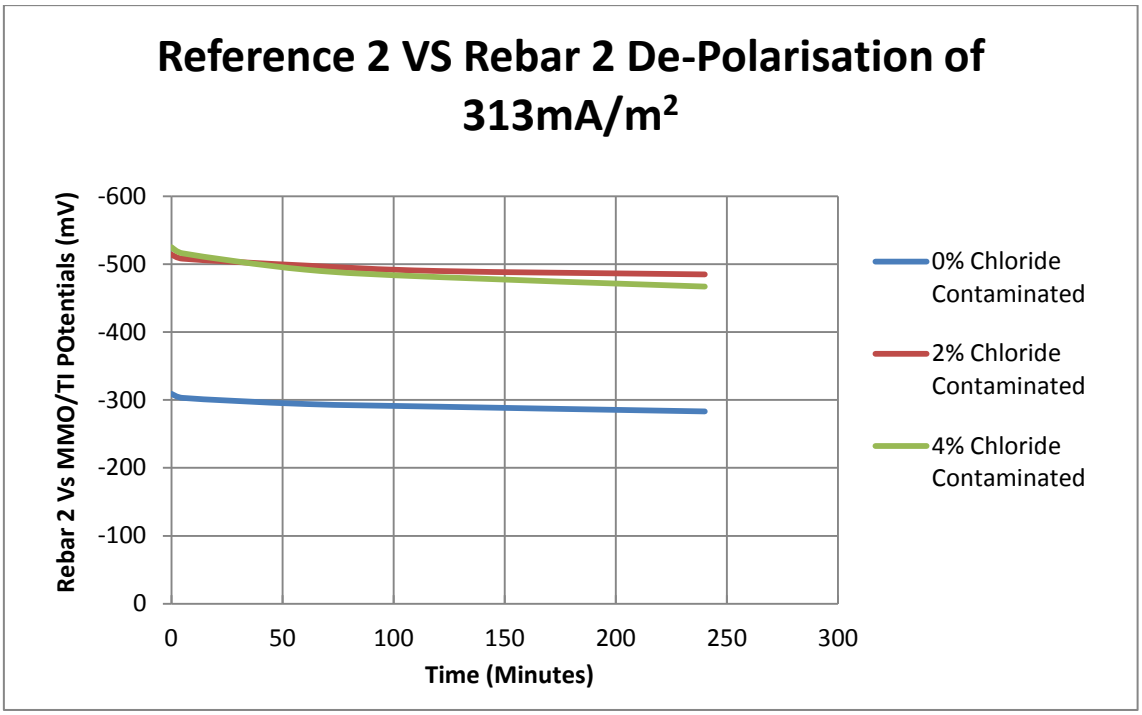

Figure C48: De-polarisation potentials at 308 mA/m^2 reference 2 Vs rebar 2

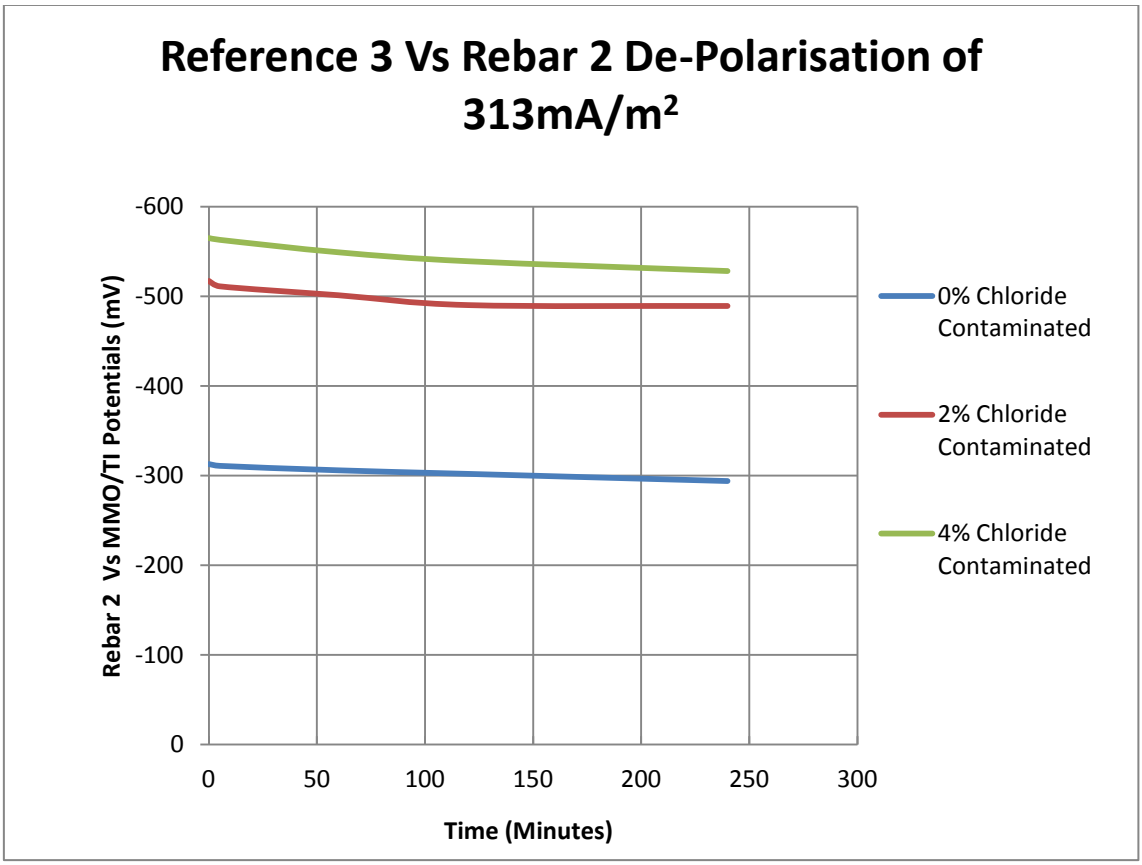

Figure C49: De-polarisation potentials at 308 mA/m^2 reference 3 Vs rebar 2

Appendix D has been removed due to third party copyright

APPENDIX E: SOME EXTRACT FROM THE ZRP COATING MANUFACTURER's TECHNICAL LITERATURES

E. 1 Technical Literatures of the proprietary ZRP Coating

ZINGA Technical data sheet	Ref.: Technische fiches/1 TF Zinga.EN 10/12/08-12	1/6

www.zinga.be

ZINGA

ZM-RE-PRO-04-A (01/08/06)

The film galvanising system Zinga is a one pack coating that contains 96% zinc in the dry film and provides cathodic protection to ferrous metals. It can be used as a unique system as an alternative to hot-dip galvanisation or metallisation, as primer in a duplex system or as a recharging system for hot-dip galvanisation or metallisation. It can be applied by brushing, rolling or spraying on a clean and rough substrate in a wide range of atmospheric circumstances. Zinga is also available as an aerosol and is sold as Zingaspray.

Physical data and technical information

- **Wet product**

Components	- zinc powder - aromatic hydrocarbons - binder
Density	2,67 Kg/dm³ (± 0,06 Kg/dm³)
Solid content	- 80% by weight (± 2%) - 58% by volume (± 2%) according to ASTM D2697
Type of thinner	Zingasolv
Flash point	≥ 40°C to < 60°C
VOC	474 gr/Lt (EPA method 24)

- **Dry film**

Colour	matt metallic grey (colour darkens after contact with humidity)
Zinc content	96% (±1%) by weight, with a purity of 99,995% Zinga gives full cathodic protection and conforms to the standard ISO 3549 in regard to its zinc purity of 99,995 % and to the standard ASTM A780 in regard of its use as repair coating for hot-dip galvanisation.
Special characteristics	- atmospheric temperature resistance - minimum : -40°C - maximum : 120°C with peaks up to 150°C - pH resistance in immersion: from 5,5 pH to 9,5 pH - pH resistance in atmospheric circumstances: from 5,5 pH to 12,5 pH - excellent UV resistance
Non-toxicity	A dry layer of Zinga is not toxic and can be used in contact with potable water, according to the standard BS 6920.

- **Packing**

500 ml	aerosol
1/4 Kg	available as sample (on request)
1 Kg	available, packed in undividable boxes of 12 x 1 Kg
2 Kg	available, packed in undividable boxes of 6 x 2 Kg
5 Kg	available
10 Kg	available
25 Kg	available

- **Conservation**

Storage	store in a cool and dry place
Shelf life	unlimited In case of long time storage it is recommended to shake the unopened tin in an automatic shaker at least once every 3 years.

Application data

- **System recommendations**

Unique system	- Zinga is used as a stand-alone system, applied in 2 or 3 layers to obtain a total maximum DFT* of 120 to 180 µm. - This system is strongly recommended because of the easy maintenance. In time the layer will become thinner as the Zinga sacrifices itself due to the cathodic protection. A new layer of Zinga can be directly applied once the surface has been properly cleaned and it will re-liquidise and recharge the previous Zinga layer. The DFT of Zinga that should be applied depends upon the remaining Zinga layer. - The system Zinga 2 x 60 µm DFT conforms to the standards NORSOK M-501 syst. 7 and ISO 12944 cat. Im2 and Im3.
Duplex system	- In a duplex system, Zinga should be applied in **one single application**, preferably by spraying, to obtain a maximum DFT of 60 to 80 µm. - The surface of the Zinga should be free of zinc salts and other contaminations prior to application of a topcoat. - Zinga can be topcoated with a wide range of compatible sealers and topcoats. To avoid pinholes when topcoated, use the **mist coat & full coat technique**.
Stripe-coat	It is recommended to apply a stripe-coat of Zinga by brush on all sharp edges, nuts and bolts and weld areas before the application of the first full layer of Zinga.
Recharging system	Zinga can be applied on top of a hot-dip galvanising layer, a metallisation layer or an old Zinga layer in order to renew or enhance the cathodic protection. The DFT of Zinga that should be applied depends upon the existing galvanising layer.

*DFT & WFT : dry film thickness and wet film thickness ; to be measured **above the peaks** of the roughness profile

- **Coverage and consumption**

Theoretical consumption	- for 60 µm DFT : 0,28 Kg/m² or 0,10 Lt/m² - for 120 µm DFT : 0,55 Kg/m² or 0,21 Lt/m²
Theoretical coverage	- for 60 µm DFT : 3,62 m²/Kg or 9,67 m²/Lt - for 120 µm DFT : 1,81 m²/Kg or 4,83 m²/Lt
Practical coverage	depends upon the roughness profile of the substrate and the application method

- **Environmental conditions during application**

Ambient temperature	- minimum -15°C - maximum 40°C
Relative humidity	- maximum 95%
Surface temperature	- minimum 3°C above the dew point - no visual presence of water or ice - maximum 60°C
Product temperature	During application the temperature of the Zinga liquid must remain between 15 and 25°C. A lower or higher temperature of the product will influence the smoothness of the film when drying.

- **Drying process and overcoating**

Drying process	Zinga dries by evaporation of the solvent. The drying process is influenced by the total WFT, the number of coats applied, the ambient air and surface temperatures and the air circulation.
Drying time	for 40 µm DFT at 20°C in a well-ventilated environment: - touch-dry: after 10 min. - dry to handle: after 1 hour - fully cured: after 48 hours - ready for immersion: after 2 hours
Overcoating	- with a new layer of Zinga : - brush : 1 hour after touch dry - spray gun : 1 hour after touch dry - with a compatible paint : after 6 to 24 hours depending on the drying conditions
Reliquidisation	Each new layer of Zinga reliquidises the former Zinga layer so that both layers form one homogeneous layer.

Instructions for use

- **Surface preparation**

Cleanliness	- The most common method to obtain a clean (and at the same time rough) surface for the application of Zinga is: The metal substrate should first be **degreased**, preferably by **steam-cleaning** at 140 bar at 80°C. After that it should be **grit-blasted** or **slurry-blasted** to cleanliness degree SA 2,5 according to the standard ISO 8501-1 or to the cleanliness degree described in the standards SSPC-SP10 and NACE nr 2. This means that the surface must be free from rust, grease, oil, paint, salt, dirt, mill scale and other contaminants. Once the grit-blasting is completed the surface should be **de-dusted** with non contaminated compressed air according to the standard ISO 8502-3 (class 2) or in case of slurry-blasting the surface should be **dried** with non-contaminated compressed air. - Another method to obtain a clean surface is **UHP water-jetting** to cleanliness degree WJ2 according to the standards NACE nr 5 and SSPC-SP12 level SC1. But keep in mind that this method does **not** create surface roughness. - This high degree of cleanliness is not needed when Zinga is applied on a hot-dip galvanisation or a metallisation layer, or when it is applied on top of an existing Zinga layer. Please consult with the Zingametall representative. - For substrates that will not be immersed Zinga can be applied on mild flash rust (FWJ-2) occurring in the allowed time limit. For applications that will be immersed Zinga can only be applied on an SA 2,5 prepared surface with contaminants to NACE No5/SSPC SP-12 level SC1 unless otherwise agreed with the Zingametall representative. - On small areas or on non-critical applications Zinga can be applied on a surface that is manually prepared to degree St 3 according to ISO 8501-1. Please consult with the Zingametall representative.
Roughness	- Zinga should be applied on a metal substrate that has roughness degree Rz 50 to 70 µm (for total DFT < 280 µm) or Rz 60 to 80 µm (for total DFT > 280 µm) according to the standard ISO 8503-2. This can be obtained by **grit-blasting** (with sharp particles) but not by shot-blasting (with spherical particles). Make sure that the surface is degreased **before** the grit-blasting. - This high degree of roughness is not needed when Zinga is applied on a hot-dip galvanisation or a metallisation layer, or when it is applied on top of an existing Zinga layer. Please consult with the Zingametall representative. - On small areas or on non-critical applications Zinga can be applied on a surface that is manually prepared e.g. with a needle gun or a grinding disk, in order to obtain an adequate roughness for Zinga. Please consult with the Zingametall representative.

Maximum time to application	Apply the Zinga as soon as possible on the prepared surface. - in dry circumstances : depending on the location - in case of water-cleaning or if the relative humidity is close to 80%: max. 4 hours waiting time If contamination occurs before coating, the surface must be cleaned again as described above. Flash rust can be removed by means of a wire brush.

- **Special instructions**

Stirring	- Zinga must be thoroughly stirred to achieve a homogeneous liquid before application. After a maximum of 20 min. re-mixing is necessary. - During the spraying application, the product must be stirred continuously.

Dilution	Zinga can be diluted with 0 to 5% (volume on volume) of Zingasolv when using airless spray equipment and 0 to 25% for air supported applications. The Zingasolv must be added whilst stirring.
Rinsing of tools and equipment	Before and after using the spraying equipment, it must be rinsed with Zingasolv. Brushes and rollers should also be cleaned with Zingasolv. Never use White Spirit.
Special demands for spraying equipment	- Pour the Zinga through a filter of 100 mesh (150 µm) into the drum. - For the spraying of Zinga, it is better to remove all filters from the pistol and from the drum to avoid blockage. - The spray gun must be equipped with reinforced needle springs.

- **Application by brush and roller**

Viscosity	Zinga is ready for use when applied by brush or roller. Do not dilute.
First layer	The first layer must never be applied by roller, only by brush, in order to fill the cavities of the roughness profile and to wet the surface.
Type of brush and roller	- short hair roller (mohair) - industrial round brush

- **Application by spraying with spray gun with gravity cup**

Dilution	0 to 25% (volume on volume)
Spray viscosity	25 to 35 sec. Ford cup nr. 4 at 20°C
Pressure at the nozzle	2 to 4 bar
Nozzle opening	1,7 to 2,5 mm

- **Application by spraying with spray gun with pressure pot**

Dilution	0 to 25% (volume on volume)
Spray viscosity	25 to 35 sec. Ford cup nr. 4 at 20°C
Pressure at the nozzle	3 to 4 bar
Pot pressure	0,8 to 1,5 bar
Nozzle opening	1,7 to 2,5 mm

- **Application by airless spraying**

Dilution	0 to 5% (volume on volume)
Pressure at the nozzle	112 to 280 bar
Nozzle opening	0,017 to 0,031 inch (0,43 to 0,78 mm)

- **Other application methods**

Please consult with the Zingametall representative.

For more specific and detailed recommendations concerning the application of Zinga, please contact the Zingametall representative. For detailed information about the health and safety hazards and precautions for use, please refer to the Zinga **safety data sheet**.

Waiver*

* The information on this sheet is merely indicative and is given to the best of our knowledge based on practical experience and testing. The conditions or methods of handling, storage, use or disposal of the product cannot be controlled by us and are therefore outside our responsibility. For these and other reasons we retain no liability in case of loss, damage or costs that are caused by or that are linked in any way to the handling, storage, use or disposal of the product. Any claim concerning deficiencies must be made within 3 months upon reception of the goods quoting the relevant batch number. We retain the right to change the formula if properties of the raw material are changed. This data sheet replaces all former specimens.

E. 2 Characteristic Properties of the proprietary ZRP Coating

ZINGA is a single-pack zinc coating that is easy to apply by brush, roller, spraying or dipping under any atmospheric condition. It offers a better cathodic protection than hot-dip galvanisation. This was proven in Europe, in the USA and in Asia, both in laboratory and in field testing. This relates mainly to direct application on steel structures. A dry ZINGA layer consists of 96% zinc, pure to 99.995% and homogeneously dispersed throughout the layer.

According to the manufacturer's, Zinga is a unique form of corrosion protection because it provides both Active and Passive protection in a form that's as easy to apply as paint, but Zinga is not a paint.

Zinga is an active zinc performance coating which works in conjunction with the metal beneath whereas paints are only passive barriers. Regardless of how thick paints are applied, they remain as barriers. Once they are breached corrosion sets in immediately. Despite this significant difference Zinga is still often mistaken for paint simply because it's liquid and comes in a tin. But there are other more subtle differences. For example it does not "skin over" in the tin because Zinga has an unlimited pot-life and it doesn't go "tacky" like paint.

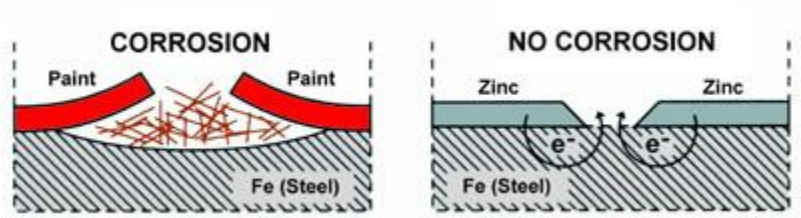

Figure E1: Corrosion behaviour of steel with 'ordinary paint' and 'Zinga'.

Active Protection

Cathodic protection, or active protection, arises from the zinc (the anode) sacrificing itself in favour of the base metal (the cathode) with the resulting flow of electrons preventing corrosion's chemical reaction. In this way the protection of the metal is guaranteed, even when the zinc layer is slightly damaged. Other well established methods of cathodic protection include hot-dip galvanising (HDG) and zinc thermal spraying both of which exhibits a constant sacrificial rate of the zinc layer.

Within Zinga though this sacrificial rate reduces dramatically after the zinc layer has oxidised and the natural porosity have been filled with zinc salts. Additionally the zinc particles within the Zinga layer are protected by the organic binder without adversely affecting the electrical conductivity. This enables Zinga to create nearly the same galvanic potential between the zinc and the steel as hot dip galvanising but with a lower rate of zinc loss because, put simply, the binder acts as a “corrosion inhibitor” to the zinc. "The zinc in Zinga becomes the sacrificial anode in relation to the steel but it corrodes at a much slower rate than would otherwise be expected" (JJB Ward, Oxfordshire, Jan '92).

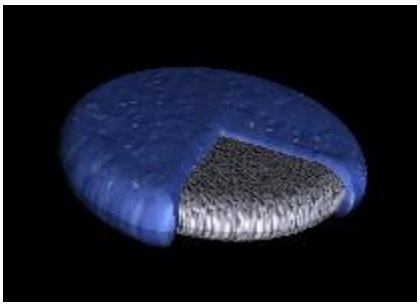

Figure E2: This illustration shows the minute elliptical zinc particle encased in the protective organic binder. This covering does not adversely affect the electrical conductivity between neighbouring particles or the steel substrate but does ensure that the zinc in Zinga is better protected than pure zinc from the weather, abrasion, pH etc.

If the Zinga layer is sufficiently damaged to expose the base metal below, the steel would form a layer of surface rust but no corrosion would take place beneath it. In other words if the surface discolouration was removed the steel below would not be pitted or eroded. This is called "throw" and enables Zinga to protect bare metal up to 3 - 5mm or so away from where the coating ends – slightly less than new HDG. Zinc sacrificial anodes used on the steel hulls of boats below the waterline work on the same principle to protect metal in the surrounding area. Zinga is simply a different form of these anodes and is therefore sometimes referred to as a liquid anode or sheet anode when used in immersed conditions. However, it should be noted that like all forms of zinc protection, Zinga should not be used uncovered in immersed conditions above 65 degrees C as that is the inversion point where the steel starts to be sacrificed to protect the zinc. The ability of zinc to provide galvanic protection is a function of its weight per given area. Dry Zinga contains a minimum of 96% medicinal quality zinc by weight, the particles of which are significantly smaller and purer than those found in normal "zinc rich" coatings. The Zinga particles small size and elliptical profile ensures maximum contact between both the individual particles

and the substrate. This greater density of active zinc per given area combined with the good conductivity of the layer ensures that charge flows through every millimetre that has been coated and therefore provides excellent cathodic protection.

Passive Protection

Passive protection, such as paints and cladding, creates a "barrier" between the steel substrate and the elements. Once this barrier is compromised then the moisture and atmospheric salts will be able to start corroding the steel beneath the damaged area. This corrosion will then begin to creep extensively beneath the coating.

With Zinga, the organic binder and the zinc oxide layer that forms on the surface create an impervious barrier by blocking the zinc's natural porosity with oxide particles. Unlike other passive coatings, once breached the zinc oxide layer simply renews itself by re-oxidising. This layer of oxides is the reason behind the matt appearance of Zinga as opposed to the shiny hot-dipped finish.

Predicted Service Life

The corrosion rates of zinc in various environments have been well researched over the years. As a result it is possible to chart the predicted service life for a zinc layer at a given dry film thickness (DFT) in a particular situation. The chart below is based on Hot-Dip Galvanised steel but, as it has already been explained in the Active Protection section, Zinga performs at least as well as HDG in normal atmospheric conditions and even better in marine environments. Please note that the minimum acceptable DFT would normally be 50 microns i.e. the structure should be re-loaded with new Zinga once the zinc has depleted to 50um from its original DFT (normally >120um if using Zinga without topcoats). This is an important point as otherwise this chart could be misleading.

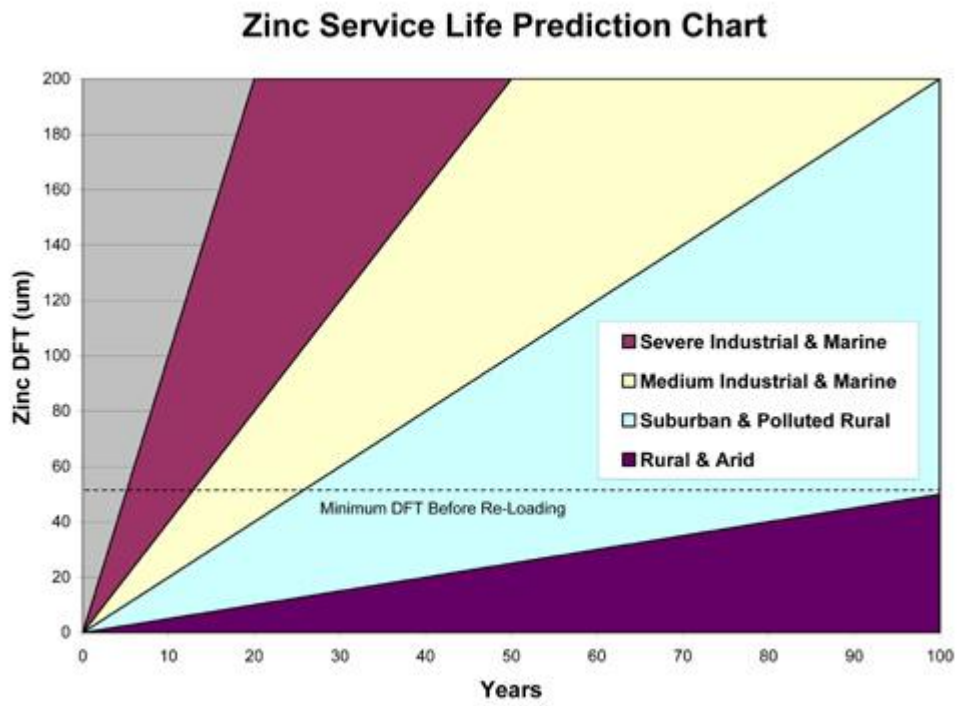

Figure E3: Source: SGS Axa-Med. Service Life is defined as the time to 5% rusting of the steel surface.

Duplex Systems

If Zinga is used as part of a duplex system, i.e. is over-coated with another compatible product, the top-coat provides the initial barrier but the zinc oxide will form a secondary barrier if the first layer is compromised for any reason. As the top-coat becomes naturally porous over time, the Zinga fills the pores from below with zinc oxides enabling the top coat to last longer. Additionally the Zinga does not even start to sacrifice itself until the topcoat is damaged exposing the bare zinc to the elements. It is because of this that Zingametall in Belgium state that the lifetime of a duplex system can be 50% more than the sum of the individual lives of Zinga and the topcoat.

Re-Liquidising of Zinga

Another of Zinga's unique characteristics is its ability to re-liquidise when a new coat of Zinga is applied to form a single homogenous layer. This ensures a massive cost saving in on-going maintenance because the old Zinga layer does not have to be removed before re-coating with Zinga. This also means that once the initial abrasive blasting has been completed the surface will never have to be blasted again.

The following microscopic photos demonstrate the total integration of multiple layers of Zinga:

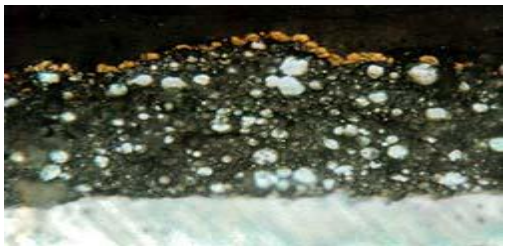

Figure E4: A thin film of gold dust was applied on top of the first coating of Zinga

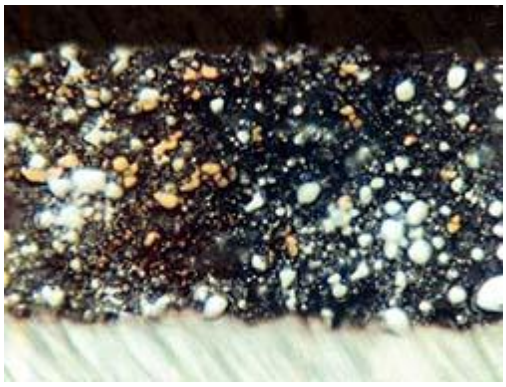

Figure E5: Seven days later a second coating of Zinga was applied on top of the gold dust. It can be clearly seen that the gold dust has mixed completely within the two Zinga layers.

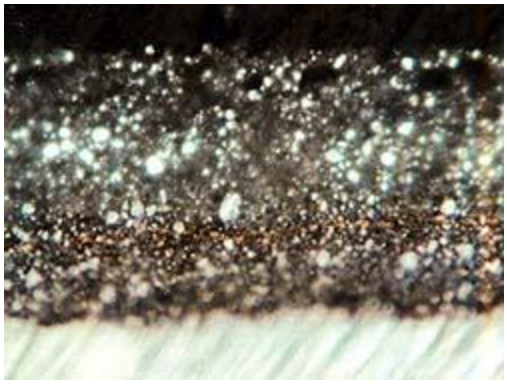

Figure E6: The same test was done with a zinc-rich paint. The gold film remains intact between the two coats demonstrating that they remain as separate layers.

As protection to concrete reinforcement bars (rebars)

Widely used in countries where the available aggregate for concrete can be saline (e.g. Iran, India, Saudi Arabia etc.), Zinganising the steel re-bars before assembly and immersion in concrete ensures vastly increased protection from corrosion without reducing the pull-out strength of the bars. Recent tests in three independent laboratories showed that Zinga had at least twice the corrosion protection of either galvanised or epoxy coated rebars.

The above description and the merits of Zinga is based on the performance of the paint applied directly on the steel surface.

APPENDIX F: ENVIRONMENTAL CHAMBER DETAILED SPECIFICATION

2 DESCRIPTION OF THE TEST SYSTEM

2.1 Structure

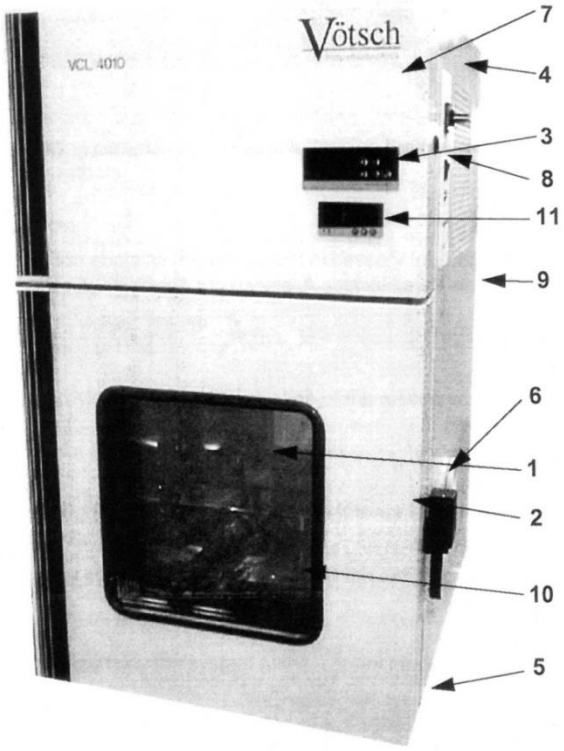

Fig 2-1
100-ltr test system

1 Test space
2 Test space door
3 Control unit »Mincontrol«
4 Mechanical section
5 Feet
6 Entry port
7 Electrical section
8 Main switch panel
9 Reservoir for demineralized water [2)]
10 Temperature and humidity sensors [2)]
11 Adjustable temperature limiter

1) option
2) climatic test systems only

2.2.9 Temperature and humidity sensors

The temperature and humidity sensors are located at the rear of the test space.

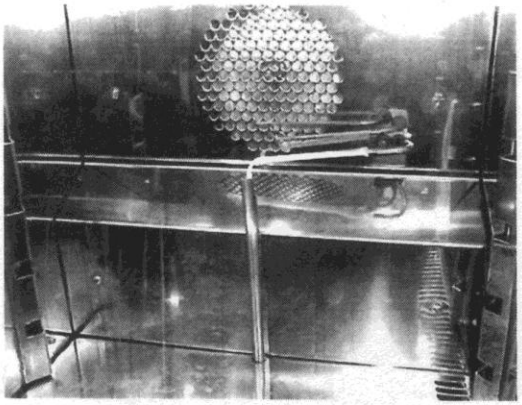

Fig 2-3
Sensor on 34-ltr and 64-ltr test systems

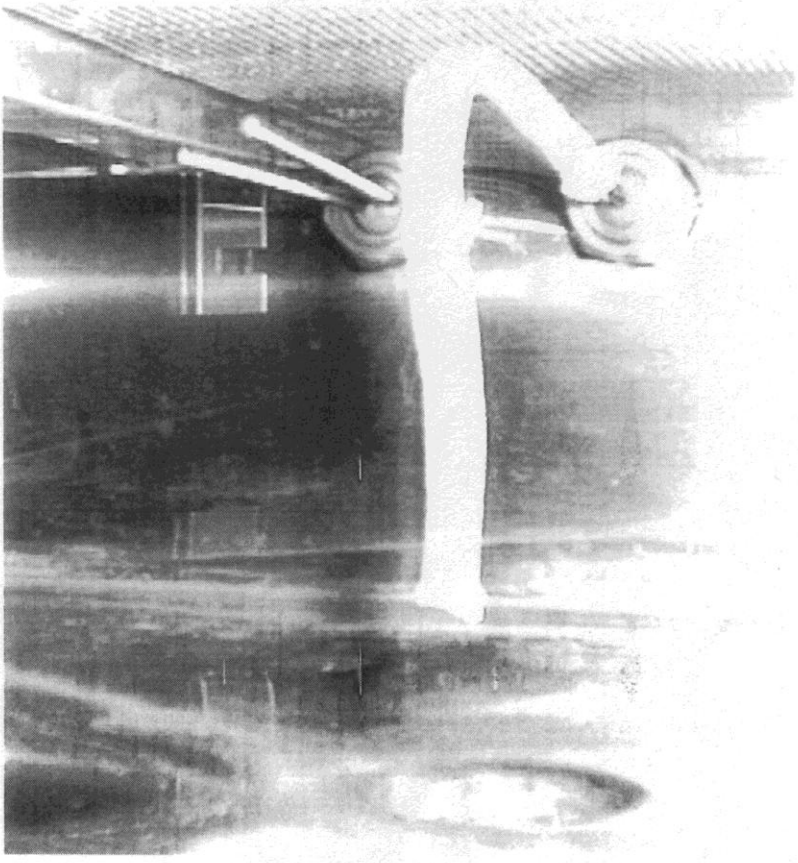

Fig 2-4
Sensor on 100-ltr test system

1) option
2) climatic test systems only

3 TECHNICAL DATA

These figures represent average values of standard test systems based on an ambient temperature of +25 °C. Rated voltage → *3.3 Operating data (page 14)*, without test specimen, without options.

NOTE
The dimensions are specified in the layout.

3.1 General characteristics

Temperature test system **Climatic test system**	**VCL 0003**	**VTL 4003** **VCL 4003**	**VTL 7003** **VCL 7003**
Test space volume	approx. 34 ltr	approx. 34 ltr	approx. 34 ltr
Weight	110 kg	110 kg	140 kg

Temperature test system **Climatic test system**	**VCL 0006**	**VTL 4006** **VCL 4006**	**VTL 7006** **VCL 7006**
Test space volume	approx. 64 ltr	approx. 64 ltr	approx. 64 ltr
Weight	120 kg	120 kg	150 kg

Temperature test system **Climatic test system**	**VCL 0010**	**VTL 4010** **VCL 4010**	**VTL 7010** **VCL 7010**
Test space volume	approx. 100 ltr	approx. 100 ltr	approx. 100 ltr
Weight	170 kg	190 kg	210 kg

3.2 Mechanical loads

Temperature test system **Climatic test system**	**VCL 00..**	**VTL 40..** **VCL 40..**	**VTL 70..** **VCL 70..**
Maximum load (evenly distributed over the entire surface)			
on test space floor	10 kg	10 kg	10 kg
on each insert shelf	10 kg	10 kg	10 kg
total shelf load	50 kg	50 kg	50 kg

1) option
2) climatic test systems only

3.3 Operating data

Temperature test system **Climatic test system**	**VCL 0003**	**VTL 4003** **VCL 4003**	**VTL 7003** **VCL 7003**
Temperature test system **Climatic test system**	**VCL 0006**	**VTL 4006** **VCL 4006**	**VTL 7006** **VCL 7006**
Test space illumination	Halogen lamp 12V, 20W		
Emitted interference, interference immunity	see Declaration of Conformity		
Rated voltage	1/N / PE AC 230 V ± 10 % 50 Hz or 1/N / PE AC 254 V ± 10 % 60 Hz[1)]		
Rated power	1.8 kW	1.8 kW	2.7 kW
Rated current	8 A	8 A	11,7 A
On-site fuse protection	16A slow		
Protection class switchgear cabinet Protection class control unit	IP 22 IP 54		
Heat dissipation on air-cooled test systems			
max. heat dissipation to surroundings	800 W	800 W	1700 W

Temperature test system **Climatic test system**	**VCL 0010**	**VTL 4010** **VCL 4010**	**VTL 7010** **VCL 7010**
Test space illumination	Halogen lamp 12V, 20W		
Emitted interference, interference immunity	see Declaration of Conformity		
Rated voltage	1/N / PE AC 230 V ± 10 % 50 Hz oder 1/N / PE AC 254 V ± 10 % 60 Hz[1)]		
Rated power	2.7 kW	3 kW	3.5 kW
Rated current	11.7 A	13 A	15.2 A
On-site fuse protection	16A träge		
Protection class switchgear cabinet Protection class control unit	IP 22 IP 54		
Heat dissipation on air-cooled test systems			
max. heat dissipation to surroundings	1700 W	2000 W	2500 W

1) option
2) climatic test systems only

3.6.1 Humidity diagram

The following humidity ranges may be used:

- range 1: standard range
- range 2: extended performance with compressed air dryer[1)] and capacitive humidity measuring system [1)]

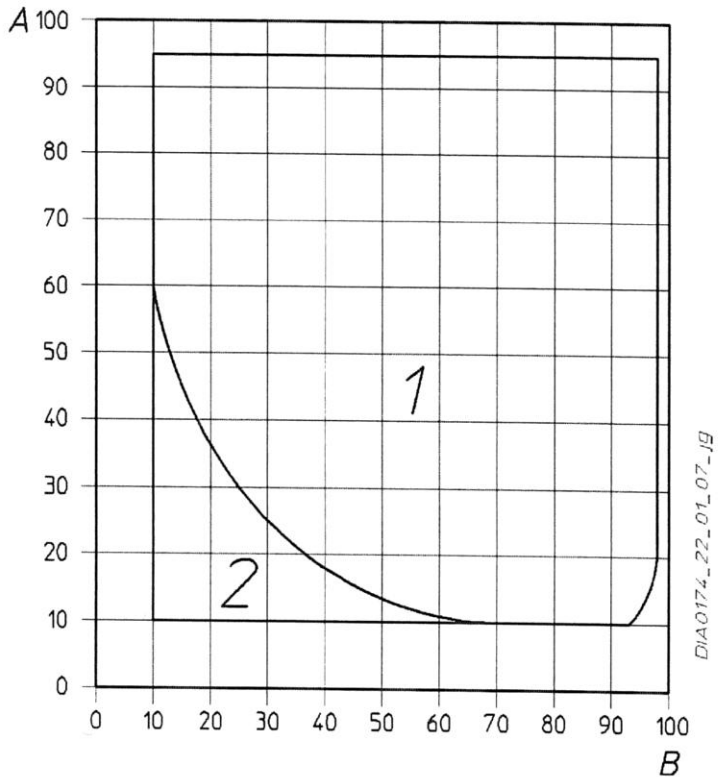

Fig 3-1
Humidity range

A Test space temperature in °C

B Relative humidity in %

1) option
2) climatic test systems only

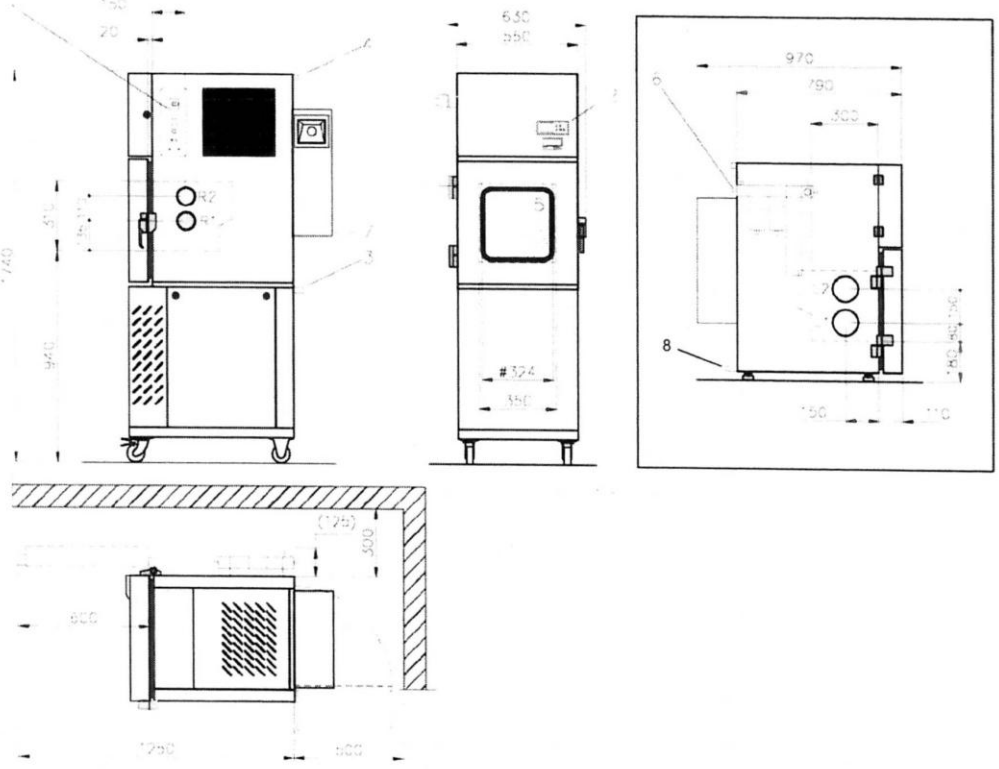

Fig. 4-2
Layout 34-ltr test system

R1: NW 50 mm - entry port installed in basic version
R2[1)], R3[1)] additional installation positions, right
L1[1)], L2[1)], L3[1)] additional installation positions, left

1 Main switch panel
2 Control unit
3 Condensate drain
4 Electrical connection, cable length approx. 3.5 m
5 Door with window
6 Connection for compressed air[1)]
7 Reservoir for humidification water[2)]
8 Connection for automatic water replenishment[1) 2)]
Useful width

1) option
2) climatic test systems only